

Application of the structural stress concept for cruciform joints subjected to fatigue loading under the specific evaluation of influences from imperfections on the component behaviour

Niclas Rausch

Vollständiger Abdruck der von der TUM School of Engineering and Design der
Technischen Universität München zur Erlangung eines
Doktors der Ingenieurwissenschaften (Dr.-Ing.)
genehmigten Dissertation.

Vorsitz: Prof. Dr.-Ing. Oliver Fischer

Prüfer*innen der Dissertation:

1. Prof. Dr.-Ing. Martin Mensinger
2. Prof. Dr. techn. Andreas Taras
3. Prof. Dr.-Ing. Markus Feldmann

Die Dissertation wurde am 02.03.2023 bei der Technischen Universität München
eingereicht und durch die TUM School of Engineering and Design am 12.09.2023
angenommen.

Abstract

This thesis addresses the application of the structural stress concept for fatigue loaded cruciform joints including the underlying structural stress-oriented assessment approaches. The objective is to eliminate existing uncertainties in the structural stress concept and to develop more expedient regulations. In this respect, the differing specifications provided in normative regulations, guidelines and the literature for FE modelling and stress determination as well as for the classification of fatigue resistances and their consideration of imperfections and thickness effects in many cases prevent a consistent economic and reliable implementation of fatigue verification. For this reason, particular emphasis is placed on the effects of manufacturing-related imperfections under clamping conditions in testing machines as well as under practice-relevant support conditions, since the resulting influence on structural stresses is insufficiently considered in standardisation. The thesis is based on the results of the IGF research project No. 20336N [1].

According to the objective, feasible local methods for the evaluation of structural stresses are discussed in detail and are assessed for their practical applicability. In addition, specifications from normative regulations, guidelines and the literature are introduced and discrepancies are identified. In order to eliminate uncertainties regarding the modelling in the structural stress concept, relevant boundary conditions are investigated within the scope of the finite element analysis and applicable methods for the development of expedient shell and solid models are determined. Furthermore, possible imperfections of cruciform joints are analysed and evaluated for relevant support conditions both directly by means of finite element analyses and indirectly by analytical stress concentration factors. Extensive parameter studies are conducted for these purposes. The numerical results of the studies are verified by evaluations of experimentally executed fatigue tests on cruciform joints. Therefore, the influence of imperfections on the resulting structural stresses is evaluated through test series with intentional axial misalignment. To this end, data from laser scan measurements of each test specimen enables an accurate assessment of the unintentional imperfections related to the manufacturing process. In this way, stress concentration factors for the indirect determination of stress-increasing effects can be determined precisely and existing regulations can be verified. Moreover, by means of the fatigue tests, the economic feasibility of the structural stress concept can be verified against the nominal stress concept, in addition to verifying its practicability.

Through comprehensive evaluations in this thesis, it can be demonstrated that based on the fatigue resistances according to DIN EN 1993-1-9 [2], guidelines of the International Institute of Welding [3] and prEN 1993-1-9 [4], more economical results can be expected in many cases with structural stresses than with the nominal stress concept, provided that no imperfections are to be encountered. However, this conclusion necessitates a reliable assessment of the fatigue resistance of cruciform joints in the structural stress concept, which cannot be verified in all cases by the fatigue tests evaluated. In addition, the normative specifications on the considered influences of imperfections on the resistance side are subjected to a wide dispersion across the regulations and can result in a misjudgement of the respective fatigue strength.

Consequently, there is a considerable risk of unreliable fatigue verification in the structural stress concept, as a realistic determination of probable load cycles cannot always be ensured. Deviating information in the literature on the indirect consideration of stress-increasing effects furthermore lead to uncertainties in the structural stress evaluation if imperfections are not directly considered in the finite element analysis. However, by systematic verification of the specifications for the determination of influences from imperfections according to the literature, ranges of application can be identified in which the indirect evaluation of stress-increasing effects can be implemented geometry-independently. In this respect, the consideration of normatively disregarded straightening effects should be included in the design, especially in the case of large expected imperfections of cruciform joints, in order to enable an economic and reliable assessment based on the structural stress concept. Nevertheless, the evaluations confirm that the structural stress concept is not economically feasible if cruciform joints with major imperfections are examined.

Although this thesis reveals that the general applicability of the structural stress concept is to be scrutinised critically in some matters, expedient optimisations for a practical application can still be developed. In this way, it is feasible to considerably minimise uncertainties within the concept. Accordingly, the achieved results should be included in the standardisation in order to ensure a more reliable fatigue verification with structural stresses.

Acknowledgment

At this point I would like to express my gratitude to all those who have supported me in the process of writing my dissertation.

My special thanks go to Prof. Dr.-Ing. Dipl. Wirt.-Ing. (NDS) Martin Mensinger for the opportunity, trust and support during the course of my entire research at the Chair of Metal Structures at the Technical University of Munich.

I would also like to thank Prof. Dr. techn. Andreas Taras and Prof. Dr.-Ing. Markus Feldmann for their kind involvement in the examination committee.

Furthermore, I would like to thank all my colleagues at the Chair of Metal Structures, especially Florian Oberhaidinger, for the positive discussions, both professional and private. Thanks also to all my bachelor and master students who wrote their theses under my supervision.

I sincerely thank my mentor, Dr. Christian Gaigl, for his exceptional guidance.

In addition, I would like to take this opportunity to express my gratitude to Magalie Karr, who supported me greatly with much consideration and words of encouragement.

And finally, the sincerest appreciation goes to my friends and family. They have always encouraged and believed in me and provided me with support not only during my dissertation, but also throughout my entire life. Special thanks therefore go to my parents Tinka and Martin and to my wonderful sister Svenja.

Preface

The research for this thesis was completed during my time at the Chair of Metal Structures of the Technical University of Munich. Parts of the associated research were accompanied by the IGF project 20336N of the “Forschungsvereinigung Stahlanwendung e.V.” (FOSTA), which was funded by the AiF as part of the "Industrielle Gemeinschaftsforschung" (IGF) of the Federal Ministry of Economic Affairs and Climate Action. Some of the results have already been presented or published in the course of the research project. My thanks also go to everyone involved in the realisation of the project.

Content

Abstract.....	i
Acknowledgment.....	iii
Preface.....	iv
Content.....	I
Abbreviations and symbols	IV
1 Introduction	1
1.1 Problem specification and objective	1
1.2 Layout of the thesis	2
2 State of science	4
2.1 Economic significance of the targeted scientific results.....	4
2.2 Standard verification for the assessment of fatigue safety	5
2.2.1 Fatigue resistance	5
2.2.2 Failure probability	8
2.2.3 Effective stress range.....	9
2.2.4 Linear damage accumulation	10
2.2.5 Fatigue verification of metal structures.....	11
2.3 Methods of verification	11
2.3.1 Nominal stress concept.....	12
2.3.2 Modified nominal stress concept.....	13
2.3.3 Structural stress concept.....	14
2.3.4 Effective notch stress concept.....	23
2.4 Normative standards and guidelines for fatigue verification	25
2.4.1 DIN EN 1993-1-9.....	25
2.4.2 Guidelines of the IIW	28
2.4.3 prEN 1993-1-9 and prEN 1993-1-14	32
2.4.4 Guideline of the FKM.....	35
2.4.5 DNVGL.....	36
2.4.6 Differences in the guidelines and normative regulations	38
2.5 Imperfections.....	39
2.5.1 Cause of imperfections.....	39
2.5.2 Possible imperfections	40
2.5.3 Imperfections in normative regulations and guidelines.....	42
2.6 Thickness effect	65
2.6.1 General cause of the thickness effect	65

2.6.2	Approaches for the determination of the thickness effect	66
2.6.3	Regulatory and guideline specifications for the thickness effect	68
3	Principles of the finite element analysis	77
3.1	Selection of element type	77
3.1.1	Shell elements	78
3.1.2	Solid elements	82
3.2	Meshing	84
3.2.1	Meshing according to the stress extrapolation	84
3.2.2	Further local methods	88
3.3	Implementation of finite element analysis	89
3.3.1	Element classification in the applied FE software ANSYS	90
3.3.2	Modelling of imperfections	90
3.3.3	Implementation of the support conditions and load application	91
3.3.4	Specification of the local method	94
3.3.5	Choice of sensible shell models	104
3.3.6	Managing thickness effects	116
3.3.7	Implementation in ANSYS APDL and Python	118
4	Experimental fatigue tests on cruciform joints	121
4.1	Evaluation methodology of the fatigue tests	121
4.1.1	Perfect FE models without unintentional imperfections	122
4.1.2	Imperfect FE models including unintentional imperfections	123
4.1.3	Determination of equivalent imperfections	124
4.2	Cruciform joints examined under fatigue loading	124
4.2.1	Overview	124
4.2.2	Detected imperfections	127
4.3	Test procedure	129
4.3.1	Static preliminary tests	131
4.3.2	Fatigue tests	132
4.4	Validation of the FE models	138
4.4.1	Clamping process	139
4.4.2	Tensile load	141
4.5	Evaluation of the fatigue tests	144
4.5.1	Nominal stress concept	144
4.5.2	Structural stress concept	161
4.5.3	Method with equivalent imperfections	177

4.6	Summary of experimental fatigue tests	183
5	Effects of imperfections on cruciform joints.....	187
5.1	Clamping processes.....	187
5.1.1	Evaluation of impact due to clamping processes	188
5.1.2	Evaluation of stress concentration factors.....	191
5.2	Practical support conditions.....	202
5.2.1	Evaluation of stress concentration factors.....	203
5.2.2	Evaluation of support parameters.....	211
5.3	Summary.....	225
6	Conclusion and perspective.....	228
6.1	Conclusion.....	228
6.2	Perspective.....	234
	Appendix	236
	Appendix A: Execution plans	236
	Appendix B: Case studies on support parameters	242
	List of figures.....	VIII
	List of tables.....	XVII
	Bibliography	XX

Abbreviations and symbols

In the further course of this thesis, only relevant abbreviations and symbols will be mentioned in the content of the text. Information on relevant abbreviations and symbols is provided in the following list. Characteristic units are indicated, while non-dimensional quantities are denoted with [–].

Abbreviations

<i>FE</i>	Finite Element
<i>FEA</i>	Finite Element Analysis
<i>S-N curve</i>	Woehler curve equivalent to fatigue resistance curve
<i>SCF</i>	Stress Concentration Factor
<i>APDL</i>	Ansys Parametric Design Language
<i>WM</i>	Welding Method for shell models
<i>WP</i>	Work Package
<i>SG</i>	Strain Gauge
<i>cf.</i>	confer
<i>resp.</i>	respectively
<i>etc.</i>	et cetera
<i>et al.</i>	et alii, and others

Symbols

<i>FAT</i>	characteristic value of fatigue strength for 2×10^6 stress cycles [<i>MPa</i>]
<i>m</i>	gradient of characteristic fatigue resistance curve [–]
σ	stress [<i>MPa</i>]
$\Delta\sigma$	stress range of fatigue testing [<i>MPa</i>]
$\sigma_{i,Ed}$	spectrum of stress ranges [<i>MPa</i>]
σ_{\perp}	stress component perpendicular to the weld [<i>MPa</i>]
γ_{Ff}	partial factor for applied stress ranges [–]
γ_{Mf}	partial factor for fatigue resistance [–]
<i>R</i>	stress ratio [–]
ε	strain [$\mu m/m$]
<i>N</i>	stress cycles [–]
$N_{i,Ed}$	step frequency [–]

$N_{i,Rd}$	maximum tolerable number of stress cycles [–]
N_{P_s}	stress cycle number with defined survival probability [–]
D	accumulated fatigue damage due to varying stress ranges [–]
D_i	partial collective of fatigue damage [–]
T_σ	application-related scatter band index [–]
P_f	probability of failure [%]
P_s	survival probability [%]
j_σ	safety factor [–]
s_σ	standard deviation to Gaussian normal distribution [–]
$s_{\log N, GG, s}$	standard deviation of the logarithms for stress cycles [–]
u, β	generally defined quantile [–]
$\Delta x_i, \Delta z$	distance to the weld notch in longitudinal resp. thickness direction [mm]
δ	defined distance for structural stress determination [mm]
R, r	notch radius for modification of the notch sharpness of welds [mm]
F	load level [kN]
ΔF	fatigue load level [kN]
f	linear force [kN]
m	linear moment [kNm]
time, t	progression over time [s]
ΔF_{factor}	factor for the consideration of straightening effects [–]
E	young's modulus [GPa]
I	second moment of area [cm ⁴]
W	moment of resistance [cm ³]
f_y	actual or specified yield strength of material [MPa]
f_u	ultimate strength of material [MPa]
ϑ	transverse contraction coefficient [–]
A	cross-sectional area [mm ²]
T, t	plate thickness [mm]
t_s, t_a	connection thickness to account for thickness effects [mm]
t_1	damaging crack depth for the determination of structural stresses [mm]
L_{total}	total length between clamping sections [mm]
L_{clamp}	length of the clamping section [mm]
L_c	length between weld notch and clamping section [mm]

l, L	effective connection length for fatigue classification [mm]
L_t, d	effective connection length to account for thickness effects [mm]
w	width of plates resp. elements [mm]
a, A	weld thickness [mm]
θ	weld angle [°]
e, δ	axial misalignment between welded-on plates of cruciform joints [mm]
e_0, δ_0	permissible axial misalignment [mm]
$e_{equivalent}$	equivalent misalignment for the determination of straightening effects [mm]
α	simplified bending angle for bending of the ground plate [°]
β	angular misalignment of welded-on plates of cruciform joints [°]
θ	misalignment through rotation around the axis in longitudinal direction [°]
Δ	deviation from straightness [mm]
SCF_R	stress concentration factor on the action side [–]
SCF_C	potential stress concentration factor on the resistance side [–]
k_f, K_m, K, K_s	stress concentration factor resp. notch factor [–]
c	coefficient for deviating weld angles [–]
k_m	stress concentration factor to account for imperfections [–]
λ, κ	support parameter for indirect consideration of imperfections [–]
$factor$	factor for modification of indirect consideration of clamping processes [–]
$f(R)$	modification of fatigue strength in relation to effective stress ratio [–]
K_t	stress concentration factor due to thickness effects [–]
$f(t), k_s, K_t$	stress concentration factor to account for thickness effects [–]
n, k, β	exponent for modification to account for thickness effects [–]

Indices

nom	assessment according to nominal stress concept
hs	assessment according to structural stress concept
en	assessment according to effective notch stress concept
m	membrane component
b	bending component
nl	non-linear component
R	applied damage-equivalent range
C	characteristic reference value for fatigue strength for 2×10^6 stress cycles

<i>E</i>	damage-equivalent constant fatigue value
<i>D</i>	characteristic constant amplitude fatigue limit
<i>L</i>	characteristic fatigue resistance limit value
50%, 97.5%	assessment with the respective survival probability P_s
<i>FEA</i>	result determined by FE analysis
<i>test</i>	result from experimental data of fatigue tests
<i>SG</i>	result measured by strain gauges
<i>e_{equivalent}</i>	result determined by equivalent misalignments
<i>k_m</i>	with consideration of normatively considered influences due to imperfections
<i>f(t)</i>	with consideration of thickness effects
<i>max</i>	maximum value
<i>min</i>	minimum value
<i>x, y, z</i>	determination in x_{global} -, y_{global} -, resp. z_{global} -direction
<i>x', y', z'</i>	x_{global} -, y_{global} -, resp. z_{global} in distance δ derived from nodal force
<i>top</i>	on the top side
<i>bottom</i>	on the bottom side
<i>direct</i>	direct consideration of imperfections as identified through the FEA
<i>indirect</i>	indirect consideration of imperfections as identified in literature
<i>perfect</i>	without consideration of influences of unintentional misalignments
<i>imperfect</i>	consideration of influences of detected misalignments
<i>intended</i>	deliberate value
<i>predefined</i>	predefined value
<i>detected</i>	detected value
<i>axial, e</i>	consideration of axial misalignment of welded-on plates
<i>angular, α</i>	consideration of angular misalignment of welded-on plates
<i>eff</i>	effective value
<i>ref</i>	reference value
<i>default</i>	default value
<i>mod</i>	modified value
<i>assess</i>	assessed value
<i>already covered</i>	already covered effects in the fatigue strength resulting from imperfections
<i>IIW</i>	according to guidelines of the IIW [3]
<i>Xing&Dong</i>	according to Xing and Dong [5]

1 Introduction

The objective of this thesis is to further elaborate the structural stress-oriented evaluation approach for steel structures under fatigue loading and to provide adequate guidelines. The scope is focused on cruciform joints. For this purpose, concepts are to be further developed to ensure a simple, economical and safe application of the structural stress concept. This should give users the capability to validate and perform own FE calculations with standard commercial software.

1.1 Problem specification and objective

Fatigue failure refers to the initiation and propagation of cracks as a result of dynamic loadings and the resulting failure of the damaged component. These are locally occurring effects that are primarily dependent on the geometry, the load and the material of the investigated detail. In many areas of engineering, such as crane and bridge construction, these processes are relevant for the design. For safe and economical dimensioning, it is important that the local effects are considered as realistically as possible when assessing fatigue strength. In practice, fatigue verifications are usually performed on the basis of the design rules of the so-called nominal stress concept without explicitly considering local effects. An alternative is offered by concepts for stress calculation based on the finite element analysis (FEA). The effect of local effects is partially or completely included in the calculation model and thus more accurate. The relevant stress at the location of the fatigue failure is usually significantly higher than in the remaining component, which can be attributed to the geometric relations and the notch effect of welds. In terms of cruciform joints, the relevant region of the detail is at the transition of the weld to the base plate. Due to the progress in the computer-aided analysis of structures, stress increases can be realistically determined through the FEA. The structural stress concept uses a theoretical stress at the critical point of the notch, the so-called hot-spot. In civil engineering, the application of the structural stress concept is specified in the current standard DIN EN 1993-1-9 [2] only in terms of structural details defined for the structural stress concept. No further information is provided. In literature, different approaches to the local stress calculation using the structural stress concept are proposed [6–10]. It depends on the field of engineering which approach is preferred. The applicability and comparability of the fatigue strength evaluation is difficult to overview and assess [11]. In addition, most procedures do not have general applicability and are, for the most part, not statistically verified. Therefore, in civil engineering, more profound methods are needed to evaluate local stresses and strains in terms of fatigue strength and durability. As a result, the application of local approaches for fatigue design fails to meet the capabilities of computer-aided structural analysis that are available in the meantime. [6, 12, 13]

The intention of normative regulations and guidelines [3, 9] must be to provide guidance for engineers to apply the structural stress concept in practice. This requires basic principles for modelling and stress calculation as well as for the consideration of

misalignments and thickness effects. The revised draft of prEN 1993-1-9 [4], which is relevant for fatigue, deals with the structural stress concept in more detail. Furthermore, a new part prEN 1993-1-14 [14] is introduced in the Eurocode to support the implementation of finite element analyses. In both drafts, numerous aspects are adopted from the guidelines of the International Institute of Welding (IIW) [3], which provide detailed information on the structural stress concept in order to determine the decisive fatigue life. With regard to the modification of the fatigue strength, due to thickness effects, different approaches are considered which need to be evaluated. Furthermore, the influence of imperfections on the fatigue strength of cruciform joints is dealt with inadequately in the normative regulations and guidelines. Consequently, stress-increasing effects are to be determined and suitable procedures for managing imperfections are to be formulated.

1.2 Layout of the thesis

Within the scope of this thesis, numerical investigations are performed on cruciform joints with explicit consideration of the structural stress concept. The focus is particularly on the effects of manufacturing-related imperfections, which are investigated by means of suitable FE analyses and stress concentration factors. Experimental fatigue tests are intended to provide input for the evaluation of structural stress calculations and to determine further influences on the fatigue strength.

For a systematic thesis structure, the current state of science (cf. Chapter 2) is initially discussed in order to demonstrate the essential coherences. In addition to the economic significance of the targeted results (cf. Chapter 2.1), the basics of conventional standard verifications for the assessment of fatigue safety are presented (cf. Chapter 2.2). Based on the information provided, Chapter 2.3 presents relevant fatigue design concepts for steel structures and the corresponding normative standards and guidelines for fatigue verification are described in Chapter 2.4. Apart from possible approaches for the consideration of imperfections (cf. Chapter 2.5), the normatively required modification of the fatigue strength due to the thickness effects (cf. Chapter 2.6) is additionally assessed.

A substantial part of the thesis represents Chapter 3 on the principles of the finite element analysis. In addition to specifications for the general selection of element types in solid and shell models and the approach to welds regarding shell elements (cf. Chapter 3.1) as well as general mesh requirements (cf. Chapter 3.2), the associated implementation and evaluation of numerical FE models used in this thesis is described in detail in Chapter 3.3. The associated objective is to provide consistent FE models. This allows experimental tests to be recalculated, congruent geometric parameter studies to be performed and solution strategies to be developed for determining the consequences of imperfections and thickness effects. In this respect, the applied element classifications (cf. Chapter 3.3.1), the approach to imperfections (cf. Chapter 3.3.2) as well as to support situations and the load introduction (cf. Chapter 3.3.3), the selection of a suitable evaluation method (cf. Chapter 3.3.4), the choice of a reasonable weld modelling in shell models (cf. Chapter 3.3.5), the approach to thickness effects (cf. Chapter 3.3.6) and the implementation of the calculations in ANSYS APDL and Python (cf. Chapter 3.3.7) are described in more detail.

Chapter 4 focuses on the experimental fatigue tests performed on cruciform joints and the evaluation of the obtained results. In this respect, the selected evaluation methodology is introduced (cf. Chapter 4.1). Besides an overview of the investigated test series with their imperfections (cf. Chapter 4.2), the selected test procedure is presented (cf. Chapter 4.3). To ensure the validity of the numerical FE models, a substantial verification is carried out (cf. Chapter 4.4). The evaluation of the fatigue safety for the conducted tests according to the nominal and structural stress concept is presented in Chapter 4.5. This allows the applicability of the structural stress concept to be verified in relation to cruciform joints under fatigue loading. In addition, influences due to straightening effects on the resulting stress ranges are investigated in more detail.

In Chapter 5, the influence of imperfections on cruciform joints is investigated more specifically. To this end, the influence of imperfections on clamping processes in testing machines is analysed and compared with existing analytical approaches (cf. Chapter 5.1). For this purpose, the experimental data of the fatigue tests from Chapter 4 are utilised. In addition to evaluations relating to clamping processes, further parametric studies on the influence of imperfections on cruciform joints under more practical support conditions are conducted in Chapter 5.2. Therefore, numerical FE calculations of stress concentration factors in case of axial and angular misalignment are evaluated and compared with available analytical solutions (cf. Chapter 5.2.1). Support parameters for further common mounting conditions of cruciform joints are analysed substantially (cf. Chapter 5.2.2). This way, geometric influences and effects of imperfections with regard to testing machines and practical support conditions can be better evaluated in the future.

In conclusion of the thesis, Chapter 6 summarises the obtained results on cruciform joints (cf. Chapter 6.1). In addition, the general applicability of the structural stress concept for metal structures is critically analysed. Finally, a perspective on further research possibilities is given in Chapter 6.2.

2 State of science

In the following chapter, the current state of science is initially discussed in order to identify essential interrelations. In addition to the economic significance of the targeted scientific results (cf. Chapter 2.1) the fundamentals of conventional standard verifications for the assessment of fatigue safety are presented (cf. Chapter 2.2). In this context, a basic understanding of fatigue strengths with the relevant stress ranges (cf. Chapter 2.2.1 and Chapter 2.2.3) and linear damage accumulations (cf. Chapter 2.2.4) is to be created. Relevant fatigue concepts for steel structures are discussed in Chapter 2.3. In addition to the nominal stress concept (cf. Chapter 2.3.1) and the modified nominal stress concept (cf. Chapter 2.3.2), the structural stress concept (cf. Chapter 2.3.3) and effective notch stress concept (cf. Chapter 2.3.4) are described. The associated normative regulations and guidelines for the nominal and structural stress concept are introduced in the following Chapter 2.4. In Chapter 2.5, approaches for the consideration of imperfections are described. In addition to the possible imperfections of cruciform joints (cf. Chapter 2.5.2), both the influences from imperfections already considered in the normative fatigue classes (cf. Chapter 2.5.3.1) and their indirect determination by means of suitable stress concentration factors (cf. Chapter 2.5.3.2) are examined. Finally, the normatively required modification of the fatigue strength due to the thickness effect (cf. Chapter 2.6) is demonstrated.

2.1 Economic significance of the targeted scientific results

Structural stresses are already part of engineering practice in many areas (mechanical engineering, offshore support structures, wind energy). In civil engineering, however, their application has not been sufficiently regulated to date. There is a general deficit of guidance on modelling, stress determination and approaches to manage misalignments and thickness effects.

Due to the currently insufficient regulations regarding the structural stress concept, there are substantial uncertainties in practice. The final report "Verbesserung der Praxistauglichkeit der Baunormen durch pränormative Arbeit" of a research project of the BBSR (Bundesinstitutes für Bau-, Stadt- und Raumforschung) [15] states that the existing formulations of DIN EN 1993 1 9 [2] regarding the structural stress concept are not sufficient for a general safe application. Therefore, the research report proposes that all substantive sections on the structural stress concept are to be deleted. This would lead to the structural stress concept no longer being normatively regulated. Significant effects on practice are to be expected. A fatigue concept would be omitted, that can provide a verification for typical structural steel joints that is more economical than the nominal stress concept. This is especially true for unusual connections where the structural stress concept provides a standard approach. Particularly in bridge and crane structures, constructional details are frequently realised that cannot be verified

adequately with the nominal stress concept. In these cases, the structural stress concept provides a necessary and effective design option.

For the design of structural steel joints subject to fatigue loading, it is therefore necessary to provide a concept that exceeds the nominal stress concept and contains precise and practice-oriented regulations for its application. In this respect, the focus must be on the revision of the structural stress concept in Annex B of DIN EN 1993-1-9 [2]. With additional guidelines and statements on the implementation of FE modelling, a systematic application has to be assured. Annex B can be further extended with this additional information. This would meet the request of the BBSR [15] for a more detailed definition of the FE methodology in part 1-9 of the standard. In addition, it might be beneficial to include local concepts into DIN EN 1993-1-9 [2] to provide a safe stress determination. Another publication on the structural stress concept [16], which pleads for the preservation of the verification method by means of structural stresses in DIN EN 1993-1-9 [2], also requires further guidance.

In the new draft prEN 1993-1-9 [4], additional information on the structural stress concept is provided in addition to partially corrected fatigue strengths according to the nominal and structural stress concept. Part B of the draft deals in more detail with the determination of structural stresses. Furthermore, more detailed information on the design of the FEA is given in the draft prEN 1993-1-14 [14]. Compared to the guidelines of the IIW [3], a different approach is considered to determine the influence of thickness effects. The drafts also lack detailed information on how to manage influences of imperfections. The systematic revision of the structural stress concept in DIN EN 1993-1-9 [2] is intended to provide an economical fatigue analysis for steel structures that can offer advantages to engineering offices and manufacturers as well as approval authorities.

2.2 Standard verification for the assessment of fatigue safety

Fatigue describes the loss of material resistance due to dynamic loading. Along with corrosion and abrasion, material fatigue is one of the primary sources of damages to load-bearing elements in metal structures. In general, the ratio of applied stress to fatigue strength is relevant for the fatigue verification. Therefore, the fatigue stress must be compared to a fatigue strength, which has to be obtained from fatigue strength curves, so-called S-N curves. The S-N curve is selected according to design-related fatigue classes that attribute a strength to specified design details under constant fatigue loading. The main factors influencing the fatigue procedure are the stress range and the number of resulting cycles. In addition to the magnitude of the load, the stress range at the relevant section is also significantly influenced by local effects such as stress increases due to changes in the cross-section, imperfections or the notch effect of welds. Furthermore, welding defects such as inclusions or lack of fusion often result in fatigue cracks. [17, 6, 18]

2.2.1 Fatigue resistance

The fatigue evaluation of welded components and structures is generally based on S-N curves. These fatigue strength curves describe the quantitative relationships between a constant stress range and the number of stress cycles leading to fatigue

failure. The curves are listed in normative regulations and guidelines and were mostly obtained from representative fatigue tests. The verification for the assessment of fatigue safety is satisfied if the applied stress does not exceed the corresponding fatigue strength. Since fatigue failure is caused by a dynamic load and consequently by the sum of the resulting stress ranges, a specific fatigue safety evaluation must be carried out for each construction detail. The fatigue strength $\Delta\sigma_C$ depends on the type of detail being examined and can differ significantly. The relevant fatigue strengths are given by defined fatigue categories, which are provided with corresponding S-N curves. These S-N curves are based on stress ranges with constant amplitudes and represent a quantitative relationship between the applied damage-equivalent stress range $\Delta\sigma_R$ and the number of cycles until failure N_R in a double logarithmic scale. Instead of graphical S-N curves, the maximum number of stress cycles N_R can also be determined on the basis of the mathematical doubled logarithmic relationship between the constant stress range $\Delta\sigma_R$ and the characteristic reference value of the fatigue strength $\Delta\sigma_C$. [6, 18–20]

$$N_R = \frac{\Delta\sigma_C^m \cdot 2 \cdot 10^6}{\Delta\sigma_R^m} \quad (2-1)$$

Therefore, the stress range $\Delta\sigma_R$ of a structural detail with a fatigue strength of $\Delta\sigma_C$ leads to fatigue failure at N_R stress cycles. The reference value of the fatigue strength can also be referred to as the fatigue class or fatigue resistance $\Delta\sigma_C$ and refers to the characteristic fatigue stress at 2×10^6 stress cycles. The gradient m of the S-N curve has an additional influence on the sustainable stress cycles and can be found in Figure 2-1. [2]

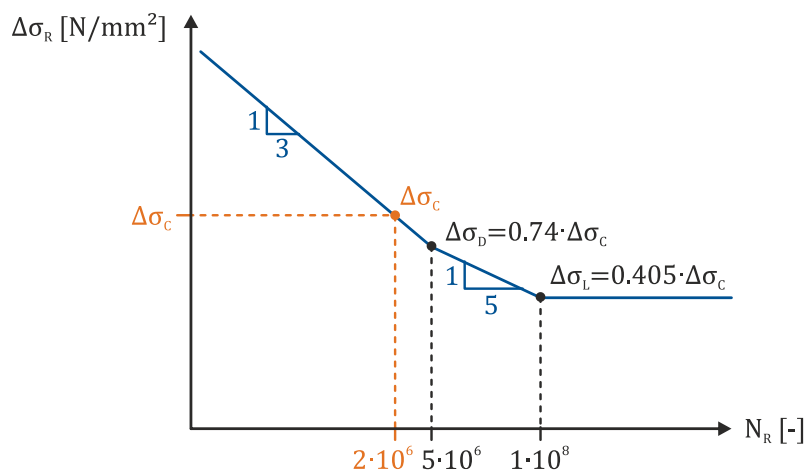


Figure 2-1: Standardised fatigue resistance curve [21]

S-N curves maintain their validity only for a single-step loading and are used to convert a stress collective into a damage-equivalent constant fatigue stress $\Delta\sigma_E$ (cf. Chapter 2.2.4) [2]. The standardised fatigue strength curve shown as an example in Figure 2-1 correlates the permissible stress cycles $\Delta\sigma_R$ with the expected fatigue life N_R and refers to a fatigue class.

S-N curves are represented by a double logarithmic scale and are divided into different sections. If the examined structure is subjected solely to constant stress ranges that do not exceed the stress range associated with this limit value, there will be negligible fatigue damage. Depending on the design specification, the characteristic, position and

number of available fatigue classes differ. The characteristic reference value of the fatigue strength $\Delta\sigma_C$ corresponds in all cases to the stress range of the fatigue strength curve at $N_R = 2 \times 10^6$ stress cycles.

According to DIN EN 1993-1-9 [2], S-N curves are classified by three sections. For this reason, an additional characteristic constant amplitude fatigue strength $\Delta\sigma_D$ at $N_D = 5 \times 10^6$ is defined, which results in a change of the gradient of the fatigue curve from $m = 3$ to $m = 5$, as fatigue failure becomes less likely. The section up to the transition to the characteristic constant amplitude fatigue strength $\Delta\sigma_D$ is called short-term fatigue range. The subsequent section of the S-N curve is interpreted as the characteristic constant amplitude fatigue range. At the threshold value of the variable amplitude fatigue limit $\Delta\sigma_L$ at $N_L = 1 \times 10^8$ stress cycles, fatigue failure is no longer expected (cf. Figure 2-1). It may be noted that the definitions of the sections can be modified or more specifically defined in other standards and guidelines. For example, the endurance limit $\Delta\sigma_D$ according to the IIW [3] is defined at $N_R = 1 \times 10^7$ (cf. Figure 2-2) and no threshold value $\Delta\sigma_L$ is specified.

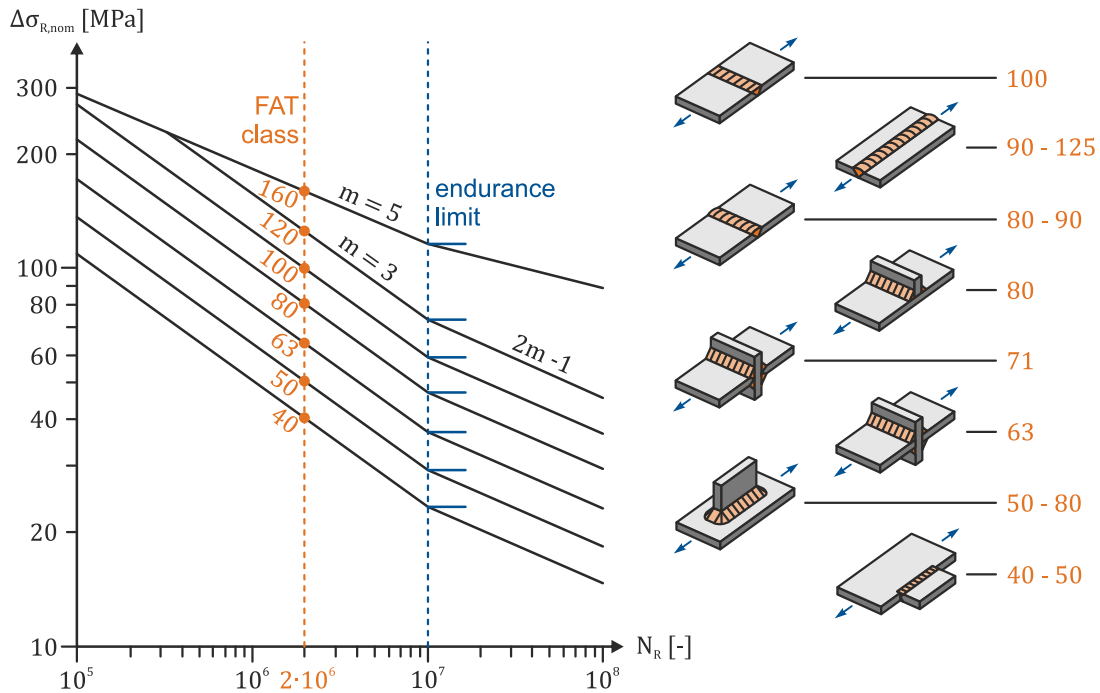


Figure 2-2: Design S-N curves (left) and different fatigue resistances (right) for the nominal stress concept according to guidelines of the IIW [3] summarised by [6]

Standard deviations, component geometries and residual stresses are considered in the S-N curves and all specifications according to EN 1990 [22] regarding the minimum number of specimens required for a statistically reliable design are satisfied. In addition, local stress concentrations due to the weld geometry as well as resulting from weld imperfections, which are in accordance with manufacturing standards, are included in the S-N curves. S-N curves are essentially independent of the static tensile strength of the material and are limited to $\Delta\sigma_{nom} \leq 1.5 \cdot f_y$, $\Delta\sigma_{hs} \leq 2 \cdot f_y$ and $\sigma_{nom,max} \leq f_y$. In addition, it is important to ensure that no corrosive environmental influences, such as humid-corrosive, saline or strong chemical conditions as well as elevated temperatures (greater than 150 °C) are to be encountered. [21, 23, 6, 20]

2.2.2 Failure probability

S-N curves result from scatter bands of tolerable stress ranges. Within the scatter band, a Gaussian normal distribution with corresponding standard deviation s_σ is assumed. The standard deviation refers to the stress range $\Delta\sigma_R$ and is determined according to Formula (2-2). In addition, an application-related scatter band index T_σ is introduced in accordance with Formula (2-3).

$$s_\sigma = \frac{1}{2.56} \cdot \log \frac{1}{T_\sigma} \quad (2-2)$$

$$T_\sigma = \frac{\Delta\sigma_{C,10\%}}{\Delta\sigma_{C,90\%}} \quad (2-3)$$

The permissible stress ranges $\Delta\sigma_{C,10\%}$ and $\Delta\sigma_{C,90\%}$ of the scatter band index T_σ refer to the failure probabilities $P_f = 10\%$ and $P_f = 90\%$. In principle, when verifying the fatigue strength, it must be ensured that the actual stress range $\Delta\sigma_R$ does not exceed the permissible stress range $\Delta\sigma_C$. In this respect, $\Delta\sigma_C$ is characterised by a certain acceptable failure probability P_f . [6]

$$\Delta\sigma_R \leq \Delta\sigma_C \quad (2-4)$$

The actual stress ranges $\Delta\sigma_R$ are derived from the permissible stress ranges $\Delta\sigma_C$ by introducing a safety factor j_σ , which depends on the scatter band index T_σ and the failure probability P_f :

$$\Delta\sigma_R = \Delta\sigma_C \cdot j_\sigma \quad (2-5)$$

Figure 2-3 gives a graphical overview of the permissible stress ranges according to DIN EN 1993-1-9 [2], guidelines of the IIW [3] and prEN 1993-1-9 [4] for welded steel joints. The $\Delta\sigma_C/\Delta\sigma_{R,50\%}$ curve illustrated is based on a scatter band index $T_\sigma = 1:1.5$, typical for welded steel joints, as a function of the failure probability P_f . This results in permissible stress ranges with failure probabilities of $P_f = 2.3\%$ resp. $P_f = 2.5\%$. The corresponding mean value can generally be assigned a two-sided confidence level of 75 – 95 %. With regard to S-N curves, probabilities of failure P_f are replaced by survival probabilities $P_s = (100 - P_f)\%$. The accepted survival probability depends strongly on the consequences of failure. [6]

The determination of the fatigue strengths or fatigue classes is based on a merely statistical evaluation of fatigue data published worldwide, which was analysed using the assessment procedure specified in Annex D of EN 1990 [22]. The foundation for the fatigue curves from DIN EN 1993-1-9 [2] is the fatigue behaviour statistically evaluated as 95 % quantile for survival. This is considered for the logarithm of the number of stress cycles N_R with a two-sided confidence probability of 75 % for 2×10^6 stress cycles. Thus, the scatter of the test results according to DIN EN 1993-1-9 [2] is accounted for with a survival probability of approximately $P_s \cong 97.5\%$ of the characteristic value of the fatigue strength [17, 2, 24].

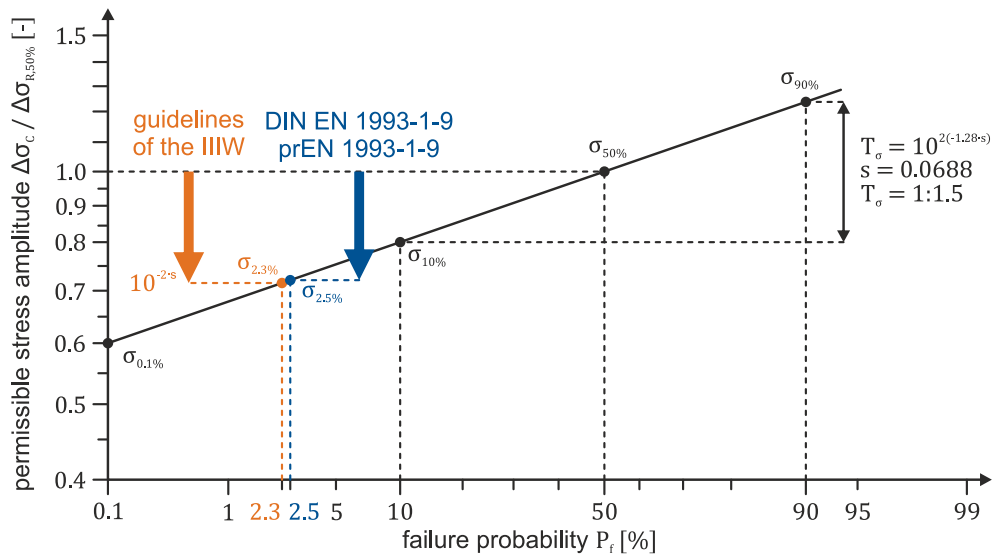


Figure 2-3: Permitted stress ranges derived from actual stress ranges according to a variety of design regulations [25, 26]

According to the guidelines of the IIW [3], the survival probability of the 95 % quantile for survival with a 75 % confidence probability results in $P_s \cong 97.7 \%$ (cf. Figure 2-4).

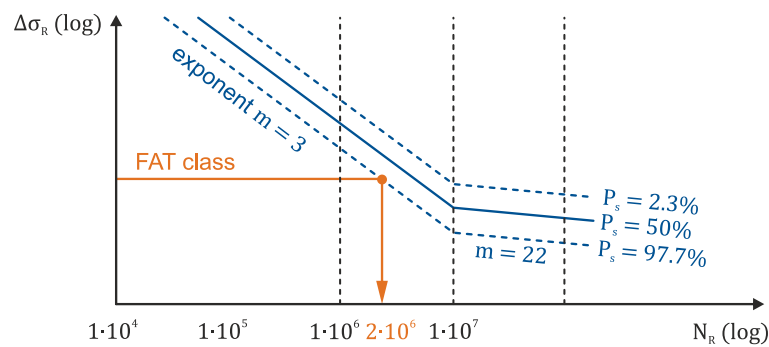


Figure 2-4: Scatter range in S-N curves according to IIW [3]

In order to be able to generate adequate S-N curves from fatigue tests, DIN 50100 [27] can be applied. This helps in conducting and evaluating fatigue tests. If the cyclic fatigue loading of the test refers to different load levels of the fatigue stress range, the so-called string-of-pearls method can be used for the evaluation. By conducting a least squares regression in the direction of the stress cycles, the population can be estimated. In this way, the mean value, the standard deviation and the gradient of the S-N curve can be determined. In order for the S-N curves to be compatible with the normative regulations and guidelines, values with a 75 % confidence probability are solely used to generate a regression line with a statistical survival quantile of 95 %. This approach consequently represents the normative safety level. [28]

2.2.3 Effective stress range

The effective design value of the stress range $\Delta\sigma_R$ required for the fatigue verification represents the relevant action characteristic value for fatigue tests. It is calculated by subtracting the minimum stress σ_{min} from the maximum stress σ_{max} according to Figure 2-5. [29]

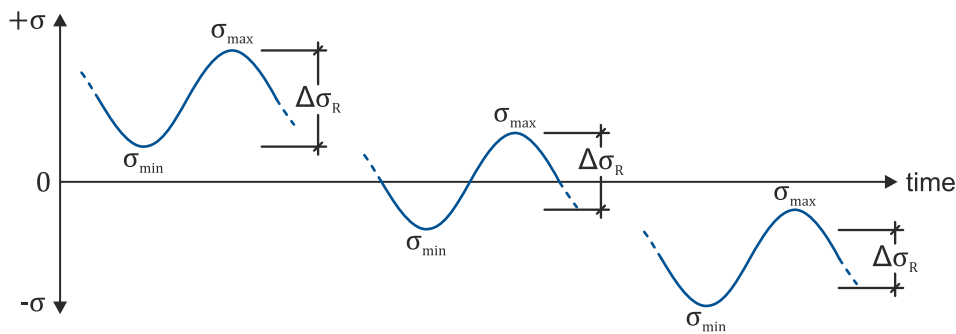


Figure 2-5: Effective design value of the stress range [4]

The effective design value is also dependent on the stress ratio R . This ratio is used for additional characterisation of stress cycles and is calculated by the ratio of minimum stress σ_{min} to maximum stress σ_{max} . While critical tensile mean stresses lead to a significant reduction in fatigue strength, it is important to note that the less critical compressive component of a stress range, if present, is only considered with 60 % of its magnitude (cf. Figure 2-5). For welded components, the mean stress σ_m and the stress ratio R generally have no significant influence on the fatigue resistance. However, for non-welded and stress-relieved components, a positive effect on the fatigue behaviour can be determined. [17, 30, 31]

2.2.4 Linear damage accumulation

In order to provide reliable information on the durability of dynamically loaded structures, fatigue tests are required. In order to conduct these tests in a realistic setting, random load tests or real time experiments with different load collectives are generally required, since structures are subject to cyclic loading with variable amplitudes during normal operation. When using S-N curves, cyclic loads with constant amplitude and therefore rectangular load collectives are assumed. In order to ensure a universally valid transferability of the results obtained, a computational assessment of the fatigue life is required, which predicts an arbitrary sequence of stresses on the basis of S-N curves up to the crack. Thus, a hypothesis is necessary to capture the damage process. Due to the difficulty of detecting damaging material mechanisms, these lifetime predictions assume a linear accumulation of damage.

The linear damage accumulation according to Palmgren [32] and Miner [33] is intended for the evaluation of the influence of load collectives on the fatigue life of a structure. It is based on the assumption of partial damage increasing linearly with the number of load cycles. Thus, they are independent of the sequence and can be accumulated. For this purpose, a spectrum of stress ranges $\Delta\sigma_{i,Ed}$ is divided into individual rectangular collectives with constant amplitudes and ordered in descending order. Peak values of the stress ranges may be neglected if they account for less than 1 % of the total damage. The approximation of the linear accumulation is to calculate a partial damage D_i for each subcollective by dividing the step frequency $N_{i,Ed}$ by the maximum tolerable number of cycles $N_{i,Rd}$ with respect to the design S-N curve at $\Delta\sigma_{i,Ed}$ (cf. Figure 2-6). [34]

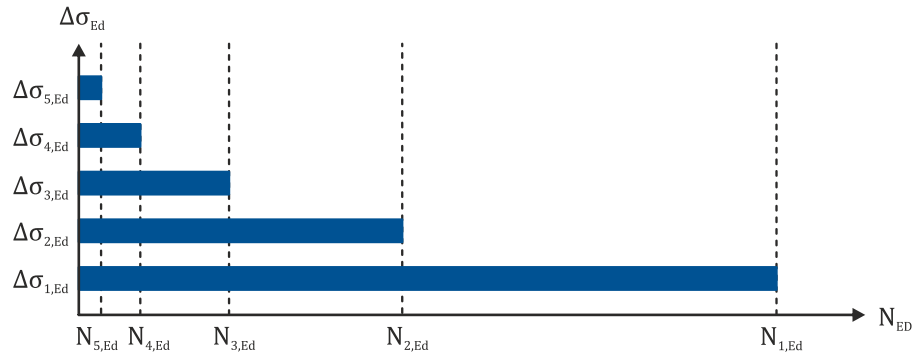


Figure 2-6: Exemplary spectrum of stress ranges [21]

Subsequently, the total damage D of the structure is calculated by the summation of the partial damages D_i . This is characterised as a constant stress range, which would lead to the identical fatigue life as the spectrum of non-constant stress ranges. From $D > 1.0$, the theoretical fatigue life is utilised and component failure is to be expected. [2, 35, 4]

$$D = \sum D_i = \sum \frac{N_{i,Ed}}{N_{i,Rd}} \leq 1.0 \quad (2-6)$$

S-N curves are mainly based on the results of cyclic fatigue tests under constant amplitudes. The experimental fatigue tests carried out are based on constant dynamic load amplitudes as well. For this reason, the linear damage accumulation is only of minor importance. [31]

2.2.5 Fatigue verification of metal structures

The fatigue verification is verified if the damage equivalent load range $\Delta\sigma_E$ is smaller than the tolerable stress of the structural detail $\Delta\sigma_C$ at 2×10^6 load cycles. Safety factors are considered both on the action side and on the resistance side. The partial safety factor for damage equivalent stress ranges γ_{Ff} is calculated according to the nationally specified standards for stresses. In Germany, the normative standard DIN EN 1090 [22] is applied in this context. The recommendation for γ_{Mf} -factors for the definition of damage consequence classes depend on the applied normative regulation or guideline for fatigue verification and may differ (cf. Chapter 2.4). The fatigue verification to be performed results according to DIN EN 1993-1-9 [2] in:

$$\gamma_{Ff} \cdot \Delta\sigma_R \leq \frac{\Delta\sigma_C}{\gamma_{Mf}} \quad (2-7)$$

The fatigue verification based on damage accumulation according to Chapter 2.2.4 then results with a double-symmetric gradient of $m = 3$ in the following equation:

$$\gamma_{Ff} \cdot \Delta\sigma_R \leq \sqrt[m]{D} \cdot \frac{\Delta\sigma_C}{\gamma_{Mf}} \quad (2-8)$$

2.3 Methods of verification

Fatigue verification in metal structures is usually carried out as a stress verification in the component and in the weld. Generally, there are different approaches to stress determination. For the evaluation of fatigue safety, different computational concepts are

available nowadays. In the following, general approaches for the stress determination and verification of fatigue-endangered components according to the nominal stress concept, the modified nominal stress concept, the structural stress concept and the effective notch stress concept are presented. The definition of the fatigue-relevant stresses is graphically illustrated in Figure 2-7. An overview of the effective stresses and verification methods is given in the following Table 2-1. [30]

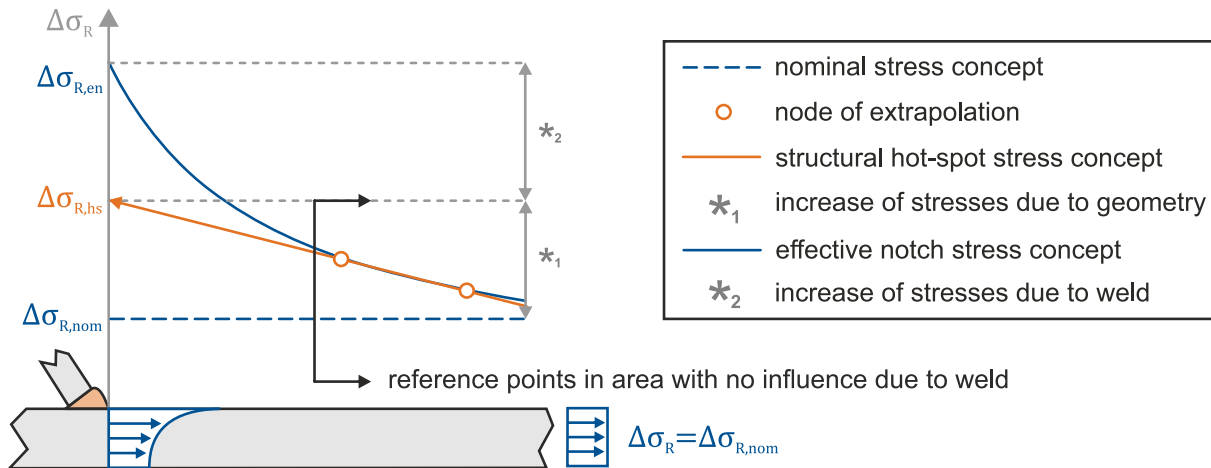


Figure 2-7: Fatigue-relevant stresses at the notch [36]

Table 2-1: Fatigue verifications in metal structures according to [3]

Type	Stress concentration	Stress determination	Assessment procedure
A	None	Gross average stress from sectional forces, calculated using general theories, e.g. beam theory	Not applicable for fatigue analysis of joints, only for component testing
B	Macro-geometrical effects due to the design of the component, but excluding stress concentrations due to the welded joint itself	Range of nominal stress $\Delta\sigma_{R,nom}$ (also modified or local nominal stress)	Nominal stress approach
C	B + structural discontinuities due to the structural detail of the welded joint, but excluding the notch effect of the weld toe transition	Range of structural hot-spot stress $\Delta\sigma_{R,hs}$	Structural hot-spot stress approach
D	B + C + notch stress concentration due to the weld bead notches (a) actual notch stress (b) effective notch stress	Range of elastic notch stress $\Delta\sigma_{R,en}$ (total stress)	(a) Fracture mechanics (b) Effective notch stress

2.3.1 Nominal stress concept

The standard procedure of DIN EN 1993-1-9 [2] for the evaluation of fatigue strength is the nominal stress concept. The concept is included in most normative regulations and guidelines and is the commonly used fatigue verification method for metal structures under fatigue loading. Structural details are referenced to S-N curves with the help of fatigue class catalogues and assigned a characteristic fatigue strength. The verification is conducted with damage equivalent stress ranges $\Delta\sigma_{E,2}$ or $\Delta\tau_{E,2}$ on the action side, which are compared with reference values of the fatigue strength $\Delta\sigma_C$ or $\Delta\tau_C$ at 2×10^6 load cycles on the resistance side.

$$\frac{\gamma_{Ff} \cdot \Delta \sigma_{E,2}}{\Delta \sigma_C / \gamma_{Mf}} \leq 1.0 \quad \text{resp.} \quad \frac{\gamma_{Ff} \cdot \Delta \tau_{E,2}}{\Delta \tau_C / \gamma_{Mf}} \leq 1.0 \quad (2-9)$$

The relevant stress is calculated according to the elastic stress theory without considering the local notch effect. The verification is based on the net cross-sectional area of the location where a potential crack might occur. In the case of significant changes in the cross-section of the structure, there are regions with stress concentrations which, in the case of purely static assessment, are reduced by plastic redistribution. On the other hand, local stress peaks must be considered under dynamic loading.

According to the nominal stress concept, this is not done by mathematical means, but by safety considerations on the resistance side of the structural detail to be evaluated. Thus, local stress concentrations are accounted for in the corresponding fatigue strength curves. In addition, imperfections from manufacturing tolerances according to DIN EN 1090-2 [37] or off-centre force introduction as well as structural imperfections from residual stresses due to welding processes are already included in the fatigue classes. In certain cases, the nominal stress concept is not applicable because the examined detail cannot be accurately assigned to any of the tabulated fatigue classes. In addition, geometric non-linearities in complex details may lead to large local stress changes that are not covered by the fatigue resistance. If this is insufficiently addressed in the stress calculation, it may lead to an invalid assessment of the fatigue strength of the component. In such cases, the modified nominal stress concept, the structural stress concept or the effective notch stress concept can be applied. The mentioned concepts are based on design S-N curves, but require a detailed, local stress determination.

2.3.2 Modified nominal stress concept

The modified nominal stress concept is particularly suited for abrupt cross-sectional changes that do not result from the structural detail itself. For example, openings in profiles or bent beam flanges are among such cross-sectional changes. These are not included in the structural details of the nominal stress concept. For this reason, the normative fatigue strengths must be additionally modified with a stress concentration factor k_f when applying the modified nominal stress concept.

$$k_f \cdot \frac{\gamma_{Ff} \cdot \Delta \sigma_{E,2}}{\Delta \sigma_C / \gamma_{Mf}} \leq 1.0 \quad \text{resp.} \quad k_f \cdot \frac{\gamma_{Ff} \cdot \Delta \tau_{E,2}}{\Delta \tau_C / \gamma_{Mf}} \leq 1.0 \quad (2-10)$$

The stress concentration factor k_f can be determined according to specifications given in literature or by means of suitable FE calculations. The non-linear stress distribution of the structure is determined using an ideal folded structure calculation, without the explicit consideration of the weld in the FE model. The resulting stress is compared to the fatigue class from the nominal stress catalogue. In the generally applicable normative regulations and guidelines, the procedure is not sufficiently clearly regulated. There is a lack of meshing specifications and information on the method of determining stresses. This leads to uncertainties and incorrect application. [17, 38]

2.3.3 Structural stress concept

For increasingly complex welded joints, the nominal stress and modified nominal stress cannot always be determined precisely. Additionally, complicated details often fail to be assigned to a classified fatigue class. Therefore, an alternative solution is provided by the structural stress concept, which considers stress increases due to the component structure at the weld transition, but excludes stress effects due to the weld geometry itself. The required structural stresses are calculated with technical formulae. The stresses can be measured during component tests with strain gauges (*SG*) or can be determined with the help of finite element analysis. The main areas of application of the structural stress concept are hollow sections in offshore engineering, structural engineering and bridge construction as well as dynamically loaded welded joints in crane construction made of high-strength and ultra-high-strength steel. [17, 38–40]

When applying the structural stress concept, the non-linear stress distribution is considered by performing a finite element calculation. The actual structural detail (e.g. stiffness or similar) must be included in the FE analysis. The non-linearities that can be caused by the weld are covered by the associated fatigue class of the structural detail and therefore do not require explicit consideration in the FE model. As a result, the structural stresses include a membrane and bending stress component excluding the non-linear stress peak caused by the weld geometry itself. Structural or geometric discontinuities may result in concentrated membrane stresses and can generate additional secondary bending stresses. [41]

In most cases, the fatigue resistance specified in the structural stress concept is only applicable for crack initiation at the weld transition and does not apply for crack initiation at the weld root followed by crack growth through the weld. This failure mechanism must be prevented by the design of the structure. Furthermore, stress increases due to imperfections (e.g. geometric misalignments, permissible tolerances, etc.) are not covered by the fatigue class, or may only be covered to a certain extent. For this reason, these imperfections must be considered in the stress determination in the FE model or must be computed by means of suitable stress concentration factors (cf. Chapter 2.5). This makes both modelling and calculation more difficult and sensitive to errors when compared to the nominal stress concept. With the exception of full penetration butt welds, there is no specification for the structural stress concept to distinguish between different weld qualities in this respect. Furthermore, FE calculations with plane folded structural models are unable to take potential thickness effects into account. Nevertheless, specifications on the plate thickness dependence, provided for example in the fatigue classes of the nominal stress concept, are only partially considered in the normative regulations and guidelines regarding the structural stress concept. In addition, the same uncertainties arise in the process of generating the FE mesh as in the modified nominal stress concept. [42]

The currently valid version of DIN EN 1993-1-9 [2] does not provide any information on the determination of structural stresses. Neither does the draft version prEN 1993-1-9 [4]. However, reference is made to the part prEN 1993-1-14 [14], which is to address information on finite element calculations in the future. At the time of this thesis, these standards are available only as draft versions. The recommendations of the IIW [3]

refer to the so-called stress extrapolation (cf. Chapter 2.3.3.1) and provide a detailed specification in the Designer's Guide [9].

In literature various methods for the determination of structural stresses can be found. The thesis is primarily focused on the linear surface extrapolation, which is described in detail in the following Chapter 2.3.3.1. Further methods such as the one-point stress determination (cf. Chapter 2.3.3.2), the internal linearisation through the plate thickness (cf. Chapter 2.3.3.3), the one-millimetre method (cf. Chapter 2.3.3.4), the δ -method (cf. Chapter 2.3.3.5) and the CAB method (cf. Chapter 2.3.3.6) are analysed in the subsequent sections as well. Figure 2-8 shows three of the existing methods for a structural stress determination schematically.

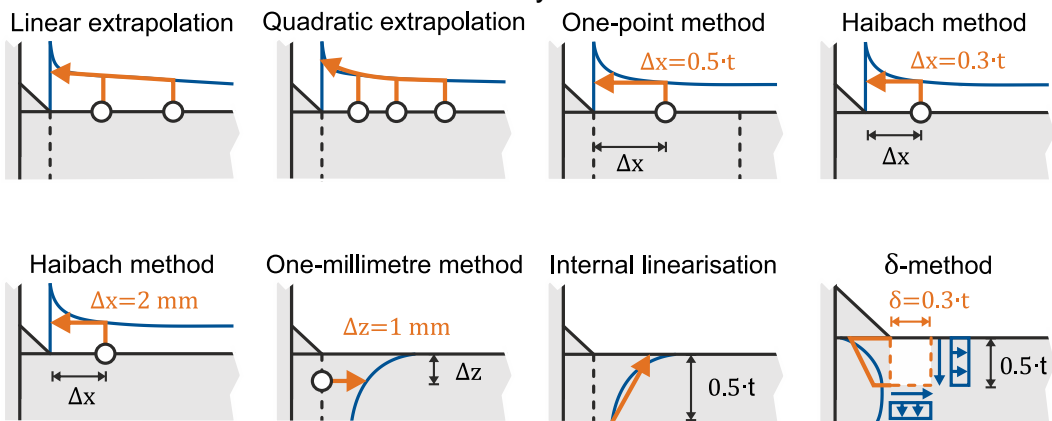


Figure 2-8: Surface methods (top row and bottom left), methods through plate thickness (bottom centre), δ -method (bottom right)

The possible procedures for structural stress determinations are explained in more detail in the following chapters and are not regulated by standards in the civil engineering industry so far.

2.3.3.1 Stress extrapolation

The conventional method for determining structural stresses is the stress extrapolation, which belongs to the surface methods. With the help of the extrapolation of surface stresses, the decisive structural stress is determined and compared to specified fatigue classes. To ensure that stress values at the critical point (hot-spot) are not influenced by the high numerical stresses at the stress peak, the stress is evaluated at reference points. The structural stress is then extrapolated (cf. Figure 2-9). The hot-spot represents the critical area at the weld transition where a fatigue crack is to be expected. Linear and quadratic extrapolation are both possible and will be explained in more detail below. [3, 9, 43]

To calculate the structural stress by means of a linear stress extrapolation, the surface stress is determined at two reference points at distances Δx_1 and Δx_2 (cf. left side of Figure 2-9) that are extrapolated to the weld transition using a linear extrapolation function. For most structural details and loading situations, a linear extrapolation is generally sufficient.

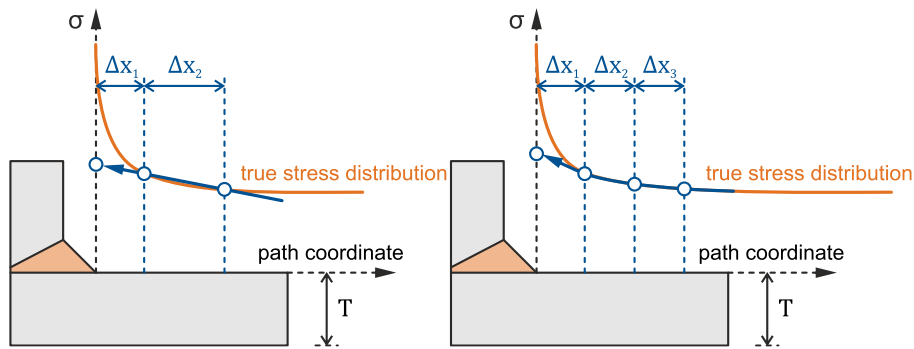


Figure 2-9: Linear stress extrapolation (left) and quadratic stress extrapolation (right) [44]

A quadratic extrapolation with a stress determination at three reference points at distances Δx_1 , Δx_2 and Δx_3 (cf. right side of Figure 2-9) is only recommended for thick plates or for severely curved stress distributions resulting mostly from significant bending loads. Therefore, the quadratic extrapolation is proposed, for example, in situations with an abrupt structural change or with large local loads. The distance Δx_1 of the reference point closest to the weld must be positioned in a way that any non-linear influence of the weld notch is decayed. In addition, the extrapolation needs to distinguish between two different types of hot-spots. A distinction is made based on the plate position and orientation in relation to the weld transition, as shown in Figure 2-10. [3, 14, 31]

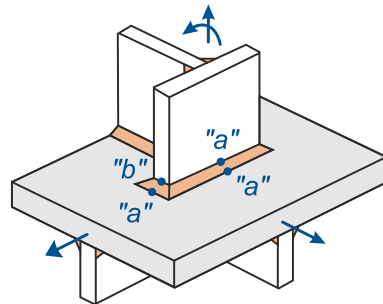


Figure 2-10: Hot-spot types *a* and *b* [14]

The classification is made by hot-spot type *a* and hot-spot type *b*. Expected fatigue cracks at weld transitions located on a plate surface are defined as hot-spot type *a*. The stress distribution through the thickness is dependent on the plate thickness t , thus the positions of the corresponding extrapolation points are defined as a direct function of the plate thickness. As cracks progress, significant changes in normal stresses throughout the thickness of the structural detail are to be expected. [28]

Verifications at weld notches located at plate edges are defined as hot-spot type *b*. Since the corresponding stress distribution is unaffected by the plate thickness t , the extrapolation points are independent as well and are always defined at an absolute distance from the weld transition. Welds defined as hot-spot type *b* are classified as load carrying if the length of the plate is $L > 100 \text{ mm}$. However, in complex details, the direction of the normal stresses may change between the extrapolation points, so that the hot-spot type cannot be defined accurately. [9, 28]

By means of this classification, a hot-spot type can be determined depending on the type of structural detail being investigated. The selected extrapolation method and the choice of meshing then result in a number of different extrapolation formulae according

to the normative regulations and guidelines. These are further described in Chapter 2.4.

2.3.3.2 One-point stress determination

While a disadvantage of the stress extrapolation is that the stress cannot be derived directly from the FE model, which requires additional effort in the evaluation of the FE results, the one-point stress determination is presented below as a simplified concept and further surface method. Suggestions on how to determine the structural stresses were made by Maddox, Lotsberg and Sigurdsson. This approach can also be found in the field of maritime engineering [45].

With this method, the structural stress is derived directly in the FE model at a specified distance from the hot-spot. According to [46, 47], the surface stress is determined at a distance of 0.5 times the plate thickness t and thus outside the influence range of the non-linearities of the notch. For this purpose, appropriate FE models are meshed with coarse shell elements using element sizes of $t \times t$ and a quadratic initial function. This allows the stress to be evaluated directly at a distance of $0.5 \cdot t$ in front of the intersection of the shell middle planes. [6, 3]

Due to the increasing gradient of the surface stress distribution perpendicular to the hot-spot, the stress at a distance of $0.5 \cdot t$ is lower than at the weld transition. To compensate for the underestimated structural stress, the fatigue strength must be reduced by one fatigue class. This corresponds to an applied structural stress increase of approximately 1.12, which is shown on the left side of Figure 2-11. [9, 41]

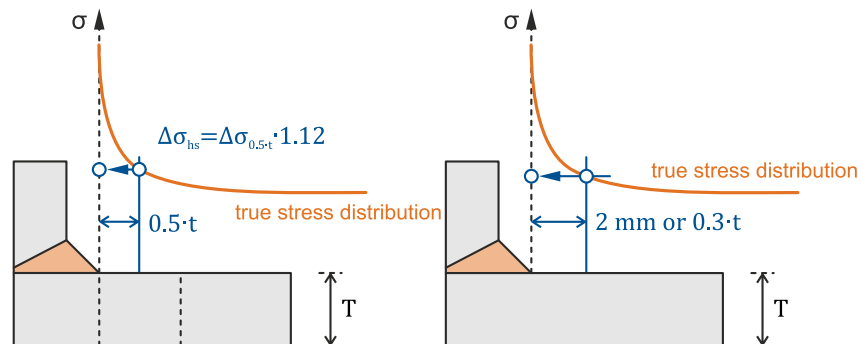


Figure 2-11: One-point stress determination [41] (left) and method of Haibach [10, 44] (right)

Alternatively, Haibach [10] proposes to derive the structural stress at an absolute distance from the weld transition directly from the FE model. This approach dates back to the 1960s and is based on the application of strain gauges. At that time, the fixed defined distance resulted from the dimension of the measuring devices. For thick-walled structures this concept is well applicable, as the plate thickness influence is supposed to be directly included in the structural stress and does not have to be considered by an additional factor. Extensive measurements in literature have defined a distance of 2 mm from the weld transition at which the local notch effect has decayed. This can be seen on the right side of Figure 2-11. In addition, this distance is specified as plate thickness dependent with $0.3 \cdot t$ in [48]. Subsequently, structural stresses are to be compared with Haibach's strain-survival curves developed as a result of measurements of actual fatigue test. [3, 49]

2.3.3.3 Linearisation of stresses in the through-thickness direction

As an alternative to determining the structural stress at the plate surface, the structural stress can be evaluated by linearising the stresses through the plate thickness. This method thus differs from the surface methods. According to the guidelines of the IIW [3], it is recommended that the structural stresses are to be calculated by this approach in the case of narrowly positioned welds. In contrast to the one-point stress determination, the internal linearisation of the stresses requires a greater additional effort for the evaluation of the FE results. Radaj et al. [6, 8] and Dong et al. [50, 51], among others, have published different strategies for this approach. In general, these solutions can only be applied at critical locations of hot-spot type *a* (cf. Chapter 2.3.3.1). The different approaches of linearisation through the plate thickness are presented in the following. [52]

Regardless of the applied method, the critical stress at the hot-spot can be divided into three stress components. These include membrane and bending stress components σ_m and σ_b as well as a non-linear component σ_{nl} . To calculate the structural stress σ_{hs} according to Radaj et al. [6, 8], in contrast to the effective notch stress concept, the component of the non-linear stress peaks σ_{nl} must be neglected (cf. Figure 2-12).

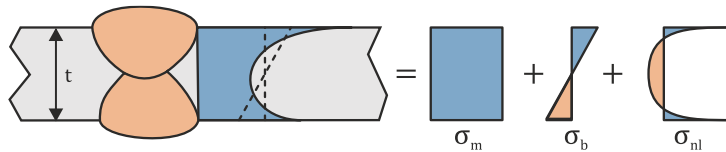


Figure 2-12: Distinction between structural and notch stresses [9, 49]

The approach is based on a linearisation of the stress distribution through the thickness of the plate at the point of expected crack initiation. In this process, the stress linearisation is performed by using the equilibrium conditions so that the integration of the non-linear stress components σ_{nl} are compensated by the membrane (σ_m) and bending stresses (σ_b) (cf. Figure 2-13). [41]

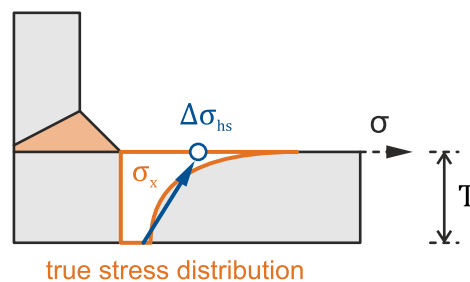


Figure 2-13: Structural stress determination by stress linearisation over the thickness at the notch [41]

The structural stress σ_{hs} is derived from the sum of the membrane stress σ_m and the shell bending stress σ_b and can be approximated via the internal linearisation of the stress distribution at the relevant point of the notch through the thickness. [41, 9, 53]

$$\sigma_{hs} = \frac{1}{t} \cdot \int_0^t \sigma_x(y) dy + \frac{6}{t^2} \cdot \int_0^t \sigma_x(y) \cdot \left(\frac{t}{2} - y\right) dy \quad (2-11)$$

Consequently, the resulting notch stresses are neglected under the assumption of a linear stress distribution over the plate thickness. According to [6], the structural

stresses determined by this method are slightly higher than with the application of the stress extrapolation.

The concept of internal linearisation through the plate thickness was investigated by Dong et al. [50, 51, 54]. As in Radaj et al. [6, 8], the relevant structural stress is approximated in the direction of the crack propagation at the weld notch. For shell elements (cf. Chapter 3.1), a linearised stress distribution over the component thickness is given by the definition. However, since non-linear stress peaks at the notch cannot be determined with sufficient accuracy by shell elements, these models are generally not recommended. In FE models with solid elements, according to [6] three or more elements should be defined over the thickness of the component. In addition, the determined stress must be increased by a notch-related and crack-depth-dependent enlargement factor. [6]

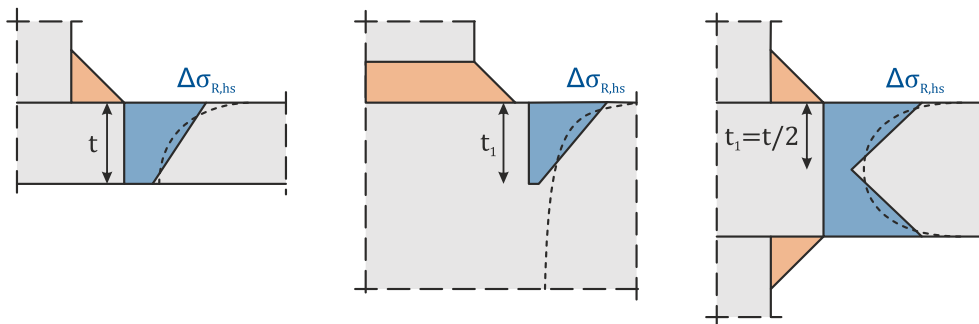


Figure 2-14: Definition of the structural stress according to Dong et al. [6] with continuous stress decrease (left), non-constant stress decrease (middle) and symmetrical stress curve (right)

According to Figure 2-14, the procedure depends on the stress distribution over the plate thickness at the critical point of the notch. In the case of a continuously decreasing stress distribution (cf. left side of Figure 2-14), as can occur for example with edge attachments, the entire plate thickness is used for the linearisation to predict the fatigue life. In the case of a non-steady decrease (cf. centre of Figure 2-14), as can be expected in the case of thick plates with attachments on both sides, only a linearisation over a defined depth t_1 is conducted for the durability analysis, which has to correspond to the damaging crack depth. In order to determine the membrane and bending stress components in the case of a symmetrical stress distribution (cf. right side of Figure 2-14), which may occur in symmetrical constructions, a general value of half the plate thickness t is applied for t_1 . As a result, the selected value of t_1 has a considerable influence on the structural stress in the case of non-steady stress decrease at the notch. Results from fatigue tests show that no universal thickness t_1 can be determined for structural details for this purpose. Since the damaging crack depth can only be determined on the basis of relevant fatigue tests, the method is not generally applicable. [6, 3, 41]

2.3.3.4 One-millimetre method

A further method for evaluating structural stresses is proposed by Xiao and Yamada [7] and is based on a generalised crack propagation analysis of the transition area of the weld. The approach was developed for longitudinal and transverse stiffeners and is based on the stress 1 mm below the surface at the location of the stress peak to

determine the structural stress. It is assumed that the fatigue life can be represented by the crack propagation along the expected crack path, perpendicular to the plate surface at the notch, since the corresponding stress gradient neglects the non-linear stress component of the structural detail. The structural stress is determined on fine meshed models with element sizes $\leq 0.5 \text{ mm}$, for which singularities at the weld transition can be avoided. However, this approach is not suitable for thin base plates with $t \leq 5 \text{ mm}$. According to the recommendations of the IIW [3], a reduction of the defined fatigue class is recommended when using this method. The following Figure 2-15 illustrates the procedure of the one-millimetre method. [6, 31, 19]

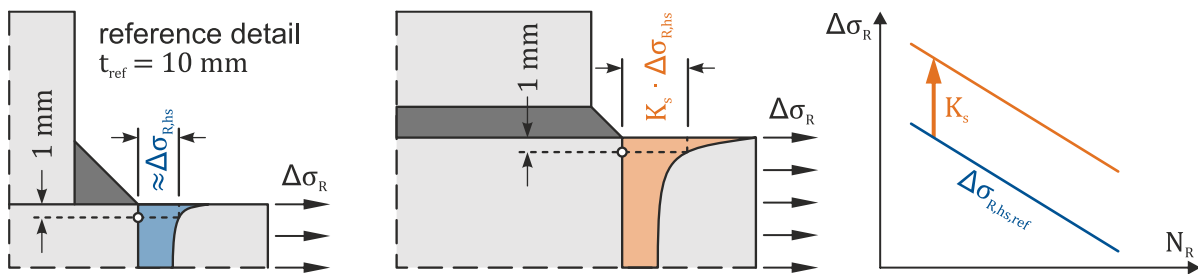


Figure 2-15: One-millimetre method with reference detail (left), examined detail (middle) and trend of the associated double logarithmic S-N curves (right) [6]

The crack propagation of an examined detail is related to a specified reference detail. A non-load-bearing cruciform joint with a plate thickness of $t = 10 \text{ mm}$ is used for this purpose, as the reference stress occurring 1 mm below the surface approximately corresponds to the normal stress of the reference detail (cf. left side of Figure 2-15). As a result, a corresponding stress concentration factor K_s can be determined for the analysed detail (cf. middle of Figure 2-15) and can be used directly for the determination of the fatigue life (cf. right side of Figure 2-15). Compared to the surface methods, the proposed one-millimetre method has the advantage of taking into account thickness effects evident in the fatigue of welded joints. [6, 7, 41, 55]

2.3.3.5 δ -method

The so-called δ -method was developed by Dong [51, 54] for the determination of structural stresses. This method is based on an equilibrium of forces and stresses at a considered element in front of the weld transition. The length of the element in the direction of the applied stress is marked with δ and depends on the expected crack depth. According to the internal linearisation through the thickness, plane longitudinal sections perpendicular to the weld notch are analysed. However, the linearised structural stress, as a combination of membrane stress σ_m and bending stress σ_b , is determined at the distance δ away from the notch by the evaluation of equilibrium conditions (cf. left side of Figure 2-16). By integrating the shear stress distribution over the thickness, the resulting force is determined, which generates a corresponding bending moment that must also be considered. The shear stresses in the section plane are to be neglected. [56, 57]

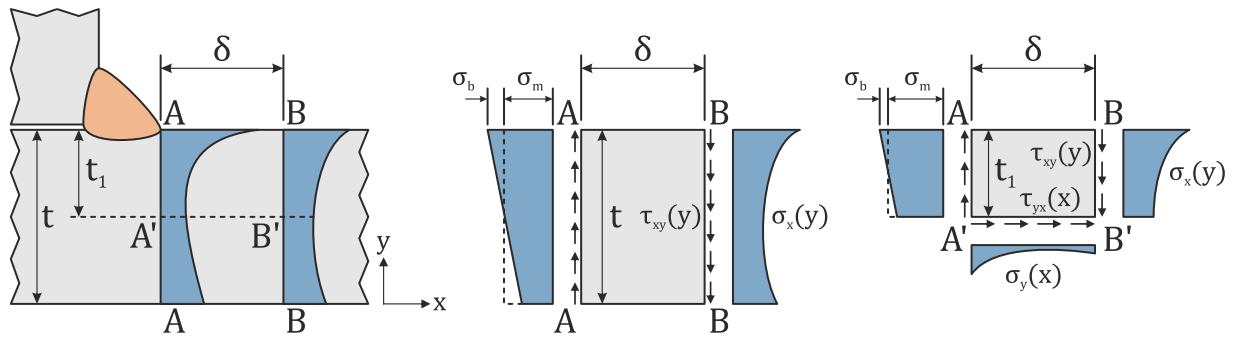


Figure 2-16: δ -method with stress distribution at the weld notch and at distance δ over the thickness t (left), linearised structural stress over the plate thickness t at the weld notch (A-A) determined by equilibrium conditions (B-B) (centre) and linearised structural stress by equilibrium conditions over the variable thickness t_1 (right) [42, 6]

The structural stresses are determined at the weld notch by deriving the normal and shear stresses according to the equilibrium conditions at the distance δ . For solid models (cf. Chapter 3.1) with a homogeneous stress distribution over the thickness t , the membrane stresses σ_m and bending stresses σ_b can be calculated according to the following formula. [42]

$$\sigma_m = \frac{1}{t} \cdot \int_0^t \sigma_x(y) \cdot dy \quad (2-12)$$

$$\sigma_m \cdot \frac{t^2}{2} + \sigma_b \cdot \frac{t^2}{6} = \int_0^t \sigma_x(y) \cdot y \cdot dy + \delta \cdot \int_0^t \tau_{xy}(y) \cdot dy \quad (2-13)$$

Additional requirements apply when the equilibrium conditions are evaluated at a distance δ and at a variable depth of $t_1 \leq t$. The depth t_1 is defined, according to the internal linearisation through the thickness, with regard to the crack propagation analysis. It is intended to be equivalent to the crack size that is assumed to represent the failure criterion. In the case of symmetrical stress distributions over the thickness, t_1 corresponds to half the plate thickness t . Figure 2-16 illustrates the stress distributions that occur in the area of the weld transition (section A – A) and in the reference section B – B (cf. left side of Figure 2-16). In section A – A the non-linear notch stresses are significantly more evident. In addition, the linearised structural stress over the depth of t_1 is visualised, resulting on the basis of the equilibrium conditions of the original stresses at section B – B' and A' – B' of the rectangular plate A – A' – B' – B (cf. right side of Figure 2-16). The structural stress determination is carried out at a depth of t_1 as follows. [6, 58, 59, 42]

$$\sigma_m = \frac{1}{t_1} \cdot \int_0^{t_1} \sigma_x(y) \cdot dy + \frac{1}{t_1} \cdot \int_0^\delta \tau_{yx}(x) \cdot dx \quad (2-14)$$

$$\sigma_m \cdot \frac{t_1^2}{2} + \sigma_b \cdot \frac{t_1^2}{6} = \int_0^{t_1} \sigma_x(y) \cdot y \cdot dy + \delta \cdot \int_0^{t_1} \tau_{xy}(y) \cdot dy + \int_0^\delta \sigma_y(x) \cdot x \cdot dx \quad (2-15)$$

Alternatively, the δ -method can be conducted on shell models (cf. Chapter 3.1). The corresponding procedure is shown schematically in Figure 2-17. [42]

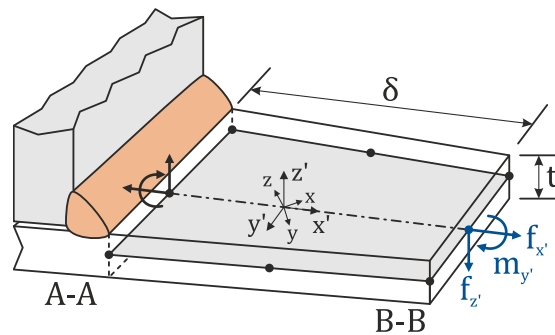


Figure 2-17: δ -method on shell models according to Dong [42]

If the FE analysis is performed with shell elements, the calculation of the structural stress is carried out in a local coordinate system with local x' -axis and y' -axis. The linear forces $f_{x'}$ and $f_{z'}$ derived from the nodal forces and moments in section $B - B$ as well as the linear moment $m_{y'}$ can be converted into the structural stress in section $A - A$. The membrane component σ_m and bending component σ_b of the shell elements at the weld notch are calculated according to the following formula. [42, 43]

$$\sigma_{hs} = \sigma_m + \sigma_b = \frac{f_{x'}}{t} + \frac{6 \cdot (m_{y'} + \delta \cdot f_{z'})}{t^2} \quad (2-16)$$

Furthermore, Dong [50] introduces a calculation of the structural stress directly based on the element nodal forces. The structural stress then results in a simplified form. [50, 60]

$$\sigma_{hs} = \sigma_m + \sigma_b = \frac{f_{x'}}{t} + \frac{6 \cdot m_{y'}}{t^2} \quad (2-17)$$

2.3.3.6 CAB-method

The so-called CAB method is a procedure from the guideline of the FKM [11] on analytical static and fatigue strength assessments procedures of components made of steel. The method was developed to calculate the fatigue strength of components used in mechanical engineering and can be implemented in civil engineering. The aim of the procedure is to interpret the decisive notch stress as being the relevant structural stress by means of a fictitious, almost notch-free modelling of the weld transition. The notches require to be rounded with a radius of $R = \sqrt{2} \cdot a$. Figure 2-18 is intended to illustrate the stress distribution for a fictitious weld rounding, showing the structural stress determined by the CAB method. [44, 11]

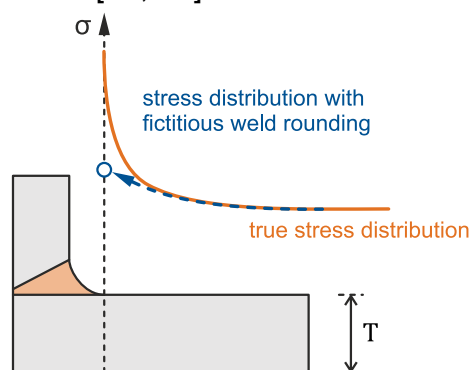


Figure 2-18: Procedure for the CAB method [44]

The weld residual stresses are neglected in the detected concept and only the critical stresses of fillet welds at the weld transitions are considered, rather than at the root of the weld. [44, 11]

2.3.3.7 *Summary of the structural stress determination*

The described approaches provide the foundation for the structural stress determination at the hot-spot. In addition to the surface methods (extrapolation method and one-point stress determination), stress evaluations through the plate thickness (internal linearisation, one-millimetre method, δ -method) offer the possibility to estimate structural stresses.

In general, there are two requirements for the responsible handling of these local approaches. On the one hand, an overview of available methods and of the input parameters necessary for the individual application is required. On the other hand, the methods should be standardised as far as possible in order to integrate them into normative regulations and guidelines.

For industrial users, it should be possible to choose the local approach that most appropriately represents the individual fatigue problem. Anyhow, apart from the stress extrapolation according to the IIW [3], as of now there is no generally accepted theory on which a uniform analytical procedure could be based. Therefore, only sufficiently validated parts of the procedures are suitable for standardisation respectively for the definition of appropriate guidelines. Following the stress extrapolation concept regulated in the guidelines of the IIW [3], which is also included in the guideline of the FKM [11] and in the draft of prEN 1993-1-9 [2, 4], significant progress has been made in the standardisation of analytical static and fatigue strength assessments procedures on the basis of local stresses. In addition, the complexity of the mentioned approaches is in the choice of an adequate FE modelling, as the results heavily depend on the quality of the chosen model. If the selection of the element type, initial function or meshing is incorrect, further deviating stresses can result amongst the different approaches. [6]

The corresponding meshing recommendations of the introduced local methods are presented in Chapter 3.2. In addition, more detailed analyses and a comparison of the structural stresses determined with the described local procedures are provided in Chapter 3.3.4. However, due to many uncertainties in the local methods, the main part of this thesis is based on the stress extrapolation according to Chapter 2.3.3.1, as this method is implemented in the commonly used codes and guidelines.

2.3.4 **Effective notch stress concept**

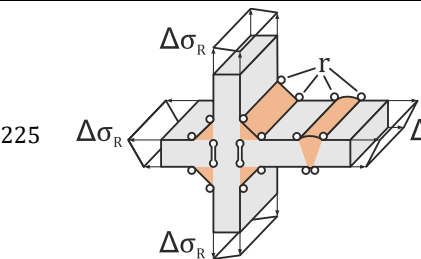
As a further alternative, the fatigue strength of components can be assessed using the effective notch stress concept. In addition to the macroscopic stress increases caused by the structure, local stress effects, e.g. as a result of the weld geometry, are considered in a computer-aided linear elastic FE calculation.

The concept is commonly used in mechanical engineering and is described in detail in the guidelines of the IIW [3] and the guideline of the FKM [11]. While the method with effective notch stresses $\Delta\sigma_{en}$ is not included in the current DIN EN 1993-1-9 [2], it will

be considered in the upcoming version of prEN 1993-1-9 and prEN 1993-1-14 [4, 14]. The concept is verified solely for ground plate thicknesses of $t > 5 \text{ mm}$ and should not be applied if significantly large stress components exist parallel to the weld.

In the effective notch stress concept, notch stresses $\Delta\sigma_{R,en}$ are calculated, that are defined as the maximum total stresses of a structure at the critical weld transition or in the weld root, including the stress concentrations from the local notch. Thus, the structural stresses $\Delta\sigma_{R,hs}$ already presented are extended by the non-linear stress component and ought to be approximately 1.6 times the structural stress at the critical point. In order to determine the effective notch stress $\Delta\sigma_{R,en}$ required for the notch stress verification, linear elastic material behaviour is to be assumed in the FE analysis. Although welds are considered in an idealised shape similar to the structural stress concept, they are modelled in a geometrically more precise way, since all notches at weld transitions and weld roots have to be rounded with an effective notch radius of $r = 1 \text{ mm}$ (cf. Table 2-2). In addition, a much finer meshing is required.

Table 2-2: Fatigue strength and notch roundness on the basis of the effective notch stress concept according to table C.1 of prEN 1993-1-9 [4]

$\Delta\sigma_{C,en}$	Structural detail	Description	Requirements
225		<p>Principal stresses are to be evaluated.</p> <p>Without post-weld treatment.</p> <p>Effective notch radius of 1 mm replaces notches at weld transitions and weld roots.</p>	<p>The calculated notch stresses must take into account imperfections that exceed the specifications of EN 1090-2. It is recommended to use the nominal value of the eccentricity in case of axial misalignment in joints.</p>

In order to make the notch effect detectable, very fine FE meshing is required in the section of the critical area. According to prEN 1993-1-14 [14], element sizes of 0.25 mm are recommended for hexahedral elements with quadratic initial function, while element sizes of 0.25 mm should be used for linear initial function and tetrahedra with quadratic initial function (cf. Table 2-3). Due to the rounding and fine meshing, the relevant effective notch stress in the FE model can be derived directly at the critical notch. Due to the required exact consideration of the geometry, including all potential imperfections, the effective stresses are uniformly compared to a fatigue strength of $\Delta\sigma_{C,en} = 225 \text{ N/mm}^2$. This applies to all structural details, both according to the IIW [3] and prEN 1993-1-9 [4].

Table 2-3: Meshing recommendations for element sizes at critical locations according to the effective notch stress concept according to Figure 7.7 of prEN 1993-1-14 [14]

Element type and initial function	Maximum element size	
Hexahedra	quadratic	0.25 mm
	linear	0.15 mm
Tetrahedra	quadratic	0.15 mm

In contrast to the concepts mentioned so far, the effective notch stress approach makes it possible to capture the local stress peaks due to the weld more accurately. However, the required detailed modelling of the weld in combination with a very fine meshing leads to a significantly increased modelling effort, which is often not economically justifiable for constructions in civil engineering. [61]

2.4 Normative standards and guidelines for fatigue verification

In civil engineering as well as in mechanical engineering, different normative regulations and guidelines are available for the assessment of components under cyclic fatigue loading. While the guideline of the FKM [11] and guidelines of the IIW [3] regarding the effective notch stress concept (cf. Chapter 2.3.4) are commonly used in mechanical engineering, DIN EN 1993-1-9 [2] generally applies in civil engineering. Consequently, for the design and construction of metal structures with regard to material fatigue, DIN EN 1993-1-9 [2] including the national Annex DIN EN 1993-1-9/NA [2] must be complied within the Free State of Bavaria. This ensures verification of Article 3 on general requirements and Article 10 on stability of the Bavarian Building Regulation [62], in accordance with the Bavarian Technical Construction Regulation [63]. The guidelines of the IIW [3] often represent the technical foundation of the structural stress concept. In the following, an overview is given of the most important standards and guidelines where fatigue verifications are specified. In this respect, only the relevant specifications for cruciform joints with fully penetrated welds are discussed in more detail. Nonetheless, for the purpose of completeness, information on cruciform joints without full penetration welds are also provided tabularly.

2.4.1 DIN EN 1993-1-9

The currently valid DIN EN 1993-1-9 [2] deals with verification methods for determining the fatigue strength of components, connections and joints that are subject to fatigue stress. This type of stress can be caused, for example, by the effects of road traffic, wind or waves and result from the operation of cranes. DIN EN 1993-1-9 [2] describes fatigue as a process of crack initiation and propagation in a structural component caused by repetitive dynamic stress ranges. The relevant potential crack locations are those where a local stress concentration is detected due to notch effects. These include joints, in particular weld transitions, whereby the notch effects can be of a geometric or metallurgical nature. Elastic component behaviour is assumed when determining the fatigue-relevant stresses. In principle, the verifications on structural steels of steel grades $f_y = 235 \text{ N/mm}^2$ to $f_y = 700 \text{ N/mm}^2$ [64] may be applied, although the yield strength f_y has no influence on the fatigue strength according to the current standard.

According to DIN EN 1993-1-9 [2], fatigue verifications are to be carried out according to the concept of adequate safety against fatigue failure without prior notice, in addition to the concept of damage tolerance. The corresponding fatigue verification is conducted on the basis of longitudinal stress ranges $\Delta\sigma$ or on shear stress ranges $\Delta\tau$. These are determined either on the basis of nominal stresses, modified nominal stresses or structural stresses. The stresses must be restricted under consideration of the associated fatigue strengths $\Delta\sigma_C$ or $\Delta\tau_C$ on the basis of S-N curves and the yield strength f_y . The corresponding partial safety factor γ_{Mf} for conducting fatigue

verifications in accordance with Chapter 2.2.5 is calculated in conformity with DIN EN 1993-1-9 [2] according to the following Table 2-4.

Table 2-4: Table 3.1 of DIN EN 1993-1-9 [2] for γ_{Mf} -factors with an influence on the fatigue strength

Design concept	Consequence of failure	
	low	high
Damage tolerance	1.00	1.15
Safety against fatigue failure without prior notice	1.15	1.35

The verifications for the damage tolerance and safety against fatigue failure without prior notice are only differentiated between low and high damage consequences (cf. Table 2-4).

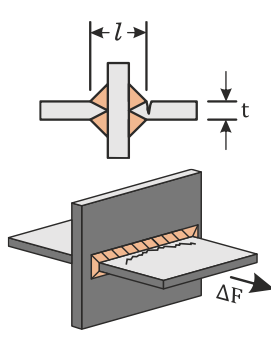
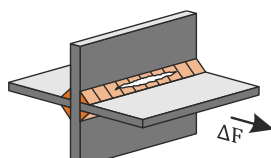
2.4.1.1 **Nominal stress concept**

The currently valid standard DIN EN 1993-1-9 [2] deals in detail with the nominal stress concept described in Chapter 2.3.1. DIN EN 1993-1-9 [2] defines nominal stress ranges $\Delta\sigma_{nom}$ as stresses in the base material arising directly at the expected crack location. These are determined according to the elastic stress theory without the consideration of local notch effects. Due to the fact that local stress peaks do not need to be evaluated, FE calculations are not required. Consequently, depending on the relevant geometric boundary conditions, the fatigue classes in the nominal stress concept are classified in detail in order to take essential influencing factors into account.

The nominal stress concept provides the simplest way of fatigue verification, as it is based on a large number of frequently encountered structural details. The corresponding fatigue classes include fatigue strengths that consider only geometric deviations explicitly described for each construction type. If geometric variations have to be considered, DIN EN 1993-1-9 [2] additionally provides the modified nominal stress concept according to Chapter 2.3.2. By means of a geometric notch factor k_f , design-related stress increases that are no longer covered by the fatigue class can be considered. The corresponding fatigue strengths can be found in the structural details of the nominal stress concept.

In the case of full penetration welded cruciform joints, a distinction is made according to the plate thickness t in addition to the connection length l in order to account for all relevant geometric influencing factors regarding the nominal stress concept. According to [2], cruciform joints with fully penetrated welds are assigned to the fatigue classes 40 to 80 and the corresponding fatigue strength varies between $\Delta\sigma_{C,nom} = 40 \text{ N/mm}^2$ and $\Delta\sigma_{C,nom} = 80 \text{ N/mm}^2$ depending on the plate thickness and connection length (cf. Table 2-5). With regard to potential effects caused by imperfections, reference is made to Chapter 2.5. [4]

Table 2-5: Excerpt from Table 8.5 according to DIN EN 1993-1-9 [2] on the fatigue strength of cruciform joints applying the nominal stress concept

$\Delta\sigma_{C,nom}$	Structural detail		Description	Requirements
80	$l \leq 50$	all t		After inspection, clear of discontinuities and misalignments exceeding the tolerances according to EN 1090.
71	$50 < l \leq 80$	all t		
63	$80 < l \leq 100$	all t		
56	$100 < l \leq 120$	all t		
56	$l > 120$	$t \leq 20$		
50	$120 < l \leq 200$	$t > 20$		
	$l > 200$	$20 < t \leq 30$		
45	$200 < l \leq 300$	$t > 30$		Two fatigue verifications required: verification against crack of the weld root and verification at the weld transition.
40	$l > 300$	$t > 50$		
36	all l	all t		

The eccentricity of the loaded plates must be $\leq 15\%$ of the thickness of the intermediate plate.

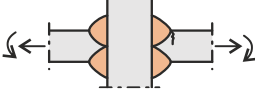
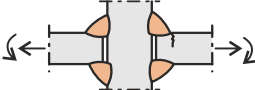
2.4.1.2 Structural stress concept

DIN EN 1993-1-9 [2] does not provide the term structural hot-spot stress concept (h_s). It solely specifies the corresponding structural stress. This is defined as the maximum principal stress at the potential crack location of the weld transition. To determine the design value $\gamma_{Ff} \cdot \Delta\sigma_{R,hs}$ (cf. Chapter 2.3.3), DIN EN 1993-1-9 [2] merely indicates a stress concentration factor k_f , which is multiplied by the equivalent constant stress range of the nominal stress concept $\gamma_{Ff} \cdot \Delta\sigma_{R,nom}$ according to the following formula:

$$\gamma_{Ff} \cdot \Delta\sigma_{R,hs} = k_f \cdot (\gamma_{Ff} \cdot \Delta\sigma_{R,nom}) \quad (2-18)$$

No information is given on the origin or determination of this stress concentration factor k_f . Assuming that the stress concentration factor k_f proposed for the modified nominal stress concept corresponds to the same factor, it is suggested that appropriate values are to be taken from literature or from suitable FE calculations. Due to the required FEA, geometric influences are already included in the modelling. Consequently, the fatigue tables for the structural stress concept are significantly reduced. The fatigue strength $\Delta\sigma_{C,hs}$ for structural stresses of cruciform joints with full penetration welds according to Table B.1 from Annex B of the currently valid standard [2] are shown in Table 2-6. However, the fatigue strength only covers crack initiation at the weld transition (cf. Note 2 of Table 2-6). Consequently, the structural stress concept can only be applied to structural details for which crack initiation at the weld root followed by crack growth through the weld can be excluded. The fatigue classes take into account geometric and structural notch effects and imperfections resulting from the weld formation as well as residual stresses caused by the welding process. [2]

Table 2-6: Extract from fatigue classes for the structural stress concept on cruciform joints according to Annex B as specified in DIN EN 1993-1-9 [2]

$\Delta\sigma_{C,hs}$	Structural detail	Description	Requirements
100		Cruciform joint with full penetration K-welds	- Attachment angle $\leq 60^\circ$ - In case of misalignments, see NOTE 1 - See also NOTE 2
90		Cruciform joints with stressed fillet welds	

NOTE 1 The table does not include misalignments; they must be explicitly considered in the stress calculation.
NOTE 2 The table does not apply to crack initiation at the weld root followed by crack growth through the weld.

Reference is made to Chapter 2.5 for the consideration of influences from imperfections in the structural stress concept. Yet, DIN EN 1993-1-9 [2] lacks information on how to deal with these influences. The general approach to thickness effects is described in Chapter 2.6. Nonetheless, DIN EN 1993-1-9 [2] does not provide any information in this respect either. According to Table 2-6, cruciform joints with full penetration welds are assigned to the fatigue class $\Delta\sigma_{C,hs} = 100 \text{ N/mm}^2$ based on 2 million stress cycles.

2.4.2 Guidelines of the IIW

As an international technical and scientific association for welding, brazing and related joining technologies, the International Institute of Welding (IIW) is dedicated to providing guidance on fatigue design. The "Recommendations for Fatigue Design of Welded Joints and Components" [9, 3] provide the principles for the design and analysis of welded structures. The recommendations of the IIW [3] provide general methods for the assessment of fatigue behaviour of welded components with regard to stability and serviceability. The guidelines are applicable for steel grades up to $f_y = 960 \text{ N/mm}^2$. In addition to the nominal stress concept, the guidelines of the IIW [3] deal with structural and notch stresses in detail. The related concepts of fatigue verification based on specific S-N curves are defined as structural hot-spot stress and effective notch stress concept. No explicit recommendations are given for fatigue loading on the action side. With regard to the partial safety factors for the fatigue strength γ_{Mf} and effective stress γ_{Ff} , no values are specified. The recommendation is to derive them from an applicable design specification. [3]

2.4.2.1 Nominal stress concept

In contrast to DIN EN 1993-1-9 [2], the IIW [3] deals with both nominal stresses and modified or local nominal stresses holistically with the nominal stress concept. The basic procedure is the same and macro-geometric effects as well as stress arrays in the section of concentrated loads have to be additionally considered in the linear elastic stress determination. Stress concentrations from the welded joint itself do not have to be considered. In the guidelines of the IIW [3], a structural stress concentration factor is suggested to represent the ratio of structural stresses to local or modified nominal stresses. A more detailed description of this procedure is omitted. It is solely pointed

out that in case of a calculation of nominal stress ranges with the use of FE calculations, the more accurate structural stress concept should be applied. The tabulated fatigue strengths for the nominal stress concept of the IIW [3] are based on uniform structural details identical to DIN EN 1993-1-9 [2]. However, stress increases due to imperfections are already included in the corresponding fatigue strengths by the factor $k_{m,already\ covered}$. This factor is described in Chapter 2.5 in more detail. If the permissible stress increase is exceeded, imperfections must be accounted for in the stress calculation. In addition, the IIW [3] specifies correction factors $f(t)$ for the modification of the fatigue strength with regard to thickness effects, provided that the specified reference thickness of 25 mm is exceeded by the load-bearing plate (cf. Chapter 2.6). Consequently, plate thickness effects according to [3] only become relevant if the analysed plate thickness is larger than the specified reference thickness. With regard to cruciform joints, merely full penetration welds without post weld treatment are examined in this thesis. According to the IIW [3], these details are assigned to a fatigue strength of $\Delta\sigma_{C,nom} = 71\text{ N/mm}^2$ according to the following Table 2-6. The influence of imperfections on the structural stress is further described in Chapter 2.5.

Table 2-7: Excerpt from Table 3.1 of the IIW [3] on the fatigue strength of cruciform joints applying the nominal stress concept

Structural detail	Description	$\Delta\sigma_{C,nom}$	Requirements
	Cruciform joint with full penetration K-butt welds, weld toes ground, potential failure from weld toe	80	Advisable to ensure that intermediate plate was checked against susceptibility to lamellar tearing
	Cruciform joint with full penetration K-butt welds, potential failure from weld toe	71	
	Cruciform joint with fillet welds or partial penetration K-butt welds, potential failure from weld toe	63	Misalignment < 15 % of primary plate thickness
	Cruciform joint with fillet welds or partial penetration K-butt welds including toe ground joints, potential failure from weld root For $a/t \leq 1/3$	36 40	For more information see detail no. 414 in Table 3.1 [3].

The guidelines of the IIW [3] also recommend procedures for modifying the fatigue strength. For an effective stress ratio $R < 0.5$, for example, a fatigue improvement factor $f(R)$ can be used to consider the total of the load and residual stress level of the analysed component. In addition, recommendations are made to account for influences from imperfections and for thickness effects, which are described in more detail in the later Chapters 2.5 on imperfections and 2.6 on thickness effects. The influence of elevated temperatures and possible post-treatment methods that can affect fatigue

strength are also provided in the guidelines of the IIW [3]. Due to the lack of application, these are not described further in this thesis.

2.4.2.2 Structural stress concept

Detailed information on the determination of the structural stresses is provided by the IIW [3]. Due to the currently insufficient results for thin plates, the solution approaches only apply for plate thicknesses of at least 3 mm. Nevertheless, in mechanical engineering the structural stress concept is also used for thinner plate structures [9, 3]. With regard to the structural stress concept, the IIW specifications are based on the surface stress extrapolation described in Chapter 2.3.3.1. Further local methods, such as the one-point stress determination according to Haibach [10], the one-millimetre method according to Xiao and Yamada [7] and the internal linearisation according to Radaj [8] are only referred to briefly [9, 3].

According to the IIW [3], the structural stress is determined at specified reference points on the surface. In practical design, the required first principal stress σ_1 is almost perpendicular to the weld. Considerable deviations may be detected in the case of a biaxial stress state at the plate surface. In this situation, it is recommended to use the first principal stress for the structural stress determination as long as no angle larger than $\pm 60^\circ$ to the weld is encountered (cf. Figure 2-19). Otherwise, an additional fatigue verification parallel to the weld is recommended. For larger angles, the stress component σ_\perp perpendicular to the weld becomes relevant. [3, 34]

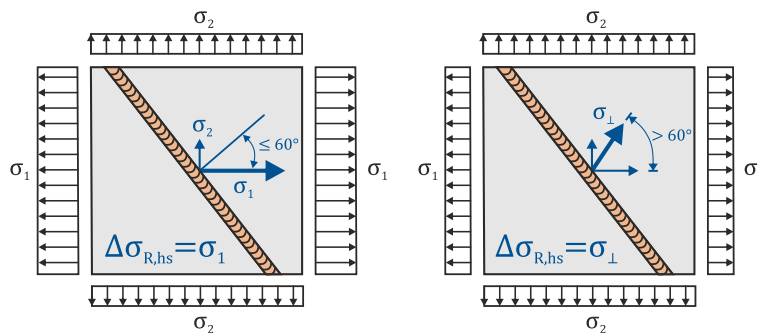


Figure 2-19: First principal stress as relevant stress component (left) and resulting relevant perpendicular stress (right) for structural stress calculation [9]

The result of the stress extrapolation is also significantly influenced by the choice of reference points and the corresponding type of meshing (cf. Chapter 3.2). For relatively coarse meshes, solely the linear extrapolation approach is applicable. The surface stress is determined at the centre nodes of the first and second element and extrapolated towards the weld. Due to the singularity at the weld transition, the stress at the first element node is rather excessive. This error is compensated by the relatively large distances of the extrapolation points of the linear stress extrapolation to the weld. For hot-spot type *a*, the following formula results for the determination of the relevant structural stress $\Delta\sigma_{R,hs}$ [3, 59]:

$$\Delta\sigma_{R,hs} = 1.50 \cdot \sigma_{0.5-t} - 0.50 \cdot \sigma_{1.5-t} \quad (2-19)$$

Due to the required coarse mesh of hot-spot type *b*, the extrapolation formula according to Table 3-1 results in [3]:

$$\Delta\sigma_{R,hs} = 1.50 \cdot \sigma_{5\text{ mm}} - 0.50 \cdot \sigma_{15\text{ mm}} \quad (2-20)$$

The extrapolation equations (2-19) and (2-20) are not to be used in combination with fine element meshes, as there is a risk of underestimating the structural stress. [3]

In contrast to a relatively coarse mesh, the reference points in fine meshed FE models are not dependent on the element size. Consequently, the distance of the extrapolation point closest to the notch is chosen in a way that any influence of the weld notch has decayed. The specifications of the IIW [3] are based on practical experience [65]. The latter has shown that the non-linear part of the notch stress is no longer present at a distance of approximately 40 % of the plate thickness $\Delta x_1 \approx 0,4 \cdot t$ [3]. The linear stress extrapolation for a hot-spot type *a* thus results in the following structural stress $\Delta\sigma_{R,hs}$:

$$\Delta\sigma_{R,hs} = 1.67 \cdot \sigma_{0,4 \cdot t} - 0.67 \cdot \sigma_{1,0 \cdot t} \quad (2-21)$$

In addition, with fine meshed FE models and the hot-spot type *a*, quadratic extrapolations can be useful if a significant non-linear stress increase in the direction of the weld transition is to be expected. The quadratic extrapolation according to the following formula is also recommended for strong directional changes of the structure and thick-walled components. Only fine meshes are possible for the quadratic extrapolations. [3]

$$\Delta\sigma_{R,hs} = 2.52 \cdot \sigma_{0,4 \cdot t} - 2.24 \cdot \sigma_{0,9 \cdot t} + 0.72 \cdot \sigma_{1,4 \cdot t} \quad (2-22)$$

It shall be mentioned that linear extrapolation is generally sufficient for fatigue analysis. Moreover, the SN curves provided by IIW [2] are based on a conservative linear extrapolation. Therefore, it is recommended to verify fatigue tests with the use of the uniform extrapolation points.

For fine meshed models with hot-spot type *b*, no extrapolation points proportional to the plate thickness can be defined due to its independence. The guidelines of the IIW [3, 65] suggest fixed distances of 4 mm, 8 mm and 12 mm. The extrapolation formula results in:

$$\Delta\sigma_{R,hs} = 3 \cdot \sigma_{4\text{ mm}} - 3 \cdot \sigma_{8\text{ mm}} + \sigma_{12\text{ mm}} \quad (2-23)$$

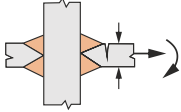
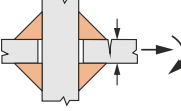
The surface stresses for stress extrapolation according to the IIW [3] are evaluated with the help of FE calculations. The corresponding FE model should be constructed as close to reality as practicable so that geometric boundary conditions and load parameters correspond to the investigated detail. Subsequently, the relevant structural stress $\Delta\sigma_{R,hs}$ is calculated by the respective valid extrapolation formula. In the assessment of fatigue safety, the applied structural stress $\Delta\sigma_{R,hs}$ is compared with the fatigue resistance $\Delta\sigma_{C,hs}$ of the structural stress concept. For this purpose, the IIW [3] provides the following catalogue (cf. Table 2-8). The fatigue strength for the structural stress concept given in Table 2-8 is defined in accordance to DIN EN 1993-1-9 [2] for 2 million stress cycles and refers to the base components of the structure. High tensile residual stresses and their resulting effects are already considered on the resistance side. If the investigated detail cannot be attributed to a reference detail, a fatigue class should be selected that is intended to be similar in terms of geometric boundary and loading conditions. FE models with the identical initial element function, meshing and

load are to be generated for both the reference detail and the detail to be analysed in order to determine the structural stresses $\Delta\sigma_{R,hs,ref}$ and $\Delta\sigma_{R,hs,assess}$ according to the stress extrapolation. The required fatigue strength $\Delta\sigma_{C,hs,assess}$ for 2 million load cycles can then be determined by the fatigue strength of the reference detail $\Delta\sigma_{C,hs,ref}$ according to the following formula:

$$\Delta\sigma_{C,hs,assess} = \frac{\Delta\sigma_{R,hs,ref}}{\Delta\sigma_{R,hs,assess}} \cdot \Delta\sigma_{C,hs,ref} \quad (2-24)$$

According to the IIW [3], cruciform joints with full penetration welds are specified with a fatigue strength of $\Delta\sigma_{C,hs} = 100 \text{ N/mm}^2$ (cf. Table 2-8). This is in accordance with the specifications of DIN EN 1993-1-9 [2]. For more information on the effects of imperfections, reference is made to Chapter 2.5. In addition, detailed specifications on thickness effects are given in the guidelines of the IIW [3]. The exact procedure is discussed in more detail in Chapter 2.6.

Table 2-8: Excerpt from Table 3.1 of the IIW [3] on the fatigue strength of cruciform joints according to the structural stress concept

No.	Structural detail	Description	Requirements	$\Delta\sigma_{C,hs}$
2		Cruciform joint with full penetration K-butt welds	K-butt welds, no lamellar tearing	100
6		Cruciform joints with load-carrying fillet welds	Fillet welds, as welded	90

NOTE 1 The table does not cover larger effects of misalignment than those specified in Sect. 3.8.2. They have to be considered explicitly in the determination of the hot-spot stress range.

2.4.3 prEN 1993-1-9 and prEN 1993-1-14

The final documents of the future Eurocode generation prEN 1993-1-9 [4] and prEN 1993-1-14 [14] provide equally detailed information regarding the structural stress concept and the effective notch stress concept as given by the guidelines of the IIW [3]. With regard to the nominal stress concept, there are only minor changes with partly deviating classifications in fatigue strengths. In addition, there are modified partial safety factors. According to the following Table 2-9 according to prEN 1993-1-9 [4], the classification was supplemented by a further consequence of failure with medium effect. In addition, the level of the partial safety factor γ_{Mf} was partially increased (cf. Table 2-9).

Table 2-9: γ_{Mf} -factors with regard to the fatigue strength according to prEN 1993-1-9 [4]

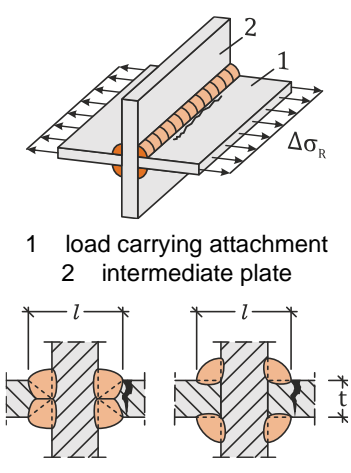
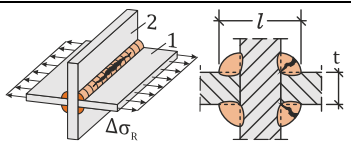
Design concept	Consequence of failure		
	low	medium	high
Damage tolerance	1.00	1.15	1.25
Safety against fatigue failure without prior notice	1.15	1.25	1.35

2.4.3.1 Nominal stress concept

In the final document prEN 1993-1-9 [4], nominal stress ranges $\Delta\sigma_{R,nom}$ continue to be calculated using a linear elastic analysis and do not include stress-increasing effects. However, thickness effects must be considered in the new draft in the nominal stress concept as well as in the structural stress concept (cf. Chapter 2.6).

The fatigue strengths $\Delta\sigma_{C,nom}$ of cruciform joints when applying the nominal stress concept are given in Table 10.6 of prEN 1993-1-9 [4]. The corresponding excerpt is summarised in Table 2-10. No changes have been made with regard to DIN EN 1993-1-9 [2] (cf. Table 2-5).

Table 2-10: Extract from Table 10.6 of prEN 1993-1-9 [4] for the fatigue strength of cruciform joints applying the nominal stress concept

Structural detail	$\Delta\sigma_{C,nom}$	Description	Requirements	
 <p>1 load carrying attachment 2 intermediate plate</p>	80	$l \leq 50 \text{ mm}$	<p>$\Delta\sigma$ should be calculated using the normal stress in the load carrying attachment.</p> <p>The eccentricity of the load carrying attachments should not exceed 15 % of the thickness of the intermediate plate.</p> <p>For load carrying attachments with partial penetration butt welds or fillet welds, weld root failure should additionally be checked, see NOTE 2.</p>	
	71	$50 < l \leq 80$		
	63	$80 < l \leq 100$		
	56	$100 < l \leq 120$		
	50	$l > 120 \text{ mm}$		$t \leq 20 \text{ mm}$
		$120 < l \leq 200$		$t > 20 \text{ mm}$
		$l > 200 \text{ mm}$		$20 < t \leq 30$
		$200 < l \leq 300$		$t > 30 \text{ mm}$
	45	$l > 300 \text{ mm}$		$30 < t \leq 50$
	40	$l > 300 \text{ mm}$		$t > 50 \text{ mm}$
	36	all l	<p>$\Delta\sigma$ should be calculated using the normal stress in the weld.</p> <p>For further information see Table 10.6 [4].</p>	

NOTE 1 Typical example: symmetrical load carrying attachments at opposite surfaces of a plate (cruciform joint).

NOTE 2 For load carrying attachments with partial penetration butt welds or fillet welds, weld toe failure only occurs for great weld sizes $a > 0.7 \cdot t$. For normal weld sizes, weld root failure is expected. Effective full penetration butt welds according to EN 1993-1-8 are considered as partial penetration butt welds in respect of fatigue.

2.4.3.2 Structural stress concept

While the current version of DIN EN 1993-1-9 [2] deals with the structural stress concept only very superficially and without application recommendations, the new draft prEN 1993-1-9 [4] addresses the design concept comprehensively. The fatigue strengths $\Delta\sigma_{C,hs}$ for the structural stress concept from prEN 1993-1-9 [4] are derived from fatigue tests that already consider effects from geometric and structural imperfections as well as from defects in the material production and the welding

process [14]. In addition to prEN 1993-1-9 [4], the new draft prEN 1993-1-14 [14] is currently being completed as well. The standard [14] is to contain rules and application recommendations for numerical finite element analyses in order to be able to model and verify steel structures with regard to their load-bearing capacity, serviceability and fatigue safety. In the specifications for the structural stress determination according to prEN 1993-1-9 [4], reference is consequently made to the draft version prEN 1993-1-14 [14].

The design standard [14] contains information on FE analysis and thus guidance on stress determination, initial element functions and meshing specifications when applying the structural or effective notch stress concept. In prEN 1993-1-14 [14], only the stress extrapolation presented in Chapter 2.3.3.1 is integrated. According to the recommendations, linear surface extrapolation is sufficient for most details and loading situations. According to [14], quadratic extrapolation should only be used for highly curved stress distributions. The information provided is based on the verification concept of prEN 1993-1-9 [4] and is strongly oriented towards the recommendations of the IIW [3].

Since the distance of the required reference points and the corresponding extrapolation formulae of prEN 1993-1-14 [14] do not differ from the procedure of the recommendations of the IIW [3], they will not be further discussed in this chapter. According to prEN 1993-1-14 [14], further rules and recommendations regarding the FEA are to be considered, which will be specified in Chapter 3.

The structural stress concept (hot-spot stress method) is described in Annex B of prEN 1993-1-9 [4], which is also oriented towards the recommendations of the IIW [3]. The terms geometric stress respectively structural stress and stress at a critical point $\Delta\sigma_{hs}$ (hot-spot stress) are defined separately. Structural stresses are considered to be elastic stresses of a welded structural detail, which include stress increases from joint-geometric and macro-geometric effects as well as influences from concentrated loads. Macro-geometric effects comprise imperfections from the manufacturing process as well as misalignments of connected structures, that are no longer covered by the fatigue strength (cf. Chapter 2.5). On the other hand, stresses at a critical point $\sigma_{R,hs}$ are defined as structural stress at a weld transition, which are determined by means of an extrapolation of stresses (cf. Chapter 2.3.3.1). When calculating the structural stress, it is recommended to use the first principal stress according to prEN 1993-1-9 [4]. Deviating from the guidelines of the IIW [3], the maximum stress perpendicular to the notch is relevant beginning at an angle $\alpha > \pm 45^\circ$ for multi-axial stress conditions (cf. Figure 2-20).

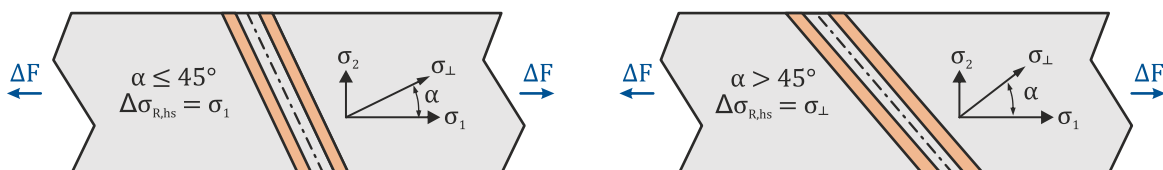
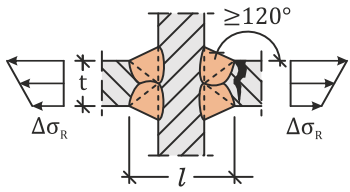
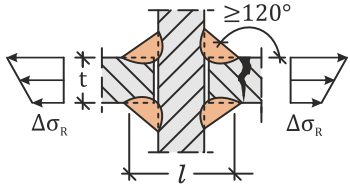


Figure 2-20: Relevant structural stress at multi-axial stress state for main plate with welded-on component according to prEN1993-1-9 [4] with first principal stress σ_1 longitudinal to the direction of tension and σ_2 transverse to the direction of tension as well as stress σ_{\perp} perpendicular to the weld

Table 2-11 shows an extract from Table B.1 of prEN 1993-1-9 [4] on cruciform joints. The reference value of the fatigue strength is defined for 2 million stress cycles. Furthermore, all specifications of the currently valid DIN EN 1993-1-9 [1] are valid. Thus, notch geometric effects from the notch geometry and material effects, e.g. different yield strengths in the heat-affected zone are already considered in the fatigue strengths. If an exact allocation is not possible, Annex G of prEN 1993-1-9 [4] adopts the procedure of the IIW [3].

Table 2-11: Excerpt from Table B.1 of prEN 1993-1-9 [4] on the fatigue strength cruciform joints applying the structural stress concept

FAT	$\beta^{1)}$	Structural detail	Description	Requirements
100	0.3		Cruciform joint with full penetration butt welds, welded from both sides	Weld flank angle $\geq 120^\circ$, see Note 2. The eccentricity of the load carrying plates due to fabrication to be neglected if $\leq 15\%$ of the thickness of the intermediate plate (with reference to Section B.3.2.9)
90	0.3		Cruciform joint with load-carrying partial penetration butt welds and fillet welds	For more information see constructional detail no. 4 in Table B.1 [4]

¹⁾ The thickness correction only applies to hot-spot type *a* (with reference to Section B.4.3).

NOTE 1 Fatigue resistance curve with slope parameter $m_1 = 3$ unless otherwise stated in detail category

NOTE 2 For load carrying attachments with partial penetration butt welds or fillet welds, for weld sizes $a > 0.7 \cdot t$ weld root failure shall also be checked.

The analysed structural detail cruciform joint is assigned the fatigue strength of $\Delta\sigma_{C,hs} = 100 \text{ N/mm}^2$ according to Table 2-11. In the case of potential cracks at the weld root, reference is made to the nominal stress concept or effective notch stress concept. Furthermore, the draft [4] specifies that axial misalignment may be neglected if it amounts to less than 15 % of the thickness of the intermediate plate. The specifications for managing the influence of imperfections are analysed in more detail in Chapter 2.5. Supplementary to DIN EN 1993-1-9 [2], a factor β is introduced for the thickness-dependent reduction of the fatigue strength. Although the underlying formula is identical to the guidelines of the IIW [3], the effective thickness t_{eff} is calculated using a different approach. More detailed information on the thickness effect is presented in Chapter 2.6.

2.4.4 Guideline of the FKM

The FKM (Forschungskuratorium Maschinenbau e.V.) provides a guideline for fatigue verification [11] which is commonly applied in mechanical engineering. The guideline includes static verifications and fatigue strength verifications for cast iron, steel and temperature castings as well as for rolled steels without special requirements regarding corrosion and heat resistance. For a verification with local stresses, the FKM [11] recommends the use of structural stresses and defines them as local stresses that can

occur in welded components. Nevertheless, no more detailed information on the procedure and on modelling requirements is provided. In addition, the guideline [11] lists tables for component fatigue classes. Reference is made to the fatigue class catalogue by Hobbacher [3]. Therefore, a more detailed consideration is omitted. Thickness effects are explicitly considered in the guideline of the FKM [11] (cf. Chapter 2.6).

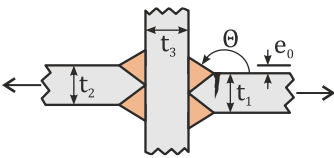
2.4.5 DNVGL

In the field of shipbuilding and offshore steel structures, there are further guidelines that deal with fatigue. DNVGL-CG-0129 [45] applies to shipbuilding, while DNVGL-RP-C203 [66] should be mentioned for offshore steel structures. However, the underlying details sometimes deviate significantly from the designs commonly used in civil engineering.

2.4.5.1 Nominal stress concept

In the following, cruciform joints are assigned to the nominal stress fatigue class tables from DNVGL-CG-0129 [45] and DNVGL-RP-C203 [66]. The additionally specified K -factors are described in the next Section 2.4.5.2 regarding the structural stress concept.

Table 2-12: Extract from Table 8 on cruciform joints according to DNVGL-CG-0129 applying the nominal stress concept [45]

Geometry	Description of joint	K -factor	FAT [MPa]
	<p>Cruciform joint with K-butt welds with full penetration or defined incomplete root penetration.</p> <p>The effective weld thickness may be assumed as the thickness of the abutting plate t_1 minus f, where f is the incomplete root penetration of $0.2 \cdot t_1$ with a maximum of 3 mm, which should be balanced by equally sized double fillet welds on each side.</p> $e = \frac{t_1}{2} + e_0 - \frac{t_2}{2} \quad \text{for } t_1 \leq t_2$ $e_0 \leq 0.3 \cdot t_1; \quad K_{m\alpha} = 1.0; \quad K_{me} = 1.45; \quad \theta = 45^\circ \text{ } ^1)$	1.27	71
	<ol style="list-style-type: none"> 1) For weld angle deviating from 45° the K factor should be multiplied by $c = 1/1.2 \cdot (0.6 + 0.6 \cdot \tan(\theta)^{1/4})$. For correction of the FAT class, the FAT class should be multiplied with $1/c$. 2) For weld angle deviating from 45° the K factor should be multiplied by $c = 1/1.67 \cdot (0.8 + 0.87 \cdot \tan(\theta)^{1/4})$. For correction of the FAT class, the FAT class should be multiplied with $1/c$. 3) If the misalignment is different than the default value then the K factor can be multiplied with $K_{me,mod}/K_{me}$ and the FAT class can be multiplied with $K_{me}/K_{me,mod}$. 4) For angular misalignment reference is made to detail no. 9 in Table 3 (cf. Chapter 2.5). If both angular and axial misalignment is considered, then K_m should be calculated by $K_m = K_{m\alpha} + K_{me} - 1$. 		

The detail specified in shipbuilding [45] for cruciform joints in accordance with Table 8 of the guideline is summarised in Table 2-12. In the nominal stress concept, the detail is classified geometry-independently in the fatigue strength of $\Delta\sigma_{C,nom} = 71 \text{ N/mm}^2$ and is thus neither dependent on the plate thickness t nor on the effective notch distance l (cf. Table 2-12). The classification therefore deviates from the division according to DIN EN 1993-1-9 [2] and prEN 1993-1-9 [4] and corresponds to the regulations of the IIW

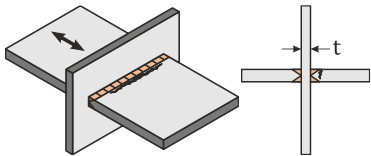
[3]. In addition, information is provided on how to manage influences caused by imperfections. These are discussed in Chapter 2.5.

Table 2-13: Fatigue resistance and structural stress concentrations according to Table 2-1 DNVGL-RP-C203 [66]

Fatigue resistance class	Assigned fatigue strength at 10 million load cycles [N/mm^2]	Calculated fatigue strength $\Delta\sigma_C$ at 6 million load cycles [N/mm^2]	Structural stress concentration factor (SCF) [-]
<i>E</i>	46.78	80	1.13
<i>F</i>	41.52	71	1.27

DNVGL-RP-C203 [66] deals with fatigue behaviour of offshore steel structures. However, the fatigue strengths are defined for a number of 10 million load cycles. The stress ranges $\Delta\sigma_C$ converted to 2 million load cycles are given for the detail categories *E* to *F* in the following Table 2-13. In addition, the stress concentration factors for the structural stress concept (cf. Chapter 2.4.5.2) are provided. According to DNVGL-RP-C203 [66], the associated structural stress σ_{hs} can be determined by multiplying the nominal stress σ_{nom} by the structural stress factor (SCF).

Table 2-14: Extract from Table A-8 on cruciform joints according to DNVGL-RP-C203 applying the nominal stress concept [66]

FAT	Structural detail	Description	Requirement
		Full penetration butt welded cruciform joint	Inspected and found free from significant defects. The detail category is given for: - Edge distance $\geq 10\text{ mm}$ - For edge distance $< 10\text{ mm}$ the detail category shall be downgraded with one S-N curve.
<i>E</i>	$t \leq 25\text{ mm}$		
<i>F</i>	$t > 25\text{ mm}$		

NOTES ON POTENTIAL MODES OF FAILURE

Failure in cruciform joints with full penetration welds will normally initiate at the weld toe. In joints made with load-carrying fillet or partial penetration butt welds, cracking may initiate either at the weld toe or propagate into the plate, or at the weld root and propagate through the weld. In welds parallel to the direction of the applied stress, however, weld failure is uncommon. In this case, cracks normally initiate at the weld end and propagate into the plate perpendicular to the direction of applied stress. The stress concentration is increased, and the fatigue strength is therefore reduced, if the weld end is located on or adjacent to the edge of a stressed member rather than on its surface.

DESIGN STRESSES

In the design of cruciform joints, which are not aligned, the stresses shall include the effect of any eccentricity. The maximum value of the eccentricity may normally be taken from the fabrication tolerances. The design stress may be obtained as the nominal stress multiplied by the stress concentration factor due to the eccentricity.

With regard to cruciform joints for offshore steel structures (cf. Table 2-14), a subdivision is made in DNVGL-RP-C203 [48] according to the thickness t of the intermediate plate. For $t \leq 25\text{ mm}$, the fatigue resistance class $FAT = E = 80\text{ N/mm}^2$ is assigned. If $t > 25\text{ mm}$, the fatigue class $FAT = F = 71\text{ N/mm}^2$ becomes relevant. The differentiation of cases according to the thickness t of the intermediate plate thus deviates from the classifications of the previously mentioned procedures. In addition,

the fatigue classes must be reduced by one class if an edge distance of $> 10 \text{ mm}$ is not satisfied. In addition, detailed information is given on possible modes of failure. These refer to both full penetration and non-full penetration welds as well as fillet welds under longitudinal and transverse loading. Furthermore, information is given on how to manage axial misalignments of cruciform joints (cf. Table 2-14). Reference is made to appropriate stress concentration factors.

2.4.5.2 Structural stress concept

In the guidelines for shipbuilding [45] and offshore structures [66], the linear stress extrapolation of surface stresses at defined reference points is applied. The guidelines preferentially address coarsely meshed shell models.

The tables detected for the nominal stress concept from DNVGL-CG-0129 [45] (cf. Table 2-12) additionally specify K -factors which allow the corresponding structural stress $\Delta\sigma_{hs}$ to be determined on the basis of the nominal stress $\Delta\sigma_{nom}$. This is achieved with the help of the following formula:

$$\Delta\sigma_{hs} = K \cdot \Delta\sigma_{nom} \quad (2-25)$$

In addition, imperfection coefficients for axial misalignment K_{me} and angular misalignment $K_{m\alpha}$ are specified for cruciform joints (cf. Table 2-12). These are analysed in Chapter 2.5.

2.4.6 Differences in the guidelines and normative regulations

In the following, the specifications from DIN EN 1993-1-9 [2], prEN 1993-1-9 [4] and from the guidelines of the IIW [3] are tabularly summarised for the nominal and structural stress concept with regard to cruciform joints with full penetration and without weld toes ground, as this dissertation focuses on these constructions (cf. Table 2-15).

Table 2-15: Fatigue classes in normative regulations and guidelines of the nominal and structural stress concept with regard to cruciform joints with full penetration without weld toes ground

	DIN EN 1993-1-9 [2]		Guidelines of the IIW [3]		prEN 1993-1-9 [4], prEN 1993-1-14 [14]	
	$\Delta\sigma_C$	Requirement	$\Delta\sigma_C$	Requirement	$\Delta\sigma_C$	Requirement
Nominal stress concept	80	$l \leq 50 \text{ mm}$	71	–	80	$l \leq 50 \text{ mm}$
	71	$50 < l \leq 80 \text{ mm}$			71	$50 < l \leq 80 \text{ mm}$
	63	$80 < l \leq 100 \text{ mm}$			63	$80 < l \leq 100 \text{ mm}$
	56	$100 < l \leq 120 \text{ mm}$			56	$100 < l \leq 120 \text{ mm}$
Structural stress concept	100	–	100	–	100	–

Differences are detected in the fatigue resistance classification of cruciform joints in the nominal stress concept according to the IIW [3], which can lead to uncertainties. In addition, the specifications of the normative regulations and guidelines differ in both the nominal and the structural stress concept with regard to the consideration of imperfections (cf. Chapter 2.5).

2.5 Imperfections

Inaccuracies in the fabrication of welded joints as well as intended imperfections may cause stress increases that can lead to an early component failure under fatigue loading [3]. Consequently, both manufacturing-related imperfections and intended imperfections must be considered in the assessment of welded joints.

In the conventional nominal stress concept (cf. Chapter 2.3.1), influences resulting from imperfections might be covered by safeties in the fatigue classes up to a certain normative specified limit. However, the extent to which imperfections are considered in the fatigue strength is not always apparent. Due to insufficient permitted imperfections, some details in crane and bridge construction cannot be adequately verified. [2]

To allow a more precise determination of the critical fatigue stresses, the structural stress concept (cf. Chapter 2.3.3) can be applied. Thus, eccentricities that exceed the limits of the nominal stress concept can also be considered. Due to the stress determination by means of FE analyses, the concept enables a direct calculation of the stress increases due to imperfections. In addition, the influence of misalignment can be included indirectly by a stress intensification factor through analytical formulae. Nevertheless, it is generally difficult to determine structural discontinuities with analytical methods, as suitable parametric formulae are rarely available. Therefore, the FEA usually is required.

For the consideration of imperfections, reasonable assumptions have to be made in any case. Since the structural stress is normally determined on the basis of an idealised and perfectly aligned FE model, misalignments must be explicitly modelled or applied by suitable stress concentration factors. This applies in particular to cruciform joints, as the influence from imperfections can be significant. The use of the maximum permissible manufacturer tolerances according to DIN EN 1090-2 [37] can hereby lead to uneconomical results. Therefore, this chapter will provide an overview of the possible approaches to consider geometric and material-specific imperfections in the analysis of structural stresses.

2.5.1 Cause of imperfections

Due to the idealisation of FE models in the structural stress concept, the dimensions may not correspond to the actual component geometry. This leads to inconsistent results between FE analyses and real experiments. The deviation between model and reality can be caused by possible geometric discontinuities. These can be caused by inaccuracies in the welding process respectively by welding distortions or can be deliberate as intended misalignments. In the case of axially loaded welds, these discontinuities can lead to negatively impacting secondary bending stresses and thus to early component failure. [67, 46]

Consequently, engineers responsible for the design of components subjected to fatigue loading always need to consider the type and degree of imperfections to be expected in the required stress calculations. For this purpose, the maximum permissible manufacturer's tolerances according to DIN EN 1090-2 [37] should provide an approximate reference value. The standard defines requirements for the design of steel structures to ensure a sufficient level of static load-bearing capacity and stability as well

as serviceability and fatigue strength. In addition, DIN EN ISO 5817 [68] provides information on evaluation groups of irregularities in fusion welded steel joints. However, not all possible imperfections can be assessed according to DIN EN 1090-2 [37] and DIN EN ISO 5817 [68]. Therefore, typical geometric imperfections of cruciform joints are examined in more detail below.

2.5.2 Possible imperfections

Depending on the design, different component imperfections can occur. According to the structural stress concept, both intended misalignments due to a structural joint itself and misalignments from the manufacturing process should be considered [4].

Angular misalignment can occur in cruciform joints due to welding distortion in the manufacturing process. This can be accentuated by unrelated bending of the ground plates. Inaccuracies in the welding process can also cause axial misalignment between the welded-on plates, which can lead to significant secondary bending stresses. Furthermore, rotations of the welded-on plates in longitudinal direction are possible. Both DIN EN 1090-2 [37] and DIN EN ISO 5817 [68] provide suitable information on axial and angular misalignment. Merely the rotation of the welded-on plates in longitudinal direction is not regulated by standards. In the following, possible imperfections of cruciform joints are identified. These can be present in different combinations and degrees. In addition, they have a correlating effect on each other.

2.5.2.1 Angular misalignment

Angular misalignment of the welded-on plates can be represented by a rotation around the global y -axis (cf. Figure 2-21). This angular misalignment is defined according to DIN EN ISO 6520-1 [69] and denoted with β according to DIN EN ISO 5817 [68]. The displacement is defined by the rotation around the transverse axis as illustrated below (cf. left side of Figure 2-21).

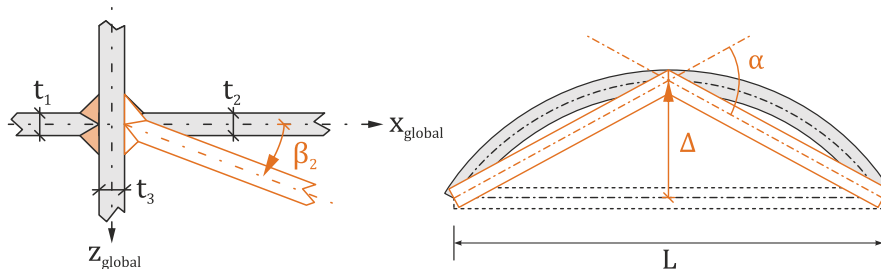


Figure 2-21: Potential angular misalignment β of cruciform joints (left) and Potential bending of plates for laterally unsupported components according to DIN 1090-2 [37] systematically for the FEA (right)

According to DIN EN ISO 6520-1 [69], angular misalignments of cruciform joints are declared with the reference number 508. In DIN EN ISO 5817 [68], the definition of the reference number is referred to as ordinal number. It specifies the maximum permissible angle β depending on the applied evaluation group. These evaluation groups characterise the quality of a weld based on the type, size and quantity of selected irregularities. Evaluation group B corresponds to the highest requirements for welds. According to this evaluation group, the maximum tolerance for welds is not permitted to exceed $\beta \leq 1^\circ$. By application of the evaluation group C, angular misalignments twice the size are allowed with $\beta \leq 2^\circ$. [68]

In addition, deflections may be detected from the manufacturing process of the plates. Since there is no restriction of bending by the construction, this can be modelled in a simplified way by separate sharp bends at the weld transitions. According to DIN EN 1090-2 [37], the resulting deviation from straightness Δ depends on an angle α for laterally not supported structural components (cf. right side of Figure 2-21). The calculation of the maximum permissible deflection of plates is given in [37]:

$$\Delta = \pm L/750 \quad (2-26)$$

Based on the simplified assumption that the welded-on plates are approximated with a continuous ground plate, the length-independent maximum permissible angle α for cruciform joints is thus obtained according to the following formula and results in $\alpha = 0.3^\circ$.

$$\alpha = 2 \cdot \tan^{-1}\left(\frac{L}{\frac{750}{L}}\right) = 0.30^\circ \quad (2-27)$$

Angular misalignments from welding distortion and bending of plates approximated by sharp bends at the weld transitions are particularly critical in cruciform joints. This is especially true if the component is to be tested by a testing machine, as large additional stresses result from the clamping process.

2.5.2.2 Axial misalignment

For cruciform joints, axial misalignment is defined as the relative offset in the global z -direction between the welded-on plates (cf. Figure 2-22). According to DIN EN 1090-2 [37], a permissible manufacturer's tolerance for axial misalignment of half the thickness of the welded-on plate is specified with $e = \pm t/2$. Analogous to angular misalignments, significantly higher structural stresses result with axial misalignment under clamping conditions in testing machines than with practically encountered support conditions.

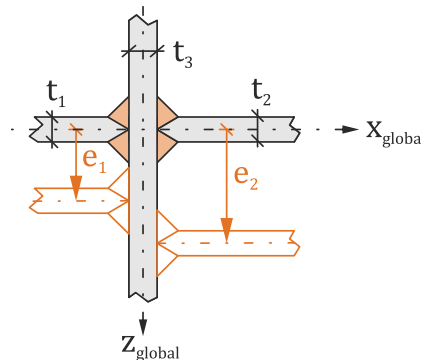


Figure 2-22: Potential axial misalignment e of cruciform joints

2.5.2.3 Rotation

In addition to the imperfections mentioned so far, a rotation of the welded-on plates around their global x -axis is also possible (cf. Figure 2-23). This torsion of the plates around their longitudinal axis is defined in this thesis with the variable θ . There are currently no normative regulations or guidelines with regard to this imperfection.

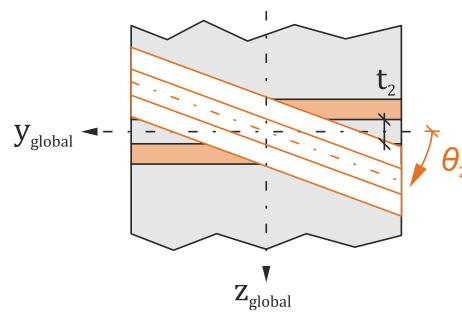


Figure 2-23: Rotation of the welded-on plates around the global x -axis

2.5.3 Imperfections in normative regulations and guidelines

The approach to possible influences caused by imperfections differs significantly in the normative regulations and guidelines. There are two possibilities for taking imperfections into account. These can be explicitly analysed in the FE model or indirectly determined by suitable analytical stress concentration factors, which are then subjected to the stresses of the perfect FE model (cf. Chapter 2.5.3.2).

In this regard, a certain extend of imperfections can already be accounted for by means of normatively reduced fatigue strengths. This is only the case with axial misalignments of cruciform joints and is not equally pursued in normative regulations and guidelines. However, if the influence is greater than the stresses accounted for, these imperfections must be fully included in the stress determination. The same applies if no influence is considered in the fatigue class of the applied normative regulation or guideline.

In order to provide a safe and simultaneously economical fatigue verification, the influences from imperfections already accounted for in reduced fatigue resistances must be identified. Therefore, the following Chapter 2.5.3.1 will provide an overview of how influences from geometric and material-specific imperfections are to be considered in the fatigue analysis. For this purpose, the respective specifications of the normative regulations of DIN EN 1993-1-9 [2], prEN 1993-1-9 [4] and prEN 1993-1-14 [14] as well as the guidelines of the IIW [3] are analysed in detail and compared with each other.

2.5.3.1 Considered imperfections on the resistance side

In DIN EN 1993-1-9 [4], prEN 1993-1-9 [4] and prEN 1993-1-14 [14] as well as in the guidelines of the IIW [3], influences from imperfections are already partly taken into account by the fatigue resistances in the nominal as well as in the structural stress concept. These influences are subsequently analysed in more detail, separately by the normative regulations and guidelines.

2.5.3.1.1 DIN EN 1993-1-9

With regard to component tolerances, the current DIN EN 1993-1-9 [2] generally refers to EN 1090 [37] and to additional information in the tables of the structural details. In the fatigue class catalogues regarding the nominal stress concept for cruciform joints (cf. Table 2-5 in Chapter 2.4.1.1), it is explicitly stated that the imperfections are not permitted to exceed the tolerances according to EN 1090-2 [37]. Furthermore, the maximum permissible axial misalignment e is limited to $e \leq 15\%$ of the thickness of the intermediate plate $t_{intermediate\ plate}$. Consequently, stress increases of 15%, due to

axial offset, are already covered by the fatigue resistance within the nominal stress concept. According to Note 1 of Table 2-6 (cf. Chapter 2.4.3.2), the fatigue classes of the structural stress concept with regard to cruciform joints do not include any stress increases due to misalignment. Unlike the nominal stress concept, these must be explicitly considered in the FEA to the full extent when determining the structural stress. No further specifications are provided in DIN EN 1993-1-9 [2] on the procedure for dealing with imperfections.

2.5.3.1.2 Guidelines of the IIW

The guidelines of the IIW [3] define misalignment as imperfections that may be detected as a result of detail design or fabrication. In the fatigue class catalogues for the nominal stress concept, the maximum permissible axial misalignment of cruciform joints is limited to 15 % of the primary plate thickness (cf. Table 2-7 in Chapter 2.4.2.1). It is not specified whether the thickness of the welded-on plates $t_{welded-on\ plates}$ or the thickness of the intermediate plate $t_{intermediate\ plate}$ of cruciform joints is meant to be the primary plate thickness. But based on the designation, it is assumed to refer to the thickness $t_{welded-on\ plates}$.

In addition, Chapter 3.8.2 of the guidelines [3] provides further information on how to handle influences from imperfections. The specifications refer to the nominal stress concept as well as to the structural and effective notch stress concept. It is stated that when applying the nominal stress concept according to the IIW [3], a defined stress concentration factor $k_{m,already\ covered}$ is already considered in the fatigue resistance of cruciform joints. This factor is integrated in the form of resulting secondary bending stresses. The handling of the corresponding effective stress concentration factor $k_{m,eff}$ is described in more detail in the following Section 2.5.3.2. An extract of table 3.20 of the IIW [3] with regard to cruciform joints is presented in Table 2-16.

Table 2-16: Extract from Table 3.20 of the IIW [3] on specifications for stress concentration factors due to imperfections

	$k_{m,already\ covered}$ already covered in FAT class of nominal stress concept	$k_{m,already\ covered}$ already covered in S-N curves of structural and effective notch stress method	Effective default resp. minimum value $k_{m,eff,default}$ for structural and effective notch stress method
Cruciform joints	1.45	1.05	1.40 *

* but not more than $(1 + 2,5 \cdot e_{max}/t)$, where e_{max} = permissible misalignment and t = wall thickness of loaded plate = $t_{welded-on\ plates}$ in this thesis

For cruciform joints according to the IIW [3], the nominal stress concept already covers $k_{m,already\ covered} = \Delta\sigma_{R,imperfect}/\Delta\sigma_C \leq 1.45$ concentrated stresses due to misalignment (cf. Table 2-16). When applying the structural stress or effective notch stress concept, effects caused by misalignment are already covered by the specified stress concentration factor $k_{m,already\ covered}$ as well (cf. Note 1 of Table 2-8 in Chapter 2.4.2.2). This factor is specified in Table 3.20 of the IIW [3] as $\Delta\sigma_{R,imperfect}/\Delta\sigma_C \leq 1.05$ (cf. Table 2-16). Only if $k_{m,already\ covered}$ is exceeded, all imperfections must be explicitly considered in the stress determination. In addition, an effective default respectively minimum value $k_{m,eff,default}$ is specified in Table 2-16. However, its

application is insufficiently specified in the guidelines [3]. This effective minimum value is analysed in more detail in Section 2.5.3.2. [70]

2.5.3.1.3 prEN 1993-1-9 and prEN 1993-1-14

PrEN 1993-1-9 [4] introduces a distinction between misalignments. The differentiation is made between "imperfections caused by the manufacturing process" and "eccentricities resulting from an offset of joints". Further details are given in prEN 1993-1-14 [14]. In the structural stress concept, imperfections that generate a stress increase of up to 5 % are already covered by the fatigue resistance [14]. If the influence due to imperfections exceeds this limit, reference is made to the procedures of the guidelines of the IIW [3]. In addition, in prEN 1993-1-9 [4] is stated that axial misalignment e , due to manufacturing inaccuracies, may be neglected to an extent of $e \leq 0,15 \cdot t_{intermediate\ plate}$. Thus, the equivalent influence must already be covered by the fatigue resistance of the structural stress concept regarding cruciform joints. This differs from DIN EN 1993-1-9 [2], as the currently valid standard [2] requires all imperfections to be included in the stress determination.

The additional reference in the fatigue class catalogue of the structural stress concept to Section B.3.2(9) [4] (cf. Table 2-11 in Chapter 2.4.3.2) leads to the remark that macro-geometric effects not covered by the detail category must be calculated directly by the FE analysis or taken into account indirectly by stress concentration factors k_f from Annex D [4] or from appropriate literature. It cannot be assumed in this regard that the manufacturer's tolerances according to DIN EN 1090-2 [37] are already covered by the fatigue resistance. However, Section B.3.2(9) [4] points out that the structural stress calculation should only consider the extent of imperfections that exceed the more adverse tolerances from the detail category and from the specifications of DIN EN 1090-2 [37]. This excludes the axial misalignment of welded constructions, which is to be applied with its full extent.

2.5.3.1.4 Summary

The following Table 2-17 systematically summarises the information on misalignment provided by the normative regulations and guidelines just described. It becomes evident that there are significant differences in the way imperfections are approached.

Table 2-17: Stress concentration due to imperfections already considered in the fatigue resistances of cruciform joints

	DIN EN 1993-1-9 [2]	Guidelines of the IIW [3]	prEN 1993-1-9 [4], prEN 1993-1-14 [14]
Nominal stress concept	no misalignment outside of EN 1090 is permitted and / or $e \leq 0.15 \cdot t_{intermediate\ plate}$	$\Delta\sigma_{R,imperfect}/\Delta\sigma_C \leq 45\%$ and / or $e \leq 0.15 \cdot t_{welded-on\ plates}$	$e \leq 0.15 \cdot t_{intermediate\ plate}$
Structural stress concept	no effect due to misalignment is covered by fatigue resistance	$\Delta\sigma_{R,imperfect}/\Delta\sigma_C \leq 5\%$	$\Delta\sigma_{R,imperfect}/\Delta\sigma_C \leq 5\%$ and / or $e \leq 0.15 \cdot t_{intermediate\ plate}$

2.5.3.2 Imperfections considered by a stress concentration factor

As already stated, the direct consideration of the influence of geometric imperfections can be achieved by using finite element analysis. This results in a large modelling and calculation effort and requires a high degree of expertise for the correct representation of possible misalignments. However, exact effects due to imperfections can be accurately determined, which is particularly beneficial for complex constructions. The corresponding stress concentration factor $k_{m,direct}$, directly assessed in the FE model, is identified by the ratio of the fatigue stress of the imperfect model $\Delta\sigma_{R,FEA,imperfect}$ to the stress of the perfect FE model $\Delta\sigma_{R,FEA,perfect}$.

$$k_{m,direct} = \frac{\Delta\sigma_{R,FEA,imperfect}}{\Delta\sigma_{R,FEA,perfect}} \quad (2-28)$$

Since structural stresses are generally determined with idealised and therefore perfectly aligned FE models, imperfections that exceed the stress increases covered by the fatigue resistance can also be considered indirectly. In order to determine the required stress concentration factor $k_{m,indirect}$, the guidelines of the IIW [3], inter alia, tabularly specify analytical values for different types of imperfections and support conditions (cf. Section 2.5.3.2.1) [6]. In addition, DNVGL [66] (cf. Section 2.5.3.2.2), BS7910 [71] (cf. Section 2.5.3.2.3) as well as Xing and Dong [5] (cf. Section 2.5.3.2.4 and Section 2.5.3.2.5) provide methods for the indirect determination of stress-increasing effects resulting from imperfections. Thus, the misaligned geometry does not have to be analysed by extensive FE calculations.

For the correct determination of the stress-increasing effects, an effective stress concentration factor $k_{m,eff}$ is required. In order to calculate this relevant factor, the already covered influences due to imperfections in the fatigue resistance $k_{m,already\ covered}$ (cf. Chapter 2.5.3.1) must be divided out of the directly or indirectly assessed k_m values. By this method, an overestimation of the influences is avoided. Section 3.8.2 of the guidelines of the IIW [3] provides a possible approach to estimate the influence of imperfections by means of this analytical effective stress concentration factor $k_{m,eff,direct/indirect}$. Formula (2-29) of the IIW [2] was developed for this purpose.

$$k_{m,eff,direct/indirect} = \frac{k_{m,direct/indirect}}{k_{m,already\ covered}} \quad (2-29)$$

Depending on the weld design and type, additional effective default values $k_{m,eff,default}$ are provided according to Table 2-16, which must satisfy a specified limit value (cf. remark in Table 2-16). Since the guidelines of the IIW [3] do not specify the application of $k_{m,eff,default}$, the procedure of Taras [70] is consulted. In [70], the information of the IIW [3] is interpreted that the effective default value $k_{m,eff,default}$ is always to be considered. This also applies if the significant fatigue stress is determined by a FE model which includes imperfections. According to [70], the effective default value given in Table 2-16 represents the maximum applicable value for $k_{m,eff,default}$. However, it is limited according to the defined limit value (cf. remark in Table 2-16). The default value must always be considered when determining $k_{m,eff,default}$.

For cruciform joints, this effective default value $k_{m,eff,default}$ satisfying the defined limit value depends on the plate thickness $t_{welded-on\ plates}$ of the loaded plates as well as on

the maximum eccentricity e_{max} permitted by manufacturer tolerances. The source of the maximum permitted eccentricity is not further specified according to the IIW [3]. Consequently, the minimum value results as follows. [70]

$$k_{m,eff,default} = 1 + 2.5 \cdot e_{max}/t_{welded-on plates} \leq 1.40 \quad (2-30)$$

If no axial misalignment is permitted, the maximum allowable eccentricity equals $e_{max} = 0$. In this case, no stress intensification is required, as the default value to be applied is calculated as $k_{m,eff,default} = 1.0$. The maximum permitted default value $k_{m,eff,default} = 1.40$ (cf. Table 2-16) results in this respect at an eccentricity of approximately $e_{max} \approx 0.15 \cdot t_{welded-on plates}$. Larger values for $k_{m,eff,default}$ are not allowed. Consequently, according to the IIW [3], it is essential to define a limit value e_{max} for axial misalignment of cruciform joints. In the structural stress determination, the corresponding standard value $k_{m,eff,default}$ is then required as a minimum. [70]

According to Taras [70], the data of the IIW [3] are further interpreted that the effective stress concentration factor $k_{m,eff,direct/indirect}$ determined for misaligned cruciform joints has to be collated with the effective default value $k_{m,eff,default}$. If the effective stress concentration factor $k_{m,eff,direkt/indirekt}$ is smaller than the calculated effective default value $k_{m,eff,default}$, the latter must be used for the design. The evaluation is then independent of the actually identified stress concentration factor $k_{m,eff,direkt/indirekt}$. The factor $k_{m,eff}$ is consequently obtained according to Formula (2-31).

$$k_{m,eff} = \begin{cases} k_{m,eff,default}, & k_{m,eff,direct/indirect} \leq k_{m,eff,default} \\ k_{m,eff,direct/indirect}, & k_{m,eff,direct/indirect} > k_{m,eff,default} \end{cases} \quad (2-31)$$

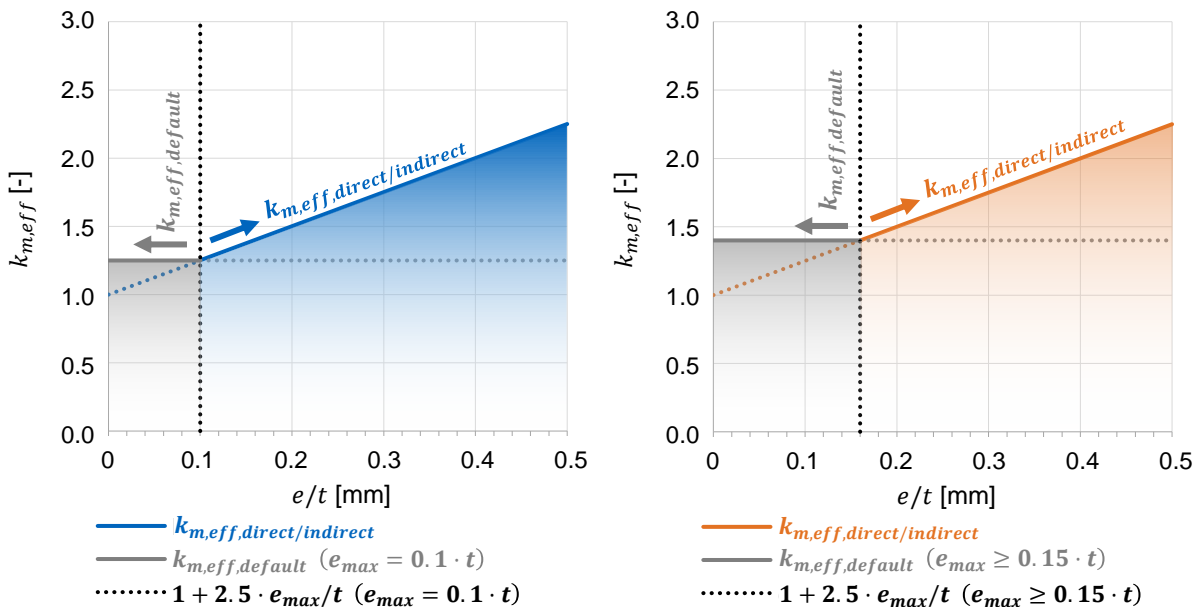


Figure 2-24: Determination of the effective stress concentration factor $k_{m,eff}$ for permitted axial misalignment of $e_{max} = 0.1 \cdot t_{welded-on plates}$ (left) and $e_{max} \geq 0.15 \cdot t_{welded-on plates}$ (right)

To visualise the proposed procedure, Figure 2-24 illustrates the significant effective stress concentration factors $k_{m,eff}$ for permissible axial misalignment of $e_{max} = 0.1 \cdot t_{welded-on plates}$ (cf. left side of Figure 2-24) and $e_{max} \geq 0.15 \cdot t_{welded-on plates}$ (cf. right

side of Figure 2-24), whereby the standard value $k_{m,eff,default} = 1.40$ is always relevant for the latter. In order to consider influences due to imperfections, the effective stress concentration factor $k_{m,eff}$ can either be applied to reduce the fatigue strength $\Delta\sigma_C$ according to Formula (2-32) or to increase the effective stress $\Delta\sigma_{R,perfect}$ assessed at a perfect FE model by Formula (2-33).

$$\Delta\sigma_{C,imperfect} = \frac{\Delta\sigma_C}{k_{m,eff}} \quad (2-32)$$

$$\Delta\sigma_{R,imperfect} = \Delta\sigma_{R,perfect} \cdot k_{m,eff} \quad (2-33)$$

However, a modification of the fatigue resistance is not recommended at this point, since in accordance to [9] stress increases only apply to the ratio of membrane stresses σ_m and not bending stresses σ_b (cf. Figure 2-12).

Consequently, imperfections should be considered according to the following Formula (2-34) to avoid an additional increase of already contained bending stresses σ_b .

$$\Delta\sigma_{R,imperfect} = \sigma_m \cdot k_{m,eff} + \sigma_b \quad (2-34)$$

Including the default value $k_{m,eff,default}$ specified in the IIW [2], the applied fatigue stress range $\Delta\sigma_{R,imperfekt}$ required for the structural stress verification results as follows.

$$\Delta\sigma_{R,imperfect} = \begin{cases} \sigma_m \cdot k_{m,eff,default} + \sigma_b, & k_{m,eff} \leq k_{m,eff,default} \\ \sigma_m \cdot k_{m,eff} + \sigma_b, & k_{m,eff} > k_{m,eff,default} \end{cases} \quad (2-35)$$

In the following sections, procedures for the indirect consideration of influences from imperfections are presented. This is done separately according to normative regulations and guidelines of the IIW [2] (cf. Section 2.5.3.2.1), DNVGL [66] (cf. Section 2.5.3.2.2), BS7910 [71] (cf. Section 2.5.3.2.3) as well as Xing and Dong [5] (cf. Section 2.5.3.2.4 and Section 2.5.3.2.5). The application of the $k_{m,indirect}$ values needs to be done according to the methodology just presented. In order to keep the following contents straightforward, $k_{m,indirect}$ is replaced by means of $k_{m,axial}$ and $k_{m,angular}$ according to the specifications from the literature on axial and angular misalignment.

2.5.3.2.1 k_m -factors in the guidelines of the IIW

With regard to cruciform joints, formulae for the analytical determination of the influence of axial and angular misalignment are given in the IIW [3]. These are based on the assumption of two plane welded-on plates with the identical thickness t , subjected strictly to axial tensile loading. The formulae recommended by Hobbacher [3] are based on a two-dimensional stress analysis and are intended for the calculation of indirect stress concentration factors $k_{m,axial}$ and $k_{m,angular}$ of misaligned welded joints. The relevant extract from Table 6.5 of the IIW [3] is presented in Table 2-18. According to IIW [3], the left plate is defined as plate 1 with a length of l_1 and a thickness of t_1 and the right plate as plate 2 with a length of l_2 and a thickness of t_2 . This is important to note as the definitions in the normative codes and guidelines are not uniform. The additional classifications (a) to (k) provided are necessary for a later comparison and are derived in accordance with Xing and Dong [5] from Table 2-23.

Table 2-18: Extract from Table 6.5 of the IIW [3] on axial and angular misalignment of cruciform joints

Stress concentration factors k_m for axial misalignment e ($k_{m,axial}$) and angular misalignment α ($k_{m,angular}$)

(a) – (f)		$k_{m,axial} = 1 + \lambda \cdot \frac{e \cdot l_1}{t \cdot (l_1 + l_2)}$ <p>λ varies from $\lambda = 3$ with full restraint to $\lambda = 6$ with no restraint. For unrestrained remotely loaded joints assume: $l_1 = l_2$ and $\lambda = 6$. Valid for $l_1 \leq l_2$</p>
(g) – (k)		$k_{m,angular} = 1 + \lambda \cdot \alpha \cdot \frac{l_1 \cdot l_2}{t \cdot (l_1 + l_2)}$ <p>If the in-plane displacement of the intermediate plate is restricted, λ varies from $\lambda = 0.02$ to $\lambda = 0.04$. Otherwise λ varies from $\lambda = 3$ to $\lambda = 6$.</p>

Axial misalignment

In contrast to the calculation of k_m -factors for angular misalignment between flat plates according to [3], the straightening effect of the structure is not considered regarding cruciform joints. Consequently, the reduction of misalignment due to straightening of joints under tensile load is disregarded. Therefore, only the length of the welded-on plates l_i , the plate thickness t and the support condition of the structure are relevant for the determination of the influences. The latter is defined by a support factor λ . In investigations of axial misalignment, the shorter plate length of the welded-on plates is always defined as l_1 by the specification $l_1 \leq l_2$ (cf. Table 2-23). The stress concentration factor $k_{m,axial}$ results for an axial misalignment e as follows:

$$k_{m,axial} = 1 + \lambda \cdot \frac{e \cdot l_1}{t \cdot (l_1 + l_2)} \quad (2-36)$$

For cruciform joints with axial misalignment the support factor λ is estimated according to Table 2-23. With no restraint, $\lambda = 6$ applies. In this context, the corresponding factor can also be derived analytically. For a statically determined system (a) with axial misalignment, articulated welded-on plates and without any support of the intermediate plate, the support factor λ can simply be derived according to Table 2-19.

Table 2-19: Derivation of the λ -factor for a statically determined cruciform joint with axial misalignment

Derivation of the λ -factor for case (a)

(a)		$\sum H = 0: A_h = -\Delta F$ $\sum M_A = 0: B_v = \frac{\Delta F \cdot e}{l_1 + l_2} = -A_v$ $M_{i-i} = \frac{\Delta F \cdot e \cdot l_2}{l_1 + l_2}$ $\sigma = \sigma_m + \sigma_b = \sigma_m + \frac{M_y}{I_y} \cdot z = \frac{\Delta F}{t \cdot b} + \frac{\frac{\Delta F \cdot e \cdot l_2}{l_1 + l_2}}{\frac{b \cdot t^3}{12}} \cdot \left(\frac{t}{2}\right) = \frac{\Delta F}{t \cdot b} + \frac{6 \cdot \Delta F \cdot e \cdot l_1}{(l_1 + l_2) \cdot t}$ $\sigma = \sigma_m \cdot \left(1 + 6 \cdot \frac{e \cdot l_1}{(l_1 + l_2) \cdot t}\right)$ $k_{m,axial} = 1 + \lambda \cdot \frac{e \cdot l_1}{t \cdot (l_1 + l_2)} \rightarrow \lambda = 6$
-----	--	---

However, if the displacement is restrained, the support factor λ decreases to $\lambda = 3$ (cf. Table 2-23). In this regard, the guidelines of the IIW [3] do not specify which type of restraint is relevant. This could refer to the welded-on plates as well as to the intermediate plate.

Angular misalignment

In addition, Table 2-23 illustrates the influence of angular misalignment α . The following formula is recommended in order to calculate the corresponding factor $k_{m,angular}$:

$$k_{m,angular} = 1 + \lambda \cdot \alpha \cdot \frac{l_1 \cdot l_2}{t \cdot (l_1 + l_2)} \tag{2-37}$$

In the indirect determination of influences from angular misalignment, the type of support is also decisive and is defined by the support factor λ . In contrast to the conditions regarding axial misalignment, the support factor is additionally specified with $\lambda = 0.02$ and $\lambda = 0.04$, if the displacement of the intermediate plate is to be restrained. Further guidance of the IIW [3] on how to approach the λ -values is missing in this context.

Table 2-20: Derivation of the λ -factor for a statically determined cruciform joint with angular misalignment

Derivation of the λ -factor for case (g)	
	$\sum H = 0: A_h = -\Delta F$ $\sum M_A = 0: B_v = \frac{\Delta F \cdot \tan\left(\frac{\alpha}{2}\right) \cdot (l_1 - l_2)}{l_1 + l_2} = -A_v$ $M_{i-i} = -\Delta F \cdot \tan\left(\frac{\alpha}{2}\right) \cdot l_2 + \frac{\Delta F \cdot \tan\left(\frac{\alpha}{2}\right) \cdot (l_2 - l_1)}{l_2 + l_1} \cdot l_2 = \frac{2 \cdot \Delta F \cdot \tan\left(\frac{\alpha}{2}\right) \cdot l_1 \cdot l_2}{l_2 + l_1}$ <p>with small-angle approximation: $\tan\left(\frac{\alpha}{2}\right) = \frac{\alpha}{2}$:</p> $M_{i-i} = \frac{2 \cdot \Delta F \cdot \frac{\alpha}{2} \cdot l_1 \cdot l_2}{l_2 + l_1}$ $\sigma = \sigma_m \cdot \left(1 + 6 \cdot \alpha \cdot \frac{l_1 \cdot l_2}{(l_1 + l_2) \cdot t}\right)$ $k_{m,angular} = 1 + \lambda \cdot \alpha \cdot \frac{l_1 \cdot l_2}{t \cdot (l_1 + l_2)} \rightarrow \lambda = 6$

It is also possible to analytically determine the support factor λ for the statically determined system (g) with angular misalignment shown in Table 2-20.

If axial and angular misalignment exist, they must be considered in combination according to the guidelines of the IIW [3] using the following Formula (2-38).

$$k_m = 1 + (k_{m,axial} - 1) + (k_{m,angular} - 1) \tag{2-38}$$

2.5.3.2.2 k_m -factors in DNVGL

In addition, DNVGL-RP-C203 [66] (cf. Chapter 2.4.5) provides information on a stress concentration factor regarding cruciform joints with axial misalignment. However, the specifications are limited to details with articulated welded plates as well as an articulated intermediate plate according to system (d) of Table 2-23. In contrast to the IIW [3], in DNVGL-RP-C203 [66] the definitions of the load-bearing main plates are

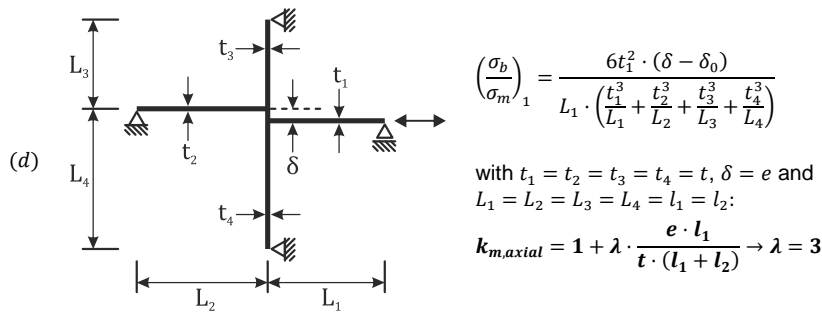
reversed. The right plate is therefore defined as plate 1. In order to take the different definition into account, the associated lengths are denoted with L_i instead of l_i in this thesis. In addition, the plate lengths and thicknesses of the intermediate plate are introduced as plate 3 and plate 4. When approaching axial misalignment, the S-N curves for cruciform joints of [66] already include some effects of misalignment δ_0 equal to $\delta_0 = 0.15 \cdot t_1$. The difference between δ and δ_0 thus corresponds to the procedure of the IIW [3] with regard to $k_{m,already\ covered}$ and $k_{eff,default}$ (cf. Chapter 2.5.3.2). According to [66], the stress concentration factor is determined by the ratio of the secondary bending stress σ_b and the existing membrane stress σ_m . Consequently, in order to remain in conformity with stress concentration factor k_m of the guidelines of the IIW [3], the following applies:

$$k_m = 1 + \left(\frac{\sigma_b}{\sigma_m} \right) \quad (2-39)$$

The following Table 2-21 summarises the procedure of DNVGL-RP-C203 [66]. In this regard, the notation for the stress concentration factor k_m , the support parameter λ and the lengths l_i are additionally adapted in accordance with the guidelines of the IIW [3]. Due to the geometric boundary conditions, the support factor λ transitions into a factor that also considers the influence of the intermediate plate. It can be seen that this geometric factor is $\lambda = 3$ for articulated supports. This corresponds to the specifications of the IIW [3].

Table 2-21: Specifications on imperfections of cruciform joints according to DNVGL-RP-C203 [66]

Cruciform joint with axial misalignment and articulated support conditions



In addition to DNVGL-RP-C203 [66] specifications for the evaluation of cruciform joints with axial misalignment, information on angular misalignment is not provided.

DNVGL-CG-0129 [45] also provides information on misalignment. However, the stress concentration factor K_m due to axial and angular misalignment is defined as the ratio of the hot-spot stress range $\Delta\sigma_{R,hs}$ to the nominal stress range $\Delta\sigma_{R,nom}$ according to the following formula. This differs from the other methods presented, in which the stress concentration factor according to Formula (2-34) refers to the defined stress increase within a concept. [57]

$$K_m = \frac{\Delta\sigma_{R,hs}}{\Delta\sigma_{R,nom}} \quad (2-40)$$

According to Table 2-12, in case of angular misalignment, reference is made to another

detail. In accordance with the corresponding information, the effects from angular misalignment can be determined with K_{me} according to the following formula.

$$K_{m\alpha} = 1 + \frac{\lambda}{4} \cdot \alpha \cdot \frac{(l_1 + l_2)}{t} \quad (2-41)$$

Nevertheless, the evaluation of angular misalignment differs only slightly from the guidelines of the IIW [3] and is slightly more conservative. The associated support parameter is specified as $\lambda = 6$ for articulated supports and $\lambda = 3$ for restrained ends of the load-bearing welded-on plates. In this context, the influence of axial misalignment K_{me} and angular misalignment $K_{m\alpha}$ is combined into a stress concentration factor K_m according to [3] with the formula below (cf. Table 2-12).

$$K_m = K_{me} + K_{m\alpha} - 1 \quad (2-42)$$

As presented in Chapter 2.4.5, the fatigue class catalogues from [45] already define fixed values for K_{me} and $K_{m\alpha}$ (cf. Table 2-12). Regarding cruciform joints, $K_{me} = 1.45$ and $K_{m\alpha} = 1.0$ are specified. In addition, it is noted that the axial misalignment e is limited to $e_0 \leq 0.3 \cdot t_1$. If deviating values for axial misalignment are to be expected, both the factor K_m and the fatigue strength FAT must be modified with $K_{m,mod} = K_m \cdot K_{me,mod}/K_{me}$ and $FAT_{mod} = FAT \cdot K_{me}/K_{me,mod}$. The corresponding axial misalignment is obtained according to DNVGL-CG-0129 [45] according to the following formula and is limited to $t_1 \leq t_2$.

$$e = \frac{t_1}{2} + e_0 - \frac{t_2}{2} \quad (2-43)$$

In addition, [45] provides information on case (d) from DNVGL-RP-C203 [66], which has already been presented. The specifications of DNVGL-CG-0129 [45] are consistent with the indications of Table 2-21.

2.5.3.2.3 k_m -factors in the BS 7910

Furthermore, BS 7910 [71] provides guidance on how to approach imperfections of cruciform joints. Both axial and angular misalignment is analysed for this purpose. The factor for the support conditions is defined as κ instead of λ in [71]. The length definitions l_i and thickness definition t correspond to the specifications of the IIW [3]. The following Table 2-22 summarises the information and converts it into the notation of IIW [3]. The specifications of the BS 7910 [71] for cruciform joints with axial misalignment are only valid for details with $l_1 \leq l_2$. This corresponds to the regulations of the IIW [3]. In this context, BS 7910 [71] states clearly that the factor for the support condition λ of the IIW [3] must be dependent on the support condition of the intermediate plate regarding cruciform joints with axial misalignment. However, in case (c) with a singly restrained and a singly articulated welded-on plate without support of the intermediate plate, $\lambda = 6.75$ exceeds the specified range of $3 \leq \lambda \leq 6$ defined in the guidelines of the IIW [3].

With regard to angular misalignments, the information on the support factor λ of the IIW [3] can be extended. In the case of restrained displacement of the intermediate plate, support factors $0.02 \leq \lambda \leq 0.04$ are also assumed for cases (i) and (k) of the BS 7910 [71]. Nonetheless, case (j) with restrained ends of the welded-on plates and restrained

but longitudinally displaceable intermediate plate leads to a support factor of $\lambda = 3$. This deviates significantly from the specifications of the IIW [3] with $0.02 \leq \lambda \leq 0.04$.

Table 2-22: Specifications for misalignment of cruciform joints according to BS 7910 [71]

Cruciform joints with axial misalignment	
	$\left(\frac{\sigma_b}{\sigma_m}\right) = \frac{\kappa \cdot e \cdot l_1}{t \cdot (l_1 + l_2)}$ <p>with $l_1 \leq l_2$ and $\kappa = \lambda$:</p> $k_{m,axial} = 1 + \lambda \cdot \frac{e \cdot l_1}{t \cdot (l_1 + l_2)}$ <p>→ (a) $\lambda = 6.00$ → (c) $\lambda = 6.75$ → (d, f) $\lambda = 3.00$ → (e) $\lambda = 2.95$</p>
Cruciform joints with angular misalignment	
	$\left(\frac{\sigma_b}{\sigma_m}\right) = \frac{\kappa \cdot \alpha \cdot l_1 \cdot l_2}{t \cdot (l_1 + l_2)}$ <p>with $\kappa = \lambda$:</p> $k_{m,angular} = 1 + \lambda \cdot \alpha \cdot \frac{l_1 \cdot l_2}{t \cdot (l_1 + l_2)}$ <p>→ (g) $\lambda = 6.00$ → (i) $\lambda = 0.02$ → (j) $\lambda = 3.00$ → (k) $\lambda = 0.04$</p>

2.5.3.2.4 k_m -factors by Xing and Dong

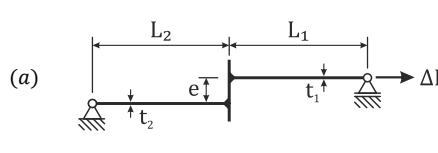
Additionally, Xing and Dong [5] provide further analytical solution methods for the evaluation of influences due to misalignment. With the law of conservation of energy, calculation methods are proposed based on Castigliano's second theorem. In this context, support conditions and stress situations are explicitly described. The cases according to [5] are presented in the following. In addition, the support factor λ is calculated according to the guidelines of the IIW [3]. This is realised for constant thicknesses $t_1 = t_2 = t_3 = t_4 = t$ and identical lengths $L_1 = L_2 = L_3 = L_4 = L$. To ensure reasonable comparability between the analysed approaches, the defined indices of the components must be consistent. While the IIW [3] and the BS 7910 [71] assign index "1" to the left plate, this applies to the right plate according to Xing and Dong [5]. Consequently, the notation corresponds with L_i to DNVGL-RP-C203 [66]. By this selective simplification of the relevant boundary conditions, it is therefore possible to provide a comparison to the specifications of the IIW [3] in order to obtain general formulations. The results are separately presented below for axial and angular misalignment.

Axial misalignment

Table 2-23 presents investigations from [5] on cruciform joints with axial misalignment and with different support conditions of the welded-on plates and the intermediate plate. In all cases, the subjected fatigue load is applied at the end of plate 1 as a tensile load. The varying systems are assigned classifications (a) to (f) in order to allow a well-defined identification.

Table 2-23: Investigations on axial misalignment of cruciform joints with varying support conditions

Cruciform joint, axial misalignment, articulated ends of load-bearing plates, no support of intermediate plate

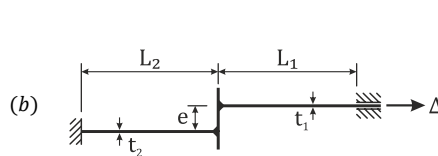


$$\left(\frac{\sigma_b}{\sigma_m}\right)_i = \left(\frac{6L_i t_i}{(L_1 + L_2) \cdot t_i^2}\right) \cdot e, i = 1,2$$

with $t_1 = t_2 = t$ and $L_1 = L_2 = L_i$:

$$k_{m,axial} = 1 + \lambda \cdot \frac{e \cdot L_1}{t \cdot (L_1 + L_2)} \rightarrow \lambda = 6$$

Cruciform joint, axial misalignment, restrained ends of load-bearing plates, no support of intermediate plate

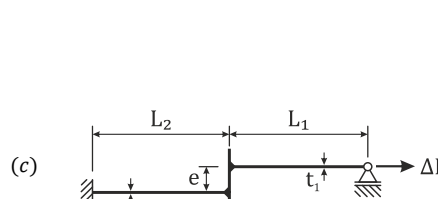


$$\left(\frac{\sigma_b}{\sigma_m}\right)_i = \left(\frac{6t_i L_1 L_2 t_i \cdot \left(4 \cdot \frac{L_i^3 t_i^3 t_i^3}{t_i^3} + 3 \cdot \frac{L_i L_1 L_2 t_i^3 t_i^3}{t_i^3} + \frac{L_1^3 L_2^3 t_i^3}{L_i^3}\right)}{L_i \cdot \left(L_1^4 t_i^6 + 4L_1^3 L_2 t_i^3 t_i^3 + 6L_1^2 L_2^2 t_i^3 t_i^3 + 4L_1 L_2^3 t_i^3 t_i^3 + L_2^4 t_i^6\right)}\right) \cdot e, i = 1,2$$

with $t_1 = t_2 = t_i = t$ and $L_1 = L_2 = L_i$:

$$k_{m,axial} = 1 + \lambda \cdot \frac{e \cdot L_1}{t \cdot (L_1 + L_2)} \rightarrow \lambda = 6$$

Cruciform joint, axial misalignment, one-sided restrained end and one-sided articulated end of load-bearing plates, no support of intermediate plate



$$\left(\frac{\sigma_b}{\sigma_m}\right)_2 = \left(\frac{3t_1 \cdot (2L_1^3 t_2^4 + 3L_1 L_2^2 t_1^4 + 2L_2^3 t_1^4)}{t_2^2 \cdot (L_1^3 t_2^4 + 3L_1^2 L_2 t_1^4 + 3L_1 L_2^2 t_1^4 + L_2^3 t_1^4)}\right) \cdot e$$

with $t_1 = t_2 = t$ and $L_1 = L_2$:

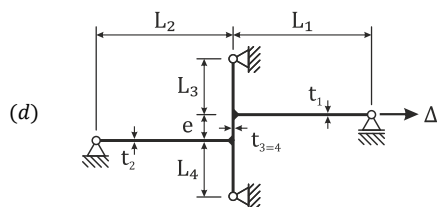
$$k_{m,axial} = 1 + \lambda_2 \cdot \frac{e \cdot L_2}{t \cdot (L_1 + L_2)} \rightarrow \lambda_2 = 5.25$$

$$\left(\frac{\sigma_b}{\sigma_m}\right)_1 = \left(\frac{9L_1 L_2 t_1^3 \cdot (2L_1 + L_2)}{L_1^3 t_2^4 + 3L_1^2 L_2 t_1^4 + 3L_1 L_2^2 t_1^4 + L_2^3 t_1^4}\right) \cdot e$$

with $t_1 = t_2 = t$ and $L_1 = L_2$:

$$k_{m,axial} = 1 + \lambda_1 \cdot \frac{e \cdot L_1}{t \cdot (L_1 + L_2)} \rightarrow \lambda_1 = 6.75 > \lambda_2$$

Cruciform joint, axial misalignment, restrained ends of load-bearing plates, articulated intermediate plate

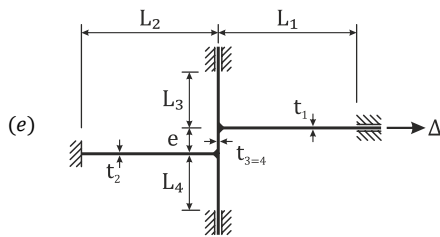


$$\left(\frac{\sigma_b}{\sigma_m}\right)_i = \left(\frac{6L_1 L_2 L_3 L_4 t_i t_i}{L_i \cdot (L_1 L_2 L_3 t_4^3 + L_1 L_2 L_4 t_3^3 + L_1 L_3 L_4 t_2^3 + L_2 L_3 L_4 t_1^3)}\right) \cdot e, i = 1,2,3,4$$

with $t_1 = t_2 = t_3 = t_4 = t_i = t$ and $L_1 = L_2 = L_3 = L_4 = L_i$:

$$k_{m,axial} = 1 + \lambda \cdot \frac{e \cdot L_1}{t \cdot (L_1 + L_2)} \rightarrow \lambda = 3$$

Cruciform joint, axial misalignment, restrained ends of load-bearing plates, restrained but longitudinally displaceable intermediate plate



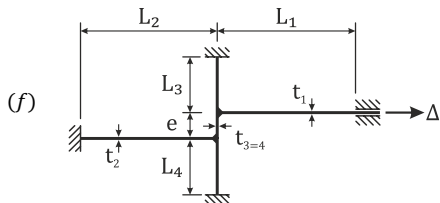
$$\left(\frac{\sigma_b}{\sigma_{m,i}}\right) = \left(\frac{6L_1L_2L_3L_4t_it_1 \cdot \left(4 \cdot \frac{L_i^3t_i^3t_3^3}{t_i^3} + 3 \cdot \frac{L_iL_1L_2t_i^3t_2^3}{t_i^3} + \frac{L_i^3L_3^3t_i^3}{L_i^3}\right)}{L_i \cdot \left(4L_1^4L_2L_3t_2^3t_4^3 + 4L_1^4L_2L_4t_2^3t_3^3 + L_1^4L_3L_4t_2^6\right)} \right) \cdot e, i = 1,2$$

$$\left(\frac{\sigma_b}{\sigma_{m,i}}\right) = \left(\frac{24L_1L_2L_3L_4t_it_1 \cdot (L_1t_2 + L_2t_1) \cdot \left(\frac{L_1^2t_2^2}{L_1^2} + \frac{L_1L_2t_1t_2}{L_1L_2}\right)}{L_i \cdot \left(4L_1^4L_2L_3t_2^3t_4^3 + 4L_1^4L_2L_4t_2^3t_3^3 + L_1^4L_3L_4t_2^6\right)} \right) \cdot e, i = 3,4$$

with $t_1 = t_2 = t_3 = t_4 = t_i = t$ and $L_1 = L_2 = L_3 = L_4 = L_i$:

$$k_{maxial} = 1 + \lambda \cdot \frac{e \cdot L_1}{t \cdot (L_1 + L_2)} \rightarrow \lambda = 3$$

Cruciform joint, axial misalignment, restrained ends of load-bearing plates, restrained intermediate plate



$$\left(\frac{\sigma_b}{\sigma_{m,i}}\right) = \left(\frac{6L_1L_2L_3L_4t_it_1}{L_i \cdot (L_1L_2L_3t_4^3 + L_1L_2L_4t_3^3 + L_1L_3L_4t_2^3 + L_2L_3L_4t_1^3)} \right) \cdot e, i = 1,2,3,4$$

with $t_1 = t_2 = t_3 = t_4 = t_i = t$ and $L_1 = L_2 = L_3 = L_4 = L_i$:

$$k_{maxial} = 1 + \lambda \cdot \frac{e \cdot L_1}{t \cdot (L_1 + L_2)} \rightarrow \lambda = 3$$

The analytical calculations of [5] are mostly consistent with the specifications of the IIW [3] and BS 7910 [71] (cf. Table 2-26). However, the values for λ given in Table 2-23 only apply under the condition that both the plate lengths $L_1 = L_2 = L_3 = L_4$ and the plate thicknesses $t_1 = t_2 = t_3 = t_4$ are equal. The respective definitions of the geometric dimensions can be derived from Table 2-23. Consequently, due to the analytical correlations, varying plate thicknesses L_i and plate thicknesses t_i result in differing analytically determined geometric support factors λ depending on the investigated support condition according to [5] (cf. Table 2-26).

Figure 2-25 illustrates the dependencies of λ according to the influence of the plate length L_2 with $L_2 \neq L_1 = L_3 = L_4$ separately for the decisive support factor $\lambda_{plate 1}$ of plate 1 (cf. left side of Figure 2-25) and $\lambda_{plate 2}$ of plate 2 (cf. right side of Figure 2-25) in logarithmic scale. The evaluation is presented for the support conditions (a) to (f) with axial misalignment according to Table 2-23. The specification of the IIW [3] and the BS 7910 [71] with respect to $l_1 \leq l_2$ results in the indirect determination of influences due to axial misalignment according to Xing and Dong [5] only being comparable if the plate length L_1 is at least as long as the plate length L_2 . Thus, only the range $L_2/L_1 \leq 1.0$ of Figure 2-25 according to [5] can be used for the comparability of the normative regulations and guidelines mentioned. To ensure completeness, the investigations for $L_2 > L_1$ are also illustrated in Figure 2-25. However, when selecting the methodology for the indirect consideration of imperfections, attention must be paid to the respective definition in order to avoid possible errors.

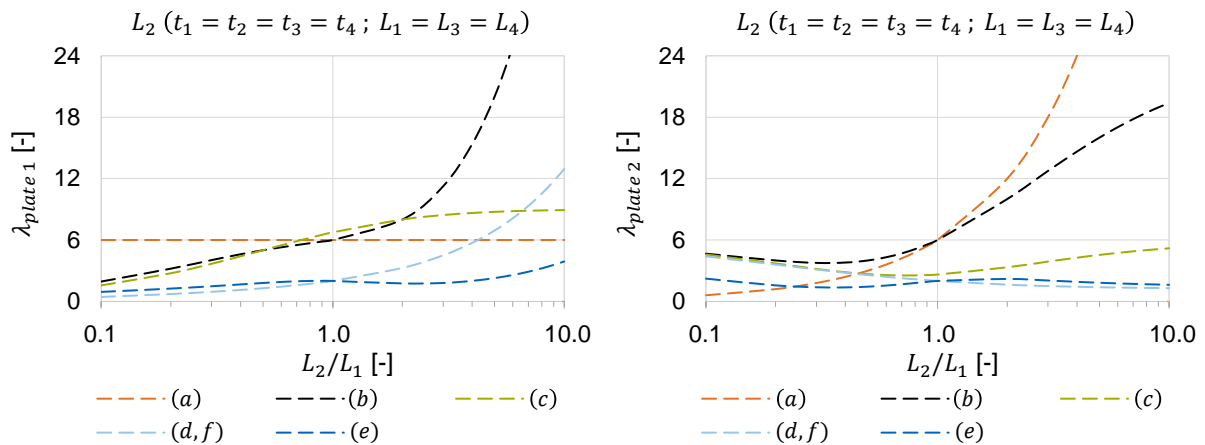


Figure 2-25: λ -factor with axial misalignment and constant plate thicknesses $t_1 = t_2 = t_3 = t_4$ according to Xing and Dong [5] as a function of L_2/L_1 of plate 1 (left) and plate 2 (right)

Furthermore, there is a theoretical possibility for the relevant support parameter λ to occur at plate 3 or plate 4. This is only plausible in the cases (d), (e) and (f), as these provide a defined type of support of the intermediate plate. However, the numerical results of the comparative calculations from Chapter 5.2.2 demonstrate that the fatigue stress of the intermediate plates is not relevant in any of the analysed cases. Consequently, the evaluation of the corresponding support parameter λ of the intermediate plate can be disregarded.

Figure 2-25 shows that the plate length $L_2 \neq L_1 = L_3 = L_4$ has a significant influence on the support factor λ . Only system (a) is independent of L_2 for the investigation of plate 1. In all further cases, λ and thus the stress concentration factor k_m increases both at plate 1 and at plate 2 with larger L_2/L_1 ratios. This is due to the reduced stiffness of plate 2. In this context, it depends on the support condition at which plate the significant support factor λ occurs. The limitation of IIW [3] and BS 7910 [71] is therefore essential, as the support parameter of $\lambda \gg 6$ is in most cases significantly larger than specified in the normative regulations and guidelines.

In the following Figure 2-26, the effect of the t_2/t_1 ratio is examined. In this case, the ratio of t_2/t_1 with constant plate thickness $t_3 = t_4$, is analysed for both plate 1 (cf. left side of Figure 2-26) and plate 2 (cf. right side of Figure 2-26).

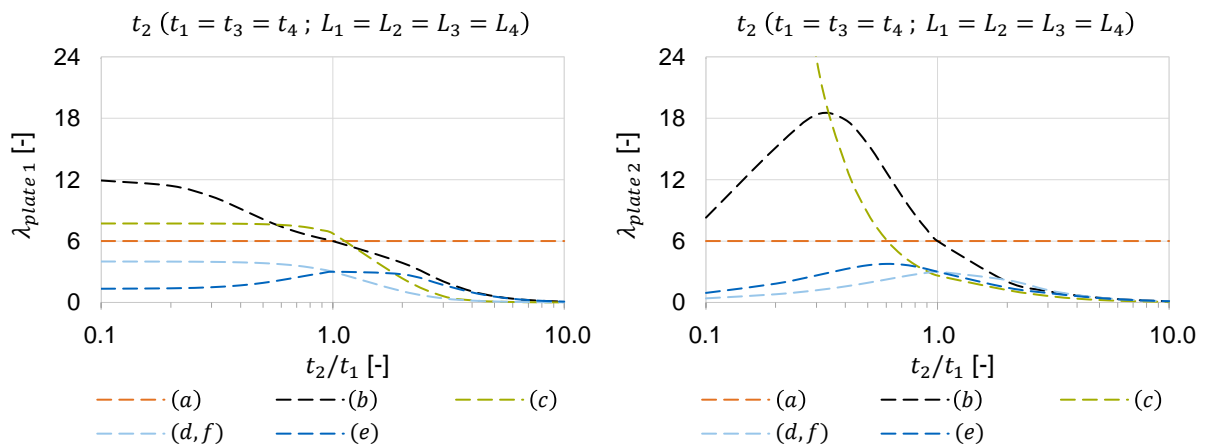


Figure 2-26: λ -factor with axial misalignment and constant plate lengths $L_1 = L_2 = L_3 = L_4$ according to Xing and Dong [5] as a function of t_2/t_1 of plate 1 (left) and plate 2 (right)

The investigations confirm that with increasing thickness t_2 and the associated increasing stiffness of plate 2, higher stress concentration factors k_m are to be expected. This is particularly evident in systems (b) and (c). Due to the restraint of plate 2, these systems react gradually like a cantilever as the stiffness increases.

In order to evaluate the relevant maximum values for λ of the total construction for the L_2/L_1 and t_2/t_1 ratio, the maxima of plate 1 (cf. left side of Figure 2-27) and plate 2 (cf. right side of Figure 2-27) are summarised in the following Figure 2-27. The position of the significant support factor can no longer be determined from the graphs.

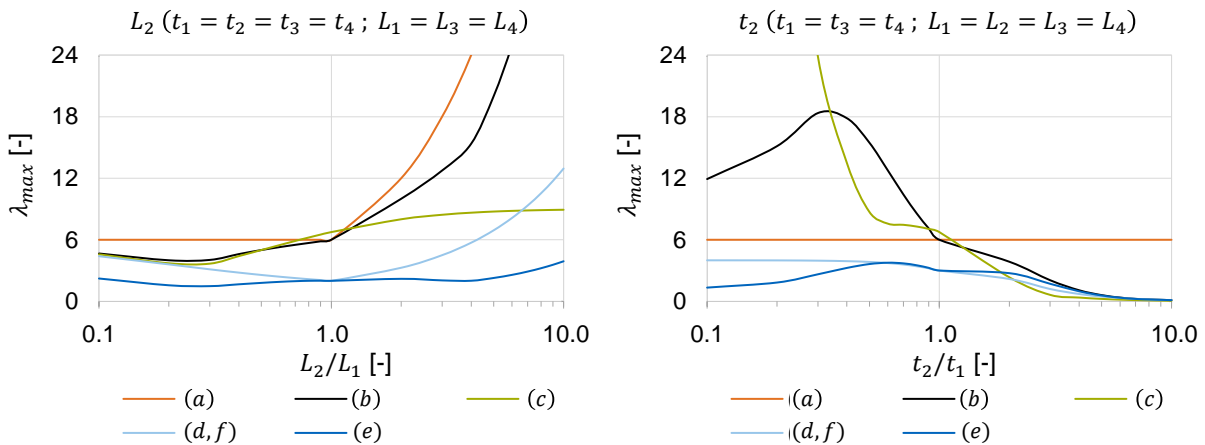


Figure 2-27: Maximum λ -factor of plate 1 and plate 2 with axial misalignment according to Xing and Dong [5] as a function of L_2/L_1 (left) and t_2/t_1 (right)

In addition, Figure 2-28 shows the results for axial misalignment of $L_3 = L_4 \neq L_1 = L_2$ and $L_3 \neq L_1 = L_2 = L_4$ for constant plate thicknesses $t_1 = t_2 = t_3 = t_4$ (cf. left side of Figure 2-28) and the influence of $t_3 = t_4 \neq t_1 = t_2$ for constant plate lengths $L_1 = L_2 = L_3 = L_4$ (cf. right side of Figure 2-28) in logarithmic space. For plate 1 and plate 2 the support factor λ is identical.

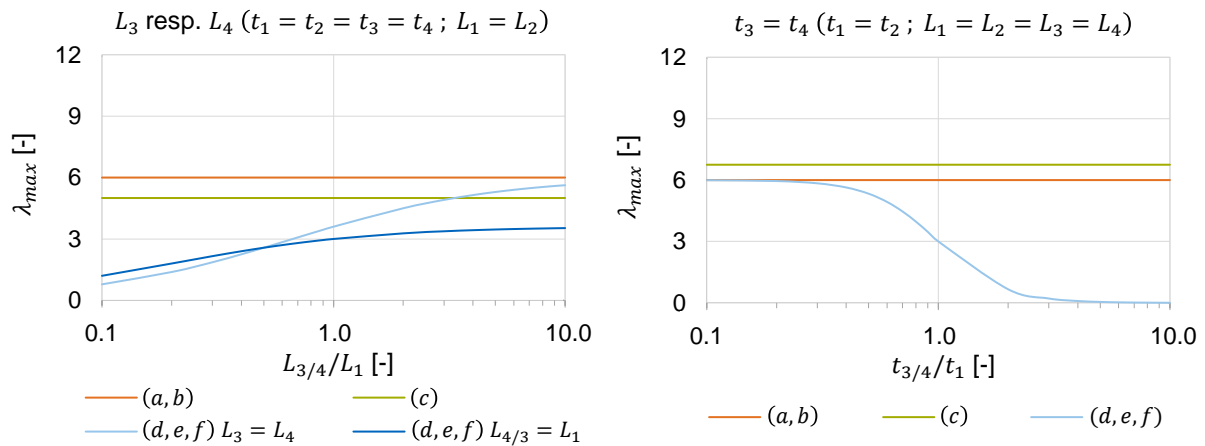


Figure 2-28: λ -factor for axial misalignment according to Xing and Dong [5] as a function of $L_{3/4}/L_1$ (left) and $t_{3/4}/t_1$ (right)

On the left side of Figure 2-28, both the influence of $L_3 \neq L_1 = L_2 = L_4$ (equivalent to $L_4 \neq L_1 = L_2 = L_3$) and the influence of $L_3 = L_4 \neq L_1 = L_2$ are analysed. For systems (a), (b) and (c) there are no dependencies due to the missing support of the intermediate plate. For systems (d), (e) and (f) the influence is independent of the

support of the intermediate plate and increases with higher $L_{3/4}/L_1$ ratios. Consequently, the stress concentration factor k_m will increase with larger lengths L_3 and L_4 and the support factor λ will converge to the characteristics without support of the intermediate plate due to the decreasing influence of the support conditions.

In the investigation of the $t_3/t_1 = t_4/t_1$ ratio (cf. right side of Figure 2-28), it is expected that the thickness of the intermediate plate of cruciform joints is identical. While the behaviour of systems (a), (b) and (c) remain constant due to the lack of support of the intermediate plate, the λ -values of systems (d), (e) and (f) decrease with higher $t_{3/4}$ ratios, since the stresses are being absorbed by the support conditions of the intermediate plate. Thus, the investigations confirm that higher stress concentration factors k_m can be expected with increasing stiffness of the intermediate plate.

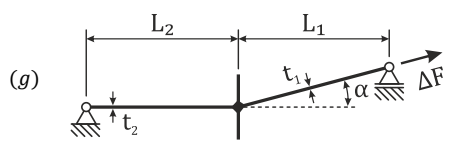
All results for the indirect consideration of influences from axial imperfections according to Xing and Dong [5] are being verified in Chapter 5.2.2 by means of numerical verification calculations.

Angular misalignment

In addition to the studies on axial misalignment, the investigations of Xing and Dong [5] on cruciform joints with angular misalignment are presented below (cf. Table 2-24).

Table 2-24: Investigations on angular misalignment of cruciform joints with varying support conditions

Cruciform joint, angular misalignment, articulated ends of load-bearing plates, no support of intermediate plate

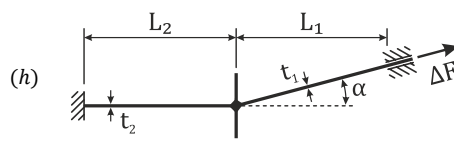


$$\left(\frac{\sigma_b}{\sigma_m}\right)_i = \left(\frac{6L_1L_2t_1}{(L_1 + L_2) \cdot t_1^2}\right) \cdot \alpha, i = 1,2$$

with $t_1 = t$ and $L_1 = L_2$:

$$k_{m,angular} = 1 + \lambda \cdot \alpha \cdot \frac{l_1 \cdot l_2}{t \cdot (l_1 + l_2)} \rightarrow \lambda = 6$$

Cruciform joint, angular misalignment, restrained ends of load-bearing plates, no support of intermediate plate

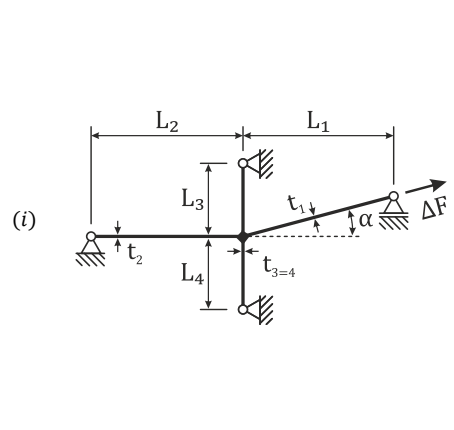


$$\left(\frac{\sigma_b}{\sigma_m}\right)_i = \left(\frac{12L_1^2L_2^2t_1^4t_2^3 \cdot (L_1 + L_2)}{(L_1^4t_2^6 + 4L_1^3L_2t_1^3t_2^3 + 6L_1^2L_2^2t_1^3t_2^3 + 4L_1L_2^3t_1^3t_2^3 + L_2^4t_1^6)t_1^2}\right) \cdot \alpha, i = 1,2$$

with $t_1 = t_2 = t_i = t$ and $L_1 = L_2$:

$$k_{m,angular} = 1 + \lambda \cdot \alpha \cdot \frac{l_1 \cdot l_2}{t \cdot (l_1 + l_2)} \rightarrow \lambda = 3$$

Cruciform joint, angular misalignment, restrained ends of load-bearing plates, articulated intermediate plate



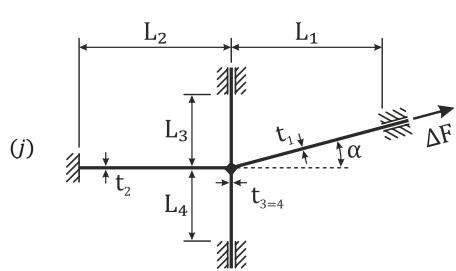
$$\left(\frac{\sigma_b}{\sigma_m}\right)_i = \left(\frac{\frac{3}{2}L_3L_4t_1t_2 \cdot (L_3t_3 + L_4t_4) \cdot \left(\frac{L_1L_3L_4t_1^3t_2^3}{t_i^3} + \frac{L_1^2L_2L_3L_4t_4^3}{L_i^2}\right)}{L_1L_2t_3t_4 \cdot (L_3 + L_4)^2 \cdot \left(\frac{L_1L_2L_3t_4^3 + L_1L_2L_4t_3^3}{L_i^3} + \frac{L_1^2L_2^2L_4t_3^3}{L_i^2} + \frac{L_2L_3L_4t_1^3t_2^3}{t_i^3}\right)}\right) \cdot \alpha, i = 1,2$$

$$\left(\frac{\sigma_b}{\sigma_m}\right)_i = \left(\frac{\frac{3}{2}L_3^2L_4^2t_1t_2 \cdot (L_3t_3 + L_4t_4) \cdot (L_1^2t_2^3 - L_2^2t_1^3)}{L_1L_2t_3t_4 \cdot (L_3 + L_4)^2 \cdot \left(\frac{L_1L_2L_3t_4^3 + L_1L_2L_4t_3^3}{L_i^3} + \frac{L_1L_3L_4t_2^3}{L_i^2} + \frac{L_2L_3L_4t_1^3}{L_i^2}\right)}\right) \cdot \alpha, i = 3,4$$

with $t_1 = t_2 = t_3 = t_4 = t_i = t$ and $L_1 = L_2 = L_3 = L_4 = L_i$:

$$k_{m,angular} = 1 + \lambda \cdot \alpha \cdot \frac{l_1 \cdot l_2}{t \cdot (l_1 + l_2)} \rightarrow \lambda = 1.5$$

Cruciform joint, angular misalignment, restrained ends of load-bearing plates, restrained but longitudinally displaceable intermediate plate



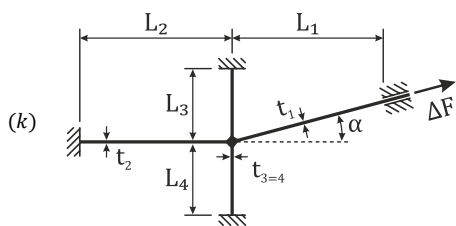
$$\left(\frac{\sigma_b}{\sigma_m} \right)_i = \left(\frac{12L_1^2 L_2^2 t_i t_1 \cdot \left(\frac{L_1 L_3 L_4 t_1^3 t_2^3}{t_i^3} + \frac{L_1^2 L_2^2 L_3 t_4^3}{L_i^2} \right)}{4L_1^4 L_2 L_3 t_2^3 t_4^3 + 4L_1^4 L_2 L_4 t_2^3 t_3^3 + L_1^4 L_3 L_4 t_2^6 + 4L_1^3 L_2 L_3 L_4 t_1^3 t_2^3 + 6L_1^2 L_2^2 L_3 L_4 t_1^3 t_2^3 + 4L_1 L_2^4 L_3 t_1^3 t_4^3 + 4L_1 L_2^4 L_4 t_1^3 t_3^3 + 4L_1 L_2^3 L_3 L_4 t_1^3 t_2^3 + L_2^4 L_3 L_4 t_1^6} \right) \cdot \alpha, i = 1,2$$

$$\left(\frac{\sigma_b}{\sigma_m} \right)_i = \left(\frac{12L_1^2 L_2^2 L_3 L_4 t_i t_1 \cdot (L_1^2 t_2^3 - L_2^2 t_1^3)}{4L_1^4 L_2 L_3 t_2^3 t_4^3 + 4L_1^4 L_2 L_4 t_2^3 t_3^3 + L_1^4 L_3 L_4 t_2^6 + 4L_1^3 L_2 L_3 L_4 t_1^3 t_2^3 + 6L_1^2 L_2^2 L_3 L_4 t_1^3 t_2^3 + 4L_1 L_2^4 L_3 t_1^3 t_4^3 + 4L_1 L_2^4 L_4 t_1^3 t_3^3 + 4L_1 L_2^3 L_3 L_4 t_1^3 t_2^3 + L_2^4 L_3 L_4 t_1^6} \right) \cdot \alpha, i = 3,4$$

with $t_1 = t_2 = t_3 = t_4 = t_i = t$ and $L_1 = L_2 = L_3 = L_4 = L_i$:

$$k_{m,angular} = 1 + \lambda \cdot \alpha \cdot \frac{L_1 \cdot L_2}{t \cdot (L_1 + L_2)} \rightarrow \lambda = 3$$

Cruciform joint, angular misalignment, restrained ends of load-bearing plates, restrained intermediate plate



$$\left(\frac{\sigma_b}{\sigma_m} \right)_i = \left(\frac{3L_3 L_4 t_i t_1 \cdot \left(\frac{L_1 L_3 L_4 t_1^3 t_2^3}{t_i^3} + \frac{L_1^2 L_2^2 L_3 t_4^3}{L_i^2} \right)}{L_1 L_2 \cdot (L_3 t_4 + L_4 t_3) \cdot \left(\frac{L_1 L_2 L_3 t_4^3 + L_1 L_2 L_4 t_3^3}{L_1 L_3 L_4 t_2^3 + L_2 L_3 L_4 t_1^3} \right)} \right) \cdot \alpha, i = 1,2$$

$$\left(\frac{\sigma_b}{\sigma_m} \right)_i = \left(\frac{3L_3^2 L_4^2 t_i t_1 \cdot (L_1^2 t_2^3 - L_2^2 t_1^3)}{L_1 L_2 L_i \cdot (L_3 t_4 + L_4 t_3) \cdot \left(\frac{L_1 L_2 L_3 t_4^3 + L_1 L_2 L_4 t_3^3}{L_1 L_3 L_4 t_2^3 + L_2 L_3 L_4 t_1^3} \right)} \right) \cdot \alpha, i = 3,4$$

with $t_1 = t_2 = t_3 = t_4 = t_i = t$ and $L_1 = L_2 = L_3 = L_4 = L_i$:

$$k_{m,angular} = 1 + \lambda \cdot \alpha \cdot \frac{L_1 \cdot L_2}{t \cdot (L_1 + L_2)} \rightarrow \lambda = 3$$

The analytical calculations from [5] for angular misalignments of cruciform joints with varying support conditions are consistent with the data from BS 7910 [71] for systems (g), (h) and (j). However, if system (i) or (k) is present, the factor for the support condition λ and consequently the stress concentration factor k_m differs significantly (cf. Table 2-27).

Figure 2-29 illustrates the dependence of the λ -factor on the plate length L_2 for cruciform joints with angular misalignment for both plate 1 (cf. left side of Figure 2-29) and plate 2 (cf. right side of Figure 2-29). It shows that a decreasing plate length L_2 generally leads to increasing support factors λ . Only system (g), which is not influenced by the plate length L_2 , and system (h), which reaches its maximum λ -value with constant plate lengths $L_1 = L_2 = L_3 = L_4$, deviate in this respect.

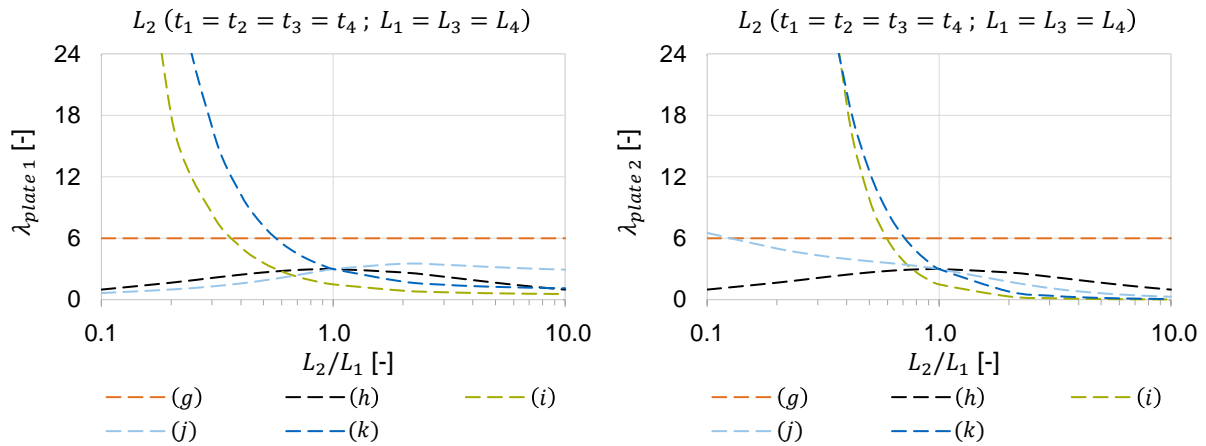


Figure 2-29: λ -factor with angular misalignment and constant plate thicknesses $t_1 = t_2 = t_3 = t_4$ according to Xing and Dong [5] as a function of L_2/L_1 of plate 1 (left) and plate 2 (right)

In addition, Figure 2-30 presents the influence of the plate thickness $t_2 \neq t_1 = t_3 = t_4$ on the λ -value of cruciform joints with angular misalignment. The evaluation is performed separately according to the support condition for plate 1 (cf. left side of Figure 2-30) and plate 2 (cf. right side of Figure 2-30). It is evident that the results are significantly dependent on the given system.

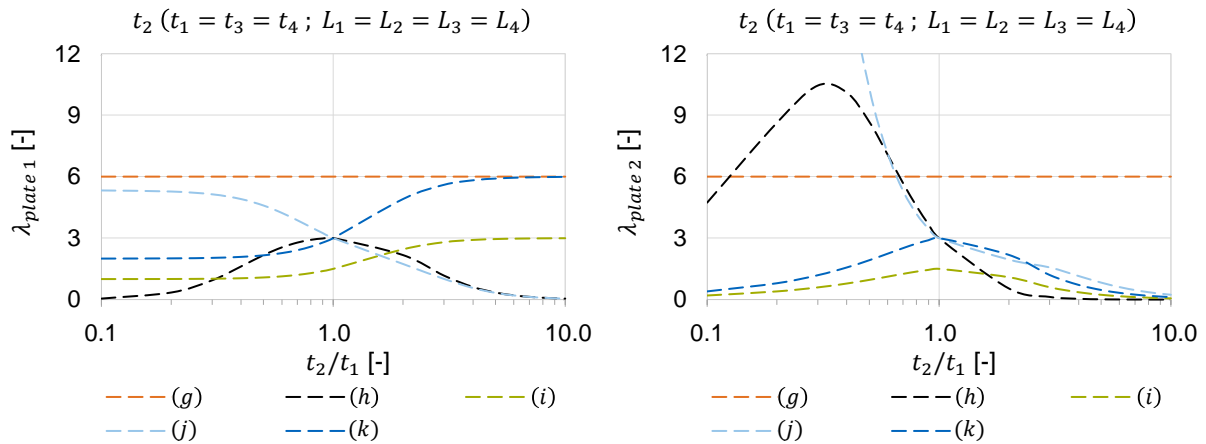


Figure 2-30: λ -factor with angular misalignment and constant plate lengths $L_1 = L_2 = L_3 = L_4$ according to Xing and Dong [5] as a function of t_2/t_1 of plate 1 (left) and plate 2 (right)

While the λ -values of plate 1 increase with higher t_2/t_1 ratios for systems (i) and (k), they decrease for system (j) (cf. left side of Figure 2-30). For plate 1 of system (h), identical plate thicknesses $t_1 = t_2 = t_3 = t_4$ result in the largest stress concentration factor k_m . The articulated and thus statically determined system (g) is independent of the plate lengths L_i and thicknesses t_i and can be assumed to be constant with $\lambda = 6$. The support factor λ increases significantly for plate 2 of system (h) and (j) with decreasing t_2/t_1 ratio and, according to Xing and Dong [5], decreases again for system (h) starting at a ratio of $t_2/t_1 < 0.3$ (cf. right side of Figure 2-30). The maximum λ -value for the L_2/L_1 and t_2/t_1 ratio is summarised in Figure 2-31.

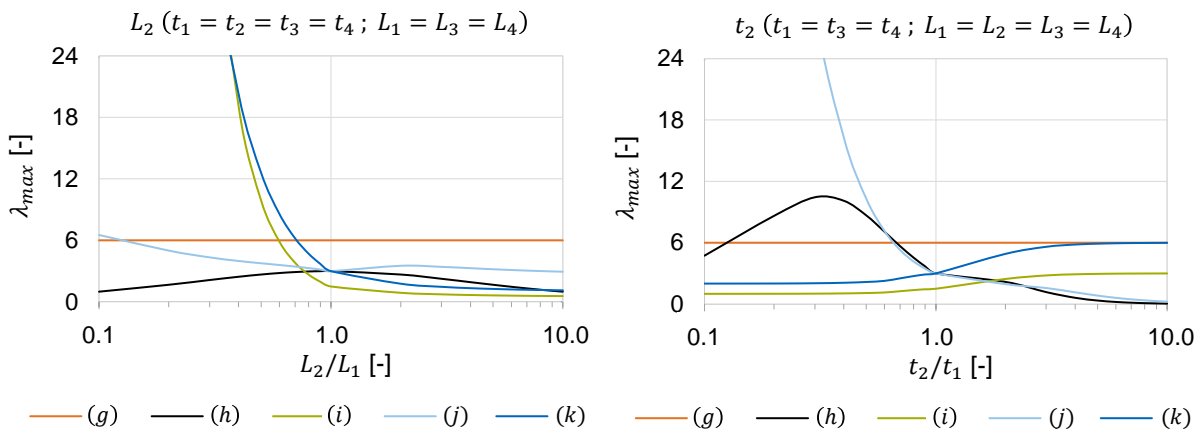


Figure 2-31: Maximum λ -factor of plate 1 and plate 2 with angular misalignment according to Xing and Dong [5] as a function of L_2/L_1 (left) and t_2/t_1 (right)

In addition, Figure 2-32 shows the results for angular misalignment of $L_3 = L_4 \neq L_1 = L_2$ and $L_3 \neq L_1 = L_2 = L_4$ for constant plate thicknesses $t_1 = t_2 = t_3 = t_4$ (cf. left side of Figure 2-32) and the influence of $t_3 = t_4 \neq t_1 = t_2$ for constant plate lengths $L_1 = L_2 = L_3 = L_4$ (cf. right side of Figure 2-32). The relevant stresses of Figure 2-32 are identical for plates 1 and 2 in the evaluation of the plate length (cf. left side of Figure 2-32) and plate thickness (cf. right side of Figure 2-32). Corresponding to the results for axial misalignment, the reduced stiffness of longer respectively thinner intermediate plates results in greater stresses in the welded-on plates. For systems (i) and (k) it is not apparent why the support factor λ exceeds the values of unsupported intermediate plates of system (g) and (h) above a certain $L_{3/4}/L_1$ ratio at constant plate lengths $L_3 = L_4$ (cf. left side of Figure 2-32). The same effect can be observed with decreasing plate thicknesses $t_3 = t_4$ (cf. right side of Figure 2-32). Consequently, according to the analytical calculations of Xing and Dong [5], large plate lengths $L_3 = L_4$ or small plate thicknesses $t_3 = t_4$, can lead to results that are larger than with unsupported intermediate plates.

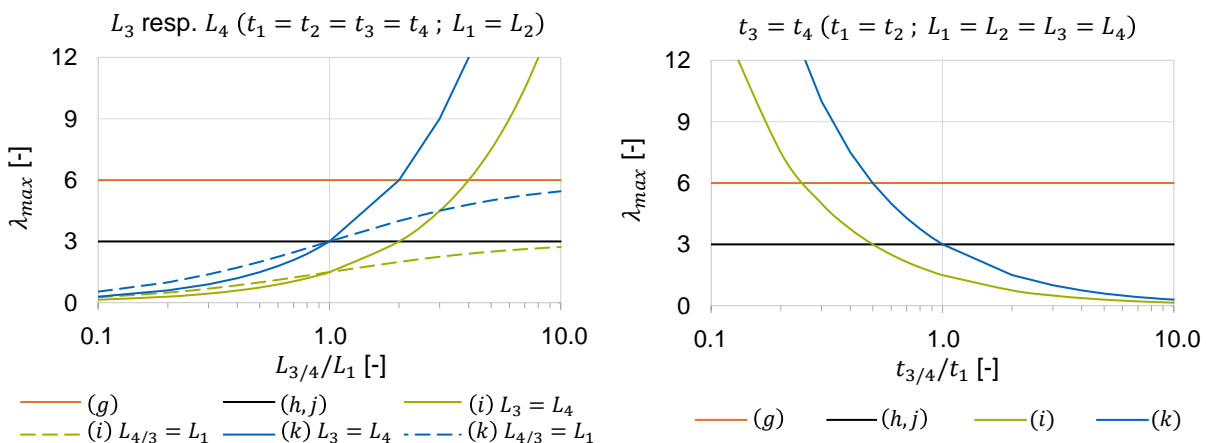


Figure 2-32: λ -factor for angular misalignment according to Xing and Dong [5] as a function of $L_{3/4}/L_1$ (left) and $t_{3/4}/t_1$ (right)

All results for the indirect consideration of influences from angular misalignments according to Xing and Dong [5] are verified in Chapter 5.2.2 by means of extensive numerical verification calculations.

2.5.3.2.5 k_m -factors for the clamping process in testing machines

In addition, Xing and Dong [5] provide an analytical calculation to determine the interaction between the stress concentration factor k_m and the clamping process of testing machines. In this clamping process, test specimens are restrained by mostly hydraulic clamps. Through possible imperfections, additional stresses can result during this process. This procedure is not considered in any normative regulations or guidelines. The process is induced by the perfect alignment of the clamps in the load axis and results in a displacement and possible rotation of the clamping area, which leads to secondary bending stresses in an unloaded component. This pre-deformation respectively pre-rotation is caused by axial misalignment e and angular misalignment α and can be reduced in the case of axial imperfections by inserting intermediate layers. The following Table 2-25 summarises the corresponding calculation methods from Xing and Dong [5] according to Castigliano's second theorem. However, the methods are limited to $t_1 = t_2 = t_3 = t_4$. In addition, a conversion into the standard form of the stress concentration factors $k_{m,axial}$ and $k_{m,angular}$ of the IIW [3] is performed under the assumption that the plate length L_1 corresponds to half the total plate length L . In addition, the distance L_c , which is defined as the distance between the end of the clamps and the intermediate plate, is replaced by $L_c \approx L_1$, since the deviation between L_1 and L_c merely corresponds to half the plate thickness $t_{intermediate\ plate}/2$. It needs to be pointed out that all plate lengths L_i from [5] are only defined up to the beginning of the clamping area. This differs from the previously presented methods.

Table 2-25: Interaction between λ -factor and clamping process

Clamping process for cruciform joint with axial misalignment	
	$\left(\frac{\sigma_b}{\sigma_m}\right) = \left(\frac{3 \cdot \left(11L^3 - 40L^2L_1 - 12L^2L_c + 30LL_1^2\right) + 60LL_1L_c + 30LL_c^2 - 60L_1^2L_c - 20L_c^3}{5L^3t}\right) \cdot e$ <p>with $L_1 = L/2$:</p> $\left(\frac{\sigma_b}{\sigma_m}\right) = \left(\frac{3 \cdot (-3L^3 + 6L^2L_c + 60LL_c^2 - 40L_c^3)}{10L^3t}\right) \cdot e$ <p>with $L_1 = L/2$ and $L_c \approx L_1$:</p> $k_{m,axial} = 1 + \lambda \cdot \frac{e \cdot l_1}{t \cdot (l_1 + l_2)} \rightarrow \lambda = 6$
Clamping process for cruciform joint with angular misalignment	
	$\left(\frac{\sigma_b}{\sigma_m}\right) = \left(\frac{4 \cdot (L^4 - 9L^3L_c + 39L^2L_c^2 - 60LL_c^3 + 30L_c^4)}{5L^3t}\right) \cdot \alpha$ <p>with $L_c \approx L/2$:</p> $k_{m,angular} = 1 + \lambda \cdot \alpha \cdot \frac{l_1 \cdot l_2}{t \cdot (l_1 + l_2)} \rightarrow \lambda = 2$

In the following, the influence of the ratio of the plate length L_1 to the total plate length L regarding the clamping process in testing machines is investigated. Again, the simplification is made that the plate length L_1 corresponds approximately to the

distance L_c . Both system (l) with axial misalignment and system (n) with angular misalignment are examined. The results are shown in Figure 2-33.

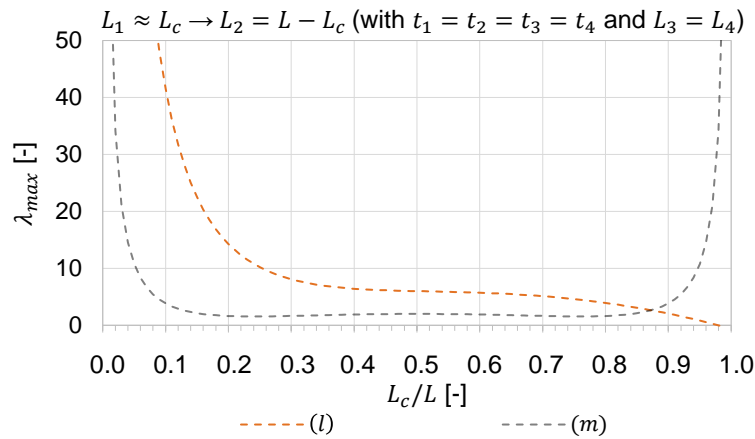


Figure 2-33: λ -factor as a function of the L_c/L -ratio in relation to the clamping process of cruciform joints with axial misalignment (l) and angular misalignment (n) with the simplification $L_c = L_1$ according to Xing and Dong [5]

Figure 2-33 shows that the selected length L_1 or L_2 for L_c is irrelevant for cruciform joints with angular misalignment, as the support factor λ_{max} of system (n) behaves symmetrically around $L_c/L = 0.5$. In contrast, with regard to cruciform joints with axial misalignment according to system (l), the shorter length of L_1 or L_2 should always be set to L_c , since greater stress concentration factors k_m are to be expected as a result.

2.5.3.2.6 Summary

In Chapters 2.5.3.2.1 to 2.5.3.2.5 different procedures were presented to indirectly consider effects resulting from imperfections. It is evident that the stress concentration factor k_m is significantly dependent on the support conditions and the corresponding support factor λ . In this respect, the normative regulations and guidelines differ at many points, which can lead to considerable errors. In addition, the specifications of the IIW [3] and BS 7910 [71] are only valid for axial misalignment under the constraints $l_1 \leq l_2$, which is equal to $L_2 \leq L_1$ according to the definition of Xing and Dong [5]. It is not clarified in [3] or [71] how to proceed with deviating systems. Furthermore, according to the guidelines of the IIW [3], it is not explicitly defined how the factor for the support condition λ is to be applied. Furthermore, the normative regulations and guidelines do not sufficiently consider the influence of deviating plate lengths and plate thicknesses.

In order to provide a better understanding of the results for different approaches, the λ -factors for uniform lengths l_i as well as for a doubled length l_2 with $l_1 = l_2/2 = l_3 = l_4$ and doubled length l_1 with $l_1/2 = l_2 = l_3 = l_4$ for axial misalignment are summarised in Table 2-26. According to the notation of DNVGL-RP-C203 [66] and Xing and Dong [5] $l_2/2$ corresponds to $L_1/2$ and $l_1/2$ to $L_2/2$. The evaluation is carried out under the condition $t_1 = t_2 = t_3 = t_4$. The clamping process in testing machines is disregarded in the comparative evaluation.

The specifications of the guidelines of the IIW [3] are interpreted in terms of the factor λ being $\lambda = 6$ with no support of the intermediate plate. If the displacement of the intermediate plate is restrained, $\lambda = 3$ is assumed, although the IIW [3] refers to a full restraint. Due to the analytical formulae, deviating plate lengths $l_1 = L_2$ and $l_2 = L_1$

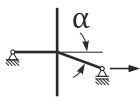
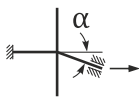
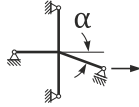
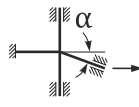
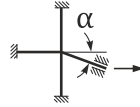
solely result in modified values for the procedure of Xing and Dong [5] and DNVGL-RP-C203 [66] (cf. Table 2-26).

Table 2-26: Comparison of normative regulations and guidelines regarding the factor of the support condition λ of cruciform joints with axial misalignment

l_1 resp. L_1	Guideline	(a)	(b)	(c)	(d)	(e)	(f)
$l_1 = l_2 = l_3 = l_4$ $L_1 = L_2 = L_3 = L_4$	IIW [3]	6.00	6.00	6.00	3.00	3.00	3.00
	DNVGL [66]	-	-	-	3.00	-	-
	BS 7910 [71]	6.00	-	6.75	3.00	2.95	3.00
	Xing [5]	6.00	6.00	6.75	3.00	3.00	3.00
$l_1 = l_2/2 = l_3 = l_4$ $L_1/2 = L_2 = L_3 = L_4$	IIW [3]	6.00	6.00	6.00	3.00	3.00	3.00
	DNVGL [66]	-	-	-	1.29	-	-
	BS 7910 [71]	6.00	-	6.75	3.00	2.95	3.00
	Xing [5]	6.00	5.00	5.00	2.57	1.80	2.57
$l_1/2 = l_2 = l_3 = l_4$ $L_1 = L_2/2 = L_3 = L_4$	IIW [3]	-	-	-	-	-	-
	DNVGL [66]	-	-	-	5.14	-	-
	BS 7910 [71]	-	-	-	-	-	-
	Xing [5]	6.00	8.00	8.00	5.14	3.60	5.14

For systems with $l_1 > l_2$, according to Xing and Dong [5], significantly larger values for the support factor λ result than are covered by the normative regulations and guidelines (cf. Table 2-26). Thus, the specification of the IIW [3] and BS7910 [71] that $l_1 \leq l_2$ must apply can be confirmed in order to verify the requirements for the support factor λ . Consequently, the associated procedures may only be used within the specified range. With regard to angular misalignments of cruciform joints, there are also significant differences in the normative regulations and guidelines. The results are summarised in Table 2-27 according to the evaluation of axial misalignment in Table 2-26. Since the guidelines of the IIW [3] do not provide any coherent information on the application of the support factor λ , the systems (i), (j) and (k) are represented by $0.02 \leq \lambda \leq 0.04$ in this thesis. While $\lambda = 3$ for axial misalignment refers to a full restraint of the intermediate plate, for angular misalignment this statement is assumed to refer to restrained plate ends of the welded-on plates. Thus, system (g) is specified with $\lambda = 6$ and system (h) as $\lambda = 3$ (cf. Table 2-27). The analytical calculations according to Xing and Dong [5] again result in modified λ -factors according to Table 2-27 with deviating lengths $l_1 = L_2$ and $l_2 = L_1$.

Table 2-27: Comparison of normative regulations and guidelines regarding the factor of the support condition λ of cruciform joints with angular misalignment

l_i resp. L_i	Guideline	(g)	(h)	(i)	(j)	(k)
						
$l_1 = l_2 = l_3 = l_4$ $L_1 = L_2 = L_3 = L_4$	IIW [3]	6.00	3.00	0.02 – 0.04	0.02 – 0.04	0.02 – 0.04
	DNVGL [66]	–	–	–	–	–
	BS 7910 [71]	6.00	–	0.02	3.00	0.04
	Xing [5]	6.00	3.00	1.50	3.00	3.00
$l_1 = l_2/2 = l_3 = l_4$ $L_1/2 = L_2 = L_3 = L_4$	IIW [3]	6.00	3.00	0.02 – 0.04	0.02 – 0.04	0.02 – 0.04
	DNVGL [66]	–	–	–	–	–
	BS 7910 [71]	6.00	–	0.02	3.00	0.04
	Xing [5]	6.00	2.67	6.11	4.48	7.07
$l_1/2 = l_2 = l_3 = l_4$ $L_1 = L_2/2 = L_3 = L_4$	IIW [3]	6.00	3.00	0.02 – 0.04	0.02 – 0.04	0.02 – 0.04
	DNVGL [66]	–	–	–	–	–
	BS 7910 [71]	6.00	–	0.02	3.00	0.04
	Xing [5]	6.00	2.67	0.88	3.52	1.77

In the case of angular misalignment, there are also considerable differences in the support factor λ according to the normative regulations and guidelines (cf. Table 2-27). The values are solely consistent for the statically determined system (g). The significant deviations in systems (i), (j) and (k) are particularly noticeable. In addition, the relevant influence of the component geometry is evident.

For the indirect consideration of imperfections, the general procedure of the IIW [3] according to Chapter 2.5.3.2 is appropriate. Nevertheless, the corresponding specifications for the determination of the stress concentration factor k_m are not defined with sufficient precision. In this respect, the information provided by Xing and Dong [5] is more adequate, as solution approaches are provided for many relevant support conditions and geometries. Since the comparison of Table 2-26 and Table 2-27 indicates that the support factor λ is subject to significant discrepancies, extensive FE calculations are presented in Chapter 5.2.2 and a comparison is provided with the regulations presented. In addition, in Chapter 5.2.1 k_m factors according to the guidelines of the IIW [3] and Xing and Dong [5] for support conditions common in practice are verified by numerical calculations. Furthermore, a numerical verification of the indirect determination of influences from imperfections due to clamping processes (cf. Section 2.5.3.2.5) is carried out in chapter 5.1.2.

2.6 Thickness effect

Following the implementation of the so-called thickness effect in the standardisation of offshore structures [66], intensive research has been carried out on the subject in recent decades. This research has generally confirmed the existence of a thickness-dependent influence [72–82]. In addition to the influence of the surface roughness, the influence of the thickness effect on the fatigue resistance is composed of a statistical, a technological and a geometric component. It was identified that these thickness effects depend on the load bearing plate thickness T , the thickness of the intermediate plate t as well as on the type of dynamic loading.

Concerning this matter, there are many different recommendations in the literature on how to deal with this effect. This is due to the extensive dispersion of fatigue data, which complicates the formulation of reliable recommendations. Due to the large loads required for axial tensile tests on thick plates, many experimental results are based on cyclic bending tests. The analysis of these results shows that the influence of the effect is more evident in bending tests than in pure tensile tests [72–82]. Consequently, most normative regulations and guidelines on fatigue verification only give simplified recommendations on the thickness effect. [12]

The thickness effect is addressed in the guidelines of the IIW [3], DIN EN 1993-1-9, prEN 1993-1-9 [4], the guideline of the FKM [11] and DNVGL-RP-C203 [66]. The majority of the normative regulations and guidelines refer to the investigations of Gurney [77, 78, 76], who already developed suitable procedures based on linear-elastic fracture mechanics. In addition, Berge et al. [72–74], Gordon et al. [75], Lotsberg [12] and Kugler [49], among others, have developed further methods to take the influence into account. The theoretical principles of thickness effects and their consideration in fatigue verification will be explained in the following sections.

2.6.1 General cause of the thickness effect

For the accurate determination of the thickness effect, macro-structural effects such as component thickness, residual stresses and further relevant stress states would have to be included. In addition, the consideration of microstructural factors such as grain size, microcracks and pores or inclusions would also be required. If the effect of different surface roughness of a component can be excluded, for instance because corrosion is prevented, the cause of the thickness effect can be divided in theory into the components already mentioned. These are briefly described below. [39, 49, 17, 9]

2.6.1.1 *Statistical size effect*

The statistical size effect is based on the fact that larger component dimensions result equally in an increase of the component volume and the component surface. Consequently, the statistical probability of defects increases. As a result, the risk of fatigue crack initiation is statistically higher. [39]

2.6.1.2 *Technological size effect*

The manufacturing process of steel causes differences in the steel structure. These can cause different coarse grain sizes, lower notched impact strengths, higher residual

stresses and a lower yield strength in the case of larger plate thicknesses. This effect is classified as a technological component. [17, 39]

2.6.1.3 Geometric size effect

The geometric size effect is generally the decisive component. This stress-mechanical influence is due to deviating stress gradients throughout the component thickness of plates of different thicknesses. In Figure 2-34, the stress distribution of a butt joint with a thin plate of thickness T_1 is compared to that of a thick plate with T_2 . Thus, $T_1 < T_2$ applies. [17, 39]

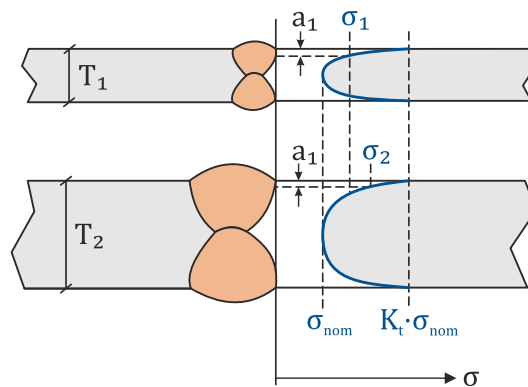


Figure 2-34: Geometric size effect [39]

Despite identical surface stresses $K_t \cdot \sigma_{nom}$ and equal normal stresses σ_{nom} in the centre of the plate, it is evident that due to the flatter stress gradient of the thicker plate T_2 , at shallow depth a_1 near the surface, significantly higher stresses σ_2 are to be expected (cf. bottom part of Figure 2-34) than for the thinner plate with σ_1 (cf. top of Figure 2-34). This can consequently lead to larger deformations and an associated increased stress level, which often leaves the geometric size effect to be significant. [17, 39, 9]

2.6.2 Approaches for the determination of the thickness effect

Since, in principle, neither microstructural nor macrostructural information is available for structural components, it is almost impossible to take statistical (cf. Chapter 2.6.1.1) and technological thickness effects (cf. Chapter 2.6.1.2) into account in a finite element calculation. Only the influence of the geometric component (cf. Chapter 2.6.1.3) could theoretically be captured by FE calculations.

However, this effect is only noticeable in a local stress determination via the plate thickness. Consequently, this is considered, for example, on the action side in the structural stress approaches of Radaj et al [6, 8] (cf. Chapter 2.3.3.3), Xiao and Yamada [7] (cf. Chapter 2.3.3.4) and Dong [50] (cf. Chapter 2.3.3.5). With further methods, such as the stress extrapolation according to the guidelines of the IIW [3], the geometric size effect can consequently only be determined to a limited extent due to the stress determination on the surface. Nevertheless, according to [9], applying the extrapolation method is intended to account for thickness effects, as the nearer reference point, at a smaller distance from the weld notch, is expected to accommodate parts of the non-linear notch stresses that are supposed to depend on the thickness of the component. In this respect, the underlying procedure for the exact determination of the thickness

effect is not defined. Furthermore, [65] confirms that the distance of the reference points is designed such that any non-linear effect is already decayed. In addition, the geometric thickness effect, as a result of flatter stress gradients over the component thickness, should not be noticeable on the plate surface.

Therefore, it is assumed in this thesis that no effects due to deviating component sizes are detectable if the stress is determined by extrapolation at the plate surface. Consequently, when applying local stress determinations at the plate surface, all thickness effects need to be covered by the fatigue strength $\Delta\sigma_C$. Since this is not to be reasonably expected for thicker plates, either a corresponding modification of the fatigue strength $\Delta\sigma_C$ or an increase of the applied stress range $\Delta\sigma_R$ is imperative. If a modification of the fatigue strength $\Delta\sigma_C$ is required due to thickness effects, the fatigue strength $\Delta\sigma_{C,mod}$ is modified by a thickness correction factor $f(t)$ according to the following Formula (2-44).

$$\Delta\sigma_{C,mod} = \Delta\sigma_C \cdot f(t) \quad (2-44)$$

Alternatively, if the applied stress ranges $\Delta\sigma_R$ are to be increased, the thickness correction factor $f(t)$ is applied as follows.

$$\Delta\sigma_{R,mod} = \Delta\sigma_R \cdot f(t) \quad (2-45)$$

In most normative regulations and guidelines, only a reduction of the fatigue strength $\Delta\sigma_C$ or an increase of the applied stress range $\Delta\sigma_R$ is permitted. However, in the guidelines of the IIW [3] and in the guideline of the FKM [11], for example, a modification with a beneficial effect is permitted for minor plate thicknesses.

Many investigations have been conducted to evaluate the influence of thickness. The approaches generally describe the presence of the size effect as a function of the plate thickness T at the hot-spot and the effective connection length L respectively the connection plate thickness t (cf. Figure 2-35).

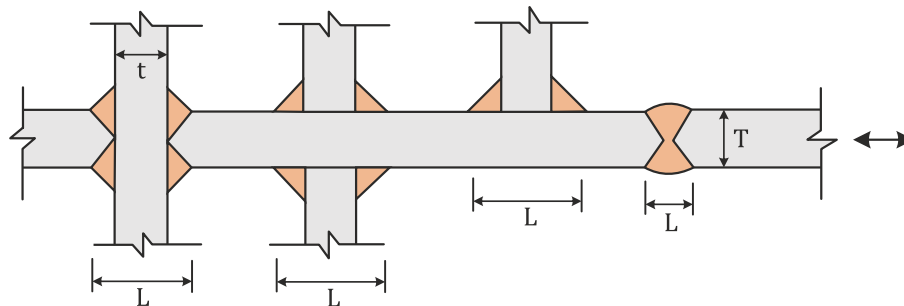


Figure 2-35: Relevant parameters for the determination of the thickness effect [39]

Gurney [76–78], Gordon et al. [75], Lotsberg [12], Kugler [49] and Yamamoto et al. [82], among others, propose different procedures for determining this thickness correction factor $f(t)$. In the field of mechanical engineering, references to thickness effects can also be found, for example, in the design standard for ships [83] of the International Association of Classification Societies (IACS). However, the information from the literature differs with regard of the modification. According to Gurney [76–78], Gordon et al. [75] and Kugler [49], the fatigue strength $\Delta\sigma_C$ requires modification. In the further approaches mentioned, the applied stress range $\Delta\sigma_R$ is to be increased. The thickness correction factor $f(t)$ is in some cases calculated using an effective plate thickness

t_{eff} . In addition, $f(t)$ is partly dependent on the adverse connection length L (cf. Figure 2-35).

In the following Table 2-28, the approaches from the literature are presented, with the respective information about the type of modification, determination of the thickness correction factor $f(t)$ with the corresponding reference thickness t_{ref} as well as, if necessary, about the effective plate thickness t_{eff} . The definition of the required main plate thickness T , the effective connection length L and the connection thickness t can be found in Figure 2-35. In addition, the thickness correction exponent k is given if explicitly specified in the relevant literature source. Where k differs for varying structural details, the full permissible range is provided in Table 2-28.

Table 2-28: Methods for the determination of the thickness correction factor $f(t)$ according to specifications from the literature

Reference	Modification	$f(t)$ [-]	t_{ref} [mm]	t_{eff} [mm]	k [-]
Gurney [76–78]	$\Delta\sigma_{C,mod}$	$f(t) = \left(\frac{t_{ref}}{t_{eff}}\right)^k$	22	$\frac{L}{T} \leq 2$: $\max(0.5 \cdot L; t_{ref})$ $\frac{L}{T} > 2$: T	0.25
Gordon et al. [75]	$\Delta\sigma_{C,mod}$	$f(t) = \left(\frac{25}{T}\right)^{0.23} \cdot \left(\frac{T}{t}\right)^{0.13}$	25	–	–
Lotsberg [12]	$\Delta\sigma_{R,mod}$	$f(t) = \left(\frac{t_{eff}}{t_{ref}}\right)^k$	25	$\min(14\text{mm} + 0.66 \cdot L; T)$	0.10 – 0.30
Kugler [49]	$\Delta\sigma_{C,mod}$	$f(t) = \left(\frac{25}{T}\right)^{0.2} \cdot \left(\frac{15}{L}\right)^{0.16}$	25	$\min(14\text{mm} + 0.66 \cdot L; T)$	–
Yamamoto et al. [82]	$\Delta\sigma_{R,mod}$	$f(t) = \left(\frac{T}{t_{ref}}\right)^k$	22	–	0.00 – 0.25
IACS [83]	$\Delta\sigma_{C,mod}$	$T > t_{ref}$: $t(f) = \left(\frac{T}{t_{ref}}\right)^k$	22	$\min\left(\frac{L}{2}; T\right)$	0.00 – 0.25

It is evident that the specifications from the literature differ. While Gurney [76–78] and Yamamoto et al. [82] define the reference thicknesses t_{ref} to be 22 mm, in the further approaches t_{ref} is given by $t_{ref} = 25$ mm. The thickness correction factor $f(t)$ is also determined in a number of different methods according to Table 2-28. Since research results from [76–78] were able to confirm that starting from an effective connection length $L > 2 \cdot T$ there is no further decrease in fatigue strength, a distinction for t_{eff} is to be made according to Gurney. Lotsberg [12] and Kugler [49] modify this specification to $L > (T - 14 \text{ mm})/0.66$ (cf. Table 2-28).

In the following section, the specifications from normative regulations and guidelines are presented, which are based on the introduced methods from the literature.

2.6.3 Regulatory and guideline specifications for the thickness effect

The influence of the thickness effect results in a reduced fatigue life of components under cyclic loading (cf. Section 2.6.2). Since different procedures for the determination

of the corresponding thickness correction factor $f(t)$ result from the literature, the corresponding specifications of DIN EN 1993-1-9 [2], prEN 1993-1-9 [4], the guidelines of the IIW [3] respective the Designers Guide [9, 65], DNVGL [45, 66] and the guideline of the FKM [11] are presented below. This is followed by a tabular comparison of the normative regulations and guidelines.

2.6.3.1 DIN EN 1993-1-9 and prEN 1993-1-9

In the currently valid version of DIN EN 1993-1-9 [2], the so-called size dependence is considered solely in the nominal stress concept. For this purpose, the fatigue strength $\Delta\sigma_C$ is reduced by the thickness correction factor k_s to $\Delta\sigma_{C,red}$ according to Formula (2-44). The corresponding formulae for the determination of the thickness correction factor k_s are provided at the relevant sections in the fatigue class catalogues for the structural details. However, according to Formula (2-46) this is only the case for bolts and threaded rods under tension and in accordance with Formula (2-47) for transverse and full joints of plates and flat steels. For all further details, no influence resulting from the thickness effect has to be considered. In contrast to the nominal stress concept, the application of the thickness correction factor is not implemented into the structural stress concept by any means. [2]

$$k_s = \left(\frac{30}{\emptyset}\right)^{0.25} \quad (2-46)$$

$$k_s = \left(\frac{25}{t}\right)^{0.2} \quad (2-47)$$

In the new draft of DIN EN 1993-1-9 [2], prEN 1993-1-9 [4], the approach to the thickness factor k_s has not changed in the nominal stress concept. However, according to prEN 1993-1-9 [4], the thickness correction is also specifically addressed in the structural stress concept. The implemented method is based on a combination of the approaches of Gurney [76–78] and Lotsberg [12] (cf. Section 2.6.2). In addition, a limitation is specified that a thickness correction is only required for hot-spot type *a* (cf. Chapter 2.3.3.1). This is due to the fact that the load-bearing plate thickness for hot-spot type *b* only has a minor influence on the applied stress range $\Delta\sigma_R$.

The corresponding Formula (2-48) for the determination of the thickness correction factor k_s regarding the structural stress concept is given below. With the specification $t > t_{ref}$, the application is solely valid for primary plate thicknesses t greater than the reference thickness $t_{ref} = 25 \text{ mm}$. Consequently, only a reduction of the fatigue strength $\Delta\sigma_C$ is possible. The relevant parameters can be taken from Figure 2-35. According to prEN 1993-1-9 [4], the thickness of the main plate T is defined as t and the effective connection length L is denoted by l .

$$k_s = \left(\frac{t_{ref}}{t_{eff}}\right)^\beta \quad (2-48)$$

The thickness correction factor k_s is additionally dependent on an effective plate thickness t_{eff} according to the procedure of Lotsberg [12]. This effective plate thickness t_{eff} must be greater than the reference thickness t_{ref} with $t_{eff} \geq t_{ref}$. According to Formula (2-49), t_{eff} results from the minimum of $14 \text{ mm} + 0.66 \cdot l$ and the primary plate

thickness t . The determination is dependent on the effective connection length l .

$$t_{eff} = \min(14 + 0.66 \cdot l; t) \quad (2-49)$$

The thickness exponent k is defined as β according to prEN 1993-1-9 [4] and results from the corresponding fatigue class catalogue for the structural stress concept. For the structural detail cruciform joint investigated in this thesis $\beta = 0.3$ applies.

2.6.3.2 Guidelines of the IIW and Designers Guide

According to the guidelines of the IIW [3], the thickness correction factor $f(t)$ must be considered in both the nominal and the structural stress concept. In the effective notch stress concept, by contrast, the influence of thickness effects is already included in the applied stress range $\Delta\sigma_R$ due to the method of stress determination (cf. Chapter 2.3.4). For this reason, a modification of effective notch stresses is not necessary. Since the IIW [3] specifies the reference thickness as $t_{ref} = 25 \text{ mm}$, the associated fatigue resistance curves are applicable up to a main plate thickness $t \leq 25 \text{ mm}$. If thicker components with $t > 25 \text{ mm}$ are investigated, it is essential to take the thickness effect into account in the nominal and structural stress concept. As in prEN 1993-1-9 [4], the corresponding correction factor $f(t)$ modifies the fatigue strength $\Delta\sigma_C$ to $\Delta\sigma_{C,mod}$ in accordance with equation (2-44). The modification of the fatigue strength $\Delta\sigma_C$ is done according to the following formula.

$$\Delta\sigma_{C,mod} = \Delta\sigma_C \cdot f(t) \quad (2-50)$$

According to the IIW [3], a positive influence of the thickness effect is also possible. Thus, for plate thicknesses $t < 25 \text{ mm}$, an increase of the fatigue strength $\Delta\sigma_C$ is permitted. In this regard, however, the results have to be verified by adequate component tests.

The corresponding approach to the thickness effect given in the guidelines of the IIW [3] is generally based on Gurney's procedure [76–78]. To this end, under the condition $L/t \geq 2$ the maximum of half the effective connection length $0.5 \cdot L$ and the primary plate thickness t is to be applied. In contrast, Gurney [76–78] selects the maximum of $0.5 \cdot L$ and the reference thickness t_{ref} (cf. Chapter 2.6.2). In addition, the signs of the case distinction L/t are reversed when determining the effective plate thickness t_{eff} . This results in the case distinction for calculating the effective plate thickness t_{eff} according to the following formulae.

$$\begin{aligned} \frac{L}{t} < 2: & \quad t_{eff} = t \\ \frac{L}{t} \geq 2: & \quad t_{eff} = \max(0.5 \cdot L; t) \end{aligned} \quad (2-51)$$

The associated thickness correction factor $f(t)$ is calculated, depending on the effective plate thickness t_{eff} and the reference thickness t_{ref} with the corresponding thickness correction exponent n , according to the following formula.

$$f(t) = \left(\frac{t_{ref}}{t_{eff}} \right)^n \quad (2-52)$$

In further contrast to Gurney [76–78] with a fixed exponent of $n = 0.25$, the thickness

correction exponent n according to the IIW [3] varies depending on the type of weld joint and hot-spot and is generally to be determined according to Table 2-29.

Table 2-29: Specifications for the thickness correction exponent n for determining the thickness correction factor $f(t)$ according to the guidelines of the IIW [3]

Type of welded joint	Condition	n	
hot-spot type a	Cruciform joints, transversely loaded T-joints, plates with transverse attachments, ends of longitudinal stiffeners	as-welded	0.3
	Cruciform joints, transversely loaded T-joints, plates with transverse attachments, ends of longitudinal stiffeners	toe ground	0.2
	Transverse butt welds	as-welded	0.2
	Butt welds ground flush, base material, longitudinal welds, attachments to plate edges	any	0.1
hot-spot type b	Cruciform joints, transversely loaded T-joints, plates with transverse stiffeners, ends of longitudinal stiffeners, transversely loaded butt joints, plate-ground butt joints, base material, longitudinally stressed welds, attachments at plate edges	any	0.1

As the fatigue resistance $\Delta\sigma_C$ of components failing due to cracks at the weld transition decreases with an increasing primary plate thickness t , the modification of the fatigue resistance is of greater relevance for hot-spot type a than for hot-spot type b . Nevertheless, according to the IIW [3], a thickness correction is to be performed for hot-spot type b as well. However, this must be done with a reduced thickness correction exponent of $n = 0.1$.

In contrast to the guidelines of the IIW [3], the Designers Guide [9, 65] remains consistent with Gurney [76–78] in determining the effective plate thickness t_{eff} . Consequently, in accordance with Section 2.6.2, t_{eff} results as follows.

$$\begin{aligned} \frac{L}{t} > 2: & \quad t_{eff} = t \\ \frac{L}{t} \leq 2: & \quad t_{eff} = \max(0.5 \cdot L; t_{ref}) \end{aligned} \quad (2-53)$$

The modification of the fatigue strength to $\Delta\sigma_{C,mod}$ according to Formula (2-50) and the calculation of the thickness correction factor $f(t)$ according to Formula (2-52) are identical to the specifications of the IIW [3]. However, the Designers Guide [9, 65] classifies the thickness exponent n of longitudinal stiffeners as $n = 0.1$.

2.6.3.3 DNVGL

Deviating from prEN 1993-1-9 [4] and the guidelines of the IIW [3], the applied stress range $\Delta\sigma_R$ is modified by the thickness correction factor according to DNVGL-RP-C203 [66]. The applied stress range $\Delta\sigma_R$ is defined as $\Delta\sigma$ according to [66]. The corresponding reference thickness t_{ref} is set at $t_{ref} = 25 \text{ mm}$. Due to the specification that $t = t_{ref}$, if the primary plate thickness t is smaller than the reference thickness t_{ref} , a reduction of the stress range $\Delta\sigma$ according to DNVGL [66] is not permitted. The number of stress cycles N , taking into account the thickness effect according to [66], is determined according to the following formula.

$$\log(N) = \log(\bar{a}) - m \cdot \log\left(\Delta\sigma \cdot \left(\frac{t}{t_{ref}}\right)^k\right) \quad (2-54)$$

In this regard, $\log(\bar{a})$ corresponds to the intersection of the design S-N curve with the $\log(N)$ axis and m to the negative slope of the S-N curve. Accordingly, the corresponding thickness correction factor $f(t)$ for the increase of the stress range $\Delta\sigma$ can be given as follows and depends on the thickness exponent k .

$$f(t) = \left(\frac{t}{t_{ref}}\right)^k \quad (2-55)$$

According to DNVGL-RP-C203 [66], the thickness exponent k depends solely on the fatigue resistance class and not on the type of construction examined. In the case of cruciform joints, k can therefore be determined in accordance with the fatigue resistance class to be applied from Chapter 2.4.5.2. The required thickness exponent k is summarised in the following Table 2-30.

Table 2-30: Thickness correction factor k according to DNVGL-RP-C203 [66]

Fatigue resistance class	Calculated fatigue strength $\Delta\sigma_C$ at 6 million load cycles [N/mm ²]	Thickness correction factor k [-]
E	80	0.20
F	71	0.25

Figure 2-36 shows the influence of the thickness correction factor $f(t)$ on the allowable stress cycles N according to Formula (2-55) of DNVGL-RP-C203 [66] as a function of the main plate thickness t for different thickness exponents k . The results are based on the assumption of a structural detail with a utilisation ratio of $\Delta\sigma_R/\Delta\sigma_C = 100\%$.

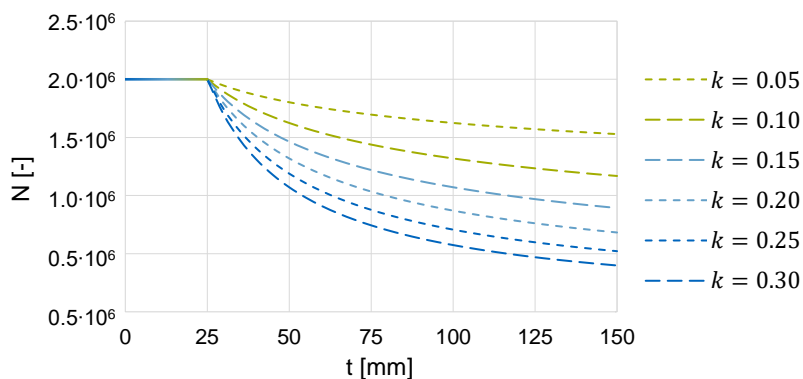


Figure 2-36: Reduction of the allowable stress cycles N due to the thickness effect $f(t)$ with different thickness exponents k according to [66]

Since no reduction of the applied stress range $\Delta\sigma$ is possible, stress cycles of $N = 2 \cdot 10^6$ are obtained up to a primary plate thickness of $t = 25 \text{ mm}$. The larger the thickness exponent k , the more the achievable load cycles N are reduced (cf. Figure 2-36).

With regard to cruciform joints, DNVGL-RP-C203 [66] additionally specifies an effective plate thickness t_{eff} , which replaces Formula (2-55) with Formula (2-56).

$$f(t_{eff}) = \left(\frac{t_{eff}}{t_{ref}}\right)^k \quad (2-56)$$

This is due to the increasing influence of the effective connection length L_t (cf. Figure 2-37). Without taking L_t into consideration, the thickness effect $f(t)$ for cruciform joints is likely to be overestimated.

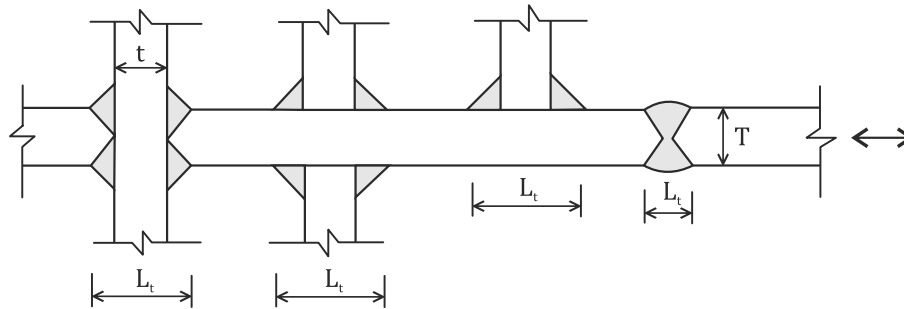


Figure 2-37: Relevant parameters for the effective connection length L_t , the connection thickness t and the main plate thickness T according to DNVGL-RP-C203 [66]

The corresponding effective plate thickness t_{eff} is determined according to Formula (2-49) in accordance with prEN 1993-1-9 [4] and is limited to $t_{eff} \geq t_{ref}$. The calculation according to DNVGL-RP-C203 [66] is given below with the correct parameter designation.

$$t_{eff} = \min ((14 \text{ mm} + 0.66 \cdot L_t); T) \quad (2-57)$$

Figure 2-38 shows the associated correlation between the attainable load cycles N_R and the effective plate thickness t_{eff} .

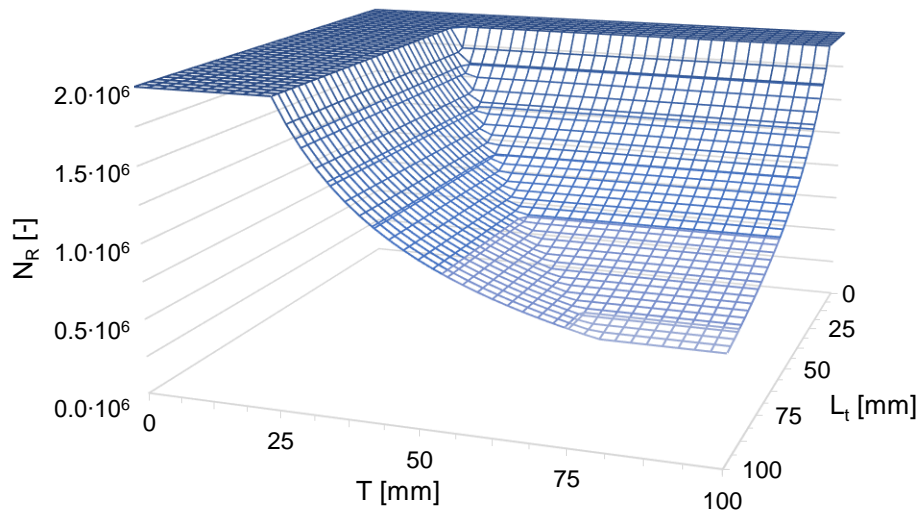


Figure 2-38: Reduction of the attainable stress cycles N_R due to the thickness effect $f(t)$ using t_{eff} with thickness exponent $k = 0.3$ according to [66]

According to Formula (2-57), the effective plate thickness t_{eff} depends on both the main plate thickness T and the effective connection length L_t . Figure 2-38 illustrates that small plate thicknesses $T < 25 \text{ mm}$ and small effective connection lengths $L_t < 16.6 \text{ mm}$ do not result in an increase of the applied stress range $\Delta\sigma$ and thus do not reduce the tolerable load cycles N_R . In comparison, large plate widths T in combination with large effective connection lengths L_t have a significant negative effect on the

fatigue behaviour. For example, with $T > 80 \text{ mm}$ and $L_t = 100 \text{ mm}$, only $N_R = 7 \cdot 10^5$ load cycles can be obtained.

DNVGL-CG-0129 [45] for offshore steel structures also provides information on the thickness effect using the factor f_{thick} . According to [45], the fatigue strength $\Delta\sigma_C$ depends to some extent on the plate thickness t . The local geometry of the weld in relation to the thickness of the adjacent plates is considered responsible for this effect. In addition, the thickness effect depends on the stress gradient across the thickness, which can differ for axial and bending stress (cf. Chapter 2.6.2). According to DNVGL-CG-0129 [45], the component-specific fatigue strength $\Delta\sigma_C$ consequently covers component thicknesses up to $t \leq 25 \text{ mm}$. Starting with $t > 25 \text{ mm}$, the applied stress range $\Delta\sigma_R$ must be increased according to Formulae (2-54), (2-55), (2-56) and (2-57) already presented. However, for the effective connection length d , which corresponds to L_t according to [48] (cf. Figure 2-39), three times the connection thickness t_a is suggested for cruciform joints. Thus, the effective connection length d results in $d = 3 \cdot t_a$.

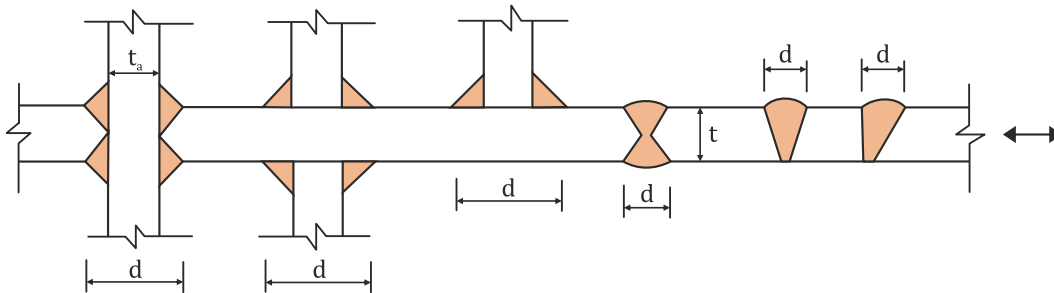


Figure 2-39: Relevant parameters for the effective connection length d , the connection thickness t_a and the main plate thickness t according to DNVGL-CG-0129 [45]

Furthermore, the thickness exponent $n = 0.2$ of DNVGL-CG-0129 [45] differs from the specifications of DNVGL-RP-C203 [66].

2.6.3.4 Guideline of the FKM

The guideline of the FKM [11] also has implemented the thickness factor f_t to consider the influence of the plate thickness on the fatigue strength $\Delta\sigma_C$. According to [11], the thickness effect must be taken into consideration starting at a decisive thickness of 25 mm . This applies to both the nominal and the structural stress concept. The fatigue strength $\Delta\sigma_C$ of structures with primary plate thicknesses $t > 25 \text{ mm}$ must consequently be modified according to Formula (2-44). Cases *A* and *B* are available in the guideline of the FKM [11] for this purpose. While case *A* may be used without further conditions, case *B* is only applicable if own or industry-specific experience is available.

According to case *A* from [11], the thickness correction factor f_t is determined with the following formula.

$$f_t = \left(\frac{25 \text{ mm}}{t} \right)^n \quad (2-58)$$

According to the guideline of the FKM [11] in the determination of the thickness correction factor $f(t)$ the plate thickness t is directly included in Formula (2-58). The additionally required thickness exponent n is defined in Table 2-31.

Table 2-31: Thickness exponent n for the thickness correction f_t according to guideline of the FKM [11]

Type of welded joint	n [-]
Cruciform and transverse loaded T-joints, plates with transverse attachments, ends of longitudinal stiffeners	
- as-welded	0.3
- ground weld transition	0.2
Transversely loaded butt joints, as-welded	0.2
Plate-flat ground butt joints, longitudinally stressed welds or welded-on parts	0.1

In addition, the FKM [11] defines further formulae for the additionally specified case B , which allow an increase in the fatigue strength $\Delta\sigma_C$ for a plate thickness t of less than $t < 25 \text{ mm}$. However, the industry-specific experience required for applying Case B is predominantly available in automotive or rail vehicle construction. Although there is limited experience in the construction field, the defined formulae are presented below.

$$\begin{aligned}
 t \leq 10 \text{ mm}: & \quad f_t = 1.1 \\
 10 \text{ mm} < t \leq 25 \text{ mm}: & \quad f_t = \left(\frac{25 \text{ mm}}{t}\right)^{0.1} \\
 t > 25 \text{ mm}: & \quad f_t = \left(\frac{25 \text{ mm}}{t}\right)^n
 \end{aligned} \tag{2-59}$$

Figure 2-40 illustrates the influence of the main plate thickness t on the thickness correction factor $f(t)$ for case A according to formulae (2-58) and case B according to formulae (2-59) for all available thickness exponents k according to the FKM [11].

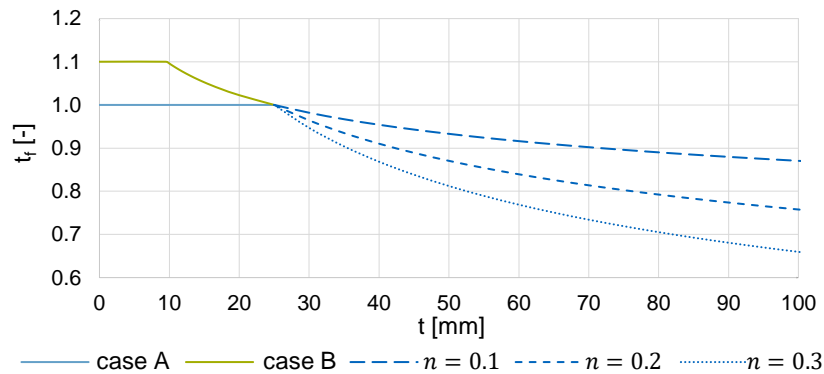


Figure 2-40: Factor f_t for case A and B for relevant thickness exponents n according to the FKM [11]

Due to the possible increase of the fatigue resistance $\Delta\sigma_C$ for plate thicknesses $t < 25 \text{ mm}$ according to case B , thickness correction factors up to $t_f = 1.1$ can be attained. Consequently, by applying case B , it would be permissible to increase the fatigue strength to 110% (cf. Figure 2-40). By contrast, the fatigue strength of case A remains constant until $t = 25 \text{ mm}$. However, in both cases there is an identical reduction of the fatigue strength $\Delta\sigma_C$ for plate thicknesses $t > 25 \text{ mm}$, which depends on the thickness exponent n according to Table 2-31. This modification of $\Delta\sigma_C$ can be significant. For example, the fatigue strength of a cruciform joint without post-weld treatment and a load-bearing plate thickness of $t = 100 \text{ mm}$ must be reduced to at least 66 % according to the thickness correction of the guideline of the FKM [11].

2.6.3.5 Summary

Table 2-32 provides a tabular summary of the presented specifications of the normative guidelines and regulations. As described in Section 2.6.2 (cf. Table 2-28), there are also significant differences in the normative determination of the thickness correction factors.

Table 2-32: Summary for the normative determination of the thickness effect of cruciform joints according to different normative regulations and guidelines

Normative regulations or guidelines	Modification	$\Delta\sigma_{nom}$	$\Delta\sigma_{hs}$	Thickness correction factor $f(t)$ resp. k_s [-]	Reference thickness t_{ref} [mm]	Effective plate thickness t_{eff} [mm]	Thickness exponent β resp. n resp. k [-]
DIN EN 1993-1-9 [2]	$\Delta\sigma_C$	✓	–	–	–	–	–
prEN 1993-1-9 [4]	$\Delta\sigma_C$	✓	✓	$k_s = \left(\frac{t_{ref}}{t_{eff}}\right)^\beta$ $t > t_{ref}$	25.0	$\min\left\{\frac{14\text{ mm} + 0.66 \cdot l}{t}\right.$ $t_{eff} \geq t_{ref}$	0.3
Guidelines of the IIW [3]	$\Delta\sigma_C$	✓	✓	$f(t) = \left(\frac{t_{ref}}{t_{eff}}\right)^n$	25.0	$\frac{L}{t} < 2$: t $\frac{L}{t} \geq 2$: $\max\left\{\frac{L}{2}, t\right\}$	0.3
Designer's Guide [9, 65]	$\Delta\sigma_C$	✓	✓	$f(t) = \left(\frac{t_{ref}}{t_{eff}}\right)^n$	25.0	$\frac{L}{t} > 2$: t $\frac{L}{t} \leq 2$: $\max\left\{\frac{L}{2}, t_{ref}\right\}$	0.3
DNVGL-RP-C203 [66]	$\Delta\sigma_R$	✓	✓	<i>in general:</i> $f(t) = \left(\frac{t}{t_{ref}}\right)^k$ $t \geq t_{ref}$ <i>cruciform joints:</i> $f(t) = \left(\frac{t_{eff}}{t_{ref}}\right)^k$	25.0	$\min\left\{\frac{14\text{ mm} + 0.66 \cdot L_t}{t}\right.$ $t_{eff} \geq t_{ref}$	0.25
DNVGL-CG-0129 [45]	$\Delta\sigma_R$	✓	✓	<i>in general:</i> $f(t) = \left(\frac{t}{t_{ref}}\right)^k$ $t \geq t_{ref}$ <i>cruciform joints:</i> $f(t) = \left(\frac{t_{eff}}{t_{ref}}\right)^k$	25.0	$\min\left\{\frac{14\text{ mm} + 0.66 \cdot L_t}{t}\right.$ $d = 3 \cdot t_a$ $t_{eff} \geq t_{ref}$	0.2
Guideline of FKM [11]	$\Delta\sigma_C$	✓	✓	$f(t) = \left(\frac{t_{ref}}{t_{eff}}\right)^n$	25.0	–	0.3

3 Principles of the finite element analysis

In contrast to the application of the nominal stress concept, finite element analysis is required for the determination of structural stresses. This chapter therefore refers specifically to the design of adequate FE models associated with the structural stress concept. The objective is to create uniform FE models that can be used to carry out congruent parameter studies, to recalculate experimental test data and to develop solution strategies for determining effects of imperfections and varying thicknesses. The main focus is on the linear stress extrapolation, addressed in the guidelines of the IIW [3], in prEN 1993-1-9 [4] as well as in prEN 1993-1-14 [14]. However, information is also provided on further local methods.

In addition to the method of stress determination, the structural stress in the FE model depends to a large extent on practical meshing and an appropriate choice of the element type with its properties. For this purpose, effective element types with their corresponding initial function are presented (cf. Section 3.1). Section 3.2 provides normative meshing recommendations for the stress extrapolation (cf. Chapter 3.2.1) as well as for additional local procedures (cf. Chapter 3.2.2), whereby the way in which the relevant structural stresses are determined represents an important factor for the correct choice of meshing. Section 3.3 addresses the associated implementation of the finite element analysis in this thesis. This includes information on the selected element classifications (cf. Section 3.3.1), the procedures for a suitable consideration of imperfections (cf. Section 3.3.2) and for the support definition and load introduction in the FEA (cf. Section 3.3.3). Furthermore, the comparative evaluation and determination of suitable local methods (cf. Section 3.3.4) the sensible weld modelling of shell models (cf. Section 3.3.5) and the handling of thickness effects (cf. Section 3.3.6) are explained in more detail. Finally, Section 3.3.7 presents the implementation of the FE calculations using ANSYS APDL (Ansys Parametric Design Language) as a partial function in associated Python scripts.

3.1 Selection of element type

In general, applying the structural stress concept requires a relatively high level of expertise on the part of the FEA user [3]. In principle, the application of models with 2D shell elements as well as with 3D solid elements is feasible, as both can determine the required normal and principal stresses consisting of membrane and bending stresses. However, some local methods (cf. Chapter 2.3.3) only enable solid models. This can be attributed to the required stress distribution over the component thickness, which cannot be sufficiently determined by shell elements.

Whereas shell models allow for less time-consuming FE calculations, solid models are better suited for the analysis of complex structures. Therefore, the use of local submodels is often recommended when applying the structural stress concept. Thus, coarsely meshed shell models are sufficient for calculating the global load-bearing

behaviour. Using adequate submodels, the local structural stress of a complex constructional detail can nevertheless be captured with reasonable accuracy using a finely meshed solid model. Consequently, the computational and modelling complexity of extensive constructions can be minimised by submodels. [49]

Accordingly, basic information on the normative specifications and initial functions is given for shell elements (cf. section 3.1.1) as well as for solid elements (cf. section 3.1.2). The contents are based on the guidelines of the IIW [3, 9, 65] and prEN 1993-1-14 [14].

3.1.1 Shell elements

Shell models are composed of simplified two-dimensional shell elements whose modelled centre is placed in the centre plane of plates. These elements are particularly suitable if one component dimension is significantly smaller than the other two. The advantage of these elements is the reduced number of degrees of freedom (DOF) and the resulting shorter calculation time.

3.1.1.1 General application

In general, shell elements with four nodes and associated degrees of freedom are possible. Degrees of freedom are defined respectively by the translations in x -, y - and z -direction as well as by the rotations around the x -, y - and z -axis. According to prEN 1993-1-14 [14] it is specified that elements must have at least five or six of these degrees of freedom. However, in order to be able to identify the increasing stress gradient at the hot-spot in front of the notch, elements with eight nodes and a corresponding quadratic initial function with six degrees of freedom per node are recommended. The resulting nodes are located at the corners as well as in the middle of the edges of the element (cf. Figure 3-1). Thus, only quadratic distributions in the local x - and y -direction can be determined with these elements. [6, 3, 14, 84]

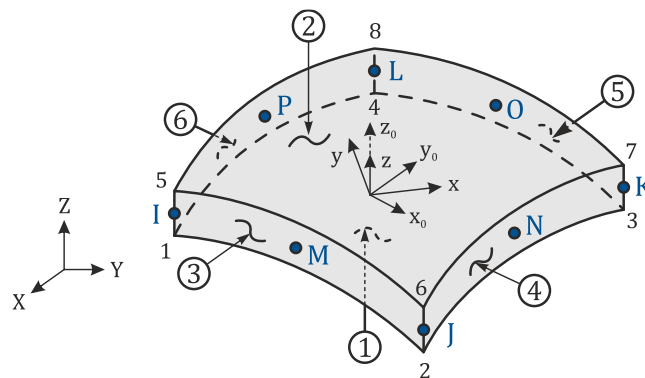


Figure 3-1: Illustration of eight node shell elements [85]

Due to the specified alignment of the nodes in the centre plane (cf. Figure 3-1), the component thickness is included in the FE calculation as a pure element parameter. As a result, only constant membrane and linear bending stress distributions, as well as their combination, are feasible in the local z -direction. Accordingly, non-linear notch stress characteristics are suppressed over the plate thickness. Shared nodes of adjacent elements must have the same displacement in this respect. As a consequence, it is important that adjoining parts are extended to the centre plane of

the connection component or are coupled together by rigid links. With shell elements, it must also be ensured that the relevant stress is analysed, since these have a total of three defined stresses at each specified node. These are located on the upper and lower as well as on the middle surface of the elements. According to prEN 1993-1-14 [14] the stresses corresponding to the expected crack location are to be evaluated in this regard. [6, 3, 14]

3.1.1.2 Consideration of welds

According to the guidelines of the IIW [3, 9, 65] and prEN 1993-1-14 [14], the explicit modelling of welds can be omitted in simplified FE models. However, this simplified procedure is only permissible if the expected results are not influenced by local bending and/or if welds are located too close to each other. In addition, welds should be modelled without exception if they are the main source of stress concentration. Figure 3-2 illustrates examples where the weld has a decisive effect on the global system and therefore must not be neglected.

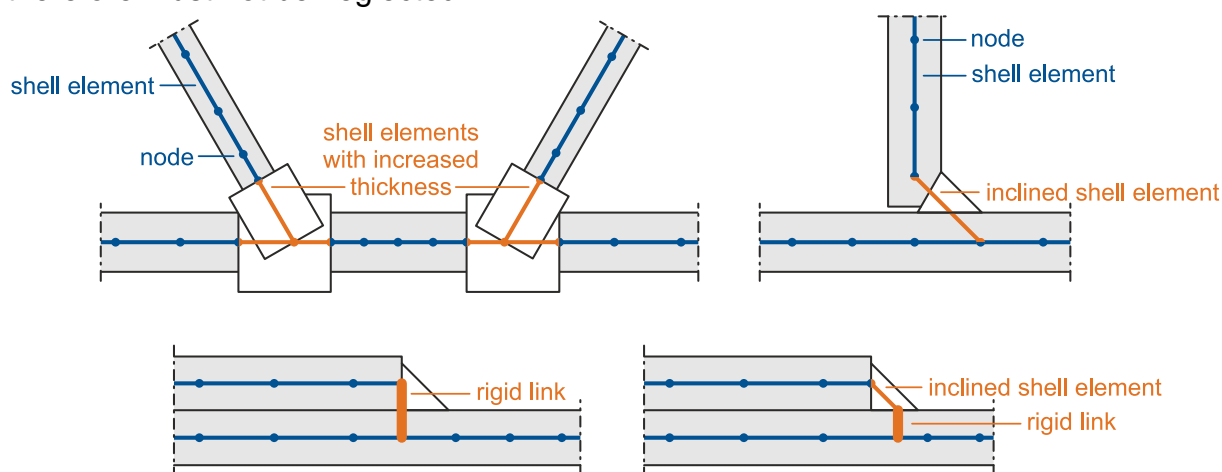


Figure 3-2: Exemplary shell models for a K-joint (top left), a welded-on T-joint (top right) and a cover plate joint (bottom) with required modelling of the welds due to the decisive effect on the detail [6]

According to Figure 3-2, the actual stiffness of welds should be considered as realistically as possible, for example in the case of K-joints with a small distance between the adjacent welds (cf. top left side of Figure 3-2), in the case of T-joints welded on one side (cf. top right side of Figure 3-2), in the case of cover plate joints (cf. bottom of Figure 3-2) or in the case of axial misalignment between two plates. In addition to the simplified modelling without welds (cf. Section 3.1.1.2.1), different methods are available in this respect. These include the consideration of enhanced stiffness through an increased cross-sectional area in the region of the welds (cf. top left side of Figure 3-2 and Section 3.1.1.2.2), the connection of plates through inclined shell elements (cf. top right side of Figure 3-2 and Section 3.1.1.2.3), as well as the connection of components by rigid links (cf. bottom left side of Figure 3-2 and Section 3.1.1.2.4). In addition, welds can be modelled by a combination of rigid links and inclined shell elements (cf. bottom right side of Figure 3-2 and Section 3.1.1.2.4). The different methods for weld modelling with shell elements are presented in more detail below.

3.1.1.2.1 No consideration of welds

Since welds do not need to be explicitly modelled in this procedure, this represents the simplest modelling method. As a consequence, the welded-on plates of cruciform joints are only connected to the intermediate plate at the intersection of the centre planes. This results in the disadvantage that adjacent components are only connected with a single array of element nodes, which can lead to a significant overestimation of the membrane stresses, especially in the case of small load introduction areas. For this reason, the guidelines of the IIW [3] recommend taking the mean value of the stresses across the full thickness span of the welded-on component if there is a narrow load introduction. This is due to the fact that associated joints in reality often contain surrounding welds and the corresponding load introduction width is consequently composed of the lateral welds in addition to the thickness of the component. However, these specifications are not considered in this thesis due to the large load application width of cruciform joints. In addition, investigations in IGF research project No. 20336N [1] without the explicit consideration of welds in shell models indicate an underestimation of the stiffness in the area of the weld, which can lead to incorrect results. With regard to surface methods for the structural stress determination according to chapter 2.3.3, [1] further demonstrates that the required reference points for thin primary plates in combination with thick intermediate plates of cruciform joints are located too closely to the weld in the area influenced by the transverse strain restraint. Consequently, in many cases no realistic results can be achieved compared to solid models with modelled welds. For these reasons, further modelling variants are introduced below.

3.1.1.2.2 Increased cross-sectional area

The required increased stiffness in the area of the welds is implemented in this method by enlarging the cross-sectional area (cf. top left side of Figure 3-2). In the case of cruciform joints, this applies to both the area of the intermediate plate and of the welded-on plates. The enlarged cross-sectional area is implemented according to [86, 87] by an increased thickness of the shell elements by the value of the weld thickness a . The corresponding procedure is shown in Figure 3-3. The modelling effort is only slightly higher compared to the method without the explicit consideration of welds (cf. Section 3.1.1.2.1). However, there are no specifications in the literature on how to apply the methodology if imperfections are to be expected.

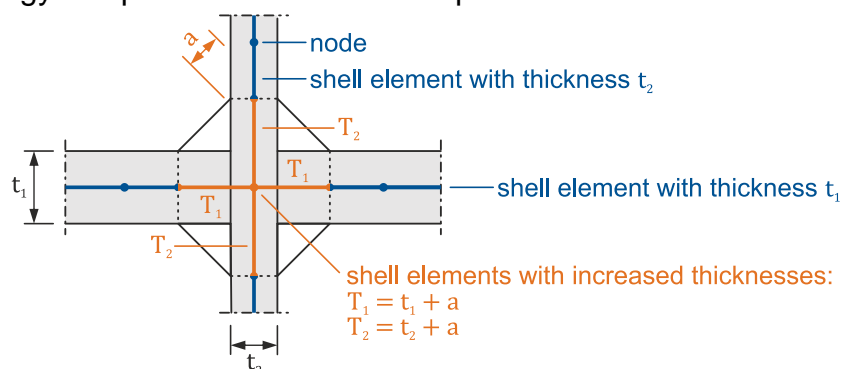


Figure 3-3: Modelling of welds in shell models by increasing the element thickness to ensure an enlarged stiffness in the area of the weld [87]

3.1.1.2.3 Vertical or inclined shell elements

According to the guidelines of the IIW [3, 9], welds can also be implemented by vertical or inclined shell elements with an appropriate stiffness, if the modelling of welds is required (cf. top right side of Figure 3-2). prEN 1993-1-14 [14] proposes this approach as well, but does not provide any information on the particular implementation. The procedure according to the IIW [3, 9] is illustrated in Figure 3-4.

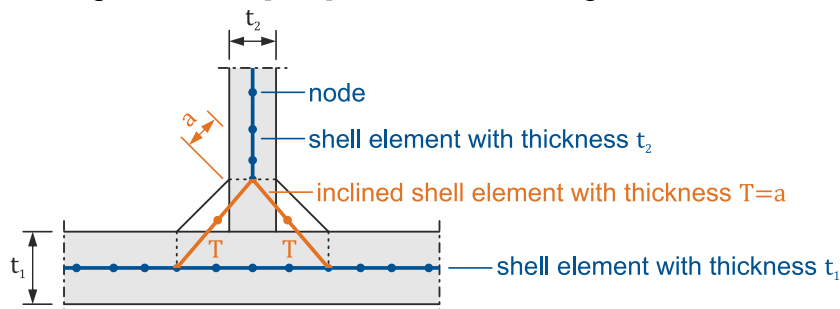


Figure 3-4: Modelling of welds in shell models by inclined shell elements between the centre planes of the plates [3]

Figure 3-4 shows the weld modelling of a shell model for a T-joint connected by fillet welds without full penetration. Due to the lack of a full penetration, the attached plate is only linked to the primary plate through the inclined shell elements on either side (cf. right side of Figure 3-5). The thickness of the inclined elements is considered to be equal to the weld thickness $T = a$.

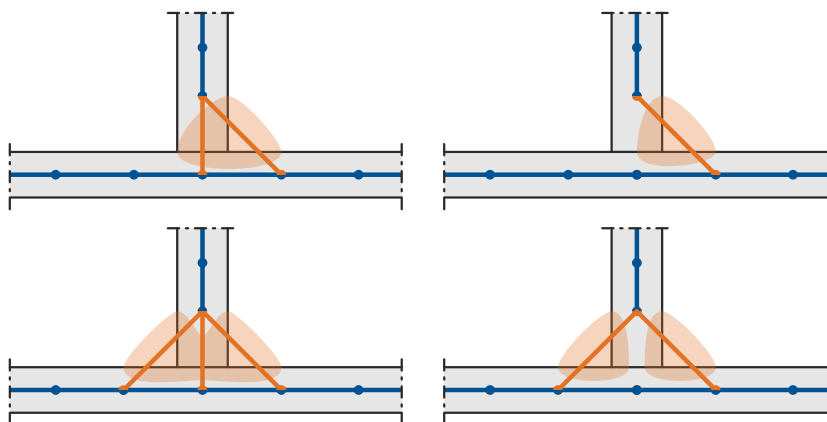


Figure 3-5: Modelling of welds in shell models by inclined shell elements for full penetration welds (left) and fillet welds (right) [88]

In the case of single-sided or double-sided full penetration welds, the FE connection of the joint is realised according to the left side of Figure 3-5. In this respect, in addition to the connection through the inclined shell elements, the centre plane of the attached plate is directly connected to the centre plane of the main plate. Again, the thickness of the inclined shell elements T is associated with the fillet weld thickness a .

According to [9], however, it is possible that the load-bearing capacity of longitudinally stressed welds is overestimated in the presented method with vertical or inclined shell elements due to the exaggerated modelling of the cross-sectional area of the weld. This can result in an inaccurate evaluation of longitudinally loaded welds. In addition, significantly differing plate thicknesses of the primary plate and the welded-on plates can result in an unrealistic high or low inclination of the shell elements.

3.1.1.2.4 Rigid links

In order to avoid the difficulties of an excessive cross-sectional area as described in Section 3.1.1.2.3, the guidelines of the IIW [3] as well as prEN 1993-1-14 [14], among others, recommend the introduction of constrained equations respectively rigid links for the coupling of nodal displacements of the weld (cf. bottom side of Figure 3-2). This enables the weld to be modelled with its true cross-sectional area in its actual position and length. However, this modelling method is time-consuming and complex, as additional nodes and rigid links have to be integrated into the FE model.

When the method is applied, welds only have to be modelled in the area of fillet welds by means of inclined shell elements. For this purpose, the thickness of the shell elements T of the welds is to be arranged with the actual weld thickness a in the centre of gravity of the weld. The end nodes are then connected to the centre plane of the joining plates through rigid links. The corresponding procedure is illustrated in Figure 3-6. [61]

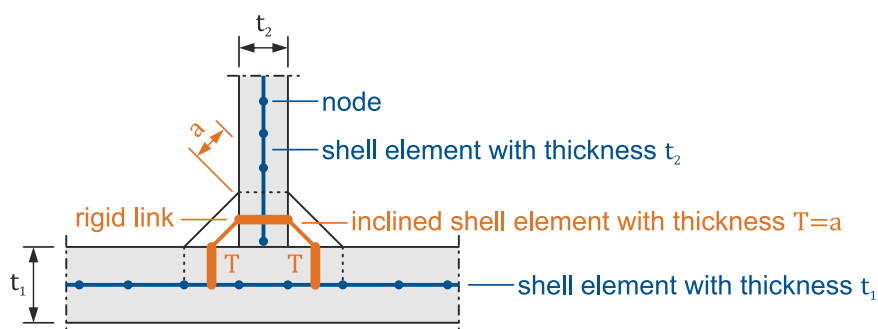


Figure 3-6: Modelling of welds in shell models by inclined shell elements in combination with rigid links connecting the centre planes of the plates [3]

According to Figure 3-6, the end nodes of the inclined shell elements are each coupled by rigid links to the shell elements of the adjacent components. In addition, there are details, including cover plate joints, that allow a direct connection through rigid links without requiring the integration of inclined shell elements (cf. bottom left side of Figure 3-2).

3.1.2 Solid elements

According to [9], higher order elements are generally to be used when solid elements are applied in FE calculations. As a result, steep stress gradients over the thickness of components can be determined. In this respect, isoparametric elements with twenty nodes are recommended, each defined with three translational degrees of freedom (cf. left side of Figure 3-7). This also ensures the implementation of relatively coarse meshes according to the guidelines of the IIW [3], as a quadratic stress distribution over the plate thickness can be guaranteed even with only one solid element over the thickness. In addition, solid elements with eight nodes can be used, which are based on a linear initial element function (cf. right side of Figure 3-7). Critical effects can be caused if these first-order elements are subjected to bending loads. If solid elements with eight nodes are fully integrated, the so-called shear locking effect can result (cf. left side of Figure 3-8).

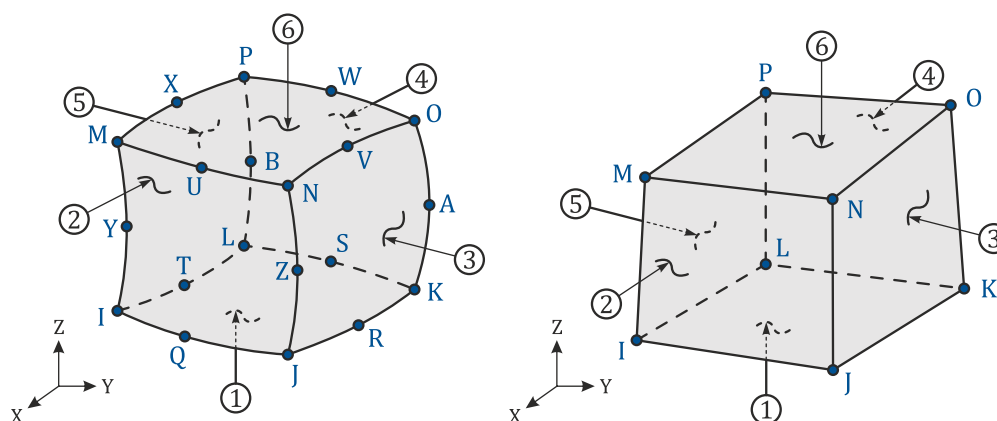


Figure 3-7: Solid element with twenty nodes and a quadratic initial element function (left) and solid node with eight nodes and a linear initial element function (right) [85]

This effect is due to induced shear strains that occur because the element edges do not enable bending. This can lead to an overestimation of the element stiffness. The shear locking effect could be circumvented with first-order elements and a reduced integration. However, with first-order elements and a reduced integration, the so-called hourglassing effect can arise (cf. right side of Figure 3-8). In this case, the resulting single integration point can lead to strain-free deformation modes, since neither the lengths nor the angles change due to the applied deformation. As a consequence, the results may be significantly distorted. Accordingly, to avoid the shear locking and hourglassing effect in coarsely meshed FE solid models, second order elements should be implemented.

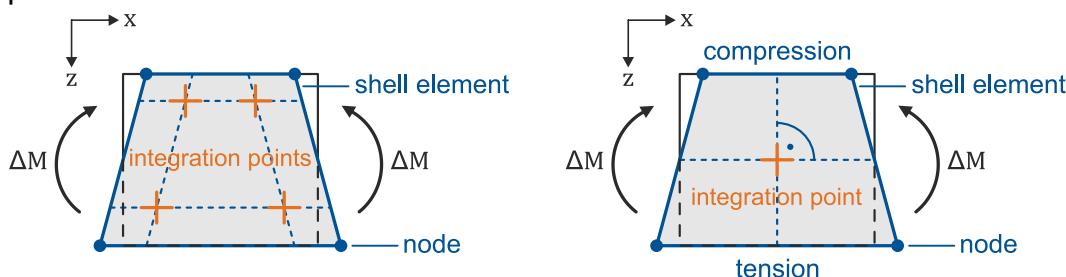


Figure 3-8: Shear locking effect with fully integrated first-order element (left) and hourglassing with reduced integrated first-order element (right) under bending loading

According to prEN 1993-1-14 [14], the choice of the initial element function (linear or quadratic) is left to the user, provided that a relatively fine mesh with solid elements is utilised for the evaluation of the structural stress. In case of a deviating meshing choice, also higher order initial element functions are recommended. Furthermore, [14] explicitly states that the loads and support conditions must be compatible with the degrees of freedom of the applied elements.

The application of solid elements in FE models also enables a more accurate modelling of the welds, as they can be represented in actual size and with their true stiffness without extensive considerations. This enables even complex welding details to be analysed in great detail. Consequently, it is generally recommended for solid models that the welds are modelled as accurately as possible in the FE model. This is especially true if they are the decisive source for the stress concentration or are required to capture the correct stiffness of a detail. On this matter, it is noted in [9] that for round modelled welds, the location of the critical structural stress may be less

apparent. For the stress extrapolation (cf. Chapter 2.3.3.1), extrapolation up to the intersection of the plate surfaces is recommended in this respect in order to avoid underestimating the stress due to the resulting lack of stiffness. [3]

3.2 Meshing

In addition to the choice of element type and the associated initial element function, the degree of FE meshing is a significant factor and depends on the local method applied to determine the relevant structural stress. Therefore, suitable meshing specifications for shell and solid models are presented separately below for the local concepts introduced in Chapter 2.3.3.

3.2.1 Meshing according to the stress extrapolation

Since a large number of normative regulations and guidelines are based on the stress extrapolation according to the IIW [3], the associated meshing specifications are presented in more detail below. The new draft prEN 1993-1-14 [14] also solely addresses the stress extrapolation (cf. Chapter 2.3.3.1). However, since the meshing specifications differ in some aspects, the recommendations are listed separately according to IIW [3] and prEN 1993-14 [14].

3.2.1.1.1 Guidelines of the IIW

For the structural stress determination, both shell and solid models are available for the extrapolation according to the guidelines of the IIW [3]. Although a linear stress distribution in the direction of the plate thickness would be sufficient for determining the structural stress on the surface of the plate, it is important to ensure that the elements and the associated element arrangement allow steep stress gradients and plate bending according to [3, 6]. In addition, the type of the mesh influences the selection of the reference points and their extrapolation (cf. Chapter 2.4.2.2). Depending on a fine or coarse meshing, as well as on the type of hot-spot present, this results in different distances between the reference points and the notch. These are illustrated in Figure 3-9. According to Figure 3-9, the guidelines of the IIW [3] for hot-spot type *a* and type *b* each specify two alternative meshing approaches for the determination of the structural stress by extrapolation method. These are differentiated according to a relatively coarse and a relatively fine mesh. While the distances of the reference points required for the stress extrapolation always depend on the thickness for hot-spot type *a*, these are defined at fixed distances to the notch for hot-spot type *b*, which have to be independent of the plate thickness. This is true regardless of the meshing method applied (cf. Chapter 2.4.2.2). As illustrated in Figure 3-9, the lengths of the elements are dependent on the position of the reference points required for the stress evaluation. To avoid interference by the stress singularity of the notch with a relatively fine mesh, the length of the first element equals its distance from the first reference point (cf. left side of Figure 3-9). If even finer meshes are applied, a refinement in the direction of the thickness is also necessary according to the IIW [3]. Relatively coarse meshes are possible as well. However, higher order elements are required in these cases, as the necessary stresses have to be determined at the centre node of the elements (cf. right side of Figure 3-9). [3]

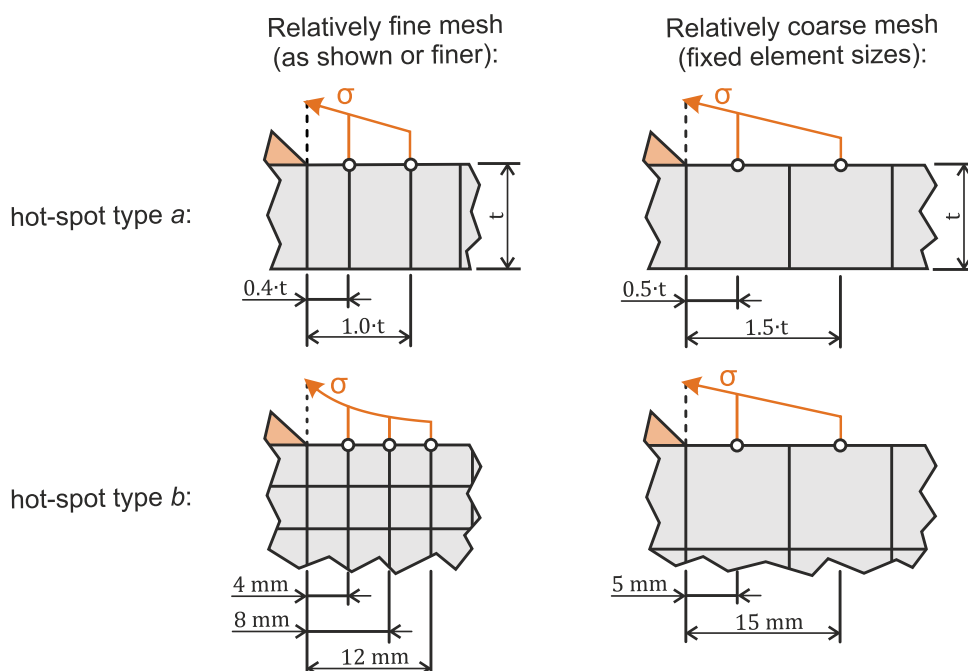


Figure 3-9: Position of reference points and associated meshing recommendations for the stress extrapolation according to the IIW [3]

Table 3-1 provides the associated specifications for element sizes regarding shell and solid models with a relatively fine and course mesh. [3]

Table 3-1: Recommended element sizes for relatively fine and relatively coarse models [9]

Type of model and weld toe	Relatively fine models		Relatively course models		
	Type a	Type b	Type a	Type b	
Element size	Shells	$\leq 0.4 \cdot t \cdot x \cdot t$ $\leq 0.4 \cdot t \cdot x \cdot w/2$	$\leq 4 \text{ mm} \times 4 \text{ mm}$	$\leq t \cdot x \cdot t$ $\leq t \cdot x \cdot w/2$	$10 \text{ mm} \times 10 \text{ mm}$
	Solids	$\leq 0.4 \cdot t \cdot x \cdot t$ $\leq 0.4 \cdot t \cdot x \cdot w/2$	$\leq 4 \text{ mm} \times 4 \text{ mm}$	$\leq t \cdot x \cdot t$ $\leq t \cdot x \cdot w$	$10 \text{ mm} \times 10 \text{ mm}$

$$w = \text{longitudinal attachment thickness} + 2 \cdot \text{leg length of the weld}$$

Furthermore, the element width w is of essential importance and can cause blurred results with excessive dimensioning. This is especially true for steep stress gradients across the component width, as caused, for example, by transverse strain restraint. For relatively coarsely meshed solid models, the maximum permissible element width w in the area of the critical structural stress should therefore not exceed the sum of the longitudinal connection thickness plus twice the weld leg length (cf. right side of Figure 3-10). In all other cases, the maximum width w is set at $w/2$. [3]

In Figure 3-10, typical extrapolation paths for determining the structural stress on shell and solid models on the component surface and at the plate edge are additionally illustrated by arrows. In this respect, when modelling shell elements without the explicit consideration of welds (cf. Section 3.1.1.2.1), the guidelines of the IIW [3] recommend a stress extrapolation to the intersection of the plate centre surfaces. This avoids the underestimation of the structural stress due to the missing stiffness of the weld (cf. left side of Figure 3-10). [3]

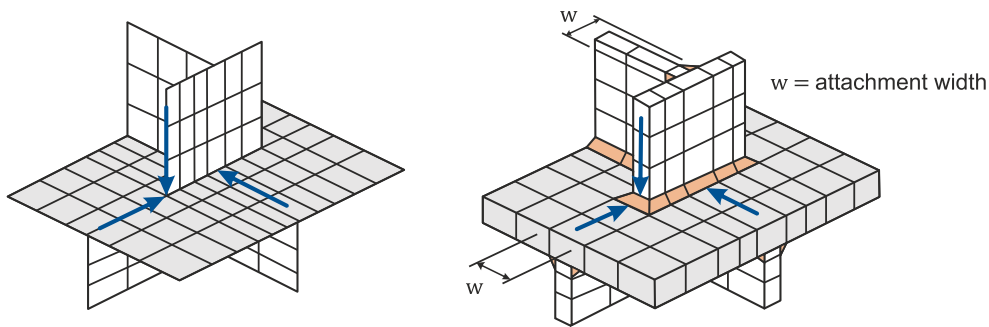


Figure 3-10: Characteristic meshing and stress extrapolation paths for shell element models without modelling of the weld (left) and solid element models with modelling of the weld (right) according to the guidelines of the IIW [3]

For the extrapolation paths according to the IIW [3], a mesh-dependent linear or quadratic extrapolation formula is required for each type of hot-spot. The necessary case distinctions were presented in Chapter 2.4.2.2. Where implementable, the paths required for the extrapolation of surface stresses are to be placed directly on element edges in order to evaluate the stresses at the centre or edge nodes of elements. Thus, an otherwise necessary interpolation of results can be avoided.

3.2.1.1.2 prEN 1993-1-14

According to chapter 2.4.3.2, the draft prEN 1993-1-14 [14] deals only with the stress extrapolation according to the guidelines of the IIW [3]. Analogous to the classification of details according to [3], the design standard [14] distinguishes between hot-spot types *a* and *b* (cf. Chapter 2.3.3.1). The corresponding classification is identical to the specifications of the IIW [3]. The associated meshing recommendations of [14] can be derived from Figure 3-11 regarding the linear stress extrapolation and from Figure 3-12 regarding the quadratic stress extrapolation. These can be applied to both shell models and solid models.

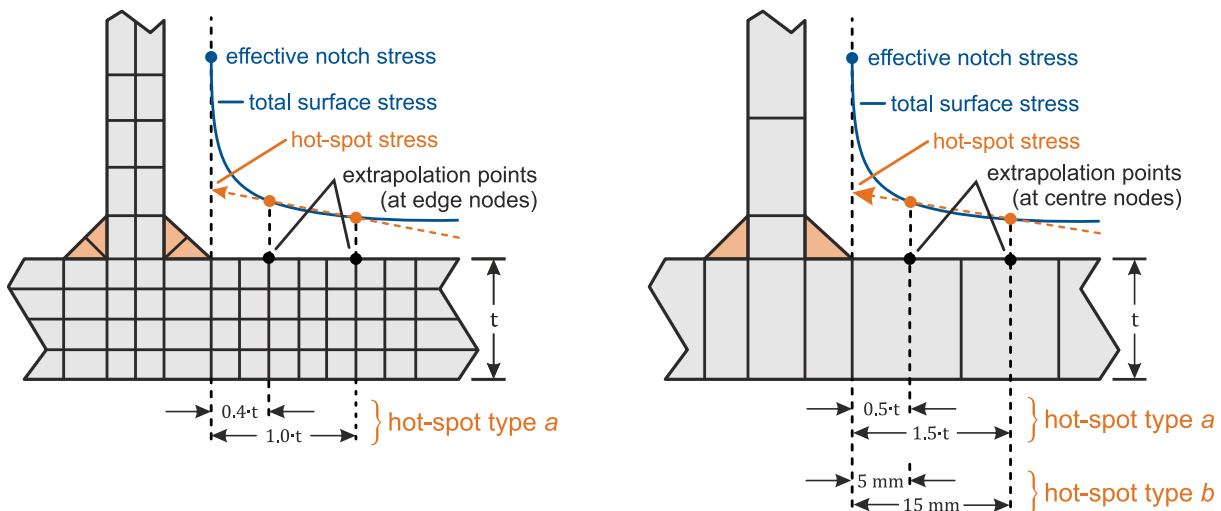


Figure 3-11: Linear stress extrapolation to determine the structural stress with a fine mesh model (left) and a coarse mesh model (right) according to prEN 1993-1-14 [14]

According to Figure 3-11, prEN 1993-1-14 [14] distinguishes between fine meshes (cf. left side of Figure 3-11) and coarse meshes (cf. right side of Figure 3-11) regarding the linear stress extrapolation. However, in the case of fine meshes according to [14],

significantly more elements are proposed over the plate thickness in the decisive area of the stress extrapolation than in [3] (cf. left side of Figure 3-11).

Whereas the surface stresses are determined at the edge nodes of the elements in the case of fine meshes, this is done at the centre nodes of the elements in the case of coarse meshes. The latter necessarily requires elements with a quadratic initial function. With a hot-spot type *b*, only coarse meshes are possible for the linear stress extrapolation according to prEN 1993-1-14 [14]. In this respect, the distances of the reference points are defined independently of the plate thickness. If a quadratic extrapolation is carried out according to prEN 1993-1-14 [14] (cf. Figure 3-12), in general considerably more elements are to be arranged than according to the guidelines of the IIW [3] (cf. Figure 3-9). Since only fine meshes are applicable, the corresponding distinction is only made according to the hot-spot type *a* (cf. left side of Figure 3-12) or hot-spot type *b* (cf. right side of Figure 3-12). In both cases, the surface stresses are determined at the edge nodes of the elements. In accordance with the specifications of the IIW [3], the specifications of the required reference points of [14] for hot-spot type *b* are independent of the plate thickness (cf. right side of Figure 3-12).

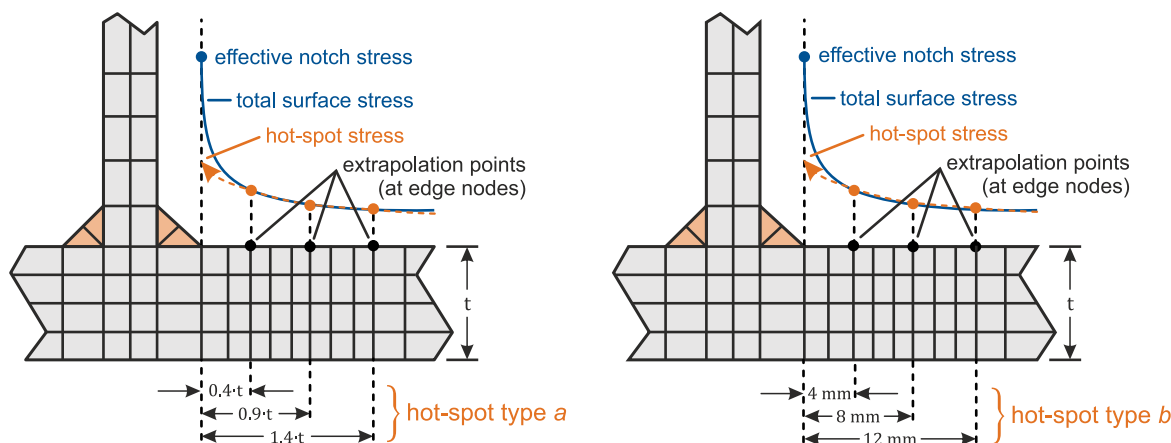


Figure 3-12: Quadratic stress extrapolation to determine the structural stress for hot-spot type *a* (left) and hot-spot type *b* (right) according to prEN 1993-1-14 [14]

Table 3-2 presents the associated extrapolation formulae in a tabular form. Since no distinction from the guidelines of the IIW [3] is discernible, the specifications are not analysed in more detail.

Table 3-2: Specifications for linear and quadratic stress extrapolation according to prEN 1993-1-14 [14]

Hot-spot type	Linear stress extrapolation		Quadratic stress extrapolation
	Fine mesh	Coarse mesh	Fine mesh
Type <i>a</i>	$0.4 \cdot t$ and $1.0 \cdot t$	$0.5 \cdot t$ and $1.5 \cdot t$	$0.4 \cdot t$, $0.9 \cdot t$ and $1.4 \cdot t$
	$1.67 \cdot \sigma_{0.4t} - 0.67 \cdot \sigma_{1.0t}$	$1.5 \cdot \sigma_{0.5t} - 0.5 \cdot \sigma_{1.5t}$	$2.25 \cdot \sigma_{0.4t} - 2.24 \cdot \sigma_{0.9t} + 0.72 \cdot \sigma_{1.4t}$
Type <i>b</i>	–	5 mm and 15 mm	4 mm, 8 mm and 12 mm
	–	$1.5 \cdot \sigma_{5mm} - 0.5 \cdot \sigma_{15mm}$	$3.0 \cdot \sigma_{4mm} - 3.0 \cdot \sigma_{8mm} + 1.0 \cdot \sigma_{12mm}$

According to prEN 1993-1-14 [14], care must also be taken to ensure that the reference points required for the stress extrapolation are located at the centre side or edge nodes of the elements in order to avoid averaged results. With regard to the allowable aspect ratios of finite elements, it is recommended that the ratio of the longest to the shortest element edge in the global model is less than three. If a relatively coarse mesh is chosen, even smaller aspect ratios are suggested. In this case, the ratio should not be greater than one within the critical range of the stress extrapolation and remain less than two in the rest of the FE model. Transition areas between fine and coarse meshes are not to be located near reference points and should be arranged as consistently as practicable. [14, 61, 41]

3.2.2 Further local methods

The following section provides the meshing specifications and the choice of element type for the local methods presented in Chapter 2.3.3. The information is applicable to both solid and shell models. With regard to the specifications for the linear and quadratic stress extrapolation, reference is made to Chapter 3.2.1.

For many designs, FE calculations with solid elements are more practical than with shell elements, as complex structures and welds can be modelled more realistically. However, when applying local methods in IGF research project No. 20336N [1], it was observed that two-dimensional FE calculations with shell elements behave relatively insensitive to the mesh size as long as predefined limits are being satisfied [42]. With regard to three-dimensional FE analyses using solid elements, on the other hand, strict meshing requirements must be satisfied in order to obtain consistent results. Table 3-3 lists these recommended initial element functions and meshing recommendations for solid models according to the local methods presented in Chapter 2.3.3. In this respect, the mesh specifications in the thickness direction as well as in the length and width direction for fine and course meshes in the critical area of the structural stress determination are presented.

Table 3-3: Meshing specifications for models with three-dimensional solid elements according to generally existing local methods without the stress extrapolation

Local method	Element type	Mesh specifications		
		Fine	Coarse	Thickness
One-point stress determination with $\Delta\sigma_{R,hs} = 1.12 \cdot \sigma_{0.5 \cdot t}$	20-node	$0.5 \cdot t \times 0.5 \cdot t$	$t \times t$	$\leq t/2$
One-point stress determination with $\Delta\sigma_{R,hs} = \sigma_{2mm}$	20-node	$0.5mm \times 0.5mm$	–	$\leq t/3$
One-point stress determination with $\Delta\sigma_{R,hs} = \sigma_{0.3 \cdot t}$	20-node	$0.3 \cdot t \times 0.3 \cdot t$	$t \times t$	$\leq t/3$
Internal linearisation with $\Delta\sigma_{R,hs} = \sigma_{linearised}$	20-node	$0.3 \cdot t \times 0.3 \cdot t$	–	$\leq t/3$
One-millimetre method with $\Delta\sigma_{R,hs} = \sigma_{1mm}$	20-node	$1mm \times 1mm$	–	$\leq 1mm$
δ -method based on equilibrium conditions at distance δ	20-node	$0.3 \cdot t \times 0.3 \cdot t$	–	$\leq t/2$

Deviating from the stress extrapolation according to Section 3.2.1, 20-node solid elements are specified for the further local methods presented (cf. Table 3-3). Although these elements allow relatively accurate stress distributions due to their quadratic displacement function, finer meshes are required for all local methods in thickness direction. Thus, sufficiently accurate results cannot be obtained with coarse meshes for most local methods, making time-consuming fine meshes unavoidable. The more exact stress distribution in the thickness direction of the fine meshes, however, facilitates the determination of the structural stress directly at the weld notch as required in some local methods. [89]

In addition, Table 3-4 defines the meshing specifications and choice of element type for shell models according to the local methods described in Chapter 2.3.3. In this respect, no meshing specifications are defined in the thickness direction, as the thickness is included as a mere parameter in FE models with shell elements. Due to the missing possibility of meshing in the thickness direction, the internal linearisation through the plate thickness and the one-millimetre method cannot be implemented with shells. According to Table 3-4, isoparametric 8-node elements are recommended for the evaluation of the remaining local methods.

Table 3-4: Meshing specifications for models with two-dimensional shell elements according to generally existing local methods without the stress extrapolation

Local method	Element type	Mesh specifications	
		Fine	Coarse
One-point stress determination with $\Delta\sigma_{R,hs} = 1.12 \cdot \sigma_{0.5 \cdot t}$	8-node	$0.5 \cdot t \times 0.5 \cdot t$	$t \times t$
One-point stress determination with $\Delta\sigma_{R,hs} = \sigma_{2mm}$	8-node	$0.5mm \times 0.5mm$	–
One-point stress determination with $\Delta\sigma_{R,hs} = \sigma_{0.3 \cdot t}$	8-node	$0.3 \cdot t \times 0.3 \cdot t$	$t \times t$
Internal linearisation with $\Delta\sigma_{R,hs} = \sigma_{linearised}$	No practical implementation available, as no sufficiently fine mesh is achievable across the plate thickness.		
One-millimetre method with $\Delta\sigma_{R,hs} = \sigma_{1mm}$			
δ -method based on equilibrium conditions with $\sigma_{hs} = \frac{f_y}{t} + \frac{6 \cdot M_z}{t^2}$	8-node	$0.3 \cdot t \times 0.3 \cdot t$	–

3.3 Implementation of finite element analysis

In the IGF research project No. 20336N [1] it was concluded that due to the significant interdependence of various model-related boundary conditions, the development of generally valid reference models for cruciform joints is not practicable. Accordingly, the information on the FEA provided in the subsequent sections is intended to provide constraints for the design of sensible FE models for cruciform joints in the structural stress concept. This section therefore deals with the implementation of the FE analysis through fundamental investigations on essential boundary conditions in order to ensure consistent evaluations in this thesis. This includes the provision of information on the selected element classifications (cf. Section 3.3.1), the implementation of imperfections (cf. Section 3.3.2) and the associated load introduction and support definition in the FE

analysis (cf. Section 3.3.3). In addition, the determination of an appropriate method for the structural stress evaluation (cf. Section 3.3.4), the realistic weld modelling with shell elements (cf. Section 3.3.5) and thickness effects (cf. Section 3.3.6) are analysed. Concluding, Section 3.3.7 specifies the general implementation of the FE calculations with ANSYS APDL.

3.3.1 Element classification in the applied FE software ANSYS

The numerical computations in this thesis are performed with the FE software ANSYS. This software is designed to solve linear and non-linear problems in the field of structural mechanics. The investigations focus on materially linear-elastic simulations with an isotropic material on models with two-dimensional shell and three-dimensional solid elements. However, in the case of large preliminary deformations due to clamping processes of imperfect structures, geometrically non-linear calculations are imperative in some instances in order to ensure realistic results. The required element assignment of the analysis is carried out in the pre-processor of the FE software.

For shell elements, so-called SHELL281 elements (cf. Figure 3-1) are used in ANSYS, which are particularly useful for the analysis of thin to moderately thick shell structures. These elements consist of eight nodes, each with six degrees of freedom, three of which are translational and three rotational. This allows linear and non-linear FE applications with large rotations and/or strains. In addition to the material and element type classification, the constant thickness must be defined as an additional cross-sectional property for shell elements. It should be noted that not all FE software provides higher order shell elements. While the FE software ANSYS and Abaqus have sufficiently large element libraries, the applications Sofistik and RFEM, for example, only provide shell elements with a maximum of four nodes.

For the three-dimensional solid element models in ANSYS, so-called SOLID186 elements (cf. left side of Figure 3-7), which have a large deformation and strain capacity, are used in the FE calculations of this thesis. These elements consist of twenty nodes, each with three translational degrees of freedom. The corresponding FE calculations are performed with reduced integration by default to avoid volumetric mesh-locking in nearly incompressible cases.

3.3.2 Modelling of imperfections

According to Chapter 2.5, the principle of a perfectly aligned model must be deviated from if imperfections have a significant influence on the applied stress range $\Delta\sigma_{R,hS}$ and no additional stress concentration factor $k_{m,eff}$ is considered for an analytical stress increase due to the imperfections. Based on the contents of Chapter 2.5, the implementation of imperfections at cruciform joints directly included in the FE calculations is briefly described in the following.

Both in shell and solid models, positive axial offset is defined as displacement in the direction of the positive global axis. Rotations are specified according to the so-called right-hand rule, defined by the direction of the global axis in which the thumb points when the bent fingers of the right-hand point in the direction of the rotational movement caused by the imperfection. A positive rotation value is thus given by the curved fingers of the right hand when the thumb indicates the positive axis direction. In order to

illustrate the above, the possible imperfections of cruciform joints from chapter 2.5 are summarised in Figure 3-13 with the required pivot points and the corresponding positive and negative directions of displacement and rotation. These include angular misalignments around the y_{global} -axis (cf. top left side of Figure 3-13), axial misalignments in the direction of the z_{global} -axis (cf. top right side of Figure 3-13) and rotation of the welded-on plates around the x_{global} -axis (cf. bottom side of Figure 3-13). The deformation figures resulting from the possible imperfections are presented in Figure 3-13 as well.

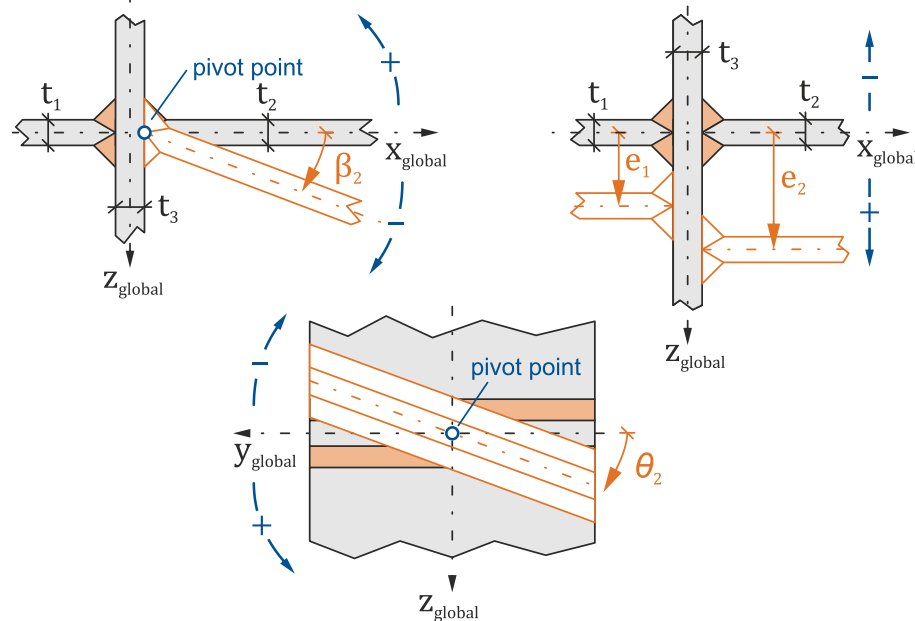


Figure 3-13: Possible imperfections of cruciform joints with associated FE modelling for angular misalignment around the y_{global} -axis (top left), axial misalignment in direction of z_{global} -axis (top left) and rotation of the welded-on plates around the x_{global} -axis (bottom)

3.3.3 Implementation of the support conditions and load application

In the following section, the procedures for both the clamping process and the load application of the conducted FE studies are explained in more detail.

The clamping range of the tensile tests from chapter 4 are simulated consistently with quadratic sections in the associated FE calculations. This corresponds to the real clamping jaw geometry of the testing machines used for the experimental fatigue tests. The same approach is applied to all further numerical studies presented in this thesis in order to ensure comparability of all results. In this respect, all element nodes in the clamping sections are provided with support conditions by means of restraints of the displacement degrees of freedom. The corresponding clamping sections for a cruciform joint are highlighted in blue in the following Figure 3-14.

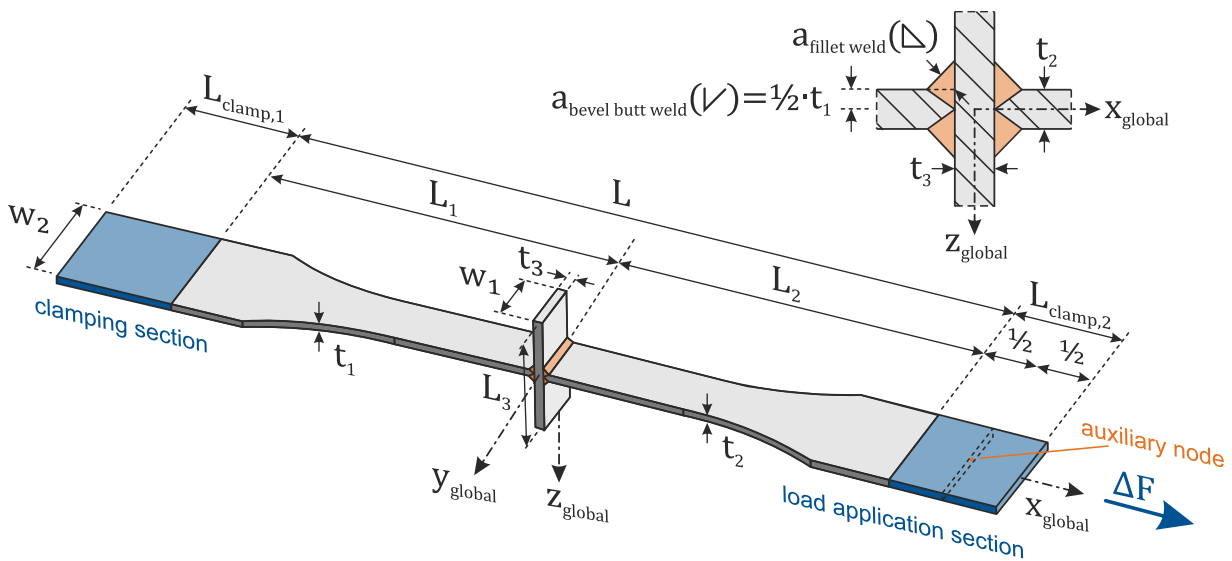


Figure 3-14: Cruciform joint geometry with required parameters in the globally arranged coordinate system and highlighted clamping and load application section as well as auxiliary node for the modelling of the clamping process

According to Figure 3-14, the clamping range in the direction of the globally negative x_{global} -axis (cf. left part of Figure 3-14) is referred to as 'clamping section' in the following. This would be equivalent to the initial fastening of the associated clamp jaws in an experimental test setting. The nodes of the clamping range in the globally positive x_{global} -direction (cf. right part of Figure 3-14), instead, are defined as 'load application section', since in real tensile tests the tension load would be applied through these corresponding clamp jaws. For FE models with solid resp. shell elements, the clamping section is specified by retaining all displacement degrees of freedom. In order to exclude displacement of the clamping section, all possible node displacements in x_{global} -, y_{global} -, and z_{global} -direction are therefore set to zero. In contrast, all nodes of the load application section are restrained solely in the y_{global} - and z_{global} -direction to enable the load application of ΔF in the x_{global} -direction.

In FE models with solid elements, the degrees of freedom of all element nodes of the clamping and load application section are used to define the degrees of freedom, since a completely pressurised plate is assumed by the hydraulically clamped jaws of the testing machine. Thus, element nodes are also selected within the clamping volumes. In contrast, in the FE models with shell elements, only the degrees of freedom of the element nodes of the clamping and load application surface are restrained, since the plate thickness is only included as a mere computational dimension. Therefore, it is not necessary to restrain rotational degrees of freedom of any nodes, as a full restraint is achieved by restraining the entire clamping and load application section.

If potential imperfections of cruciform joints (cf. Chapter 2.5.2) are to be considered numerically, clamping processes have to be included with regard to testing machinery. This is due to the hydraulic locking of the clamping jaws to allow targeted load introduction in the x_{global} -direction. According to Figure 3-15, this clamping process results in a vertical displacement Δz_{global} (displacement in z_{global} -direction) of the load introduction section in case of axial misalignment e (cf. Chapter 2.5.2.2).

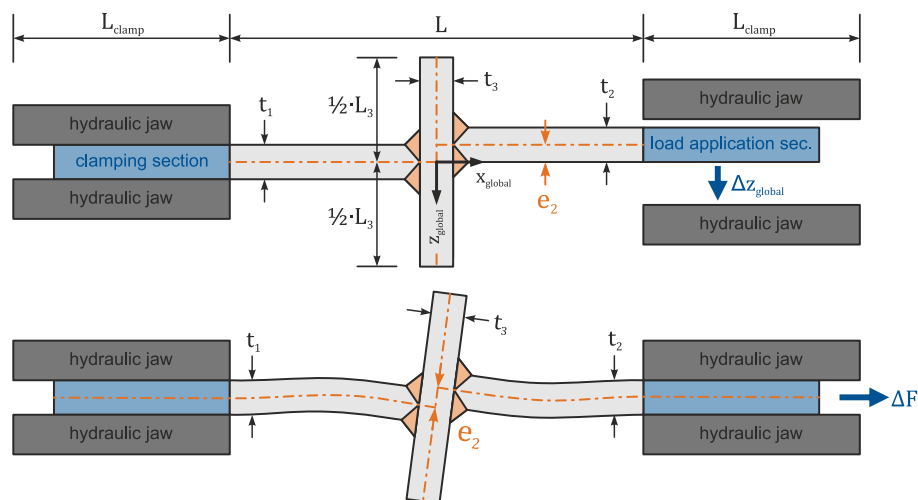


Figure 3-15: Cruciform joint geometry with axial misalignment before clamping process (top) and deformed shape after clamping process (bottom)

If there is angular misalignment α (cf. Chapter 2.5.2.1), the load application section must also be aligned in the global z-direction (cf. Figure 3-16). This is achieved by a rotation around the y_{global} -axis in addition to the displacement in z_{global} -direction according to the procedure regarding axial misalignment.

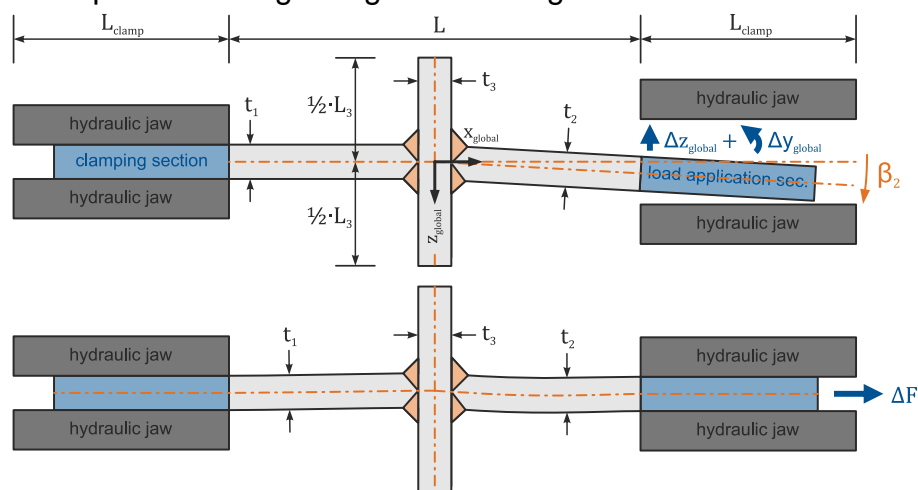


Figure 3-16: Cruciform joint geometry with angular misalignment before clamping process (top) and deformed shape after clamping process (bottom)

In addition, a rotation of the welded-on plates around the x_{global} -axis may be possible in the case of cruciform joints (cf. Chapter 2.5.2.3). In this respect, the clamping process results in an alignment of the load application area by pure rotation around the x_{global} -axis. This causes a plain rotation according to Chapter 2.5.2.3 without any additional displacement in the direction of the z_{global} -axis.

The associated numerical simulation in ANSYS is conducted using rigid beam elements. These elements are defined as MPC184 elements and are particularly suitable for large displacements and rotations, as can occur during the clamping process in testing machines. For this purpose, kinematic boundary conditions are introduced into the system of equations by means of a direct elimination method. These rigid links are defined by two element nodes with up to six degrees of freedom each. With respect to solid models, three degrees of freedom of displacement are utilised. In

contrast, for shell models a variant is selected that offers three additional degrees of freedom of rotation. As these rigid links are two-node elements, an auxiliary node must be created centrally in the load application section. This auxiliary node is located in the centre of gravity of the section and thus represents the intersection of the rotation axes around the x_{global} - and y_{global} -axes required for the clamping process (cf. Figure 3-14). The necessary MPC184 elements are generated between the auxiliary node and every node of the load application section. By defining degrees of freedom for the auxiliary node, all nodes of the load application section can then be activated directly. The numerical clamping process thus results, depending on the present imperfection, from the possible rotation and displacement of the common auxiliary node to the position and orientation of the clamping section between the clamp jaws of a testing machine. The required tensile load is also implemented by applying the entire tensile force to the shared auxiliary node. Due to the existing rigid body connections, the load is uniformly distributed to all nodes of the load application section.

If only minor imperfections are to be expected, the clamping and loading process in ANSYS can be executed within a single load step. To this end, the influence of an incremental deformation and load application is advisable to ensure that these processes can numerically be modelled correctly, irrespective of the size of imperfections. Due to the different stiffness ratios, the displacement into the vertical zero point between the clamping jaws is therefore realized in a first load step. Subsequently, the rotation into the exact horizontal position (rotation of the load application section around the y_{global} -axis) is implemented in a further load step. In a final load step, the tensile load is applied. Due to the generally large pre-deformations associated with clamping processes of imperfect cruciform joints, a geometrically non-linear calculation is inevitable in order to obtain realistic results.

Additionally, a so-called "CERIG" command for simulating the clamping process was examined more closely. In this respect, a MASS21 element of the ANSYS element library was required to define rigid element constraints between this element and all nodes of the load application section. The MASS21 element consists of a node with 6 degrees of freedom and operates as a "master" node in the intended "master-slave" relationship. However, it was observed that the associated constraint equations are strictly based on small deformations. As a result, it is not possible to simulate large geometric distortions in the clamping process, despite geometrically non-linear FE analysis. Consequently, this approach was discarded.

3.3.4 Specification of the local method

In the following section, the local methods for determining structural stresses presented in Chapter 2.3.3 are examined in more detail. Furthermore, a general comparison is made between the stress extrapolation according to the guidelines of the IIW [3] and the further presented local methods, as the main focus of most normative regulations and guidelines lies on the former method.

The associated meshes of the linear and quadratic stress extrapolation are implemented according to Section 3.2.1. The required meshing specifications of the respective local methods are based on Table 3-3 for models with solid elements and Table 3-4 for shell elements. In order to ensure better comparability of the different

methods, various dimensions are analysed. This includes the test specimen geometries of the third work package (WP3) of IGF research project No. 20336N [1] (cf. Chapter 4). For this purpose, the cruciform joint geometries of WP3_1.1 (12 – 12), WP3_2.1 (12 – 40) and WP3_3.1 (40 – 12) are utilised. In this context, the first value in brackets describes the welded-on load-bearing primary plate thickness and the second the thickness of the intermediate plate. In addition, a geometry with identical primary and intermediate plate thicknesses of 25 mm (25 – 25) is analysed. In this way, influences from deviating thickness ratios can be considered.

The evaluation is performed on idealised perfect FE models under mere tensile stress without the consideration of any potential misalignment according to Section 3.3.2. In this respect, both quadratic solid and quadratic shell elements with reduced integration are implemented (cf. Section 3.1). In order to keep the results as comprehensive as possible, models with FE shell elements are solely based on the weld modelling according to Section 3.1.1.2.3, with inclined shell elements to the centre axes of the plates. This is due to the fact that in IGF research project No. 20336N [1] reasonable results could solely be expected with this method. A detailed examination of the various weld models presented (cf. Section 3.1.1.2) is given later in Section 3.3.5. All models are subjected to a nominal stress of 1.0 N/mm^2 . The first principal stress is determined at the relevant positions respectively along the critical paths. Exclusively in the δ -method, based on the local force and stress equilibrium [50, 51], the required nodal normal stresses and nodal shear stresses are derived.

In the following, the determination of the relevant structural stresses according to the different local methods from chapter 2.3.3 is described in more detail. In this context, Section 3.3.4.1 deals with the surface methods including the linear and quadratic stress extrapolation (cf. Chapter 2.3.3.1) as well as the one-point stress determination (cf. Chapter 2.3.3.2). Section 3.3.4.2 addresses the procedures in the thickness direction by means of the one-millimetre method (cf. Chapter 2.3.3.4) and the internal linearisation (cf. Chapter 2.3.3.3) and Section 3.3.4.3 discusses the δ -method (cf. Chapter 2.3.3.5). In addition, nominal stresses and effective notch stresses can be converted to structural stresses through calculations on the resistance side. The corresponding procedure is explained in Section 3.3.4.4. Finally, in Section 3.3.4.5, the results of the local methods are compared in order to determine an appropriate approach for a consistent structural stress determination.

3.3.4.1 **Surface Methods**

Characteristic surface methods include the stress extrapolation (cf. Chapter 2.3.3.1) and the one-point stress determination (cf. Chapter 2.3.3.2).

For the determination of the structural stress by means of the linear and quadratic surface extrapolation of the IIW [3], FE models are created with solid and shell elements respectively. With regard to the linear stress extrapolation to determine structural stresses, both finely meshed and coarsely meshed solid and shell models can be considered. In contrast, according to Chapter 2.4.2.2, only models with a fine mesh can be applied for the quadratic stress extrapolation. The stress determination of the examined cruciform joints is consistently defined with hot-spot type *a* (cf. Chapter 2.3.3.1). The required distances of the extrapolation paths to the weld notch can

therefore be derived from chapter 2.4.2.2 for both the linear and quadratic extrapolation. According to the meshing specifications of prEN 1993-1-14 [14] (cf. Section 3.2.1.1.2), models with a fine as well as with a coarse mesh are evaluated.

In this respect, the mesh of solid models is generated with the help of structured meshing. For this purpose, all solids are divided into hexahedron-shaped volume elements. The welds are explicitly modelled in the FE calculations and meshed with hexahedrons as well. With regard to finely meshed solid models, extensive preliminary investigations according to IGF research project No. 20336N [1] indicate that at least four elements should be realised over the smallest component thickness of the structure. This is due to the fact that with this number of elements only minor deviations of 0.8 % are observed compared to much finer meshed FE models with up to twenty elements across the component thickness. The specifications of prEN 1993-1-14 [14] (cf. left side of Figure 3-11 and Figure 3-12) can thus be confirmed. Although, the finely meshed solid models in this thesis are implemented slightly finer in the z_{global} -direction with an element size of $0.2 \cdot t$ across the component thickness. This way, the achieved convergence of structural stresses with twenty elements over the plate thickness can be nearly matched with significantly less computational time. In order to meet the meshing requirements of prEN 1993-1-14 [14], the elements in the critical areas in front the weld notch also have a size of $0.2 \cdot t$ in the longitudinal x_{global} -direction (cf. left side of Figure 3-11 and Figure 3-12). However, with increasing distance to critical sections, significantly coarser meshes are applied in order to save further computing time. Over the component width in the y_{global} -direction, on the other hand, the models are meshed uniformly, since no significant local stress concentrations are to be expected for cruciform joints. In order to satisfy the 1:1:1 element aspect ratio recommended in prEN 1993-1-14 [14] within the critical sections, the number of elements across the component width is also defined by the element size of $0.2 \cdot t$. Influences from the transverse strain constraint can be detected sufficiently with this type of mesh. With respect to coarsely meshed solid models, meshes are implemented according to prEN 1993-1-14 [14] as illustrated on the right side of Figure 3-11. In order to satisfy the aspect ratio of 1:1:1 even with a coarse mesh, element sizes of $1.0 \cdot t$ are also applied across the component width in y_{global} -direction.

The shell models are also subdivided into quadrangular shell elements using structured meshing. The applied weld modelling with inclined shell elements up to the centre planes of the plates (cf. Section 3.1.1.2.3) are implemented with a quadrangular mesh as well. Based on prEN 1993-14 [14], when fine meshes are applied, the critical sections are meshed with a maximum element size of $0.2 \cdot t$ aiming for a maximum aspect ratio of 1:1. In terms of coarsely meshed shell models, element sizes of $1.0 \cdot t$ are implemented. Furthermore, the consistent orientation of shell elements is of great importance in order to exclude falsified results due to deviating local coordinate systems.

In addition, further finely and coarsely meshed FE models are used for the evaluation of the one-point stress determination [9, 41] (cf. Chapter 2.3.3.2). The associated meshes are created according to Section 3.2.2. In this respect, paths at a distance $\Delta x = 0.3 \cdot t$ [48] according to Haibach as well as $\Delta x = 0.5 \cdot t$ [6, 3] in front of the notch are evaluated. For shell models, the distances are defined from the intersection of the shell

middle planes of the inclined weld elements and ground plate. In addition, a further analysis is conducted on solid and shell models at a fixed distance of $\Delta x = 2 \text{ mm}$ [9, 41] according to Haibach. With the latter method, no coarse meshing is possible according to Section 3.2.2. Only in the one-point stress determination according to [4, 2], the relevant surface stress $\Delta\sigma_{0.5-t}$ is directly multiplied by the factor 1.12 to determine the critical structural stress (cf. chapter 2.3.3.2).

3.3.4.2 *Methods through the thickness direction*

With regard to the one-millimetre method of Xiao and Yamada [7] (cf. Chapter 2.3.3.4) and the linearisation of stresses in the through-thickness direction of plates [6, 8] (cf. Chapter 2.3.3.3), additional very finely meshed solid models are generated. Due to the structural stress determination in the thickness direction, shell elements cannot be implemented in a practical way with either of these methods.

According to Chapter 2.3.3.4, the required stresses for the one-millimetre method are evaluated on a path at a fixed distance of 1 mm below the weld transition. Consequently, the associated FE model is created with a maximum element size of 1 mm in the critical area of the notch (cf. Section 3.2.2). Due to the path defined over the component width, the relevant structural stress can be determined directly from the FE model according to the one-millimetre method.

The internal linearisation is carried out by means of linear regression on half the ground plate thickness, as a symmetrical stress distribution through the thickness is to be expected for cruciform joints. The linearised value at the surface then consequently corresponds to the structural stress (cf. Chapter 2.3.3.3). The very finely meshed models of the one-millimetre method are used for the associated evaluations. Since, due to the design of cruciform joints, it is not possible to estimate at which position across the component width the maximum structural stress is to be expected, a large number of paths across the component width must be arranged for the internal linearisation. Consequently, many linearisation processes need to be performed in order to determine the relevant structural stress. This makes the method very time-consuming in practical application.

3.3.4.3 *δ -method*

For the δ -method according to Dong [50, 51] (cf. Chapter 2.3.3.5) further solid and shell models are created. Since the method is based on a local equilibrium of forces and stresses, both the normal and shear stresses at the cut-free element edges are evaluated. The corresponding length of the element in the direction of the applied stress is marked with δ and depends on the expected crack depth. This is assumed to be $\delta = 0.3 \cdot t$ and also defines the required element size of the FE models with solid or shell elements in the global x-direction. The thickness t_1 of the element edge is defined with regard to the crack propagation analysis. It is to be equivalent to the crack size assumed as failure criterion. In case of a symmetrical stress distribution across the thickness, t_1 corresponds to half the plate thickness $t/2$. Accordingly, the solid models are created with two elements over the plate thickness. By means of embedded evaluation paths in the solid model, the decisive normal and shear stress distributions at the element edges can be determined. Since the thickness of shell models is

included as a mere parameter, the element nodes on the cut edges of the shell elements can be evaluated directly. Finally, the relevant structural stress is calculated from the stress distributions of the solid and shell models according to chapter 2.3.3.5. In line with the method for internal linearisation of stresses, the delta method also requires numerous paths across the width of the component in order to determine the relevant structural stress. Once again, this leads to a questionable practical implementation of this method.

3.3.4.4 **Converted nominal and effective notch stresses**

To provide a further assessment of the local methods, the nominal stress concept (cf. Chapter 2.3.1) and effective notch stress concept (cf. Chapter 2.3.4) are applied to subsequently convert the results to the equivalent level of the structural stress concept. This allows an additional comparison with the differing methods of verification. The necessary conversion to the relevant structural stress $\Delta\sigma_{R,hs}$ is carried out by the systematic adjustment of the respective resistance sides $\Delta\sigma_C$. The procedure for the nominal and effective notch stress concept is explained in more detail below.

According to Section 3.3.4, the loading of the cruciform joints to be investigated is specified in a way that a nominal stress of $\Delta\sigma_{R,nom} = 1 \text{ N/mm}^2$ results in the decisive load-bearing components. Thus, the applied nominal stress $\Delta\sigma_{R,nom}$ can be converted into an applied structural stress $\Delta\sigma_{R,hs}$ by multiplying it by the ratio of the normative fatigue class of the structural stress concept $\Delta\sigma_{C,hs}$ to the normative fatigue class of the nominal stress concept $\Delta\sigma_{C,nom}$ according to the following formula.

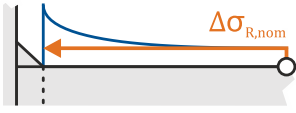

$$\Delta\sigma_{R,hs} = \Delta\sigma_{R,nom} \cdot \frac{\Delta\sigma_{C,hs}}{\Delta\sigma_{C,nom}} \quad (3-1)$$

The required numerical evaluation of the effective notch stresses $\Delta\sigma_{R,en}$ is conducted on additionally created FE models, with the meshing specifications of prEN 1993-1-14 [14] in accordance with the notch stress concept. The notches of these very finely meshed FE models are smoothed by applying a radius of 1 mm. At the applied stress, which leads to a nominal stress range of $\Delta\sigma_{R,nom} = 1 \text{ N/mm}^2$ in the relevant components, applied effective notch stress ranges $\Delta\sigma_{R,en}$ of 2.69 N/mm² (12 – 12), 2.73 N/mm² (12 – 40), 3.51 N/mm² (40 – 12) and 3.27 N/mm² (25 – 25) result. By means of these effective stresses, the same procedure can be followed for the numerically determined effective notch stress ranges $\Delta\sigma_{R,en}$ as for the nominal stress ranges $\Delta\sigma_{R,nom}$. However, the conversion is based on the multiplication with the ratio of the fatigue classes $\Delta\sigma_{C,hs}/\Delta\sigma_{C,en}$ in accordance with the formula below.

$$\Delta\sigma_{R,hs} = \Delta\sigma_{R,en} \cdot \frac{\Delta\sigma_{C,hs}}{\Delta\sigma_{C,en}} \quad (3-2)$$

The resulting structural stresses $\Delta\sigma_{R,hs}$ are summarised for the evaluated cruciform joints WP3_1.1 (12 – 12), WP3_2.1 (12 – 40), WP3_3.1 (40 – 12) and (25 – 25) in Table 3-5. Due to the uniform nominal stress of $\Delta\sigma_{R,nom} = 1 \text{ N/mm}^2$, the resulting structural stresses $\Delta\sigma_{R,hs}$ correspond equally to the stress concentration factor $\Delta\sigma_{R,hs}/\Delta\sigma_{R,nom}$. Consequently, this represents the factor by which the results of the structural stress concept are larger or smaller than those of the nominal stress concept.

Table 3-5: Evaluation of the structural stresses resp. the stress concentration factor with the nominal and effective notch stress concept

Verification Method		Calculated structural stress $\Delta\sigma_{R,hs}$ resp. stress concentration factor $\Delta\sigma_{R,hs}/\Delta\sigma_{R,nom}$ [N/mm ²] resp. [-]	
Nominal stress concept		(12 – 12) 1.250 – 1.408	(12 – 40) 1.250 – 1.408
		(40 – 12) 1.223 – 1.409	(25 – 25) 1.250 – 1.408
Effective notch stress concept		(12 – 12) 1.194	(12 – 40) 1.213
		(40 – 12) 1.354 – 1.558	(25 – 25) 1.452

Since the respective fatigue strengths $\Delta\sigma_C$ of DIN EN 1993-1-9 [2], the guidelines of the IIW [3] and prEN 1993-1-9 [4] may differ (cf. Chapter 2.4), the obtained results for $\Delta\sigma_{R,hs}$ are depicted in the permissible ranges (cf. Table 3-5). For example, the nominal stress fatigue strength $\Delta\sigma_{C,nom}$ of the investigated details is defined as 71 N/mm^2 and 80 N/mm^2 (cf. Chapter 2.4.1.1, 2.4.2.1 and 2.4.3.1), which consequently provides varying results. By contrast, in the structural stress and effective notch stress concept, all examined details are classified uniformly in the applied normative regulations and guidelines. In this respect, the fatigue classes $\Delta\sigma_{C,hs} = 100 \text{ N/mm}^2$ (cf. Chapter 2.4.1.2, 2.4.2.2 and 2.4.3.2) and $\Delta\sigma_{C,en} = 225 \text{ N/mm}^2$ (cf. Chapter 2.3.4) apply. However, Table 3-5 indicates that the stress concentration factors based on a conversion to the structural stress concept from the nominal stress and notch stress concept are largely subject to a wide dispersion range. This complicates the general assessment of the correctness and applicability of the different local methods.

In addition, thickness effects are considered in the evaluation of *WP3_3.1* (40 – 12), since the load-bearing plate thickness $t = 40 \text{ mm}$ exceeds the general reference thickness $t_{ref} = 25 \text{ mm}$. This leads to further deviating results in Table 3-5 (cf. Chapter 2.6). Furthermore, for some local methods, thickness effects are already considered by the corresponding procedures and consequently do not need to be accounted for by correction factors. This further complicates the comparison for details with load-bearing plate thicknesses $t > 25 \text{ mm}$.

3.3.4.5 Comparison of local methods

The relevant structural stresses of the local methods for solid and shell models according to the previous Sections 3.3.4.1, 3.3.4.2 and 3.3.4.3 are summarised in Table 3-6. The evaluation is performed for finely meshed and, if applicable, also for coarsely meshed FE models regarding the cruciform joint geometries *WP3_1.1* (12 – 12), *WP3_2.1* (12 – 40) and *WP3_3.1* (40 – 12) according to Chapter 4 in addition to a further geometry with (25 – 25) (cf. Section 3.3.4). The applied local methods are defined in a relevant way and supplemented by information on the type of mesh as well as by illustrations of the procedure (cf. Chapter 2.3.3). Due to the uniform nominal stress of $\Delta\sigma_{R,nom} = 1 \text{ N/mm}^2$, again the resulting structural stresses $\Delta\sigma_{R,hs}$ equally correspond to the stress concentration factor $SCF = \Delta\sigma_{R,hs}/\Delta\sigma_{R,nom}$. Possible thickness

effects are not considered in any form in order to ensure comparability of the results. Table 3-6 is thus intended to provide a comparison for the evaluation of structural stresses by means of alternative local methods.

Table 3-6: Evaluation of structural stresses resp. stress concentration factors according to different local methods for varying geometries (12 – 12), (12 – 40), (40 – 12) and (25 – 25) separately for finely and coarsely meshed solid and shell elements

Method	Structural stress $\Delta\sigma_{R,hs}$ resp. $SCF = \Delta\sigma_{R,hs}/\Delta\sigma_{R,nom}$ [N/mm ²] resp. [-]							
	Solid elements				Shell elements			
	Fine mesh		Coarse mesh		Fine mesh		Coarse mesh	
Linear stress extrapolation	(12 – 12)	(12 – 40)	(12 – 12)	(12 – 40)	(12 – 12)	(12 – 40)	(12 – 12)	(12 – 40)
	1.044	1.002	1.037	1.033	1.039	1.013	1.040	1.023
	(40 – 12)	(25 – 25)	(40 – 12)	(25 – 25)	(40 – 12)	(25 – 25)	(40 – 12)	(25 – 25)
	1.034	1.020	1.030	1.025	1.011	1.012	1.032	1.025
Quadratic stress extrapolation	(12 – 12)	(12 – 40)	-	-	(12 – 12)	(12 – 40)	-	-
	1.065	1.011	-	-	1.052	1.015	-	-
	(40 – 12)	(25 – 25)	-	-	(40 – 12)	(25 – 25)	-	-
	1.059	1.043	-	-	1.014	1.018	-	-
One-point method	(12 – 12)	(12 – 40)	(12 – 12)	(12 – 40)	(12 – 12)	(12 – 40)	(12 – 12)	(12 – 40)
	1.161	1.141	1.152	1.137	1.143	1.131	1.144	1.132
	(40 – 12)	(25 – 25)	(40 – 12)	(25 – 25)	(40 – 12)	(25 – 25)	(40 – 12)	(25 – 25)
	1.141	1.130	1.153	1.145	1.134	1.133	1.135	1.137
Haibach $\Delta x = 0.3 \cdot t$	(12 – 12)	(12 – 40)	(12 – 12)	(12 – 40)	(12 – 12)	(12 – 40)	(12 – 12)	(12 – 40)
	1.092	1.069	1.091	1.071	1.027	1.011	1.032	1.011
	(40 – 12)	(25 – 25)	(40 – 12)	(25 – 25)	(40 – 12)	(25 – 25)	(40 – 12)	(25 – 25)
	1.063	1.058	1.074	1.073	1.008	1.010	1.013	1.012
Haibach $\Delta x = 2 \text{ mm}$	(12 – 12)	(12 – 40)	-	-	(12 – 12)	(12 – 40)	-	-
	1.247	1.199	-	-	1.031	1.010	-	-
	(40 – 12)	(25 – 25)	-	-	(40 – 12)	(25 – 25)	-	-
	1.395	1.301	-	-	1.003	1.005	-	-
One-millimetre method	(12 – 12)	(12 – 40)	-	-	-	-	-	-
	1.017	1.082	-	-	-	-	-	-
	(40 – 12)	(25 – 25)	-	-	-	-	-	-
	0.986	1.042	-	-	-	-	-	-
Internal linearisation	(12 – 12)	(12 – 40)	-	-	-	-	-	-
	1.090	1.068	-	-	-	-	-	-
	(40 – 12)	(25 – 25)	-	-	-	-	-	-
	1.076	1.069	-	-	-	-	-	-
δ -method	(12 – 12)	(12 – 40)	-	-	(12 – 12)	(12 – 40)	-	-
	1.320	1.123	-	-	1.121	1.087	-	-
	(40 – 12)	(25 – 25)	-	-	(40 – 12)	(25 – 25)	-	-
	1.136	1.124	-	-	1.086	1.094	-	-

According to Table 3-6, large deviations between the different methods become apparent, which make a general assessment of the respective applicability difficult. Additionally, the geometry has a significant effect, as distinct differences can be observed in the results of the FE models evaluated for (12 – 12), (12 – 40), (40 – 12) and (25 – 25). In this respect, tendencies can only be determined to a limited extent. Nevertheless, the structural stresses tend to decrease with thicker main and/or intermediate plates and are highest at (12 – 12) for most methods (cf. Table 3-6). Furthermore, the results for shell elements are in the majority of cases lower than for solid elements. An exception to this is (12 – 40), where FE shell models mostly result

in larger structural stresses than solid models (cf. Table 3-6). However, in the applied method for modelling the weld with inclined shell elements to the centre axes of the plates (cf. Section 3.1.1.2.3), this is due to the relatively steep gradient of these shells. The steep gradient derives from the differing plate thicknesses in combination with a significantly thicker intermediate plate, which leads to a greater stress peak. Moreover, the results for coarsely meshed FE models indicate that only minor differences to fine meshes are to be expected (cf. Table 3-6). In this respect, it depends on both the method and the geometry whether larger or smaller structural stresses are to be expected. With the one-millimetre method, it can further be determined for test specimen (40 – 12) that a stress concentration factor $SCF = \Delta\sigma_{R,hs} / \Delta\sigma_{R,nom} = 0.986$ smaller than 1.00 is identified (cf. Table 3-6). Since the expected structural stress $\Delta\sigma_{R,hs}$ of cruciform joints is unlikely to be lower than the applied nominal stress $\Delta\sigma_{R,nom}$, the general practicability of this method is questionable.

The guidelines of the IIW [3] as well as prEN 1993-1-9 [4] and prEN 1993-1-14 [14] are primarily addressing the generally accepted stress extrapolation (cf. Chapter 2.3.3.1). Nonetheless, apart from the one-millimetre method, the associated structural stresses prove to be the lowest of all local methods (cf. Table 3-6). The corresponding $SCFs$ are only slightly above 1.00 despite a significantly higher fatigue strength $\Delta\sigma_{C,hs}$ within the structural stress concept than with $\Delta\sigma_{C,nom}$ in the nominal stress concept (cf. Chapter 2.4). On the one hand, this fact may indicate a significantly more economical applicability of the structural stress concept compared to the nominal stress concept. However, Table 3-5 indicates that significantly higher $SCFs$ are to be expected according to the nominal stress and effective notch stress concept. Consequently, on the other hand, this may point to an exaggerated fatigue strength in the structural stress concept or an incorrect determination of the structural stress by the linear stress extrapolation. To verify the latter and to ensure a better comparison of the local methods, the results of the linear stress extrapolation with finely meshed solid models are defined as reference values in the further course of this section. In this way, it can be identified whether other local approaches are more effective for the determination of structural stresses. Therefore, the associated differences of the local methods are summarised in Table 3-7. The results represent the percentage of deviations of the local methods to the structural stress of the linear stress extrapolation. The comparison is carried out with the structural stresses calculated on finely meshed solid models using the linear stress extrapolation for the respective test specimen geometries (12 – 12), (12 – 40), (40 – 12) and (25 – 25). The resulting deviations can additionally provide a tendency, if a non-standard local method is selected for the structural stress determination.

According to Table 3-7, it can be seen that the element selection as well as the type of mesh do not have a decisive influence on the linear and quadratic stress extrapolation, as only minor deviations from the finely meshed solid models can be identified. In this regard, [3] recommends that the quadratic stress extrapolation, in contrast to the linear stress extrapolation, should be applied for details with significantly curved stress distributions. Typical examples proposed are details with an abrupt structural change or with large local loads, which are not provided in the cruciform joints investigated in this study. Since the examined details are additionally exposed to a pure tensile stress,

no large deviations should be evident. Nevertheless, it is noticeable that with regard to all geometries, a slight stress increase of approximately 2 % can be determined with the quadratic extrapolation compared to the linear extrapolation (cf. Table 3-7).

Table 3-7: Deviation of the structural stresses resp. $SCFs$ of different local methods and the nominal stress and effective notch stress method from the results of the linear stress extrapolation for various geometries (12 – 12), (12 – 40), (40 – 12) and (25 – 25) separately for finely and coarsely meshed solid and shell elements

Geometry and meshing		Linear stress extrapolation	Quadratic stress extrapolation	One-point method	Haibach $\Delta x = 0.3 \cdot t$	Haibach $\Delta x = 2 \text{ mm}$	One-millimetre method	Internal linearisation	δ -method	Nominal stress concept	Effective notch stress concept	
(12 – 12)	Solid	fine	100%	102%	111%	105%	119%	97%	104%	126%	120% – 135%	114%
		coarse	99%	–	110%	105%	–	–	–	–		
	Shell	fine	100%	101%	109%	98%	99%	–	–	107%		
		coarse	100%	–	110%	99%	–	–	–	–		
(12 – 40)	Solid	fine	100%	101%	114%	107%	120%	108%	107%	112%	120% – 135%	121%
		coarse	103%	–	113%	107%	–	–	–	–		
	Shell	fine	101%	101%	113%	101%	101%	–	–	108%		
		coarse	102%	–	113%	101%	–	–	–	–		
(40 – 12)	Solid	fine	100%	102%	110%	103%	135%	95%	104%	110%	118% – 136%	131% – 151%
		coarse	100%	–	112%	104%	–	–	–	–		
	Shell	fine	98%	98%	110%	97%	97%	–	–	105%		
		coarse	100%	–	110%	98%	–	–	–	–		
(25 – 25)	Solid	fine	100%	102%	111%	104%	128%	102%	105%	110%	120% – 135%	142%
		coarse	100%	–	112%	105%	–	–	–	–		
	Shell	fine	99%	100%	111%	99%	99%	–	–	107%		
		coarse	100%	–	111%	99%	–	–	–	–		

With the one-point stress determination [9, 41], the structural stresses that are determined with $\Delta x = 0.5 \cdot t$ [4, 2] are between 10 % and 15 % larger than in the linear stress extrapolation. This fact is due to the computational stress intensification by a factor of 1.12, which is fundamental to this approach (cf. Chapter 2.3.3.2). In this respect, it also becomes apparent that the choice of element type and the kind of mesh are of subordinate importance, since the results for finely resp. coarsely meshed solid resp. shell models are within the specified range of deviation (cf. Table 3-7). In contrast, Haibach's methods with $\Delta x = 0.3 \cdot t$ [48] and $\Delta x = 2 \text{ mm}$ [9, 41] are strongly dependent on the selected type of element. While the structural stresses determined with shell elements are in the range of the linear stress extrapolation, the results for solid models deviate considerably (cf. Table 3-7). In this respect, the deviations in the stress determination at a distance of $\Delta x = 0.3 \cdot t$ vary between 3 % and 7 %, whereas the results at a distance of $\Delta x = 2 \text{ mm}$ deviate significantly between 19 % and 35 %. The

latter demonstrates that with increasing thickness of the load-bearing primary plate, a thickness-independent specification of the distance fails to provide reasonable results. This is due to the fixed proximity to the weld notch, which results in large structural stresses, especially with thicker plates.

With regard to the one-millimetre method [7], widely varying values between 95 % and 108 % can be expected, depending on the dimensions of the cruciform joint to be evaluated (cf. Table 3-7). Since $SCFs = \Delta\sigma_{R,hs} / \Delta\sigma_{R,nom} < 1.00$ cannot be excluded, this method appears to be unsuitable for a uniform structural stress determination. The equally complex internal linearisation [6, 8], on the other hand, provides more uniform values with deviations between 4 % and 7 % to the linear stress extrapolation. However, the assessment of structural stresses is very intricate and requires detailed meshing, which is hardly feasible in economic and practical terms.

The same applies to the δ -method, which can only be implemented in a time-consuming manner and with complicated calculational procedures (cf. Chapter 2.3.3.5). In this respect, the results determined with solid elements differ greatly with a deviation between 110 % and 126 % (cf. Table 3-7). In addition, the structural stresses evaluated from solid models vary significantly from those determined from shell models, which only show deviations between 5 % and 8 %. Consequently, this approach also appears to be ineffective for a general applicability of the structural stress concept for metal structures with a required universal validity.

In addition to the local methods, the valid value ranges according to the nominal stress concept and effective notch stress concept from Table 3-5 are converted into deviations from the linear stress extrapolation (cf. Table 3-7). In this respect, the resulting smaller value can be regarded as the limit at which lower structural stresses allow economic applicability of the structural stress concept in all cases. Nonetheless, according to the nominal and effective notch stress concept, significantly greater structural stresses are generally expected than can be achieved using most local methods (cf. Table 3-7). The expected deviations are between 118 % and 136 % in the nominal stress concept and between 114 % and 151 % in the effective notch stress concept and thus significantly above the determinable structural stresses. Comparably large results are calculated only with solid elements according to Haibach with $\Delta x = 2 \text{ mm}$ (cf. Table 3-7). However, this approach is not considered to be appropriate in this thesis due to its missing thickness dependence. Since all other local methods are far below the $SCFs$ to be expected according to the nominal and effective notch stress concept, the economic applicability of the structural stress concept should generally apply if the methods are capable of realistically representing structural stresses. But due to the large scatter of results obtained by the applied local methods, this cannot simply be assumed to be the case.

The evaluations thus show that a general assessment of the validity of local methods is difficult, as no clear tendencies are discernible. In this respect, the determination of the structural stress by all methods must be questioned, as it seems unrealistic that the economic efficiency, compared to the nominal and effective notch stress concept, is improved to such a large extent. In addition, there is a deficiency of confirmed reference values that could be determined exclusively on the basis of experimental trials. However, it is impossible to determine stresses in the thickness direction on

experimental fatigue tests. Consequently, only surface stresses can be considered to verify structural stress determination methods. Since, alongside the applied structural stress $\Delta\sigma_{R,hs}$, the fatigue strength $\Delta\sigma_{C,hs}$ is equally to be investigated, an exact assessment is therefore practically impossible.

To still be able to implement sensible evaluations with structural stresses $\Delta\sigma_{R,hs}$ and to provide an evaluation of the associated fatigue strength $\Delta\sigma_{C,hs}$, the generally accepted stress extrapolation will be used in the further course of this thesis. In the author's view, this methodology offers the largest benefits in comparison to the other local approaches investigated. One reason for this is its simple implementation, which does not require a great degree of meshing. In addition, resulting stress distributions can be verified by strain measurements, as stresses are recorded on the surface. Furthermore, the minimally scattering results of the linear and quadratic stress extrapolation for fine and coarse meshes with solid and shell elements allow a generally valid application, which is imperative for a normative realisation. In this respect, the structural stress determination by means of stress extrapolation offers the additional advantage that it is already normatively anchored in prEN 1993-1-9 [4] and prEN 1993-1-14 [14] as well as in the guidelines of the IIW [3]. Suggestions for improved design may thus be implemented in a more effective and simpler process. Accordingly, in the further course of this thesis, only the linear stress extrapolation with the meshing specifications of fine meshes according to Section 3.3.4.1 is investigated further. However, the results presented in this section can be considered as indications for the applicability of alternative local methods.

3.3.5 Choice of sensible shell models

The aim of this section is to identify which modelling methods for welds are suitable for a realistic FE calculation with shell elements. For this purpose, results generated with finely meshed solid models are used to validate the weld models for shell elements presented in Section 3.1.1.2. On the basis of Section 3.3.4, the linear stress extrapolation is used for the associated structural stress determination. To allow a uniform analysis, the FE shell models are also evaluated using the linear stress extrapolation with the meshing properties according to Section 3.3.4.1. In order to enable an explicit allocation, the methods from Section 3.1.1.2 are abbreviated in the further course of this thesis. In this respect, the method with no consideration of welds (cf. Section 3.1.1.2.1) is defined as weld method one with *WM1*. Accordingly, the approach with an increased cross-sectional area (cf. Section 3.1.1.2.2) is defined as *WM2*, the method with inclined shell elements (cf. Section 3.1.1.2.3) as *WM3* and the procedure with rigid links (cf. Section 3.1.1.2.4) as *WM4*. To ensure a sensible comparability, thickness effects (cf. Chapter 2.6) are not considered in this Section. Furthermore, in the following Section 3.3.5.1, solely idealised perfect cruciform joints without any imperfections are considered to avoid additional influences. In order to also identify the influence of axial and angular misalignment on the different weld models, the effects of imperfections on the resulting structural stresses are investigated in Section 3.3.5.2. The associated evaluations are based on the results of IGF research project No. 20336N [1] and only address the two most effective methods. In conclusion, the obtained results are summarised in Section 3.3.5.3.

3.3.5.1 Evaluation without consideration of imperfections

The evaluation of the different weld approaches for shell element models is performed with the dimensions according to the following Table 3-8. In this respect, solely cruciform joints without imperfections are examined in this section. The corresponding allocation of the given parameters is in accordance with Figure 3-14.

Table 3-8: Dimensions of cruciform joints for the parametric study of different weld modelling methods

Welded-on primary plates				Intermediate plate			Weld	
$t_1 = t_2$ [mm]	$w_1 = w_2$ [mm]	$L_1 = L_2$ [mm]	L_{clamp} [mm]	t_3 [mm]	w_1 [mm]	L_3 [mm]	$a_{fillet\ weld}$ [mm]	$a_{butt\ weld}$ [mm]
12				12			5	
(12)				(40)			(5)	
[40]	100	150	100	[12]	100	$200\ mm + (t_1 = t_2)$	[14]	$(t_1 = t_2)/2$
{40}				{40}			{14}	
25				25			8	

The parameters from Table 3-8 that applied collectively are listed below each other and are marked with uniform brackets. While the length L_3 of the intermediate plate represents the total length of this component, the individual plate lengths L_1 and L_2 of the welded-on primary plates are specified up to the intersection with the centre plane of the intermediate plate (cf. Figure 3-14). The weld thickness $a_{fillet\ weld}$ corresponds to the thickness of the fillet welds and is required for generating the FE models (cf. Figure 3-14). In contrast, the thickness of the bevel butt weld $a_{butt\ weld}$ is not considered in the FEA, as a homogeneous material is assumed in the models. This is due to the fact that the welds of the cruciform joints investigated are fully penetrated (cf. Chapter 2.3). Consequently, no distinction is made within the component between the plate and the weld.

The results are summarised for varying thicknesses of the welded-on primary plates. The corresponding evaluation is provided for intermediate plate thicknesses of $12\ mm$ (Figure 3-17) and $40\ mm$ (Figure 3-18). In this respect, both finely and coarsely meshed shell models are assessed using weld methods *WM1* (cf. Section 3.1.1.2.1), *WM2* (cf. Section 3.1.1.2.2), *WM3* (cf. Section 3.1.1.2.3) and *WM4* (cf. Section 3.1.1.2.4). To enable a comparison with the results of FEA with solid elements, the results for a finely meshed solid model are also presented. According to section 3.3.4, the evaluation is based on stress concentration factors (*SCF*), which represent the ratio of the applied structural stress $\Delta\sigma_{R,hs}$ to the applied nominal stress $\Delta\sigma_{R,nom}$.

According to Figure 3-17 and Figure 3-18, the results of the finely meshed solid models are relatively independent of the thicknesses of the welded-on plates and the intermediate plate. The corresponding stress concentration factors vary in a small range between $SCF \approx 1.01$ and $SCF \approx 1.05$. However, depending on the weld model, considerable differences become apparent with regard to the FE models with shell elements. To this end, the stress concentration factors range between $SCF \approx 1.01$ and $SCF \approx 1.26$, indicating the significant influence of the selected welding method. In this respect, overestimates are considered to be less critical, as they solely result in an uneconomical design. In contrast, underestimations lead to uncertain results being

obtained with shell elements, which can cause an incorrect estimation of the structural stress. These cases are therefore to be considered particularly critical in the following.

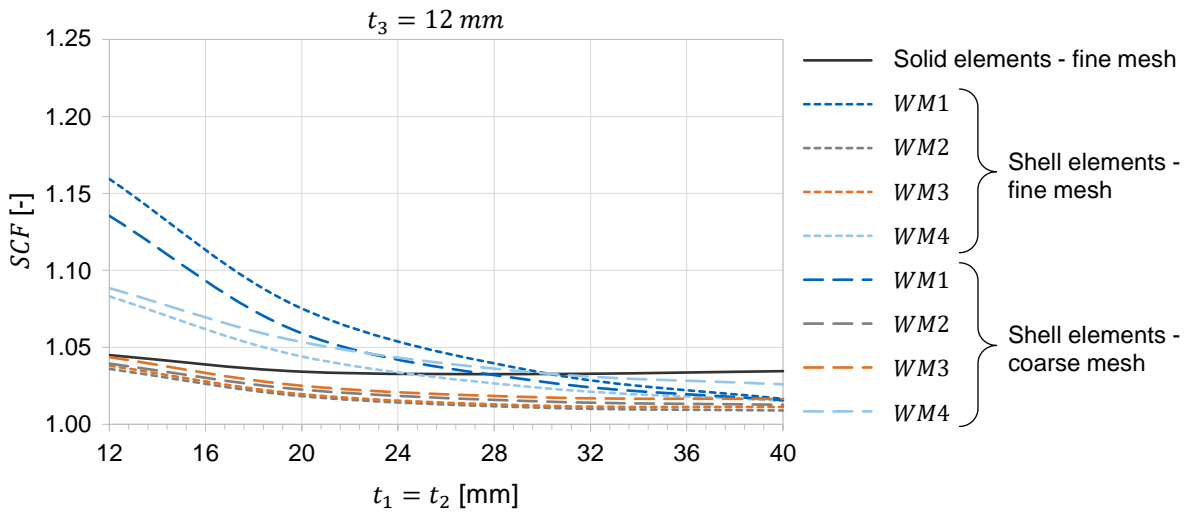


Figure 3-17: Parameter study on stress concentration factors (SCF) of weld methods $WM1$ to $WM4$ with finely and coarsely meshed shell models and comparison to finely meshed solid model for different primary plate thicknesses $t_1 = t_2$ with an intermediate plate thickness of $t_3 = 12$ mm

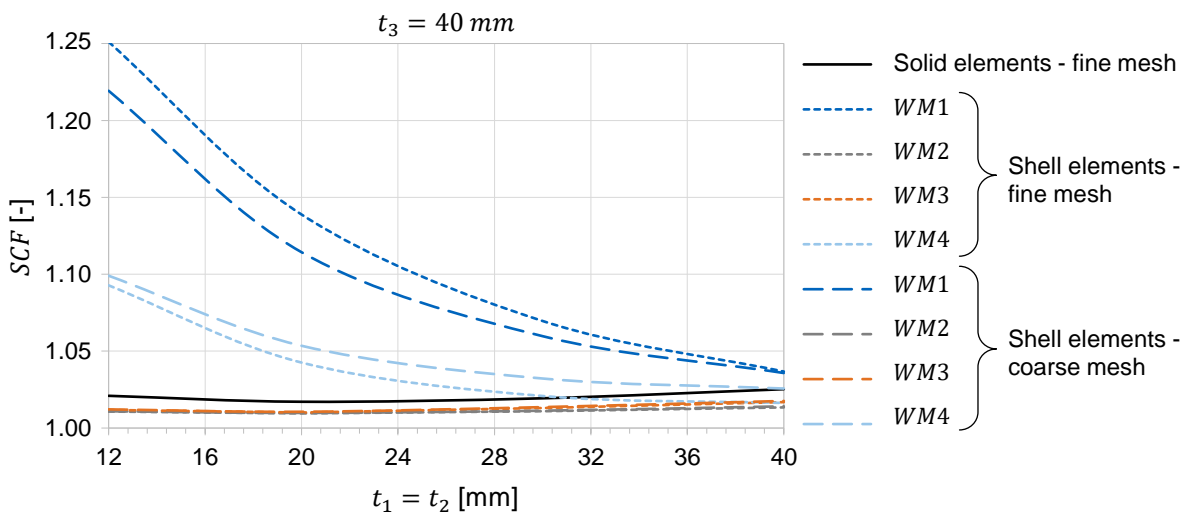


Figure 3-18: Parameter study on stress concentration factors (SCF) of weld methods $WM1$ to $WM4$ with finely and coarsely meshed shell models and comparison to finely meshed solid model for different primary plate thicknesses $t_1 = t_2$ with an intermediate plate thickness of $t_3 = 40$ mm

Figure 3-17 and Figure 3-18 further show that, with regard to meshing in general, no explicit statement can be provided that applies to all methods investigated. For most methods, however, the results for the finely meshed shell models are lower than the results with coarse meshing, irrespective of the selected thicknesses $t_1 = t_2$ and t_3 (cf. Figure 3-17 and Figure 3-18). This is true for $WM2$, $WM3$ and $WM4$. Only in the method without modelling welds ($WM1$) does a finer mesh lead to larger stress concentration factors. In order to identify the cause, the required stress distributions of the linear stress extrapolation (cf. Chapter 2.3.3.1) are investigated for a fine and for a coarse mesh across the component width. In this respect, both $WM1$, with larger stress concentration factors for coarse meshes, and $WM4$, as a representative method with larger stress concentration factors for fine meshes, are evaluated. The evaluation is

carried out on cruciform joints with $t_1 = t_2 = 12 \text{ mm}$ and $t_3 = 40 \text{ mm}$, as the most distinct difference between a fine and coarse mesh are present in *WM1* with these dimensions. The corresponding results are illustrated below for *WM4* (left side of Figure 3-19) and *WM1* (right side of Figure 3-19).

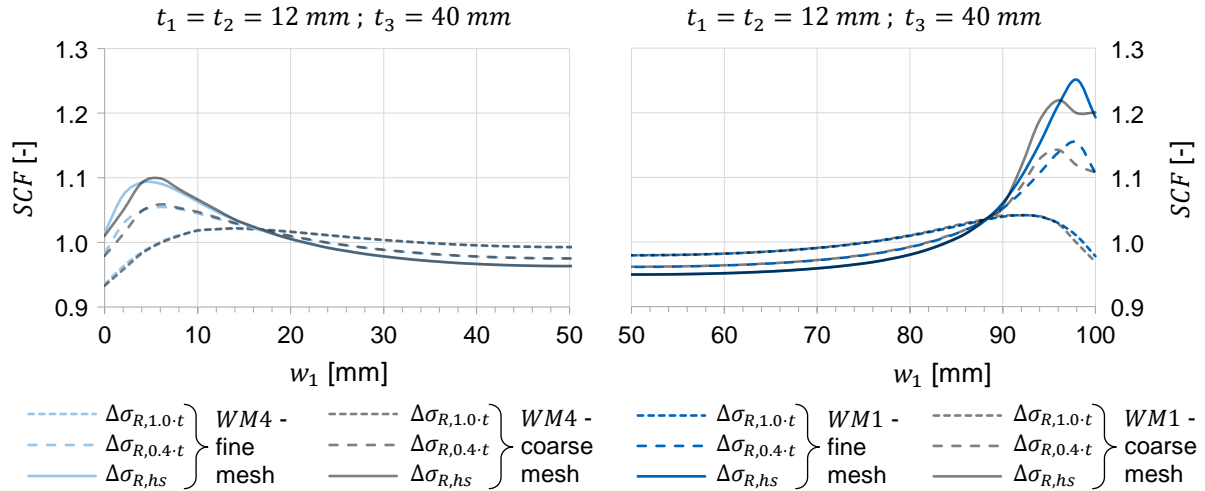


Figure 3-19: Stress distributions of the stress concentration factor for $\Delta\sigma_{R,1.0-t}$, $\Delta\sigma_{R,0.4-t}$ and $\Delta\sigma_{R,hs}$ over the component width for the linear stress extrapolation for finely and coarsely meshed *WM4* (left) and *WM1* (right) with $t_1 = t_2 = 12 \text{ mm}$ and $t_3 = 40 \text{ mm}$

The right side of Figure 3-19 illustrates that in contrast to the stress distributions of finely meshed models with *WM1*, the stress peaks at a distance of $0.4 \cdot t$ cannot be accurately detected with this method if a coarse mesh is applied. This results in a lower structural stress $\Delta\sigma_{R,hs}$ for method *WM1* and is due to the abrupt change in stiffness at the intersection of the plates. This fact leads to the most significant differences between the results for fine and coarse meshes of *WM1* (cf. Figure 3-17 and Figure 3-18). In the evaluation presented, the difference amounts between $\Delta SCF \approx 2.6 \%$ and $\Delta SCF \approx 0.1 \%$. In this respect, the largest deviations are obtained with a thickness of the welded-on primary plates of $t_1 = t_2 = 12 \text{ mm}$ and a concurrent intermediate plate thickness of $t_3 = 40 \text{ mm}$ (cf. Figure 3-18). [55]

On the other hand, with methods *WM2*, *WM3* and *WM4*, both models with fine and coarse meshing are able to accommodate the stress peaks at $0.4 \cdot t$ (cf. left side of Figure 3-19). In this respect, coarse meshing only leads to less accurate results than fine meshes. The corresponding structural stresses $\Delta\sigma_{R,hs}$ are therefore slightly lower due to the more evenly distributed stiffness increases and limited number of elements across the width of the component. With *WM4*, the differences between a fine and a coarse mesh are somewhat smaller than *WM1*, but with stress concentration factors between $\Delta SCF \approx 1.1 \%$ and $\Delta SCF \approx 0.5 \%$ still significant (cf. Figure 3-18). In contrast, only small differences $\Delta SCF < 0.5 \%$ are detected with *WM2* and *WM3* (cf. Figure 3-17 and Figure 3-18). Consequently, these methods can be considered relatively insensitive to the choice of meshing.

In general, however, it can be assumed that FE models with a finer mesh lead to more accurate results, as considerably more element nodes can be evaluated. This leads to more realistic stress distributions for the structural stress determination in the critical area in front of the weld notch. Since, with respect to shell elements, fine meshes require only slightly more computational effort with almost no change in modelling

complexity, fine meshing should consequently be used in all cases. For this reason, further evaluations on shell models are implemented solely with fine meshes. [55]

Based on the results, the following sections provide a detailed evaluation of the results from Figure 3-17 and Figure 3-18 separately for the methods investigated. In this respect, *WM1* is evaluated in Section 3.3.5.1.1, *WM4* in Section 3.3.5.1.2 and *WM2* as well as *WM3* in Section 3.3.5.1.3.

3.3.5.1.1 *WM1*

Figure 3-17 and Figure 3-18 demonstrate that the FE models with *WM1*, without explicitly modelled welds, significantly overestimate the expected structural stress of the finely meshed solid models in the majority of cases. In this regard, the maximum overestimation amounts to +22.5 % with a finely meshed shell model with *WM1*. Only thin intermediate plates $t_3 = 12 \text{ mm}$ with relatively thick welded-on primary plates $t_1 = t_2 > 30 \text{ mm}$ lead to an underestimation of a minimum of -1.8% (cf. Figure 3-17). This is due to the significant influence of the transverse strain constraint with method *WM1*. In the associated shell models, the stiffness from the intermediate plate is concentrated solely on the intersection with the welded-on primary plates. This can lead to large stresses transverse to the longitudinal direction of the primary plate. Consequently, the stress peaks in the decisive area of the structural stress determination of the linear stress extrapolation are significantly too high if the stiffness of the welded-on primary plates is far lower than that of the intermediate plate. Therefore, the results of solid elements are maximally overestimated with shell elements if thin primary plates with $t_1 = t_2 = 12 \text{ mm}$ and a low stiffness are connected to a relatively thick intermediate plate with $t_3 = 40 \text{ mm}$ and a large stiffness (cf. Figure 3-18).

This behaviour is further illustrated in Figure 3-20. In this respect, the required stress distributions of the linear stress extrapolation are evaluated over the component width. In this way, the distributions of *WM1* can be compared to the results using solid elements. In both cases, the FE models are finely meshed. The most unfavourable case investigated is presented with the highest overestimation of the occurring structural stress $\Delta\sigma_{R,hs}$ with a thickness of the primary plates of $t_1 = t_2 = 12 \text{ mm}$ and an intermediate plate thickness of $t_3 = 40 \text{ mm}$.

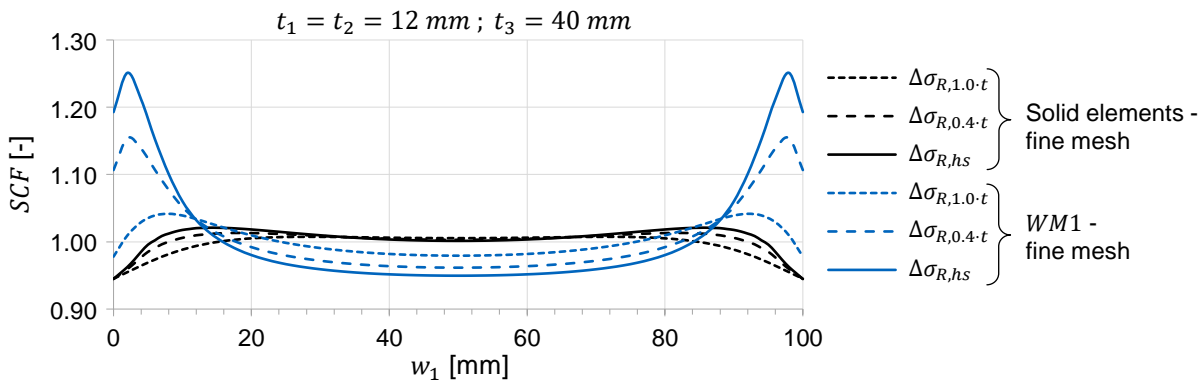


Figure 3-20: Stress distributions of the stress concentration factor for $\Delta\sigma_{R,1.0-t}$, $\Delta\sigma_{R,0.4-t}$ and $\Delta\sigma_{R,hs}$ over the component width for the linear stress extrapolation for finely meshed *WM1* and solid model with $t_1 = t_2 = 12 \text{ mm}$ and $t_3 = 40 \text{ mm}$

The difference in stiffness between the welded-on primary plates and the intermediate plate is therefore greatest in the evaluation from Figure 3-20. Although a slight stress increase at the edges can also be observed in the solid model, this is significantly less severe than in the shell model. Thus, with $SCF \approx 1.26$, significantly higher stress concentration factors are generated than with $SCF \approx 1.02$ of the finely meshed models with solid elements.

Furthermore, the distance of the reference points of the extrapolation method depends only on the thickness of the welded-on primary plates $t_1 = t_2$. For small primary plate thicknesses, the distances of the extrapolation paths are consequently too close to the intermediate plate and the associated critical area. This additionally leads to the fact that the stress peaks at the edges are too steep with method *WM1*.

Due to the aforementioned aspects, method *WM1* is thus hardly economically applicable. This applies in particular to cruciform joints with relatively high stiffness of the intermediate plate and comparably low stiffness of the welded-on primary plates. However, since the procedure of method *WM1* represents a significant time saving due to the lack of weld modelling, the distances of the reference points for the linear stress extrapolation are checked for their applicability in the following. Therefore, the aim is to exploit the potential of this method by adjusting resp. correcting the recommended distances. In this respect, the results from IGF research project No. 20336N [72] indicate that by changing the position of the structural stress path as a function of the intermediate plate thickness t_3 , better conformities can be achieved compared to the solid model. This is due to the reduced influence of the transverse strain constraint on the stress peaks (cf. Figure 3-20).

In Table 3-9 the stress concentration factors SCF of the finely meshed solid model are compared to the results of *WM1* with a fine mesh for different main and intermediate plate thicknesses. In the corresponding evaluation, on the one hand and in accordance with the normative specifications and guidelines, the positions of the linear stress extrapolation paths of method *WM1* remain unmodified at $0.0 \cdot t$. On the other hand, the results are listed in which the paths are uniformly positioned further away from the intersection of the plates by $0.25 \cdot t$ because, according to [72], this provided the most favorable results.

Table 3-9: Comparison of the stress concentration factors SCF of the solid model to shell models with *WM1* and normative positions of the required structural stress paths at $0.00 \cdot t_3$ as well as adjusted positions at distance $0.25 \cdot t_3$ for different cruciform joint geometries

$t_1 = t_2$ [mm]	t_3 [mm]	Finely meshed solid model with unmodified stress extrapolation paths SCF [-]	Finely meshed shell model with <i>WM1</i>			
			Stress extrapolation paths $0.00 \cdot t_3$ from intersection of plates		Stress extrapolation paths $0.25 \cdot t_3$ from intersection of plates	
			SCF [-]	Deviation	SCF [-]	Deviation
12	12	1.045	1.159	+10.9 %	1.085	+3.8 %
12	40	1.021	1.251	+22.5 %	1.045	+2.3 %
25	25	1.023	1.081	+5.7 %	1.032	+0.9 %
40	12	1.035	1.016	-1.7 %	1.010	-2.4 %
40	40	1.025	1.037	-1.1 %	1.013	-1.2 %

According to Table 3-9, the evaluation for *WM1* without the adjustment of the paths required for the linear stress extrapolation results in deviations ranging from 22.5 % (12 – 40) to –1.7 % (40 – 12) compared to the solid model. By correcting the positions of the structural stress paths to an ideal distance of $0.25 \cdot t_3$ to the line of intersection of the plates, the maximum deviation can be reduced to +3.8 % (12 – 12) without the underestimation being more than –2.4 % (40 – 12) (cf. Table 3-9). This significantly smaller deviation from the relevant structural stresses of the solid models is more likely to allow the applicability of method *WM1*. Furthermore, an increase of the structural stresses by a correction factor of 1.025 would be possible. In this way, the results of the shell models of method *WM1* could be modified by adjusting the positions of the evaluation paths of the linear stress extrapolation and by an additional general increase of the structural stresses to $\Delta\sigma_{R,hs,eff} = 1.025 \cdot \Delta\sigma_{R,hs}$ in order not to allow uncertain results with *WM1* at any of the examined cruciform joints. However, since the structural stress $\Delta\sigma_{R,hs}$ is already overestimated up to +3.8 % with thin plates $t_1 = t_2$ and t_3 , only relatively uneconomical results can be achieved in this range. Nevertheless, a general applicability of *WM1* would be conceivable through the adjustments.

3.3.5.1.2 *WM4*

For method *WM4*, Figure 3-17 and Figure 3-18 also demonstrate that there is a significant overestimation of the structural stresses $\Delta\sigma_{R,hs}$ of the finely meshed solid models associated with thin welded-on primary plates. In this respect, the maximum overestimation amounts to +7.6 % for FE models with coarsely meshed shell elements. The corresponding cause is illustrated in Figure 3-21, with the stress concentration factors of the paths required for the linear stress extrapolation evaluated over the component width. For this purpose, the evaluation paths of the finely meshed solid model are compared to method *WM4*, also with a fine mesh. The analysis is carried out for a cruciform joint with $t_1 = t_2 = 12 \text{ mm}$ and $t_3 = 40 \text{ mm}$.

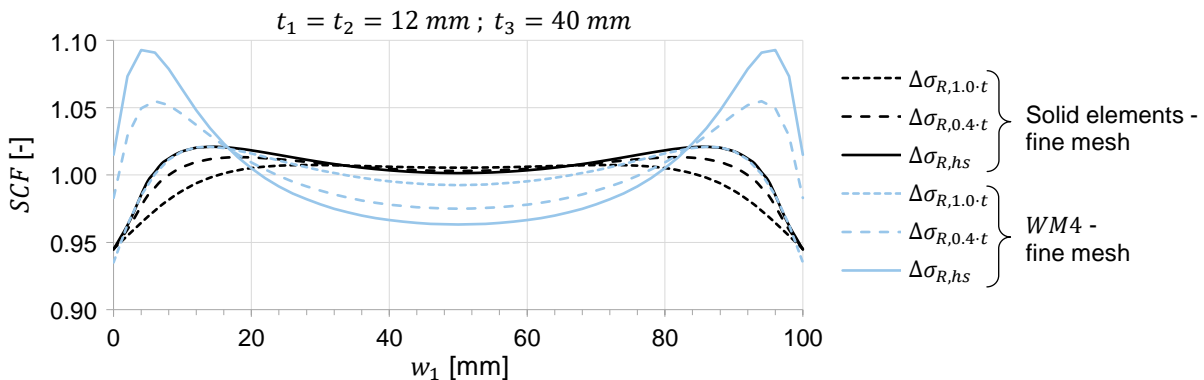


Figure 3-21: Stress distributions of the stress concentration factor for $\Delta\sigma_{R,1.0-t}$, $\Delta\sigma_{R,0.4-t}$ and $\Delta\sigma_{R,hs}$ over the component width for the linear stress extrapolation for finely meshed *WM4* and solid model with $t_1 = t_2 = 12 \text{ mm}$ and $t_3 = 40 \text{ mm}$

According to Figure 3-21, a similar behaviour can be observed with method *WM4* as with method *WM1*, since the stress peaks of the finely meshed solid model are also overestimated significantly with thin welded-on primary plates $t_1 = t_2$. This is due to the fact that the inclined shell elements of the welds are connected to the welded-on primary plates and intermediate plate by attached rigid links, which makes the system

behaviour significantly stiffer than it is the case with the solid model. This leads to an overestimation of the structural stresses $\Delta\sigma_{R,hs}$ transverse to the tensile direction. In addition, the fixed distance of the reference points of the linear stress extrapolation to the intermediate plate is smaller for method *WM4* than for FE models with solid elements, as the distances of the extrapolation paths are defined to the connection point of the rigid links (cf. Section 3.1.1.2.4).

Depending on the thickness of the intermediate plate t_3 and the selected mesh, the structural stresses of the solid models are additionally underestimated starting at approximately $t_1 = t_2 \approx 30 \text{ mm}$ (cf. Figure 3-17 and Figure 3-18). To this end, the maximum underestimation of -1.9% for finely meshed shell models with *WM4* is somewhat less significant than the overestimation.

Although the deviations of *WM4* from the results of the finely meshed solid models are not quite as critical as for *WM1*, rectifications are not considered expedient for this method due to the above-average modelling effort and large deviations from the solid model.

3.3.5.1.3 *WM2* and *WM3*

According to Figure 3-17 and Figure 3-18, *WM2* and *WM3* provide the most consistent results of the investigated methods with the finely meshed solid models. However, in all cases there is an underestimation of the results. While this amounts to a maximum of -2.5% for method *WM2*, a maximum deviation of -2.3% results for *WM3*. The maximum differences in this respect occur with thick welded-on primary plates $t_1 = t_2 = 40 \text{ mm}$ in combination with thin intermediate plates $t_3 = 12 \text{ mm}$. Although the stress concentration factors are generally slightly underestimated, the structural stress distributions have a similar tendency (cf. Figure 3-17 and Figure 3-18).

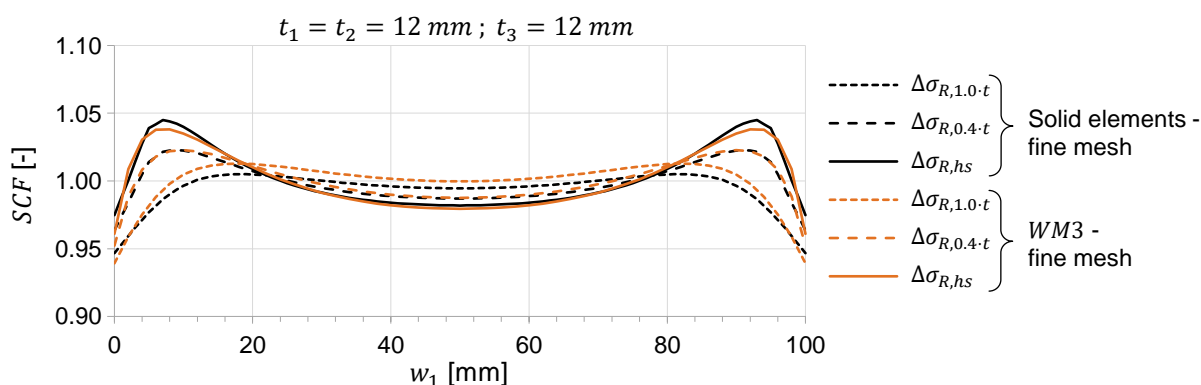


Figure 3-22: Stress distributions of the stress concentration factor for $\Delta\sigma_{R,1.0-t}$, $\Delta\sigma_{R,0.4-t}$ and $\Delta\sigma_{R,hs}$ over the component width for the linear stress extrapolation for finely meshed *WM3* and solid model with $t_1 = t_2 = 12 \text{ mm}$ and $t_3 = 12 \text{ mm}$

Figure 3-22 and Figure 3-23 show the decisive stress distributions of the paths for the linear stress extrapolation over the component width. The evaluation is carried out with the finely meshed FE model for *WM3*, representative of the methods investigated in this section. This is sufficient because *WM2* and *WM3* practically provide the same systematic behaviour. In addition, the results for the finely meshed solid model are presented for comparability. For the analysis, a cruciform joint with $t_1 = t_2 = 12 \text{ mm}$ (cf. Figure 3-22) as well as with $t_1 = t_2 = 40 \text{ mm}$ (cf. Figure 3-23) is considered. In both

cases the thickness of the intermediate plate is defined with $t_3 = 12 \text{ mm}$. According to Figure 3-22, the distribution of the stress concentration factor at a distance of $0.4 \cdot t$ sufficiently corresponds to the results of the model with finely meshed solid elements. Nevertheless, since the stresses at a distance of $1.0 \cdot t$ are higher than in the solid model, the structural stresses $\Delta\sigma_{R,hs}$ with *WM3* are slightly underestimated. Similar behaviour can be detected with method *WM2*.

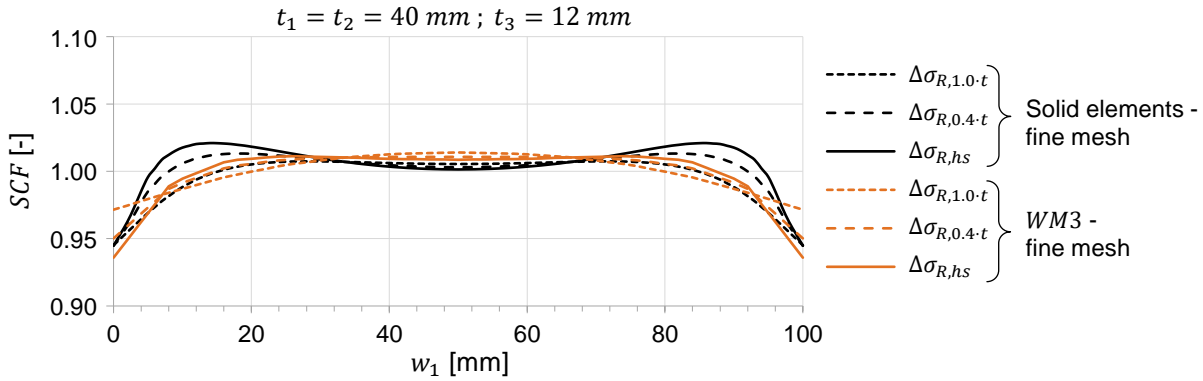


Figure 3-23: Stress distributions of the stress concentration factor for $\Delta\sigma_{R,1.0-t}$, $\Delta\sigma_{R,0.4-t}$ and $\Delta\sigma_{R,hs}$ over the component width for the linear stress extrapolation for finely meshed *WM3* and solid model with $t_1 = t_2 = 40 \text{ mm}$ and $t_3 = 12 \text{ mm}$

Concerning this matter, Figure 3-23 illustrates that with thick welded-on primary plates $t_1 = t_2$ in combination with a thin intermediate plate t_3 , there is an increasing tendency for the maximum structural stress $\Delta\sigma_{R,hs}$ to shift towards the centre of the plate. Consequently, the stress peaks in the edges of the plate are no longer detected accurately by *WM2* and *WM3*. This leads to the fact that the structural behaviour can no longer be represented accurately with increasing thicknesses $t_1 = t_2$ of the welded-on primary plates in combination with a thin intermediate plate t_3 . However, this only leads to minor deviations of the structural stresses $\Delta\sigma_{R,hs}$ from the solid model (cf. Figure 3-23).

In general, for the cruciform joints examined, the percentage deviations of *WM2* from the solid model are slightly higher than for *WM3*. Moreover, since the significantly higher modelling effort of *WM2* compared to *WM3* is not justified, method *WM3* thus delivers the most effective results.

Since the deviations of *WM3* from the FE models with solid elements are relatively consistent, the implementation of a correction factor is also reasonable, corresponding to the procedure for *WM1* (cf. Section 3.3.5.1.1). In this respect, a general stress increase of the results for shell elements with *WM3* to 102.5% would cover all deviations from solid models determined in the investigated range of cruciform joints. The linear stress extrapolation for a hot-spot type *a* thus would result in the following structural stress $\Delta\sigma_{R,hs,eff}$:

$$\Delta\sigma_{R,hs,eff} = 1.025 \cdot \Delta\sigma_{R,hs} = 1.025 \cdot (1.67 \cdot \sigma_{0.4-t} - 0.67 \cdot \sigma_{1.0-t}) \quad (3-3)$$

This way, the structural stress $\Delta\sigma_{R,hs}$ determined with FE shell models could be modified to $\Delta\sigma_{R,hs,eff}$ to ensure sufficient concordance with the results of solid models without generating uneconomic results, as this would be the case with method *WM1* and *WM4*. However, these general statements apply solely to perfect cruciform joints

without the consideration of potential imperfections. The influence of misalignments on structural stresses is therefore examined in more detail in the following section for the most auspicious methods *WM1* and *WM3*.

3.3.5.2 Evaluation with consideration of imperfections

According to section 3.3.5.1, the influences of imperfections on the results using methods *WM1* and *WM3* are presented subsequently. The results are based on the evaluations from IGF research project No. 20336N [1]. In this respect, it was discovered that the type of support is crucial for the evaluation of effects regarding imperfections. The associated imperfect FE models with the consideration of clamping processes in testing machines are based on the contents from section 3.3.2. For the further evaluations of more common support conditions, all systems from Chapter 2.5.3.2.4 according to Xing and Dong [5] are applied to create and evaluate the models with finely meshed solid and shell elements. In this context, only influences of axial (cf. Chapter 2.5.2.2) and angular (cf. Chapter 2.5.2.1) misalignment on the structural stresses of cruciform joints are assessed. The associated parameter range investigated for the analysis of imperfections includes a maximum axial misalignment of $e = 0.5 \cdot t_{1=2}$ (cf. Figure 2-22) and a maximum angular misalignment of $\beta = 2.5^\circ$ (cf. Figure 2-21). Thus, the maximum permissible manufacturer tolerances of $e/t = \pm 0.5$ for axial misalignment according to DIN EN 1090-2 [37] are considered. In addition, the entire range of the specification $\beta \leq 2^\circ$ of evaluation group C according to DIN EN ISO 5817 [68] for angular misalignment is also under consideration. Analysed are the cruciform joints with the dimensions from Table 3-8. In addition, the parameter range is extended by thicker welded-on primary plates up to $t_1 = t_2 = 80 \text{ mm}$ and by lengths $L_1 = L_2$ up to 1000 mm . This is due to the fact that particularly the thickness of the primary plates $t_1 = t_2$ and the lengths $L_1 = L_2$ between the clamping section and the critical notch in the area of the welds have a significant influence on the relevant structural stresses under the influence of imperfections.

The resulting maximum underestimations, which are to be regarded as particularly critical, are summarised for the investigated support conditions in the following Table 3-10. The percentage differences are the deviations of the modified method *WM1* and unmodified method *WM3* to the results of the solid models. In this respect, the finely meshed solid models are each supported in the same way as the shell models and the identical imperfections are implemented.

Table 3-10: Maximal underestimation of the relevant structural stress $\Delta\sigma_{R,hs}$ of finely meshed shell models with the modified method *WM1* and unmodified method *WM3* to finely meshed solid models

Misalignment	Support condition	Maximal underestimation [%]	
		Modified <i>WM1</i>	<i>WM3</i>
No misalignment	No influence	-2.4	-2.3
	Testing machine	-17.3	-1.9
Axial: $e = 0.5 \cdot t_{1=2}$	Common practice	-	-5.3
	Testing machine	-11.5	-11.0
Angular: $\beta = 2.5^\circ$	Common practice	-	-5.8

According to Table 3-10, significant differences between the examined methods *WM1* and *WM3* are evident. In this respect, the determined limit values are consistently identified with the maximum investigated axial and angular imperfections. Due to the large deviations in the investigations of the clamping process for shell models with *WM1* (cf. Table 3-10), both with axial and angular misalignment, the extensive evaluations of practical support conditions according to Chapter 2.5.3.2.4 [5] are not further investigated for *WM1*. Consequently, the respective assessment is only carried out for the more applicable method *WM3*. The results on the influence of imperfections from Table 3-10 are described separately for *WM1* (cf. Section 3.3.5.2.1) and *WM3* (cf. Section 3.3.5.2.2).

3.3.5.2.1 *WM1*

When evaluating perfect FE model with finely meshed shell models of the modified method *WM1*, an underestimation of the finely meshed solid models of -2.4% was determined (cf. Section 3.3.5.1.1). However, the investigations of influences resulting from imperfections indicate that a realistic evaluation is not possible with *WM1*, as the system behaviour can only be implemented with significant deviations from the solid model. In this respect, axial misalignment of $e = 0.5 \cdot t$ leads to an underestimation of up to -17.3% (cf. Table 3-10). An angular misalignment of $\beta = 2.5^\circ$, on the other hand, still results in a deviation of -11.5% to the solid model. Consequently, a correction factor would have to be very conservative to cover the insufficient structural stresses $\Delta\sigma_{R,hs}$. In practice, this would result in inefficient design in most cases, which is why the applicability of shell models without explicitly considered welds is considered questionable in studies on imperfections.

3.3.5.2.2 *WM3*

In contrast to the evaluations with *WM1*, with method *WM3*, for the most part, sufficient conformities to the finely meshed solid models can be achieved, even if imperfections are to be considered (cf. Table 3-10). However, when imperfections are taken into account, the deviations are in some cases also considerably more critical than with -2.3% for the perfect FE models. In this respect, smaller deviations of up to -1.9% can only be determined with axial misalignment $e = 0.5 \cdot t$ in combination with the clamping process in testing machines. If angular misalignment $\beta = 2.5^\circ$ is analysed, considerably larger deviations of up to -11.0% result with regard to clamping processes (cf. Table 3-10). In this context, this large value only applies with $t_1 = t_2 < t_3/4$ when very thin primary plates are welded to a relatively thick intermediate plate and significantly better values of less than -5.0% can be achieved with $t_1 = t_2 \leq t_3/2$. Nevertheless, corrections of $\Delta\sigma_{R,hs,eff} = 1.11 \cdot \Delta\sigma_{R,hs}$ would have to be applied to cover all probabilities of the cruciform joints investigated. For this reason, the general use of shell elements with possible angular misalignments in testing machines is not recommended. With regard to practical support conditions according to Chapter 2.5.3.2.4 of Xing and Dong [5], the differences of -5.3% for axial misalignment and -5.8% for angular misalignment are relatively small. Consequently, with a stress-increasing correction for shell models with *WM3* amounting to $\Delta\sigma_{R,hs,eff} = 1.06 \cdot \Delta\sigma_{R,hs}$, the majority of the critical underestimated structural stresses for practical support conditions could be covered. As a result, method *WM3* would be suitable for studies on

imperfections as long as a correction of the structural stresses is applied. Only in the case of cruciform joints with angular misalignment in combination with a clamping process in testing machines should solid models be used in all cases to ensure realistic results.

3.3.5.3 *Summary*

In the evaluations of the investigated weld methods *WM1*, *WM2*, *WM3* and *WM4* for FE models with shell elements, large differences can be observed, even without the consideration of possible misalignment (cf. Section 3.3.5.1). In the evaluations of the normative procedure of the linear stress extrapolation with *WM1*, there is a significant overestimation as well as an underestimation of the results of solid models depending on the component dimensions of the examined cruciform joints. For this reason, modelling without welds is not recommended if no modification of the structural stress determination is implemented. However, by a suitable adjustment of the distances for the evaluation paths of the linear stress extrapolation, significantly better results can be achieved with *WM1*. In this respect, a general structural stress increase to 102.5 % would allow safe applicability as long as no imperfections have to be considered (cf. Section 3.3.5.1.1). In contrast, it appears that method *WM4* is not suitable for a practical design, due to the very complex modelling in combination with the major deviations from the investigated solid models (cf. Section 3.3.5.1.2). Consequently, this method will not be considered in the further course of this thesis. In the evaluations of *WM2* and *WM3*, on the other hand, a very similar system behaviour is observed, which only has minor differences to the results of the solid models. In addition, these methods are very insensitive to different meshing options, which is conducive to practical application. However, since the modelling effort of method *WM2* is considerably greater than that of *WM3* and since the results for *WM3* additionally provide a slightly better accordance with the solid models, only *WM3* will be further investigated in this thesis with regard to these two methods. In this respect, a correction of the resulting structural stresses $\Delta\sigma_{R,hs}$ to 102.5 % would be sufficient in the assessments of *WM3* to compensate for all underestimations, without the consideration of influences due to imperfections (cf. Section 3.3.5.1.3).

In the evaluations of the influence of imperfections on *WM1* and *WM3*, however, it becomes evident that higher corrections are required to ensure a reliable design. Both axial misalignments up to $0.5 \cdot t_{1=2}$ and angular misalignments up to $\beta = 2.5^\circ$ were investigated in this regard (cf. Section 3.3.5.2). Method *WM1* would lead to very uneconomical results in most cases, as a very large structural stress correction up to 117.5 % would be necessary to cover possible underestimations of the results of solid models during clamping processes in testing machines (cf. Section 3.3.5.2.1). In contrast, the FE models with *WM3* are sufficiently effective in capturing influences from imperfections. In this respect, deviations of more than 10 % only result if angular misalignment is examined in combination with a clamping process in testing machines. Moreover, this only applies with $t_1 = t_2 < t_3/2$ when very thin primary plates are welded to a thick intermediate plate. In all other cases, influences from imperfections can be covered with a correction of the structural stresses to 106 %, independent of the selected support type (cf. Section 3.3.5.2.2).

The relatively simple modelling with inclined shell elements as well as the low sensitivity to the choice of meshing with also a high accordance to the investigated solid models therefore does not require a correction of the general methodology of *WM3* or the linear stress extrapolation. Since in addition, even in investigations with included imperfections, only underestimations are to be expected in comparison to the solid models, it is possible to ensure a reliable but not unnecessarily uneconomical design by means of a suitable correction of the structural stresses $\Delta\sigma_{R,hs}$. For these reasons, *WM3* is considered the most practical of the investigated methods. The evaluations with shell elements presented subsequently are therefore based on this method. In this respect, the validation based on strain measurements conducted on experimental fatigue tests of imperfect cruciform joints also provides satisfactory results (cf. Chapter 4.4). This fact further verifies the statements presented in this section.

3.3.6 Managing thickness effects

According to Chapter 2, statistical, technological and geometric thickness effects lead to an increasing probability of fatigue failure in components with increasing component thickness (cf. Chapter 2.6). However, according to the current state of science, only the geometric thickness effect can be assessed by numerical calculations with a finite element analysis. This is due to the lack of precise information regarding the statistical and technological thickness effect in practice. For instance, in the majority of projects, no information is available on the number and position of defects, inclusions, different coarse grain sizes or component residual stresses from manufacturing or welding processes of the investigated components. This is especially true for the relevant engineering phase, as there is no possibility to extensively inspect the elements to be installed. Consequently, a correction of structural stresses at increasing plate thicknesses should be implemented to cover statistical and technological thickness effects, as far as these effects are not already considered by the fatigue class. With regard to geometric thickness effects, this chapter discusses whether an analytical consideration is required or if the method of structural stress determination in the FEA includes corresponding thickness effects.

In this respect, comprehensive parameter studies of IGF research project No. 20336N [1] indicate that the linear stress extrapolation applied for structural stress determination is unable to capture geometric thickness effects. The corresponding studies on different parameter ranges demonstrate that no significant increase in structural stress can be detected with increasing plate thicknesses. Indeed, in most cases there is a minor reduction of the resulting structural stresses [1]. Furthermore, Section 3.3.4 implies that neither of the further investigated local methods is able to capture geometric effects. Only the Haibach surface method with the single-point stress determination at a distance of $\Delta x = 2 \text{ mm}$ [9, 41] generates slightly higher values with thicker welded-on plates (cf. Table 3-6). With all other methods, there is a reduction in structural stresses with greater plate thicknesses compared to thinner plates. Similar behaviour can also be seen in the evaluation of Section 3.3.5 for finely and coarsely meshed shell and solid models. In the corresponding evaluations, there are no significant increases in the expected structural stress that are expected to result from increasing plate thicknesses (cf. Figure 3-17 and Figure 3-18). Accordingly, it can be substantiated that increasing

plate thicknesses of cruciform joints cause a slight decrease rather than the expected increase of structural stresses.

In addition, the dimensions of the fatigue-tested cruciform joints of IGF research project No. 20336N [1] were specifically designed to enable the general potential for thickness effects to be evaluated (cf. Chapter 4). However, the associated evaluations revealed that it was practically impossible to precisely determine thickness effects. On the one hand, too few varying test specimen dimensions were available to enable precise conclusions. On the other hand, it was not possible to isolate significantly more conspicuous influences from axial and angular imperfections. This is due to the fact that the thickness of the welded-on plates also has a negative effect on the clamping process in testing machines. Thus, it was hardly possible to identify the effects to be attributed to the thickness effect and to establish conclusive predictions about the effect of different thicknesses on the structural stress concept.

Concerning this matter, comparative calculations with the effective notch stress concept were carried out in [1]. In order to establish comparability between the effective notch stress and the structural stress concept, the respective utilisation factors were determined by means of the corresponding fatigue classes for a uniform fatigue loading. The identical resulting thickness correction factors for the examined cruciform joints according to the IIW [3] and prEN 1993-1-9 [4] (cf. Chapter 2.6.3) were applied to the structural stresses on the action side. This was not in accordance with the normative specifications, as the resistance side is generally to be reduced by the thickness correction factor. Nevertheless, the result remains consistent with a calculation of the degree of utilisation with a reduced fatigue class. The associated evaluations demonstrate that the structural stresses resulting from increasing thicknesses of the welded-on plates $t_1 = t_2$ remain approximately constant [1]. In the structural stress concept, this applies independently to the investigated thicknesses of the intermediate plate t_3 . In contrast, the effective notch stress increases non-linearly starting at $t_1 = t_2 = 12 \text{ mm}$ and is directly influenced by the thickness of the intermediate plate t_3 . In this respect, the notch stresses are slightly higher with thicker intermediate plates. In the structural stress concept, the thickness correction factor is consequently intended to capture the stress increase that can be determined in the effective notch stress concept as a result of increasing thicknesses. However, the results of the comparative calculations according to [1] show that with a reference thickness of $t_{ref} = 25 \text{ mm}$ the actual stress increase is expected significantly too late. In this context, a considerably improved correlation between the utilisation rates of the structural stress concept and the effective notch stress concept is obtained when the thickness correction factor is calculated with an adjusted reference thickness of $t_{ref} = 12 \text{ mm}$. Consequently, in IGF research project No. 20336N [1], the targeted comparative investigations did not confirm satisfactory compliance with the specifications according to the normative regulations and guidelines. It should be noted, however, that the aforementioned results from [1] are difficult to verify, as it cannot be validated to what extent the consideration of thickness effects can be effectively implemented in the effective notch stress concept. In addition, Chapter 4 on fatigue tests on cruciform joints indicates that due to the thickness correction according to the IIW [3] and prEN 1993-1-9 [4], the experimentally determined fatigue strengths can be represented adequately by the

numerical verification calculations (cf. Chapter 4.5). Contrary to the results according to [1], this could signify that the normative determination of a thickness correction can be applied appropriately. The same is true for the evaluation of the structural stress concept by means of equivalent imperfections described in Chapter 5 (cf. Chapter 4.5.3).

In order to be able to verify the stated conclusions about the thickness effect and to gather further detailed information, additional experimental tests with a wide range of plate thicknesses and only minimal imperfections would be required. Furthermore, extensive evaluations with the effective notch stress concept would be essential in order to determine the influence of the thickness effect in a more effective way. However, the results of the parametric FE calculations from [1] confirm that an analytical correction of the structural stresses is imperative in order to cover not only the statistical and technological but also the geometric thickness effect. Therefore, in the further course of this thesis, thickness effects are considered by the normatively regulated specifications according to the IIW [3] and prEN 1993-1-9 [4]. This is due to the fact that according to [1] no verified corrections could be identified and the results from Chapter 4 and Chapter 5 indicate a reasonable applicability of the normative specifications.

3.3.7 Implementation in ANSYS APDL and Python

All FE calculations presented in this thesis are performed using ANSYS APDL as a partial function of a Python script. In addition, Python's internal PyANSYS library is accessed for the static analyses. Through the implementation in Python, essential results regarding the structural stress concept can be evaluated directly and provided as a comprehensive report. In the following, the corresponding procedures for the ANSYS Preprocessor (cf. Section 3.3.7.1), ANSYS Solver (cf. Section 3.3.7.2) and ANSYS Postprocessor (cf. Section 3.3.7.3) with the corresponding Python evaluation are presented.

3.3.7.1 ANSYS Preprocessor

Finite element analysis provides the basis for the evaluations. With the integration of the PyANSYS library, parametric Python scripts are implemented in this regard. For this process, the so-called ANSYS Preprocessor requires information about the material and the geometry of the structure to be investigated in order to be able to perform adequate FE calculations.

With respect to the material, all models are based on a linear elastic material behaviour defined by at least two material constants. These include the Young's modulus, the shear modulus and the Poisson's ratio. In the FE models of this thesis, the Young's modulus is set at a general value of 210000 N/mm^2 , unless more precise results from material test specimens are present. The Poisson's ratio is assumed to be constant in all FE calculations with $\nu = 0.3$.

With regard to the geometry, coordinates in three-dimensional space are automatically calculated by means of specified auxiliary parameters for lengths, widths, thicknesses, etc. Through the use of loops, this parameterisation enables a rapid setup of different FE systems. In addition to the required coordinates of the specimen geometry, a large

number of auxiliary points are defined to enable structured meshing and to provide evaluation paths for the linear stress extrapolation. Furthermore, coordinate points are defined at the positions of the strain gauges applied to the real test specimens to ensure a simplified validation of the FE results. Relevant matrix and vector operations convert the coordinates without imperfections into imperfect node coordinates if potential misalignments have to be considered. Moreover, the coordinates of the overall geometry are modified in space in case of imperfections so that the centre of gravity of the clamping section (cf. Figure 3-14) is horizontally aligned on the vertical origin of the z_{global} -axis. This procedure facilitates the correct modelling of the required clamping process (cf. Chapter 3.3.3) by the clamp jaws of the testing machine. It also allows for the load application section (cf. Figure 3-14) to be subjected to uniform tensile stress in the longitudinal direction of the plate (x_{global} -direction). So-called Keypoints are created at the positions of the defined spatial coordinates in order to generate the necessary surfaces for shell models resp. volumes for solid models. By using the generated auxiliary points, the component surfaces resp. volumes are then meshed with so-called mapped or swept meshes according to the meshing specifications of Section 3.2. For this purpose, the element classification from section 3.1 is implemented for solid resp. shell models.

3.3.7.2 ANSYS Solver

In the ANSYS Solver, boundary conditions of the analysed system have to be defined. Based on the system and the boundary conditions, the solution of the equilibrium system can subsequently be determined by ANSYS. In a first step, the degrees of freedom of the clamping section are specified according to section 3.3.3. In a second step, it is automatically verified whether existing imperfections require a geometrically non-linear calculation. In this respect, a distinction is made between the following two cases.

The explicit modelling of the load application section by means of rigid body connections (cf. Section 3.3.3) is omitted, if a linear FE calculation is sufficient. This is true if no large pre-deformations are to be expected from the clamping process due to imperfections. Therefore, the small angle approximation remains valid. In this case, the restriction of the vertical displacement in the z_{global} -direction and horizontal displacement in the y_{global} -direction is defined exclusively on the front side of the load application section facing the clamping section. The required tensile load is subsequently applied to this surface in the x_{global} -direction. In order to avoid stress concentrations in the centre and at the edges of the surface, it is important to ensure that the resulting nodal forces are generated according to their element sizes and resulting load catchment areas. In this respect, the application of a tensile load on the surface is suitable, as the distribution of the individual forces is performed according to their element size within ANSYS. Once all boundary conditions are defined, the geometric linear analysis is executed. Due to the avoidance of a geometrically non-linear calculation with required rigid body connections, considerable calculation time can be reduced.

However, if the investigated system is affected by imperfections that lead to relatively large pre-deformations in the clamping process, it is essential to perform a

geometrically non-linear calculation. Otherwise, unrealistic deformations and distortions result in the FE models, as the element formulation based on the small-angle approximation no longer provides realistic solutions. The geometric non-linear analysis is executed following the definition of the support and load application according to section 3.3.3.

3.3.7.3 **ANSYS Postprocessor and Python evaluation**

By solving the equilibrium conditions of the FE calculation in ANSYS, it is possible to extract the computed results from the ANSYS postprocessor with Python. For the general evaluation, the data of the element nodes are considered, which are determined by the linearly extrapolated results of the associated integration points at which the FE analysis is performed. In this respect, both the required extrapolation paths of the stress extrapolation and the nodes at the strain gauge positions of the experimentally conducted tests are evaluated. The necessary results are determined on the defined selection paths. If the associated path subdivision coincides with element nodes, the node values are extracted directly. If this is not the case, a linear interpolation of the nearest node results is conducted, whereby the interpolated values have sufficient accuracy with a reasonably fine mesh. As normatively specified, the first principal stress σ_1 is generally evaluated on the extrapolation paths required for the stress extrapolation. In contrast, the normal stresses σ_x are analysed in the x_{global} -direction in order to validate the FE calculations against the actual strain measurements. This is due to the applied strain gauges being positioned in the loaded longitudinal direction of the plate.

Based on the specified input of the path stresses, the structural stresses are calculated automatically by Python scripts using the linear extrapolation. The overall evaluation with all input data and predefined results is subsequently exported automatically to an Excel file. Besides providing a summary sheet with the relevant characteristic values and parameters, all structural stress results with the corresponding stress paths are stored separately according to the clamping process and the ensuing tensile load. Furthermore, a summary of all relevant structural stress results is provided in the form of stress plots and screenshots from different viewpoints on deformations and stresses. This enables a reliable verification of the accuracy of the system assumptions and consequently serves as an overview, visual control and evaluation strategy.

4 Experimental fatigue tests on cruciform joints

In IGF research project No. 20336N [1], extensive fatigue tests were carried out on cruciform joints with different geometries. The subsequent chapter summarises the identified research results. The objective is to verify the economic and safe applicability of the structural stress concept through extensive FE calculations. The evaluation is based on both the structural stress concept to be investigated and the generally accepted nominal stress concept to allow classification. The fatigue tests also specifically target the influence of imperfections on the resulting structural stresses. In this way, influences from misalignment can be considered in the respective evaluations. This further allows the information on imperfections presented in Chapter 2.5 to be critically questioned.

In order to verify the applicability of the structural stress concept on the basis of the fatigue tests from [1], the principles of the selected evaluation methodology are initially presented in Section 4.1. An overview of the fatigue-tested cruciform joints with dimensions, material and the detected imperfections is provided in Section 4.2. Additionally, Section 4.3 deals with the corresponding experimental test procedures. Furthermore, in Section 4.4 the developed FE models (cf. Chapter 3.3) are validated against the actual fatigue tests to ensure the general validity of the numerics. Based on the verified models, the fatigue tests are evaluated in Section 4.5. In this respect the fatigue tests are evaluated applying the nominal stress concept to provide a first assessment (cf. Section 4.5.1). Subsequently, the evaluation is conducted according to the structural stress concept (cf. Section 4.5.2). In order to be able to realistically consider imperfections, Section 4.5.3 additionally investigates the influence of imperfections on the conducted fatigue tests. The objective of the investigations is to enable an evaluation of the applicability of the structural stress concept in comparison to the nominal stress concept for cruciform joints. To this end, section 4.6 provides a summary of the derived results.

4.1 Evaluation methodology of the fatigue tests

The evaluation of the fatigue tests from IGF research project No. 20336N [1] with the nominal stress concept (cf. Section 4.5.1) and structural stress concept (cf. Section 4.5.2) is performed with the experimental applied fatigue load ΔF and a geometric non-linear analysis in order to numerically include realistic straightening effects. This is essential as imperfections significantly influence the evaluation of fatigue tests of cruciform joints. In order to specifically determine the influence on the fatigue strength, the fatigue tests are evaluated for both perfect and imperfect FE models. The selected methodology for the evaluation within the nominal resp. structural stress concept thus analyses, on the one hand, perfect FE models that are modelled exclusively with the specified imperfections resulting from the design process. The corresponding evaluation methodology is described in Section 4.1.1. On the other hand, FE analyses

are also realised with imperfect FE models that include all detected imperfections. These also incorporate unintentional imperfections, which were determined in [1] using 3D laser scan measurements of all cruciform joint specimen. A more detailed description of the corresponding methodology can be found in section 4.1.2. In this way, the normative specifications on the fatigue resistance can be verified with regard to perfect and imperfect nominal resp. structural stresses. Through the perfect and imperfect evaluation, verification is equally possible for the normative specified fatigue classes (cf. Chapter 2.4) as well as for the corresponding specifications for normatively already considered influences on the resistance side due to imperfections (cf. Chapter 2.5.3.1).

In addition, in Section 4.5.3 a self-developed methodology for a more accurate determination of the influence of imperfections is presented. For this purpose, an equivalent imperfection $e_{equivalent}$ is introduced. This equivalent imperfection $e_{equivalent}$ allows the influence of imperfections on the nominal stress resp. structural stress of imperfect test specimens to be determined more realistically. The approach is based on the fact that straightening effects of imperfect cruciform joints can lead to a reduction of the stress ranges $\Delta\sigma_R$ of experimental fatigue tests. This is due to the load-dependent changes in the influence of imperfections on the component behaviour due to varying straightening effects. However, by using the method described in Section 4.1.3, it is possible to determine the experimental and numerical stress ranges $\Delta\bar{\sigma}_R$ more accurately. It should be noted that these effects are currently not considered in the standardised procedures of the nominal or structural stress concept, as evaluations are to be performed exclusively under the uncorrected fatigue loading of ΔF . This can lead to a significant overestimation of the resulting stresses if cruciform joints with imperfections are analysed.

Therefore, the objective of Chapter 4 is to evaluate the applicability of the design-relevant specifications of the structural stress concept on the basis of the fatigue tests conducted in [1] and to identify the influence of imperfections on the nominal and structural stress concept. In this respect, for the experimental series with plate thicknesses $t_1 = t_2 > t_{ref} = 25 \text{ mm}$, thickness effects are considered uniformly for all methods according to the IIW [3] and prEN 1993-1-9 [4] (cf. Chapter 3.3.6). The associated procedures can be accessed in Chapter 2.6. For better comprehensibility, the different evaluation methods for the perfect evaluation (cf. Section 4.1.1), imperfect evaluation (cf. Section 4.1.2) and evaluation by means of equivalent imperfections (cf. Section 4.1.3) are described in more practical terms below.

4.1.1 Perfect FE models without unintentional imperfections

The evaluation of perfect FE models without the consideration of unintentional imperfections is based on geometrically non-linear calculations, as straightening effects may also exist due to possible intentional imperfections. The associated exposure is defined by the experimental fatigue tests with the uncorrected fatigue loading ΔF . Since there is generally no available information on unintentional imperfections in the design of fatigue loaded components, the verification must typically be achieved with the perfect nominal stress ranges $\Delta\sigma_{R,nom,FEA,perfect}$ resp. perfect structural stress ranges

$\Delta\sigma_{R,hs,FEA,perfect}$. In this respect, only influences from intentional imperfections that are specified in the design phase are included in the FE models.

To this end, the required perfect nominal stress $\Delta\sigma_{R,nom,FEA,perfect}$ is determined on perfect FE models by averaging the first principal stress over the component width. This is done at the evaluation path relevant for the linear stress extrapolation at a distance of $1,0 \cdot t$ before the weld, since at this distance all non-linear effects due to the notch have subsided. The required perfect structural stress $\Delta\sigma_{R,hs,FEA,perfect}$ is determined by the linear stress extrapolation (cf. Chapter 2.3.3.1). The comparison of the effective stresses with the respective fatigue strengths of the nominal stress concept $\Delta\sigma_{C,nom,FEA,perfect}$ resp. structural stress concept $\Delta\sigma_{C,hs,FEA,perfect}$ is based on the normative fatigue classes according to DIN EN 1993-1-9 [2], IIW [3] and prEN 1993-1-9 [4]. With this approach, no correction is applied regarding normatively already included influences from imperfections, as no unintentional imperfections are considered on the action side. For the required corrections due to imperfections, the specifications from chapter 2.5.3.1 are applied.

The fatigue tests conducted in [1] can therefore verify the applicability of the normative fatigue classes in the design phase for cruciform joints in the nominal and structural stress concept. If large stress-increasing effects from imperfections are to be expected, however, this approach can lead to unreliable results, as unintentional imperfections are not explicitly considered.

4.1.2 Imperfect FE models including unintentional imperfections

In contrast to the procedure of Section 4.1.1, the imperfections of the experimentally tested cruciform joints can also be determined more precisely, as exact measurement records are available in [1]. This is implemented in the evaluation of imperfect FE models including unintentional imperfections. In this respect, the imperfect nominal stress $\Delta\sigma_{R,nom,FEA,imperfect}$ resp. imperfect structural stress $\Delta\sigma_{R,hs,FEA,imperfect}$ is determined for imperfect FE models, which include all intentional and unintentional imperfections of the experimentally tested specimens.

The assessment is carried out according to Section 4.1.1 with a geometrically non-linear calculation in order to include straightening effects under the experimental fatigue loading of ΔF . The imperfect nominal stress $\Delta\sigma_{R,nom,FEA,imperfect}$ and imperfect structural stress $\Delta\sigma_{R,hs,FEA,imperfect}$ as well as the corresponding fatigue strengths $\Delta\sigma_{C,nom,FEA,imperfect}$ resp. $\Delta\sigma_{C,hs,FEA,imperfect}$ are also determined according to Section 4.1.1. To this end, in contrast to Section 4.1.1, the applied stresses are determined using the imperfect FE model with unintended imperfections. Furthermore, the fatigue strengths are modified by normatively considered influences from imperfections on the resistance side (cf. Chapter 2.5.3.1), as all imperfections are accounted for on the action side.

Consequently, with this methodology, the normative specifications can be verified with regard to any imperfections already covered through the fatigue classes. Furthermore, this procedure leads to more realistic results than Section 4.1.1, since the experimentally determined stress cycles $N_{R,test}$ are affected by imperfections as well. However, the experimental stress range $\Delta\sigma_{R,test}$ may be overestimated, as

straightening effects are only determined under the defined fatigue loading ΔF (cf. Section 4.1.3). This can cause an equivalent overestimation of the imperfect nominal stress $\Delta\sigma_{R,nom,FEA,imperfect}$ resp. imperfect structural stress $\Delta\sigma_{R,hs,FEA,imperfect}$. The same applies to Section 4.1.1 for cruciform joints with intended imperfections. For this reason, an additional methodology is presented below in Section 4.1.3.

4.1.3 Determination of equivalent imperfections

In the evaluations of the fatigue tests from IGF research project No. 20336N [1], straightening effects are detected that lead to a deviating stress range $\Delta\sigma_{R,test}$ for the nominal or structural stress concept. This is due to the fact that a smaller imperfection $e_{equivalent}$ is present at the maximum load level F_{max} than at the minimum load level F_{min} . Consequently, the resulting maximum stress σ_{max} increases only slightly due to imperfections, while a significantly larger minimum stress σ_{min} is to be expected. Accordingly, in the experimental tests, the applied stress range $\Delta\sigma_R = \sigma_{max} - \sigma_{min}$ appears to be considerably lower than would be expected by generally applying the fatigue load ΔF . In order to numerically determine this behaviour, a geometrically non-linear evaluation of equivalent imperfections $e_{equivalent}$ under the static loading of F_{max} and F_{min} is necessary. In this way, it is possible to accurately assess fatigue loads in order to realistically evaluate cruciform joints with defined imperfections. Consequently, stress-increasing effects from imperfections can be considered accurately, resulting in realistic nominal fatigue strengths $\Delta\sigma_{C,nom,FEA,e_{equivalent}}$ resp. structural fatigue strengths $\Delta\sigma_{C,hs,FEA,e_{equivalent}}$. The methodology developed for this purpose to determine $e_{equivalent}$ and the associated evaluations are presented in Section 4.5.3.

4.2 Cruciform joints examined under fatigue loading

In the following sections 4.2.1 and 4.2.2 all relevant data of the test specimens tested for fatigue in IGF research project No. 20336N [1] and their imperfections are presented. For more detailed information, reference is made to [1].

4.2.1 Overview

The cruciform joints tested experimentally in the IGF research project No. 20336N [1] were manufactured by different companies. In this respect, a detailed manufacturing concept was specified to ensure a standardised production of the test specimens in order to allow for comparability. Figure 4-1 documents parts of the test specimen fabrication. All components were preheated before the welding process in order to minimise welding residual stresses (cf. centre of Figure 4-1). In addition, outlet plates were installed to ensure a smooth execution of the weld seams in the edge areas.

Since the fatigue tests were part of the third work package (WP3) of the IGF research project No. 20336N [1], the original designations of the research project are retained in this thesis. The 77 examined cruciform joints were manufactured in S355J2+N (material no.: 1.0577) and divided into three different test series $WP3_1$, $WP3_2$ and $WP3_3$. The corresponding test specimens differentiated according to the thickness of the primary plates $t_1 = t_2$ and the intermediate plate t_3 . In order to be able to determine the influences of imperfections, the individual test series were each designed in two

different variations, each including twelve test specimens. In this respect, both perfect cruciform joints without intentional imperfections and imperfect cruciform joints with intentional axial misalignment $e_{intended}$ (cf. Chapter 2.5.2.2) were manufactured. To this end, the test groups $WP3_1.1$, $WP3_2.1$, $WP3_3.1$ were manufactured without intentional imperfections $e_{intended} = 0 \text{ mm}$. In contrast, the test specimens for $WP3_1.2$, $WP3_2.2$, $WP3_3.2$ were executed with intentional imperfections amounting to a quarter of the welded-on plate thickness $e_{intended} = t_{1=2}/4$. Due to the insufficient execution quality of the test specimens $WP3_2.2$, five additional cruciform joints were supplied and designated with $WP3_2.2NL$. The corresponding materials and intentional misalignments of each test group are summarised in the following Table 4-1.

Table 4-1: Overview of experimental fatigue tests on cruciform joints

Test group	Material	Material number	$t_1 = t_2$ [mm]	t_3 [mm]	$e_{intended}$ [mm]	Quantity [-]
$WP3_1.1$	S355J2+N	1.0577	12	12	0	12
$WP3_1.2$	S355J2+N	1.0577	12	12	3	12
$WP3_2.1$	S355J2+N	1.0577	12	40	0	12
$WP3_2.2$	S355J2+N	1.0577	12	40	3	12
$WP3_2.2NL$	S355J2+N	1.0577	12	40	3	5
$WP3_3.1$	S355J2+N	1.0577	40	12	0	12
$WP3_3.2$	S355J2+N	1.0577	40	12	10	12



Figure 4-1: Staped test specimens before the welding process (left) preheating process to reduce welding residual stresses (middle) and welding process (right)

The execution plans of the test series $WP3_1$, $WP3_2$ and $WP3_3$, which are subjected to fatigue loading, are provided in 0. The corresponding component thicknesses of the welded-on plates $t_1 = t_2$ and the intermediate plate t_3 are listed in Table 4-1. The component widths w_1 (cf. Figure 3-14) in the critical area of the welds were specified consistently with 100 mm in order to ensure comparability between the varying test groups. Since possible fatigue failure at the clamping section was to be avoided, the end sections of all cruciform joints were designed with a width of $w_2 = 150 \text{ mm}$. Therefore, w_2 corresponded to the width of the quadratic clamping jaws of the applied testing machines. Furthermore, the lengths $L_1 = L_2$ (cf. Figure 3-14) of the welded-on plates were uniformly determined through extensive preliminary studies. In this respect, a length of 150 mm between the fillet and the intermediate plate was sufficient to ensure a smooth stress distribution over the length of the component, unaffected by the clamping sections or fillets. The fillet between the clamping section and the critical

section was implemented uniformly with a radius of 400 mm over a length of 136 mm. All notches were ground over in these areas in order to avoid fatigue failure at the fillets. To facilitate the clamping process, the lengths $L_{clamp,1=2}$ (cf. Figure 3-14) were universally defined with 200 mm. The test series WP3_1 and WP3_3 therefore had uniform total lengths $L_{total} = L + L_{clamp,1} + L_{clamp,2} = 984 \text{ mm}$ due to the identical thickness of the intermediate plates $t_3 = 12 \text{ mm}$. In contrast, due to thicker intermediate plates $t_3 = 40 \text{ mm}$, the total length of WP3_2 increases to $L_{total} = 1012 \text{ mm}$. The length of the intermediate plate L_3 (cf. Figure 3-14) was kept constant at 200 mm regardless of the test group.

In accordance with the execution plans in Appendix A, the junctions of the welded-on plates were realised by full penetration bevel butt welds with additional fillet welds. In this respect, all bevel butt welds were welded with a thickness $a_{bevel \text{ butt weld}}$ (cf. Figure 3-14) of half the plate thickness of the welded-on plates $t_{1=2}/2$. In the test series WP3_1 and WP3_2 with plate thicknesses $t_{1=2} = 12 \text{ mm}$, all fillet weld thicknesses $a_{fillet \text{ weld}}$ (cf. Figure 3-14) were welded with 5 mm. In contrast, the fillet welds of test series WP3_3, due to the large component thickness $t_{1=2} = 40 \text{ mm}$, were significantly thicker with $a_{fillet \text{ weld}} = 14 \text{ mm}$. All welds were manufactured in accordance with DIN EN ISO 5817 [68] according to evaluation group B without post-weld treatment.

In order to verify the predefined material characteristics of the test specimens, tensile tests were conducted on all applied steel batches. The circular tensile specimens were fabricated according to DIN 50125 [90] in order to implement the tensile tests according to DIN EN ISO 6892-1 [91]. To ensure statistical validation, five samples were tested for each batch, both longitudinally and transversely to the direction of rolling. The corresponding tests were executed on a Zwick Roell universal testing machine 100 kN. With the help of the mean value of the five available measurement results, both longitudinally and transversely to the rolling direction, statistically validated characteristic values could be determined for all specimens. The only exception was the test group WP3_3.2, where no material tests could be provided for the material batch of the thin intermediate plates. The results of the tensile tests are summarised in the following Table 4-2.

Table 4-2: Material properties of the steel batches of the fatigue tests according to [1]

Test groups	Plate thickness [mm]	f_y [Mpa]	f_u [Mpa]	E-modulus [GPa]
WP3_1.1, WP3_1.2, WP3_2.1, WP3_2.2	12	409.2	551.8	205.5
WP3_2.1, WP3_2.2	40	390.6	532.2	210.0
WP3_2.2NL	12	396.8	545.4	204.7
WP3_3.1	12	368.3	585.6	207.5
WP3_3.1	40	374.6	527.5	205.0
WP3_3.2	40	378.8	539.0	201.9

4.2.2 Detected imperfections

The 3D laser scan measurements conducted in IGF research project No. 20336N [1] made it possible to determine the imperfections of the test specimens of the fatigue tests. Based on the identified imperfections, imperfect FE models could be generated. By superposing the imperfect FE models with the point clouds of the measurement records, it was also checked whether inconsistencies in the models had to be corrected. Figure 4-2 illustrates the validation of the measurement records against the point clouds produced.

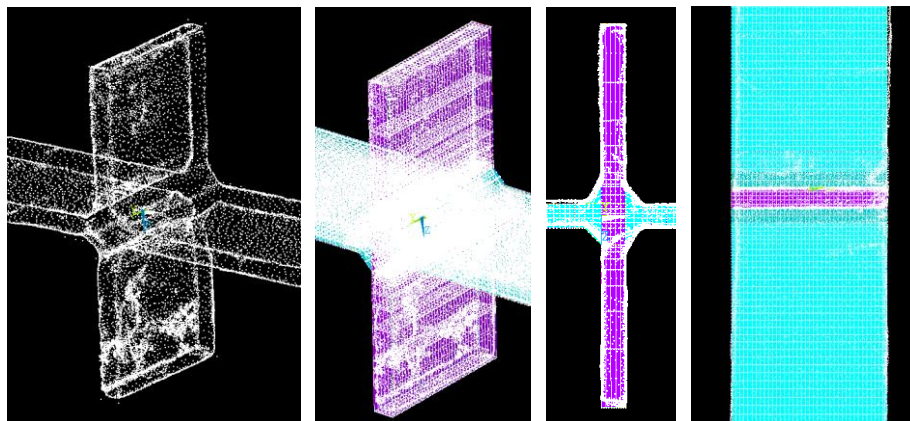


Figure 4-2: Validation of the measurement data records by superposition of the point clouds of the measurements with imperfect FE models

In the following Table 4-3 the detected axial misalignments $e_{detected}$ and angular misalignments $\alpha_{detected}$ are summarised separately according to the test groups of [1]. The results represent the absolute values from the combined imperfections of both welded-on plates. This is reasonable, as in comprehensive comparative calculations no influence of the respective plate side could be determined. Consequently, it does not matter in the evaluation whether plate 1 or plate 2 features all axial or angular imperfections or whether these are proportionally distributed to both plates. Furthermore, since the sense of direction is irrelevant in the evaluation with imperfections, only the absolute values are stated. In the later evaluations of the test specimens from [72], however, the true imperfections of the respective plates are used. In addition, the intended imperfections $e_{intended}$ and the resulting deviation in relation to axial misalignment are indicated in Table 4-3. Since no angular imperfections were intended, $\alpha_{detected}$ is considered unintentional in all cases.

The evaluated imperfections from Table 4-3 indicate that it is generally difficult to avoid unintentional imperfections. On the one hand, this can be identified by the large deviations of the detected axial misalignments $e_{detected}$ from the intended axial misalignments $e_{intended}$. Therefore, due to the plates being welded on both sides of the intermediate plate, an unintentional axial misalignment can hardly be avoided even in workshop conditions. Since all test specimens for WP3_2.2, with the exception of WP3_2.2_06, had significantly too low misalignments $e_{detected}$ (cf. Table 4-3), a subsequent delivery was essential in order to be able to ensure conclusive evaluations of the influence of imperfections. However, the test specimen WP3_2.2NL_01 also did not meet the intended axial misalignment $e_{intended}$.

Table 4-3: Axial and angular misalignment as cumulative absolute values of the two welded-on plates

Misalignment	01	02	03	04	05	06	07	08	09	10	11	12	
WP3_1.1	$e_{intended}$ [mm]	0.00											
	$e_{detected}$ [mm]	0.74	0.69	1.17	1.13	0.53	0.94	0.62	1.07	0.68	0.22	0.11	0.03
	Deviation [mm]	+0.74	+0.69	+1.17	+1.13	+0.53	+0.94	+0.62	+1.07	+0.68	+0.22	+0.11	+0.03
	$\alpha_{detected}$ [°]	0.38	0.04	0.38	0.26	0.24	0.66	1.03	0.76	0.75	0.23	0.59	0.42
WP3_1.2	$e_{intended}$ [mm]	3.00											
	$e_{detected}$ [mm]	2.08	3.28	3.69	3.56	3.06	3.37	2.26	2.06	2.88	3.69	3.23	7.30
	Deviation [mm]	-0.92	+0.28	+0.69	+0.56	+0.06	+0.37	-0.74	-0.94	-0.12	+0.69	+0.23	+4.30
	$\alpha_{detected}$ [°]	0.98	0.86	4.17	1.55	1.38	0.78	1.07	1.85	1.95	2.86	2.47	2.37
WP3_2.1	$e_{intended}$ [mm]	0.00											
	$e_{detected}$ [mm]	0.07	0.40	0.46	0.48	0.48	0.37	1.02	0.12	0.20	0.12	0.58	0.37
	Deviation [mm]	+0.07	+0.40	+0.46	+0.48	+0.48	+0.37	+1.02	+0.12	+0.20	+0.12	+0.58	+0.37
	$\alpha_{detected}$ [°]	1.24	0.74	0.80	0.10	0.64	0.83	0.18	0.33	1.12	0.21	0.73	0.06
WP3_2.2	$e_{intended}$ [mm]	3.00											
	$e_{detected}$ [mm]	0.08	0.74	1.30	1.05	0.12	3.19	1.45	0.68	0.28	0.78	0.65	0.96
	Deviation [mm]	-2.92	-2.26	-1.70	-1.95	-2.88	+0.19	-1.55	-2.32	-2.72	-2.22	-2.35	-2.04
	$\alpha_{detected}$ [°]	0.65	3.16	0.59	0.19	0.24	0.56	0.27	0.14	0.24	3.65	2.85	0.40
WP3_2.2NL	$e_{intended}$ [mm]	3.00											
	$e_{detected}$ [mm]	0.52	3.65	3.10	3.27	2.89							
	Deviation [mm]	-2.48	+0.65	+0.10	+0.27	-0.11							
	$\alpha_{detected}$ [°]	0.31	0.21	0.82	0.82	0.68							
WP3_3.1	$e_{intended}$ [mm]	0.00											
	$e_{detected}$ [mm]	0.09	0.06	0.24	0.43	0.01	0.05	0.18	0.19	0.16	0.05	0.15	0.16
	Deviation [mm]	+0.09	+0.06	+0.24	+0.43	+0.01	+0.05	+0.18	+0.19	+0.16	+0.05	+0.15	+0.16
	$\alpha_{detected}$ [°]	0.01	0.26	0.71	0.31	0.06	0.20	0.31	0.03	0.18	0.05	0.17	0.26
WP3_3.2	$e_{intended}$ [mm]	10.00											
	$e_{detected}$ [mm]	9.84	10.05	9.79	9.96	10.24	9.61	10.30	9.07	9.23	10.59	10.80	10.05
	Deviation [mm]	-0.16	+0.05	-0.21	-0.04	+0.24	-0.39	+0.30	-0.93	-0.77	+0.59	+0.80	+0.05
	$\alpha_{detected}$ [°]	0.02	0.45	0.39	0.16	0.30	0.64	0.37	0.17	0.09	0.51	0.36	0.23

On the other hand, welding distortions in particular lead to unintentional rotations of the welded-on plates. Accordingly, unintentional angular offsets $\alpha_{detected}$ are identified in all examined test specimens. For the thin welded-on plates of WP3_1 and WP3_2 with $t_{1=2} = 12 \text{ mm}$, these are considerably larger than for WP3_3 with $t_{1=2} = 40 \text{ mm}$ (cf. Table 4-3). For example, in the test group WP3_1.2, angular misalignments $\alpha > 1,0^\circ$ are reached in nine out of twelve specimens. This could be due to the greater influence of welding distortion on thinner plates or to difficulties in production implementation.

Consequently, based on the decisive influence of imperfections on the structural stress and the relatively large unintentional imperfections, the measurement records are imperative to ensure valid evaluations of the fatigue tests (cf. Section 4.1).

4.3 Test procedure

This section presents the implementation of the experimental fatigue tests of the IGF research project No. 20336N [1]. In this respect, static preliminary tests were carried out for each cruciform joint (cf. Section 4.3.1) in order to assess local plastic component behaviour. In addition, the preliminary tests enabled the determination of influences of the clamping process on the stress distributions of the cruciform joints. To provide additional information on the fatigue behaviour, the components were subsequently tested for fatigue (cf. Section 4.3.2). With the exception of test group *WP3_3.2*, all tests were conducted using a two-column Instron hydropulse machine $\pm 1000\text{ kN}$ from Schenck at the University of the Federal Armed Forces in Munich. Due to the limited clamping width of this testing machine, the test specimens of *WP3_3.2* were tested at the Materials Testing Office MPA BAU of the Technical University of Munich on a four-column universal testing machine of the company RK MFL of the type EVO 1600 with a maximum tensile force of 1600 kN .

In general, both the test specimens without intentional imperfections (*WP3_1.1*, *WP3_2.1*, *WP3_3.1*) and the cruciform joints with intentional axial misalignment $e = 3\text{ mm}$ (*WP3_1.2*, *WP3_2.2*, *WP3_2.2NL*) were clamped directly with no further modification of the clamping process. However, in the test group *WP3_3.2*, a large bending stiffness EI_y was existent around the global y_{global} -axis due to the relatively short lengths between the clamping sections and the decisive welding notches in combination with a relatively thick plate thickness of $t_{1=2} = 40\text{ mm}$. Because of the additional large axial misalignments $e_{intended} = t_{1=2}/4 = 10\text{ mm}$, critical stresses would have resulted from the clamping process. Consequently, this would have caused a very unbeneficial number of stress cycles. For this reason, two support elements with a thickness of $t_{support\ element} = e_{intended}/2 = 5\text{ mm}$ were manufactured in S690QL (material no.: 1.8928). In this respect, the respective width and length of 150 mm was based on the dimensions of the clamp jaws of the testing machines. Before the clamping process and in accordance with the axial misalignment $e_{intended}$, the support elements were fixed on opposite sides at both ends of the test specimens of *WP3_3.2* and included in the test procedure (cf. Figure 4-3). This way, the influence of the intended eccentricity could be compensated in the clamping section.

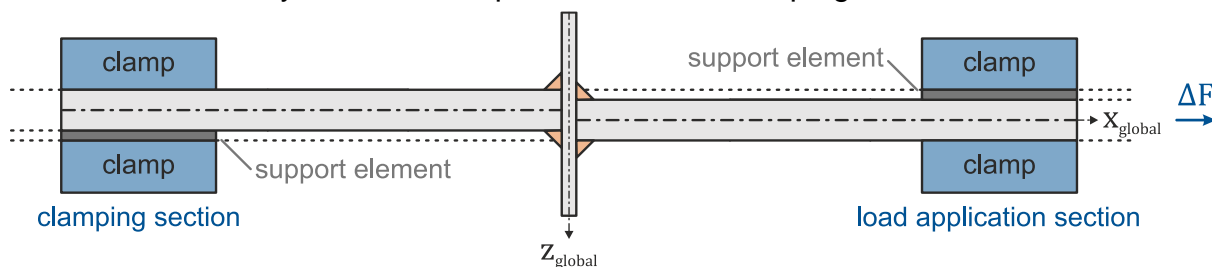


Figure 4-3: Arrangement of support elements to compensate for the effects of axial misalignment of test group *WP3_3.2*

Furthermore, strain gauges (*SG's*) were attached to all test specimens for strain measurements to determine more specific information about the behaviour of the cruciform joints. The measuring length of the strain gauges was chosen with 1 mm . In this way, the specifications of the IIW [3] regarding the maximum permissible measuring length $\leq 0.2 \cdot t_{1=2}$ were satisfied. The configuration was based on the linear stress

extrapolation at a distance of $0.4 \cdot t_{1=2}$ as well as $1.0 \cdot t_{1=2}$ to the weld notches (cf. Figure 4-4). The recordings and associated evaluations were performed for both the static preliminary tests and the fatigue tests.

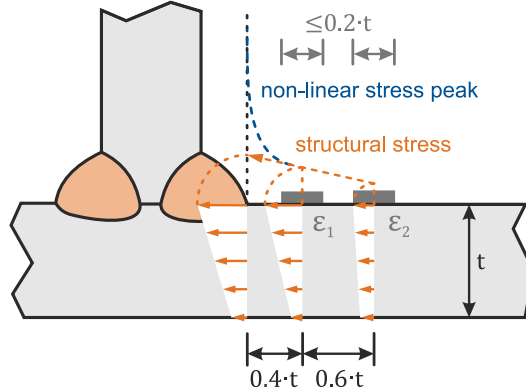


Figure 4-4: Strain gauge position for linear extrapolation to determine the structural stress [9]

The strain gauges were installed on all cruciform joints according to the position plan illustrated in Figure 4-5.

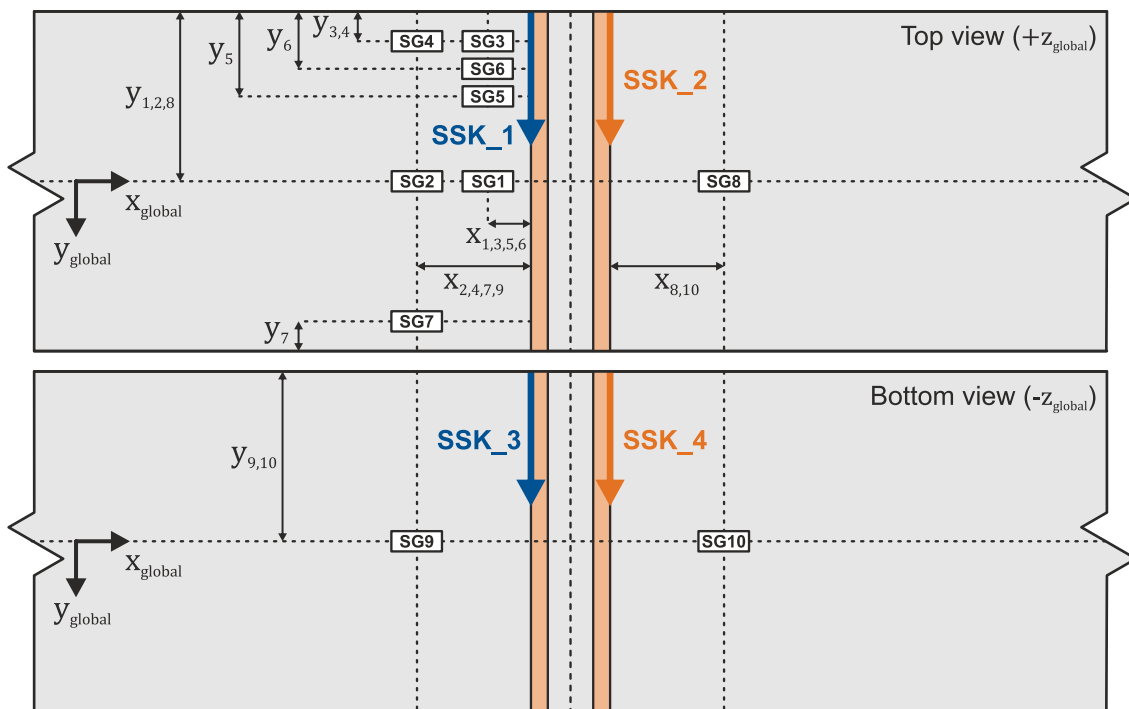


Figure 4-5: Standardised position plan of the strain gauges for fatigue tests from [1]

Accordingly, ten strain gauges were positioned on each test specimen. In order to determine effects from secondary bending, *SG2* and *SG9* as well as *SG8* and *SG10* were placed on opposite sides of the welded-on plates (cf. Figure 4-5). To minimise non-linear influences due to the notch, these strain gauges were placed at a distance of $1,0 \cdot t$ to the welds. These strain gauges also allowed the determination of the decisive side with the relevant structural stresses. Due to the limited number of strain gauges available, it was still essential to obtain information about the strain distribution over the component width on at least one plate side. For this reason, strain gauges *SG1*, *SG3*, *SG5* and *SG6* were positioned in the area of the expected relevant structural stresses at

a distance of $0,4 \cdot t$ to the notch (cf. Figure 4-5). In this respect, the positions across the component width resulted from numerical pre-calculations. In addition, it was experimentally possible to determine structural stresses through the *SG1* and *SG2* strain gauges as well as *SG3* and *SG4* (cf. Figure 4-5). Furthermore, *SG7* was fixed at the same distance from the component edge as *SG4* in order to assess the effect of a possible rotation around the longitudinal axis of the welded-on plates (x_{global} -axis). This was realised at a distance of $1.0 \cdot t_{1=2}$ in front of the weld (cf. Figure 4-5). Through the systematic arrangement of the strain gauges, important component effects under tensile stress could be determined. In addition, sufficiently accurate estimates of the total strain distribution could be derived. The standardised strain gauge layout for all cruciform joints also ensured good comparability of the different test specimens. Furthermore, the experimental data can be used in the later Section 4.4 to provide validation of the numerical FE models.

4.3.1 Static preliminary tests

In the preparation of the fatigue tests, preliminary static tests were conducted for each test specimen in IGF research project No. 20336N [1]. As a result, it was possible to systematically identify local plasticity effects and influences from the clamping process. For this purpose, all test specimens were exposed to the maximum load F_{max} of the fatigue tests for a definite period of time. Consequently, the subsequent fatigue tests were carried out in the purely elastic range, as local plasticising effects had been concluded. The following Figure 4-6 illustrates the selected procedure for the force of the testing machine over the test time. In this respect, the test progression is subdivided into *Phase 1* to *Phase 7*.

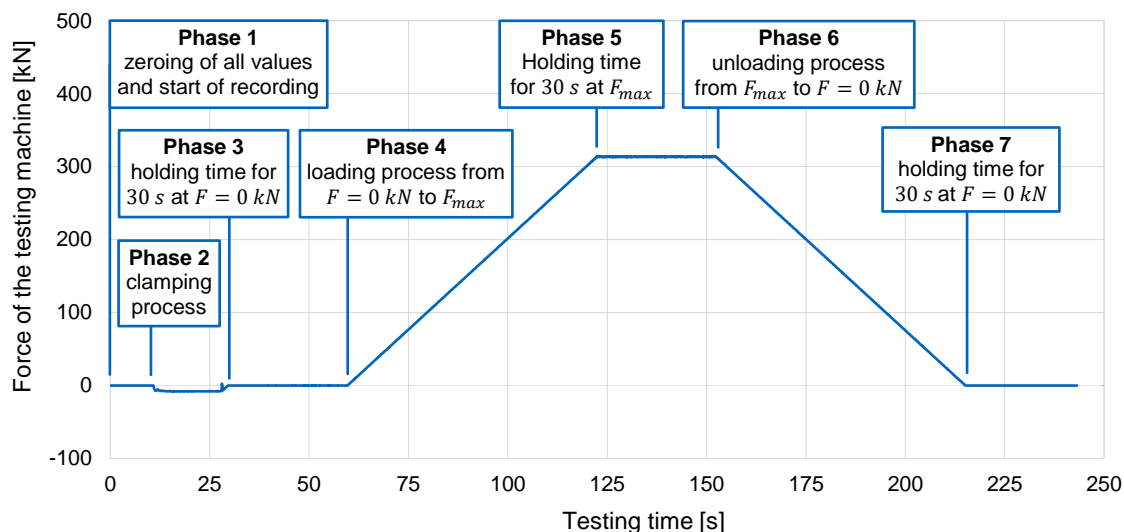


Figure 4-6: Standardised test force sequence plan for static preliminary tests exemplarily for test specimen WP3_1.1_01

According to Figure 4-6, the records of test force, test displacement, test time and strain gauges are initiated before the clamping process. All experimental data is set to zero before starting the measurements (cf. *Phase 1* of Figure 4-6). Following the clamping process of the testing machine (cf. *Phase 2* of Figure 4-6), it can be observed that a compressive force is present, as part of the weight of the load-applying traverse of the testing machine is applied to the test specimen. To compensate for this compression,

the test force was directly adjusted to 0 kN and then maintained at this level for thirty seconds (cf. *Phase 3* of Figure 4-6). This allowed the strain of the strain gauges resulting from the clamping process to be determined over a definite period of time. Subsequently, a load of 300 kN/min was applied in order to subject the cruciform joints to the maximum load F_{max} of the fatigue tests (cf. *Phase 4* of Figure 4-6). F_{max} was also maintained for a further thirty seconds (cf. *Phase 5* of Figure 4-6) to ensure that the majority of the plasticising effects had redistributed. Finally, the test specimens were unloaded with 300 kN/min (cf. *Phase 6* of Figure 4-6) and maintained constantly at 0 kN for another thirty seconds (cf. *Phase 7* of Figure 4-6).

Figure 4-7 presents the corresponding strain curves of *SG1* to *SG10* exemplarily for the test specimen *WP3_1.1_01*. In order to ensure sufficient measurement results, the frequency of the strain gauges was selected at 10 Hertz for the static preliminary tests.

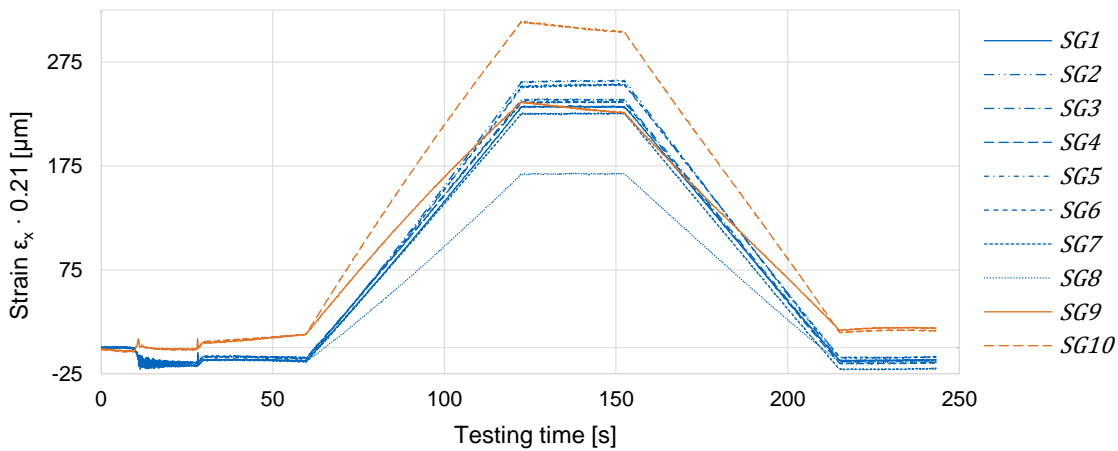


Figure 4-7: Strain measurements for *SG1* to *SG10* of static preliminary tests exemplarily for test specimen *WP3_1.1_01*

By the deviation of the resulting strains from *Phase 7* to *Phase 3* (cf. Figure 4-6), the plasticised strains can be determined according to the following formula. The modified strains $\varepsilon_{Phase\ 5,mod}$ are necessary to validate numerical comparative calculations under tensile load F_{max} (cf. Section 4.4.2).

$$\varepsilon_{Phase\ 5,mod} = \varepsilon_{Phase\ 5} - (\varepsilon_{Phase\ 7} - \varepsilon_{Phase\ 3}) \quad (4-1)$$

This correction is necessary because plastic strains cannot occur in a purely linear-elastic material behaviour as assumed in the FEA, without external load and unchanged clamping situation.

4.3.2 Fatigue tests

Subsequent to the static preliminary tests, the fatigue tests were conducted in the IGF research project No. 20336N [1]. In this respect, the evaluation of the respective strain measurements was of importance in addition to the total number of stress cycles $N_{R,test}$ attained. In the following, both the implementation of the tests (cf. Section 4.3.2.1) and the procedure for evaluating the experimental data (cf. Section 4.3.2.2) are presented.

4.3.2.1 Test implementation

All fatigue tests were carried out with a stress ratio of $R = 0.1$ under a sinusoidal oscillation. The predefined varying stress ranges $\Delta\sigma_{R,test}$ were determined according to the nominal stress concept of DIN EN 1993-1-9 [2]. For this purpose, based on the relevant fatigue strengths $\Delta\sigma_C$ of the examined cruciform joints as well as with the predefined stress cycles $N_{R,predefined}$, the stress ranges $\Delta\sigma_{R,test}$ required for the fatigue tests could be calculated for a survival probability of $P_s = 50\%$. The fatigue strengths according to DIN EN 1993-1-9 [2] are based on fatigue tests and are defined as the 95 % survival quantile of the test results with a probability of confidence of 75 % assuming a logarithmic normal distribution (cf. Chapter 2.2.2). To ensure a valid calculation of the experimentally required stress ranges $\Delta\sigma_{R,test}$, a conversion of the fatigue strengths $\Delta\sigma_C$ to the 50 % survival quantile was necessary.

Since there is no specific information on the standard deviation that was encountered in the normative regulations and guidelines and only test results with a confidence level of 75 % were used to determine the regression line, a simplified conversion of the fatigue strengths is implemented. A 95 % survival quantile in combination with a confidence probability of 75 % can be approximated with a survival probability of $P_s = 97.5\%$ according to [92]. Consequently, this corresponds to a probability of failure of $P_f = 2.5\%$. Based on DIN 50100 [27], which deals specifically with the evaluation of fatigue tests, the number of cycles N_{Pf} is defined as a conversion variable (cf. Chapter 2.2.2). In this way, slightly more conservative values are obtained than using the approach according to FOSTA Report P 778 [93], which is based on the direct conversion of the fatigue strength $\Delta\sigma_C$ (cf. Chapter 2.2.2). The comparison of both approaches is summarised exemplary for a normative fatigue strength according to the nominal stress concept of $\Delta\sigma_{C,97.5\%} = 71 \text{ N/mm}^2$ in Table 4-4.

Table 4-4: Comparison of different approaches to convert normative fatigue classes $\Delta\sigma_C$ to a survival probability of $P_s = 50\%$ based on the example of a fatigue class $\Delta\sigma_{C,97.5\%} = 71 \text{ N/mm}^2$

Database	Standard deviation	Index of reliability	Approach	$N_{R,50\%}$ [-]	$\Delta\sigma_{C,50\%}$ [N/mm ²]
DIN 50100 [27]	$s_{\log N,GG,P_f=2.5\%} = 0.18$	$u = -1.95996$	$N_{50\%} = 10^{\log(N_{Pf}) - u \cdot s_{\log N,GG}}$	4506328	93.08
FOSTA P 778 [93]	$s = 0.0688$	$\beta = -1.95996$	$\Delta\sigma_{50\%} = 10^{\log(\Delta\sigma_{Pf}) - \beta \cdot s}$	5076516	96.85

According to Table C.1 of DIN 50100 [27], a standard deviation of the logarithms of the stress cycles $s_{\log N,GG} = 0.18$ is specified for the required failure probability of $P_f = 2.5\%$ for linear welds with steel plate thicknesses of more than 5 mm. The corresponding index of reliability is $u = -1.95996$. Accordingly, after the conversion of formula (66) from [27], the number of cycles for the 50 % survival quantile can be generally determined according to the following formula.

$$N_{C,P_f} = 10^{\log(N_{C,50\%}) + u \cdot s_{\log N,GG}} \quad (4-2)$$

Since the normative fatigue strengths are based on $N_{C,97.5\%} = 2 \cdot 10^6$ number of cycles (cf. Chapter 2.2.1), this results in $N_{C,50\%} = 4506328$ with a 50 % survival quantile. Applying formula (2-1) specified in section 7.1 of DIN EN 1993-1-9 [2], the required

fatigue strength $\Delta\sigma_{C,50\%}$ for the relevant number of cycles of $N_{C,50\%} = 2 \cdot 10^6$ can be determined as follows.

$$\Delta\sigma_{C,50\%} = \sqrt[m]{\frac{(\Delta\sigma_{C,97.5\%})^m \cdot N_{C,50\%}}{2 \cdot 10^6}} \quad (4-3)$$

The gradient of the fatigue strength curve m is uniformly defined as $m = 3$ in the normative regulations and guidelines for the considered strength range. Thus, a back calculation from $N_{C,50\%} = 4.51 \cdot 10^6$ to $N_{C,50\%} = 2.00 \cdot 10^6$ load cycles is performed to be able to determine the relevant fatigue strength $\Delta\sigma_{C,50\%}$. Accordingly, an exemplary fatigue strength $\Delta\sigma_{C,nom,50\%} = 93.08 \text{ N/mm}^2$ results for the nominal stress fatigue class 71. The stress cycles $N_{R,predefined}$ were specified to be $1 \cdot 10^5$, $2 \cdot 10^5$ and $5 \cdot 10^5$ in order to be able to generate conclusive S-N curves in a reasonable amount of time. Nevertheless, in case of unexpected test results $N_{R,test}$, the predefined stress ranges $N_{R,predefined}$ were modified for the individual test groups.

The potential test velocity was determined on the basis of the maximum test displacement of the static preliminary tests under the maximum load F_{max} . On the Instron hydro-pulse machine, the sinusoidal oscillations of the fatigue tests could be conducted at 2 Hertz. On the EVO 1600 universal testing machine, however, only 1 Hertz was possible. Depending on the test velocity, the scanning frequency of the strain gauges was defined. In order to comply with the so-called sampling theorem and to capture the peak values of the sinusoidal oscillations, the sampling frequency was set at 300 Hertz for the Instron hydro-pulse machine and at 150 Hertz for the EVO 1600 universal testing machine. To limit the resulting large amount of data, a cycle-dependent memory plan was set up. It is presented in Table 4-5 below.

Table 4-5: Memory plan for fatigue tests of [1]

Cycles	1 – 100	101 – 1000	1001 – 100000	100000 – 5000000
Memory plan	all cycles	1 full cycle every 10 cycles	2 full cycles every 100 cycles	10 full cycles every 1000 cycles

By recording the cycles according to Table 4-5, it was possible to determine the initiation time of cracks accurately as well as effects resulting from imperfections (cf. Section 4.3.2.2). In addition, a peak value detection was set up in order to be able to determine load cycles $N_{R,test}$ independently of the experimental results of the testing machines. In this respect, it was also possible to evaluate strain measurements as a function of cycles. The associated evaluation method of the experimental data on the strain measurements is explained in more detail in the following Section 4.3.2.2.

4.3.2.2 Evaluation method of the experimental data

In order to process the large amount of data from the strain measurements of the fatigue tests, suitable Python scripts were developed in the IGF research project No. 20336N [1]. The associated evaluation in Python is realised on the basis of the text documents generated by HBM's QuantumX measurement data acquisition system Catman for each test. By directly analysing the text files, a concise and efficient analysis of all test results is possible. The solution in Python allows both the evaluation of

individual cycles (cf. Section 4.3.2.2.1) as well as evaluations over several cycles (cf. Section 4.3.2.2.2). In this respect, all experimental data can be assigned to the respective associated cycles by means of the configured peak value detection. For this purpose, defined measurands must be assigned to the memory channels specified in the text documents. The measurands test time, test force, test displacement and strain of a recorded strain gauge are available for the respective assignment. Based on the linear law of elasticity, an instant conversion of the measured strains ε_x into stresses σ_x is performed by Python. In this way, both strains and stresses can be analysed. To simplify the further utilisation of the results, a feature is provided that allows the analysed data to be automatically exported to Excel. In the Python evaluation, it is also possible to display the selected experimental data in tabular form or as a plot in order to verify the results directly. The procedure for single-cycle and multi-cycle evaluation is presented below in more detail.

4.3.2.2.1 Individual cycles

The Python script offers the possibility to perform a single cycle evaluation. In this respect, it is verified automatically whether the requested cycle was covered by the memory plan and is therefore included in the data file. If a cycle is not included in the experimental records, the next smaller and larger cycle is suggested. In the single cycle evaluation, all input parameters can be displayed over the time of a single cycle. This includes the test force, the test displacement and the strains resp. stresses of all strain gauges applied to the test specimen. In addition, structural stresses can be calculated automatically through the Python evaluation. In the present evaluation, this is possible for strain gauges *SG 1* and *SG 2* as well as for *SG 3* and *SG 4*, as these pairs were systematically positioned at a distance of $0.4 \cdot t$ and $1.0 \cdot t$ to the notch at the identical width of the component (cf. Figure 4-5). The associated calculation by linear stress extrapolation is performed according to specifications of the guidelines of the IIW [3] resp. prEN 1993-1-9 [4].

Furthermore, according to the proposed evaluation procedure of Section 4.1.3, the time-dependent behaviour of imperfections can be investigated by means of the Python evaluation. With the present arrangement of the strain gauges (cf. Figure 4-5), this can be implemented by evaluating the strain gauge pairs *SG 2* with *SG 9* as well as *SG 8* with *SG 10*, as these are positioned on opposite sides of the plates. Consequently, the calculated stresses of the strain gauges can be used to determine an equivalent misalignment $e_{equivalent}$ by subdividing the determined stress distribution over the component thickness into a membrane and bending component $\sigma_{SG,m}$ resp. $\sigma_{SG,b}$. The associated approach is presented in Figure 4-8.

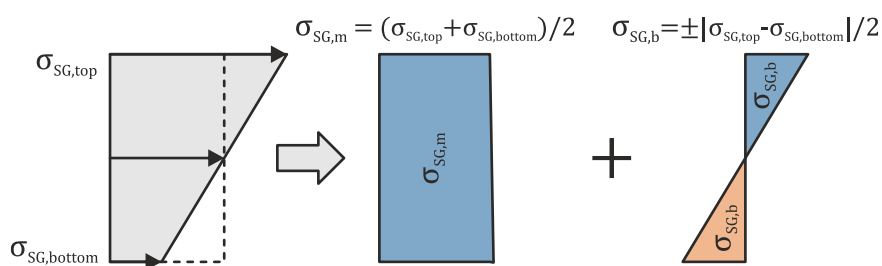


Figure 4-8: Determination of the equivalent misalignment $e_{equivalent}$ by calculated stress measurements on opposite plate sides

The correlation in Figure 4-8 can be used to determine both membrane and bending stresses around the weak axis of the welded-on plates. The bending component $\sigma_{SG,b}$ as a function of time of the strain gauges is therefore given by the following formula.

$$\sigma_{SG,b}(time) = \frac{e_{equivalent}(time) \cdot F(time)}{W_y} = \frac{|\sigma_{SG,top} - \sigma_{SG,bottom}|}{2} \quad (4-4)$$

To enable the determination of $e_{equivalent}(time)$ independently of the force of the testing machine, the applied force $F(time)$ can equivalently be determined by the calculated membrane stress component $\sigma_{SG,m}$ of the strain measurements.

$$F(time) = \sigma_{SG,m}(time) \cdot A = \left(\frac{\sigma_{SG,top} + \sigma_{SG,bottom}}{2} \right) \cdot A \quad (4-5)$$

Combining the two formulae and solving for the equivalent imperfection $e_{equivalent}(time)$ results in the following equation.

$$e_{equivalent}(time) = \frac{|\sigma_{SG,top} - \sigma_{SG,bottom}| \cdot W_y}{2 \cdot \left(\frac{\sigma_{SG,top} + \sigma_{SG,bottom}}{2} \right) \cdot A} \quad (4-6)$$

Through this evaluation implemented in Python, existing imperfections can be examined in detail in the later Section 4.5.3.

However, it was noticed in the evaluations of the experimental data from [1] that the two applied measurement data acquisition systems did not record sufficiently synchronised data. Consequently, there were time-related deviations in the experimental measurements between the first and second measuring devices. This time-delayed behaviour is exemplarily shown on the left side of Figure 4-9.

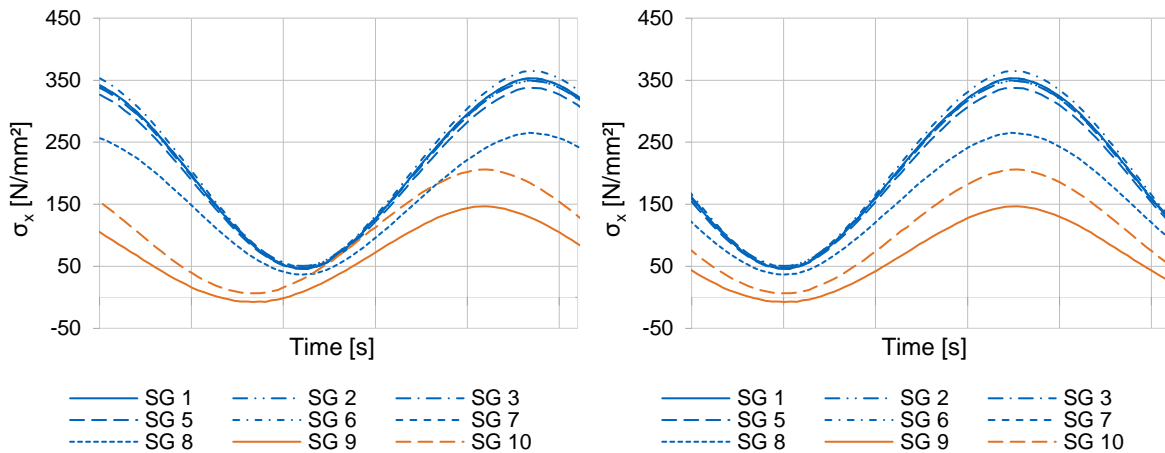


Figure 4-9: Exemplarily delayed measurement results for strain gauges *SG 1* to *SG 10* due to inaccurate synchronisation between the used measurement data acquisition systems (left) and corrected experimental data (right)

Figure 4-9 demonstrates that in contrast to *SG 9* and *SG 10*, the results of strain gauges *SG 1* to *SG 8* were stored with a time-dependent increase in delay. This is due to the fact that machine force and machine displacement as well as *SG 9* and *SG 10* were connected to the first measuring device and all other strain gauges *SG 1* to *SG 8* were connected to the second. However, the experimental data generated could be manually corrected for *SG 1* to *SG 8* by selectively deleting individual cycles of the delaying

QuantumX. The modified experimental data is shown on the right side of Figure 4 22. In this way, synchronised experimental data can be provided.

4.3.2.2.2 Several cycles

In addition to the evaluation of individual cycles, the Python evaluation can also be used to analyse results over several cycles. Besides the possible evaluation variables according to the single cycle assessment (cf. Section 4.3.2.2.1), the minimum and maximum values as well as the mean values for stresses and strains can be determined. Furthermore, structural stresses and equivalent imperfections according to Section 4.3.2.2.1 can also be analysed over several cycles.

Although the Catman data acquisition system allows peak detection to assign the respective cycles, there is a possibility that not only complete cycles may be recorded. For this reason, minimum, average and maximum values over several cycles may be calculated incorrectly if cycles have not been captured entirely. In the evaluation over several cycles, it is therefore important to ensure that a reasonable significance criterion is defined. This is characterised by a maximum permissible deviation of the single-cycle-dependent loading to the specified maximum load F_{max} and minimum load F_{min} of the fatigue test. Therefore, the significance criterion is defined in absolute values as an admissible tolerance. Through this screening progress, only cycles are included in the evaluation in which both the maximum and minimum load levels are within the defined range.

Figure 4-10 illustrates results for the maximum stresses $\sigma_{x,max}$ and minimum stresses $\sigma_{x,min}$ of each individual cycle over all reached cycles for all applied strain gauges.

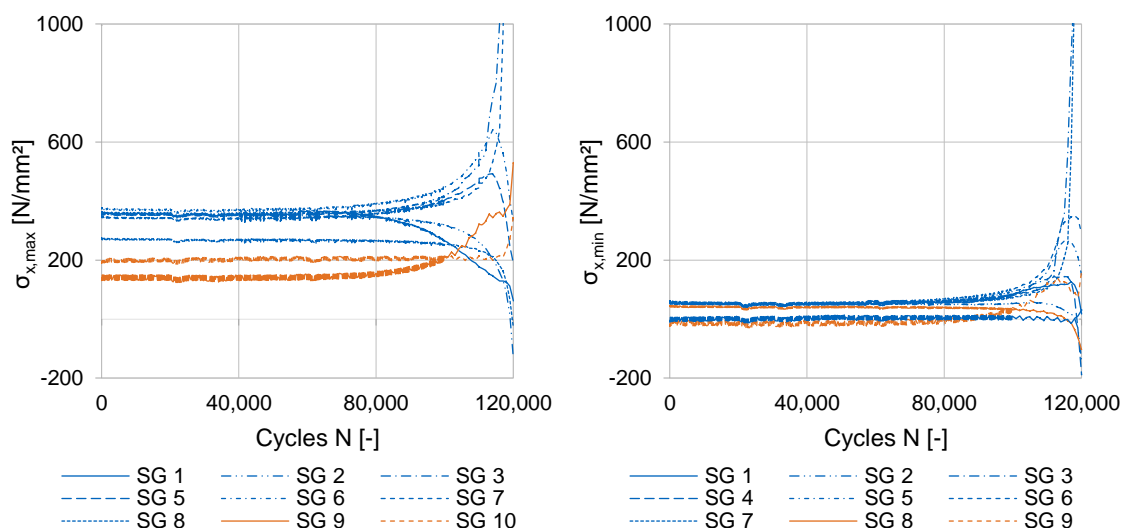


Figure 4-10: Exemplary evaluation of the maximum single cycle stresses (left) and minimum single cycle stresses (right) of all strain gauges over all cycles of the fatigue test

According to Figure 4-10, it is evident that the maximum and minimum stresses remain relatively constant over a wide period of time. Only after a large number of load changes do local stress redistributions result, leading to an increase or decrease in stresses. Through the exact cycle-dependent allocation of the measured strains of all attached strain gauges, the defined crack of the test specimens can therefore also be determined accurately. In this respect, the crack initiation is defined by the change of the machine

displacement $u \geq 0.1 \text{ mm}$. Based on this definition, the time point of the crack initiation can be determined. This procedure is exemplarily shown in the following Figure 4-11.

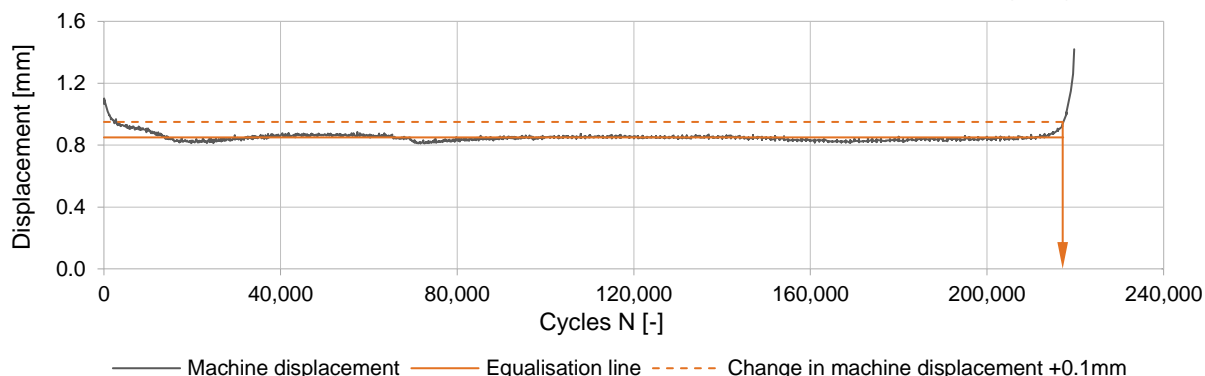


Figure 4-11: Definition for the evaluation of the initial crack

The evaluations indicated that the required reduction of the achieved number of load cycles until component failure to the cycles until crack initiation is relatively low across all test series.

4.4 Validation of the FE models

The validation of the imperfect FE models for the fatigue tests of the IGF research project No. 20336N [1] was performed according to the test procedure for static preliminary tests presented in Section 4.3.1. For this purpose, both the clamping process and the subsequent tensile stress under load F_{max} were simulated numerically. The required imperfections were modelled according to the evaluation from the 3D laser scan measurements (cf. Section 4.2.2). In addition to imperfect solid models, imperfect shell models were generated to determine the capability of shells to represent the correct structural stress. The FE models required in each case were created in accordance with Chapter 3.3. For the validation, the data of the experimental strain gauges as well as the strains ε_x of the FE models are considered. On the one hand, the validation is performed at the time point without external load in order to validate the numerical clamping simulation (cf. Section 4.4.1). This corresponds to *Phase 3* of Figure 4-6. On the other hand, the FE models are evaluated at time point F_{max} in order to validate the FE models under maximum load (cf. Section 4.4.2). For this purpose, the results from *Phase 5* are evaluated according to Figure 4-6. Since the structural stress concept is based on linear elastic material behaviour in the FEA and local plasticisation effects were partially detected in the area of the strain gauges due to large residual welding stresses, the experimental measurement results under tensile load additionally had to be modified according to formula (4-1).

In the validation presented below, the exact locations of the strain gauges are evaluated. Since the strain gauges were applied by hand, inaccuracies could not be excluded. For this reason, the test bodies attached with strain gauges were measured in order to determine the exact positions. Consequently, the evaluation is performed at the identical locations. In the following, the validation results achieved in [1] are presented in an abbreviated form, exemplarily and separately according to the clamping process (cf. Section 4.4.1) and tensile load (cf. Section 4.4.2). The evaluation includes the measured experimental data of the ten strain gauges *SG1* to *SG10* and the

associated results of the imperfect solid and shell models. The imperfections and maximum tensile load F_{max} of the exemplarily validated cruciform joints are summarised in Table 4-6.

Table 4-6: Imperfections and maximum load F_{max} for exemplarily presented cruciform joints through the clamping process

Specimen	$t_1 = t_2$ [mm]	t_3 [mm]	e_1 [mm]	e_2 [mm]	α_1 [°]	α_2 [°]	F_{max} [kN]
WP3_1.1_07	12	12	+0.60	-0.02	-1.18	-0.14	232.82
WP3_1.2_05	12	12	+1.26	-1.80	-0.69	+0.70	184.40
WP3_2.1_03	12	40	+0.61	+0.80	-0.32	+0.47	350.53
WP3_2.2NL_03	12	40	+1.09	-2.01	+0.41	-0.41	117.14
WP3_3.1_09	40	12	-0.37	-0.53	-0.21	-0.03	596.92
WP3_3.2_07	40	12	+5.34	-4.96	+1.35	+0,98	618.25

According to Table 4-6, only one validation is presented for each test group. With regard to the incorrectly produced test group WP3_2.2, only a test specimen of the subsequent delivery WP3_2.2NL with sufficiently large axial misalignment is validated. For a more detailed analysis, reference is made to the final report of the IGF research project No. 20336N [1].

4.4.1 Clamping process

In the following, the comparison between the experimental test results and the FEA at the time point of the clamping process is presented. The associated validation results are summarised for the test specimens of Table 4-6 in the following Figure 4-12 to Figure 4-17. In the validations for the clamping process (cf. Figure 4-12 to Figure 4-17) it is evident that there is generally a satisfactory congruence between the results of the FE shell and solid models. Consequently, it can be confirmed that the selected method of modelling the welds with inclined shell elements in the FE shell models (cf. Chapter 3.3.5) provides representative results. Despite the presence of unwanted angular misalignments $\alpha < 1.5^\circ$, with regard to the selected welding method WM3, no correction of the resulting strains is necessary to ensure good congruence with the solid models. According to the evaluation from Table 3-10, the minor axial misalignments of $e = 0.25 \cdot t$ also provide a reasonable correlation to the solid models for the FE models with shell elements.

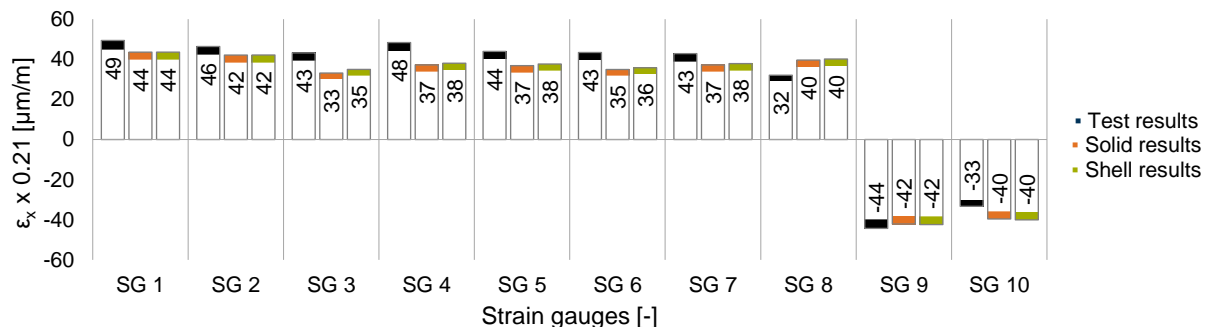


Figure 4-12: Validation of the clamping process for WP3_1.1_07 representatively for WP3_1.1

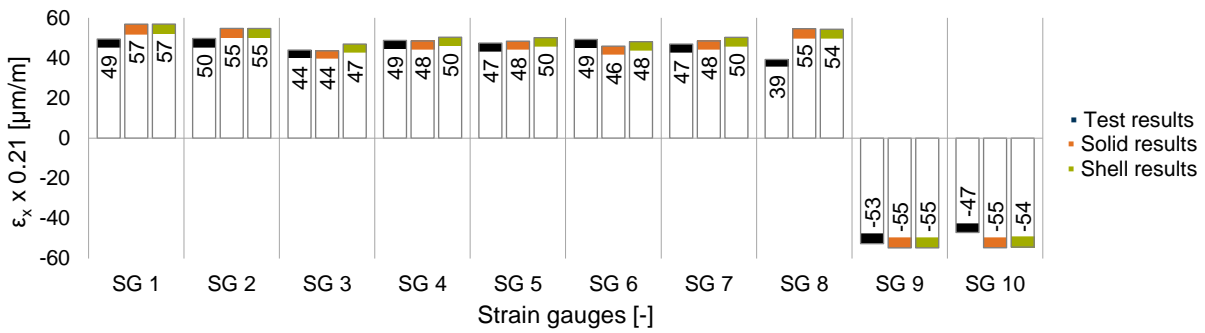


Figure 4-13: Validation of the clamping process for WP3_1.2_05 representatively for WP3_1.2

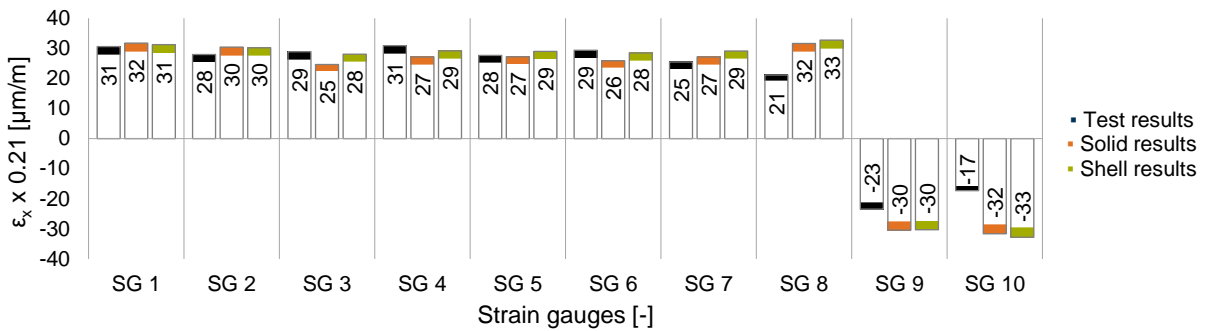


Figure 4-14: Validation of the clamping process for WP3_2.1_03 representatively for WP3_2.1

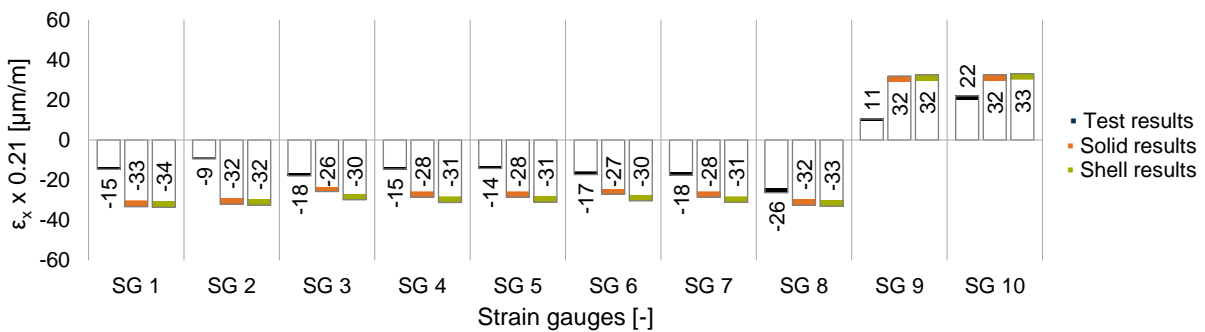


Figure 4-15: Validation of the clamping process for WP3_2.2NL_03 representatively for WP3_2.2

In principle, the numerical results of the test group WP3_1 (cf. Figure 4-12 and Figure 4-13) as well as WP3_2 (cf. Figure 4-14 and Figure 4-15) correspond well with the experimental data of the static preliminary tests. In this respect, there is no systematic over- or underestimation by the numerical FE calculations and tendencies of the experimental strain distributions can be identified correctly. It is generally apparent that there is a slightly reduced congruence in the range of small experimental strains (cf. Figure 4-15). This is due to the fact that strain gauges in small strain ranges are significantly more susceptible to erroneous evaluations. If higher strains result from the clamping process, the results are consistent with the FEA. The deviations detected in the clamping process may also be attributed to imperfections that were incorrectly assumed to be too large or too small.

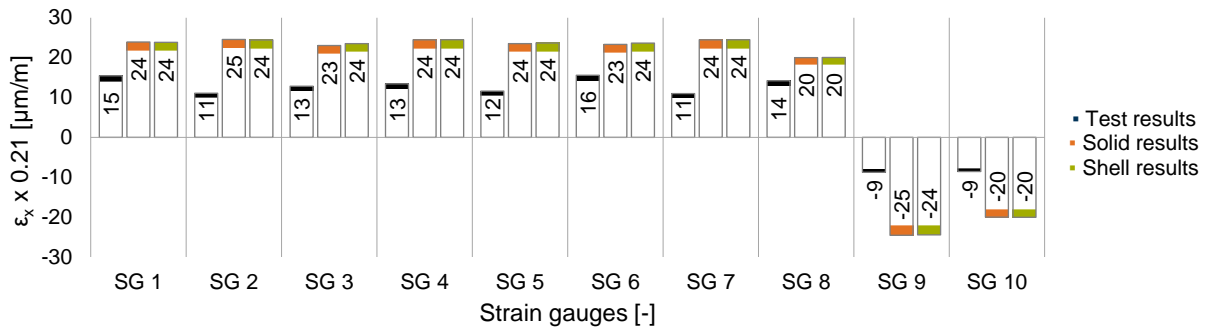


Figure 4-16: Validation of the clamping process for *WP3_3.1_09* representatively for *WP3_3.1*

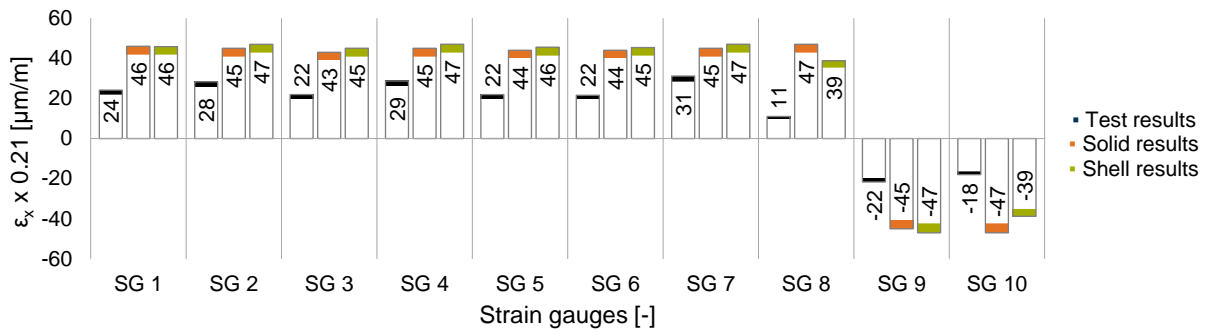


Figure 4-17: Validation of the clamping process for *WP3_3.2_07* representatively for *WP3_3.2*

In contrast to the validations of test series *WP3_1* and *WP3_2*, the results for the clamping process of *WP3_3* (cf. Figure 4-16 and Figure 4-17) are less satisfactory for most of the test specimens. In this respect, the experimental results with thicker plates $t_{1=2} = 40 \text{ mm}$ are systematically lower than in the FEA. However, the experimentally determined strains are relatively small, which appears disproportionate considering the existence of imperfections associated with thick welded-on plates (cf. Table 4-6). Two possible causes can be identified in this regard. On the one hand, there is the possibility that the evaluation of the 3D laser scan measurements incorrectly assumed too large imperfections for *WP3_3*, which consequently result in excessive strains in the inaccurately generated FE models. On the other hand, it is possible that the influence of the clamping process on the resulting strains is exaggerated in the FEA if imperfections are present. In this respect, it was observed in the experimental tests that the high stiffness of the welded-on plates during the clamping process can lead to minimal lateral deflection of the clamping jaws in the Z_{global} direction. The specified rigid restraints of the support areas in the FEA consequently results in larger strains from the clamping process, as in reality a weaker system is present. Nevertheless, the tendencies of the tensile and compression ranges of the test specimens are correctly represented by the numerics in the validations for *WP3_3*.

4.4.2 Tensile load

The validations performed with the tensile loading F_{max} are presented below. The corresponding imperfections of the selected test specimens and the values for F_{max} are summarised in Table 4-6. The generated results are illustrated in Figure 4-18 to Figure 4-23. Both imperfect solid and imperfect shell models were evaluated. In contrast to section 4.4.1, the validations include not only the measured experimental data of the strain gauges but also the experimental strains modified for plastic effects.

The validation under tensile load F_{max} for the test series $WP3_1$, $WP3_2$ and $WP3_3$ is shown in Figure 4-18 to Figure 4-23. As already noted in the validations for the clamping process (cf. Section 4.4.1), the FE calculations with shell models provide comparable results to the numerical analyses with solid elements. Consequently, shell models with weld method $WM3$ (cf. Chapter 3.3.5) are capable of providing equivalent strains as solid models, irrespective of the level of imperfections.

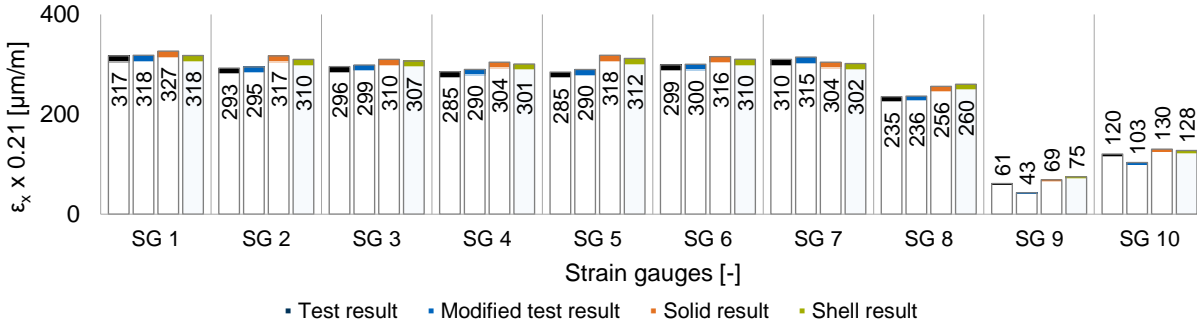


Figure 4-18: Validation of tensile load F_{max} for $WP3_1.1_07$ representatively for $WP3_1.1$



Figure 4-19: Validation for tensile load F_{max} for $WP3_1.2_05$ representatively for $WP3_1.2$

Nevertheless, the values of the strain gauges measured in the tensile tests for test group $WP3_1.1$ are slightly overestimated in the FEA, both by solid and shell elements (cf. Figure 4-18). In contrast, in the test group $WP3_1.2$, only minor differences between measured data and FEA can be observed (cf. Figure 4-19). In this respect, due to the intentional misalignments $e = 0.25 \cdot t$, some strains are measured which, using Hooke's law, would result in stresses considerably above the yield strength (cf. $SG 1$ in Figure 4-19). Consequently, local plasticisation must be present, which cannot be investigated by the chosen FE analyses. However, by correcting for the plastic strain components (cf. Section 4.3.1), good conformity can be provided.

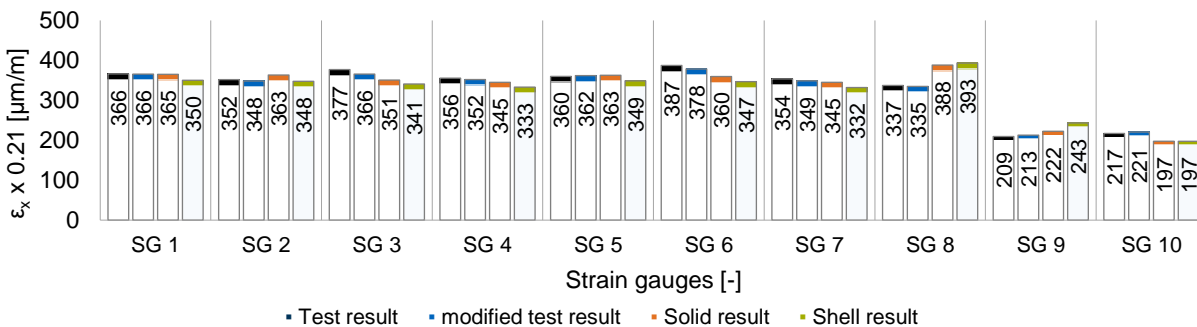


Figure 4-20: Validation for tensile load F_{max} for $WP3_2.1_03$ representatively for $WP3_2.1$

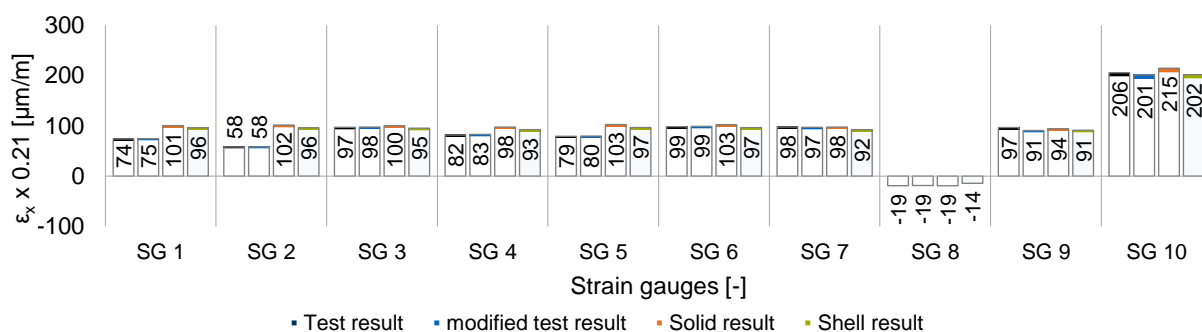


Figure 4-21: Validation for tensile load F_{max} for $WP3_2.2NL_03$ representatively for $WP3_2.2$

With regard to the test series $WP3_2$, only minor differences between the experimental results and the FEA are determined (cf. Figure 4-20 and Figure 4-21). A systematic over- or underestimation cannot be detected, which is why the deviations can be attributed to incorrectly assumed imperfections.

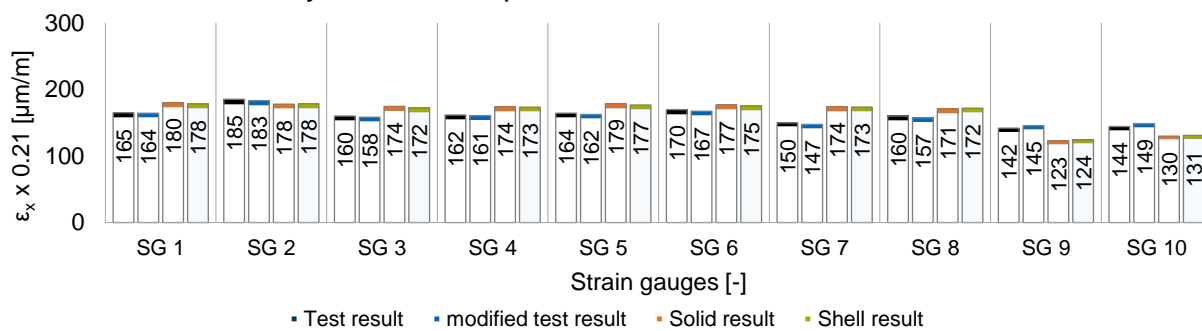


Figure 4-22: Validation for tensile load F_{max} for $WP3_3.1_09$ representatively for $WP3_3.1$

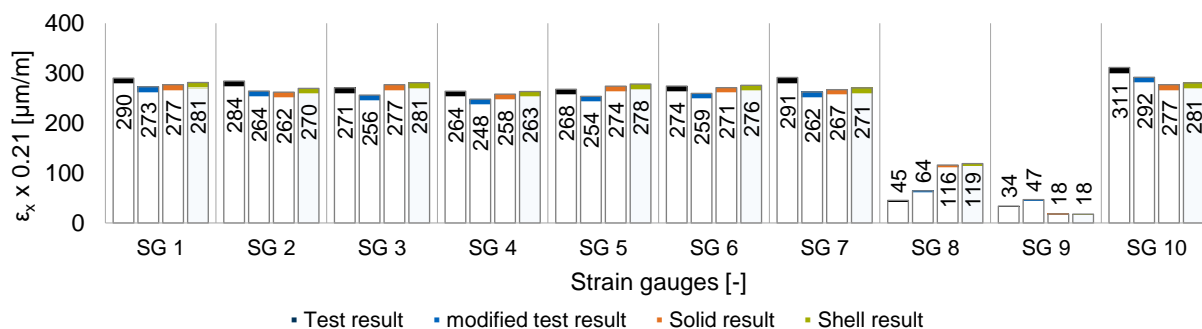


Figure 4-23: Validation for tensile load F_{max} for $WP3_3.2_07$ representatively for $WP3_3.2$

The results of the validation under tensile load of $WP3_3$ (cf. Figure 4-22 and Figure 4-23), however, show significant differences corresponding to the results of the clamping process (cf. Figure 4-16 and Figure 4-17). It is apparent that the overestimation of the secondary bending moments from the clamping process also leads to deviating results under tensile loading. This is evident in the test specimens of $WP3_3.1$ (cf. Figure 4-22) as well as in the test specimens of $WP3_3.2$ (cf. Figure 4-23). The cause can again be attributed to the lateral deflection of the upper clamping section of the testing machine (cf. Section 4.4.1). Due to the relatively high stiffness of the welded-on plates of $WP3_3$, the FEA significantly overestimates the proportion of secondary bending moments in this respect. In addition, imperfections show a greater influence on the resulting strains in the shell and solid models. Consequently, even small deviations in the measurement records lead to large differences in the validation.

In general, the evaluations demonstrate that the superposition principle between the clamping process and the tensile load is not applicable. This is due to the fact that the stress determination of the FEA is based on a geometrically non-linear calculation that includes straightening effects of the structural detail. Concerning this matter, it can be stated that an over- or underestimation of the stresses resulting from the clamping process (cf. Figure 4-12 to Figure 4-17) simultaneously results in an over- or underestimation of the validation under tensile load (cf. Figure 4-18 bis Figure 4-23).

The results of the validation thus generally show good consistency with the experimentally conducted preliminary tests. In this respect, both shell and solid models are able to evaluate the system behaviour correctly. However, it is impossible to include all effects that have an impact on the strains in the FE calculations. Among other things, welding inaccuracies, local redistributions after exceeding the yield strength, residual stresses, other imperfections besides axial misalignment and angular misalignment, as well as the test frame of the trials having significantly less stiffness than the full restraint assumed in the FEA, to deviating results. Consequently, it is nearly impossible to provide more accurate results. Nevertheless, the selected FE methodology from chapter 3.3 can be considered sufficiently validated due to the relatively good accordance with the experimental test results.

4.5 Evaluation of the fatigue tests

The evaluation of the fatigue tests performed in the IGF research project No. 20336N [1] is presented below. For this purpose, the assessment methodology from Section 4.1 is applied. In this respect, all cruciform joints according to Section 4.2 are analysed based on FE solid models. Both the evaluation based on the nominal stress concept (cf. Section 4.5.1) and the structural stress concept (cf. Section 4.5.2) are realised by means of the procedures presented in Section 4.1.1 for perfect FE models and Section 4.1.2 for imperfect FE models. The objective of the evaluation in the nominal and structural stress concept is to establish a comparison with a normatively validated procedure by means of the reliable results in the nominal stress concept. In this way, the results determined by the structural stress concept can be verified with regard to their practical applicability. In addition, Section 4.5.3 examines the influences of the straightening effect with the equivalent imperfections $e_{equivalent}$ (cf. Section 4.3.2.2.1). This is achieved with the presented procedure from Section 4.1.3 to determine more accurate results on the influence of imperfections on the fatigue behaviour of cruciform joints. Furthermore, the results from the fatigue tests are utilised in the next chapter to investigate the handling of imperfections from clamping processes in testing machines (cf. Chapter 5.1).

4.5.1 Nominal stress concept

In the following section, the fatigue tests conducted in [1] on cruciform joints are evaluated according to the nominal stress concept. For this purpose, the basic principle of evaluation according to the nominal stress concept is presented first (cf. Section 4.5.1.1). The respective assessment is then presented separately for test series *WP3_1*, *WP3_2* and *WP3_3* in Section 4.5.1.2. Section 4.5.1.3 provides a final summary of the conclusions regarding the nominal stress concept.

4.5.1.1 Basic principle

As no measurement records of structures are regularly available in the design phase, both perfect and imperfect FE models are assessed according to Section 4.1. Consequently, on the one hand, perfect nominal stress ranges $\Delta\sigma_{R,nom,50\%,FEA,perfect}$ determined with perfect FE models are related to the corresponding stress cycles $N_{R,test}$ up to crack initiation. In the resulting S-N curves, only the intentional axial misalignments of the test groups *WP3_1.2*, *WP3_2.2* and *WP3_3.2* of $e = t_{1=2}/4$ are included, without considering manufacturing-related inaccuracies. On the other hand, imperfect nominal stress ranges $\Delta\sigma_{R,nom,50\%,FEA,imperfect}$ are computed for imperfect FE models. The resulting S-N curves are also generated on the basis of the experimentally determined stress cycles $N_{R,test}$ up to crack initiation. In this respect, all detected axial and angular misalignments are considered in the FEA, including all manufacturing inaccuracies. In order to be able to provide comparability with the normative fatigue strengths, the determined experimental S-N curves with a survival probability of $P_s = 50\%$ are subsequently converted to a normative survival probability of $P_s = 97.5\%$ according to DIN 50100 [27] (cf. Section 4.3.2.1).

Since the investigated cruciform joints are attributed with varying normative fatigue classes in the nominal stress concept, the evaluation is performed in accordance with DIN EN 1993-1-9 [2], the guidelines of the IIW [3] as well as prEN 1993-1-9 [4]. The associated decisive fatigue classes on the resistance side of test series *WP3_1*, *WP3_2* and *WP3_3* are summarised in Table 4-7 below.

Table 4-7: Fatigue classes according to nominal stress concept for the fatigue tests of *WP3* according to normative regulations and guidelines

Test series	Fatigue class $\Delta\sigma_{C,nom,97.5\%}$ [N/mm ²]		
	DIN EN 1993-1-9 [2]	Guidelines of the IIW [3]	prEN 1993-1-9 [4]
<i>WP3_1</i>	80	71	80
<i>WP3_2</i>	71	71	71
<i>WP3_3</i>	71	71	71

The stresses of the fatigue tests are applied at the level of the actual fatigue load $\Delta F = F_{max} - F_{min}$. Since possible imperfections may lead to secondary bending moments, which are largest in the area of the intermediate plate, it is important to determine the nominal stress range at a small distance from the weld notch. Therefore, to determine the actual nominal stress ranges, principal stresses are averaged over the component width at a distance of $1,0 \cdot t$ in front of the notch. This is reasonable since at this distance all non-linear behaviour of the notch of the weld has subsided. Stress-increasing effects due to the structural detail, such as the existing transverse strain constraint due to the stiffness of the intermediate plate in the transverse direction, are compensated for through the use of the mean value across the width.

Furthermore, imperfections are considered to a certain extent according to DIN EN 1993-1-9 [2], guidelines of the IIW [3] and prEN 1993-1-9 [4]. Consequently, According to Chapter 2.5.3.1, the corresponding fatigue classes from Table 4-7 already include influences from imperfections on the normative resistance side. In this respect,

according to DIN EN 1993-1-9 [2] and prEN 1993-1-9 [4], 15 % of the thickness of the intermediate plate $e \leq 0.15 \cdot t_3$ is already covered as axial misalignment by the fatigue classes for cruciform joints in the nominal stress concept (cf. Chapter 2.5.3.1.1). In contrast, the already considered influences of the IIW [3] amount to an axial misalignment of 15 % of the thickness of the welded-on plates $e = 0.15 \cdot t_{1=2}$ (cf. Chapter 2.5.3.1.2). In order to estimate the magnitude of these stress-increasing effects, numerical comparative calculations were performed in [1] for the investigated test series $WP3_1$, $WP3_2$ and $WP3_3$. The required stress concentration factors $k_{m,FEA}$ were determined by the ratio of the nominal stress determined with axial misalignments $e = 0.15 \cdot t_{1=2}$ as well as $e = 0.15 \cdot t_3$ to the nominal stress without axial misalignment $e = 0.0$. Depending on the respective test series, the loading was defined in a way that a nominal stress of $\sigma_{R,nom,50\%,perfect} = 1.0 \text{ N/mm}^2$ resulted in the FE model without imperfections. Thus, the comparability of the perfect and imperfect evaluations is ensured by a consistent load level. In addition, due to the minor stress, straightening effects of the constructions can be minimised. The resulting values for $k_{m,FEA}$ are summarised in Table 4-8 below.

Table 4-8: Stress concentration factors k_m due to already considered imperfections in the fatigue classes for cruciform joints of DIN EN 1993-1-9 [2] and prEN 1993-1-9 [4] as well as of the guidelines of the IIW [3] in the nominal stress concept

Test series	DIN EN 1993-1-9 [2] and prEN 1993-1-9 [4]		Guidelines of the IIW [3]
	$k_{m,FEA} (e = 0.15 \cdot t_3) [-]$	$k_{m,FEA} (e = 0.15 \cdot t_{1=2}) [-]$	$k_{m,already\ covered} [-]$
$WP3_1$	1.40	1.40	1.45
$WP3_2$	2.25	1.37	1.45
$WP3_3$	1.09	1.32	1.45

In addition the guidelines of the IIW [3] specify in the nominal stress concept for cruciform joints that a stress concentration factor of $k_{m,already\ covered} = 1.45$ is already considered in the fatigue class (cf. Table 2-16). However, since the values for $k_{m,already\ covered}$ and $k_{m,FEA}$ tend to be approximately equal, only the more accurately determined factors $k_{m,FEA}$ are considered further.

In order to ensure the comparability of the experimental results with the normative regulations and guidelines, both the fatigue strengths increased by $k_{m,FEA}(e = 0.15 \cdot t_{1=2})$ and by $k_{m,FEA}(e = 0.15 \cdot t_3)$ are presented in the S-N curves in addition to the uncorrected normative fatigue classes. Since the evaluation of the perfect nominal stress ranges $\Delta\sigma_{R,nom,50\%,FEA,perfect}$ does not include influences from unintentional imperfections on the action side, the associated S-N curves are consequently to be related to the uncorrected normative fatigue classes. This allows a verification of the validity of the normative specifications regarding imperfections. In this respect, the normative fatigue classes should be satisfied by the experimental S-N curves, as no imperfections are present that are greater than normatively permitted. In contrast, with the imperfect nominal stress ranges $\Delta\sigma_{R,nom,50\%,FEA,imperfect}$ all imperfections are included on the action side. Consequently, the corresponding results are to be related to the modified fatigue strength according to DIN EN 1993-1-9 [2] and prEN 1993-1-9 [4] as well as according to the guidelines of the IIW [3]. Based on the adjustment of the

fatigue classes, good compliance should be achieved by evaluating the experimental tests with $\Delta\sigma_{R,nom,50\%,FEA,imperfect}$.

In addition, thickness effects must be considered, as the welded-on plates of test series *WP3_3* with a thickness of $t_{1=2} = 40 \text{ mm}$ are thicker than the standardised reference thickness $t_{ref} = 25 \text{ mm}$ (cf. Chapter 2.6). However, DIN EN 1993-1-9 [2] does not specify any thickness effects and a thickness correction according to prEN 1993-1-9 [4] is only required in the structural stress concept. In contrast, according to the guidelines of the IIW [3], thickness effects must be explicitly considered in the nominal stress concept. The consideration of the normative specified thickness effects is thus performed by the thickness correction factors $f(t)$ according to Table 4-9.

Table 4-9: Thickness concentration factor $f(t)$ of DIN EN 1993-1-9 [2], guidelines of the IIW [3] and prEN 1993-1-9 [4] according to the nominal stress concept

Test series	Thickness correction factor $f(t)$ [-]		
	DIN EN 1993-1-9 [2]	Guidelines of the IIW [3]	prEN 1993-1-9 [4]
<i>WP3_1</i>	–	–	–
<i>WP3_2</i>	–	–	–
<i>WP3_3</i>	–	$f(t) = \left(\frac{25}{40}\right)^{0.3} = 0.8685$	–

4.5.1.2 Analysis of the test series

Based on the presented procedures of Section 4.5.1.1, the results obtained by applying the nominal stress concept to the fatigue tests from the IGF research project No. 20336N [1] are presented separately for the test series *WP3_1* (cf. Section 4.5.1.2.1), *WP3_2* (cf. Section 4.5.1.2.2) and *WP3_3* (cf. Section 4.5.1.2.3).

4.5.1.2.1 *WP3_1*

In the following, the S-N curves for test series *WP3_1* are shown separately for *WP3_1.1* (cf. Figure 4-24) and *WP3_1.2* (cf. Figure 4-25), both for the perfect FE models in blue and for the imperfect FE calculations in orange. In addition, the normative fatigue classes according to DIN EN 1993-1-9 [2], guidelines of the IIW [3] and prEN 1993-1-9 [4] are illustrated both uncorrected and modified according to Section 4.5.1.1.

For the test group *WP3_1.1* without intentional imperfections, a fatigue strength of $\Delta\sigma_{C,nom,97.5\%,FEA,imperfect} = 104 \text{ N/mm}^2$ results according to Figure 4-24, with the consideration of unintentional imperfections in the FEA. With the perfect FE evaluations, on the other hand, only a fatigue strength of $\Delta\sigma_{C,nom,97.5\%,FEA,perfect} = 70 \text{ N/mm}^2$ can be determined. Consequently, with a difference of 34 N/mm^2 between the perfect and imperfect fatigue strength, there is a defined scatter band for *WP3_1.1*. This is due to the explicit consideration of the unintentional imperfections in $\Delta\sigma_{R,nom,50\%,FEA,imperfect}$, which results in greater fatigue strength than without the explicit consideration by means of $\Delta\sigma_{R,nom,50\%,FEA,perfect}$.

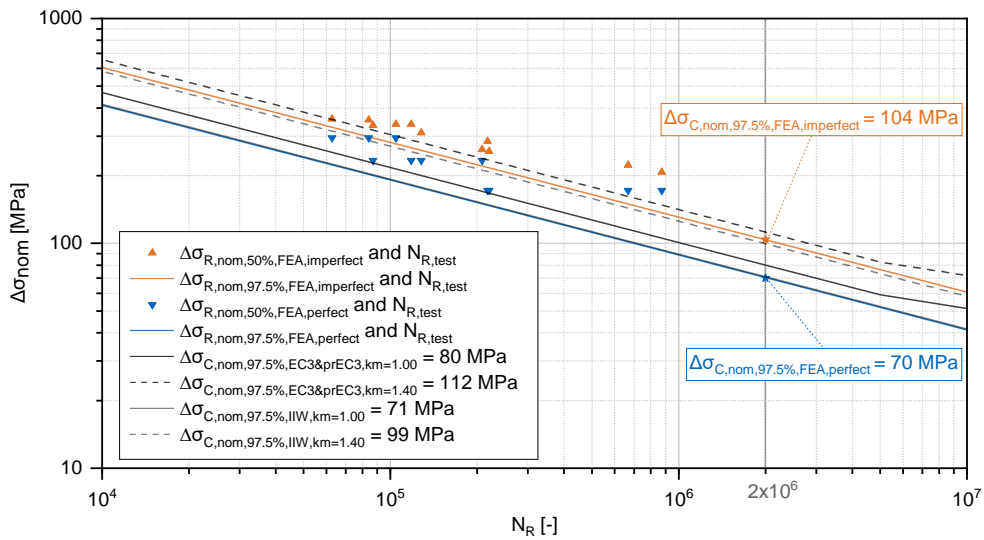


Figure 4-24: Results according to the nominal stress concept for the perfect and imperfect FE models and $N_{R,test}$ for test group $WP3_1.1$ with associated normative fatigue classes

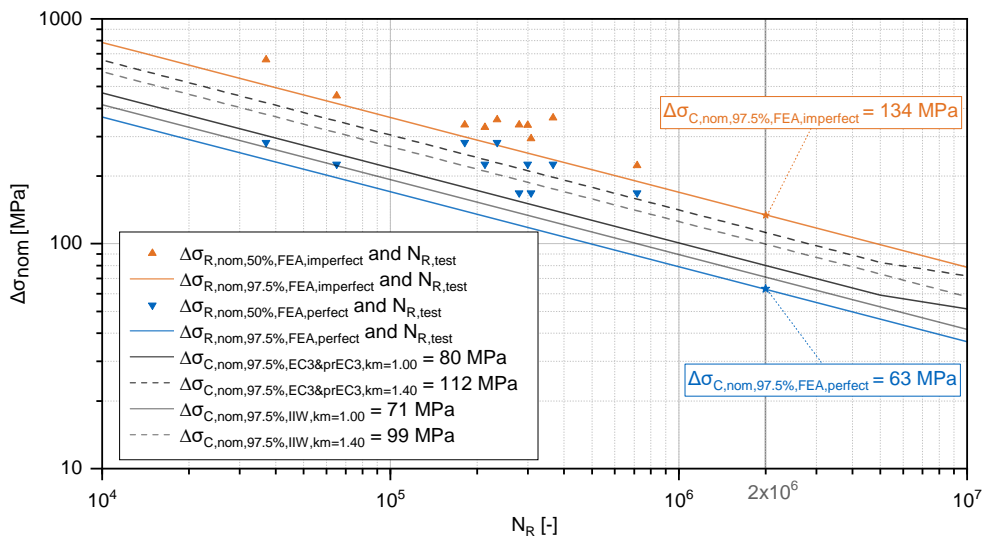


Figure 4-25: Results according to the nominal stress concept for the perfect and imperfect FE models and $N_{R,test}$ for test group $WP3_1.2$ with associated normative fatigue classes

The imperfect FE evaluation for test group $WP3_1.2$ with the explicit consideration of unintentional imperfections leads to a significantly higher fatigue strength $\Delta\sigma_{C,nom,97.5\%,FEA,imperfect} = 134 \text{ N/mm}^2$ than test group $WP3_1.1$ (cf. Figure 4-25). This is due to the larger intentional and particularly unintentional imperfections, which result in large numerical nominal stress ranges $\Delta\sigma_{R,nom,50\%,FEA,imperfect}$. Consequently, along with the experimental results for $N_{R,test}$, a high fatigue strength $\Delta\sigma_{C,nom,97.5\%,FEA,imperfect}$ is determined. This high fatigue strength indicates that despite sufficiently accurate validation of the FE models (cf. Section 4.4), there is an overestimation of the imperfect nominal stress ranges, since it cannot be expected that the test group $WP3_1.2$ with intentional imperfections has a significant higher fatigue strength than $WP3_1.1$. In contrast, the perfect fatigue strength of $\Delta\sigma_{C,nom,97.5\%,FEA,perfect} = 63 \text{ N/mm}^2$ for test group $WP3_1.2$ is lower than for $WP3_1.1$. This can especially be attributed to the test specimens $WP3_1.2_03$ and $WP3_1.2_10$, which experimentally exhibited large applied stress ranges due to their large unintentional imperfections. In this respect, these test specimens showed the largest angular misalignments of test group $WP3_1.2$ with

$\alpha_{detected} = 4.17^\circ$ and 2.86° (cf. Table 4-3). Consequently, these experimental tests resulted in low stress cycles $N_{R,test}$. However, the influences from these intentional imperfections are not considered by $\Delta\sigma_{R,nom,50\%,FEA,perfect}$, which therefore results in an underestimation of the fatigue strength. This demonstrates that the application of the perfect evaluation according to Section 4.1.1 can lead to unreliable results in the case of large imperfections, since significantly higher load cycles $N_{R,test}$ would have been expected on the basis of $\Delta\sigma_{R,nom,50\%,FEA,perfect}$. Accordingly, the relatively large difference of 71 N/mm^2 between the perfect and imperfect evaluation results in a significantly large scatter band of the test results of $WP_1.2$. To this end, since the nominal stress ranges $\Delta\sigma_{R,nom,50\%,FEA,imperfect}$ of the test specimens $WP3_1.2_03$ and $WP3_1.2_10$ with 744.67 N/mm^2 and 508.93 N/mm^2 are considerably above the yield strength, the selected approach cannot represent a realistic analysis for those experiments. For this reason, the tests $WP3_1.2_03$ and $WP3_1.2_10$ are considered as abortive tests in the further course of this thesis. The S-N curves rectified for these two test specimens are shown in Figure 4-26.

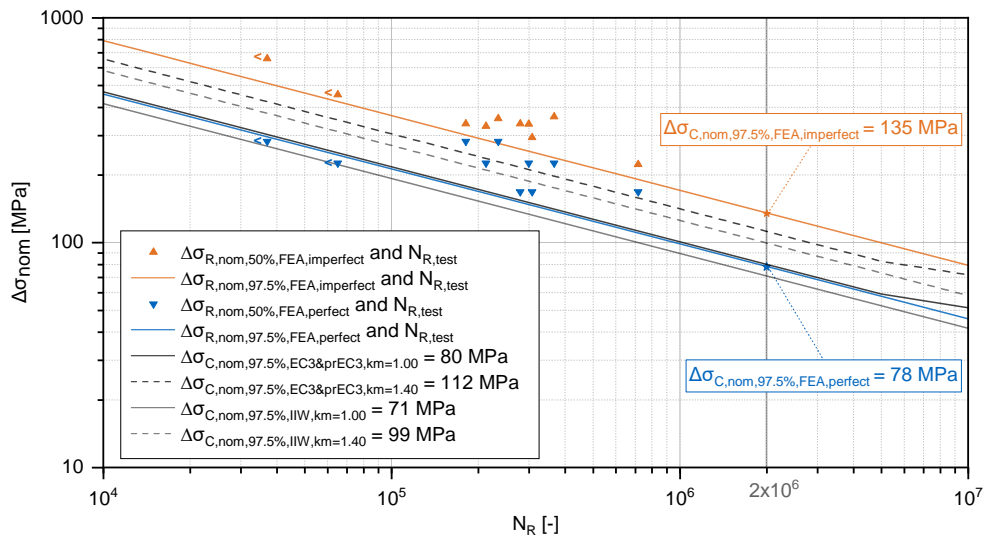


Figure 4-26: Results according to the nominal stress concept for the perfect and imperfect FE models and $N_{R,test}$ for test group $WP3_1.2$ without the abortive tests $WP3_1.2_03$ and $WP3_1.2_10$

It can be observed that the fatigue strength $\Delta\sigma_{C,nom,97.5\%,FEA,imperfect} = 135\text{ N/mm}^2$ of $WP3_1.2$ remains almost identical to that of $WP3_1.2$ with the consideration of $WP3_1.2_03$ and $WP3_1.2_10$ (cf. Figure 4-26). In contrast, the fatigue strength $\Delta\sigma_{C,nom,97.5\%,FEA,perfect} = 78\text{ N/mm}^2$ of the perfect evaluation is significantly higher than before, since the exclusion of the abortive tests leads to a smaller scatter band of the associated results. In this way, more realistic results are generated.

The S-N curves for $WP3_1$ thus indicate that the scatter band between the results for perfect FE calculations with $\Delta\sigma_{R,nom,50\%,FEA,perfect}$ and imperfect FE calculations with $\Delta\sigma_{R,nom,50\%,FEA,imperfect}$ increases with higher imperfections (cf. Figure 4-24 and Figure 4-26). This is due to the fact that with larger imperfections the resulting imperfect nominal stress ranges $\Delta\sigma_{R,nom,50\%,FEA,imperfect}$ are increasingly overestimated. The reason for this is the overestimation of the influence of imperfections, since realistic straightening effects are not considered numerically (cf. Section 4.5.3). Since the unintentional imperfections of $WP3_1.2$ are considerably larger than those of $WP3_1.1$ (cf. Table 4-3), the corresponding scatter band is significantly wider. Although larger

imperfections lead to an increase in the stress ranges $\Delta\sigma_{R,nom}$, there is an equivalent reduction in the resulting number of load cycles $N_{R,test}$. Consequently, regardless of the size of the imperfections, an approximately equal fatigue strength is generally to be expected for *WP3_1.1* and *WP3_1.2*. Thus, the realistic fatigue strengths according to the nominal stress concept are likely to be in the range between the results of the perfect and imperfect nominal stress ranges.

If the unintentional imperfections are not explicitly included in the FEA, as is the case in the evaluation of $\Delta\sigma_{R,nom,50\%,FEA,perfect}$, the uncorrected normative fatigue class 71 according to the guidelines of the IIW [3] can be satisfied by a narrow margin for both *WP3_1.1* (cf. Figure 4-24) and *WP3_1.2* (cf. Figure 4-26). In contrast, the uncorrected fatigue class 80 according to DIN EN 1993-1-9 [2] and prEN 1993-1-9 [4] can neither be confirmed for *WP3_1.1* nor for *WP3_1.2*. Consequently, the application of the nominal stress concept according to [2] and [4], without the explicit consideration of imperfections in the FEA, would be considered critical, since the fatigue classes cannot compensate for the stress-increasing effects. The lower fatigue class of the IIW [3] is therefore considered to be more reasonable than the fatigue class according to DIN EN 1993-1-9 [2] and prEN 1993-1-9 [4].

In the imperfect evaluation for $\Delta\sigma_{R,nom,50\%,FEA,imperfect}$, the fatigue strengths of *WP3_1.1* and *WP3_1.2* are higher than the corrected fatigue class 99 according to the guidelines of the IIW [3] (cf. Figure 4-24 and Figure 4-26). Thus, the corrected fatigue class also covers the large intentional imperfections $e = 0,25 \cdot t_{1=2}$ of *WP3_1.2*. This is the case even though the application limit for the nominal stress concept for cruciform joints is specified with $e < 0,15 \cdot t_{1=2}$ according to the guidelines [3]. With regard to the specifications from DIN EN 1993-1-9 [2] and prEN 1993-1-9 [4], the corrected fatigue class 112 can only be complied with in test group *WP3_1.2*. However, normative application limits of $e < 0,15 \cdot t_3$ are specified in this respect, which are only satisfied by the test specimens of test group *WP3_1.1*. Consequently, the specifications on considered imperfections according to DIN EN 1993-1-9 [2] and prEN 1993-1-9 [4] cannot be confirmed numerically by the experimental results of test group *WP3_1.1* (cf. Figure 4-24).

To further investigate the results from the nominal stress concept, resulting stress ranges $\Delta\sigma_{R,nom,50\%}$ are correlated at stress level. For this purpose, the experimentally determined load cycles $N_{R,test}$ for *WP3_1* with the associated normative fatigue classes $\Delta\sigma_{C,nom,50\%}$ are analytically converted into stress ranges $\Delta\sigma_{R,nom,50\%}$. The conversion is performed according to formula (2-1). In this context, the fatigue strengths $\Delta\sigma_{C,nom,97.5\%}$ of the normative regulations DIN EN 1993-1-1 [2] and prEN 1993-1-9 [4] as well as the guidelines of the IIW [3] are calculated to a survival probability of $P_s = 50\%$. The evaluation is performed separately for $\Delta\sigma_{R,nom,50\%,FEA,perfect}$ (cf. Figure 4-27) and $\Delta\sigma_{R,nom,50\%,FEA,imperfect}$ (cf. Figure 4-28). According to Section 4.5.1.1, the results of the perfect evaluation are compared with the uncorrected normative fatigue classes. In contrast, the imperfect evaluation is analysed with the described stress concentration factors k_m (cf. Table 4-8). These are applied to increase the fatigue classes according to DIN EN 1993-1-9 [2], IIW [3] and prEN 1993-1-9 [4] by the already considered influences with regard to imperfections. The respective keys in Figure 4-27 and Figure 4-28 provide the corresponding corrections.

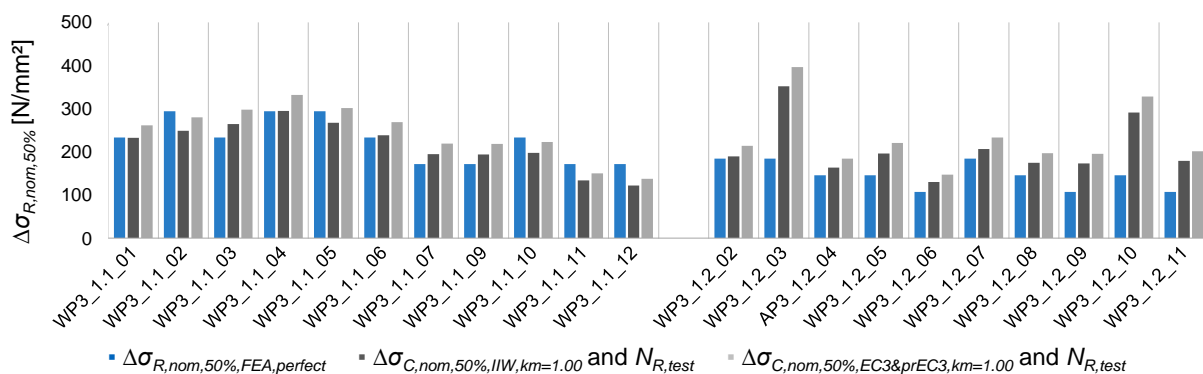


Figure 4-27: Evaluation of the numerically determined perfect nominal stress $\Delta\sigma_{R,nom,50\%,FEA,perfect}$ of the test specimens of test series $WP3_1$ in comparison to analytically determined uncorrected stress ranges of the nominal stress concept according to the normative regulations and guidelines

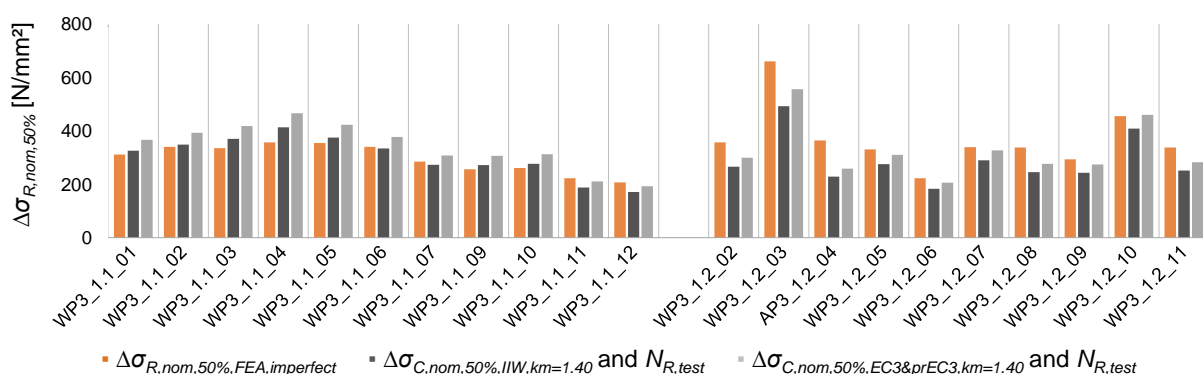


Figure 4-28: Evaluation of the numerically determined imperfect nominal stress $\Delta\sigma_{R,nom,50\%,FEA,imperfect}$ of the test specimens of test series $WP3_1$ in comparison to analytically determined corrected stress ranges of the nominal stress concept according to the normative regulations and guidelines

According to Figure 4-27 and Figure 4-28, there is generally good correlation between the uncorrected normative stress ranges and $\Delta\sigma_{R,nom,50\%,FEA,perfect}$ as well as between the corrected normative stress ranges and $\Delta\sigma_{R,nom,50\%,FEA,imperfect}$. In this respect, the results according to the guidelines of the IIW [3] provide better conformity than those of DIN EN 1993-1-9 [2] and prEN 1993-1-9 [4] in the majority of cases. However, Figure 4-27 illustrates that the perfect nominal stress ranges $\Delta\sigma_{R,nom,50\%,FEA,perfect}$ of most specimen somewhat underestimate the stress ranges calculated analytically and based on the uncorrected normative fatigue classes. This is especially true for test group $WP3_1.2$ with larger unintentional and intentional imperfections. The reason for this is that in terms of $\Delta\sigma_{R,nom,50\%,FEA,perfect}$ the unintentional imperfections are not considered. Consequently, the experimental results are underestimated. In contrast, the evaluation of the imperfect nominal stress ranges $\Delta\sigma_{R,nom,50\%,FEA,imperfect}$ of test group $WP3_1.2$ results in a uniform overestimation of the normative stress ranges corrected by the stress concentration factor k_m . As a consequence, it can be assumed that the applied imperfections numerically lead to an overestimation of the experimental stresses. Furthermore, it is again evident that $WP3_1.2_03$ and $WP3_1.2_{10}$ must be considered as abortive tests, since the perfect nominal stress ranges are clearly underestimated (cf. Figure 4-27) and the imperfect nominal stress ranges are overestimated (cf. Figure 4-28).

4.5.1.2.2 WP3_2

In accordance with Section 4.5.1.2.1, the evaluations of WP3_2.1 (cf. Figure 4-29) and WP3_2.2 including WP3_2.2NL (cf. Figure 4-30) are presented separately below.

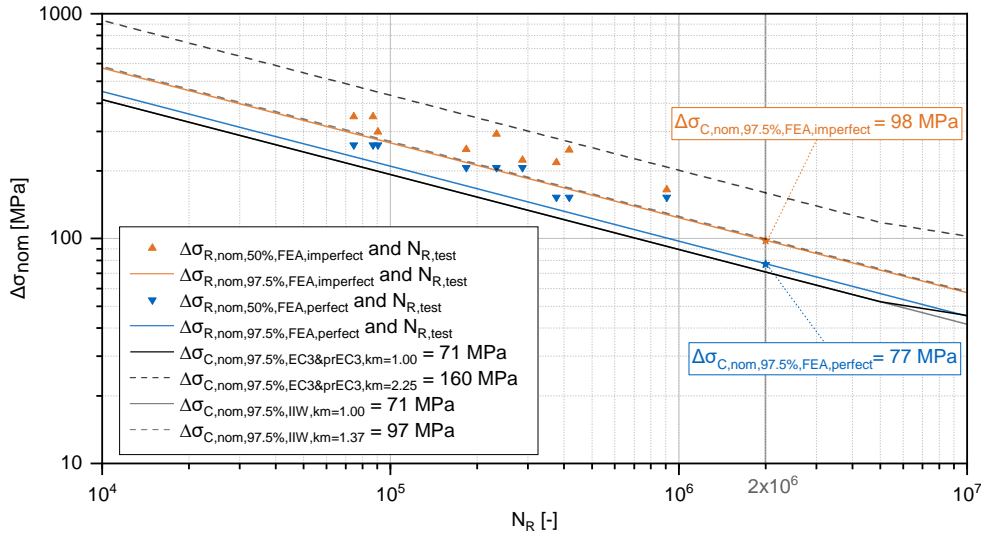


Figure 4-29: Results according to the nominal stress concept for the perfect and imperfect FE models and $N_{R,test}$ for test group WP3_2.1 with associated normative fatigue classes

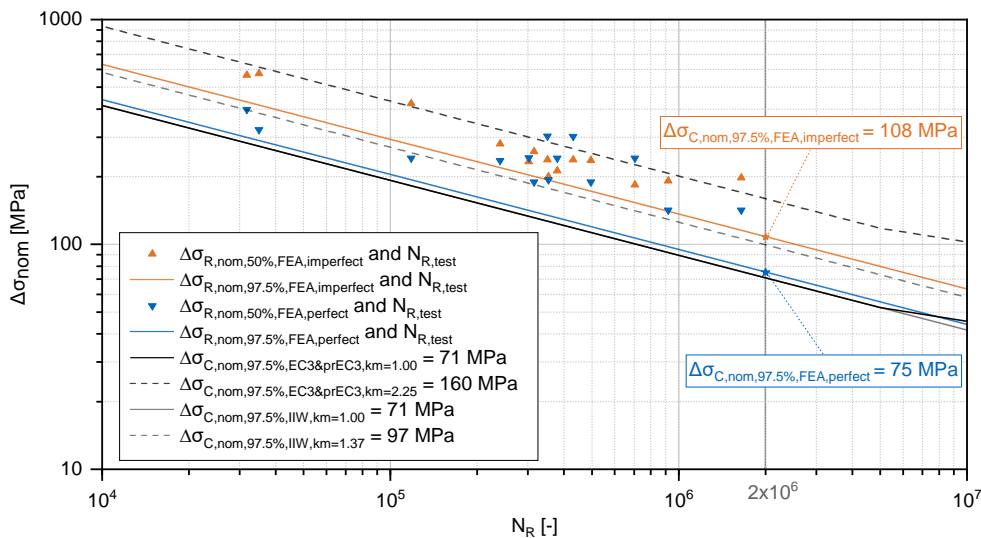


Figure 4-30: Results according to the nominal stress concept for the perfect and imperfect FE models and $N_{R,test}$ for test groups WP3_2.2 and WP3_2.2NL with associated normative fatigue classes

The results of test series WP3_2 (cf. Figure 4-29 and Figure 4-30) display similar behaviour to the S-N curves of test series WP3_1 (cf. Figure 4-24 and Figure 4-26). Whereas a fatigue strength of $\Delta\sigma_{C,nom,97.5\%,FEA,perfect} = 77 \text{ N/mm}^2$ is calculated for test group WP3_2.1 with perfect nominal stress ranges, a fatigue strength of $\Delta\sigma_{C,nom,97.5\%,FEA,imperfect} = 98 \text{ N/mm}^2$ is determined when evaluating the imperfect nominal stress ranges. In contrast, the perfect fatigue strength $\Delta\sigma_{C,nom,97.5\%,FEA,perfect}$ for WP3_2.2 with intentional imperfections is smaller with 75 N/mm^2 and the imperfect fatigue strength is larger with $\Delta\sigma_{C,nom,97.5\%,FEA,imperfect} = 108 \text{ N/mm}^2$ than for WP3_2.1. Consequently, there is a greater discrepancy between the nominal stress ranges of the perfect and imperfect FE models for the cruciform joints of WP3_2.2 with 33 N/mm^2 than for the test group WP3_2.1 with 21 N/mm^2 . This is due to the unconsidered

imperfections in the evaluation with $\Delta\sigma_{R,nom,50\%,FEA,perfect}$, which result in a larger scatter band with increasing imperfections. The resulting fatigue strengths of *WP3_2* (cf. Figure 4-29 and Figure 4-30) are also slightly lower than those of *WP3_1* (cf. Figure 4-24 and Figure 4-26). Consequently, compared to the *WP3_1* test series, the thicker intermediate plate $t_3 = 40 \text{ mm}$ of the *WP3_2* test series indicates a reduction in fatigue strength.

In the IGF research project No. 20336N [1], the evaluation of the imperfections of the test specimens of the test group *WP3_2.2* revealed that the intended imperfections of $e \approx 0.25 \cdot t_{1=2}$ were not satisfied for all specimens (cf. Table 4-3). The intended imperfection was also not achieved with the subsequent delivery *WP3_2.2NL* for one test specimen. For this reason, only the test specimens of the *WP3_2.2* and *WP3_2.2NL* are evaluated in the following Figure 4-31, where imperfections in the intended range could be determined. These include the test specimens *WP3_2.2_06* as well as *WP3_2.2NL_02* to *WP3_2.2NL_05*. The resulting S-N curves are shown in Figure 4-31 below.

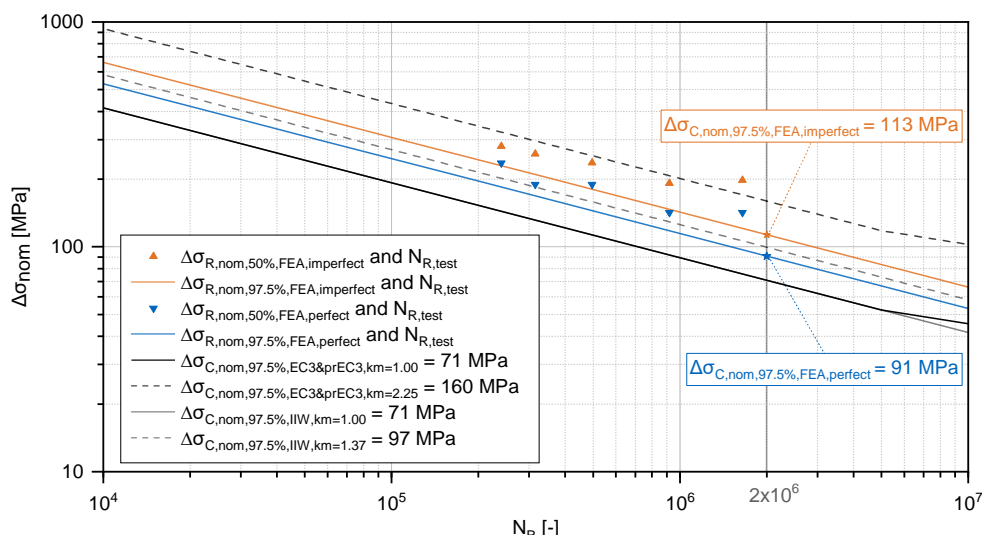


Figure 4-31: Results according to the nominal stress concept for the perfect and imperfect FE models and $N_{R,test}$ for the specimens *WP3_2.2_06* and *WP3_2.2NL_02* to *WP3_2.2NL_05* with intentional imperfections $e \approx 3 \text{ mm}$ with associated normative fatigue classes

The evaluation according to Figure 4-31 demonstrates that improved fatigue strengths are expected from both the perfect FE models with $\Delta\sigma_{C,nom,97.5\%,FEA,perfect} = 113 \text{ N/mm}^2$ and the imperfect FE models with $\Delta\sigma_{C,nom,97.5\%,FEA,imperfect} = 91 \text{ N/mm}^2$, if only test specimens with the intended axial misalignment $e \approx 3 \text{ mm}$ are evaluated. This results in a reduced scatter band with 22 N/mm^2 , which is almost identical to *WP3_2.1* (cf. Figure 4-29). Nevertheless, due to the significantly higher fatigue strengths of *WP3_2.2* (cf. Figure 4-31) compared to the test group *WP3_2.1* (cf. Figure 4-29), it must be assumed that the imperfect nominal stress ranges $\Delta\sigma_{R,nom,50\%,FEA,imperfect}$ overestimate the experimental stresses encountered in reality. Concerning this matter, the results of the evaluation according to Figure 4-31 are considered to be relevant, as the objective of the test group is to investigate intentional imperfections $e = 0.25 \cdot t_{1=2}$. The S-N curves generated with perfect nominal stress ranges $\Delta\sigma_{R,nom,50\%,FEA,perfect}$ for *WP3_2.1* (cf. Figure 4-29) and *WP3_2.2* (cf. Figure 4-31) confirm the specified uncorrected fatigue class 71 according to DIN EN 1993-1-9 [2], guidelines of the IIW

[3] and prEN 1993-1-9 [4]. However, it is noticeable in the evaluation for $WP3_2$ that the corrected fatigue classes according to DIN EN 1993-1-9 [2] and prEN 1993-1-9 [4] lead to unrealistic fatigue strengths. With the axial misalignment $e \leq 0.15 \cdot t_3$ already considered, this is due to the dependence of the stress concentration factor $k_{m,FEA}$ on the intermediate plate thickness t_3 (cf. Section 4.5.1.1). With the relatively thick intermediate plate $t_3 = 40 \text{ mm}$ compared to relatively thin welded-on plates $t_{1=2} = 12 \text{ mm}$ of test series $WP3_2$, very large imperfections are therefore permitted. Consequently, the corrected fatigue class 160 is significantly higher than the fatigue strengths achieved for the imperfect nominal stress ranges $\Delta\sigma_{R,nom,50\%,FEA,imperfect}$. Accordingly, the imperfections allegedly included by the fatigue classes do not correlate with the evaluations of $\Delta\sigma_{R,nom,50\%,FEA,imperfect}$ for $WP3_2.1$ (cf. Figure 4-29) and $WP3_2.2$ (cf. Figure 4-31). It is evident that the dependence of the stress concentration factor $k_{m,FEA}$ on the thickness of the intermediate plate t_3 leads to a significant overestimation of the feasible stress cycles. As a consequence, in the fatigue classes of the nominal stress concept for cruciform joints, imperfections are allowed which are not covered by the associated resistance side according to DIN EN 1993-1-9 [2] and prEN 1993-1-9 [4]. In contrast, the stress concentration factor $k_{m,FEA}$ according to the guidelines of the IIW [3] provides a correction that leads to reasonable conformity with the numerical results. With $e \leq 0.15 \cdot t_{1=2}$, this is attributable by the dependence of the factor on the thickness of the welded-on plates $t_{1=2}$. The associated fatigue strength of 97 can be verified by the evaluation of $\Delta\sigma_{R,nom,50\%,FEA,imperfect}$ for both $WP3_2.1$ (cf. Figure 4-29) and $WP3_2.2$ (cf. Figure 4-31). Thus, the evaluation of $WP3_2$ can also confirm that the nominal stress concept according to the IIW [3] covers stress-increasing effects of cruciform joints up to $e = 0.25 \cdot t_{1=2}$.

The following Figure 4-32 and Figure 4-33 further emphasise the previous statements. In this respect, the evaluation of the perfect and imperfect nominal stress ranges for all test specimens of $WP3_2$ is carried out according to Section 4.5.1.2.1 with $\Delta\sigma_{R,nom,50\%}$. The evaluations of the perfect nominal stress ranges $\Delta\sigma_{R,nom,50\%,FEA,perfect}$ are compared to the uncorrected fatigue classes according to DIN EN 1993-1-9 [2], guidelines of the IIW [3] and prEN 1993-1-9 [4] (cf. Figure 4-32). By contrast, the imperfect nominal stress ranges $\Delta\sigma_{R,nom,50\%,FEA,imperfect}$ are compared with the corrected normative fatigue classes according to Section 4.5.1.1 (cf. Figure 4-33).

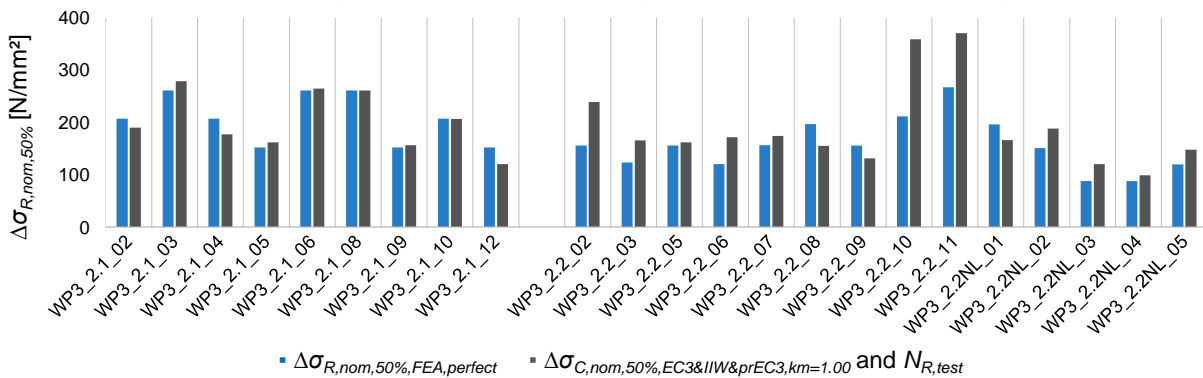


Figure 4-32: Evaluation of the numerically determined perfect nominal stress $\Delta\sigma_{R,nom,50\%,FEA,perfect}$ of the test specimens of test series $WP3_2$ in comparison to analytically determined uncorrected stress ranges of the nominal stress concept according to the normative regulations and guidelines

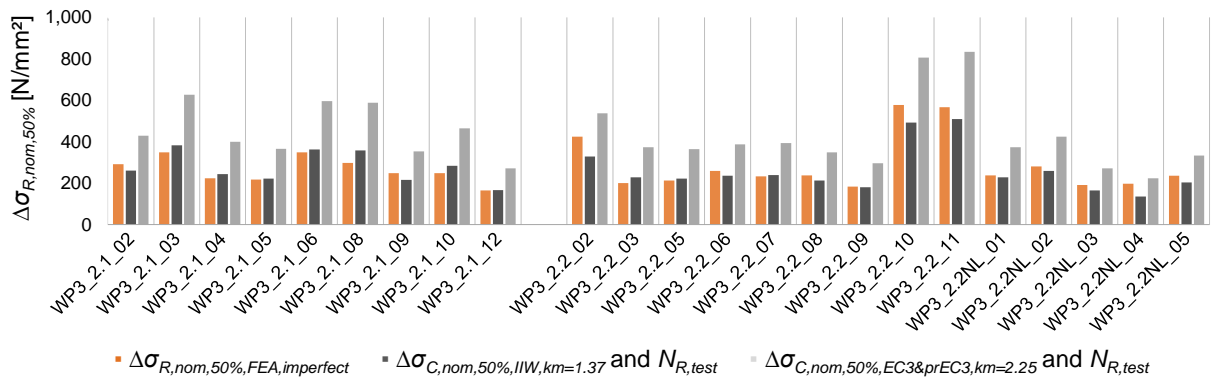


Figure 4-33: Evaluation of the numerically determined imperfect nominal stress $\Delta\sigma_{R,nom,50\%,FEA,imperfect}$ of the test specimens of test series $WP3_2$ in comparison to analytically determined uncorrected stress ranges of the nominal stress concept according to the normative regulations and guidelines

Figure 4-32 and Figure 4-33 confirm that the specifications according to the guidelines of the IIW [3] generally provide good conformities with the perfect and imperfect nominal stress ranges for the test series $WP3_2$. However, for the specimens of $WP3_2.2$ with intentional imperfections $e = 0.25 \cdot t_{1=2}$, the evaluations of $\Delta\sigma_{R,nom,50\%,FEA,perfect}$ leads to an underestimation of the uncorrected normative stress ranges (cf. Figure 4-32), as unintentional imperfections are not explicitly considered. In contrast, the imperfect nominal stress ranges $\Delta\sigma_{R,nom,50\%,FEA,imperfect}$ overestimate the corrected normative stress ranges of the IIW [3] (cf. Figure 4-33), indicating an excessive influence of the detected imperfections on the numerics. It can also be shown that the correction of the fatigue classes according to DIN EN 1993-1-9 [2] and prEN 1993-1-9 [4] leads to unrealistic stress ranges in the $WP3_2$ test series (cf. Figure 4-33). The associated fatigue classes cannot be confirmed by the numerically determined imperfect nominal stress ranges $\Delta\sigma_{R,nom,50\%,FEA,imperfect}$. Consequently, the approach according to the guidelines of the IIW [3] is considered much more reasonable.

4.5.1.2.3 WP3_3

The results for test series $WP3_2$ according to the nominal stress concept are shown separately below for $WP3_3.1$ (cf. Figure 4-34) and for $WP3_2$ (cf. Figure 4-35).

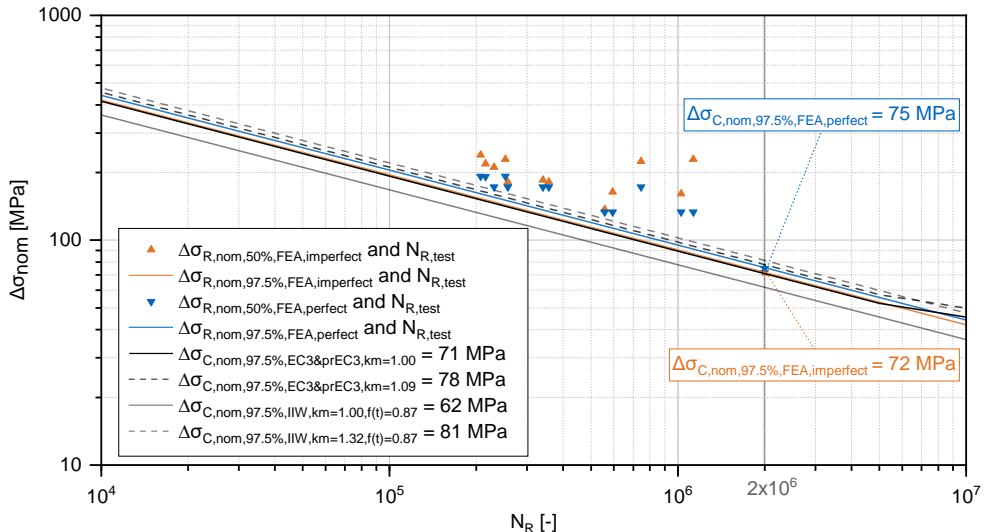


Figure 4-34: Results according to the nominal stress concept for the perfect and imperfect FE models and $N_{R,test}$ for test group $WP3_3.1$ with associated normative fatigue classes

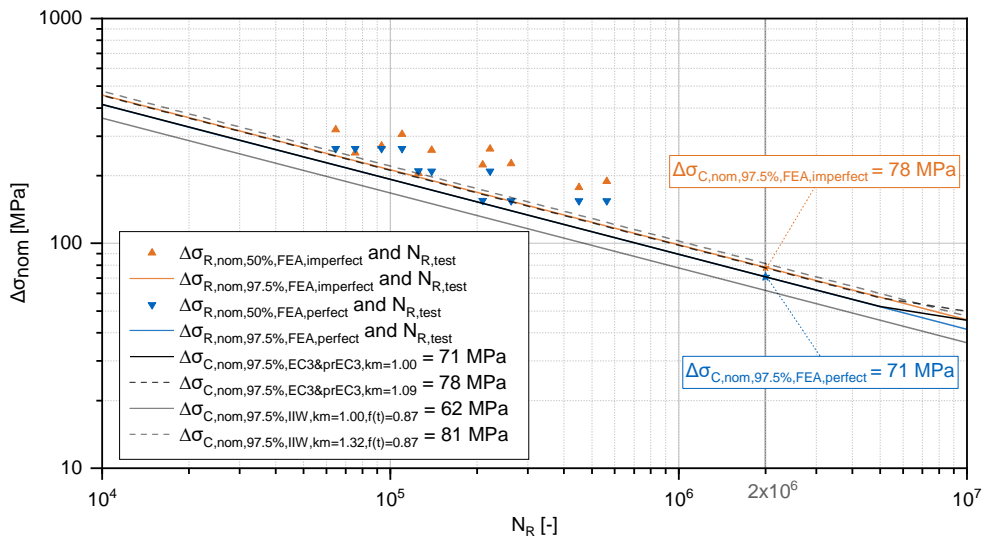


Figure 4-35: Results according to the nominal stress concept for the perfect and imperfect FE models and $N_{R,test}$ for test group $WP3_3.2$ with associated normative fatigue classes

In contrast to the test specimens of $WP3_1$ and $WP3_2$, the nominal stress ranges determined on perfect and imperfect FE models of $WP3_3$ are significantly more similar (cf. Figure 4-34 and Figure 4-35) and thus result in very small scatter bands between the fatigue strength curves. Consequently, the influence from unintentional imperfections in the nominal stress concept seems to be considerably lower for thicker welded-on plates than for thinner plate thicknesses $t_{1=2}$. Furthermore, the results for $\Delta\sigma_{R,nom,50\%,FEA,perfect}$ with respect to $WP3_3.1$ provide a slightly higher fatigue strength than the evaluation of $\Delta\sigma_{R,nom,50\%,FEA,imperfect}$. This can be attributed to the deviating gradient of the S-N curves. The fixed gradient of $m = 3$ consequently results in a wider scatter band of the test results, which would lead to significantly higher strengths if the gradient of the S-N curve was increased. It is also noticeable that the fatigue strength for $\Delta\sigma_{R,nom,50\%,FEA,imperfect}$ of the $WP3_3.2$ test group with intentional imperfections $e = 0.25 \cdot t_{1=2}$ provides slightly higher fatigue strengths than those of $WP3_3.1$ without intentional axial misalignment. Figure 4-34 and Figure 4-35 demonstrate that the normative uncorrected fatigue classes 71 according to DIN EN 1993-1-9 [2] and prEN 1993-1-9 [4] can be satisfied by the evaluation of $\Delta\sigma_{R,nom,50\%,FEA,perfect}$. Due to the large plate thicknesses of the welded-on plates $t_{1=2} = 40 \text{ mm}$, the thickness correction factor $f(t)$ has to be determined according to Table 4-9 and is to be applied to the normative fatigue strength. However, in the nominal stress concept, this thickness correction is only specified in the guidelines of the IIW [3]. In this respect, it is evident that the IIW [3] fatigue class 62 corrected for the thickness effect is significantly inferior to the numerically determined S-N curves. On the other hand, the evaluations for $\Delta\sigma_{R,nom,50\%,FEA,imperfect}$ can only be barely complied with by the corrected fatigue classes according to the DIN EN 1993-1-9 [2], IIW [3] and prEN 1993-1-9 [4] (cf. Figure 4-34 and Figure 4-35).

In order to provide a better understanding of the achievable stress ranges $\Delta\sigma_{R,nom,50\%}$ for test series $WP3_3$, Figure 4-36 and Figure 4-37 show the analytically determined values of the perfect and imperfect evaluation of all test specimens. In this respect, the perfect nominal stress ranges $\Delta\sigma_{R,nom,50\%,FEA,perfect}$ are related to the uncorrected fatigue classes and the imperfect nominal stress ranges $\Delta\sigma_{R,nom,50\%,FEA,imperfect}$ are

compared to the corrected fatigue classes according to the normative regulations and guidelines.

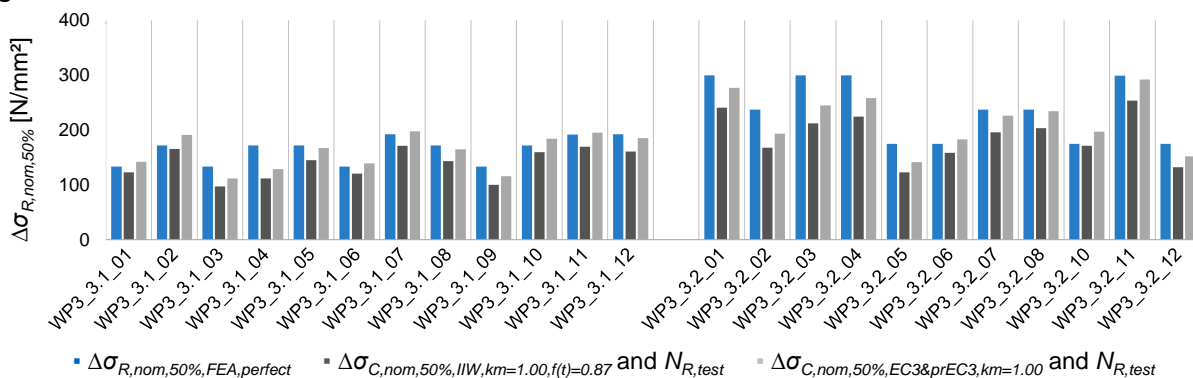


Figure 4-36: Evaluation of the numerically determined perfect nominal stress $\Delta\sigma_{R,nom,50\%,FEA,perfect}$ of the test specimens of test series $WP3_3$ in comparison to analytically determined uncorrected stress ranges of the nominal stress concept according to the normative regulations and guidelines

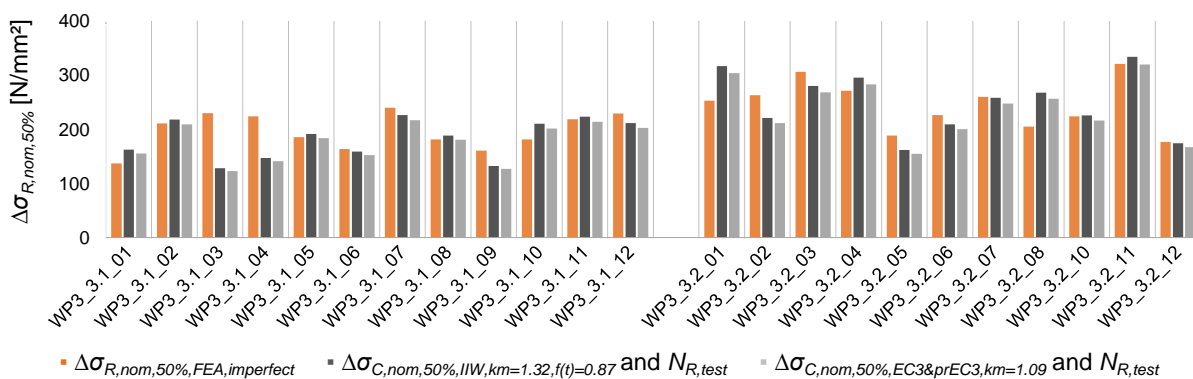


Figure 4-37: Evaluation of the numerically determined imperfect nominal stress $\Delta\sigma_{R,nom,50\%,FEA,imperfect}$ of the test specimens of test series $WP3_3$ in comparison to analytically determined uncorrected stress ranges of the nominal stress concept according to the normative regulations and guidelines

In general, there is a relatively good correlation between the numerically determined perfect and imperfect nominal stress ranges and the analytically determined results (cf. Figure 4-36 and Figure 4-37) based on the normative fatigue strengths $\Delta\sigma_{C,nom,50\%}$ and experimentally obtained load cycles $N_{R,test}$. However, it is noticeable that the perfect evaluation for $WP3_3.2$ overestimates the normative uncorrected fatigue classes (cf. Figure 4-36), which is neither the case for $WP3_1$ nor for $WP3_2$. In this respect, the omitted consideration of unintentional imperfections by $\Delta\sigma_{R,nom,50\%,FEA,perfect}$ seems to overestimate the normative values based on $N_{R,test}$ due to the large intentional axial misalignment of $WP3_3$. In addition, both Figure 4-36 for the perfect nominal stress ranges $\Delta\sigma_{R,nom,50\%,FEA,perfect}$ and Figure 4-37 for the imperfect nominal stress ranges $\Delta\sigma_{R,nom,50\%,FEA,imperfect}$ indicate that the thickness correction in the nominal stress concept according to the guidelines of the IIW [3] tends to lead to a deterioration of the verification. In this regard, better agreements are achieved with both the uncorrected fatigue classes (cf. Figure 4-36) and corrected fatigue classes (cf. Figure 4-37) according to DIN EN 1993-1-9 [2] and prEN 1993-1-9 [4]. Consequently, the necessity of a thickness correction of cruciform joints with plate thicknesses $t_{1=2} > t_{ref} = 25 \text{ mm}$ cannot be confirmed by the fatigue tests of $WP3_3.1$. Nevertheless, due to the dependence of $k_{m,FEA}$ on the thickness of the welded-on plates $t_{1=2}$ according to the IIW [3], the resulting stress concentration factor $k_{m,FEA} = 1.32$ leads to a significantly

larger correction of the normative fatigue strengths than with $k_{m,FEA} = 1.09$ according to DIN EN 1993-1-9 [2] and prEN 1993-1-9 [4]. In this respect, the thickness correction in the test specimens of $WP3_3.2$ is required to ensure a good agreement between the values of IIW [3] and the results of the imperfect nominal stress ranges $\Delta\sigma_{R,nom,50\%,FEA,imperfect}$.

4.5.1.3 Summary

In summary, the resulting fatigue strengths of the S-N curves for the nominal stress concept for the perfect evaluation with $\Delta\sigma_{R,nom,50\%,FEA,perfect}$ are presented in Figure 4-38. The results are compared with the uncorrected fatigue classes according to DIN EN 1993-1-9 [2], guidelines of the IIW [3] and prEN 1993-1-9 [4]. In this respect, for test series $WP3_3$, thickness effects are considered in the nominal stress concept according to the guidelines of the IIW [3].

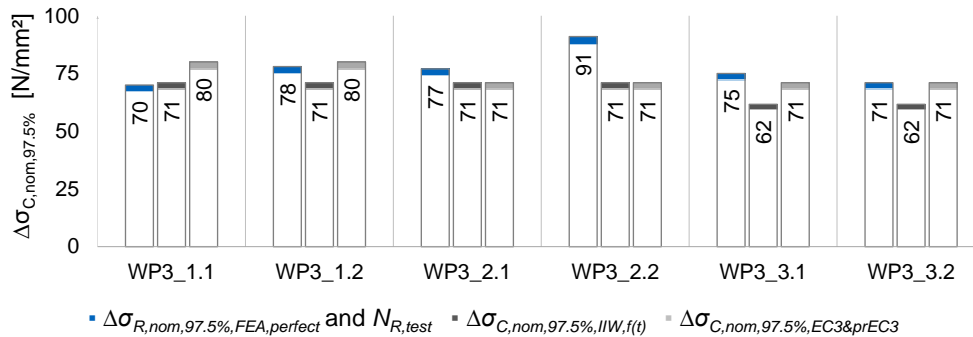


Figure 4-38: Fatigue strengths for $WP3$ following the S-N curves according to the nominal stress concept for the perfect FE models and experimentally determined load cycle numbers $N_{R,test}$ with associated uncorrected normative fatigue classes

Figure 4-38 indicates that, despite the general absence of information on imperfections in the design phase of structures, the nominal stress concept is capable of providing realistic fatigue strengths for the investigated cruciform joints. To this end, the evaluation of the perfect nominal stress ranges $\Delta\sigma_{R,nom,50\%,FEA,perfect}$ for test series $WP3_1$ leads to a fatigue strength that is in better agreement with the fatigue class according to the guidelines of the IIW [3] than with those according to DIN EN 1993-1-9 [2] and prEN 1993-1-9 [4] (cf. Figure 4-38). Therefore, the fatigue class 71 according to the IIW [3] is more appropriate for test series $WP3_1$ than the classification 80 according to DIN EN 1993-1-9 [2] and prEN 1993-1-9 [4]. The evaluations of the perfect nominal stress ranges for test series $WP3_2$ and $WP3_3$ also prove to be better than the fatigue strengths specified by the standards for the nominal stress concept (cf. Figure 4-38). However, with the exception of test group $WP3_2.2$, these are not sufficiently better to justify a higher fatigue class. Since only five cruciform joints with an intended axial misalignment $e = 0.25 \cdot t_{1=2}$ are considered in the evaluation of $WP3_2.2$, it is questionable how statistically valid the results are. In contrast, when evaluating all cruciform joints for $WP3_2.2$, the fatigue strength would be significantly lower with $\Delta\sigma_{C,nom,50\%,FEA,perfect} = 75 \text{ N/mm}^2$ and in the range of the normative fatigue classes. Furthermore, it is noticeable that the consideration of the thickness effect in test series $WP3_3$ according to [3] provides rather conservative fatigue strengths. The recommended thickness correction can therefore not be verified by the fatigue tests of $WP3_3$ (cf. Figure 4-38).

Accordingly, all test series of *WP3* are within the range of the normatively specified fatigue strengths. Thus, the nominal stress concept according to DIN EN 1993-1-9 [2], guidelines of the IIW [3] and prEN 1993-1-9 [4] provides highly economical fatigue classes for cruciform joints. In the evaluation on structural stresses (cf. Section 4.5.2), there should therefore be rather no potential to realise more economical results than in the nominal stress concept.

In addition, the evaluation of the fatigue strengths for the imperfect FE models with $\Delta\sigma_{R,nom,50\%,FEA,imperfect}$ is summarised in Figure 4-39 below. In this respect, the results are compared to the fatigue classes corrected by the stress concentration factors $k_{m,FEA}$ according to the DIN EN 1993-1-9 [2], IIW [3] and prEN 1993-1-9 [4]. The specified thickness correction of the fatigue classes for test series *WP3_3* is again applied according to the guidelines of the IIW [3].

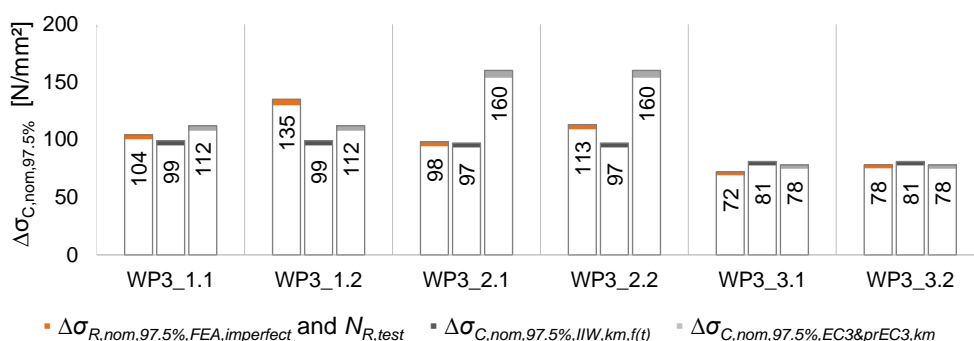


Figure 4-39: Fatigue strengths for *WP3* following the S-N curves according to the nominal stress concept for the imperfect FE models and experimentally determined load cycle numbers $N_{R,test}$ with associated corrected normative fatigue classes

In the summarised evaluation from Figure 4-39, it is noticeable how differently normative regulations and guidelines provide information on already considered imperfections in the associated cruciform joint fatigue classes. Due to the contradictory specifications, significantly different fatigue strengths result according to the guidelines of the IIW [3] compared to DIN EN 1993-1-9 [2] and prEN 1993-1-9 [4]. Only in test series *WP3_1* is the difference in the normative fatigue classes attributable to the respective fatigue class, since the stress concentration factor $k_{m,FEA}$ is identical. This is due to the equal plate thickness of the welded-on plates $t_{1=2}$ and intermediate plate t_3 . In this respect, the evaluation of test group *WP3_1.1* for imperfect nominal stress ranges $\Delta\sigma_{R,nom,50\%,FEA,imperfect}$ indicates again that the lower fatigue class 71 according to the IIW [3] provides more reasonable results than fatigue class 80 according to DIN EN 1993-1-9 [2] and prEN 1993-1-9 [4] (cf. Figure 4-39). In contrast, the fatigue strength of $\Delta\sigma_{R,nom,50\%,FEA,imperfect}$ for test series *WP3_1.2* is significantly higher than the normative corrected fatigue classes. Since the results are significantly larger than the normative fatigue classes according to the DIN EN 1993-1-9 [2], IIW [3] and prEN 1993-1-9 [4], there is a risk that the nominal stress ranges $\Delta\sigma_{R,nom,50\%,FEA,imperfect}$ might be overestimated by the imperfect FE models. Consequently, in combination with the experimentally obtained load cycles $N_{R,test}$, excessive fatigue strengths are generated. The same applies to test series *WP3_2.2* (cf. Figure 4-39). Furthermore, due to the dependence of the stress concentration factor $k_{m,FEA}$ on the intermediate plate thickness t_3 , the fatigue strength of 160 N/mm^2 for test series *WP3_2* is clearly

overstated according to DIN EN 1993-1-9 [2] and prEN 1993-1-9 [4]. The evaluation of the imperfect nominal stress ranges $\Delta\sigma_{R,nom,50\%,FEA,imperfect}$ is therefore significantly lower and indicates that considerably smaller imperfections are considered in the corresponding fatigue classes. In this respect, the fatigue resistance according to the guidelines of the IIW [3] is in a range that can be confirmed by $\Delta\sigma_{R,nom,50\%,FEA,imperfect}$ for the tested specimens of test series $WP3_2$. By the evaluation of the imperfect nominal stress ranges for the test series $WP3_3$, good accordance with the normative corrected fatigue classes can be achieved. In contrast to the $WP3_2$ test series, $WP3_3$ results in similar corrected fatigue classes for the normative regulations and guidelines (cf. Figure 4-39). To this end, due to different stress concentration factors $k_{m,FEA}$ (cf. Table 4-8), this is a result of the thickness correction factor $f(t)$ (cf. Table 4-9), which is to be applied in the nominal stress concept according to the IIW [3]. Otherwise, the fatigue strength would be significantly overstated in accordance with the specifications of [3].

However, it should generally be noted that there should be a direct correlation between the fatigue strengths of test groups $WP3_1.1$, $WP3_2.1$ and $WP3_3.1$ without intentional imperfections to the test groups $WP3_1.2$, $WP3_2.2$ and $WP3_3.2$ with intentional axial misalignment $e = 0.25 \cdot t_{1=2}$. Apart from the partly intentional axial misalignments, this is a consequence of the uniform geometry, fabrication and choice of material. Although larger stress ranges $\Delta\sigma_{R,nom,50\%,FEA}$ are expected with increased imperfections, they experimentally also result in a lower number of load cycles $N_{R,test}$. Consequently, within each of the respective test series $WP3_1$, $WP3_2$ and $WP3_3$, an almost equivalent fatigue strength $\Delta\sigma_{C,nom,97.5\%,FEA}$ should result, provided the evaluation method is accurate. In the evaluations of perfect nominal stress ranges $\Delta\sigma_{R,nom,50\%,FEA,perfect}$, this hypothesis can be verified approximately for all test series $WP3_1$, $WP3_2$ and $WP3_3$ (cf. Figure 4-38). According to Figure 4-39, the same applies for test series $WP3_3$ to the evaluation of imperfect nominal stress ranges $\Delta\sigma_{R,nom,50\%,FEA,imperfect}$. On the contrary, the fatigue strengths of the imperfect evaluation for test groups $WP3_1.2$ and $WP3_2.2$ with intentional imperfections are greater than those of test groups $WP3_1.1$ and $WP3_2.1$ without intentional imperfections (cf. Figure 4-39). This indicates that the effects from imperfections on thicker welded-on plates $t_{1=2}$ are less decisive. Nevertheless, it has to be considered that the evaluation method for imperfect nominal stress ranges $\Delta\sigma_{R,nom,50\%,FEA,imperfect}$ provides confined practical results if thin plate thicknesses $t_{1=2}$ are present. This is due to the fact that significantly more load cycles $N_{R,test}$ resulted from the experimental tests than would be expected from the overestimated numerically determined stress cycles.

Concerning this matter, the nominal stress concept according to DIN EN 1993-1-9 [2] and prEN 1993-1-9 [4] is generally only approved for axial misalignments $e < 0.15 \cdot t_3$. With the intentional imperfections $e = 0.25 \cdot t_{1=2}$, these tolerable imperfections are exceeded for test group $WP3_1.2$ and in particular for $WP3_3.2$. On the other hand, according to the guidelines of the IIW [3], only axial misalignment $e < 0.15 \cdot t_{1=2}$ is permitted in the nominal stress concept. Therefore, the permissible imperfections of all test series with intentional imperfections are exceeded. Consequently, the associated evaluations according to the nominal stress concept are considered to be purely

theoretical. Nevertheless, in most cases, good conformities of the perfect and imperfect evaluations are found with the normative specifications.

4.5.2 Structural stress concept

Furthermore, in the following section, the fatigue tests conducted in [1] on cruciform joints are evaluated according to the structural stress concept. Therefore, the basic principle of evaluation according to the structural stress concept is presented in Section 4.5.2.1. The respective assessment is then presented separately for test series *WP3_1*, *WP3_2* and *WP3_3* in Section 4.5.2.2. Finally, Section 4.5.2.3 summarises the conclusions on the structural stress concept in relation to the fatigue tests.

4.5.2.1 Basic principle

The basic principle of evaluation for the structural stress concept is based on the assessment of the nominal stress concept (cf. Section 4.5.1.1). This is expedient to ensure comparability between the results and to allow a classification of the structural stress concept against the nominal stress concept. However, in the following section, the perfect structural stress ranges $\Delta\sigma_{R,hs,50\%,FEA,perfect}$ and imperfect structural stress ranges $\Delta\sigma_{R,hs,50\%,FEA,imperfect}$ are evaluated and compared with the normative fatigue class classifications of the structural stress concept. Consequently, both perfect and imperfect FE models are evaluated according to Section 4.1. The resulting S-N curves of the perfect evaluation only include the intentional axial misalignments of the test groups *WP3_1.2*, *WP3_2.2* and *WP3_3.2* of $e = t_{1=2}/4$, without considering manufacturing-related inaccuracies. In contrast, the imperfect evaluation considers all detected axial and angular imperfections in the FEA, including all manufacturing inaccuracies. The required number of load cycles $N_{R,test}$ are defined again by the experimentally determined cycles until crack initiation (cf. Section 4.3.2.2.2). In order to ensure consistency with the normative fatigue strengths, the determined experimental S-N curves with probability of survival of $P_s = 50\%$ are subsequently converted to $P_s = 97.5\%$ in accordance with DIN 50100 [27] (cf. Section 4.3.2.1).

The decisive fatigue resistances for the structural stress concept according to DIN EN 1993-1-9 [2], guidelines of the IIW [3] and prEN 1993-1-9 [4] are given in Table 4-10 below and are consistent with $\Delta\sigma_{C,hs,97.5\%} = 100 \text{ N/mm}^2$.

Table 4-10: Fatigue classes according to structural stress concept for the fatigue tests of *WP3* according to normative regulations and guidelines

Test series	Fatigue class $\Delta\sigma_{C,hs,97.5\%}$ [N/mm ²]		
	DIN EN 1993-1-9 [2]	Guidelines of the IIW [3]	prEN 1993-1-9 [4]
<i>WP3_1</i>	100	100	100
<i>WP3_2</i>	100	100	100
<i>WP3_3</i>	100	100	100

For the evaluation according to the structural stress concept, the linear stress extrapolation is implemented (cf. Chapter 2.3.3.1). The analysis is performed on finely meshed solid models with the attributes according to Chapter 3.3. In this respect, the

stresses in the numerical calculations are applied at the level of the actual fatigue load $\Delta F = F_{max} - F_{min}$. The resulting structural stress ranges $\Delta\sigma_{R,hs,50\%,FEA}$ are then compared with the corresponding fatigue classes.

However, imperfections already considered on the resistance side must be accounted for in the evaluations. In this respect, according to the guidelines of the IIW [3] and prEN 1993-1-9 [4], imperfections are covered to a certain extent by the resistance side. Only DIN EN 1993-1-9 [2] does not specify any influences from imperfections in the fatigue resistances. In contrast, according to prEN 1993-1-9 [4], axial misalignments $e \leq 0.15 \cdot t_3$ are tolerated in the structural stress fatigue class for cruciform joints. In accordance with the procedure for the nominal stress concept (cf. Section 4.5.1.1), the stress concentration factors $k_{m,FEA}$ for the imperfections considered in [4] are determined by numerical comparative calculations. The resulting factors $k_{m,FEA}$ are summarised in Table 4-11. In addition to the numerically determined stress concentration factors $k_{m,FEA}$, prEN 1993-1-14 [14] specifies that influences from imperfections up to a stress increase of 5 % are already covered by the fatigue classes of the structural stress concept. This corresponds to a further stress concentration factor of $k_{m,already\ covered} = 1.05$ (cf. Table 4-11). As in [14], the guidelines of the IIW [3] provide a stress concentration factor of $k_{m,already\ covered} = 1.05$ for the evaluation of cruciform joints in the structural stress concept (cf. Table 4-11).

Table 4-11: Stress concentration factors k_m due to already considered imperfections in the fatigue classes for cruciform joints of normative regulations and guidelines for the structural stress concept

Test series	DIN EN 1993-1-9 [2]	Guidelines of the IIW [3]	prEN 1993-1-9 [4] and prEN 1993-1-14 [14]	
	k_m not defined [-]	$k_{m,already\ covered}$ [-]	$k_{m,FEA}$ ($e = 0.15 \cdot t_3$) [-]	$k_{m,already\ covered}$ [-]
WP3_1	1.00	1.05	1.37	1.05
WP3_2	1.00	1.05	2.38	1.05
WP3_3	1.00	1.05	1.12	1.05

Since, according to Table 4-11, the numerically determined values $k_{m,FEA}$ are significantly higher than $k_{m,already\ covered}$, only the decisive stress concentration factors $k_{m,FEA}$ are applied in the evaluations of the structural stress concept according to prEN 1993-1-9 [4]. Furthermore, the resulting stress increase resulting from $k_{m,already\ covered} = 1.05$ from [14] would be consistent with the evaluation according to the guidelines of the IIW [3].

In order to ensure the comparability of the experimental results with the normative regulations and guidelines, both the uncorrected and the corrected normative fatigue classes are presented in the evaluations for WP3 (cf. Section 4.5.2.2). Since the evaluation of the perfect structural stress ranges $\Delta\sigma_{R,hs,50\%,FEA,perfect}$ excludes influences from unintentional imperfections on the action side, the associated S-N curves are related to the uncorrected normative fatigue resistances according to the structural stress concept. By contrast, the imperfect structural stress ranges $\Delta\sigma_{R,hs,50\%,FEA,imperfect}$ include all imperfections on the action side. Consequently, the associated results are to be compared to the corrected fatigue strength according to DIN EN 1993-1-9 [2], guidelines of the IIW [3] and prEN 1993-1-9 [4].

Due to the thick welded-on plates of *WP3_3* with $t_{1=2} = 40 \text{ mm}$, the reference thickness of $t_{ref} = 25 \text{ mm}$ for the required consideration of thickness effects is exceeded (cf. Chapter 2.6). Therefore, according to the IIW [3] and prEN 1993-1-9 [4], a thickness correction factor $f(t)$ must be applied in the structural stress concept. In this respect, only DIN EN 1993-1-9 [2] does not require any thickness correction. The corresponding correction factors are determined according to Chapter 2.6.3 and are applied to reduce the respective normative fatigue classes.

Table 4-12: Thickness concentration factor $f(t)$ of DIN EN 1993-1-9 [2], guidelines of the IIW [3] and prEN 1993-1-9 [4] according to the structural stress concept

Test series	Thickness correction factor $f(t)$ [-]		
	DIN EN 1993-1-9 [2]	Guidelines of the IIW [3]	prEN 1993-1-9 [4]
<i>WP3_1</i>	–	–	–
<i>WP3_2</i>	–	–	–
<i>WP3_3</i>	–	$f(t) = \left(\frac{25}{40}\right)^{0.3} = 0.8685$	$f(t) = \left(\frac{25}{40}\right)^{0.3} = 0.8685$

4.5.2.2 Analysis of the test series

Based on the presented procedures of Section 4.5.2.1, the results obtained by applying the structural stress concept to the fatigue tests from the IGF research project No. 20336N [1] are presented separately for the test series *WP3_1* (cf. Section 4.5.2.2.1), *WP3_2* (cf. Section 4.5.2.2.2) and *WP3_3* (cf. Section 4.5.2.2.3).

4.5.2.2.1 *WP3_1*

In the following, the resulting S-N curves for the evaluation with perfect structural stress ranges $\Delta\sigma_{R,hs,50\%,FEA,perfect}$ and imperfect structural stress ranges $\Delta\sigma_{R,hs,50\%,FEA,imperfect}$ for test series *WP3_1* are presented separately for the test groups *WP3_1.1* (cf. Figure 4-40) and *WP3_1.2* (cf. Figure 4-41).

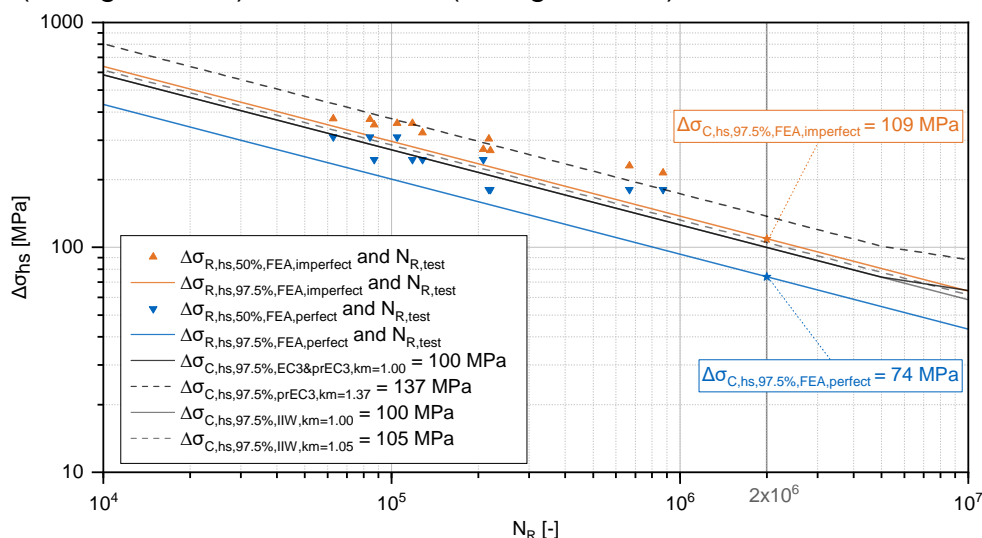


Figure 4-40: Results according to the structural stress concept for the perfect and imperfect FE models and $N_{R,test}$ for test group *WP3_1.1* with associated normative fatigue classes

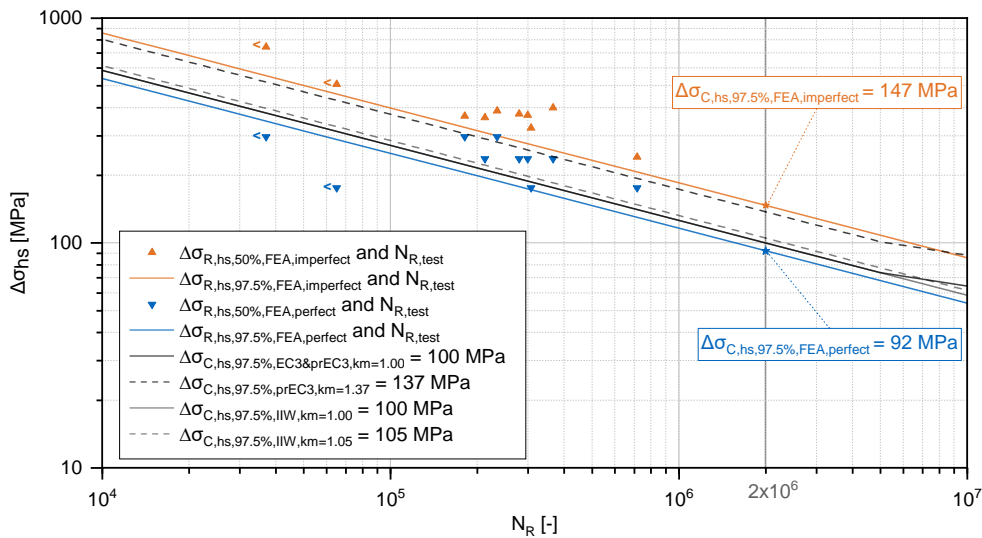


Figure 4-41: Results according to the structural stress concept for the perfect and imperfect FE models and $N_{R,test}$ for test group $WP3_1.2$ with associated normative fatigue classes

In addition to the uncorrected normative fatigue classes of DIN EN 1993-1-9 [2], IIW [3] and prEN 1993-1-9 [4], the corrected fatigue classes according to the IIW [3] and prEN 1993-1-9 [4] (cf. Section 4.5.2.1) are provided. In accordance with section 4.5.1.2.1, the experimental tests $WP3_1.2_{03}$ and $WP3_1.2_{10}$ of the test group $WP3_1.2$ are evaluated as abortive experiments and are therefore not considered in the determination of the S-N curves. For test group $WP3_1.1$ (cf. Figure 4-40), the evaluation of the perfect structural stress ranges results in a fatigue strength of $\Delta\sigma_{C,hs,97.5\%,FEA,perfect} = 74 \text{ N/mm}^2$ if unintentional imperfections are not explicitly considered in the FEA. By taking all imperfections into account, a significantly higher strength of $\Delta\sigma_{C,hs,97.5\%,FEA,imperfect} = 109 \text{ N/mm}^2$ can be determined. The same applies to the test group $WP3_1.2$, where a significantly lower fatigue strength is given by $\Delta\sigma_{C,hs,97.5\%,FEA,perfect} = 92 \text{ N/mm}^2$ than by $\Delta\sigma_{C,hs,97.5\%,FEA,imperfect} = 147 \text{ N/mm}^2$ (cf. Figure 4-41). The difference between the resulting S-N curves for perfect structural stress ranges $\Delta\sigma_{R,hs,50\%,FEA,perfect}$ and imperfect structural stress ranges $\Delta\sigma_{R,hs,50\%,FEA,imperfect}$ is thus significantly lower for test group $WP3_1.1$ with 35 N/mm^2 than for $WP3_1.2$ with 55 N/mm^2 . Consequently, corresponding to the evaluation of $WP3_1$ according to the nominal stress concept (cf. Section 4.5.1.2.1), the evaluation in the structural stress concept indicates that the resulting scatter band increases with larger imperfections. This is due to the increasing influence of the unintentional imperfections on the fatigue strength $\Delta\sigma_{C,hs,97.5\%,FEA,imperfect}$, which seems to be more significant in case of already existing intentional axial misalignment $e = 0.25 \cdot t_{1=2}$. Furthermore, the unintentional angular misalignment α is significantly larger for most specimens of test group $WP3_1.2$ than of $WP3_1.1$ (cf. Table 4-3). To this end, according to the nominal stress concept (cf. Section 4.5.1.3), it is generally expected in the structural stress concept that, depending on the selected evaluation method, equal structural stress ranges $\Delta\sigma_{C,hs,97.5\%,FEA,perfect}$ resp. $\Delta\sigma_{C,hs,97.5\%,FEA,imperfect}$ should result within the respective test series $WP3_1$, $WP3_2$ and $WP3_3$. This is based on the direct correlation between the stress ranges and the achievable number of load cycles. Therefore, with increasing imperfections, larger stress ranges $\Delta\sigma_{R,hs,50\%,FEA}$ are expected, however, experimentally these also result in a lower number of load cycles

$N_{R,test}$. Nevertheless, the fatigue strengths $\Delta\sigma_{C,hs,97.5\%,FEA,perfect}$ resp. $\Delta\sigma_{C,hs,97.5\%,FEA,imperfect}$ of the cruciform joints of test group $WP3_1.2$ are considerably larger than those of $WP3_1.1$. In contrast to the evaluation with the nominal stress concept, it is therefore evident in the structural stress concept that in addition to $\Delta\sigma_{C,hs,97.5\%,FEA,imperfect}$, $\Delta\sigma_{C,hs,97.5\%,FEA,perfect}$ also differs significantly between the test groups of the $WP3_1$ test series. This fact indicates an overestimation of the applied structural stress ranges with increasing imperfections.

Without the explicit consideration of unintentional imperfections, as is common in the design phase of constructions without exact knowledge of expected imperfections from manufacturing inaccuracies, the uncorrected normative fatigue class 100 according to DIN EN 1993-1-9 [2], guidelines of the IIW [3] and prEN 1993-1-9 [4] cannot be satisfied by the evaluation of the perfect structural stress ranges $\Delta\sigma_{R,hs,50\%,FEA,perfect}$. While the fatigue class of the structural stress concept is only missed by 8 N/mm^2 for test group $WP3_1.2$, the difference for $WP3_1.1$ amounts to a full 26 N/mm^2 . Therefore, in contrast to the investigations on perfect nominal stress ranges $\Delta\sigma_{R,nom,50\%,FEA,perfect}$ (cf. Figure 4-38), the uncorrected normative fatigue class $\Delta\sigma_{C,hs,97.5\%} = 100\text{ N/mm}^2$ cannot be verified by the evaluation of perfect structural stress ranges $\Delta\sigma_{R,hs,50\%,FEA,perfect}$ for test series $WP3_1$. This indicates an overestimated classification of the fatigue class for cruciform joints in the structural stress concept. On the other hand, the corrected normative fatigue class 105 according to the guidelines of the IIW [3] resp. prEN 1993-1-14 [14] can be complied with by the evaluations of the imperfect structural stress ranges $\Delta\sigma_{R,hs,50\%,FEA,imperfect}$ for the entire test series $WP3_1$. Due to the exclusion of influences from imperfections according to DIN EN 1993-1-9 [2], no correction of the fatigue class is feasible in this respect. Consequently, the fatigue class 100 is also satisfied by the respective test groups. In contrast, with $\Delta\sigma_{C,hs,50\%,FEA,imperfect} = 109\text{ N/mm}^2$ of test group $WP3_1.1$, the corrected fatigue class 137 according to prEN 1993-1-9 [4] cannot be validated. The specification of prEN 1993-1-9 [4] regarding the consideration of axial misalignment $e = 0.15 \cdot t_3$ is therefore not applicable.

To further investigate the results from the structural stress concept, the resulting stress ranges $\Delta\sigma_{R,hs,50\%}$ are subsequently correlated at stress level. For this purpose, the experimentally determined load cycles $N_{R,test}$ are analytically converted into stress ranges $\Delta\sigma_{R,hs,50\%}$ on the basis of the associated normative fatigue classes in the structural stress concept $\Delta\sigma_{C,hs,50\%}$. In this respect, the corresponding conversion is done according to formula (2-1). The evaluation is presented separately for the perfect structural stress ranges $\Delta\sigma_{R,hs,50\%,FEA,perfect}$ (cf. Figure 4-42) and imperfect structural stress ranges $\Delta\sigma_{R,hs,50\%,FEA,imperfect}$ (cf. Figure 4-43). According to Section 4.5.2.1, the results for perfect structural stress ranges are again compared to the uncorrected normative fatigue classes. In contrast, the evaluations of the imperfect structural stress ranges are related to the normative specifications corrected by the specified stress concentration factors k_m (cf. Table 4-12). The individual keys of Figure 4-42 and Figure 4-43 indicate the corresponding corrections.

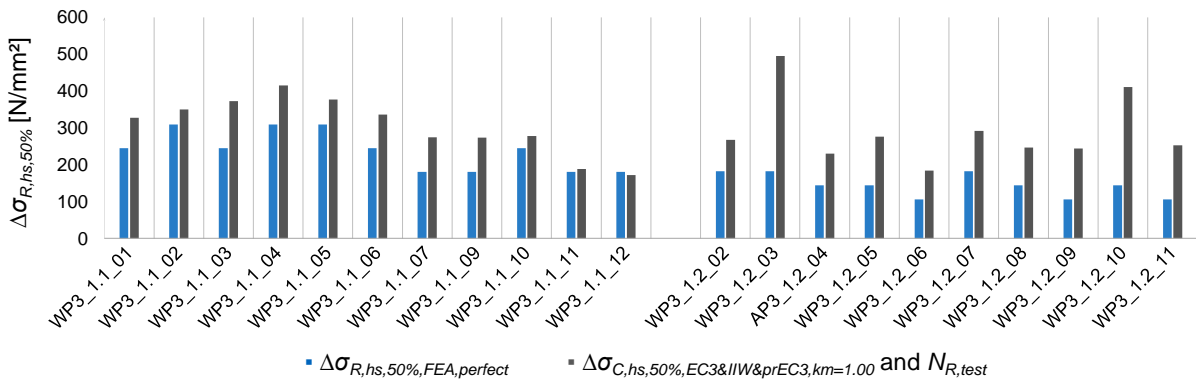


Figure 4-42: Evaluation of the numerically determined perfect structural stress $\Delta\sigma_{R,hs,50\%,FEA,perfect}$ of the test specimens of test series $WP3_1$ in comparison to analytically determined uncorrected stress ranges of the structural stress concept according to the normative regulations and guidelines

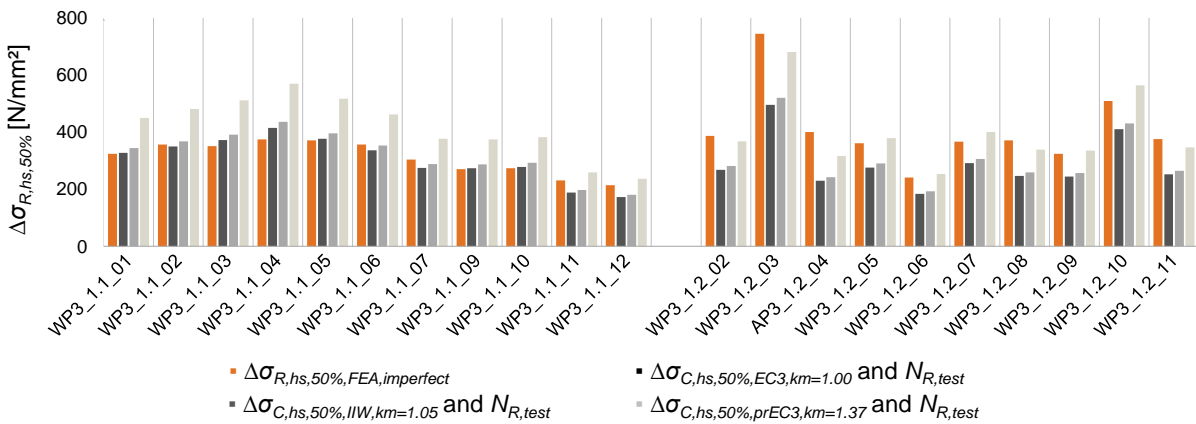


Figure 4-43: Evaluation of the numerically determined imperfect structural stress $\Delta\sigma_{R,hs,50\%,FEA,imperfect}$ of the test specimens of test series $WP3_1$ in comparison to analytically determined corrected stress ranges of the structural stress concept according to the normative regulations and guidelines

The evaluation of perfect structural stress ranges $\Delta\sigma_{R,hs,50\%,FEA,perfect}$ demonstrates that the normative expected stress ranges $\Delta\sigma_{R,hs,50\%}$ are not observed by either test group $WP3_1.1$ or $WP3_1.2$ (cf. Figure 4-42). In this respect, there is a significant underestimation of the expected stress ranges according to DIN EN 1993-1-9 [2], guidelines of the IIW [3] and prEN 1993-1-9 [4] for almost all test specimens. It can be reiterated that the test specimens $WP3_1.2_{03}$ and $WP3_1.2_{10}$ are to be evaluated as abortive tests due to their significant angular misalignments. This can be attributed to the associated low number of load cycles $N_{R,test}$, which normatively result in large expected stress ranges $\Delta\sigma_{R,hs,50\%}$. These are erroneously greater than the associated yield strength (cf. Figure 4-42). Since unintentional imperfections are neglected by the evaluation of the perfect structural stress ranges $\Delta\sigma_{R,hs,50\%,FEA,perfect}$, the stress ranges to be expected on the basis of $N_{R,test}$ can thus not be determined numerically in the structural stress concept. Since the normative fatigue classes can be satisfied in the nominal stress concept (cf. Section 4.5.1.2.1), this indicates a deficient fatigue strength in the structural stress concept.

On the other hand, the evaluation of the imperfect structural stress ranges $\Delta\sigma_{R,hs,50\%,FEA,imperfect}$ shows for test group $WP3_1.1$ that only the corrected fatigue classes 100 according to DIN EN 1993-1-9 [2] and fatigue class 105 according to the guidelines of the IIW [3] lead to a good accordance with the numerical results (cf. Figure 4-43). In this respect, the specifications according to prEN 1993-1-9 [4] result again in

a significant overestimation of the stress ranges due to the imperfections that are stated to be considered on the resistance side. In contrast, the evaluation for test group *WP3_1.2* with intentional imperfections $e = 0.25 \cdot t_{1=2}$ indicates that the specifications from DIN EN 1993-1-9 [2] and IIW [3] underestimate the numerically determined imperfect structural stress ranges $\Delta\sigma_{R,hs,50\%,FEA,imperfect}$. The corrected fatigue class 137 according to prEN 1993-1-9 [4] provides significantly better results in this regard. However, an overestimation of the imperfect structural stress ranges is to be assumed for test group *WP3_1.2*, since significantly higher fatigue strengths $\Delta\sigma_{C,hs,97.5\%,FEA,imperfect}$ are obtained than for test group *WP3_1.1*. Consequently, based on the selected evaluation method, it cannot be definitively assessed to what extent normative guidelines apply.

4.5.2.2.2 WP3_2

The evaluation of test series *WP3_2* according to the structural stress concept is presented for test group *WP3_2.1* (cf. Figure 4-44) and *WP3_2.2* (cf. Figure 4-45) below.

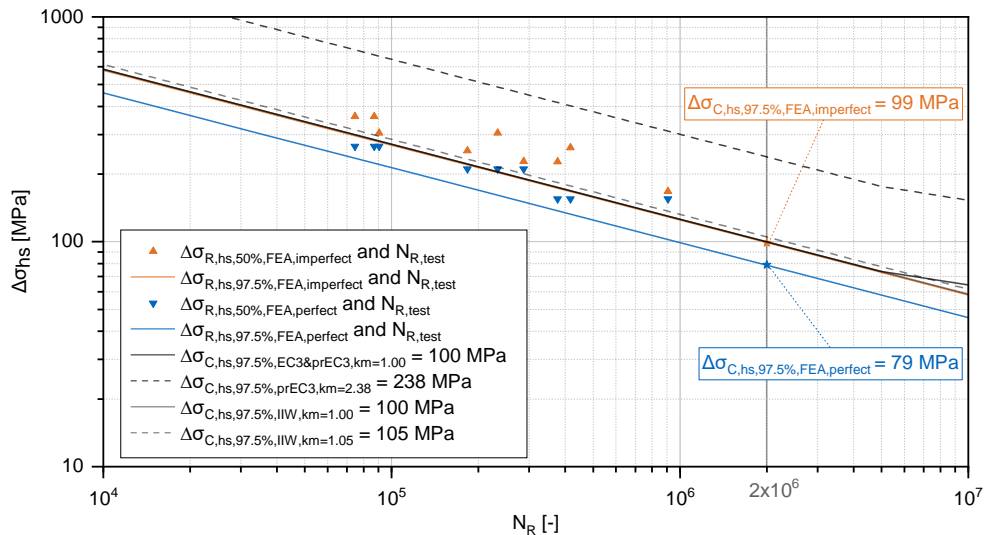


Figure 4-44: Results according to the structural stress concept for the perfect and imperfect FE models and $N_{R,test}$ for test group *WP3_2.1* with associated normative fatigue classes

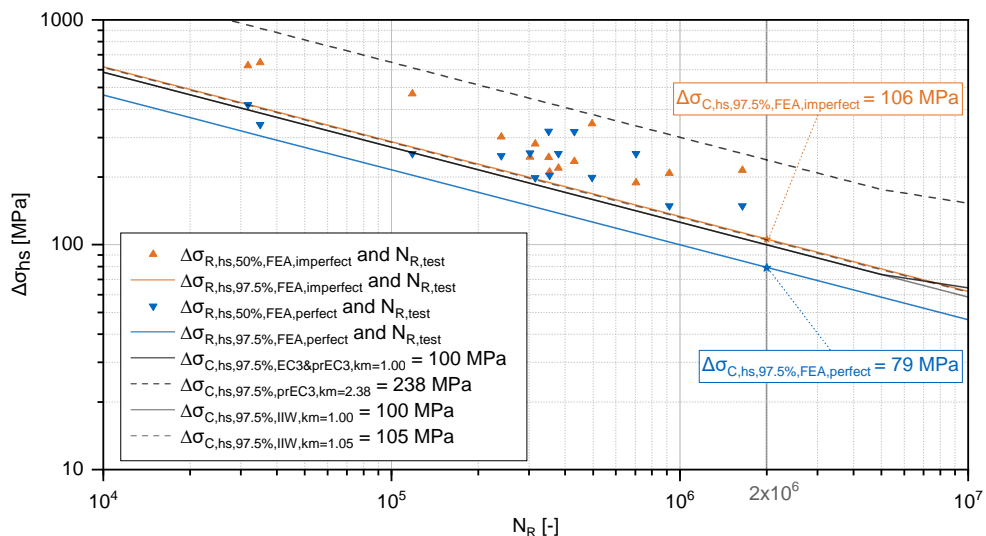


Figure 4-45: Results according to the structural stress concept for the perfect and imperfect FE models and $N_{R,test}$ for test group *WP3_2.2* and *WP3_2.2NL* with associated normative fatigue classes

According to Figure 4-44 and Figure 4-45, the evaluations of $\Delta\sigma_{R,hs,50\%,FEA,perfect}$ for the test groups $WP3_2.1$ and $WP3_2.2$ result in equal fatigue strengths of $\Delta\sigma_{C,hs,97.5\%,perfect} = 79 \text{ N/mm}^2$. In contrast, the fatigue strengths for $\Delta\sigma_{R,hs,50\%,FEA,imperfect}$ differ only slightly with $\Delta\sigma_{C,hs,97.5\%,imperfect} = 99 \text{ N/mm}^2$ for test group $WP3_2.1$ and $\Delta\sigma_{C,hs,97.5\%,imperfect} = 106 \text{ N/mm}^2$ for test group $WP3_2.2$ (cf. Figure 4-44 and Figure 4-45). This applies as long as all test specimens of test groups $WP3_2.2$ and $WP3_2.2NL$ are evaluated. However, in the IGF research project no. 20336N [1] for the test series $WP3_2.2$ and $WP3_2.2NL$, the intended axial misalignment $e \approx 0.25 \cdot t_{1=2}$ was not observed for all specimens (cf. Table 4-3). For this reason, only test specimens $WP3_2.2_06$ and $WP3_2.2NL_02$ to $WP3_2.2NL_05$ for which imperfections in the intended range could be detected are evaluated in Figure 4-46.

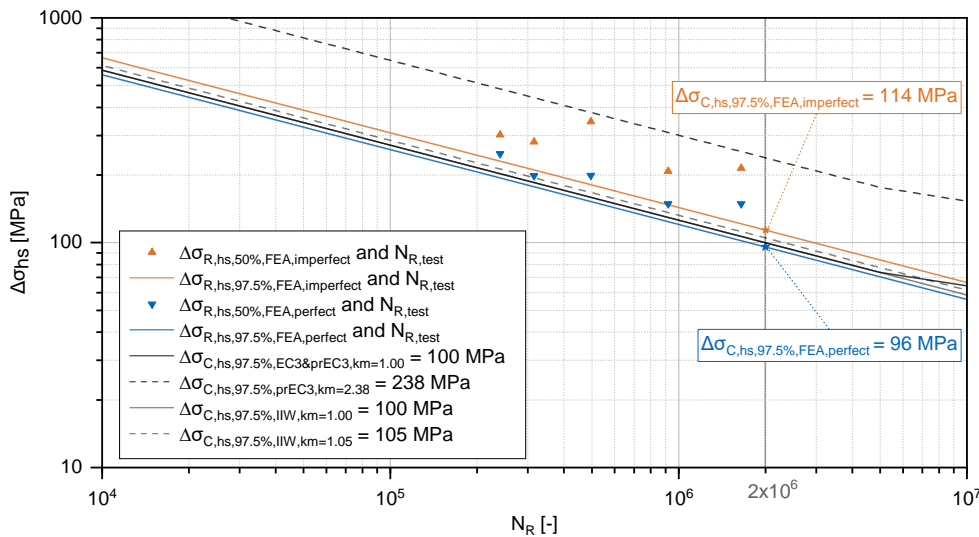


Figure 4-46: Results according to the structural stress concept for the perfect and imperfect FE models and $N_{R,test}$ for the specimens $WP3_2.2_06$ and $WP3_2.2NL_02$ to $WP3_2.2NL_05$ with intentional imperfections $e \approx 3 \text{ mm}$ with associated normative fatigue classes

By the exclusive consideration of the specimens with the intentional axial misalignment, the fatigue strengths improve both for the perfect evaluation to $\Delta\sigma_{C,hs,97.5\%,perfect} = 96 \text{ N/mm}^2$ and for the imperfect evaluation to $\Delta\sigma_{C,hs,97.5\%,imperfect} = 114 \text{ N/mm}^2$ (cf. Figure 4-46). The results obtained in this way for test series $WP3_2$ (cf. Figure 4-44 and Figure 4-46) thus tend to provide similar results to those already observed for $WP3_1$ (cf. Figure 4-40 and Figure 4-41). In this respect, the fatigue strengths of the evaluations of both perfect and imperfect structural stress ranges of test group $WP3_2.2$ with intentional imperfections are significantly better than those of $WP3_2.1$ without intentional imperfections. However, consistent fatigue strengths should be identified within test series $WP3_2$ (cf. Section 4.5.2.2.1). Consequently, the influence of imperfections on the structural stress concept appears to lead to unrealistic results. Furthermore, the difference between the stress ranges $\Delta\sigma_{R,hs,50\%,FEA,perfect}$ and $\Delta\sigma_{R,hs,50\%,FEA,imperfect}$ is equal and amounts to 20 N/mm^2 for the test group $WP3_2.1$ (cf. Figure 4-44) and 18 N/mm^2 for $WP3_2.2$ (cf. Figure 4-46). To this end, the respective scatter band of 27 N/mm^2 is somewhat larger in the evaluation for all test specimens of $WP3_2.2$ (cf. Figure 4-45).

In the investigation of perfect structural stress ranges $\Delta\sigma_{R,hs,50\%,FEA,perfect}$, the uncorrected normative fatigue classes according to the DIN EN 1993-1-9 [2], IIW [3]

and prEN 1993-1-9 [4] can neither be achieved by WP3_2.1 (cf. Figure 4-44) nor by WP3_2.2 (cf. Figure 4-45 and Figure 4-46). Like in Section 4.5.2.2.1, this indicates an overestimated fatigue class in the structural stress concept, as more economical results could be confirmed by the evaluation of perfect nominal stress ranges against the relevant fatigue classes (cf. Section 4.5.1.2.2) than with perfect structural stress ranges.

In addition, the evaluation of imperfect structural stress ranges $\Delta\sigma_{R,hs,50\%,FEA,imperfect}$ shows that the correction by the stress concentration factor $k_{m,FEA}$ according to prEN 1993-1-9 [4] with a fatigue class 238 results in unrealistically high fatigue strengths. In this respect, more reasonable fatigue strengths are given by the specifications according to DIN EN 1993-1-9 [2] and guidelines of the IIW [3]. However, these corrected fatigue classes can only be satisfied by the resulting S-N curve for the imperfect structural stress ranges of the WP3_2.2 test series (cf. Figure 4-45 and Figure 4-46).

To further investigate the presented results from the structural stress concept for test series WP3_2, the resulting stress ranges $\Delta\sigma_{R,hs,50\%}$ are again correlated at stress level. The respective analysis is performed separately for $\Delta\sigma_{R,hs,50\%,FEA,perfect}$ (cf. Figure 4-47) and $\Delta\sigma_{R,hs,50\%,FEA,imperfect}$ (cf. Figure 4-48). The results are compared with the relevant fatigue strengths according to DIN EN 1993-1-9 [2], IIW [3] and prEN 1993-1-9 [4] (cf. Section 4.5.2.1).

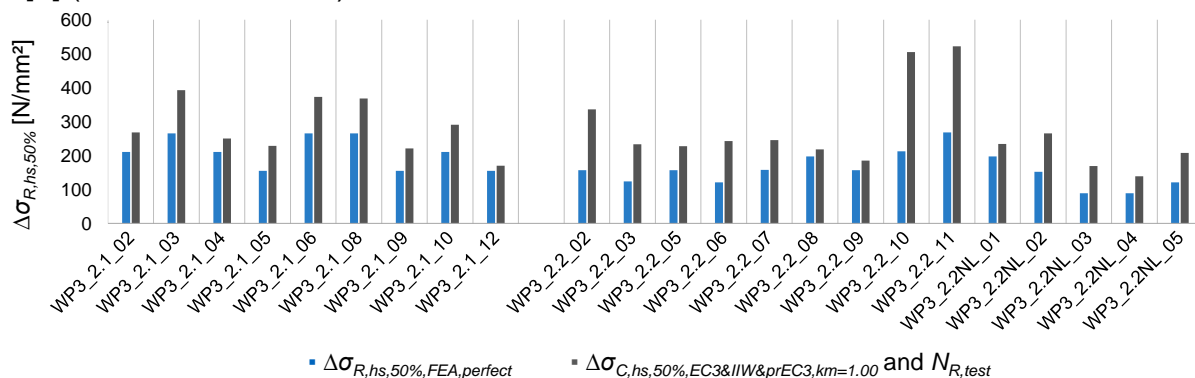


Figure 4-47: Evaluation of the numerically determined perfect structural stress $\Delta\sigma_{R,hs,50\%,FEA,perfect}$ of the test specimens of test series WP3_2 in comparison to analytically determined stress ranges of the structural stress concept according to the normative regulations and guidelines

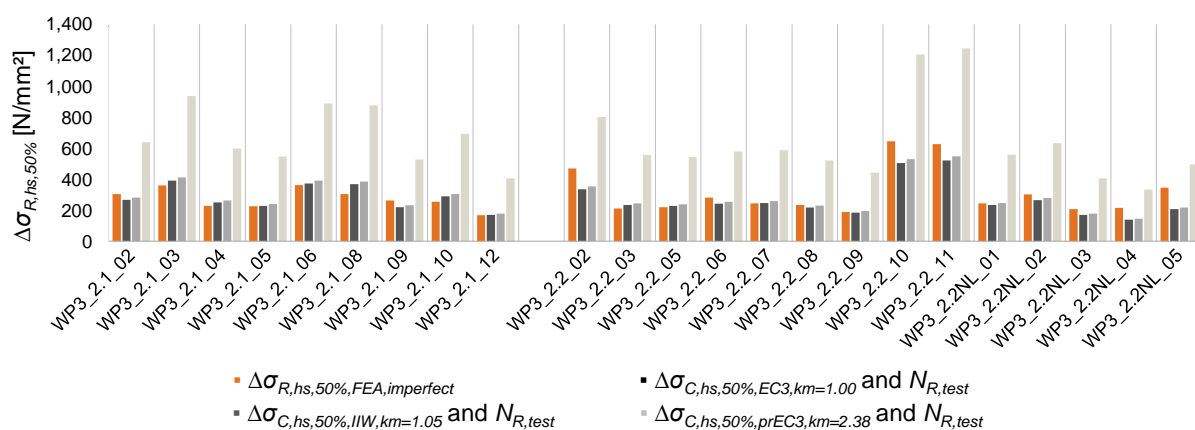


Figure 4-48: Evaluation of the numerically determined imperfect structural stress $\Delta\sigma_{R,hs,50\%,FEA,imperfect}$ of the test specimens of test series WP3_2 in comparison to analytically determined corrected stress ranges of the structural stress concept according to the normative regulations and guidelines

The evaluation of the perfect structural stress ranges $\Delta\sigma_{R,hs,50\%,FEA,perfect}$ for test series *WP3_2* shows a uniform underestimation of all expected normative stress ranges according to DIN EN 1993-1-9 [2], IIW [3] and prEN 1993-1-9 [4] on the basis of the experimental load cycles $N_{R,test}$ without any correction (cf. Figure 4-47). This corresponds to the results of test series *WP3_1* (cf. Figure 4-42). Therefore, due to the specified normative fatigue classes in the structural stress concept, significantly higher stress ranges $\Delta\sigma_{R,hs,50\%,FEA,perfect}$ should have resulted than were numerically determined. However, due to the successful validation according to Section 4.4, the numerical results are not expected to deviate significantly from the experimental tests. Consequently, the normative fatigue strengths for the structural stress concept are compromised by the results of the fatigue tests.

On the other hand, generally good accordance can be achieved between the evaluation of imperfect structural stress ranges $\Delta\sigma_{R,hs,50\%,FEA,imperfect}$ and corrected normative stress ranges according to DIN EN 1993-1-9 [2] and guidelines of the IIW [3]. In contrast, the dependence on the plate thickness t_3 of the stress concentration factor $k_{m,FEA}$ given according to prEN 1993-1-9 [4] results in a clear overestimation of $\Delta\sigma_{R,hs,50\%,FEA,imperfect}$, significantly exceeding the yield strength. This indicates incorrect specification in the fatigue class of the structural stress concept for cruciform joints. Consequently, it can be concluded that it is impossible for stress-increasing effects from $e = 0.15 \cdot t_3$ to be included in the fatigue strength of cruciform joints according to prEN 1993-1-9 [4]. It is therefore inevitable to explicitly consider all imperfections in evaluations according to the structural stress concept.

4.5.2.2.3 WP3_3

The results of the *WP3_3* test series applying the structural stress concept are shown below for the evaluation to perfect structural stress ranges $\Delta\sigma_{R,hs,50\%,FEA,perfect}$ and imperfect structural stress ranges $\Delta\sigma_{R,hs,50\%,FEA,imperfect}$. In this respect, the evaluation of the test group *WP3_3.1* without intentional axial misalignment is presented in Figure 4-49. The evaluation of *WP3_3.2* with intentional axial misalignment $e = 0.25 \cdot t_{1=2}$ is illustrated in Figure 4-50.

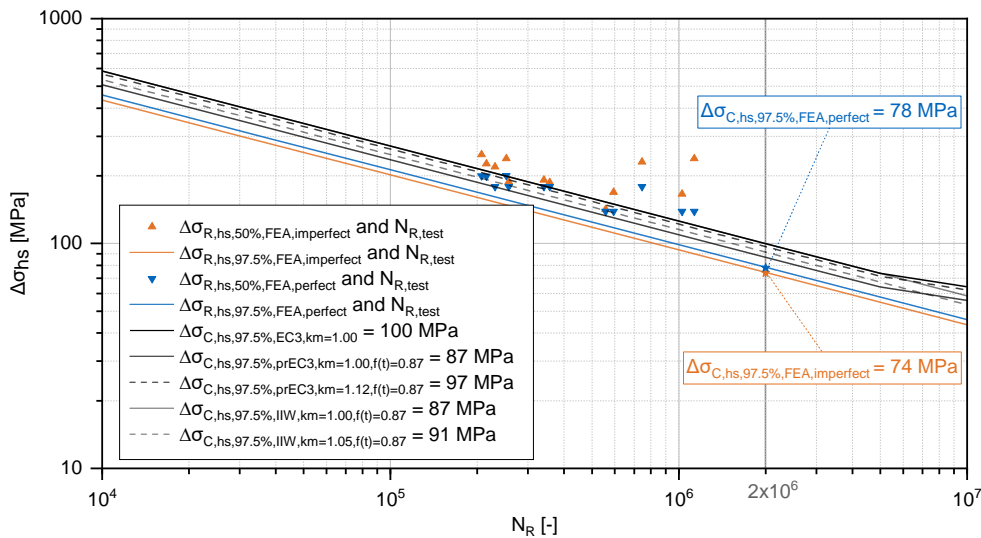


Figure 4-49: Results according to the structural stress concept for the perfect and imperfect FE models and $N_{R,test}$ for test group *WP3_3.1* with associated normative fatigue classes

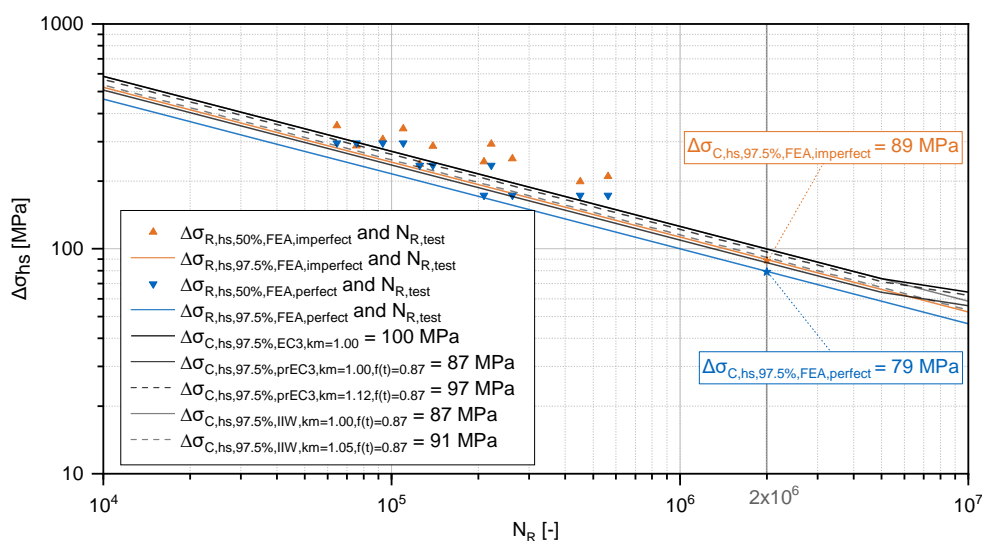


Figure 4-50: Results according to the structural stress concept for the perfect and imperfect FE models and $N_{R,test}$ for test group $WP3_3.2$ with associated normative fatigue classes

In contrast to the S-N curves for $WP3_1$ (cf. Section 4.5.2.2.1) and $WP3_2$ (cf. Section 4.5.2.2.2), the fatigue strengths of the perfect and imperfect structural stress ranges are very similar in test series $WP3_3$ (cf. Figure 4-49 and Figure 4-50). In this respect, the evaluation of the perfect structural stress $\Delta\sigma_{R,hs,50\%,FEA,perfect}$ for test group $WP3_3.1$ with $\Delta\sigma_{C,hs,50\%,FEA,perfect} = 78 \text{ N/mm}^2$ even results in a greater fatigue strength than when considering all imperfections by $\Delta\sigma_{C,hs,50\%,FEA,imperfect} = 74 \text{ N/mm}^2$ (cf. Figure 4-49). However, the unintentional imperfections do not lead to a reduction of the resulting imperfect structural stress ranges $\Delta\sigma_{R,hs,50\%,FEA,imperfect}$. Nevertheless, by the consideration of all imperfections, a larger scatter band of the test results is obtained, which leads to a lower fatigue resistance. For test group $WP3_3.2$, the resulting fatigue strengths are also similar with $\Delta\sigma_{C,hs,50\%,FEA,perfect} = 79 \text{ N/mm}^2$ and $\Delta\sigma_{C,hs,50\%,FEA,imperfect} = 89 \text{ N/mm}^2$ (cf. Figure 4-50). In addition, the test groups $WP3_3.1$ and $WP3_3.2$ within the test series $WP3_3$ result in very comparable results, as would have been expected for $WP3_1$ and $WP3_2$. Consequently, the structural stress concept seems to lead to more reasonable results for the test specimens of $WP3_3$. Furthermore, the thicker welded-on plates $t_{1=2} = 40 \text{ mm}$ of test series $WP3_3$ generally appear to cause a smaller influence due to imperfections on the structural stress ranges.

Once again, it is noticeable in the $WP3_3$ test series that the evaluation of the perfect structural stress ranges $\Delta\sigma_{R,hs,50\%,FEA,perfect}$ leads to fatigue strengths below the normative specifications according to the DIN EN 1993-1-9 [2], IIW [3] and prEN 1993-1-9 [4] (cf. Figure 4-49 and Figure 4-50). In this respect, the fatigue class 100 according to DIN EN 1993-1-9 [2] deviates most significantly from the results due to the missing thickness correction (cf. Chapter 2.6). By applying the thickness correction according to the guidelines of the IIW [3] and prEN 1993-1-9 [4], with the resulting fatigue class 87 slightly better conformities with $\Delta\sigma_{R,hs,50\%,FEA,perfect}$ can be achieved. Nonetheless, due to the apprehension of generally misclassified fatigue classes in the structural stress concept in the normative regulations and guidelines, it is not possible to verify the validity of the thickness correction. The same applies to the evaluation of imperfect structural stress ranges $\Delta\sigma_{R,hs,50\%,FEA,imperfect}$. In this respect, neither the results for

test group $WP3_3.1$ (cf. Figure 4-49) nor for $WP3_3.2$ (cf. Figure 4-50) can verify the corrected normative fatigue classes according to DIN EN 1993-1-9 [2], IIW [3] and prEN 1993-1-9 [4]. With the corrected fatigue class 91 according to the guidelines of the IIW [3], however, the best accordance with the imperfect structural stress ranges is achieved.

In the following, the evaluation of the perfect and imperfect structural stress ranges for test series $WP3_3$ is carried out at the stress level. The results are presented separately for $\Delta\sigma_{R,hs,50\%,FEA,perfect}$ (cf. Figure 4-51) and $\Delta\sigma_{R,hs,50\%,FEA,imperfect}$ (cf. Figure 4-52) and are related to the corresponding fatigue resistances according to DIN EN 1993-1-9 [2], IIW [3] and prEN 1993-1-9 [4].

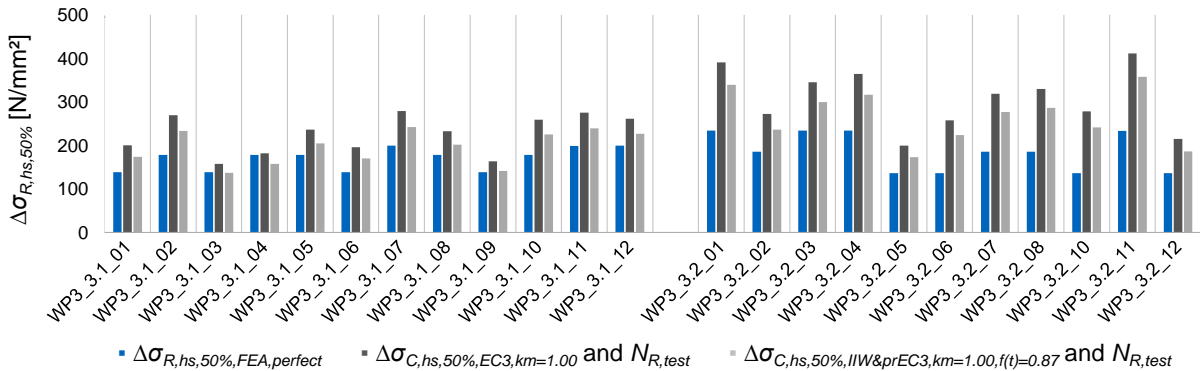


Figure 4-51: Evaluation of the numerically determined perfect structural stress $\Delta\sigma_{R,hs,50\%,FEA,perfect}$ of the test specimens of test series $WP3_3$ in comparison to analytically determined uncorrected stress ranges of the structural stress concept according to the normative regulations and guidelines

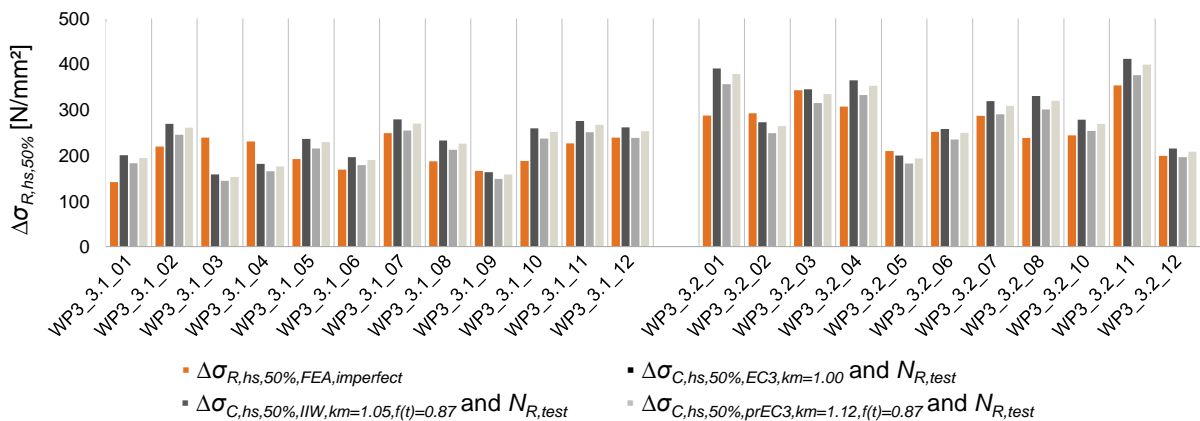


Figure 4-52: Evaluation of the numerically determined imperfect structural stress $\Delta\sigma_{R,hs,50\%,FEA,imperfect}$ of the test specimens of test series $WP3_3$ in comparison to analytically determined corrected stress ranges of the structural stress concept according to the normative regulations and guidelines

According to Figure 4-51, the evaluations of the perfect structural stress ranges $\Delta\sigma_{R,hs,50\%,FEA,perfect}$ show that the normative stress ranges $\Delta\sigma_{R,hs,50\%}$ resulting from the obtained load cycles $N_{R,test}$ and uncorrected normative fatigue classes $\Delta\sigma_{C,hs,50\%}$ are generally significantly underestimated. In this respect, however, due to the existing thickness correction, the results according to the guidelines of the IIW [3] and prEN 1993-1-9 [4] indicate better conformities than the stress ranges resulting from DIN EN 1993-1-9 [2]. In addition, the evaluation of $\Delta\sigma_{R,hs,50\%,FEA,perfect}$ demonstrates that the underestimates of test group $WP3_3.1$ are somewhat lower than those of $WP3_3.2$ (cf. Figure 4-51). Based on the number of load cycles $N_{R,test}$ and normative fatigue classes $\Delta\sigma_{C,hs,50\%}$, stress ranges $\Delta\sigma_{R,hs,50\%}$ are determined, which are often exceeding the valid

yield strength. As a result, it can be assumed that, at least in these cases, the fatigue classes cannot be valid.

According to Figure 4-52, the evaluations of imperfect structural stress ranges $\Delta\sigma_{R,hs,50\%,FEA,imperfect}$ are generally very similar to those with perfect structural stress ranges $\Delta\sigma_{R,hs,50\%,FEA,perfect}$ (cf. Figure 4-51). Again, $\Delta\sigma_{R,hs,50\%,FEA,imperfect}$ tends to underestimate the normatively determined corrected stress ranges $\Delta\sigma_{R,hs,50\%}$. However, the evaluations of the imperfect structural stress ranges result in significantly lower deviations and can be best verified by the guidelines of the IIW [3] in most cases. Due to the missing thickness correction, the results for DIN EN 1993-1-9 [2] provide the largest deviations (cf. Figure 4-52).

4.5.2.3 Summary

In summary, the resulting fatigue strengths for the perfect evaluation with $\Delta\sigma_{R,hs,50\%,FEA,perfect}$ according to the structural stress concept are shown in Figure 4-53. The comparison is presented for all test series $WP3_1$ (cf. Section 4.5.2.2.1), $WP3_2$ (cf. Section 4.5.2.2.2) and $WP3_3$ (cf. Section 4.5.2.2.3). The results are related to the uncorrected fatigue classes according to DIN EN 1993-1-9 [2], guidelines of the IIW [3] and prEN 1993-1-9 [4]. In this context, the thickness effects in the structural stress concept according to the guidelines of the IIW [2] and prEN 1993-1-9 [4] are considered for the test series $WP3_3$.

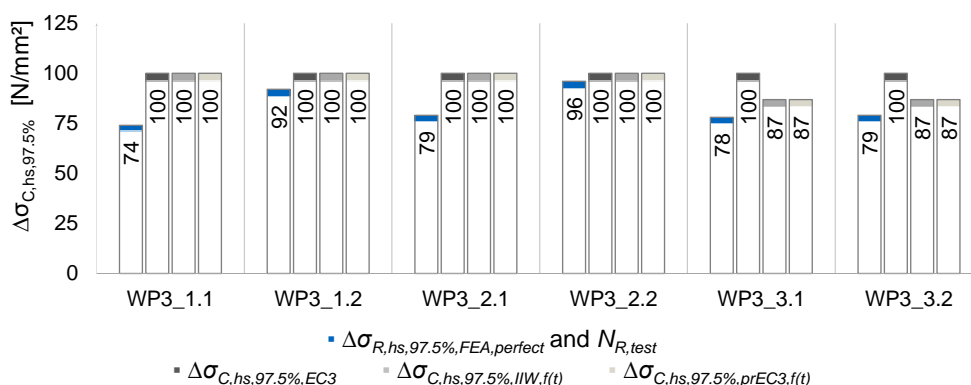


Figure 4-53: Fatigue strengths for $WP3$ following the S-N curves according to the structural stress concept for the perfect FE models and experimentally determined load cycle numbers $N_{R,test}$ with associated uncorrected normative fatigue classes

Due to the general unavailability of information on imperfections of constructions, there is often no alternative in the design phase but to assume a perfect structure in the fatigue evaluation. Consequently, the evaluation of the perfect structural stress ranges $\Delta\sigma_{R,hs,50\%,FEA,perfect}$ according to Figure 4-53 represents the foremost possibility to design according to the structural stress concept. However, in contrast to the evaluation of perfect nominal stress ranges $\Delta\sigma_{R,nom,50\%,FEA,perfect}$, the evaluation of the perfect structural stress ranges reveals that the structural stress concept specifies unrealistic fatigue strengths for the examined cruciform joints. This is based on the fact that economic results can be realised with the nominal stress concept in relation to the corresponding fatigue classes (cf. Figure 4-38). In contrast, the evaluation of the perfect structural stress $\Delta\sigma_{R,hs,50\%,FEA,perfect}$ for all test series $WP3_1$, $WP3_2$ and $WP3_3$ are considerably below the normatively specified fatigue strengths according to DIN EN

1993-1-9 [2], guidelines of the IIW [3] and prEN 1993-1-9 [4] (cf. Figure 4-53). The reason for this is that the structural stress ranges $\Delta\sigma_{R,hs,50\%,FEA,perfect}$ determined using the linear stress extrapolation are only slightly larger than the corresponding nominal stress ranges $\Delta\sigma_{R,nom,50\%,FEA,perfect}$ (cf. Table 3-6). Consequently, the significantly greater fatigue strengths of the structural stress concept compared to the nominal stress concept do not correlate to the applied stress ranges. Thus, the results of the linear stress extrapolation in combination with the applied normative fatigue classes of the structural stress concept might lead to unreliable results. Only with the test series *WP3_1.2* and *WP_2.2* slightly better correlations are observed. To this end, this fact indicates an overestimated influence of imperfections on the chosen structural stress determination, as uniform fatigue strengths would generally be expected within test series. In addition, only five cruciform joints with the intended axial misalignments $e \approx 0.25 \cdot t_{1=2}$ are included in the evaluation of *WP3_2.2* given in Figure 4-53. This causes a questionable statistical validation of the result. By evaluating all cruciform joints of *WP3_2.2*, a deviating fatigue strength $\Delta\sigma_{C,hs,50\%,FEA,perfect} = 79 \text{ N/mm}^2$ would result, which proves to be lower and equal to the fatigue strength of *WP3_2.1*. Furthermore, it is noticeable in Figure 4-53 that the consideration of the thickness effect in the fatigue strength of test series *WP3_3* leads to a better accordance with the numerical results. This effect is only specified according to the guidelines of the IIW [3] and prEN 1993-1-9 [4]. Due to the debatable classifications of the fatigue strengths in the structural stress concept, the normative specifications for the thickness correction can be roughly confirmed. Based on the fatigue tests of test series *WP3_3*, however, no more reliable conclusions can be drawn.

Furthermore, the evaluation of the fatigue strengths for the imperfect structural stress ranges $\Delta\sigma_{R,hs,50\%,FEA,imperfect}$ is presented in Figure 4-54. In this respect, the results are compared with the fatigue classes according to DIN EN 1993-1-9 [2], guidelines of the IIW [3] and prEN 1993-1-9 [4] corrected by the stress concentration factors k_m . The specified thickness correction of the fatigue classes for the test series *WP3_3* is applied according to the guidelines of the IIW [3] and prEN 1993-1-9 [4].

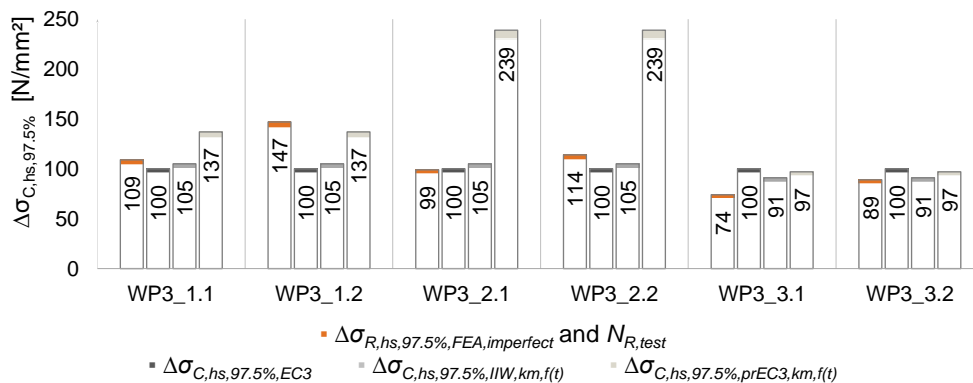


Figure 4-54: Fatigue strengths for *WP3* following the S-N curves according to the structural stress concept for the imperfect FE models and experimentally determined load cycle numbers $N_{R,test}$ with associated corrected normative fatigue classes

Due to the exact measurement results of all test specimens for the test series *WP3_1*, *WP3_2* and *WP3_3*, the evaluation from Figure 4-54 on imperfect structural stress ranges $\Delta\sigma_{R,hs,50\%,FEA,imperfect}$ provides more realistic results than the evaluation of the

perfect structural stress ranges $\Delta\sigma_{R,hs,50\%,FEA,perfect}$ from Figure 4-53. In general, with the exception of the specifications according to prEN 1993-1-9 [4], better compliance with the corrected normative specifications can be ensured by considering all axial and angular imperfections. In this respect, the corrected fatigue classes according to DIN EN 1993-1-9 [2] and guidelines of the IIW [3] can practically be verified by the evaluation of $\Delta\sigma_{R,hs,50\%,FEA,imperfect}$ for the test groups *WP3_1.1*, *WP3_2.1* and *WP3_2.2* (cf. Figure 4-54). However, the result for test group *WP3_1.2* is considerably above the normative fatigue strengths, which could indicate an overestimation of the influence of imperfections. Furthermore, in test series *WP3_1* and *WP3_2*, the fatigue strengths of the test groups with intentional imperfections differ significantly from the test groups without intentional imperfections (cf. Figure 4-54). This supports the supposition that influences from imperfections are overestimated by the applied evaluation method in the structural stress concept. Therefore, since each test series should result in equal internal fatigue strengths, no reliable evaluation can be guaranteed even if all detected axial and angular misalignments are included in the FEA. In contrast to the specifications from DIN EN 1993-1-9 [2] and IIW [3], the corrected fatigue strengths from prEN 1993-1-9 [4] provide a significant overestimation of the resistance side, which cannot be verified numerically (cf. Figure 4-54). The corresponding information on already considered imperfections in the amount of an axial misalignment of $e = 0.15 \cdot t_3$ thus proves to be invalid. The results thus indicate that all imperfections should be explicitly accounted for in the evaluation with the structural stress concept, as no stress-increasing effects are included in the normative regulations and guidelines. This can cause unreliable results in case not all imperfections can be identified in the design phase. Furthermore, in the evaluations of test series *WP3_3*, the necessity of a thickness correction can be confirmed. Nevertheless, due to the exact consideration of all determined axial and angular misalignments in the evaluation according to Figure 4-54, the minor underestimation of the numerically determined fatigue strengths for test group *WP3_3.1* and *WP3_3.2* could indicate an understated thickness correction factor. In principle, consistent utilisation rates should result in accordance with the different verification concepts for fatigue failure. Accordingly, the results for the nominal and structural stress concept should differ solely due to their economic applicability. However, in the evaluations of perfect systems without unintentional imperfections, it is noticeable that in comparison to the relevant fatigue strengths, significantly worse results are achieved according to the structural stress concept (cf. Figure 4-53) than according to the evaluation in the nominal stress concept (cf. Figure 4-38). For this reason, the normative fatigue strengths according to the structural stress concept can neither be verified by the experiments, nor can it be confirmed that realistic stress cycles N_R are determinable. In contrast, the normative fatigue strengths of the nominal stress concept accord much better with the numerical results. This could be attributed to the fact that the associated fatigue classes are based on actual fatigue test results and indicates that a more economical evaluation may not be possible for cruciform joints in general. Since the structural stress ranges determined with the linear stress extrapolation are only slightly higher than the concurrent nominal stress ranges, it is probable that the normative fatigue strength is exaggerated.

In order to allow a better comparability of the nominal and structural stress concept results, the respective utilisation rates for perfect and imperfect FE models are presented in the following Figure 4-55. The utilisation factor is calculated by the ratio of the numerically determined fatigue strengths to the corresponding normative fatigue resistances of the nominal resp. structural stress concept. In this respect, the corresponding numerically determined fatigue strengths are calculated on the basis of the resulting stress ranges of the nominal resp. structural stress concept and the experimentally identified load cycles $N_{R,test}$. Since the specifications according to the guidelines of the IIW [3] generally provide the most realistic results, only the associated normative resistances are considered in Figure 4-55.

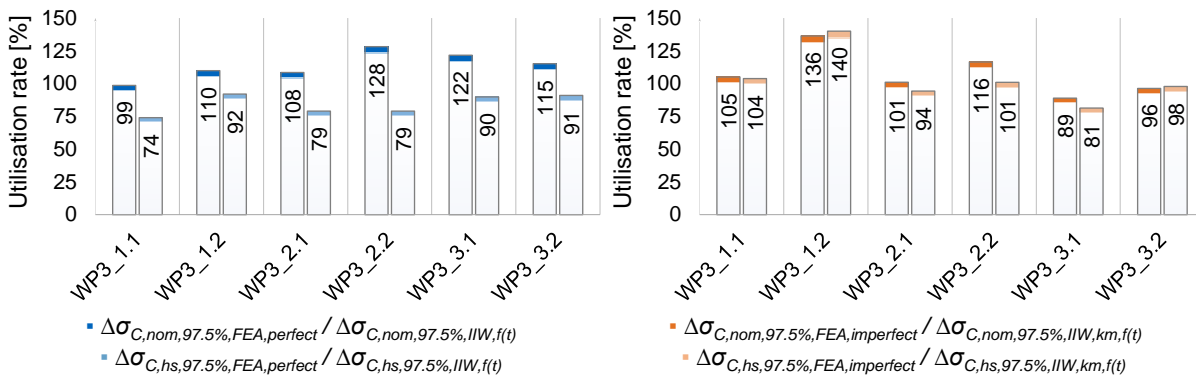


Figure 4-55: Utilisation rates for the ratio of numerically determined nominal or structural stress ranges to normative fatigue strengths according to the guidelines of the IIW [3] for an evaluation on perfect FE models without unintentional imperfections (left) and imperfect FE models (right)

According to Figure 4-55, significant differences can be observed between the evaluation of perfect and imperfect FE models in the nominal and structural stress concept. In this respect, there is good agreement between the utilisation rates of the nominal and structural stress concepts in the evaluation to imperfect FE models (cf. right side of Figure 4-55). This indicates at least that both fatigue concepts are capable of providing consistent results as long as all imperfections are accounted for in the FEA. On the other hand, the evaluation of the perfect FE models shows that due to the missing consideration of unintentional imperfections, large differences in the utilisation rates of the nominal and structural stress concept are to be expected (cf. left side of Figure 4-55). As a result, the normative fatigue strengths according to the guidelines of the IIW [3] cannot be confirmed by the structural stress concept, whereas they are verified using the nominal stress concept (cf. left side of Figure 4-55). Furthermore, due to the high number of load cycles $N_{R,test}$ obtained by the fatigue tests with intentional imperfections, the influence of imperfections appears to be significantly lower than would be expected from the numerically determined stress ranges. Therefore, since the discrepancies between the respective fatigue strengths within each test series are also evident in the perfect evaluations from Figure 4-55, it is reasonable to assume that influences from imperfections are overestimated by both the nominal and structural stress concept. In the following Section 4.5.3, equivalent imperfections $e_{equivalent}$ of the fatigue tests from the research project No. 20336N [69] are thus evaluated to determine the influence of imperfections on the applied nominal as well as structural stress ranges more accurately.

4.5.3 Method with equivalent imperfections

As already presented on the selected evaluation methods, in addition to the evaluation in the nominal and structural stress concept, a further investigation is realised regarding the influences of imperfections on the stress ranges (cf. Section 4.1). This is essential because the assessments according to the nominal stress concept (cf. Section 4.5.1) and the structural stress concept (cf. Section 4.5.2) indicate that the actual stress ranges tend to be overestimated. Therefore, it is reasonable to assume that the influence of detected imperfections on the fatigue strength is misjudged. Although the measurement records of the test specimens are utilised to generate realistic FE models that are additionally validated by means of strain gauges, it is almost impossible to ensure numerical models without idealisations or deviations from reality. In this respect, in addition to many other influencing factors such as the clamping process in testing machines, residual stresses, weld seam defects, among others, it is also not possible to consider the full range of imperfections in the FEA due to the complexity involved. However, the validation of the FEA indicates sufficiently accurate numerical models (cf. Section 4.4). Nonetheless, the numerical nominal and structural stress ranges appear to be excessive if large imperfections are present. Consequently, it can be expected that the identified imperfections have a differing influence on the resulting stress ranges of the experimental tests than on the FEA. For this reason, this section presents a specifically developed approach for a more precise determination of influences from imperfections by means of an equivalent imperfection $e_{equivalent}$. The basic principle, as already mentioned in Section 4.1.3, is described in more detail in the following Section 4.5.3.1. In this respect, the results of the strain measurement records are analysed to determine the actual stress ranges of the experimental fatigue tests. In addition, an evaluation in FEA can also be implemented. The resulting evaluations are presented in Section 4.5.3.2 for the fatigue tests of the IGF research project No. 20336N [1].

4.5.3.1 Basic principle

As already presented in Section 4.3.2.2.1, the results of the strain measurement records can be utilised to determine specified equivalent imperfections $e_{equivalent}$. As strain gauges were installed on all investigated cruciform joints, the respective evaluation is feasible for all recorded cycles. In accordance with Section 4.3.2.2.1, the results from *SG 2* and *SG 9* as well as from *SG 8* and *SG 10* are analysed for this purpose. The particular arrangement of these strain gauges can be seen in Figure 4-56 below. In this respect, the strain gauges are located in the centre of the plate.

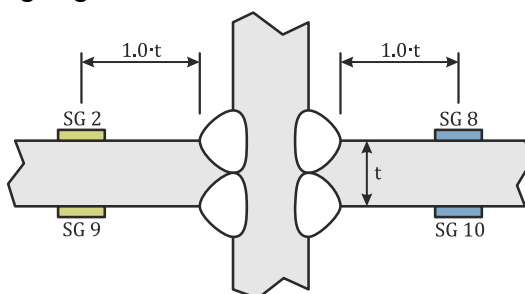


Figure 4-56: Position of strain gauges *SG 2* and *SG 9* as well as *SG 8* and *SG 10* in the centre of the welded-on plates to determine secondary bending effects

The determination of the associated equivalent imperfections $e_{equivalent}$ is performed according to Section 4.3.2.2.1. The equivalent imperfections calculated analytically by this procedure are illustrated on the left side of Figure 4-57 exemplarily for test specimen WP3_1.1_06. The results are based on cycle $N_{R,test} = 25000$ which represents approximately 10 % of the total number of achieved load cycles $N_{R,test}$ until crack initiation. In addition, left side of Figure 4-57 shows the corresponding force progression F of the testing machine during this cycle.

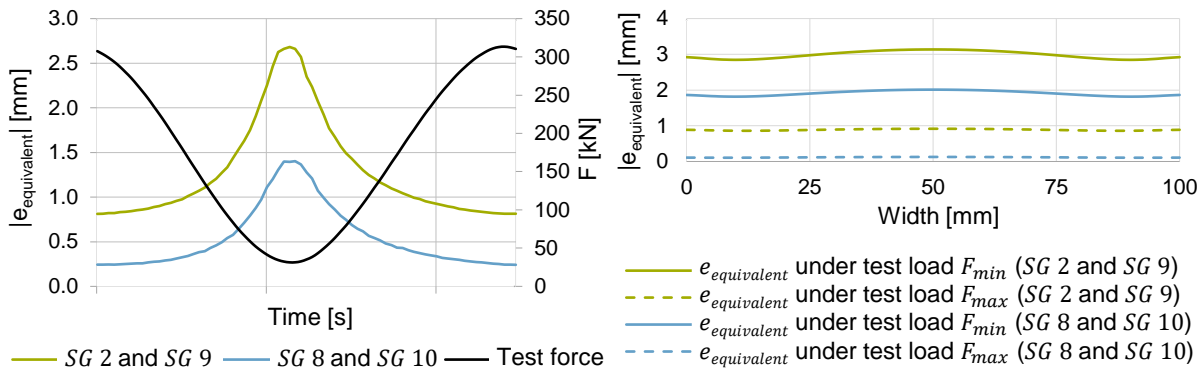


Figure 4-57: Calculated equivalent imperfections $e_{equivalent}$ for strain gauges SG 2 and SG 9 as well as for SG 8 and SG 10 and associated test force F at load cycle $N_{R,test} = 25.000$ exemplarily for test specimen WP3_1.1_06

The left side of Figure 4-57 illustrates that the influence of imperfections is not consistent on both sides of specimens, as the equivalent imperfections $e_{equivalent}$ of strain gauges SG 2 and SG 9 are dissimilar to those of SG 8 and SG 10. This is caused by the concurrence of axial misalignment and angular misalignment. It is also noticeable that the straightening effect has a decisive influence on the impact of imperfections. In this respect, the smallest influence from imperfections occurs at the time point of maximum stress on the testing machine. As a result, under the maximum test force F_{max} , the test specimen is only affected by the lowest equivalent imperfection $e_{equivalent}$ (cf. left side of Figure 4-57). The opposite applies under the minimum test force F_{min} , for which the maximum equivalent imperfection $e_{equivalent}$ has decisive influence.

Similar characteristics can be determined by the FEA. For this purpose, paths are evaluated over the component width at the locations of the respective strain gauges SG 2 and SG 9, as well as SG 8 and SG 10 at a distance of $1.0 \cdot t_{1=2}$ in front of the weld notch. The required numerical evaluations are conducted both under the maximum load F_{max} and under the minimum load F_{min} . Once again, the procedure according to Section 4.3.2.2.1 is applied for the required calculations. In this respect, geometrically non-linear FE analyses are imperative to account for straightening effects. Right side of Figure 4-57 exemplarily presents the relevant results for test specimen WP3_1.1_06. Depicted are the minimum and maximum values of the equivalent imperfections $e_{equivalent}$ for the strain gauges SG 2 and SG 9 as well as SG 8 and SG 10 over the width of the component.

The right side of Figure 4-57 indicates that the influence of imperfections in the component remains practically constant over the width of the component. However, since the strain gauges for the determination of secondary bending stresses were

arranged in the centre of the welded-on plates, the maximum equivalent imperfection $e_{equivalent}$ is determined experimentally. The agreement between the equivalent imperfections of the experimental tests and the results from the FEA generally appears to be satisfactory. Although there are slight differences between the maximum and minimum resulting equivalent imperfections according to Figure 4-57, this is mainly attributable to the shifting imperfections during the experimental tests. Left side of Figure 4-58 shows the corresponding progression of the equivalent imperfections under the loading F_{max} for all cycles.

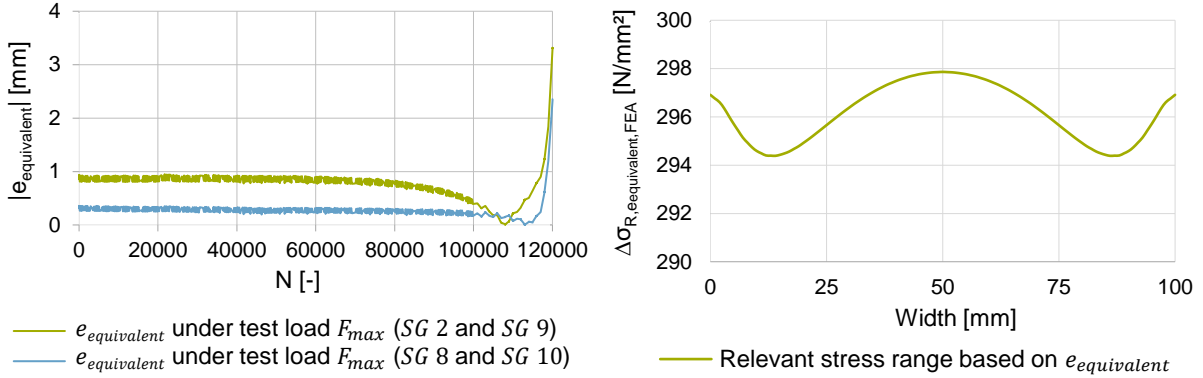


Figure 4-58: Equivalent imperfections $e_{equivalent}$ under test load F_{max} for strain gauges $SG 2$ and $SG 9$ as well as $SG 8$ and $SG 10$ over all cycles exemplarily for test specimen $WP3_1.1_06$

The left side of Figure 4-58 demonstrates that the equivalent imperfections $e_{equivalent}$ stay nearly constant for approximately 80 % of the test period before decreasing in the last 20 % and rapidly rising just before the end of the test. As the imperfections have a direct influence on the applied stress range $\Delta\sigma_{R,equivalent}$, any changes are accounted for by the linear damage accumulation according to Chapter 2.2.4. For this purpose, one cycle each is evaluated after 10 % and after 90 % of the total cycles. Since the progression of equivalent imperfections in almost all cases is linear or abruptly changes to a differing level, the evaluation of these two cycles is sufficient for a realistic assessment. Due to the purely static analysis in the FEA, no damage accumulation is to be performed in this respect.

To determine the required applied stress ranges $\Delta\sigma_{R,equivalent}$, the decisive maximum stresses $\sigma_{max,equivalent}$ and minimum stresses $\sigma_{min,equivalent}$ must be identified. For this, it must initially be ensured that the straightening effects of all experimental fatigue tests result in the minimum equivalent imperfections $e_{equivalent}$ to be expected under the maximum test load F_{max} and vice versa. In this respect, the evaluations according to Figure 4-57 for all cruciform joints confirm that this correlation is valid for all tests. According to the following formula, the maximum and minimum stresses are thus the result of the subsequent membrane and bending stress components.

$$\sigma_{max,equivalent} = \frac{F_{max}}{A} + \frac{F_{max} \cdot e_{equivalent}(\text{under load } F_{max})}{W_y} \quad (4-7)$$

$$\sigma_{min,equivalent} = \frac{F_{min}}{A} + \frac{F_{min} \cdot e_{equivalent}(\text{under load } F_{min})}{W_y} \quad (4-8)$$

Consequently, the actual stress range $\Delta\sigma_{R,e_{equivalent}}$ can be calculated by the difference of maximum stress $\sigma_{max,e_{equivalent}}$ and minimum stress $\sigma_{min,e_{equivalent}}$ as follows.

$$\Delta\sigma_{R,e_{equivalent}} = \sigma_{max,e_{equivalent}} - \sigma_{min,e_{equivalent}} \quad (4-9)$$

In this way, the decisive stress ranges $\Delta\sigma_{R,e_{equivalent}}$ can be determined both for the experimental tests and for the comparative calculations in the FEA. Following Figure 4 61 illustrates the decisive distribution of the maximum stress range $\Delta\sigma_{R,e_{equivalent},FEA}$ over the component width for test specimen *WP3_1.1_06*. According to the equivalent imperfections (cf. Figure 4-57), the stress range is largest in the centre of the component (cf. right side of Figure 4-58), which verifies the position of the strain gauges relevant for the determination of the secondary bending effects. However, the deviations at the edges of the welded-on plates amount to less than 2 %. Consequently, no major deviations would have been expected otherwise. While the maximum stress range of the test specimen *WP3_1.1_06* in the FEA results in $\Delta\sigma_{R,e_{equivalent},FEA} = 297.86 \text{ N/mm}^2$, an experimental stress range of $\Delta\sigma_{R,e_{equivalent},test} = 294.47 \text{ N/mm}^2$ can be determined by the linear damage accumulation. Thus, the respective results differ by only 1.2 % and provide reasonable agreement. This procedure can therefore also be regarded as a further validation of the FE models.

4.5.3.2 Analysis of the test series

Based on the procedure for the determination of equivalent imperfection $e_{equivalent}$ (cf. Section 4.5.3.1), the numerical results of the stress ranges $\Delta\sigma_{R,e_{equivalent},FEA}$ of the FEA are compared with the experimentally determined stress ranges $\Delta\sigma_{R,e_{equivalent},test}$. The respective assessment is presented separately for the test series *WP3_1* (cf. Figure 4-59), *WP3_2* (cf. Figure 4-60) and *WP3_3* (cf. Figure 4-61). In addition, the results of the stress ranges $\Delta\sigma_{R,nom,FEA,perfect}$ and $\Delta\sigma_{R,nom,FEA,imperfect}$ determined by perfect and imperfect FE models are given for the respective test specimens in order to compare the previously assumed limiting assumptions.

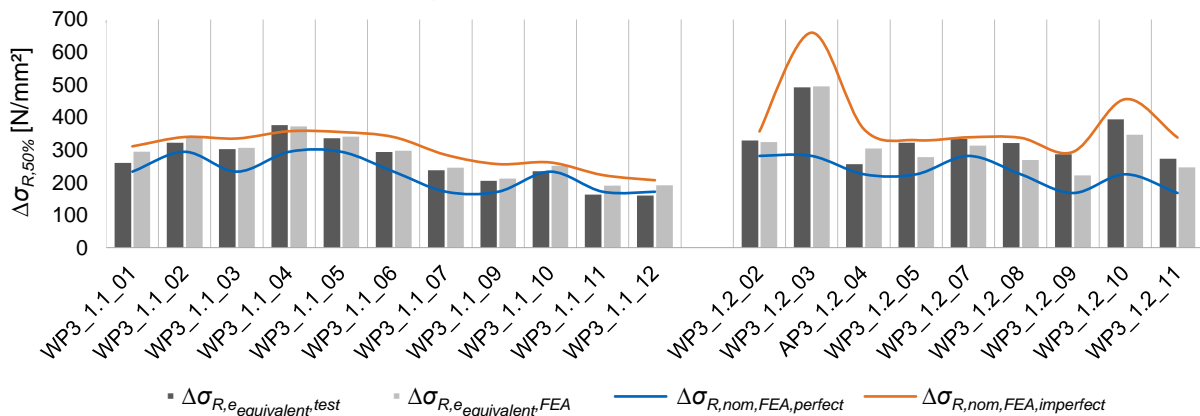


Figure 4-59: Comparison between numerical stress ranges $\Delta\sigma_{R,e_{equivalent},FEA}$ and experimental stress ranges $\Delta\sigma_{R,e_{equivalent},test}$ for test series *WP3_1* with reference to results of stress ranges determined on perfect FE models $\Delta\sigma_{R,nom,FEA,perfect}$ and imperfect FE models $\Delta\sigma_{R,nom,FEA,imperfect}$

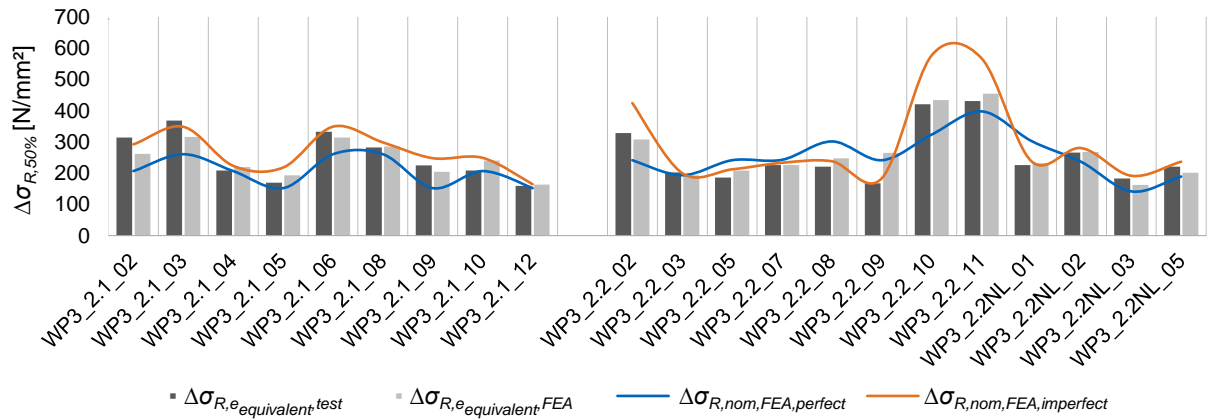


Figure 4-60: Comparison between numerical stress ranges $\Delta\sigma_{R,e_{equivalent},FEA}$ and experimental stress ranges $\Delta\sigma_{R,e_{equivalent},test}$ for test series $WP3_2$ with reference to results of stress ranges determined on perfect FE models $\Delta\sigma_{R,nom,FEA,perfect}$ and imperfect FE models $\Delta\sigma_{R,nom,FEA,imperfect}$

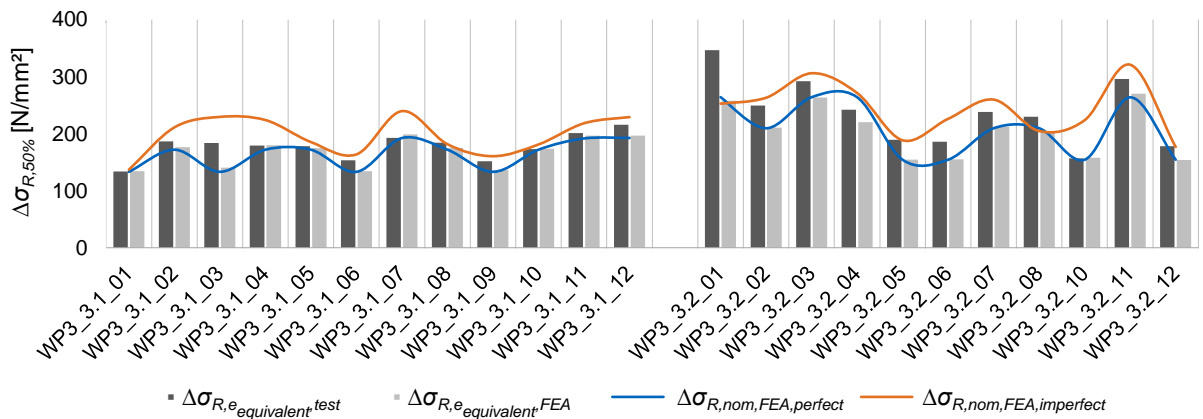


Figure 4-61: Comparison between numerical stress ranges $\Delta\sigma_{R,e_{equivalent},FEA}$ and experimental stress ranges $\Delta\sigma_{R,e_{equivalent},test}$ for test series $WP3_3$ with reference to results of stress ranges determined on perfect FE models $\Delta\sigma_{R,nom,FEA,perfect}$ and imperfect FE models $\Delta\sigma_{R,nom,FEA,imperfect}$

The results from Figure 4-59, Figure 4-60 and Figure 4-61 show very satisfactory agreements between the numerically determined stress ranges $\Delta\sigma_{R,e_{equivalent},FEA}$ and the experimentally obtained stress ranges $\Delta\sigma_{R,e_{equivalent},test}$. However, the experimental equivalent imperfections $e_{equivalent}$ could not be determined on individual test specimens due to erroneous recordings. This included the test specimens $WP3_1.2_06$, $WP3_2.2_06$ and $WP3_2.2NL_04$, which were therefore not included in the evaluation. The evaluations also demonstrate that the stress ranges $\Delta\sigma_{R,e_{equivalent}}$ determined by equivalent imperfections are in most cases within the previously assumed stress ranges for perfect and imperfect FE analyses in the nominal stress concept. In this way, significantly more accurate evaluations can be provided based on the accurate consideration of straightening effects and the resulting deviating fatigue stresses of the cruciform joints.

Therefore, the determined stress ranges $\Delta\sigma_{R,e_{equivalent}}$ allow for the determination of more accurate S-N curves. For this objective, the determined stress ranges $\Delta\sigma_{R,e_{equivalent}}$ are related to the experimental stress cycles $N_{R,test}$. The creation of these S-N curves proves that the adjusted stress ranges $\Delta\sigma_{R,e_{equivalent}}$ lead to a significant

reduction in the scatter of the test data. This confirms that in combination with the experimentally determined load cycles $N_{R,test}$, more realistic stress ranges are applied. The resulting fatigue strengths $\Delta\sigma_{C,97.5\%}$ are summarised in the following Figure 4-62 for the test series $WP3_1$, $WP3_2$ and $WP3_3$ according to the nominal stress concept. Additionally, the fatigue strengths presented in Section 4.5.1.3 are specified based on the evaluations on perfect and imperfect nominal stress ranges in order to establish a comparison to the previously assumed results.

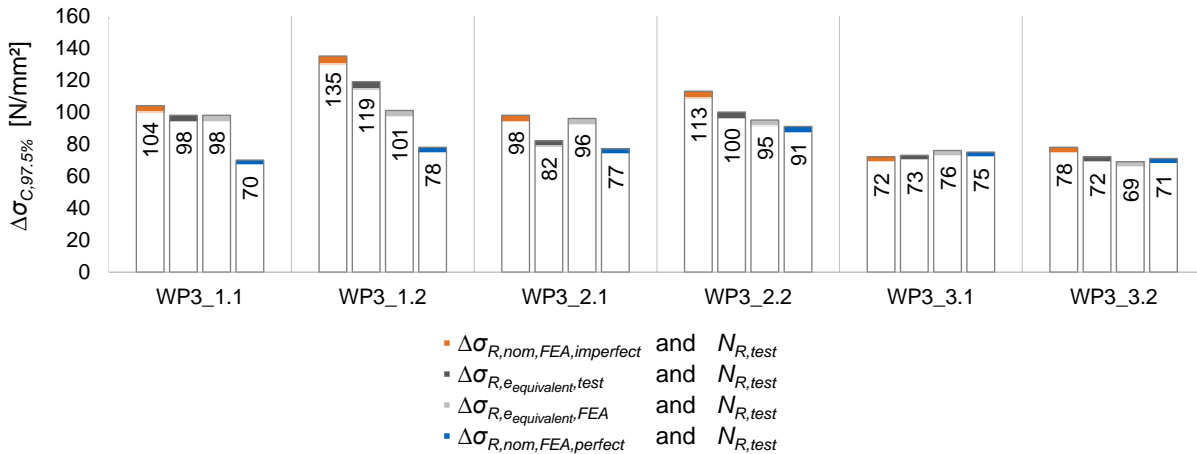


Figure 4-62: Fatigue strengths for $WP3$ following the S-N curves according to the evaluation by equivalent misalignment $e_{equivalent}$ and experimentally determined load cycle numbers $N_{R,test}$ according to the nominal stress concept

Figure 4-62 reveals that, despite the small differences between the respective numerical and experimentally determined equivalent imperfection stress ranges $\Delta\sigma_{R,equivalent}$, the resulting fatigue strengths $\Delta\sigma_{C,97.5\%}$ of the fatigue tests clearly deviate in some cases. This is especially true for the experimental groups $WP3_1.2$ and $WP3_2.1$. This fact is due to the differing scatter bands, which lead to a varying fatigue strength in the evaluation of the experimental fatigue tests compared to the numerical analysis. The reason for this mainly results from measurement inaccuracies and the simplified application of linear damage accumulation in the experimental evaluations of $e_{equivalent}$. In contrast, the results from the FEA generally provide better agreement. In this respect, there are practically no differences between the fatigue strengths within the test series $WP3_1$ and $WP3_2$ (cf. Figure 4-62). Only in test series $WP3_3$, with a deviation of $7 N/mm^2$ between the test groups $WP3_3.1$ and $WP3_3.2$, slightly worse results are obtained. In this regard, the results for $\Delta\sigma_{R,equivalent,test}$ are more favourable with a deviation of only $1 N/mm^2$. However, the evaluation according to Figure 4-62 generally confirms that the fatigue strengths to be expected in reality of the investigated cruciform joints can be assigned between the results of the perfect and imperfect FE evaluations in the nominal stress concept.

Based on the evaluation of equivalent imperfections $e_{equivalent}$, more accurate fatigue strengths are determined for the structural stress concept as well. This is accomplished by the determination of consequential stress concentration factors. These factors are calculated by the ratio of the numerical stress ranges $\Delta\sigma_{R,equivalent,FEA}$, based on the equivalent imperfections, to the nominal stress ranges $\Delta\sigma_{R,nom,FEA}$ determined without equivalent imperfections. By the multiplication with the stress ranges $\Delta\sigma_{R,hs,FEA}$ within

the structural stress concept, the associated fatigue strengths can be identified. The corresponding results are summarised in Figure 4-63 below.

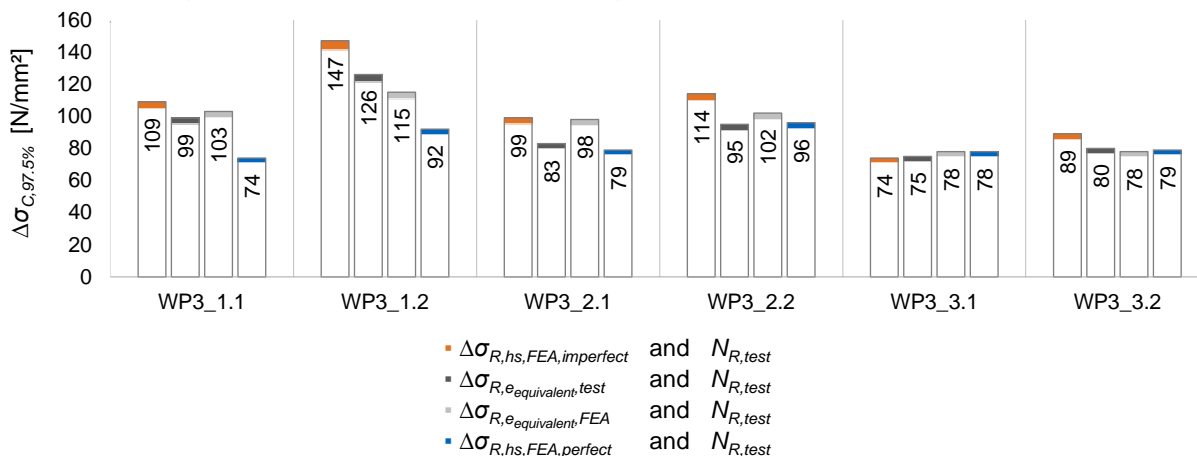


Figure 4-63: Fatigue strengths for WP3 following the S-N curves according to the evaluation by equivalent misalignment $e_{equivalent}$ and experimentally determined load cycle numbers $N_{R,test}$ according to the structural stress concept

According to Figure 4-63, it is evident that differences between the numerical and experimental results also occur in the modified fatigue strengths $\Delta\sigma_{C,97.5\%}$ according to the structural stress concept. Especially for test groups WP3_1.2 and WP3_2.1 these deviations are relatively large with a maximum of $15 N/mm^2$ and are attributable to the differing scatter bands. In addition, in contrast to the nominal stress concept, it is noticeable that the fatigue strength of WP3_1.2 in the structural stress concept is significantly greater than that of WP3_1.1, even under evaluation with equivalent imperfections $e_{equivalent}$. In this case, more comparable fatigue strengths could have been expected within test series WP3_1 due to the modified evaluation. Consequently, despite the adjustment of the procedure, the linear structural stress extrapolation does not prove to be appropriate for a realistic representation of influences resulting from considerable imperfections. However, the difference between the modified fatigue strengths of $12 N/mm^2$ can be significantly reduced compared to the results from Section 4.5.2.3. In contrast, more consistent results are observed between the respective test groups with and without intentional imperfections for test series WP3_2 and WP3_3. This indicates the validity of the adapted methodology. With the exception of test series WP3_3, the revised fatigue strengths enable the normative fatigue classes according to DIN EN 1993-1-9 [2], guidelines of the IIW [3] and prEN 1993-1-9 [4] to be complied with by narrow margin. Nevertheless, the economic applicability of the structural stress concept at cruciform joints is debatable, as significantly better results can be achieved by the application of the universally acknowledged nominal stress concept.

4.6 Summary of experimental fatigue tests

The fatigue tests of the IGF research project No. 20336N [1] are comprehensively evaluated in the previous chapter. For this purpose, different evaluation methods are elaborated in order to ensure a detailed analysis of the fatigue tests (cf. Section 4.1). In this respect, the measurement records of the cruciform joints can be utilised to

determine axial and angular misalignments accurately (cf. Section 4.2). In the analysis of the experimental fatigue test data, specially developed Python scripts facilitate a systematic evaluation. In addition to the cycle-based analysis of strains, stresses, machine force, machine displacement as well as experimental structural stress ranges and equivalent imperfections, among other things, the required cycles of the crack initiation of the test specimens can be determined with reasonable precision (cf. Section 4.3). By the validation on the basis of statically conducted preliminary tests, the created FE models can be verified for the realistic determination of numerically computed strains (cf. Section 4.4). This applies both to the strain distributions of the clamping processes in testing machines as well as under the maximum tensile stress of the fatigue loads. As a result, the imperfect FE models with the consideration of the identified imperfections can be considered as sufficiently reliable. In the detailed evaluation of the fatigue tests from [1] in Section 4.5, evaluations are performed both in the nominal stress concept (cf. Section 4.5.1) and structural stress concept (cf. Section 4.5.2) as well as with specifically defined equivalent imperfections (cf. Section 4.5.3).

The analyses of the nominal stress concept according to Section 4.5.1 demonstrate that despite the general unavailability of information on imperfections in the design phase, the concept is capable of providing realistic fatigue strengths for the investigated cruciform joints as long as perfect nominal stress ranges are assessed without the consideration of unintentional imperfections (cf. Figure 4-38). In this respect, all results of the fatigue tests are within the range of the normative fatigue resistances. Thus, the nominal stress concept according to DIN EN 1993-1-9 [2], guidelines of the IIW [3] and prEN 1993-1-9 [4] provides highly economical fatigue classes for cruciform joints. This possibly reflects the fact that the associated fatigue strengths are based on results of real tests, and indicates that a more economical assessment may be impractical for cruciform connections in general. However, it can be observed that for thin weld-on plates of test series *WP3_1* and *WP3_2*, increased fatigue strengths are determined with greater imperfections. With increasing imperfections, this indicates an overestimation of the stress-increasing effects in the nominal stress concept, since constant fatigue strengths are to be expected within test series. This could be attributed to the fact that straightening effects are not sufficiently considered. Furthermore, the evaluation method with imperfect FE models considering all intentional and unintentional imperfections provides only limited practical results for thin plate thicknesses $t_{1=2}$ (cf. Figure 4-39). The reason for this is that the experimental tests with relatively large imperfections (cf. Table 4-3) result in significantly more load cycles $N_{R,test}$ than can be expected from the numerically determined stress ranges. Consequently, the FE models with integrated misalignments increasingly overestimate the resulting nominal stress ranges with larger imperfections. Furthermore, it is noticeable in the evaluations of the nominal stress concept that the specified fatigue class 71 according to the guidelines of the IIW [3] proves to be more suitable for the cruciform joints of *WP3_1* with $l \leq 50 \text{ mm}$ (cf. Chapter 2.4) than the specified classification 80 according to DIN EN 1993-1-9 [2] and prEN 1993-1-9 [4]. In addition, it can be demonstrated that the applied normative regulations and guidelines provide considerably different information on already considered imperfections in the fatigue classes for cruciform joints. Due to the dependence of the stress concentration factor

k_m on the intermediate plate thickness t_3 , the fatigue resistances of the nominal stress concept according to DIN EN 1993-1-9 [2] and prEN 1993-1-9 [4] are clearly overestimated. In this respect, only the information on considered imperfections according to the guidelines of the IIW [3] can be confirmed by the fatigue tests. Finally, it can be stated that the consideration of the thickness effect in the nominal stress concept according to the IIW [3] provides rather conservative fatigue strengths and is therefore not advisable.

In contrast to the evaluation according to the nominal stress concept, the evaluation according to the structural stress concept from Section 4.5.2 demonstrates that unrealistic fatigue strengths are specified for the examined cruciform joints according to the normative regulations and guidelines. This applies in particular to the evaluation of perfect structural stress ranges without the consideration of unintentional imperfections (cf. Figure 4-53). Therefore, without detailed information on the actual imperfections of cruciform joints, the associated fatigue resistances in the structural stress concept cannot be verified by any test series. Consequently, it has to be concluded that no realistic determination of expected stress cycles N_R can be expected by the application of the structural stress concept. This fact can be attributed to the structural stress ranges determined on the basis of the linear stress extrapolation, which exceed the resulting nominal stress ranges by a minimum. However, since the normative fatigue classes are defined disproportionately higher, the application of formula (2-1) numerically results in a significant overestimation of the feasible load cycles compared to the experimentally determined results for $N_{R,test}$. In addition, it can be observed that increased fatigue strengths are determined for thin welded-on plates of test series *WP3_1* and *WP3_2* with increasing imperfections. This indicates an overestimation of the stress-increasing effects due to imperfections by the linear stress extrapolation in the structural stress concept, as consistent fatigue strengths are to be expected within test series. A possible reason could be the insufficient consideration of straightening effects. Thus, there is a risk of unreliable fatigue verification in the structural stress concept. Furthermore, the numerical evaluations of imperfect structural stress ranges show an exaggerated influence resulting from the consideration of unintentional imperfections (cf. Figure 4-54). In this respect, since no consistent fatigue strengths can be guaranteed within the respective test series *WP3_1*, *WP3_2* and *WP3_3*, not even the inclusion of all detected axial and angular misalignments in the FEA can ensure a reliable assessment. Consequently, the linear structural stress extrapolation is only suitable to a limited extent to realistically represent influences from imperfections. Furthermore, in contrast to the specifications of DIN EN 1993-1-9 [2] and the guidelines of the IIW [3], the included imperfections according to prEN 1993-1-9 [4] lead to a clear overestimation of the resistance side, which cannot be verified numerically by the structural stress concept. The corresponding information on cruciform joints according to [4] about already considered imperfections in the amount of an axial misalignment $e = 0.15 \cdot t_3$ thus proves to be invalid. In contrast, the consideration of the thickness effect specified according to the guidelines of the IIW [3] and prEN 1993-1-9 [4] ensures a better accordance with the numerical results and is therefore to be applied in the structural stress concept. Nonetheless, the economic applicability of the structural stress concept for cruciform joints is arguable, as much

more reasonable results can be attained by the application of the generally approved nominal stress concept.

Due to the overestimation of nominal and structural stress ranges with increasing imperfections, a specific methodology for determining equivalent imperfections is presented (cf. Section 4.5.3). This method is intended to enable better consideration of straightening effects in the case of imperfections. The associated verification of this behaviour by the experimentally measured equivalent imperfections shows that an evaluation by FEA is also capable of providing realistic results. In general, the evaluation by means of equivalent imperfections $e_{equivalent}$ in the nominal stress concept and structural stress concept proves that the realistic stress ranges are strongly influenced by straightening effects. Based on the methodology including the realistic straightening effects related to imperfections, the resulting fatigue strengths therefore range between the results of the fatigue strengths determined on perfect and imperfect FE models (cf. Figure 4-62 and Figure 4-63). This confirms that influences of imperfections on the nominal and structural stress concept can be considered more consistently by the proposed procedure than by the normatively specified assessments. Consequently, much more accurate evaluations can be provided based on the accurate consideration of straightening effects and the resulting deviating fatigue stresses of the examined cruciform joints. Straightening effects thus should be included in the design, especially in the case of large expected imperfections, in order to allow for a realistic and, especially, economical design.

5 Effects of imperfections on cruciform joints

This chapter presents the results of extensive parameter studies from the IGF research project No. 20336N [1] on the influence of imperfections on the fatigue behaviour of cruciform joints. In this respect, both clamping processes in testing machines (cf. Section 5.1) and realistic support conditions are analysed in detail (cf. Section 5.2).

Regarding clamping processes, in addition to effects from possible imperfections on the fatigue resistance (cf. Section 5.1.1), associated stress concentration factors are investigated in order to indirectly consider axial and angular misalignments (cf. Section 5.1.2). The objective is to determine direct influences from imperfections on nominal and structural stress ranges and to express them by indirect stress concentration factors. In this way, imperfections can be considered indirectly without any complex modelling assumptions in the FEA. With regard to the realistic support conditions, on the one hand stress concentration factors based on normative regulations and guidelines are verified by means of comparative calculations in the FEA (cf. Section 5.2.1). On the other hand, support parameters λ are investigated to allow indirect evaluations of influences from imperfections for all support conditions from Chapter 2.5 for different cruciform joint geometries (cf. Section 5.2.2). The objective is to investigate influences from imperfections in detail and to define stress concentration factors that allow a reliable indirect evaluation of cruciform joints with imperfections.

5.1 Clamping processes

In general, the clamping process of specimens in a testing machine does not represent a practical support configuration, since the resulting support and load situations are practically non-existent in realistic constructions. Nevertheless, the correct numerical consideration of the relevant effects is crucial in research, since testing machines are frequently used in this respect. As a result of clamping processes, if components with intentional or unintentional imperfections are investigated, additional secondary bending stresses result even before loads are applied by the testing machine. The influences resulting from different imperfections due to clamping processes in testing machines are discussed in more detail in the following Section 5.1.1. However, since the resulting modelling effort is practically impossible to implement, in addition to the direct determination of the resulting stresses by numerical FE models, an indirect consideration can be carried out by means of adequate stress concentration factors. For this purpose, in Section 5.1.2 the analytical factors proposed by Xing and Dong [5] on axial and angular misalignment are evaluated in order to verify the accuracy by parameter studies.

In order to numerically simulate the clamping process in testing machines, complex modelling of the resulting boundary conditions is generally required. In this respect, solid models are modelled with rigid beam elements that allow rigid body displacement and rotation (cf. Chapter 3.3.3). The validity of the analysis can be confirmed by the

validation of the strain distributions under restraint conditions presented in Chapter 4.4.1 for the fatigue tests on cruciform joints. The required loading of the FE models of Sections 5.1.1 and 5.1.2 is uniformly implemented with stresses that would result in nominal stress ranges of $\Delta\sigma_{R,nom} = 100 \text{ N/mm}^2$ at perfect systems without the influence of secondary bending stresses. Consequently, straightening effects are included in the investigations. These are considerably lower in the case of clamping processes in testing machines than for practical support conditions (cf. Section 5.2). In addition to the type and size of misalignment and the magnitude of the load to be investigated, the thickness $t_{1=2}$ and length $L_{1=2}$ of the welded-on plates (cf. Figure 3-14) are relevant factors influencing the extent of straightening effects. In this respect, these effects are more distinct with thinner welded-on plates $t_{1=2}$ than with thicker plates. Furthermore, increasing lengths $L_{1=2}$ between the clamping sections and critical notches of the welds result in a magnification of straightening effects. This is especially true for angular misalignments under minor loads that cause almost no straightening, as greater lengths lead to an increasing misalignment that must be aligned by the clamp jaws. With greater loads, the straightening effects compensate the influence of the length almost completely. For more detailed information, it is referred to the assessments in [1].

5.1.1 Evaluation of impact due to clamping processes

In [1], extensive parameter studies on the influence of possible imperfections under clamping conditions in testing machines are presented. In this respect, apart from angular misalignments α and axial misalignments $e/t_{1=2}$, rotations θ around the longitudinal axis of the welded-on plates also have a decisive influence on the fatigue behaviour of cruciform joints. From the results of the parameter studies from [1], stress concentration factors SCF_R are determined, which result from the ratio of applied structural stress $\Delta\sigma_{R,hs}$ to associated nominal stress $\Delta\sigma_{R,nom}$ according to the following formula.

$$SCF_R = \frac{\Delta\sigma_{R,hs}}{\Delta\sigma_{R,nom}} \quad (5-1)$$

In the associated investigations, it is generally assumed that in practice, the influences from imperfections on the resulting structural stress ranges $\Delta\sigma_{R,hs}$ under clamping conditions in testing machines can be explicitly determined by the required numerical FE models of the structural stress concept. Since, in contrast, no FE models are required in the nominal stress concept, the influences of the complex secondary bending moments caused by the restraint processes on the resulting nominal stress ranges $\Delta\sigma_{R,nom}$ cannot be determined analytically. Accordingly, despite the investigations regarding imperfections, the required nominal stress ranges are determined by the simplified normative analysis with $\Delta\sigma_{R,nom} = \Delta F/A$ to ensure a practical comparability of the results.

In order to be able to assess the economic efficiency of the structural stress concept compared to the nominal stress concept, the acting stress concentration factor SCF_R in the relevant area is analysed and related to the decisive stress concentration factor SCF_C of the resistance side. For this purpose, SCF_C is calculated according to the

following formula from the relevant normatively specified resistances in the structural and nominal stress concept.

$$SCF_C = \frac{\Delta\sigma_{C,hs}}{\Delta\sigma_{C,nom}} \quad (5-2)$$

If the acting stress concentration factor SCF_R exceeds the stress concentration factor on the resistance side SCF_C , consequently an economic applicability of the structural stress concept compared to the nominal stress concept is no longer provided. In this way, critical imperfections can be determined starting from which the structural stress concept leads to unfavourable results. In the following, the associated results on angular misalignment α (cf. Section 5.1.1.1), axial misalignment $e/t_{1=2}$ (cf. Section 5.1.1.2), rotation θ of the welded-on plates (cf. Section 5.1.1.3) and the superimposition of the mentioned imperfections (cf. Section 5.1.1.4) are presented in summarised form.

5.1.1.1 *Angular misalignment*

The evaluation of the influence of angular misalignment α of the welded-on plates around the y_{global} -axis (cf. Chapter 2.5.2.1) is conducted for a range of up to $\alpha = 5.00^\circ$. With increasing angular misalignment α , the acting stress concentration factor increases linearly to a maximum of $SCF_R = 7.00$. In this respect, besides the magnitude of the angular misalignment α , only the length $L_{1=2}$ and thickness $t_{1=2}$ of the welded-on plates significantly influence the resulting stress increase. With increasing $t_{1=2}$ and decreasing $L_{1=2}$ this is due to the resulting increase in stiffness of the restrained welded-on plates which, in combination with the clamping process, leads to greater stress concentrations.

The parameter studies in [1] demonstrate that the economic applicability of the structural stress concept compared to the nominal stress concept leads to different results depending on the fatigue classifications of the normative regulations and guidelines. Since the fatigue classes according to DIN EN 1993-1-9 [2] and prEN 1993-1-9 [4] in the nominal stress concept result through the effective connection length (cf. Chapter 2.4), the weld thickness a has a decisive influence on the corresponding classification. Accordingly, it can be determined for these normative regulations that the applicability for cruciform joints with $t_{1=2} = 12 \text{ mm}$ in combination with weld thicknesses $a \leq 8 \text{ mm}$ is only given for angular misalignments of up to $\alpha \approx 0.30^\circ$. On the other hand, for welds $a > 8 \text{ mm}$, the structural stress concept according to DIN EN 1993-1-9 [2] and prEN 1993-1-9 [4] can be applied economically up to $\alpha \approx 0.50^\circ$. According to the guidelines of the IIW [3], only the latter applies, irrespective of the weld thickness a , since no consideration of the effective connection length is required in the fatigue classes (cf. Chapter 2.4). For greater thicknesses $t_{1=2}$ and reduced lengths $L_{1=2}$ of the welded-on plates, the resulting stress concentration factors SCF_R increase non-linearly to a greater extent, which further reduces the applicability of the structural stress concept compared to the nominal stress concept. According to the evaluation class C of DIN EN ISO 5817 [68] (cf. Chapter 2.5.2.1), structural stress ranges are two and a half times greater at a permissible $\alpha = 2^\circ$ than according to the nominal stress concept. Therefore, it is evident that even specifications according to evaluation group B of [68] with $\alpha \leq 1^\circ$ can lead to results that no longer permit economic applicability of the structural stress concept.

5.1.1.2 Axial misalignment

The effects of the axial misalignment $e/t_{1=2}$ in z_{global} -direction (cf. Chapter 2.5.2.2) on the stress concentration factor are evaluated in a range of up to $e/t_{1=2} = 0.5$. This corresponds to the maximum permissible manufacturer tolerances according to DIN 50100 [27]. The corresponding results are consistent with the evaluations of the angular misalignment α . However, the maximum stress concentration factors SCF_R resulting from the parameter studies are significantly lower with $SCF_R = 3.00$.

With regard to the economic applicability of the structural stress concept, the decisive parameters for the fatigue class classification are evaluated with regard to SCF_R , and the results are compared with SCF_C according to the DIN EN 1993-1-9 [2], guidelines of the IIW [3] and prEN 1993-1-9 [4]. In this respect, the thickness of the welded-on plates $t_{1=2}$ is decisive for the thickness correction factor that may be required for SCF_C in the structural and nominal stress concept (cf. Chapter 2.6). In addition, the intermediate plate thickness t_3 must be considered, as it has a significant influence on the effective connection length of the thickness effect. For cruciform joints with $t_{1=2} = 12 \text{ mm}$, it can be verified in the associated evaluations that even small axial misalignments $e/t > 0.10$ lead to results that no longer allow for economic applicability of the structural stress concept compared to the nominal stress concept. With thicker plates $t_{1=2}$, the limit value for axial misalignment further decreases significantly. Consequently, the economic applicability of the structural stress concept is no longer ensured even far below the limit according to 50100 [27].

5.1.1.3 Rotation

A rotation θ of the welded-on plates around the x_{global} -axis (cf. Chapter 2.5.2.3) is currently not considered in any normative regulations or guidelines. However, the detectable influence of this imperfection is mainly due to the alignment effects caused by the clamping process and consequently does not significantly contribute under practical support conditions. In the associated parameter studies on clamping processes, rotations up to $\theta = 5.00^\circ$ are evaluated. The results show that stress concentration factors SCF_R increase almost linearly with increasing rotations θ of the welded-on plates. In this respect, shorter lengths $L_{1=2}$ and increasing thicknesses $t_{1=2}$ of the welded-on plates lead to increasing values. In addition, increasing weld thicknesses a , primary plate widths w_1 and intermediate plate thicknesses t_3 result in an increase of SCF_R , as the primary plate is twisted around its longitudinal axis during the clamping process. Consequently, significantly higher structural stress ranges occur on the relevant side of the plate, which are superimposed on the already increased values resulting from the transverse strain constraint. The resulting maximum stress concentration factors SCF_R from the associated parameter studies are with $SCF_R = 5.50$ between the results from angular and axial misalignments.

With regard to the economic application of the structural stress concept compared to the nominal stress concept, the weld thickness a as well as the plate thickness of the welded-on plates $t_{1=2}$ and of the intermediate plate t_3 are among the influencing parameters of SCF_C . The corresponding evaluations indicate that even small rotations of more than $\theta \approx 1^\circ$ no longer lead to economic applicability of the structural stress concept. Consequently, rotation of the welded-on plates should imperatively be

considered in studies on clamping processes, as a significant influence on the system behaviour of cruciform joints can be observed.

5.1.1.4 *Superimposition of imperfections*

In addition, in [1] superimpositions of the previously presented imperfections are evaluated in order to determine reciprocal influences. In this respect, it can be stated that only the magnitudes of the expected stress concentration factors SCF_R vary depending on the combined imperfections. However, this is due to the respective effects of the individual misalignments. Consequently, the superposition of influences from imperfections suggested according to the guidelines of the IIW [3] can be confirmed (cf. Chapter 2.5).

5.1.2 Evaluation of stress concentration factors

In addition to the evaluations of influences due to imperfections on the fatigue verification in the structural stress concept under restraint conditions (cf. Section 5.1.1), the effects from axial and angular misalignment are analysed in more detail in this section. The objective is to indirectly determine the behaviour of clamping processes by means of analytical formulae. For this purpose, numerical studies are presented and related to the information on the indirect consideration of imperfections provided in Chapter 2.5.3. Concerning this matter, Xing and Dong [5] provide the following indirect calculation approach of resulting stress increases due to clamping processes with regard to cruciform joints with axial misalignment.

$$k_{m,axial,Xing\&Dong} = 1 + \frac{3}{5} \cdot \frac{\left(11L^3 - 40L^2L_1 - 12L^2L_c + 30LL_1^2 + 60LL_1L_c + 30LL_c^2 - 60L_1^2L_c - 20L_c^3 \right)}{L^3} \cdot \frac{e}{t_{1=2}} \quad (5-3)$$

The required parameters for formula (5-3) are illustrated in Figure 5-1. In the following evaluations, the length L_c between the clamping section and the critical notch (cf. Figure 5-1) is simplified with $L_c = L_{total}/2 = L_{1=2}$. Due to the marginal difference in length between L_2 and L_c , this simplification only results in an insignificant deviation.

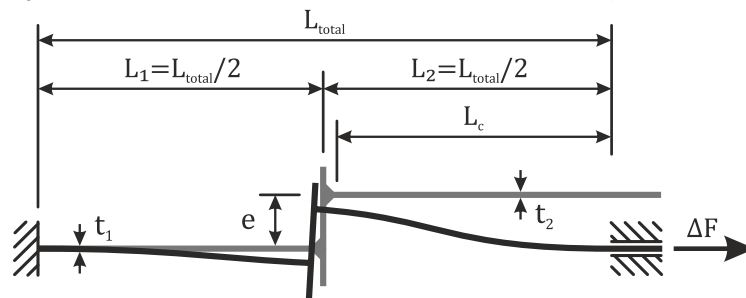


Figure 5-1: Parameter definition for indirect determination of the influence from axial misalignment according to Xing and Dong [5]

To verify the applicability of the calculation method proposed by Xing and Dong [5], parameter studies on cruciform joints with different thicknesses $t_{1=2}$ and lengths L_{total} are presented subsequently. In this respect, both axial and angular misalignments are analysed. The thickness of the intermediate plate and the constant component width are set uniformly at $t_3 = 25 \text{ mm}$ and $w_1 = 100 \text{ mm}$ to ensure comparability of the generated results. In order to numerically determine the required stress concentration

factors $k_{m,FEA}$ for both axial and angular misalignment, the structural stress ranges $\Delta\sigma_{R,hs,FEA,imperfect}$ determined on imperfect FE models are related to the structural stress ranges $\Delta\sigma_{R,hs,FEA,perfect}$ of perfect FE models excluding imperfections and therefore secondary bending moments. The relevant structural stress ranges are determined according to linear stress extrapolation for finely meshed solid models (cf. Chapter 3.3). The calculations are performed according to the following formula.

$$k_{m,FEA} = \frac{\Delta\sigma_{R,hs,FEA,imperfect}}{\Delta\sigma_{R,hs,FEA,perfect}} \quad (5-4)$$

The stress concentration factors $k_{m,FEA}$ thus describe the definite stress increase in the structural stress concept due to imperfections (cf. Chapter 2.5). The resulting stress concentration factors are generally also applicable to the nominal and notch stress concept, as the factors simply represent the percentage increase in the effective stresses due to imperfections.

In accordance with Section 5.1, the test load is uniformly specified at a level such that a nominal stress range of $\Delta\sigma_{R,nom} = 100 \text{ N/mm}^2$ is to be expected on the perfect system. In this way, a realistic load level of fatigue tests can be ensured in order to determine stress concentration factors $k_{m,FEA}$. In contrast, insufficient loading would lead to excessively large stress concentration factors $k_{m,FEA}$, as straightening effects are only insufficiently and unrealistically included in their determination. According to Figure 5-2, for example, angular misalignment of only $\alpha = 1^\circ$ with a test load leading to $\Delta\sigma_{R,nom} = 1 \text{ N/mm}^2$ results in an unrealistic overestimation of the stress concentration factor of $k_{m,angular,FEA,\Delta\sigma_{R,nom}=1\text{MPa}} \approx 45.4 \gg k_{m,angular,FEA,\Delta\sigma_{R,nom}=100\text{MPa}} \approx 1.8$.

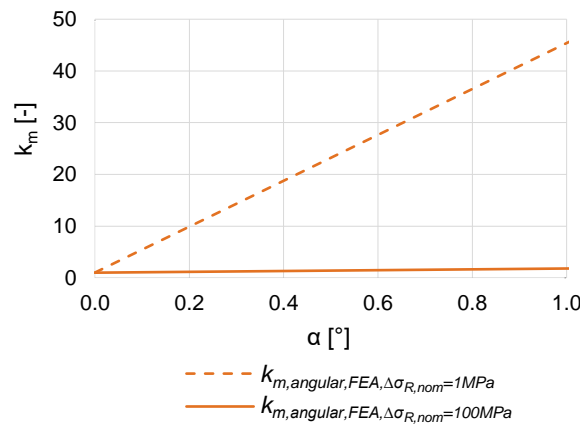


Figure 5-2: Evaluation of analytical stress concentration factors $k_{m,angular,Xing\&Dong}$ according to Xing and Dong [5] and numerical stress concentration factors $k_{m,angular,FEA}$ for nominal stress ranges of 1 N/mm^2 and 100 N/mm^2 in the FEA for cruciform joints with angular misalignment

Consequently, with a resulting stress for $\Delta\sigma_{R,nom} = 100 \text{ N/mm}^2$, more realistic stress concentration factors $k_{m,FEA}$ in the range of the analytical values of Xing and Dong [5] are identifiable, as resulting straightening effects are considered more practically. A necessary load-dependent investigation of $k_{m,FEA}$ is provided later in this section.

In the following Figure 5-3 the evaluation of axial misalignment for specimen lengths of $L_{total} = 600 \text{ mm}$ and 1400 mm is presented. In this respect, thicknesses of the welded-on plates of $t_{1=2} = 10 \text{ mm}$, 25 mm and 40 mm are evaluated. The resulting numerically

determined stress concentration factors $k_{m,axial,FEA}$ are compared to the analytical results of $k_{m,axial,Xing\&Dong}$ according to Xing and Dong [5].

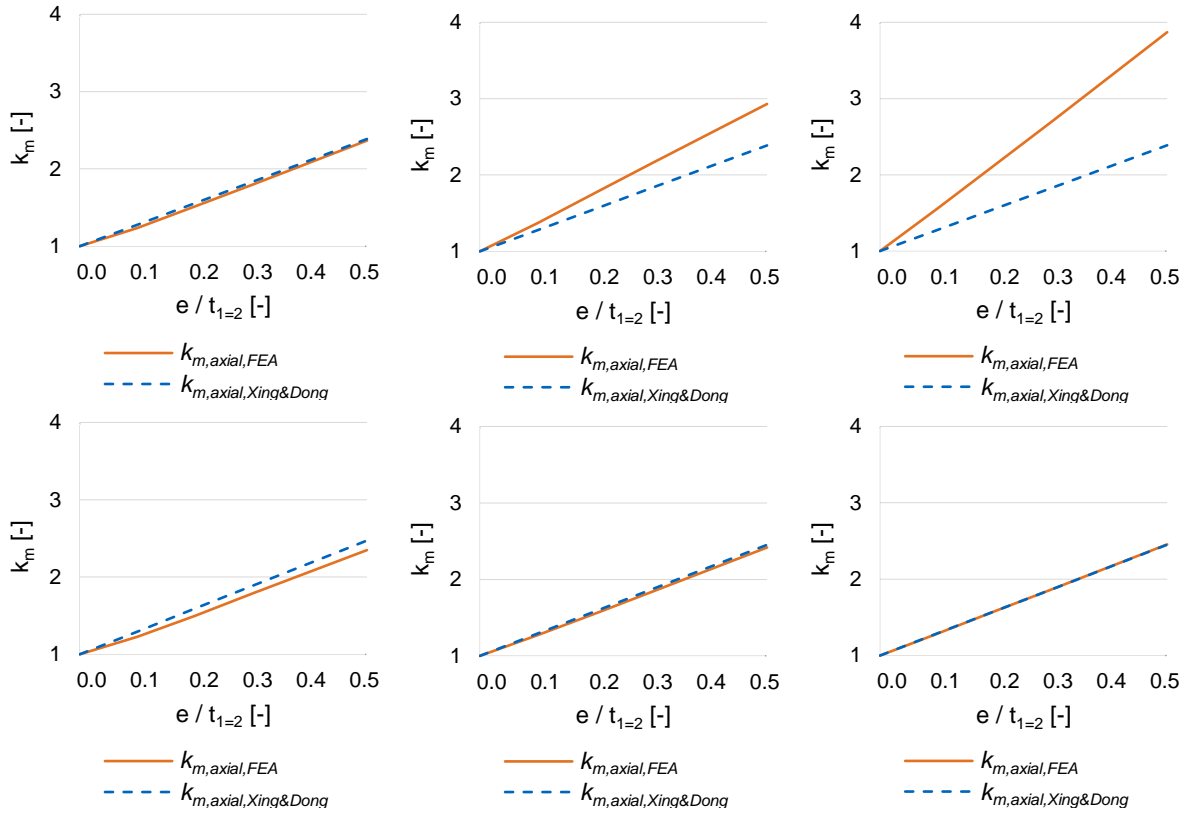


Figure 5-3: Numerical parameter study of the axial stress concentration factor $k_{m,axial,FEA}$ and comparison with $k_{m,axial,Xing\&Dong}$ from [5] for $t_{1=2} = 10$ mm (left), $t_{1=2} = 25$ mm (middle) and $t_{1=2} = 40$ mm (right) with total length $L_{total} = 600$ mm (top) and $L_{total} = 1400$ mm (bottom)

With regard to the evaluation from Figure 5-3 on axial misalignment, it can be demonstrated that with larger total lengths of the cruciform joints, numerically improved accordance can be achieved with the analytical results according to Xing and Dong [5]. With increasing stiffness of the welded-on plates, it becomes apparent that the stress concentration factors resulting from [5] cannot be verified by the numerical results for $k_{m,axial,FEA}$. In this respect, the analytical stress concentration factor of Xing and Dong [5] underestimates the large stiffness, which results in significantly larger k_m factors (cf. Figure 5-3). With increasing thicknesses, the analytical approach to $k_{m,axial,Xing\&Dong}$ according to [5] remains invariant, as the thickness only influences formula (5-3) through the relationship $e/t_{1=2}$. Consequently, stiffness influences cannot be considered sufficiently by the indirect estimation of axial misalignments under restraint conditions according to Xing and Dong [5], which requires a modification by means of a stiffness ratio $t_{1=2}/L_{total}$.

With regard to angular misalignments, Xing and Dong [5] specify the following indirect formula for determining the angular stress concentration factor $k_{m,angular,Xing\&Dong}$.

$$k_{m,angular,Xing\&Dong} = 1 + \frac{4}{5} \cdot \frac{(L^4 - 9L^3L_c + 39L^2L_c^2 - 60L_c^3L + 30L_c^4)}{L^3t_{1=2}} \cdot \alpha \quad (5-5)$$

The required parameters are defined according to the following Figure 5-4. Again, the length L_c between the clamping section and the critical notch is approximated by $L_{1=2}$.

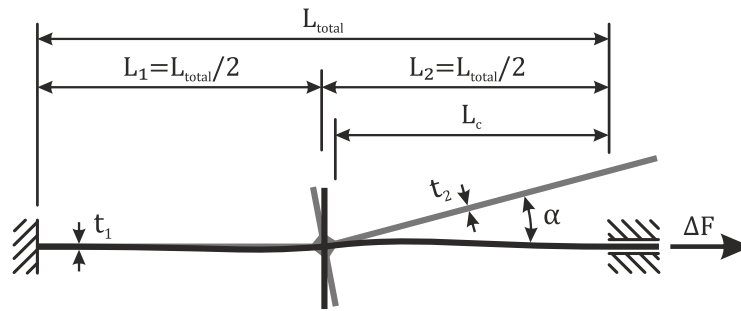


Figure 5-4: Parameter definition for indirect determination of the influence from angular misalignment according to Xing and Dong [5]

Corresponding to the studies on axial misalignment, numerical parameter studies are also carried out on angular misalignments. These are based on the investigations of axial misalignment. The corresponding results are summarised in Figure 5-5.

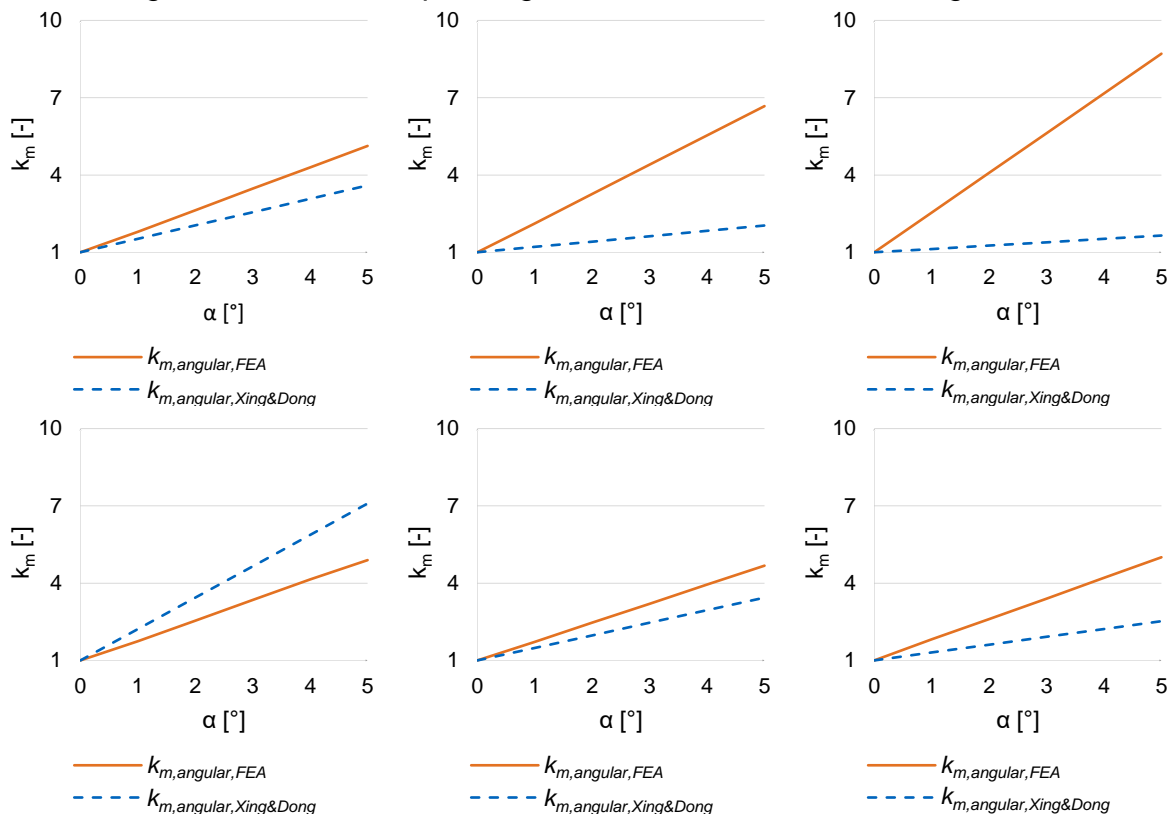


Figure 5-5: Numerical parameter study of the angular stress concentration factor $k_{m,angular,FEA}$ and comparison with $k_{m,angular,Xing\&Dong}$ from [5] for $t_{1=2} = 10\text{ mm}$ (left), $t_{1=2} = 25\text{ mm}$ (middle) and $t_{1=2} = 40\text{ mm}$ (right) with total length $L_{total} = 600\text{ mm}$ (top) and $L_{total} = 1400\text{ mm}$ (bottom)

In contrast to the results obtained for axial misalignment (cf. Figure 5-3), the deviations between the numerically determined stress concentration factors $k_{m,angular,FEA}$ and the analytically determined factors $k_{m,angular,Xing\&Dong}$ are significantly greater in terms of angular misalignment (cf. Figure 5-5). While the analytical approach according to [5] for relatively small specimen lengths generally leads to an underestimation of the numerical results, it is noticeable that increasingly larger differences result from the increasing stiffness of the welded-on plates. The results for $k_{m,angular,Xing\&Dong}$ decrease with increasing plate thicknesses $t_{1=2}$ (cf. Figure 5-5). In contrast, $k_{m,angular,FEA}$ increases significantly with thicker $t_{1=2}$, which is due to the greater

stiffness of the welded-on plates. Furthermore, the analytical values of $k_{m,angular,Xing\&Dong}$ increase with larger lengths L_{total} of the investigated cruciform joints. However, since the resulting component stiffness decreases with increasing length, this system behaviour cannot be verified numerically by the FE models. Therefore, for the cruciform joint with $t_{1=2} = 10\text{ mm}$ and a total length of $L_{total} = 1400\text{ mm}$, there is even an overestimation by the analytical k_m factors according to Xing and Dong [5] (cf. bottom left side of Figure 5-5). Consequently, the analytical derivation of formula (5-5) for angular misalignment according to [5] has to be modified with regard to stiffness effects based on the ratio $t_{1=2}/L_{total}$.

In order to carry out the necessary modifications, the deviations between the analytical formulae according to Xing and Dong [5] and the results of the FEA are evaluated. In this respect, the following formula is assessed for the analysed ratios $t_{1=2}/L_{total}$ to determine a correction factor between the FEA and Xing and Dong [5]. The evaluation is performed for the different plate thicknesses $t_{1=2} = 10\text{ mm}$, 25 mm and 40 mm for both axial and angular misalignment.

$$factor = \frac{(k_{m,FEA} - 1)}{(k_{m,Xing\&Dong} - 1)} \quad (5-6)$$

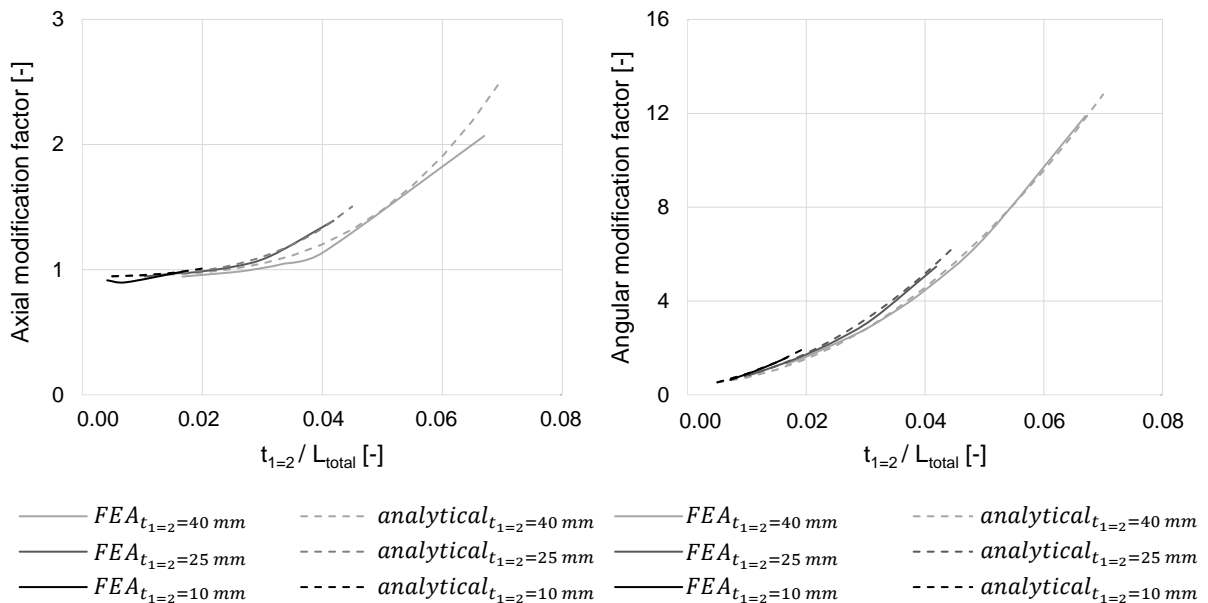


Figure 5-6: Studies on the influence of the $t_{1=2}/L_{total}$ -ratio on the correction factor between FEA and Xing and Dong [5] on axial misalignment (left) and angular misalignment (right) with analytically determined compensation curves

Figure 5-6 summarises the studies on the axial and angular modification factors between the results of the FEA and Xing and Dong [5] based on the plate thicknesses investigated. In this respect, the influence of stiffness on the modification factor is investigated by the ratio of $t_{1=2}/L_{total}$. In addition, the analytically determined compensation curves are presented in the evaluation of axial misalignment and angular misalignment. In this way, suitable correction factors are to be determined. To this end, the mathematical theorems for the $factor_{axial}$ and $factor_{angular}$ presented below can be derived based on the results for axial and angular misalignment from Figure 5-6.

$$factor_{axial} = \left[\begin{array}{c} \left(-\frac{2}{15} \cdot t_{1=2} + 11.333 \right) \cdot 1000 \cdot \left(\frac{t_{1=2}}{L_{total}} \right)^3 - \\ -125 \cdot \left(\frac{t_{1=2}}{L_{total}} \right)^2 + 2 \cdot \frac{t_{1=2}}{L_{total}} + 0.94 \end{array} \right] \quad (5-7)$$

$$factor_{angular} = \left[\begin{array}{c} \left(-\frac{1}{300} \cdot t_{1=2} + 2.5833 \right) \cdot 1000 \cdot \left(\frac{t_{1=2}}{L_{total}} \right)^2 + \\ + (-t_{1=2} + 45) \cdot \frac{t_{1=2}}{L_{total}} + \left(\frac{1}{200} \cdot t_{1=2} + 0.25 \right) \end{array} \right] \quad (5-8)$$

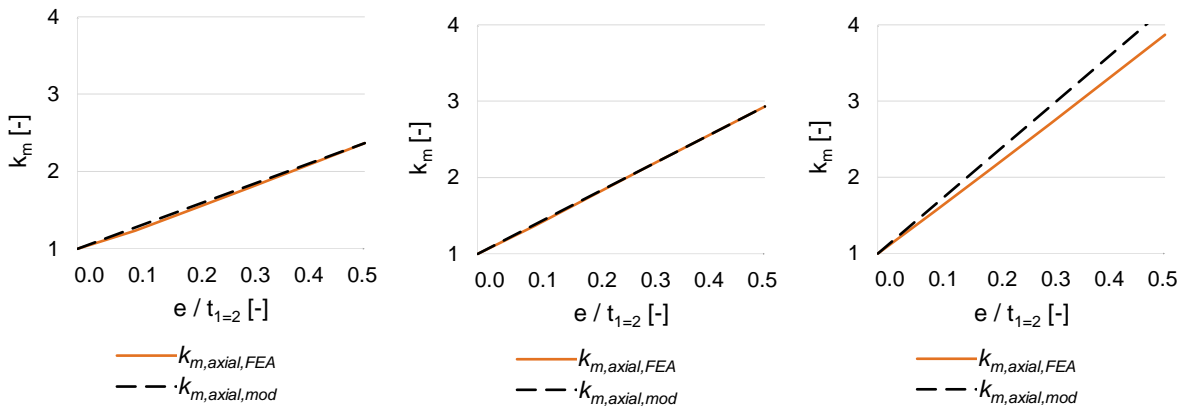
Figure 5-6 indicates that there is a significant influence of the $t_{1=2}/L_{total}$ ratio on the axial and angular modification factors. With increasing stiffness, the correction values for both axial and angular misalignment are considerably greater. In addition, there is a clear dependence on the plate thickness. Consequently, it is reasonable to modify the original formulae of Xing and Dong [5] by suitable correction factors which, according to formulae (5-7) and (5-8), dependent on both the plate thickness $t_{1=2}$ and the ratio $t_{1=2}/L_{total}$. According to Figure 5-6, the respective curves of the analytically derived formulae show a sufficiently good agreement with the results from the parameter studies.

Due to the correlation from formula (5-6), the corrected stress concentration factors $k_{m,axial,mod}$ and $k_{m,angular,mod}$ thus result according to the following formulae.

$$k_{m,axial,mod} = 1 + k_{m,axial,Xing\&Dong} \cdot factor_{axial} \quad (5-9)$$

$$k_{m,angular,mod} = 1 + k_{m,angular,Xing\&Dong} \cdot factor_{angular} \quad (5-10)$$

Through these modifications in the indirect consideration of axial and angular misalignments, the missing influences from stiffness effects can be included in the existing formulae of Xing and Dong [5]. To check the applicability of the modification, the parameter studies presented in Figure 5-3 and Figure 5-5 are recalculated with the modified mathematical correlations. The results are summarised in Figure 5-7 for axial misalignment and Figure 5-8 for angular misalignment. Through the adjustment, a sufficiently good agreement between the stress concentration factors $k_{m,FEA}$ from the FEA and $k_{m,mod}$ can be achieved. This applies to both the investigated axial misalignments (cf. Figure 5-7) and angular misalignments (cf. Figure 5-8).



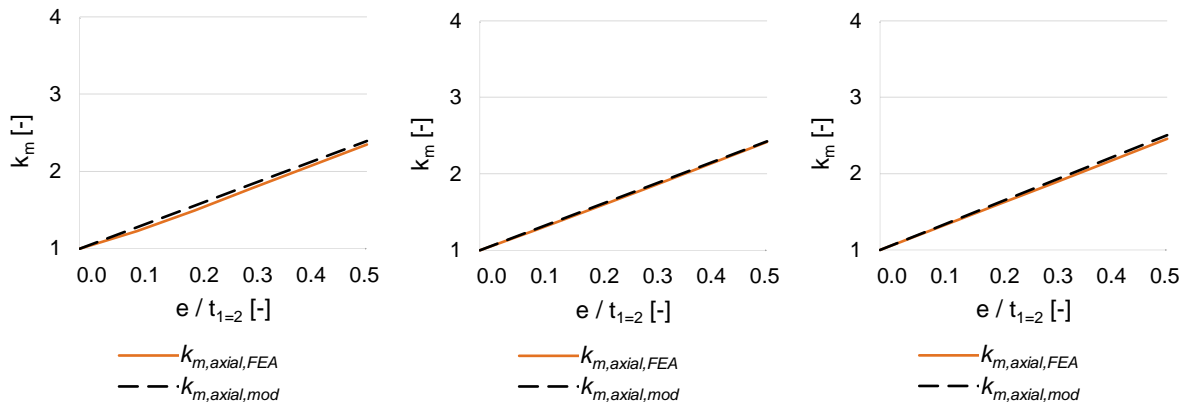


Figure 5-7: Numerical parameter study with $k_{m,axial,mod}$ for $t_{1=2} = 10$ mm (left), $t_{1=2} = 25$ mm (middle) and $t_{1=2} = 40$ mm (right) with total length $L_{total} = 600$ mm (top) and $L_{total} = 1400$ mm (bottom)

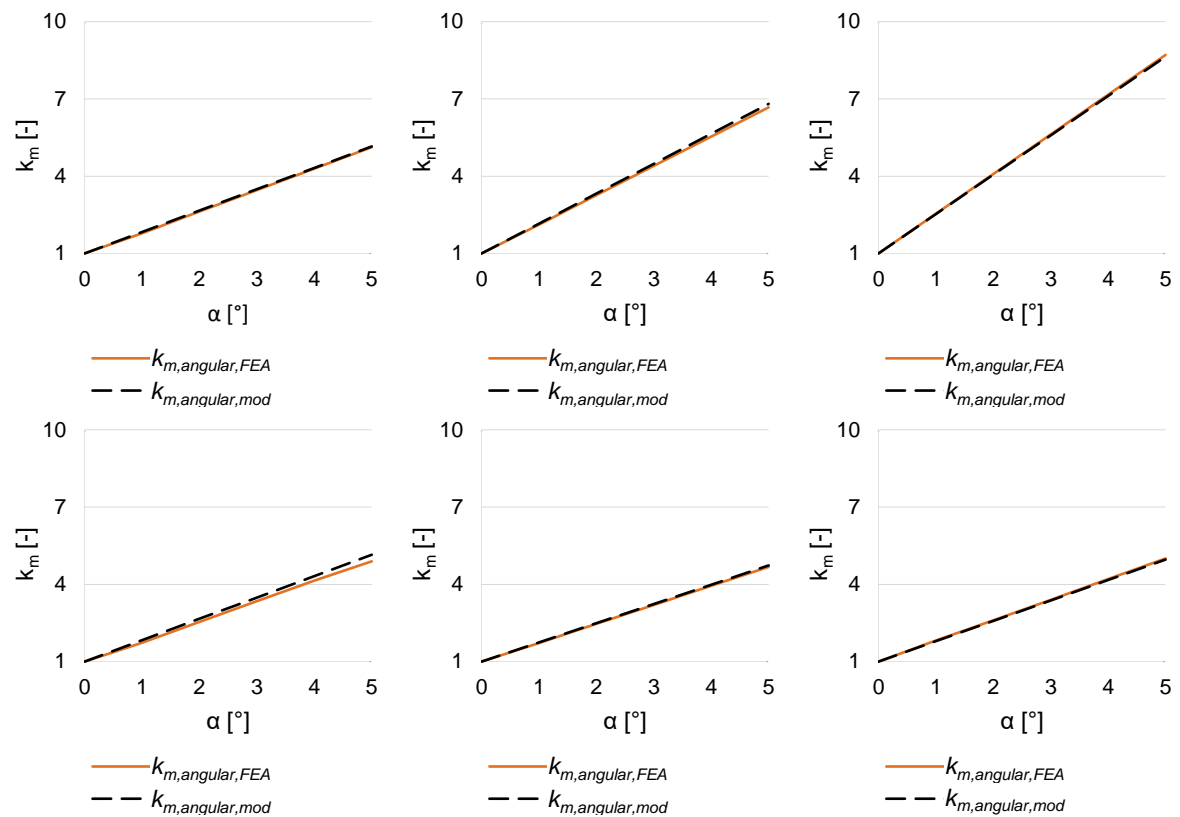


Figure 5-8: Numerical parameter study with $k_{m,angular,mod}$ for $t_{1=2} = 10$ mm (left), $t_{1=2} = 25$ mm (middle) and $t_{1=2} = 40$ mm (right) with total length $L_{total} = 600$ mm (top) and $L_{total} = 1400$ mm (bottom)

Since the parameter studies performed on the clamping process are based entirely on a stress level of $\Delta\sigma_{R,nom} = 100$ N/mm², it is also necessary to implement load-dependent factors. This is due to the fact that the stress concentration factors k_m are strongly dependent on the applied load and the associated straightening effects. With regard to lower loads, significantly larger and therefore unrealistic k_m factors are detected in clamping processes (cf. Figure 5-2). In order to be able to investigate the corresponding behaviour in more detail, the factors for axial and angular misalignment $k_{m,axial,FEA}$ and $k_{m,angular,FEA}$ are evaluated for a variety of different load levels and the resulting nominal stress ranges are related to the validated factors for $\Delta\sigma_{R,nom} = 100$ N/mm². In this way, suitable load-dependent factors ΔF_{factor} can be determined.

These factors $\Delta F_{factor,axial}$ and $\Delta F_{factor,angular}$ result from the following formula depending on the calculated imperfections.

$$\begin{aligned} \Delta F_{factor} &= \frac{k_{m,FEA}(\Delta\sigma_{R,nom})}{k_{m,FEA}(\Delta\sigma_{R,nom} = 100 \text{ N/mm}^2)} = \\ &= \frac{\left(\frac{\Delta\sigma_{R,hs,FEA,imperfect}(\Delta\sigma_{R,nom})}{\Delta\sigma_{R,hs,FEA,perfect}(\Delta\sigma_{R,nom})}\right)}{\left(\frac{\Delta\sigma_{R,hs,FEA,imperfect}(\Delta\sigma_{R,nom} = 100 \text{ N/mm}^2)}{\Delta\sigma_{R,hs,FEA,perfect}(\Delta\sigma_{R,nom} = 100 \text{ N/mm}^2)}\right)} \end{aligned} \quad (5-11)$$

Figure 5-9 exemplarily presents the corresponding evaluations of ΔF_{factor} for axial and angular misalignment for cruciform joints with thicknesses of $t_{1=2} = 10 \text{ mm}$.

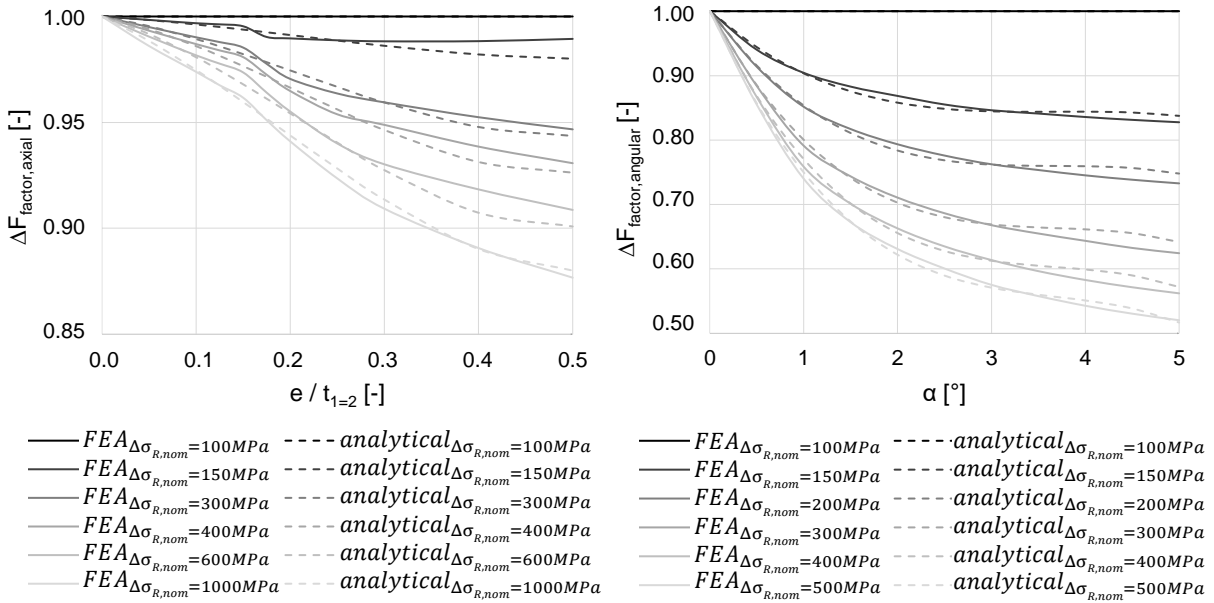


Figure 5-9: Numerical parameter study on cruciform joints with $t_{1=2} = 10 \text{ mm}$ for the load-dependent correction factor ΔF_{factor} for axial misalignment (left) and angular misalignment (right) with analytically derived results

According to Figure 5-9, the results for the load-dependent factors ΔF_{factor} for cruciform joints with plate thicknesses $t_{1=2} = 10 \text{ mm}$ are highly non-linear. Consequently, the associated correlations are difficult to represent analytically. However, the influence from straightening effects is clearly identifiable and cannot be neglected in the analysis. For this reason, the derived formula for $\Delta F_{factor,axial}$ and $\Delta F_{factor,angular}$ are very extensive. The corresponding formulae are presented below and are also illustrated in Figure 5-9.

$$\Delta F_{factor,axial,t_{1=2}=10mm} = \left[\begin{aligned} &\left(\frac{-2.9 \cdot 10^{-6} \cdot (\Delta\sigma_{R,nom})^2 + 0.00435 \cdot \Delta\sigma_{R,nom} - 0.406}{1.9 \cdot 10^{-6} \cdot (\Delta\sigma_{R,nom})^2 - 0.00275 \cdot \Delta\sigma_{R,nom} + 0.256} \right) \cdot \left(\frac{e}{t_{1=2}} \right)^3 + \\ &\left(\frac{-\Delta\sigma_{R,nom}}{6000} + \frac{6}{\Delta\sigma_{R,nom}} - 0.04333 \right) \cdot \frac{e}{t_{1=2}} + \\ &+ 1.0 \end{aligned} \right] \quad (5-12)$$

$$\Delta F_{factor,angular,t_{1=2}=10mm} = \left[\begin{array}{l} \left(\frac{0.95}{\Delta\sigma_{R,nom}} - 0.0095 \right) \cdot \left(\alpha \cdot \frac{360^\circ}{2\pi} \right)^3 + \\ + \left(-\frac{10.5}{\Delta\sigma_{R,nom}} + 0.105 \right) \cdot \left(\alpha \cdot \frac{360^\circ}{2\pi} \right)^2 + \\ + \left(-\frac{\Delta\sigma_{R,nom}}{15000} + \frac{37.5}{\Delta\sigma_{R,nom}} - 0.368333 \right) \cdot \left(\alpha \cdot \frac{360^\circ}{2\pi} \right) + 1.0 \end{array} \right] \quad (5-13)$$

Although the agreement between the analytical derivation and the results from the FEA is not always optimal, no more adequate analytical adjustments are possible due to the strongly non-linear characteristics. In addition, the evaluation is performed for plates with $t_{1=2} = 40 \text{ mm}$. The results are shown in the following Figure 5-10.

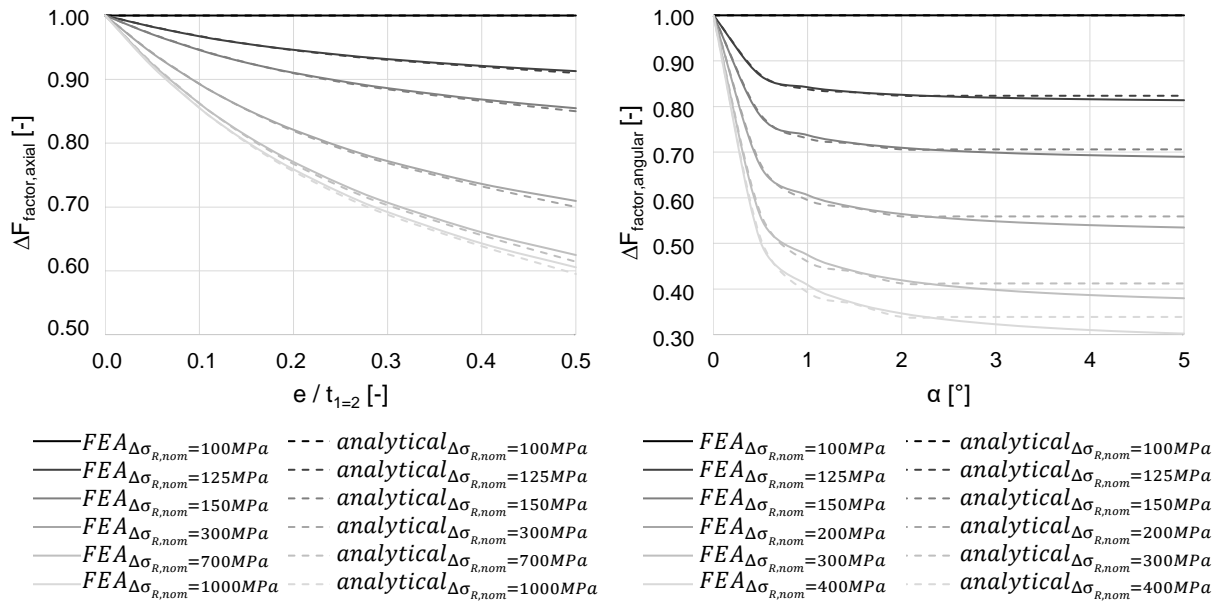


Figure 5-10: Numerical parameter study with $t_{1=2} = 40 \text{ mm}$ for the load-dependent correction factor ΔF_{factor} for axial misalignment (left) and angular misalignment (right) with analytically derived results

According to Figure 5-10, for plates with thicknesses of the welded-on plates of $t_{1=2} = 40 \text{ mm}$ there is a strong non-linear influence, corresponding to $t_{1=2} = 10 \text{ mm}$. However, the characteristics in Figure 5-10 are completely different from those in Figure 5-9. Therefore, the assessment has to be dependent on the thickness of the component, as there is a significant influence on the resulting straightening effects. Nevertheless, the attempted inclusion of thickness dependence in the formulae for ΔF_{factor} could not be achieved due to the large deviations between the results of Figure 5-9 and Figure 5-10. Therefore, the evaluations of $\Delta F_{factor,axial}$ and $\Delta F_{factor,angular}$ are only carried out for the defined plate thicknesses $t_{1=2} = 10 \text{ mm}$ (cf. Figure 5-9) and $t_{1=2} = 40 \text{ mm}$ (cf. Figure 5-10). The influences can be derived analytically using the following formulae.

$$\Delta F_{factor,axial,t_{1=2}=40mm} = \left[\begin{array}{l} \left(\frac{240}{\Delta\sigma_{R,nom}} - 2.4 \right) \cdot \left(\frac{e}{t_{1=2}} \right)^3 + \\ + \left(-\frac{320}{\Delta\sigma_{R,nom}} + 3.2 \right) \cdot \left(\frac{e}{t_{1=2}} \right)^2 + \\ + \left(\frac{190}{\Delta\sigma_{R,nom}} - 1.9 \right) \cdot \frac{e}{t_{1=2}} + 1.0 \end{array} \right] \quad (5-14)$$

$$\begin{aligned}
 \alpha \leq 2^\circ: \quad \Delta F_{factor,angular,t_{1=2}=40mm} &= \left[\begin{aligned}
 &\left(-\frac{0.335}{\Delta\sigma_{R,nom}} + 0.00335 \right) \cdot \left(\alpha \cdot \frac{360^\circ}{2\pi} \right)^6 + \\
 &+ \left(\frac{5.8}{\Delta\sigma_{R,nom}} - 0.058 \right) \cdot \left(\alpha \cdot \frac{360^\circ}{2\pi} \right)^5 + \\
 &+ \left(-\frac{39.5}{\Delta\sigma_{R,nom}} + 0.395 \right) \cdot \left(\alpha \cdot \frac{360^\circ}{2\pi} \right)^4 + \\
 &+ \left(\frac{135}{\Delta\sigma_{R,nom}} - 1.35 \right) \cdot \left(\alpha \cdot \frac{360^\circ}{2\pi} \right)^3 + \\
 &+ \left(-\frac{242}{\Delta\sigma_{R,nom}} + 2.42 \right) \cdot \left(\alpha \cdot \frac{360^\circ}{2\pi} \right)^2 + \\
 &+ \left(\frac{222}{\Delta\sigma_{R,nom}} - 2.22 \right) \cdot \left(\alpha \cdot \frac{360^\circ}{2\pi} \right) + 1.0
 \end{aligned} \right] \quad (5-15) \\
 \alpha > 2^\circ: \quad \Delta F_{factor,angular,t_{1=2}=40mm} &= \frac{88.16}{\Delta\sigma_{R,nom}} + 0.1184
 \end{aligned}$$

Based on the analytical formulae of Xing and Dong [5] with the corrections applied for stiffness, plate thickness and load dependency, it should therefore be possible to determine effects of combined axial and angular misalignment by the final stress concentration factor $k_{m,final}$. In this respect, it is important to note that the angular misalignment in the specifications according to Xing and Dong [5] for $k_{m,Xing\&Dong}$ as well as the analytical derivations for the modification factors ΔF_{factor} are specified in radians. Since in practice there are usually both axial and angular misalignments, formula (2-38) according to the IIW [3] (cf. Chapter 2.5.3.2) is used to combine the respective indirect stress concentration factors. This is reasonable as it could be demonstrated in the parameter studies on combined imperfections that a superposition of the effects of individual misalignments is possible (cf. Section 5.1.1.4). The final stress concentration factor $k_{m,final}$ is thus calculated according to the following formula.

$$k_{m,final} = 1 + \left[\begin{aligned}
 &(1 - k_{m,axial,Xing\&Dong} \cdot factor_{axial} \cdot \Delta F_{factor,axial}) + \\
 &+(1 - k_{m,angular,Xing\&Dong} \cdot factor_{angular} \cdot \Delta F_{factor,angular})
 \end{aligned} \right] \quad (5-16)$$

Numerical structural stress ranges $\Delta\sigma_{R,hs,imperfect,FEA}$ of imperfect FE models thus also should become determinable by the indirect consideration of stress-increasing effects through the multiplication of $k_{m,final}$ with the perfect structural stress $\Delta\sigma_{R,hs,perfect,FEA}$. In order to verify the effectiveness of the modification, the fatigue tests from Chapter 4 are analysed again. The corresponding evaluations are presented separately for the test series $WP3_1$, $WP3_2$ and $WP3_3$ in Figure 5-11, Figure 5-12 and Figure 5-13. Depending on the thickness of the welded-on plates $t_{1=2}$ the presented modification factors ΔF_{factor} are applied. With regard to test series $WP3_1$ and $WP3_2$ with welded-on plate thicknesses $t_{1=2} = 12\text{ mm}$, the factors presented for $t_{1=2} = 10\text{ mm}$ are assumed.

Effects of imperfections on cruciform joints

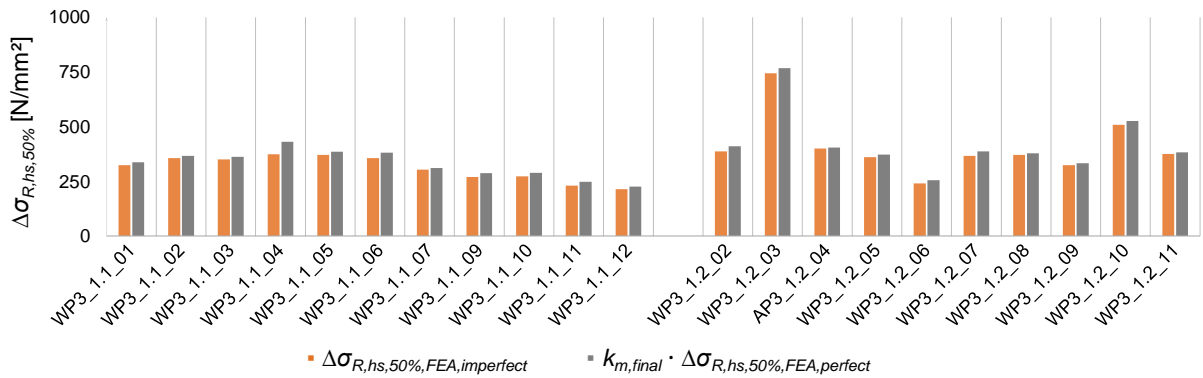


Figure 5-11: Comparison between directly determined structural stress ranges by imperfect FE models and analytically calculated structural stress ranges by stress concentration factors for $WP3_1$

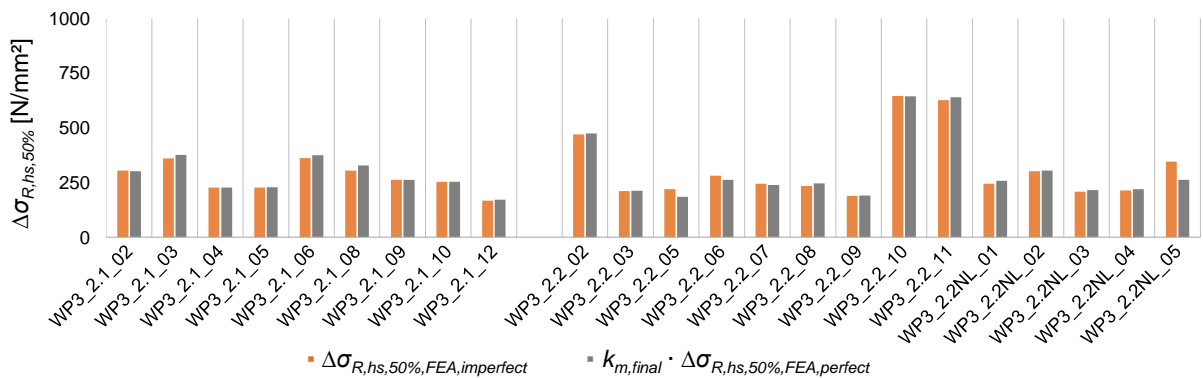


Figure 5-12: Comparison between directly determined structural stress ranges by imperfect FE models and analytically calculated structural stress ranges by stress concentration factors for $WP3_2$

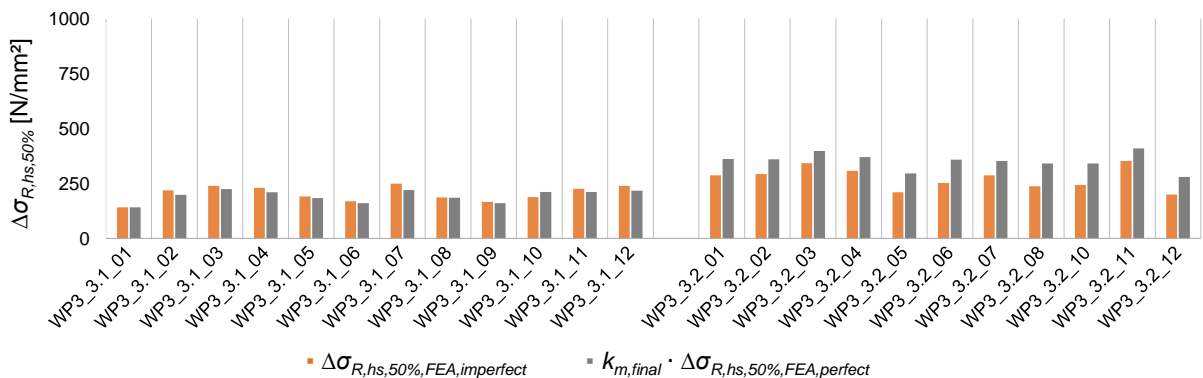


Figure 5-13: Comparison between directly determined structural stress ranges by imperfect FE models and analytically calculated structural stress ranges by stress concentration factors for $WP3_3$

For both test series $WP3_1$ (cf. Figure 5-11) and $WP3_2$ (cf. Figure 5-12), there is very good agreement between the structural stress ranges $\Delta\sigma_{R,hs,imperfect,FEA}$ determined on imperfect FE models and the stress ranges indirectly determined by the stress concentration factor $k_{m,final}$. Consequently, it is evident that the thickness of the intermediate plate t_3 of cruciform joints has no influence on the influences from imperfections resulting from clamping processes. In test group $WP3_3.1$, good conformities can be observed as well. However, the indirectly determined stress ranges lead to a slight underestimation of the imperfect structural stress ranges from the FEA. In this respect, the influence of increasing stiffness with thicker plate thicknesses may not have been sufficiently considered. Furthermore, since the fatigue tests of test group

WP3_3.2 were conducted with support elements to compensate for the large intentional misalignments (cf. Figure 4-3), it is not sufficient to apply the modified stress concentration factor. This is due to the fact that the welded-on plates with intentional imperfections are not aligned by the clamping process and consequently the resulting structural stress ranges would be significantly overestimated. For this reason, the indirect stress concentration factor $k_{m,axial}$ for the intended imperfections is determined in a simplified way by the specifications for practical support conditions of Xing and Dong [5] on axial misalignment (cf. Chapter 2.5.3.2.4). In this regard, classification (b) applies. The modified stress concentration factors $k_{m,final}$ from this section are thus determined exclusively for the unintended axial and angular misalignments. Nevertheless, it is noticeable in Figure 5-13 that larger deviations occur in test group WP3_3.2 with intentional imperfections than in the other test groups. Consequently, the system behaviour cannot be represented realistically by this simplified procedure. This can be attributed to the fact that the combination of both stress concentration factors inevitably assumes a negative mutual influence. Yet, the unintentional imperfections may also provide a positive effect on the relevant structural stress, as can be seen in Figure 5-13.

Concerning this matter, by means of the specified stress concentration factor $k_{m,final}$, the clamping processes of imperfect cruciform joints can be determined with sufficient accuracy. Since the correlations are strongly non-linear, a generally valid procedure cannot be identified from the experimental tests. However, the established formulae provide the foundation to indirectly capture relevant structural stress ranges of imperfect FE models, which could be further investigated in the future.

5.2 Practical support conditions

In contrast to clamping processes in testing machines (cf. Section 5.1), alternative support conditions are generally relevant in practice (cf. Chapter 2.5). Therefore, influences from imperfections under practical support conditions will be investigated in more detail.

With regard to the support conditions, the clamping sections of the welded-on plates of the cruciform joints are not displaced and rotated to a uniform level, as is the case in the evaluations of the clamping process. Instead, the investigated support conditions are defined in the FEA and the stresses are applied directly to the imperfect model. This allows support conditions under realistic load to be analysed. In this respect, finely meshed numerical FE models with solid elements are evaluated both with and without imperfections. The corresponding stress concentration factors $k_{m,FEA}$ determined directly in the FEA are obtained according to formula (2-28). With regard to the associated straightening effects, the IGF research project No. 20336N [1] concluded that the load-dependent behaviour is similar to that observed in clamping processes. To this end, the effect of straightening is somewhat more significant when the support conditions according to the IIW [3] and Xing and Dong [5] are analysed. This is particularly noticeable in studies on angular misalignment. However, since there are no restraint procedures that generate large secondary bending stresses, realistic stress concentration factors k_m can also be determined by small stresses. Accordingly, the evaluations in this section are implemented with a loading that leads to a nominal stress

of $\Delta\sigma_{R,nom} = 1.00 \text{ N/mm}^2$ in perfect FE models without imperfections. The stress distributions of a geometrically non-linear evaluation by the FEA thus correspond approximately to geometrically linear results. As a result, straightening effects are practically eliminated in this way. Therefore, the investigations represent a rather conservative evaluation, as smaller numerical stress concentration factors $k_{m,FEA}$ are to be expected for larger loads.

On the basis of the FEA, the analytical stress concentration factors k_m from Chapter 2.5 for the indirect consideration of imperfections according to the guidelines of the IIW [3] and Xing and Dong [5] are assessed in the following Section 5.2.1 by means of numerical calculations. In addition, support parameters λ_{direct} are determined numerically in Section 5.2.2 for all support conditions presented in Chapter 2.5. According to the guidelines of the IIW [3], λ_{IIW} specifies the stress-increasing effects of various support conditions (cf. Chapter 2.5.3.2.1). In this way, analytical $\lambda_{indirect}$ -values can be verified for uniform plate thicknesses and lengths according to Xing and Dong [5] and can be extended for deviating geometries. The results are provided for cruciform joints to allow a numerically verified indirect determination of stress-increasing effects for any support condition with axial and angular misalignments.

5.2.1 Evaluation of stress concentration factors

The numerical calculations of indirect stress concentration factors for practical support conditions are carried out separately for axial misalignment (cf. Section 5.2.1.1) and angular misalignment (cf. Section 5.2.1.2) on cruciform joints. In the case of cruciform joints with axial misalignments, systems (a) and (b) are examined according to the classification of Xing and Dong [5] (cf. Table 2-23). With regard to angular misalignments, systems (g) and (h) are analysed (cf. Table 2-24). Therefore, the systems evaluated are cruciform joints without restraint of the intermediate plate. According to the IIW [3], the information in Table 2-18 is decisive for all support conditions (cf. Chapter 2.5). For this purpose, numerical calculations are carried out for the determination of $k_{m,FEA}$ according to Section 5.2. The results are then related to indirect stress concentration factors k_m according to the guidelines of the IIW [3] and Xing and Dong [5] to verify the applicability of the respective guidelines. The corresponding analytical formulae for the indirect determination of the stress concentration factors are explained in more detail for the specifications of the IIW [3] in Chapter 2.5.3.2.1 and for the specifications of Xing and Dong [5] in Chapter 2.5.3.2.4. The influence of imperfections on the system behaviour is investigated for axial misalignment and angular misalignment, respectively with hinged supports (cf. Sections 5.2.1.1.1 and 5.2.1.2.1) and restrained support conditions (cf. Section 5.2.1.1.2 and 5.2.1.2.2).

5.2.1.1 Axial misalignment

With regard to axial misalignment, the respective fatigue classes of the normative regulations and guidelines already include influences from imperfections. This applies to the corresponding specifications from DIN EN 1993-1-9 [2], guidelines of the IIW [3] and prEN 1993-1-9 [4] both in the nominal and in part in the structural stress concept. In this respect, in the nominal stress concept according to DIN EN 1993-1-9 [2] and

prEN 1993-1-9 [4], stress-increasing effects from $e = 0.15 \cdot t_3$ are to be covered by the fatigue classes. In contrast, the guidelines of the IIW [3] specify the considered influences of axial misalignment in the nominal stress concept by the thickness of the welded-on plates $e = 0.15 \cdot t_{1=2}$. In the structural stress concept, according to DIN EN 1993-1-9 [2], no information is given on imperfections considered on the resistance side. However, prEN 1993-1-9 [4] specifies in the structural stress concept that axial misalignment up to $e = 0.15 \cdot t_3$ does not need to be considered, as related effects are already included in the fatigue class. This corresponds to the specifications from the nominal stress concept according to [4]. In addition, both prEN 1993-1-14 [14] and IIW [3] specify that influences from imperfections with stress-increasing effects of less than 5% are considered in the fatigue classes for cruciform joints in the structural stress concept. Furthermore, the guidelines of the IIW [3] provide an effective default value $k_{m,eff,default}$, which has to be applied in the structural stress concept in all cases (cf. Chapter 2.5.3.2). This amounts to formula (2-30) for cruciform joints, although the definition of e_{max} is not specified in more detail. If e_{max} is defined as the maximum permissible axial misalignment, the effective default value would be $k_{m,eff,min} = 1.40$ if the imperfections are limited to the permissible manufacturer tolerances $e_{permissible} = 0.5 \cdot t_{1=2}$ according to DIN 50100 [27]. In order to ensure a consistent evaluation, this value is provided as a reference value in the following investigations.

In the following, the evaluation for axial misalignment is carried out separately for hinged supports with freedom of rotation (cf. Section 5.2.1.1.1) as well as for restrained supports (cf. Section 5.2.1.1.2). Axial misalignments up to $e/t_{1=2} = 0.5$ are examined according to the permissible manufacturer tolerances as per DIN 50100 [27]. In the evaluations, the intermediate plate is specified uniformly with a thickness of $t_3 = 25 \text{ mm}$. The uniform component width is defined with $w_1 = 100 \text{ mm}$. The total length L_{total} of the cruciform joints is also set consistently at $L_{total} = 1200 \text{ mm}$, regardless of the support conditions investigated. In this respect, the respective plate lengths $L_{1=2}$ amount to $L_{total}/2$.

5.2.1.1.1 Hinged supports with freedom of rotation

The evaluation for systems with hinged supports is performed for the static system (a) with axial misalignment e illustrated in Figure 5-14 under fatigue load ΔF . The hinged supports are defined with freedom of rotation on both ends of the cruciform joints. The stress is applied longitudinally to plate 1 as tension load.

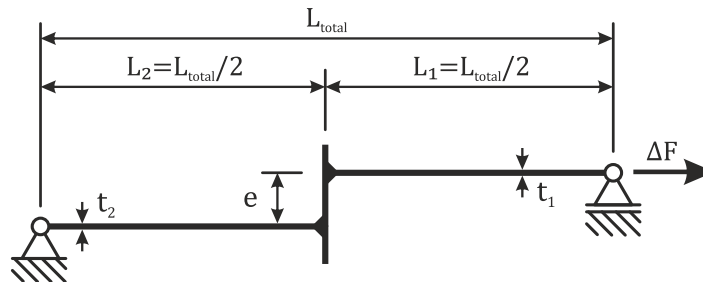


Figure 5-14: System (a) with hinged supports with freedom of rotation for axial misalignment

The results of the numerically determined stress concentration factors $k_{m,case(a),FEA}$ for axial misalignments up to $e = 0.5 \cdot t_{1=2}$ are summarised for system (a) in Figure 5-15 for welded-on plates with a thickness of $t_{1=2} = 10 \text{ mm}$ (cf. left side of Figure 5-15) and

$t_{1=2} = 40 \text{ mm}$ (cf. right side of Figure 5-15). In addition, the numerically determined results are compared to the analytical stress concentration factors $k_{m,case(a),Xing\&Dong}$ according to Xing and Dong [5] and $k_{m,case(a),IIW}$ according to the guidelines of the IIW [3]. According to [2], $k_{m,case(a),IIW}$ is evaluated with the support parameter $\lambda_{IIW} = 3$ as well as with $\lambda_{IIW} = 6$ for system (a) (cf. Chapter 2.5.3.2.1).

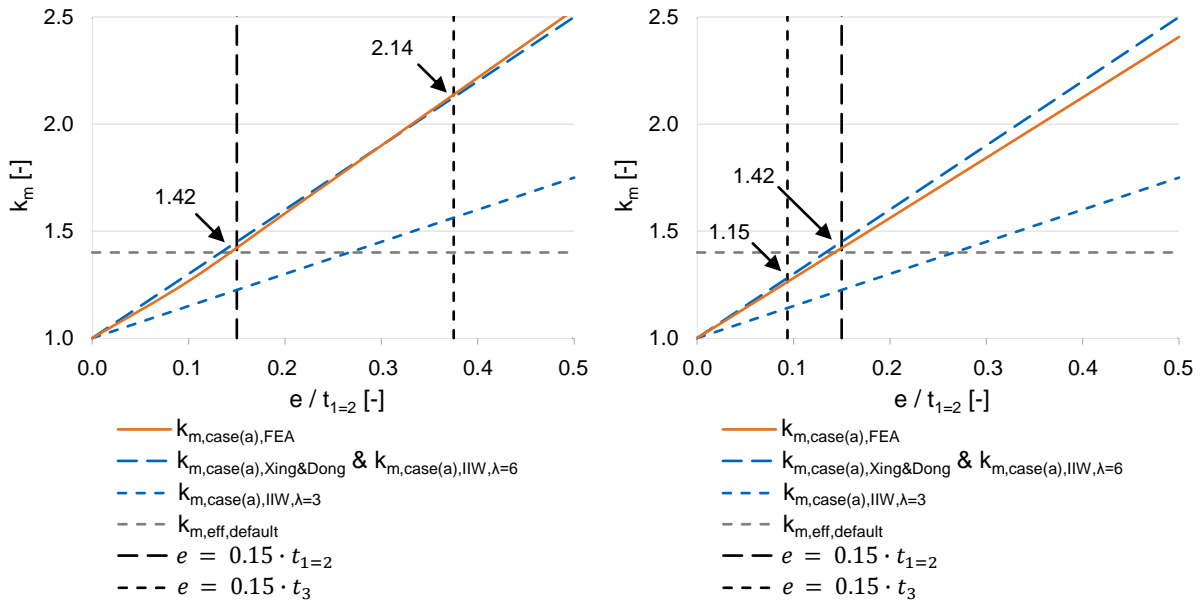


Figure 5-15: Comparison of numerical stress concentration factor $k_{m,FEA}$ to analytical factors according to IIW [3] and Xing and Dong [5] for case (a) for axial misalignment with $t_{1=2} = 10 \text{ mm}$ (left) and $t_{1=2} = 40 \text{ mm}$ (right)

According to Figure 5-15, the numerically determined $k_{m,case(a),FEA}$ factors correspond well with the analytical stress concentration factors according to the guidelines of the IIW [3] and Xing and Dong [5]. However, this applies to the specifications of the IIW [3] exclusively for the evaluation with a support parameter $\lambda_{IIW} = 6$. This corresponds to the specifications of the guidelines [3], as a support parameter of $\lambda_{IIW} = 6$ is specified for axial misalignment without restraint (cf. Table 2-18). With axial misalignment $e = 0.5 \cdot t_{1=2}$, stress concentration factors $k_{m,case(a),FEA} \approx 2.5$ result for $t_{1=2} = 10 \text{ mm}$ (cf. left side of Figure 5-15). In this respect, with thicker welded-on plates $t_{1=2} = 40 \text{ mm}$, the resulting stress concentration factor of $k_{m,case(a),FEA} \approx 2.4$ is only minimally lower (cf. right side of Figure 5-15). Due to the very similar results, only a minor thickness dependency can be detected. Therefore, the evaluation for system (a) shows that, in contrast to clamping processes in testing machines (cf. Section 5.1), no large stress concentration factors result from increasing stiffnesses of the welded-on plates.

Concerning this matter, further evaluations indicate that the analytical results tend to underestimate $k_{m,case(a),FEA}$ for thin plates with $t_{1=2} = 10 \text{ mm}$ starting from plate lengths of approximately $L_{total} = 400 \text{ mm}$. With the maximum examined total length $L_{total} = 1600 \text{ mm}$, the observed difference amounts to only 2 %, though, and is not to be regarded as critical. Furthermore, almost no straightening effects are included in the numerical evaluations due to the minor load level. These effects would result in a reduction of the $k_{m,case(a),FEA}$ values even at a marginally higher load level, which would ensure compliance with the analytical stress concentration factors. In contrast, the analytical stress concentration factors for plates with $t_{1=2} = 40 \text{ mm}$ are up to 5 % above

the numerical factors, which results in conservative results for indirect consideration. Thus, the guidelines according to the guidelines of the IIW [3] and Xing and Dong [5] for an analytical and thus indirect consideration of influences from imperfections can generally be regarded as reasonable in practice for system (a).

Although the evaluation from Figure 5-15 is carried out in the structural stress concept, the resulting k_m factors can also be applied in the nominal stress concept. Therefore, two points are highlighted in Figure 5-15 for the evaluations with $t_{1=2} = 10 \text{ mm}$ (cf. left side Figure 5-15) and $t_{1=2} = 40 \text{ mm}$ (cf. right side of Figure 5-15) respectively. These refer to the evaluation of $k_{m,case(a),FEA}$ for axial misalignment of $e/t_{1=2} = 0.15$ and $e/t_{1=2} = 0.15 \cdot t_3/t_{1=2} = 0.375$. In this way, the specifications for axial misalignment already considered by the resistance side can be verified for both the nominal and the structural stress concept.

To this end, stress-increasing effects up to a stress concentration factor of $k_{m,already\ covered} = 2.14$ are to be covered by the corresponding normative fatigue classes in the nominal stress concept according to the specifications of DIN EN 1993-1-9 [2] and prEN 1993-1-9 [4] with $t_{1=2} = 10 \text{ mm}$ (cf. left side of Figure 5-15). In contrast, the nominal stress concept according to the IIW [3] only includes stress-increasing effects of $k_{m,already\ covered} = 1.42$ (cf. left side of Figure 5-15) respectively $k_{m,already\ covered} = 1.45$ according to Table 2-17. The almost identical and significantly more conservative specifications according to the guidelines of the IIW [3] with almost equal classification of the fatigue strength indicate an incorrect dependence on the thickness t_3 of the intermediate plate according to DIN EN 1993-1-9 [2] and prEN 1993-1-9 [4] in the nominal stress concept. The evaluation for $t_{1=2} = 40 \text{ mm}$ (cf. right side of Figure 5-15) additionally reveals that the dependence on the intermediate plate thickness t_3 leads to a significantly lower factor $k_m = 1.15$ in this case. In this respect, due to the uniform intermediate plate thickness t_3 with thicker thickness of the welded-on plates $t_{1=2}$ in the evaluation according to DIN EN 1993-1-9 [2] and prEN 1993-1-9 [4], significantly lower axial misalignments are considered in the nominal stress concept than according to the guidelines of the IIW [2]. This also suggests an inappropriate applicability of the specifications in the nominal stress concept according to DIN EN 1993-1-9 [2] and prEN 1993-1-9 [4].

Whereas in the structural stress concept according to DIN EN 1993-1-9 [2] no information is provided on imperfections, prEN 1993-1-14 [14] and the guidelines of the IIW [3] specify that influences from imperfections with stress-increasing effects up to 5 % are already considered. In addition, the IIW [3] defines in the structural stress concept that an effective default value $k_{m,eff,default}$ has to be applied in any case (cf. Chapter 2.5.3.2.1). Consequently, stress-increasing effects of $k_{m,eff,default} = 1.42$ must be explicitly considered in the evaluation of the structural stress concept, even if smaller imperfections are to be expected (cf. Figure 5-15). By contrast, the specifications of prEN 1993-1-9 [4] lead to the conclusion that in the structural stress concept $k_{m,already\ covered} = 2.14$ is to be covered by the associated normative fatigue class for $t_{1=2} = 10 \text{ mm}$ (cf. left side of Figure 5-15). With an identical fatigue strength of $\Delta\sigma_C = 100 \text{ N/mm}^2$ according to DIN EN 1993-1-9 [2], IIW [3] and prEN 1993-1-9 [4], these results confirm the implications from chapter 4 regarding a significant overestimation of the achievable stress cycles N_R , applying the specifications for

considered imperfections in the fatigue class of prEN 1993-1-9 [4] at relatively thin welded-on plates. The evaluations for $t_{1=2} = 40 \text{ mm}$ (cf. right side of Figure 5-15) in the structural stress concept also lead, according to prEN 1993-1-9 [4] with $k_{m,already\ covered} = 1.15$, to greater considered influences from imperfections than with $k_{m,already\ covered} = 1.05$ according to prEN 1993-1-14 [14] and guidelines of the IIW [3]. However, the uniform fatigue class 100 according to DIN EN 1993-1-9 [2], IIW [3] and prEN 1993-1-9 [4] in the structural stress concept should not lead to different considerations of stress-increasing effects according to prEN 1993-1-9 [4]. Therefore, only the specifications according to the IIW [2] should be regarded as reasonable.

5.2.1.1.2 Restrained supports

The evaluation of case (b) is carried out for the static system shown in Figure 5-16 under tensile load ΔF and with angular misalignment e . The supports are restrained on both sides of the cruciform joint and the load is applied in the longitudinal direction of plate 1 as tensile load.

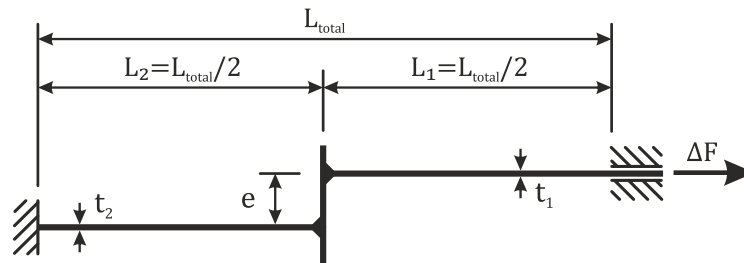


Figure 5-16: System (b) with restrained supports for axial misalignment

The corresponding results are presented in Figure 5-17 for plate thicknesses of $t_{1=2} = 10 \text{ mm}$ (cf. left side of Figure 5-17) and $t_{1=2} = 40 \text{ mm}$ (cf. right side of Figure 5-17). The analysis is consistent with the studies discussed in Section 5.2.1.1.1.

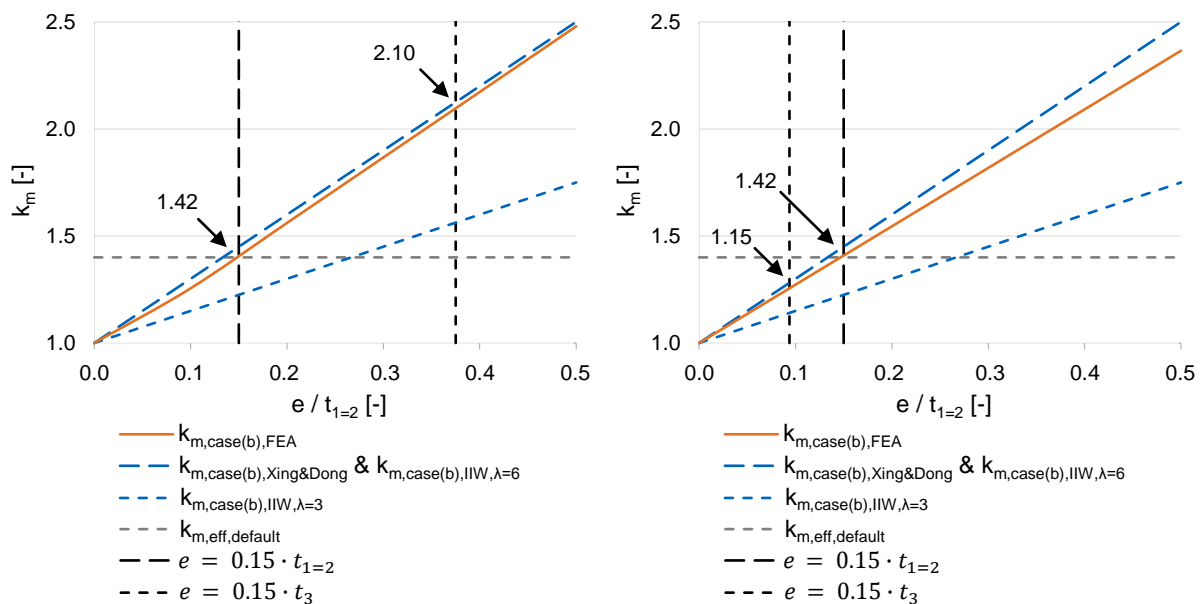


Figure 5-17: Comparison of numerical stress concentration factor $k_{m,FEA}$ to analytical factors according to IIW [3] and Xing and Dong [5] for case (b) for axial misalignment with $t_{1=2} = 10 \text{ mm}$ (left) and $t_{1=2} = 40 \text{ mm}$ (right)

According to Figure 5-17, only a slight dependence on thickness is observed for system (b). This is in accordance with the results from Section 5.2.1.1.1 for system (a). In addition, the resulting $k_{m,case(b),FEA}$ with $e = 0.5 \cdot t_{1=2}$ for system (b) are almost equal to the results for system (a). With regard to investigations of axial misalignment on systems (a) and (b), the support conditions therefore do not affect the results. Furthermore, there is good agreement between the numerically determined stress concentration factors $k_{m,case(b),FEA}$ and the analytically indirectly determined results according to the guidelines of the IIW [3] and Xing and Dong [5] (cf. Figure 5-17). However, according to the IIW [3], only the support parameter $\lambda_{IIW} = 6$ provides good accordance with the numerical results. This corresponds to the results for hinged supports with freedom of rotation (cf. Section 5.2.1.1.1). This confirms the assumptions from Chapter 2.5.3.2.1 that the defined support parameter λ_{IIW} in the case of axial misalignment refers exclusively to the degree of restraint of the intermediate plate. Accordingly, the specifications differ from those for angular misalignment, where the degree of restraint of the load-bearing welded-on plates is relevant (cf. Section 5.2.1.2). As a result, the reference to $\lambda_{IIW} = 3$ with restrained supports according to the guidelines of the IIW [3] refers exclusively to the degree of restraint of the intermediate plate. With regard to the dependencies of the considered axial misalignments on the thickness of the intermediate plate t_3 , unrealistic results are obtained again (cf. Figure 5-17). This corresponds to the conclusions on system (a) from Section 5.2.1.1.1. Thus, in analyses of axial misalignment, this can be ascertained independently of the investigated system.

5.2.1.2 Angular misalignment

In contrast to the influences from imperfections due to axial misalignment (cf. Section 5.2.1.1), the normative regulations and guidelines DIN EN 1993-1-9 [2], IIW [3] and prEN 1993-1-9 [4] do not specify explicitly the limitation of angular misalignment in the nominal or structural stress concept. However, the guidelines of the IIW [3] and Xing and Dong [5] define stress concentration factors $k_{m,angular}$ which allow the stress-increasing effects from angular misalignments to be considered indirectly (cf. Table 2-18 and Table 2-24). In this respect, the analytical formulae differ according to the support condition and are dependent on the plate lengths $L_{1=2}$. In the following, the analytical results are compared with numerical comparative calculations from the FEA for the structural stress concept. In the assessments for angular misalignment up to $\alpha = 5^\circ$, the total length is uniformly defined with $L_{total} = 1200 \text{ mm}$ with a uniform thickness of the intermediate plate of $t_3 = 25 \text{ mm}$ and width $w_1 = 100 \text{ mm}$. The evaluation is performed separately for system (g) with hinged supports (cf. Section 5.2.1.2.1) and system (h) with restrained supports (cf. Section 5.2.1.2.2) for cruciform joints.

5.2.1.2.1 Hinged supports with freedom of rotation

The evaluation for case (g) is carried out for the static system shown in Figure 5-18 with angular misalignment α under tensile load ΔF . The hinged supports with freedom of rotation are defined in the FEA at both ends of the cruciform joint and the stress is applied longitudinally to plate 1 as a tensile load.

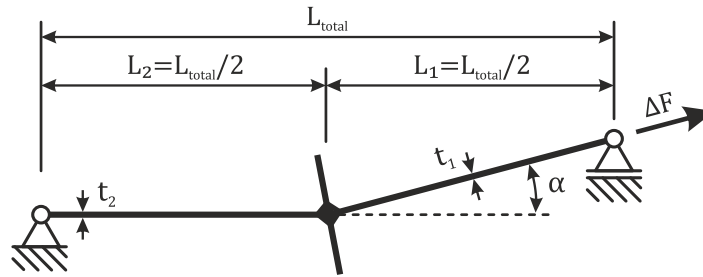


Figure 5-18: System (g) with hinged supports with freedom of rotation for angular misalignment

In accordance with the results for axial misalignment (cf. Section 5.2.1.1), the evaluation for angular misalignment in Figure 5-19 is summarised for $t_{1=2} = 10 \text{ mm}$ (cf. left side of Figure 5-19) as well as for $t_{1=2} = 40 \text{ mm}$ (cf. right side of Figure 5-19).

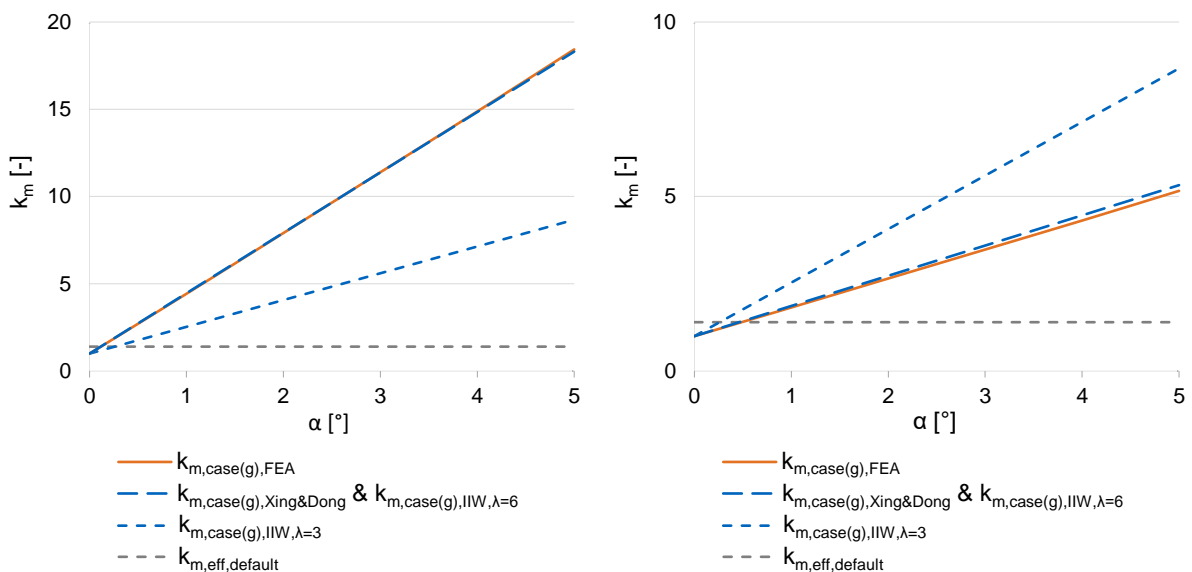


Figure 5-19: Comparison of numerical stress concentration factor $k_{m,FEA}$ to analytical factors according to IIW [3] and Xing and Dong [5] for case (g) for angular misalignment with $t_{1=2} = 10 \text{ mm}$ (left) and $t_{1=2} = 40 \text{ mm}$ (right)

According to Figure 5-19, higher stress concentration factors $k_{m,case(g),FEA} = 18.3$ are determined for plate thicknesses $t_{1=2} = 10 \text{ mm}$ (cf. left side of Figure 5-19) compared to plate thicknesses $t_{1=2} = 40 \text{ mm}$ with $k_{m,case(g),FEA} = 5.2$ (cf. right side of Figure 5-19). Therefore, in contrast to the investigations on axial misalignment (cf. Section 5.2.1.1), system (g) shows a clear dependence on the thickness of the welded-on plates. For this reason, the dependence of indirect calculations on the plate thickness of the welded-on plates is mandatory. In addition, it can be observed that there is good agreement between the numerically determined $k_{m,case(g),FEA}$ factors and the analytically determined $k_{m,case(g)}$ factors according to the IIW [3] and Xing and Dong [5] (cf. Figure 5-19). To this end, further evaluations reveal that for a short total length of $L_{total} = 800 \text{ mm}$ up to plate thicknesses of approximately $t_{1=2} = 20 \text{ mm}$, minimally higher numerical stress concentration factors $k_{m,case(g),FEA}$ are obtained than indirectly by the specifications according to the IIW [3] and Xing and Dong [5]. In addition, for thin plate thicknesses $t_{1=2} = 10 \text{ mm}$ of the welded-on plates, minimally higher numerical $k_{m,case(g),FEA}$ factors result up to a length of approximately $L_{total} = 1400 \text{ mm}$. Nevertheless, due to the minor straightening effects, the agreement is considered as

satisfactory. Regarding welded-on plates with $t_{1=2} = 40 \text{ mm}$, the analytical $k_{m,case(g)}$ factors according to the IIW [3] and Xing and Dong [5] correspond well to the numerical results. Consequently, the applicability of the indirect determination of stress-increasing effects can be confirmed for hinged supports. This enables a safe design, provided that angular misalignments are indirectly considered for supports with freedom of rotation. With regard to the guidelines of the IIW [3], however, only calculations with a support parameter $\lambda_{IIW} = 6$ provide good results for system (g). This clarifies the information according to [3] from Table 2-18. Furthermore, the defined default value $k_{m,eff,default}$ according to the IIW [3] is already exceeded at $\alpha > 0.1^\circ$ for welded-on plates with $t_{1=2} = 10 \text{ mm}$ and at $\alpha > 0.5^\circ$ for plates with $t_{1=2} = 40 \text{ mm}$. Accordingly, this factor to be considered for stress-increasing effects due to imperfections only insufficiently covers angular misalignments. Accordingly, expected angular misalignments have to be entirely considered either directly in the FEA or indirectly by stress concentration factors in order to ensure a safe design.

5.2.1.2.2 Restrained supports

The evaluation for case (h) is carried out for the static system shown in Figure 5-20 under the fatigue load ΔF for angular misalignment α . The supports are restrained on both sides of the cruciform joint and the tensile load is applied on the right edge of the component in the longitudinal direction of plate 1.

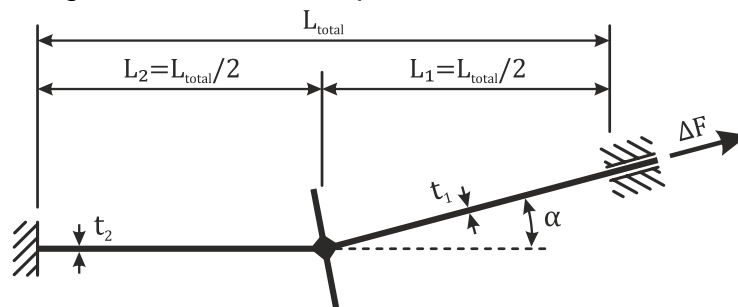


Figure 5-20: System (h) with restrained supports for angular misalignment

The evaluation of system (h) from Figure 5-20 with restrained supports and angular misalignment is presented in Figure 5-21. Again, welded-on plates with $t_{1=2} = 10 \text{ mm}$ (cf. left side of Figure 5-21) as well as $t_{1=2} = 40 \text{ mm}$ (cf. right side of Figure 5-21) are analysed. According to Figure 5-21, the results for plates with a welded-on thickness of $t_{1=2} = 10 \text{ mm}$ provide good agreement between the numerical and analytical k_m factors (cf. left side of Figure 5-21). With regard to thicker plates with $t_{1=2} = 40 \text{ mm}$, the difference is marginally greater with increasing angular misalignments (cf. right side of Figure 5-21). At a higher fatigue load level, greater straightening effects would result, leading to a further improvement of the numerical stress concentration factors $k_{m,case(h),FEA}$. Accordingly, numerical evaluation can provide more economical results for system (h) than an indirect determination of the stress-increasing effects from imperfections. Again, a thickness dependence is evident for system (h) as well (cf. Figure 5-21). However, in contrast to the results for system (g) (cf. Section 5.2.1.2.1), the differences are slightly smaller for system (h) and result in $k_{m,case(h),FEA} \approx 8.5$ for $t_{1=2} = 10 \text{ mm}$ (cf. left side of Figure 5-21) and $k_{m,case(h),FEA} \approx 2.7$ for the thicker welded-on plates $t_{1=2} = 40 \text{ mm}$ (cf. right side of Figure 5-21). Consequently, the dependence

of indirect calculations on the plate thickness of the welded-on plates is imperative for system (h).

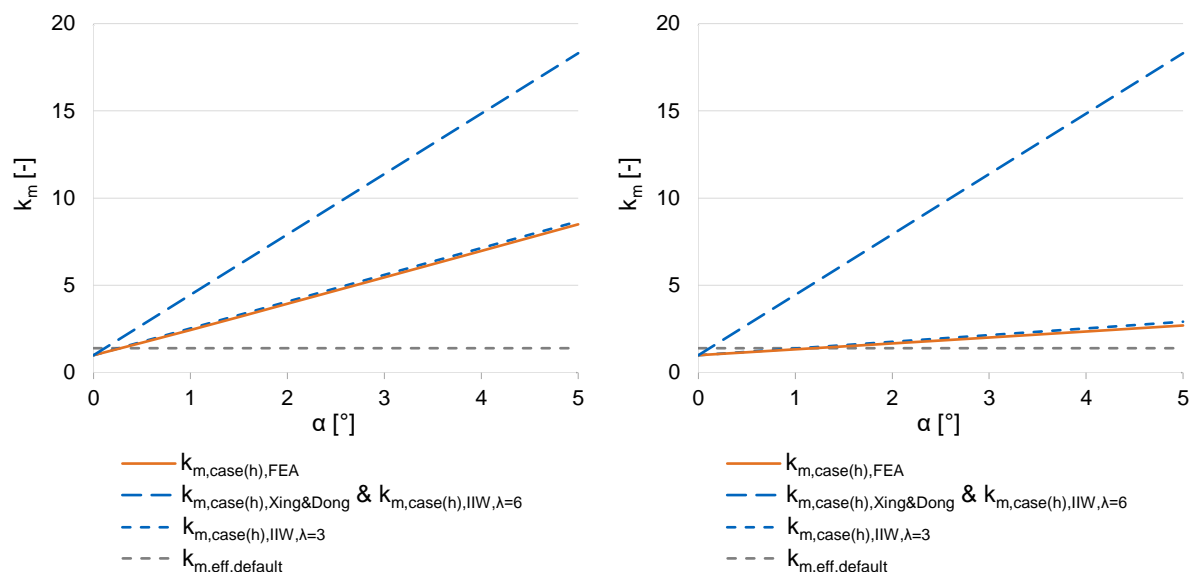


Figure 5-21: Comparison of numerical stress concentration factor $k_{m,FEA}$ to analytical factors according to IIW [3] and Xing and Dong [5] for case (h) for angular misalignment with $t_{1=2} = 10 \text{ mm}$ (left) and $t_{1=2} = 40 \text{ mm}$ (right)

Figure 5-21 also illustrates that for angular misalignment and restrained supports with a support parameter $\lambda_{IIW} = 3$ according to the IIW [3], more suitable k_m factors are obtained than with $\lambda_{IIW} = 6$. This agrees with the results from Xing and Dong [5] and allows a good approximation of the numerically determined $k_{m,case(h),FEA}$ factors. However, this differs from the results with hinged supports, where $\lambda_{IIW} = 6$ becomes relevant (cf. Section 5.2.1.2.1). In this respect, since large differences in the numerical stress concentration factors between system (g) and (h) are evident, the adjusted support parameter λ_{IIW} is essential. Therefore, the support parameter λ_{IIW} according to the IIW [3] refers to the degree of restraint of the welded-on plates (cf. Table 2-18). Thus, the decisive type of restraint differs significantly from the specifications for axial misalignment (cf. Section 5.2.1.1), as the support parameter λ_{IIW} for the latter refers to the degree of restraint of the intermediate plate. Furthermore, in accordance with the results for system (g), the default value $k_{m,eff,default}$ of the IIW [3], always to be applied, only covers the stress-increasing effects from angular misalignments to a very limited extent. Due to the very large directly resp. indirectly determined k_m factors for angular misalignment at system (h) (cf. Figure 5-21), the consideration of the resulting effects is mandatory. Nonetheless, sensible results can be achieved through the indirect calculation options, which are on a reliable basis.

5.2.2 Evaluation of support parameters

In addition to the validation of the indirect calculations of influences from imperfections by numerical calculations from Section 5.2.1, support parameters λ presented in Chapter 2.5 are analysed subsequently. The corresponding evaluations are carried out for all support conditions customary in practice listed in Chapter 2.5.3.2.4. In this respect, formula (2-36) of the IIW [3] is applied as standardised equation for the

determination of the stress concentration factor for axial misalignment $k_{m,axial}$. It is presented below in adapted notation.

$$k_{m,axial} = 1 + \lambda_{IIW} \cdot \frac{L_1}{(L_1 + L_2)} \cdot \frac{e}{t} \quad (5-17)$$

With respect to $k_{m,angular}$ for angular misalignments, formula (2-37) is applicable with the following notation. [3]

$$k_{m,angular} = 1 + \lambda_{IIW} \cdot \alpha \cdot \frac{L_1 \cdot L_2}{t \cdot (L_1 + L_2)} \quad (5-18)$$

The respective support parameter λ_{IIW} of the guidelines of the IIW [3] exclusively considers the required geometry-dependent stress correction due to possible support conditions. In addition, the thickness of the welded-on plates is uniformly specified as t without distinguishing between the welded-on plates respectively the intermediate plate. An indirect investigation of stress-increasing effects from imperfections of cruciform joints with welded-on plates of different thicknesses $t_1 \neq t_2$ or with a deviating intermediate plate thickness t_3 is therefore not possible according to [3]. The same applies to the arrangement and length L_3 of the intermediate plate (cf. Figure 3-14). For this reason, varying length and thickness ratios are examined below to ensure an enhanced evaluation. In this way, the analytical specifications according to Xing and Dong [5] for the investigated support conditions can also be verified by numerical calculations. Results are provided for cruciform joints to allow numerically verified indirect determination of stress-increasing effects for arbitrary support conditions and dimensions with axial and angular misalignment.

5.2.2.1 Basic principle

The general procedure for the determination of the support parameter λ from Chapter 2.5.3.2.1 for different plate thicknesses and lengths is presented below. The implemented evaluation methodology is presented below exemplarily for system (a) (cf. left side of Figure 5-22).

The analytical assessment of $\lambda_{indirect}$ is carried out by equating the standard form of the IIW [3] according to formula (5-17) resp. (5-18) with the system-dependent specifications according to Xing and Dong [5] (cf. Chapter 2.5.3.2.4). For this purpose, the specifications of the IIW [3] for the generally defined plate thickness t are adapted and assigned to t_1 . This method is implemented in the following exemplarily for case (a).

$$k_{m,case(a),IIW} = k_{m,case(a),Xing\&Dong} \quad (5-19)$$

$$1 + \lambda_{indirect,case(a)} \cdot \frac{L_1}{(L_1 + L_2)} \cdot \frac{e}{t_1} = 1 + \left(\frac{6L_i t_1}{(L_1 + L_2) \cdot t_1^2} \right) \cdot e \quad (5-20)$$

$$\lambda_{indirect,case(a)} = \frac{6 \cdot L_i}{L_1}$$

Consequently, $\lambda_{indirect,case(a)} = 6 \cdot L_i / L_1$, where L_i refers to the length of the plate under investigation. Thus, by simplifying the relevant boundary conditions selectively, a comparison can be derived between the evaluations according to the IIW [3] and Xing

and Dong [5] in order to obtain general formulations. On the other hand, the numerical support parameter λ_{direct} results from the conversion of formula (5-17) resp. (5-18), where the stress concentration factor $k_{m,FEA}$ is determined by the quotient of the structural stress $\Delta\sigma_{R,hs,FEA}$ of the imperfect to perfect model according to formula (5-4). For the investigation of system (a) with axial misalignment, λ_{direct} is calculated as follows.

$$\lambda_{direct,case(a)} = \frac{(k_{m,FEA} - 1) \cdot \frac{L_1}{(L_1 + L_2)} \cdot \frac{e}{t_1}}{\left(\frac{\Delta\sigma_{R,hs,FEA,imperfect,case(a)}}{\Delta\sigma_{R,hs,FEA,perfect,case(a)}} - 1 \right) \cdot \frac{L_1}{(L_1 + L_2)} \cdot \frac{e}{t_1}} \quad (5-21)$$

For the determination of the relevant perfect and imperfect structural stress ranges, the linear stress extrapolation according to the IIW [3] is applied to finely meshed solid models according to Chapter 3.3.

The assessment is performed separately for axial misalignment according to systems (a) to (f) and for angular misalignment according to systems (g) to (k). To ensure a uniform evaluation with practical imperfections, axial misalignment is specified as $e = 0.15 \cdot t_1$ and angular misalignment as $\alpha = 2^\circ$ in all studies. In the analyses, both the thickness t_1 and the length L_1 of the load initiating welded-on plate 1 are set as the primary parameters. In this respect, thicknesses of plate 1 of $t_1 = 12 \text{ mm}$ and $t_1 = 40 \text{ mm}$ are analysed. The lengths of plate 1 are specified respectively with $L_1 = 500 \text{ mm}$ as well as with $L_1 = 2.000 \text{ mm}$. The component width is uniformly defined as $w_1 = 100 \text{ mm}$. If systems with a supported intermediate plate are evaluated, structural stress ranges on the intermediate plate must be determined in addition to the evaluations on plate 1 and plate 2. This is due to the fact that the additional support conditions may lead to greater stress concentrations at the intermediate plate than at the welded-on plates. Since different lengths of the intermediate plate are possible from the intersection point of the welded-on plates, the intermediate plate is subdivided into plate 3 with the corresponding length L_3 and plate 4 with the corresponding length L_4 (cf. Figure 5-27 and Figure 5-34). Since the intermediate plate of cruciform joints consists of one component, a uniform associated thickness $t_3 = t_4$ is assumed in all cases. The investigation is carried out with factors representing the length and thickness ratios of the second welded-on plate 2 and the intermediate plate with plate 3 and plate 4. The selected factors amount to $factor = 1/4, 1/2, 2/3, 3/4, 1.00, 2.00, 3.00$ and 4.00 . Thus, the resulting lengths L_i and thicknesses t_i are calculated according to the following formulae.

$$L_i = factor \cdot L_1 \quad (5-22)$$

$$t_i = factor \cdot t_1 \quad (5-23)$$

In the evaluations, the lengths or thicknesses not analysed remain unchanged and are defined according to the associated dimensions of plate 1. This results in the geometric correlations of lengths $L_2/L_1, L_3/L_1, L_4/L_1$ as well as $L_{3=4}/L_1$ and thicknesses t_2/t_1 as well as $t_{3=4}/t_1$, which are examined subsequently. In this way, geometric effects on the influence of axial and angular misalignment on structural stress ranges under different support conditions can be determined. As the assessment is carried out on the action

side, no thickness effects are taken into account. All evaluations are interpreted in logarithmic space.

The presented approach allows a comparison between the analytical support parameters $\lambda_{indirect}$ and the numerical determined parameters λ_{direct} for varying geometries of cruciform joints. Therefore, the analytical approach for the indirect determination of stress-increasing effects from imperfections according to the IIW [3] and Xing and Dong [5] can be verified for all common support conditions.

5.2.2.2 Analysis of the support conditions

In the following, the associated support parameters λ for the systems (a) to (f) with axial misalignment and (g) to (k) with angular misalignment are evaluated in detail according to the methodology presented in Section 5.2.2.1. In this respect, the assessment is performed separately for axial misalignment (cf. Section 5.2.2.2.1) and angular misalignment (cf. Section 5.2.2.2.2). The summary of all relevant results are also provided in Appendix B on a case-by-case basis.

5.2.2.2.1 Axial misalignment

The structural stress ranges for λ_{direct} are evaluated for system (a), (b) and (c) (cf. Figure 5-22) exclusively on the welded-on plates plate 1 and plate 2, as there is no support for the intermediate plate.

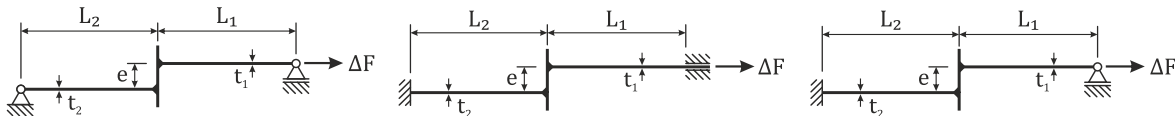


Figure 5-22: Case (a) (left), case (b) (middle) and case (c) (right) according to Xing and Dong [5]

The resulting support parameters λ_{direct} and $\lambda_{indirect}$ for the evaluation of the influence of the length ratio L_2/L_1 for system (a) (cf. left side of Figure 5-22) with axial misalignment $e/t_1 = 0.15$ are presented in Figure 5-23. The analysis is carried out separately for plate 1 (cf. left side of Figure 5-23) and plate 2 (cf. right side of Figure 5-23).

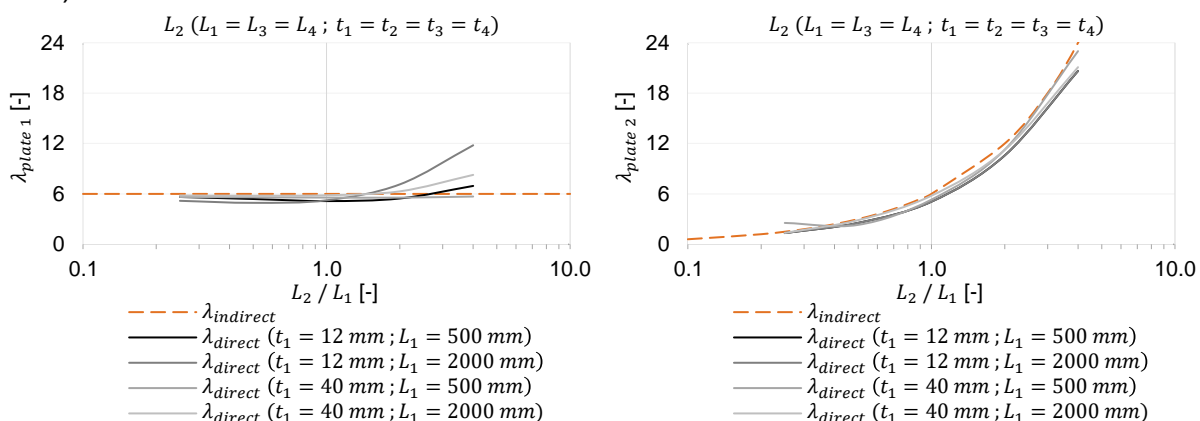


Figure 5-23: Support factor $\lambda_{plate 1}$ of plate 1 (left) and $\lambda_{plate 2}$ of plate 2 (right) for analytical support factor $\lambda_{indirect}$ with comparison to numerical support factors λ_{direct} for L_2/L_1 for case (a) with axial misalignment $e/t_1 = 0.15$

According to Figure 5-23, there is generally good agreement between the indirect and direct results. Nevertheless, starting at $L_2/L_1 > 2.0$, λ_{direct} of plate 1 deviates from the

analytical $\lambda_{indirect}$ values (cf. left side of Figure 5-23). However, the corresponding $\lambda_{plate 1}$ values are not relevant, since larger $\lambda_{plate 2}$ factors are decisive for larger plate lengths L_2 than L_1 (cf. right side of Figure 5-23). In this respect, a good agreement between the numerical λ_{direct} values and analytical factors $\lambda_{indirect}$ is obtained in the investigation on the plate length of plate 2 for system (a). In the following, the decisive λ_{max} -factors of plates 1 to 4 are presented for the identical examination of the length ratio L_2/L_1 (cf. left side of Figure 5-24). This means that the plate allocation of the decisive λ_{max} factor cannot be identified, but a better overview is ensured.

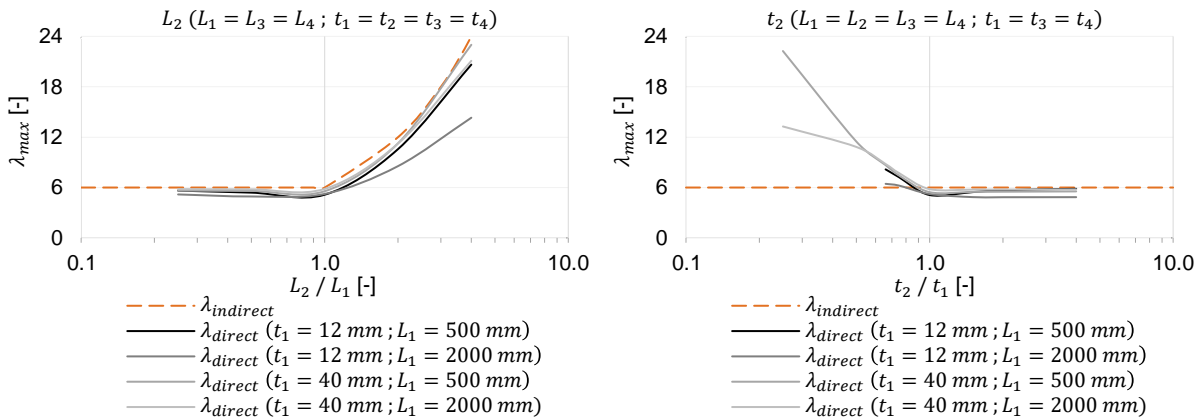


Figure 5-24: Relevant factor λ_{max} for analytical support factor $\lambda_{indirect}$ with comparison to numerical support factors λ_{direct} for L_2/L_1 ratio (left) and for t_2/t_1 ratio (right) case (a) with $e/t_1 = 0.15$

According to the left side of Figure 5-24, the analytical $\lambda_{indirect}$ factors according to Xing and Dong [5] are appropriate for all investigated plate lengths L_2 , provided that the maximum relevant structural stress ranges are considered. Deviating from this, the guidelines of the IIW [3] specify a constant support parameter $\lambda_{IIW} = 6$. However, the plate with the shorter plate length L_1 resp. L_2 is always defined as plate 2 by the specified requirement $L_2 \leq L_1$ according to the guidelines [3]. This requirement can be confirmed according to Figure 5-24. Consequently, the indirect determination of stress-increasing effects from axial misalignments for system (a) for deviating length ratios $L_1 \neq L_2$ can ensure reliable results according to Xing and Dong [5] as well as according to the guidelines of the IIW [3].

The right side of Figure 5-24 additionally illustrates the evaluation of the decisive support parameters λ_{max} for varying plate thicknesses t_2 for system (a). It can be observed that λ_{direct} determined numerically by the FEA significantly exceeds the analytically calculated $\lambda_{indirect}$ values of Xing and Dong [5] starting at a ratio of $t_2/t_1 < 1.0$. Consequently, significantly higher stress concentration factors are expected for plate thicknesses $t_2 < t_1$ than analytically specified. For this reason, it is not recommended to use the indirect determination of stress-increasing effects if the thickness t_1 is to be larger than t_2 . The same applies to the guidelines of the IIW [3] with the constant parameter $\lambda_{IIW} = 6$. Concerning this matter, it should be noted that the guidelines [3] do not differentiate between plate thicknesses and only define a general plate thickness t . In this respect, it cannot be assumed that the analytical formulae were intended for different plate thicknesses. Accordingly, for cruciform joints with a support condition according to system (a) and plate thicknesses $t_2 < t_1$, the direct determination of the imperfect structural stress ranges should be carried out by FEA if axial misalignment is to be expected. Nonetheless, provided thickness t_2 is

greater than t_1 , good analytical agreement can be ensured with the stress concentration factors according to the IIW [3] and Xing and Dong [5].

The results for case (b) (cf. centre of Figure 5-22) are presented in Figure 5-25 below. The evaluation is presented separately for different L_2/L_1 ratios (cf. left side of Figure 5-25) and t_2/t_1 ratios (cf. right side of Figure 5-25).

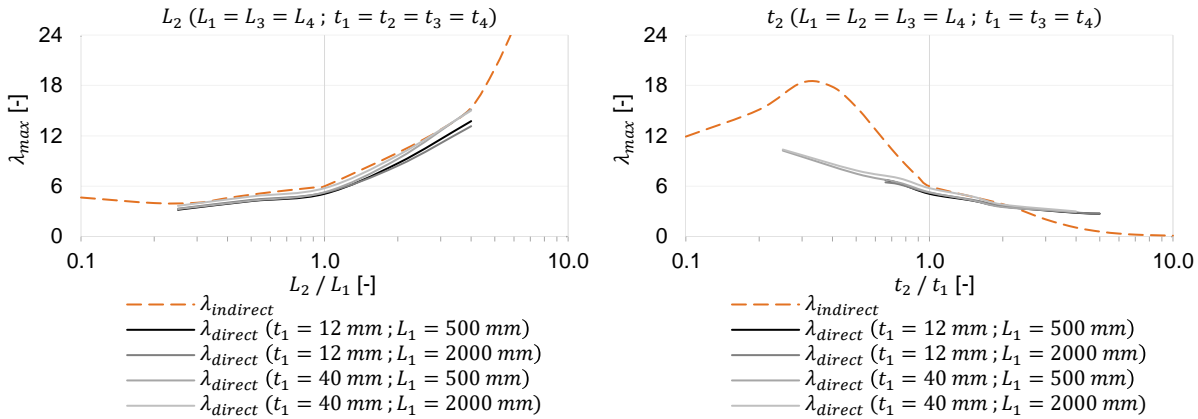


Figure 5-25: Relevant factors λ_{max} for analytical support factor $\lambda_{indirect}$ with comparison to numerical support factors λ_{direct} for L_2/L_1 ratio (left) and for t_2/t_1 ratio (right) for case (b) with $e/t_1 = 0.15$

In Figure 5-25, for varying plate lengths L_2 , $\lambda_{indirect}$ analytically provides very good agreement with the numerical results for λ_{direct} (cf. left side of Figure 5-25). The support parameter $\lambda_{IIW} = 6.0$ can also be verified numerically under the specification $L_2 \leq L_1$ according to the guidelines of the IIW [3]. However, it can be seen that there are significant deviations between the direct and indirect results for varying plate thicknesses t_2 (cf. right side of Figure 5-25). In this respect, the analytical results for $\lambda_{indirect}$ starting at $t_2 > 2 \cdot t_1$ prove to be smaller than in the numerics. Since in the case of $\lambda_{direct} > \lambda_{indirect}$ an indirect approach results in insufficient k_m -factors, the application of the analytical calculation according to Xing and Dong [5] and the IIW [3] is not considered reasonable for $t_2/t_1 > 2$. In this case, the direct consideration of the axial misalignment by the FEA is recommended. Furthermore, starting at $t_2 < t_1$ there is a clear overestimation by $\lambda_{indirect}$ compared to λ_{direct} (cf. right side of Figure 5-25). An indirect calculation of the associated stress concentration factors $k_{m,axial}$ according to Xing and Dong [5] would lead to very uneconomical results in this respect in the case of axial misalignment. Moreover, for $t_2/t_1 > 2$ the given support parameter v according to the IIW [3] cannot be verified numerically and would result in stress concentration factors significantly too low.

The evaluation of system (c) with axial misalignment (cf. right side of Figure 5-22) is summarised in Figure 5-26 for varying L_2/L_1 ratios and t_2/t_1 ratios. It shows that starting at lengths $L_2 > 2 \cdot L_1$ as well as at thicknesses $t_2 > t_1$, higher λ_{direct} values are determined by the FEA than with the indirect calculation of $\lambda_{indirect}$ according to Xing and Dong [5]. Although the support parameter $\lambda_{IIW} = 6.0$ can also be verified under the specification $L_2 \leq L_1$ according to the guidelines of the IIW [3], this only applies to plate thicknesses $t_2 > t_1$. Accordingly, computational k_m factors for system (c) with axial misalignment only should be applied to designs with $L_2 \leq 2 \cdot L_1$ according to Xing and Dong [5] respectively $L_2 \leq L_1$ according to the IIW [3] as well as with $t_2 \leq t_1$ in both cases.

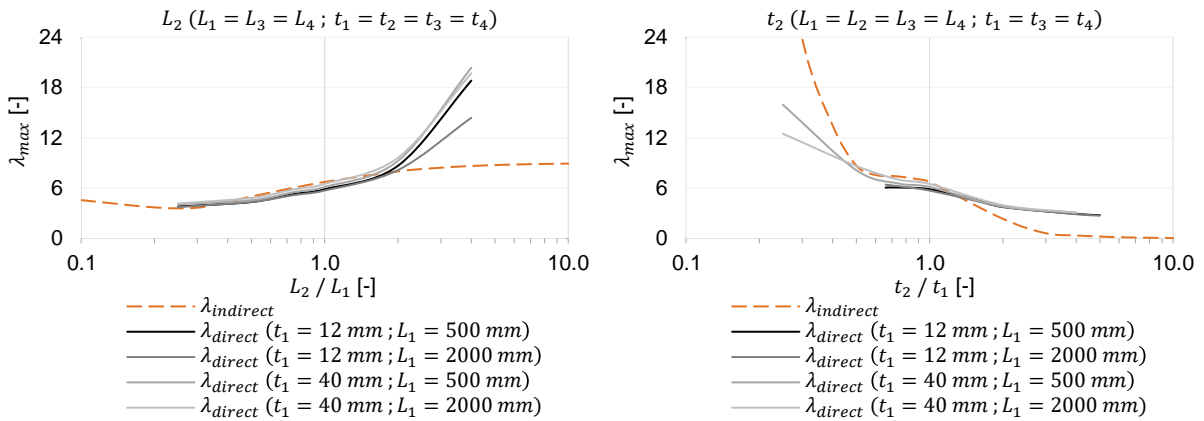


Figure 5-26: Relevant factors λ_{max} for analytical support factor $\lambda_{indirect}$ with comparison to numerical support factors λ_{direct} for L_2/L_1 ratio (left) and t_2/t_1 ratio (right) for case (c) with $e/t_1 = 0.15$

In addition to cases (a), (b) and (c) without the support of the intermediate plate (cf. Figure 5-22), in practice most systems include some support of the intermediate plate. For this purpose, systems (d), (e) and (f) according to Figure 5-27 with axial misalignment $e = 0.15 \cdot t_1$ are additionally evaluated below.

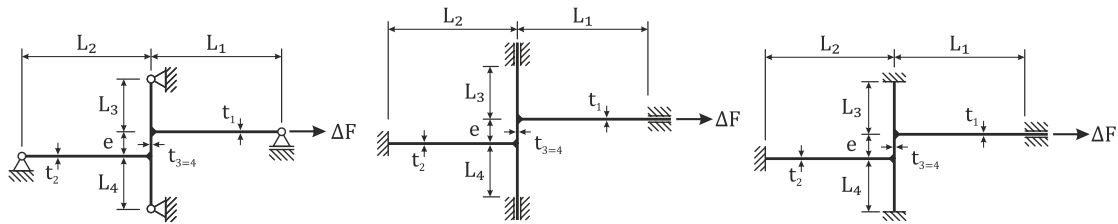


Figure 5-27: Case (d) (left) case (e) (middle) and case (f) (right) according to Xing and Dong [5]

Due to the support of the intermediate plate (cf. Figure 5-27), in addition to the L_2/L_1 and t_2/t_1 ratios, all other geometrically feasible boundary conditions that may affect the decisive λ_{max} -values are investigated for systems (d), (e) and (f). These include the ratios L_3/L_1 , L_4/L_1 , $L_3/4/L_1$ and $t_{3/4}/t_1$. All evaluations are presented in Appendix B. However, with regard to cruciform joints with a supported intermediate plate and axial misalignment, only the relevant results for case (d) (cf. Figure 5-28), case (e) (cf. Figure 5-29) and case (f) (cf. Figure 5-30) are presented below.

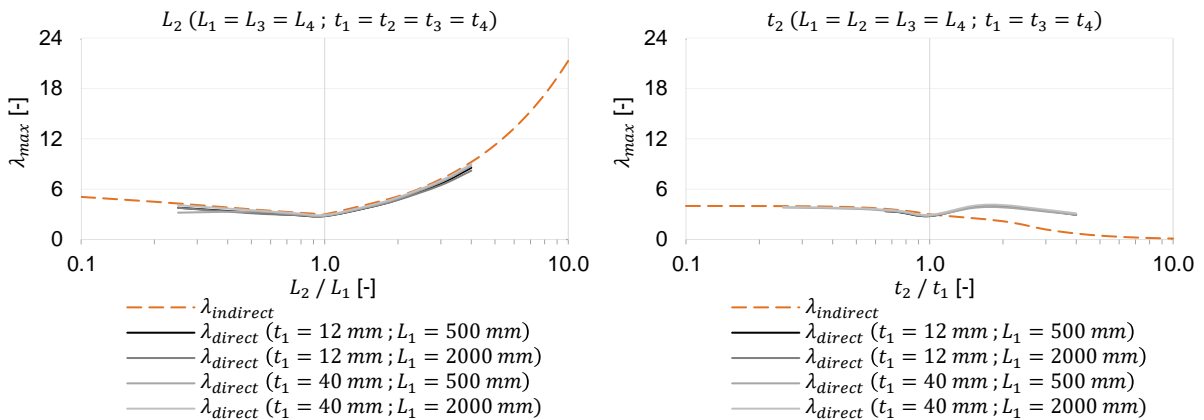


Figure 5-28: Relevant factors λ_{max} for analytical support factor $\lambda_{indirect}$ with comparison to numerical support factors λ_{direct} for L_2/L_1 ratio (left) and for t_2/t_1 ratio (right) for case (d) with $e/t_1 = 0.15$

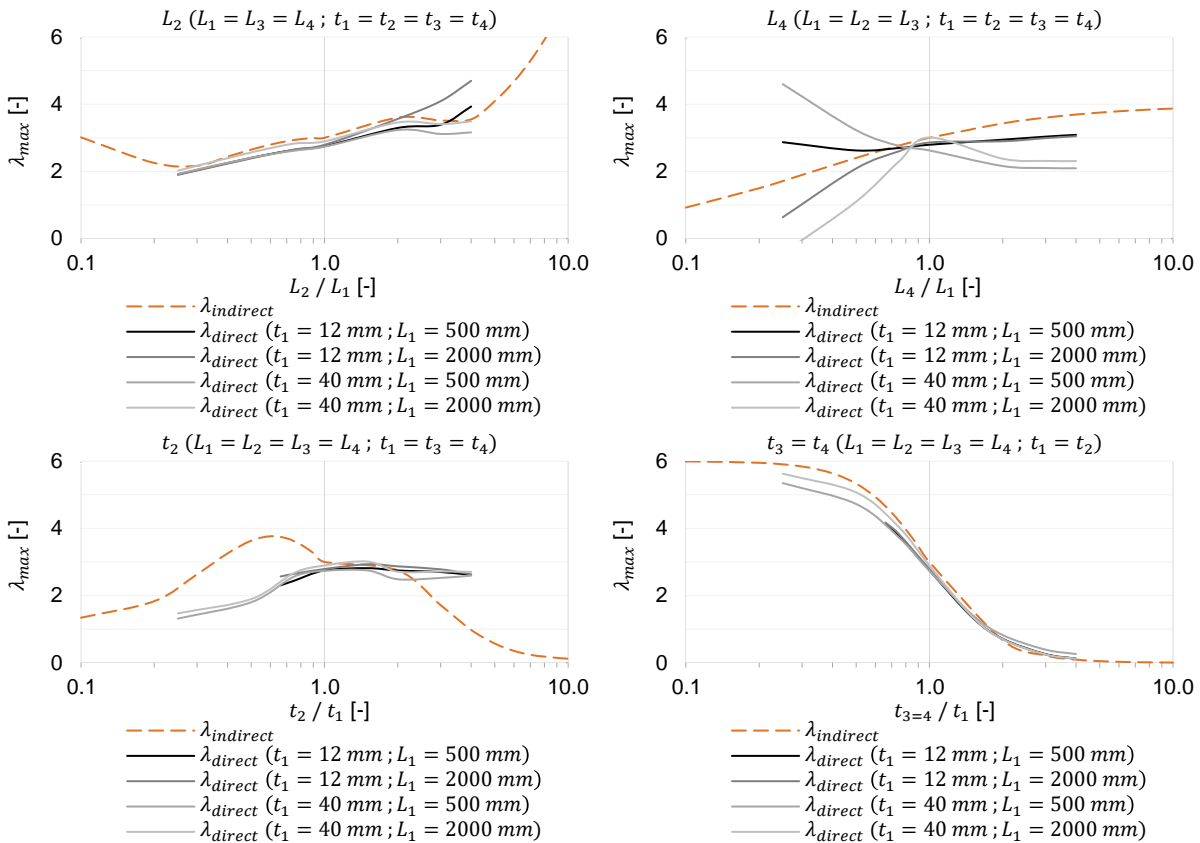


Figure 5-29: Relevant factors λ_{max} for analytical support factor $\lambda_{indirect}$ with comparison to numerical support factors λ_{direct} for L_2/L_1 ratio (top left), L_4/L_1 ratio (top right), t_2/t_1 ratio (bottom left) and for $t_{3=4}/t_1$ ratio (bottom right) for case (e) with $e/t_1 = 0.15$

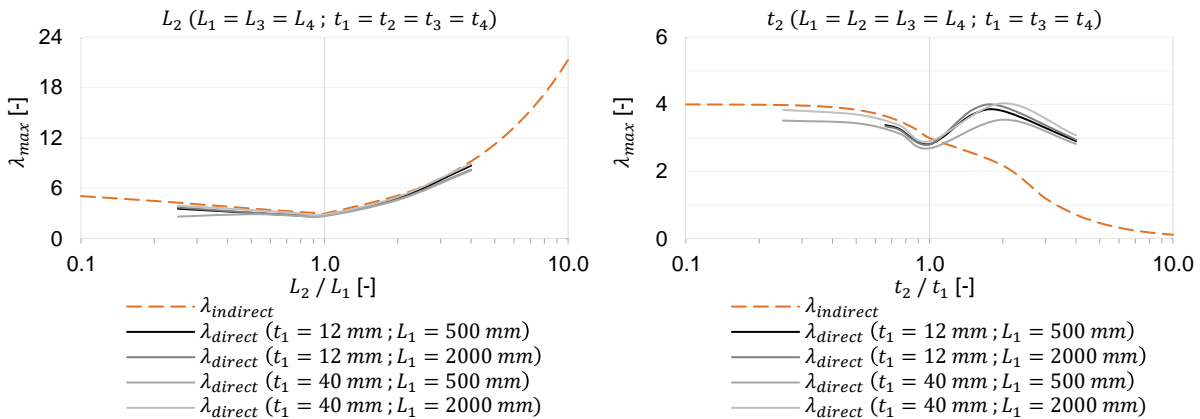


Figure 5-30: Relevant factors λ_{max} for analytical support factor $\lambda_{indirect}$ with comparison to numerical support factors λ_{direct} for L_2/L_1 ratio (left) and for t_2/t_1 ratio (right) for case (f) with $e/t_1 = 0.15$

With regard to systems (d), (e) and (f), the indirect $\lambda_{indirect}$ values of Xing and Dong [5] generally provide good agreement with the results from FEA (cf. case (d), (e) and (f) of Appendix B). This also applies to the evaluations of L_2 (cf. left side of Figure 5-28, top left side of Figure 5-29 and left side of Figure 5-30). In this respect, only with system (e) and plate thicknesses $t_1 = 12 \text{ mm}$ starting at plate lengths $L_2 > 3 \cdot L_1$ does λ_{direct} lead to minimally higher values than $\lambda_{indirect}$. In addition, the investigations of the t_2/t_1 ratio result in deviating results of the relevant structural stress ranges. For system (d) and (e), the analytical formulae should only be applied if it can be ensured that $t_2 \leq t_1$

applies (cf. right sides of Figure 5-28 and Figure 5-30). In contrast, the formulae of Xing and Dong [5] are unsuitable for system (e) starting at $t_2 \geq 2 \cdot t_1$, as they lead to an underestimation of λ_{direct} (cf. bottom left side of Figure 5-29). Generally, it is also noticeable that the results for system (d) and (f) are practically indistinguishable despite different supports of the intermediate plate. In this respect, the type of support only appears to be important in terms of freedom of displacement in z_{global} direction, as only system (e) leads to deviating results. Furthermore, the evaluations for system (e) reveal that for short plate lengths of $L_1 = 500 \text{ mm}$ and $L_4 \leq L_1$, larger values are obtained by the FEA than by $\lambda_{indirect}$ (cf. top right side of Figure 5-29). This can provide unreliable results in the indirect determination of the stress concentration factors.

With regard to the guidelines of the IIW [3], the support parameter $\lambda_{IIW} = 3$ is specified for fully restrained intermediate plates (cf. Table 2-18). For uniform plate lengths $L_1 = L_2 = L_3 = L_4$ and plate thicknesses $t_1 = t_2 = t_3 = t_4$ of cruciform this specification is always accurate for systems (d), (e) and (f) (cf. case (d), (e) and (f) of Appendix B). However, deviating plate lengths L_2 , L_3 and L_4 and plate thicknesses t_2 and $t_3 = t_4$ partially lead to significant exceeding of $\lambda_{IIW} = 3$. In addition to the previously mentioned exceedances of $\lambda_{IIW} = 6.0$ for systems (a), (b), and (c), the exceedances of systems (d), (e) and (f) according to Appendix B are summarised in Table 5-1 below. Therefore, Table 5-1 specifies all parameter ranges in which the support parameters λ_{IIW} according to the specifications from [3] cannot be complied with by numerical calculations.

Table 5-1: Exceedances of the specifications for support parameters λ_{IIW} according to the IIW [3] by numerically determined support parameters λ_{direct} for systems (a) to (e) with $e/t_1 = 0.15$

Exceedance	L_2/L_1 [-]	L_3/L_1 [-]	L_4/L_1 [-]	$L_{3=4}/L_1$ [-]	t_2/t_1 [-]	$t_{3=4}/t_1$ [-]
λ_{IIW} [-]	$\lambda_{max,(a,b,c)} = 6.0$					
(a,b,c) λ_{direct} [-]	$\lambda_{max,(a)} \approx 23.0$ $\lambda_{max,(b)} \approx 15.0$ $\lambda_{max,(c)} \approx 19.7$ ($L_2 > L_1$)	–	–	–	$\lambda_{max,(a)} \approx 22.3$ $\lambda_{max,(b)} \approx 10.4$ $\lambda_{max,(c)} \approx 8.1$ ($t_2 < t_1$)	–
λ_{IIW} [-]	$\lambda_{max,(d,f)} = 3.0$					
(d,f) λ_{direct} [-]	$\lambda_{max,(d,f)} \approx 3.5$ ($L_2 < L_1$)	$\lambda_{max,(d,f)} \approx 3.6$ ($L_3 > L_1$)	$\lambda_{max,(d,f)} \approx 3.4$ ($L_4 > L_1$)	$\lambda_{max,(d,f)} \approx 4.7$ ($L_{3=4} > L_1$)	$\lambda_{max,(d,f)} \approx 3.9$ ($t_2 < t_1$)	$\lambda_{max,(d,f)} \approx 5.6$ ($t_{3=4} < t_1$)
λ_{IIW} [-]	$\lambda_{max,(e)} = 3.0$					
(e) λ_{direct} [-]	$\lambda_{max,(d,f)} \approx 4.7$ ($L_2 > L_1$)	$\lambda_{max,(e)} \approx 3.5$ ($L_3 > L_1$)	$\lambda_{max,(e)} \approx 4.6$ ($L_4 < L_1$)	$\lambda_{max,(e)} \approx 4.7$ ($L_{3=4} > L_1$)	–	$\lambda_{max,(e)} \approx 5.6$ ($t_{3=4} < t_1$)

For constructions that are beyond the scope of [3] (cf. Table 5-1), the specifications of Xing and Dong [5] can be applied, as long as the associated validity could be verified in this section. If neither the specifications according to the IIW [2] nor Xing and Dong [53] can provide reliable results, numerical evaluation for the direct determination of influences from axial misalignment are to be preferred.

5.2.2.2.2 Angular misalignment

In this section, angular misalignments of $\alpha = 2^\circ$ are investigated. The results for the corresponding systems (g) to (k) are presented below. In accordance with Section 5.2.2.2.1, the systems without support of the intermediate plate according to Figure 5-31 are analysed at the beginning of the section. In this respect, system (g) refers to cruciform joints with hinged supports with freedom of rotation (cf. left side of Figure 5-31). In contrast, system (h) refers to cruciform joints with restrained supports of the welded-on plates (cf. right side of Figure 5-31).

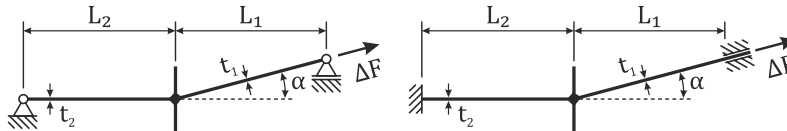


Figure 5-31: Case (g) (left) and case (h) (right) according to Xing and Dong [5]

The results for system (g) (cf. left side of Figure 5-31) can be seen in Figure 5-32. The corresponding evaluations are carried out separately for varying L_2/L_1 ratios (cf. left side of Figure 5-32) and t_2/t_1 ratios (cf. right side of Figure 5-32).

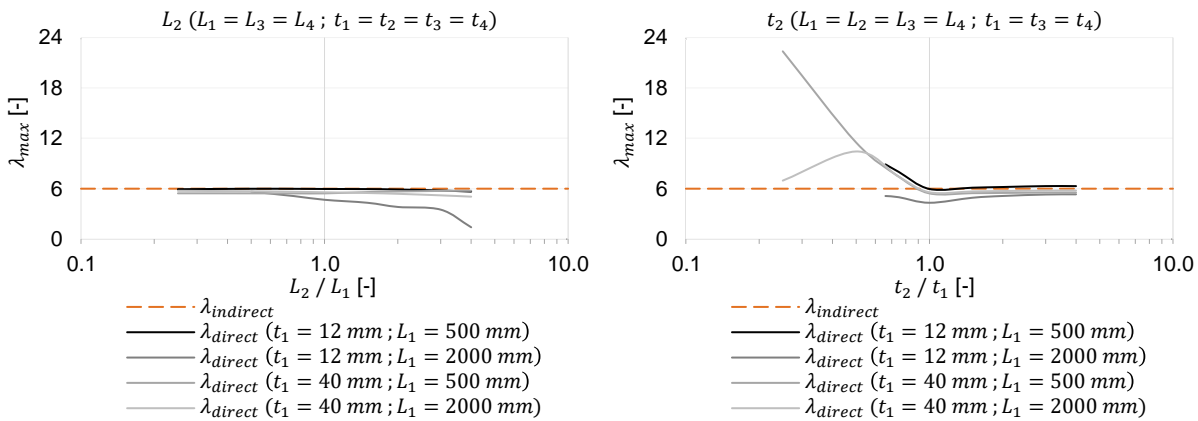


Figure 5-32: Relevant factors λ_{max} for analytical support factor $\lambda_{indirect}$ with comparison to numerical support factors λ_{direct} for L_2/L_1 ratio (left) and for t_2/t_1 ratio (right) for case (g) with $\alpha = 2^\circ$

The results show that good agreements can be achieved with the analytically determined support parameters for all lengths L_2 (cf. left side of Figure 5-32). This applies both to the indirectly determined support parameters $\lambda_{indirect}$ according to Xing and Dong [5] and to the specifications according to the guidelines of the IIW [3] with the constant factor $\lambda_{IIW} = 6.0$ for unrestrained welded-on plates (cf. Section 5.2.1.2.1). However, the analytical formulae of [5] should not be applied to cruciform joints with $t_2 \leq t_1$, as λ_{direct} can be significantly larger than $\lambda_{indirect}$ (cf. right side of Figure 5-32). With regard to thicker plates 1 than plates 2, the specification of IIW [3] for λ_{IIW} is therefore no longer appropriate either. Consequently, numerical calculations with angular misalignment should be carried out in the FEA for this type of design.

The results for case (h) (cf. right side of Figure 5-31) are presented in Figure 5-33. The evaluations are carried out separately for varying L_2/L_1 ratios (cf. left side of Figure 5-33) and t_2/t_1 ratios (cf. right side of Figure 5-33).

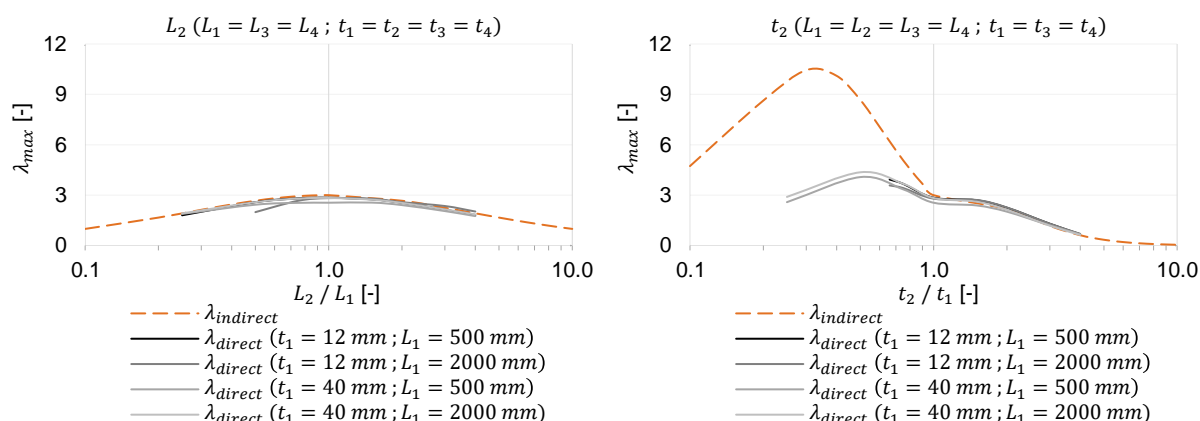


Figure 5-33: Relevant factors λ_{max} for analytical support factor $\lambda_{indirect}$ with comparison to numerical support factors λ_{direct} for L_2/L_1 ratio (left) and for t_2/t_1 ratio (right) for case (h) with $\alpha = 2^\circ$

According to Figure 5-33, the analytical $\lambda_{indirect}$ factors of Xing and Dong [5] are appropriate for evaluating different L_2/L_1 ratios (cf. left side of Figure 5-33). With regard to a varying t_2/t_1 ratio, the formulae are also suitable for $t_2 \geq t_1$ (cf. right side of Figure 5-33). However, at $t_2 < t_1$, an overestimation of the resulting structural stress ranges occurs due to the specifications according to Xing and Dong [5]. This can cause uneconomical design if angular misalignment is to be included at system (h) by means of stress concentration factors k_m . In the case of constructions with a thinner plate 2 than plate 1, incorrect results also occur when applying $\lambda_{IIW} = 3.0$ according to the guidelines of the IIW [3]. In this respect, the relevant support parameters would be underestimated unreliably.

In addition, systems (i), (j) and (k) with supported intermediate plates (cf. Figure 5-34) are evaluated subsequently. The evaluation is carried out according to the evaluation for system (d), (e) and (f) (cf. Section 5.2.2.2.1) for all relevant parameters. Additionally, all results are summarised in Appendix B and only significant results are presented below.

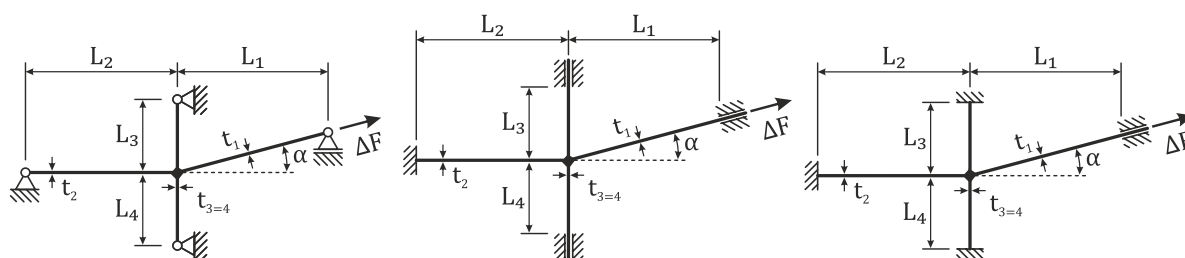


Figure 5-34: Case (i) (left), case (j) (middle) and case (k) (right) according to Xing and Dong [5]

The significant results for system (i) (cf. left side of Figure 5-34) are presented in Figure 5-35. Since the numerical λ_{direct} values for system (i) are significantly lower than the analytical $\lambda_{indirect}$ values given by Xing and Dong [5] (cf. case (i) of Appendix B), the comparison for the support parameters in Figure 5-35 is based on $0.02 \leq \lambda_{IIW} \leq 0.04$ according to the guidelines of the IIW [3] (cf. Table 2-18).

In contrast to the indirect stress concentration factors according to Xing and Dong [5] (cf. case (i) of Appendix B), the significantly lower specifications for the support parameter according to the IIW [3] are in much better accordance with the numerically determined results for λ_{direct} (cf. Figure 5-35). In this respect, only the investigations on cruciform joints with $t_1 = 40 \text{ mm}$ and $L_1 = 500 \text{ mm}$ result in support parameters

$\lambda_{direct} > 0.02$. With uniform plate lengths $L_1 = L_2 = L_3 = L_4$ and plate thicknesses $t_1 = t_2 = t_3 = t_4$, the specifications from [3] can be confirmed throughout with $\lambda_{IIW} = 0.02$. Consequently, there is almost no stress increase in system (i) due to angular misalignment α compared to the results of the perfect FE model. Due to the minor differences between the directly determined support parameters λ_{direct} to λ_{IIW} and the small effect of angular misalignments on the maximum structural stress $\Delta\sigma_{R,hs,FEA,imperfect}$, the specifications of IIW [3] can therefore be regarded as sufficiently validated numerically. In this respect, the significant overestimation of the analytical formulae of Xing and Dong [5] can be attributed to the relatively large stress increase at the intermediate plate. Nevertheless, since the relevant structural stress is still observed at the welded-on plates, the $\lambda_{indirect}$ values according to Xing and Dong [5] are certainly applicable for system (i), but provide very inefficient results. The specifications of the IIW [3] can therefore be applied more effectively in the case of system (i).

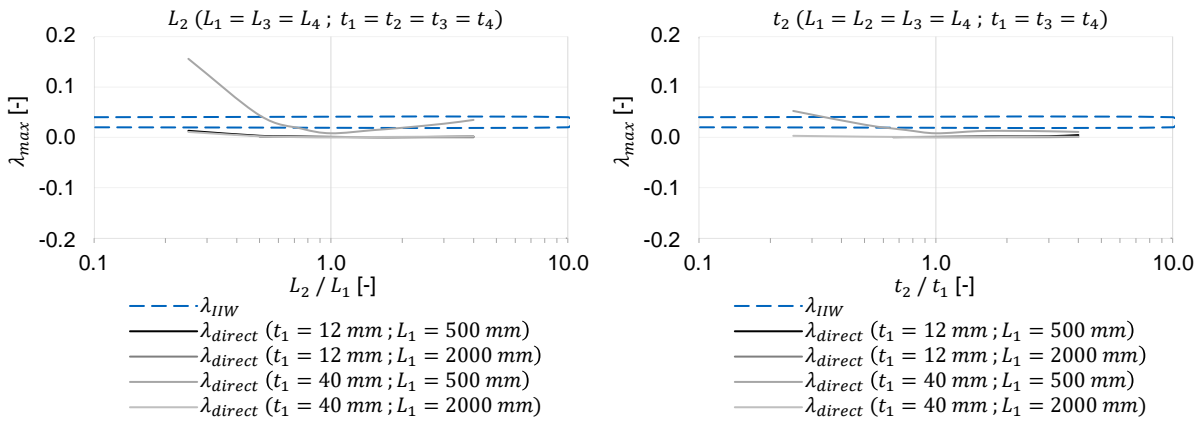


Figure 5-35: Relevant factors λ_{max} for support factors λ_{IIW} according to the IIW [3] with comparison to numerical support factors λ_{direct} for L_2/L_1 ratio (left) and for t_2/t_1 ratio (right) for case (i) with $\alpha = 2^\circ$

The relevant results for system (j) (cf. centre of Figure 5-34) are summarised in Figure 5-36. To this end, the comparison of λ_{direct} is made with the indirectly determined support parameters $\lambda_{indirect}$ since good agreements can be achieved by the specifications of Xing and Dong [5] (cf. case (j) of Appendix B). According to Figure 5-35 for system (j), the analytical formulae according to Xing and Dong [5] result in conservative and thus uneconomic results both for $L_2 < L_1$ (cf. top left side of Figure 5-35) and for $t_2 < t_1$ (cf. bottom left side of Figure 5-35). Only for $L_3 = L_4 < L_1$ analytical unreliable $\lambda_{indirect}$ values are determined, as the numerical results for λ_{direct} are larger (cf. top right side of Figure 5-35). In this range, the application of the formula of Xing and Dong [5] is not recommendable. However, the specifications according to the guidelines of the IIW [3] are not adequate for case (j), since the restriction of the support parameter to $0.02 \leq \lambda_{IIW} \leq 0.04$ underestimates the numerically obtained results significantly. Accordingly, the specifications from [3] are to be formulated more distinctly, since it is not a matter of a restricted in-plane displacement (cf. Table 2-18), but exclusively of the freedom of displacement in the z_{global} direction of the intermediate plate.

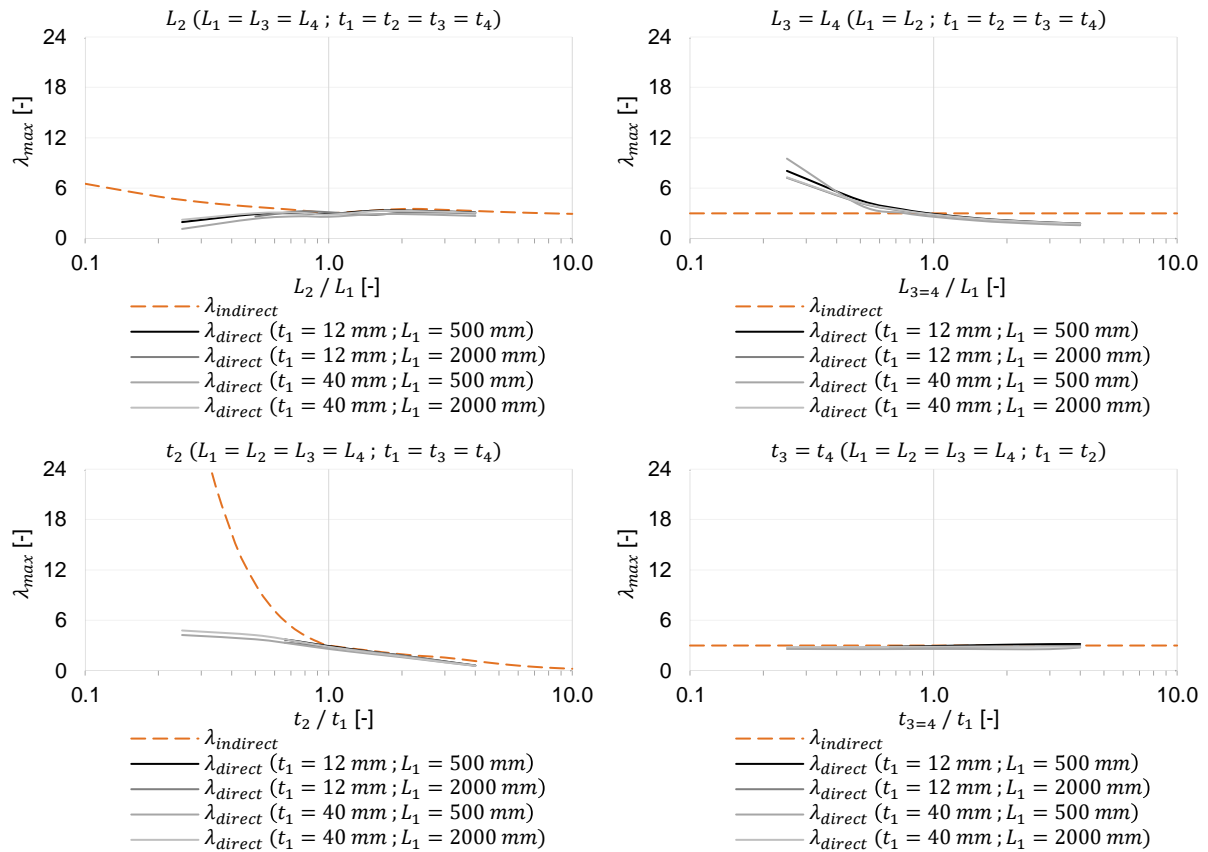


Figure 5-36: Relevant factors λ_{max} for analytical support factor $\lambda_{indirect}$ with comparison to numerical support factors λ_{direct} for L_2/L_1 ratio (top left), $L_{3=4}/L_1$ ratio (top right), t_2/t_1 ratio (bottom left) and for $t_{3=4}/t_1$ ratio (bottom right) for case (j) with $\alpha = 2^\circ$

Finally, the relevant results for system (k) (cf. right side of Figure 5-34) are presented in Figure 5-37. In accordance with the evaluation of system (i), numerically significantly lower λ_{direct} values result than those specified by Xing and Dong [5] (cf. case (k) of Appendix B). Consequently, a comparison is carried out with the more suitable specifications according to the guidelines of the IIW [3]. In the evaluations of system (k), it is apparent that the analytical $\lambda_{indirect}$ values according to Xing and Dong [5] are considerably overstated (cf. case (k) of Appendix B) and do not relate to the λ_{direct} results obtained by the FEA. The application of the formula proposed by Xing and Dong [5] would thus lead to very uneconomical results. To this end, the numerically determined results are consistent with the guidelines of the IIW [2], which specify $0.02 \leq \lambda_{IIW} \leq 0.04$ for supported intermediate plates (cf. Table 2-18). In this respect, the results of λ_{direct} (cf. Figure 5-37) are very similar to case (i) (cf. Figure 5-35). Small deviations with $\lambda_{direct} \geq \lambda_{IIW}$ only occur with a thick welded-on plate 1 with $t_1 = 40 \text{ mm}$ and associated short length $L_1 = 500 \text{ mm}$. However, with uniform plate lengths and thicknesses, $\lambda_{IIW} = 0.02$ can be confirmed by λ_{direct} in all investigations of case (k). Nevertheless, with system (k) there are almost no stress-increasing effects due to angular misalignment α , which is again due to the restricted displacement of the intermediate plate in the z_{global} direction. Therefore, the specifications from [3] can be regarded as numerically sufficiently validated despite the small deviations. Consequently, for cases with intermediate plates supported in the z_{global} direction, the

specifications of IIW [3] are considerably more applicable than those of Xing and Dong [5].

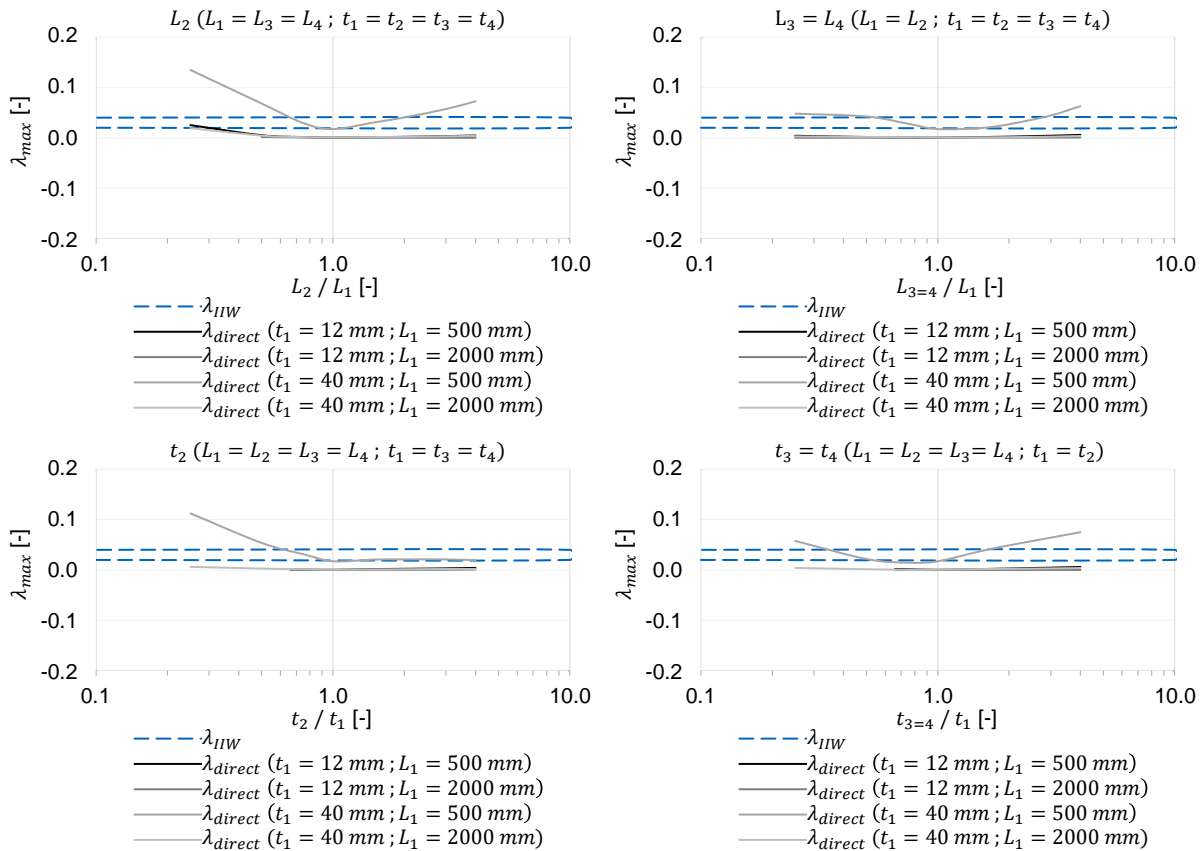


Figure 5-37: Relevant factors λ_{max} for support factor λ_{IIW} according to guidelines of the IIW [3] with comparison to numerical support factors λ_{direct} for L_2/L_1 ratio (top left), $L_{3=4}/L_1$ ratio (top right), t_2/t_1 ratio (bottom left) and for $t_{3=4}/t_1$ ratio (bottom right) for case (k) with $\alpha = 2^\circ$

In summary, the limits of the guidelines of the IIW [3] regarding the support parameter λ_{IIW} for angular misalignment are exceeded with systems (g) to (k) in the ranges defined in Table 5-2. In the ranges specified in Table 5-2, the regulations of the guidelines of the IIW [3] on angular misalignment should only be applied with deliberation. Since the specifications according to Xing and Dong [5] are only suitable to a limited extent for systems (i) and (k) and lead to very uneconomical results, the specifications of the IIW [3] are to be applied in this respect, since only very small stress-increasing effects due to angular misalignment are to be expected. If neither the analytical formulae according to Xing and Dong [5] nor the specifications according to the guidelines of the IIW [3] could be validated numerically by the support parameters λ_{direct} in this section, stress-increasing effects from angular misalignments are to be determined directly by means of the FEA.

Table 5-2: Exceedances of the specifications for support parameters λ_{IIW} according to the guidelines of the IIW [3] by numerically determined support parameters λ_{direct} for systems (g) to (k) with $\alpha = 2^\circ$

Exceedance	L_2/L_1 [-]	L_3/L_1 [-]	L_4/L_1 [-]	$L_{3=4}/L_1$ [-]	t_2/t_1 [-]	$t_{3=4}/t_1$ [-]	
(g)	λ_{IIW} [-]	$\lambda_{max,(g)} = 6.0$					
	λ_{direct} [-]	-	-	-	-	$\lambda_{max,(g)} \approx 22.4$ ($t_2 < t_1$)	-
(h)	λ_{IIW} [-]	$\lambda_{max,(h)} = 3.0$					
	λ_{direct} [-]	-	-	-	-	$\lambda_{max,(g)} \approx 4.4$ ($t_2 < t_1$)	-
(i,k)	λ_{IIW} [-]	$0.02 \leq \lambda_{max,(i,k)} \leq 0.04$					
	λ_{direct} [-]	$\lambda_{max,(i)} \approx 0.16$ $\lambda_{max,(k)} \approx 0.14$ ($L_2 < L_1$)	-	-	$\lambda_{max,(k)} \approx 0.05$ ($L_{3=4} < L_1$)	$\lambda_{max,(i)} \approx 0.05$	$\lambda_{max,(k)} \approx 0.06$ ($t_{3=4} < t_1$)
		$\lambda_{max,(k)} \approx 0.07$ ($L_2 > L_1$)	-	-	$\lambda_{max,(k)} \approx 0.06$ ($L_{3=4} > L_1$)	$\lambda_{max,(k)} \approx 0.12$ ($t_2 < t_1$)	$\lambda_{max,(i)} \approx 0.05$ $\lambda_{max,(k)} \approx 0.08$ ($t_{3=4} > t_1$)
(j)	λ_{IIW} [-]	$0.02 \leq \lambda_{max,(j)} \leq 0.04$					
	λ_{direct} [-]	$\lambda_{max,(j)} \approx 3.1$ ($L_2 < L_1$)	$\lambda_{max,(j)} \approx 3.0$ ($L_3 < L_1$)	$\lambda_{max,(j)} \approx 3.0$ ($L_4 < L_1$)	$\lambda_{max,(j)} \approx 9.5$ ($L_{3=4} < L_1$)	$\lambda_{max,(j)} \approx 4.8$ ($t_2 < t_1$)	$\lambda_{max,(j)} \approx 3.0$ ($t_2 < t_1$)
		$\lambda_{max,(j)} \approx 3.3$ ($L_2 > L_1$)	$\lambda_{max,(j)} \approx 3.0$ ($L_3 > L_1$)	$\lambda_{max,(j)} \approx 3.0$ ($L_4 > L_1$)	$\lambda_{max,(j)} \approx 3.0$ ($L_{3=4} > L_1$)	$\lambda_{max,(j)} \approx 3.0$ ($t_2 > t_1$)	$\lambda_{max,(j)} \approx 3.0$ ($t_2 > t_1$)

5.3 Summary

The objective of this chapter was to analyse the effects of possible imperfections on cruciform joints and to verify normative specifications. For this purpose, studies on clamping processes were summarised in Section 5.1. Concerning this matter, the evaluations of the extensively conducted parameter studies from the IGF research project No. 20336N [1] on clamping processes were presented in Section 5.1.1. In addition, in Section 5.1.2, the analytical specifications for the indirect determination of stress-increasing effects under clamping conditions according to Xing and Dong [5] were verified by comparative calculations in the FEA. Moreover, investigations on practical support conditions were analysed in Section 5.2. In this respect, stress concentration factors $k_{m,axial}$ and $k_{m,angular}$ were evaluated on cruciform joints with uniform plate thicknesses and lengths (cf. Section 5.2.1) as well as support parameters λ for deviating geometries (cf. Section 5.2.2).

Regarding the parameter studies from [1], the influence of possible imperfections of cruciform joints on the resulting stress concentration factors SCF_R under clamping conditions was investigated in Section 5.1.1. In the investigations on possible imperfections under tensile stress in the structural stress concept, it generally is evident that clamping processes lead to significant stress increases compared to the nominal stress concept. According to section 5.1.1.1, evaluations based on the structural stress concept with an angular misalignment of $\alpha = 5^\circ$ result in stress-increasing effects of up to seven times the associated nominal stress ranges. Consequently, evaluation classes B and C of DIN EN ISO 5817 [68] result in large stress concentration factors, which do not allow the economic applicability of the structural stress concept compared to the

nominal stress concept even for small angular misalignment. The evaluations from section 5.1.1.2 on axial misalignment $e/t_{1=2} \leq 0.5$ according to the maximum permissible manufacturer tolerances according to DIN 50100 [27] reveal similar characteristics. To this end, the maximum stress concentration factors are significantly lower with $SCF_R = 3.00$. In addition, the possible rotation of the welded-on plates of cruciform joints was evaluated in Section 5.1.1.3, which has not been considered normatively to date. In this respect, a large influence on the resulting structural stress can similarly be observed under clamping conditions. The resulting maximum stress concentration factors from the associated parameter studies up to $\Phi = 5^\circ$ are with $SCF_R = 5.50$ between those from angular and axial misalignments. However, this only applies to effects from testing machines, as in practice the welded-on plates would not be twisted back by clamping processes. The evaluations on superimposed imperfections from Section 5.1.1.4 prove that single investigations with subsequent superimposition provide sufficiently accurate results under restraint conditions and thus no combinations need to be investigated numerically. Consequently, the superposition of influences from imperfections proposed according to the guidelines of the IIW [3] can be verified.

In addition to the presentation of the results from the parameter studies from [1], the validation of the analytical procedure according to Xing and Dong [5] for the indirect determination of influences from clamping effects was reviewed in Section 5.1.2. The investigations are carried out exclusively on axial and angular misalignment, as [5] does not provide an analytical formula for rotations of the welded-on plates. Associated effects from rotations should therefore be considered directly in the FEA under clamping conditions. In the evaluations of the formulae of Xing and Dong [5], the underestimation of the stiffness of the welded-on plates of cruciform joints is apparent. In addition, straightening effects are only insufficiently included in the analysis. Accordingly, extensive adjustments to the analytical formulae according to [5] on axial and angular misalignment are essential, which compromises general applicability. Although it is possible to generate reasonable results for the cruciform joints evaluated for fatigue in Chapter 4, general applicability is to be considered questionable. Due to the highly geometric non-linear correlations, it is therefore recommended to consider all imperfections on the action side in the FEA if clamping effects are to be investigated. The results on practical support conditions from Section 5.2 are presented subsequently. According to Section 5.2.1, the investigations on stress concentration factors k_m show that the comparative calculations by FEA for axial misalignment at systems (a) and (b) as well as for angular misalignment at systems (g) and (h) agree sufficiently well with the analytical values from the guidelines of the IIW [3] respectively from Xing and Dong [5]. Nevertheless, the evaluations are carried out exclusively on cruciform joints with uniform plate lengths and thicknesses. To this end, it can be verified that the specifications for the support parameter λ_{IIW} of the IIW [3] for axial misalignment relate to the support of the intermediate plate. Consequently, for system (a) and (b) without support of the intermediate plate, $\lambda_{IIW} = 6$ applies. In contrast, the support parameter λ_{IIW} according to [3] for angular misalignment is based on the degree of restraint of the welded-on plates. Accordingly, for system (g) with hinged supports $\lambda_{IIW} = 3$ becomes decisive, whereas for restrained supports according to

system (h) $\lambda_{IIW} = 6$ provides reasonable results. In addition, with regard to axial misalignment, the specifications in the fatigue classes of the nominal and structural stress concept are investigated in relation to already considered influences. Concerning this matter, only the specifications according to the guidelines of the IIW [3] can be classified as reasonable by the numerical calculations. In contrast, the specifications according to DIN EN 1993-1-9 [2] and prEN 1993-1-9 [4] can result in a doubling of the resulting stresses in the nominal and structural stress concept. With comparable fatigue classes in the nominal stress concept and identical classification in the structural stress concept compared to the recommendations of the IIW [2], it can be argued that these effects cannot feasibly be covered by the associated fatigue resistances. Consequently, the specifications according to DIN EN 1993-1-9 [2] and prEN 1993-1-9 [4] in the nominal stress concept on already included effects from axial misalignment $e = 0.15 \cdot t_3$ are to be regarded as critical. Furthermore, the identical specification of prEN 1993-1-9 [4] on cruciform joints within the structural stress concept must be scrutinised carefully.

Finally, analyses of the support parameter λ were carried out in Section 5.2.2 for any relevant support condition. In this respect, the analytical results on $\lambda_{indirect}$ according to Xing and Dong [5] are verified by numerically determined parameters λ_{direct} . In general, the study provides good agreements. However, numerically larger λ_{direct} values are attained in individual cases than analytically by $\lambda_{indirect}$. In these ranges, the application of the analytical formulae of Xing and Dong [5] is not recommended, since the indirect determination of the influences from imperfections is expected to result in insufficient structural stress ranges. With uniform plate thicknesses and lengths, the specifications of the guidelines of the IIW [3] on λ_{IIW} also provide good agreements. Nonetheless, for system (i) and (k) the specifications according to [3] provide significantly more sensible results than the formulae according to Xing and Dong [5]. In the case of cruciform joints with intermediate plates supported in the z_{global} direction, larger percentage stress increases occur at the intermediate plate, but the relevant structural stress ranges still result at the welded-on plates. For this reason, the formulae of Xing and Dong [5] result in an uneconomical overestimation of the structural stress ranges for system (i) and (j), which is not the case according to the guidelines of the IIW [3]. In order to allow a safe application of the stress concentration factors k_m , the verified methods for the indirect determination of influences from axial misalignments and angular misalignments are listed in Appendix B. The associated results can therefore be used to verify whether influences from axial and/or angular misalignments may be indirectly considered in a given design. If the formulae of Xing and Dong [5] and specifications according to the IIW [3] are considered inadequate, the evaluation should be carried out directly by means of numerical FE models in order not to underestimate the relevant stresses and to avoid uneconomical design.

6 Conclusion and perspective

The objective of this thesis is to further develop the structural stress-oriented evaluation procedure for fatigue-loaded cruciform joints and to provide appropriate specifications for the consideration of possible imperfections. Based on the results of the IGF research project No. 20336N [1], concepts are to be developed that enable a simple, economical and reliable application of the structural stress concept in order to provide the capability to perform sensible FE calculations. For this purpose, extensive numerical investigations were conducted on expedient boundary conditions (cf. Chapter 3.3). Specific interest was focused on the effects of imperfections on the stress-increasing effects of cruciform joints (cf. Chapter 5). Based on experimental fatigue tests (cf. Chapter 4), the numerical results were verified and an assessment of the applicability of the structural stress concept was provided. Accordingly, the related conclusions identified in this thesis are summarised in the following Section 6.1. In this respect, a critical assessment of the applicability of the structural stress concept in relation to cruciform joints is provided. Finally, Section 6.2 presents a perspective on further expedient investigations.

6.1 Conclusion

According to the current state of science and standardisation (cf. Chapter 2), structural stresses are part of daily practice in many engineering fields. Nonetheless, since ambiguities persist in civil engineering with regard to modelling, stress determination, the assignment of fatigue resistances as well as the management of imperfections and thickness effects (cf. Chapter 2.1), the inferences determined in this thesis are presented in the following in order to minimise uncertainties with regard to the structural stress concept.

On the one hand, on the resistance side, it can be evidenced with different specifications from normative regulations and guidelines that the resulting fatigue strengths generally only differ insignificantly (cf. Chapter 2.4). With regard to cruciform joints, this applies according to DIN EN 1993-1-9 [2], guidelines of the IIW [3] and prEN 1993-1-9 [4] for both the nominal and the structural stress concept. Concerning this matter, it is evident that the fatigue strengths of the structural stress concept are significantly larger than those of the nominal stress concept.

On the other hand, on the action side, it can be demonstrated that many different approaches are available for the determination of the decisive effective stresses. In addition to the design procedure in the nominal stress concept (cf. Chapter 2.3.1), there are numerous potential local methods for the assessment of structural stress ranges (cf. Chapter 2.3.3). In the evaluations of these local methods, it can be identified in Chapter 3.3.4 that large discrepancies result among the results, which queries the general validity and applicability of the respective concepts for cruciform joints. To this end, only the stress extrapolation (cf. Chapter 2.3.3.1) is specified in prEN 1993-1-9 [4] and prEN 1993-1-14 [14] as well as in the guidelines of the IIW [3]. However, the normative specifications for modelling differ significantly from each other (cf. Chapter

3.2). In this context, the linear stress extrapolation with a fine mesh according to prEN 1993-1-14 [14] is considered to provide the most consistent results with comparatively low complexity. Furthermore, the results of all local methods demonstrate that the resulting structural stress ranges only increase marginally compared to the corresponding nominal stress ranges (cf. Chapter 3.3.4 and 3.3.5). Consequently, the action side is disproportionate to the resistance side, as the latter has significantly higher fatigue resistances in the structural stress concept than in the nominal stress concept.

In order to verify the normative fatigue classes, the evaluation of the fatigue tests conducted in IGF research project No. 20336N [1] is based on differing evaluation methods (cf. Chapter 4.1). In addition to the investigation of perfect and imperfect nominal and structural stress ranges, a further method is developed to consider straightening effects more realistically. The corresponding analyses are performed with adequate FE models, which are implemented according to the defined specifications for expedient boundary conditions in the finite element analysis (cf. Chapter 3.3). Through the validation performed on the basis of the fatigue tests (cf. Chapter 4.4), it can be verified that these FE models can accurately reflect the system behaviour. Associated structural stress ranges are determined by the linear stress extrapolation on finely meshed solid models according to prEN 1993-1-14 [14].

As in practice generally no information is available on unintentional imperfections, a design can in most cases only be realised by an evaluation of perfect nominal resp. structural stress ranges. In this respect, only intentional imperfections are explicitly considered in the numerical calculations in the FEA. For the nominal stress concept DIN EN 1993-1-9 [2], the guidelines of the IIW [3] and prEN 1993-1-9 [4] provide economically efficient fatigue strengths for the experimentally investigated cruciform joints (cf. Figure 4-38). However, according to the guidelines of the IIW [3], fatigue class 71 proves to be more adequate for cruciform joints with connection lengths of $l \leq 50 \text{ mm}$ than fatigue class 80 according to DIN EN 1993-1-9 [2] and prEN 1993-1-9 [4] (cf. Chapter 4.5.1). Despite the general unavailability of information on unintentional imperfections at the design stage, the nominal stress concept is still capable of providing realistic fatigue strengths. This is potentially due to the fact that the associated fatigue strengths are based on results of real tests, which were most likely subjected to unintended imperfections as well. An economic benefit of the significantly more complex evaluations in the structural stress concept is therefore generally not ensured due to the very economically specified nominal stress fatigue classes for the examined cruciform joints. The corresponding evaluation of perfect nominal stress ranges proves that the structural stress ranges determined on the basis of the linear stress extrapolation are only slightly higher than the corresponding nominal stresses (cf. Chapter 4.5.2). However, since the normative fatigue classes are defined disproportionately larger, the evaluation results in a considerable overestimation of the realisable number of stress cycles compared to the experimentally determined results. This indicates that excessive fatigue strengths are specified for the examined cruciform joints in the structural stress concept according to DIN EN 1993-1-9 [2], guidelines of the IIW [3] and prEN 1993-1-9 [4]. In addition, the evaluations of both the nominal and the structural stress concept reveal that increased fatigue strengths are determined for

thin welded-on plates with increasing imperfections. This implies an overestimation of the stress-increasing effects due to imperfections, as consistent fatigue strengths are to be expected within test series. In this context, the insufficient consideration of straightening effects can be identified as a cause.

In addition, the evaluation method with imperfect FE models considering all intentional and unintentional imperfections in the nominal as well as in the structural stress concept demonstrates that only limited practical results are determinable (cf. Figure 4-39 and Figure 4-54). The associated numerical evaluations show an overestimated influence on the fatigue strength, as straightening effects are not accounted for to the correct extent. Although the detected axial and angular imperfections are included in the FEA, no reliable evaluation can be ensured, as no consistent fatigue strengths can be provided within the respective test series investigated. In this respect, the experimental tests on cruciform joints with relatively large imperfections resulted in significantly more load cycles than would have been expected numerically from the associated stress ranges. Consequently, neither an evaluation in the nominal nor in the structural stress concept is capable of realistically representing influences from imperfections as long as straightening effects are not considered accurately.

Due to the overestimation of fatigue strengths in the nominal and structural stress concept with increasing imperfections, a further evaluation procedure is developed to realistically consider straightening effects (cf. Section 4.5.3). To this end, the validations of the approach by means of the experimentally measured effects from imperfections confirm that an evaluation by means of the FEA is capable of providing reliable results. The associated evaluation proves that the real stress ranges in the case of imperfections at cruciform joints are strongly influenced by straightening effects. This confirms that influences of imperfections on the nominal and structural stress concept can be considered more consistently by the proposed method than by the normatively specified design. Consequently, significantly more accurate assessments can be ensured for the investigated cruciform joints by the precise consideration of straightening effects and the resulting deviating fatigue stresses.

With regard to the normative information on influences from imperfections considered in the fatigue resistance, it can be observed that considerably different specifications are provided for similar fatigue classes throughout regulations and guidelines (cf. Chapter 2.5.3.1). In this respect, the specifications according to DIN EN 1993-1-9 [2], guidelines of the IIW [3] and prEN 1993-1-9 [4] differ in both the nominal and the structural stress concept. Considerable differences are also evident in the literature with regard to the feasibility of indirectly determining influences from imperfections by means of stress concentration factors (cf. Chapter 2.5.3.2). While DIN EN 1993-1-9 [2] and prEN 1993-1-9 [4] do not address this essential matter, the associated specifications according to the guidelines of the IIW [3] are not formulated in sufficient detail. In contrast, Xing and Dong [5] provide geometry-dependent formulae for cruciform joints to indirectly determine stress-increasing effects for a variety of practical support conditions (cf. Chapter 2.5.3.2.4). In the corresponding numerical comparative calculations for imperfections of cruciform joints, a significant influence on the relevant structural stress ranges can be determined (cf. Chapter 5). This fact confirms that influences from imperfections must imperatively be considered directly or indirectly

when applying the structural stress concept provided they are not covered by the resistance side. However, it is essential to distinguish between clamping processes in testing machines (cf. Chapter 5.1) and practical support conditions (cf. Chapter 5.2), as the type of support has a major influence on stress-increasing effects. The validity of the modelling of restraint conditions according to Chapter 3.3, can be verified with sufficient accuracy by the results of the fatigue tests on cruciform joints. Nevertheless, this only applies to clamping processes, as no fatigue tests were conducted for practical support conditions.

With regard to clamping conditions, possible angular and axial misalignment of cruciform joints has a significant influence on the resulting structural stress ranges (cf. Chapter 5.1.1). In addition, the rotation of the welded-on plates (cf. Chapter 2.5.2.3), which is normatively not accounted for, is to be explicitly included in the FEA as well, since large stress increases are to be expected with regard to clamping processes in testing machines. Furthermore, it can be revealed that even with small imperfections of cruciform joints, the structural stress concept no longer allows for a more economical application than the nominal stress concept. Due to the dependence on the intermediate plate thickness of the imperfections considered on the resistance side, the fatigue resistances of the nominal stress concept according to DIN EN 1993-1-9 [2] and prEN 1993-1-9 [4] are significantly overestimated under clamping conditions (cf. Chapter 4.5.1). In this respect, the specified dependence on the thickness of the welded-on plates according to the IIW [3] is more effective and can be verified by the results of the fatigue tests. Moreover, in the structural stress concept, prEN 1993-1-9 [4] specifies that stress-increasing effects resulting from axial misalignments of up to 15 % of the thickness of the intermediate plate are covered by the associated fatigue resistance. Accordingly, smaller imperfections may be disregarded. In contrast to the specifications of DIN EN 1993-1-9 [2] and the guidelines of the IIW [3] with uniform classification of the fatigue class, this reference results in a significant overestimation of the resistance side and cannot be verified by the fatigue results for cruciform joints (cf. Chapter 4.5.2). The corresponding specification according to prEN 1993-1-9 [4] thus proves to be invalid with regard to clamping conditions. The stress-increasing effects from imperfections according to the guidelines of the IIW [3] and prEN 1993-1-14 [14] can be verified. Consequently, these specifications are much more suitable for a reliable design of fatigue loaded cruciform joints. In addition, the formulae for an indirect consideration of imperfections for clamping conditions according to Xing and Dong [5] should not be applied without the proposed adjustments. Otherwise, both stiffness and straightening effects are not sufficiently evaluated by the formulae (cf. Chapter 5.1.2). Nonetheless, a general applicability cannot be ensured due to extensive geometrically non-linear correlations.

According to the investigations on clamping processes in testing machines, with regard to practical support conditions it becomes apparent that the specifications according to DIN EN 1993-1-9 [2] and prEN 1993-1-9 [4] for considered axial misalignment on the resistance side lead to unrealistic fatigue strengths (cf. Chapter 5.2.1). This applies to both the nominal and the structural stress concept. In this respect, the specifications according to the guidelines of the IIW [3] are considerably more appropriate and can be verified numerically. In addition, it can be seen that numerical results on the support

parameter partially result in inconsistencies compared to the indirect consideration of stress-increasing effects according to Xing and Dong [5] and the IIW [3] (cf. Chapter 5.2.2). Accordingly, the analytical formulae of Xing and Dong [5] cannot be verified entirely by the results of FEA. The same applies to the imprecisely formulated specifications for the support parameter according to the guidelines of the IIW [3], whose ranges of validity can be specified more accurately through the performed numerical calculations. To this end, it is evident that the support parameters according to the IIW [3] in most cases only provide sensible results for uniform plate lengths and thicknesses (cf. Table 5-1 and Table 5-2). Nevertheless, ranges are identified in which the indirect evaluations according to Xing and Dong [5] and the IIW [3] can be applied appropriately, independently of the geometry.

Furthermore, the fatigue evaluation of FE models with shell elements indicates that comparatively satisfactory agreements with the validated solid models can be ensured (cf. Chapter 3.3.5). However, this is only valid if welds of cruciform joints are explicitly considered by inclined shell elements (cf. Chapter 3.1.1) and a correction of the resulting structural stress ranges to 102.5 % is applied to compensate for underestimations compared to the solid models. This method is very insensitive to different meshes, which is conducive to practical application. The capability of the associated FE models to deliver realistic results can be confirmed by the validation on the fatigue tests on cruciform joints (cf. Chapter 4.4). In contrast, the evaluations with simplified FE models without explicitly modelled welds result in significant over- and underestimations of the solid models, depending on the component dimensions of the examined cruciform joints (cf. Chapter 3.3.5.1.1). For this reason, modelling without welds is only recommended if the introduced modification of the structural stress determination is implemented. In this respect, by adjusting the distances for the evaluation paths of the linear stress extrapolation with an additional structural stress increase to 102.5 %, a reliable applicability of shell models without explicit weld modelling can be enabled. Nonetheless, this only applies to cruciform joints where no influences from imperfections are to be considered, as significantly larger corrections are required otherwise (cf. Chapter 3.3.5.2.1). Accordingly, the exclusion of welds would lead to very inefficient results in most cases. Conversely, the FE models with inclined shell elements are sufficiently effective in capturing influences from imperfections. To this end, deviations of more than 10 % compared to results of solid models are only evident if large angular misalignment is to be investigated under clamping conditions in testing machines (cf. Chapter 3.3.5.2.2). With regard to practical support conditions, however, a factor of 1.06 is sufficient to rectify the corresponding structural stress ranges.

Moreover, studies conducted on the plate thickness of cruciform joints prove that no thickness effects can be detected using the structural stress concept (cf. Chapter 3.3.6). Accordingly, the consideration of thickness effects through a modification of the corresponding normative fatigue classes is imperative. In order to appropriately account for these effects, a broad range of normative approaches are available, some of which differ considerably from one another (cf. Chapter 2.6). In order to better assess thickness effects, fatigue tests were carried out in IGF research project No. 20336N [1] on cruciform joints with varying thicknesses. To this end, since the test results are

severely influenced by imperfections, it is not feasible to identify thickness effects unambiguously. Anyhow, it can be demonstrated that a consideration of thickness effects in the nominal stress concept according to the guidelines of the IIW [3] provides conservative fatigue strengths (cf. Chapter 4.5.1). The specifications according to DIN EN 1993-1-9 [2] and prEN 1993-1-9 [4] are more sensible in order to ensure economic results. By contrast, in the structural stress concept, consideration of the thickness effect according to the guidelines of the IIW [3] and prEN 1993-1-9 [4] ensures better agreement with the experimental results and is therefore recommended. As specifications regarding the thickness effect are not included in the currently valid DIN EN 1993-1-9 [2], it is advisable to include them in prEN 1993-1-9 [4]. Concerning this matter, with regard to the extent of thickness effects to be accounted for, no definite assessment can be provided.

Finally, it can be stated that the investigations on cruciform joints unveil that a general evaluation of the universal applicability of the structural stress concept is to be considered challenging. In this respect, the various specifications in the normative regulations and guidelines for modelling and stress determination as well as for fatigue strengths and their consideration of imperfections and thickness effects make it difficult to develop a sensible approach. Nevertheless, with regard to the application of shell elements, it can be demonstrated that by modelling welds through inclined shell elements, reasonable results can be obtained which, with a stress correction, provide good agreements compared to the results on solid models. Thus, in relation to reliable evaluations in the structural stress concept for cruciform joints, shell elements can be implemented as well. Furthermore, the extensive parameter studies on cruciform joints conducted in IGF research project No. 20336N [1] indicate that significantly lower stress concentration factors are to be expected on the action side between the structural and nominal stress concept than provided on the resistance side between the respective fatigue classes. These imply that more economical results may be achieved with the structural stress concept compared to the nominal stress concept as long as no imperfections are to be expected. However, this assumption presupposes expedient fatigue strengths in the structural stress concept, which cannot be verified for all cases by the evaluated fatigue tests (cf. Chapter 4). Accordingly, there is a considerable risk of unreliable fatigue verification in the structural stress concept, as no realistic determination of expected stress cycles can be ensured for the conducted experiments. Furthermore, the economic applicability of the structural stress concept compared to the nominal stress concept is no longer provided starting at minor imperfections (cf. Chapter 5). In the associated evaluations of imperfections, regardless of the selected support condition, it is evident that imperfections have a significant influence on the relevant structural stress ranges of cruciform joints. Nonetheless, the considerably differing specifications of normative regulations and guidelines on considered influences from imperfections on the resistance side, can lead to an incorrect estimation of the respective fatigue strength. In this respect, only the specifications according to the guidelines of the IIW [3] are considered appropriate, as the recommendations according to DIN EN 1993-1-9 [2] and prEN 1993-1-9 [4] may lead to inaccurate results. Furthermore, deviating specifications in the literature for the indirect consideration of stress-increasing effects may lead to uncertainties in the evaluation if not all imperfections are directly considered in the FEA. So far, this circumstance has severely

restricted the sensible applicability of the structural stress concept regarding cruciform joints with imperfections. Concerning this matter, by means of systematic verifications of the specifications from literature, ranges of application can be identified in which the indirect evaluation of stress-increasing effects due to imperfections according to Xing and Dong [5] as well as the guidelines of the IIW [3] can be implemented in a geometry-independent manner. It is therefore recommended to include the results on support parameters and related stress concentration factors in the standardisation. However, the consideration of straightening effects should be included in the design, especially in the case of large expected imperfections of cruciform joints, in order to enable an economic and reliable assessment based on the nominal and structural stress concept. In this way, the structural stress concept can also be applied more practically in the case of imperfections.

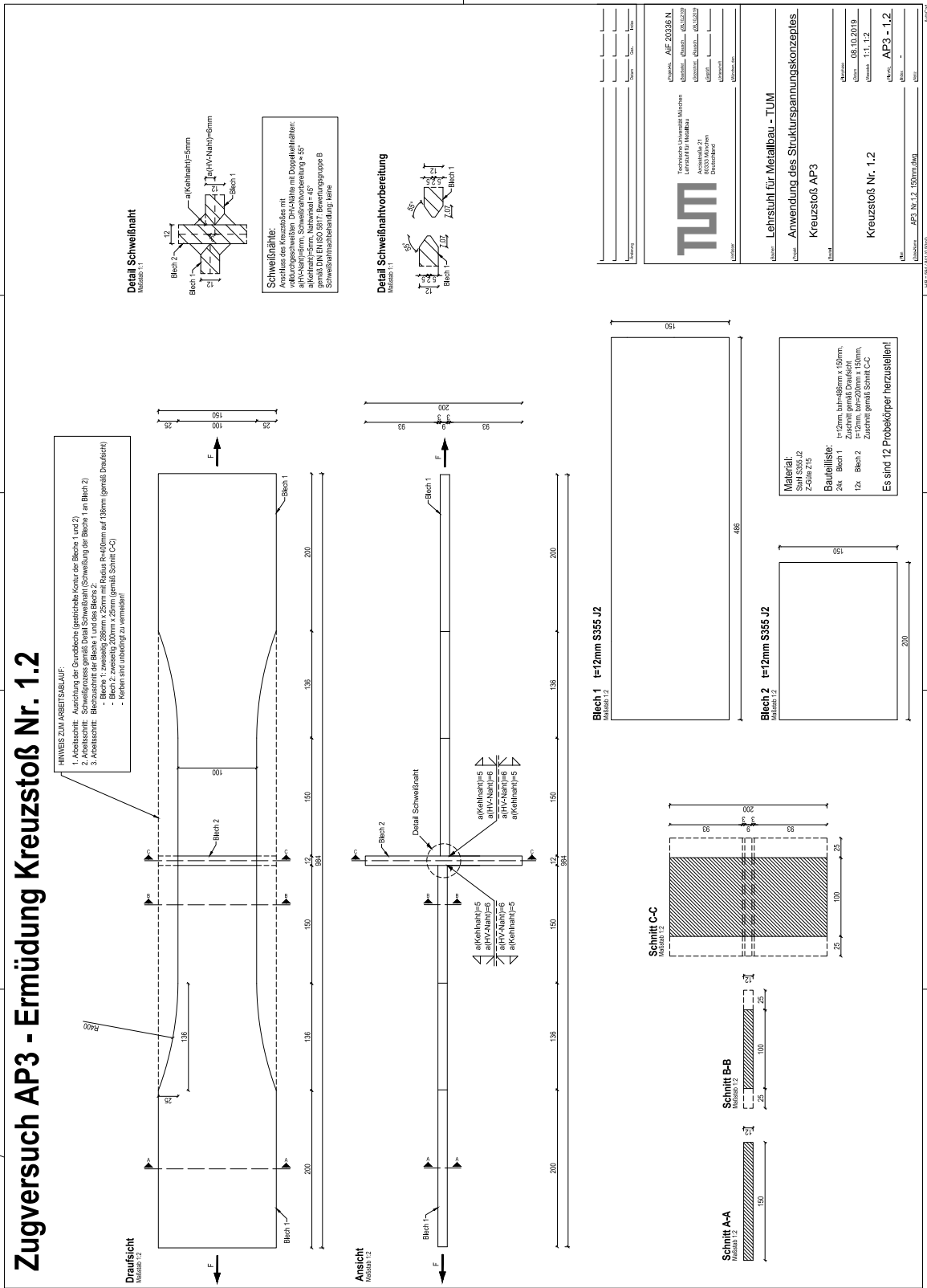
Consequently, in the course of this thesis, expedient regulations could be established to significantly reduce uncertainties within the structural stress concept. Nevertheless, in practice, the economic applicability of the structural stress concept regarding cruciform joints is generally disputable. In comparison, the application of the generally accepted nominal stress concept can ensure considerably more sensible results in many instances, with significantly less expenditure and fewer uncertainties with regard to a reasonable stress determination. Moreover, with significantly improved computational efficiency, the effective notch stress concept nowadays provides a practical alternative that can identify fatigue-relevant effects in much greater detail.

6.2 Perspective

Nonetheless, in order to provide further unambiguous information on the applicability of the structural stress concept specified in the standards, additional fatigue tests would have to be conducted on cruciform joints. In this respect, special effort would have to be directed towards accurate execution in order to avoid preventable stress-increasing effects from imperfections. To enable verification of the numerically investigated parameter ranges, experiments on further geometric parameters as well as on additional imperfections would be expedient for varying support conditions. Consequently, in order to verify the indirect consideration of imperfections under practical support conditions, it would be required to conduct tests with adapted degree of clamping respectively freedom of rotation of the supports. To this end, it would be advisable to focus on a single parameter in each experimental investigation. By contrast, in the fatigue tests of the IGF research project No. 20336N [1], several parameters were varied simultaneously in order to determine influences from imperfections as well as thickness effects. Although it is reasonable to investigate many influences with a minimum of tests, the exact assignment of resulting effects on structural stress ranges to individual parameters is hardly possible. In addition, due to the limited number of similar experimental tests, it is not yet possible to verify the normative fatigue strengths of the structural stress concept with sufficient accuracy. Thus, the results of the completed parameter studies could be verified by the implementation of further fatigue tests. In addition, it might be possible to draw further conclusions about possible influences on the fatigue strength to further minimise remaining uncertainties in the structural stress concept.

Since the results attained in this thesis on the structural stress concept indicate that an economic applicability of the structural stress concept is questionable, evaluations with the more accurate effective notch stress concept are considered by the author to be more future-oriented. The evaluation of effective notch stresses also enables an assessment of thickness effects. In this way, further investigations in the effective notch stress concept could facilitate a realistic consideration of these effects in civil engineering. Nevertheless, the outcomes of this thesis need to be included in the standardisation in order to ensure a more reliable fatigue verification with the structural stress concept. The achieved results on the influence of imperfections on the fatigue behaviour of cruciform joints can additionally be applied in the nominal and effective notch stress concept.

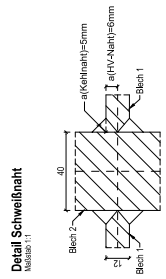
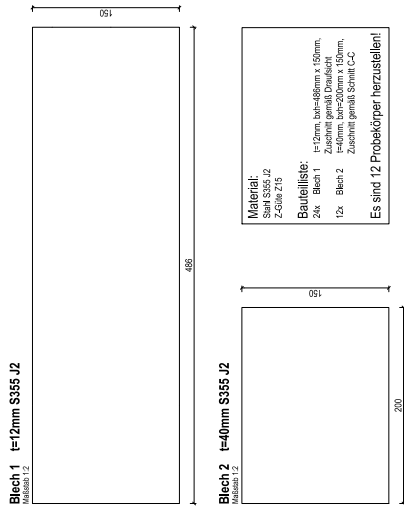
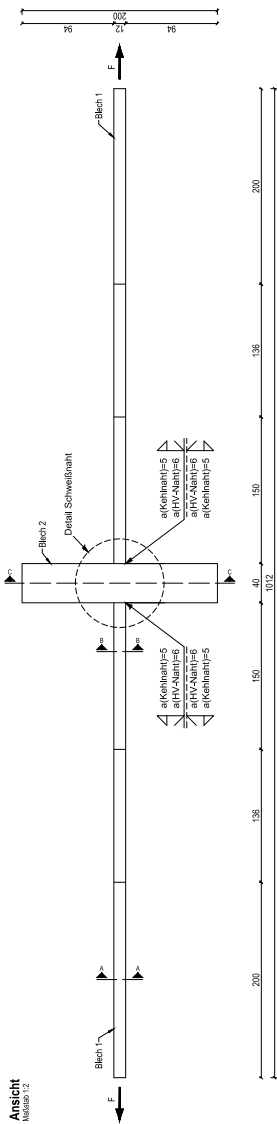
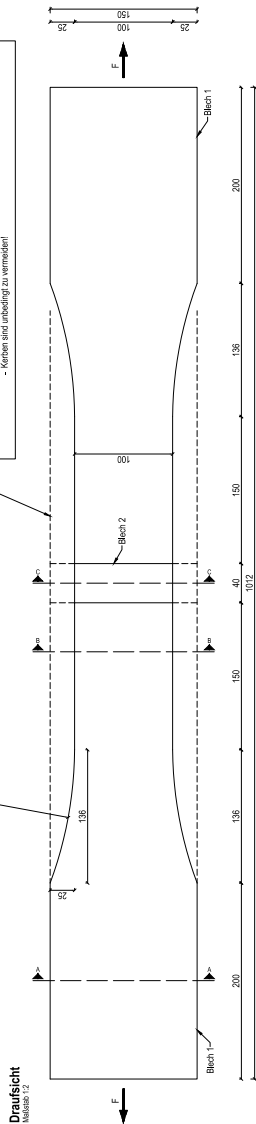
Execution plan for cruciform joints of test group WP3_1.2



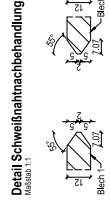
Execution plan for cruciform joints of test group WP3_2.1

Zugversuch AP3 - Ermüdung Kreuzstoß Nr. 2.1

HINWEIS ZUM ARBEITSLAUF:
 1. Anzeitschnitt: Ausrichtung der Grundfläche (gestrichelte Kontur der Bleche 1 und 2)
 2. Anzeitschnitt: Ausrichtung der Bleche 1 und 2
 3. Anzeitschnitt: Schweißnaht der Bleche 1 und 2
 4. Anzeitschnitt: Schweißnaht der Bleche 1 und 2
 5. Anzeitschnitt: Schweißnaht der Bleche 1 und 2
 - Blech 1: zweiseitig 20mm x 25mm mit Radius R=400mm auf 136mm (gemäß Schnitt C-C)
 - Blech 2: zweiseitig 20mm x 25mm (gemäß Schnitt C-C)
 - Kontur sind unbedingt zu verwenden!

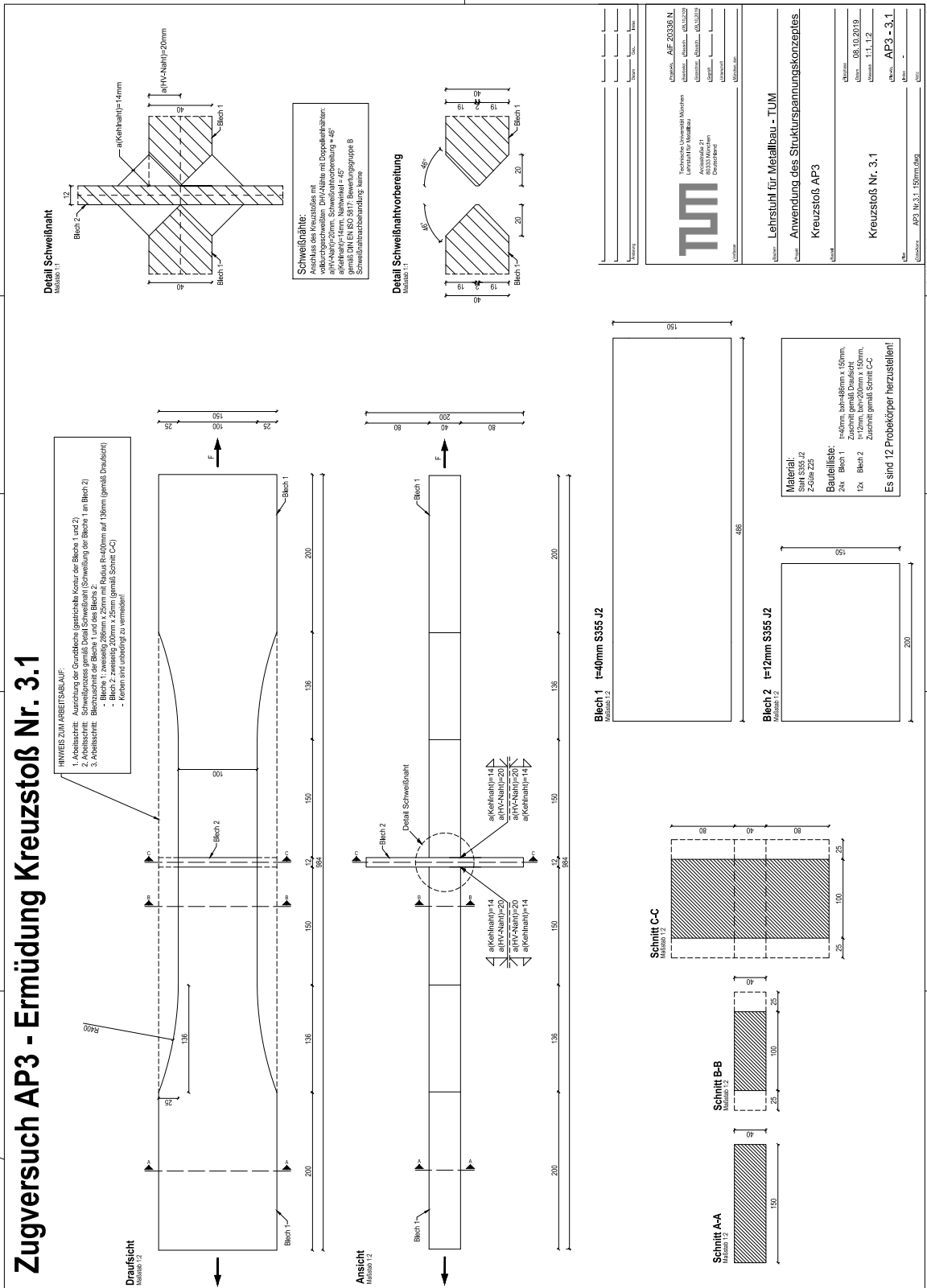


Schweißnaht:
 Anschluss des Kreuzstoßes mit
 vollrandgeschweißten DHP-Nähten mit Doppelfächerbau:
 - Winkel der Fächer: 45°
 - Fächerhöhe: 10mm
 - Fächerbreite: 10mm
 gemäß DIN EN ISO 5817: Bewertungsgruppe B
 Schweißnahtbehandlung: Kerne

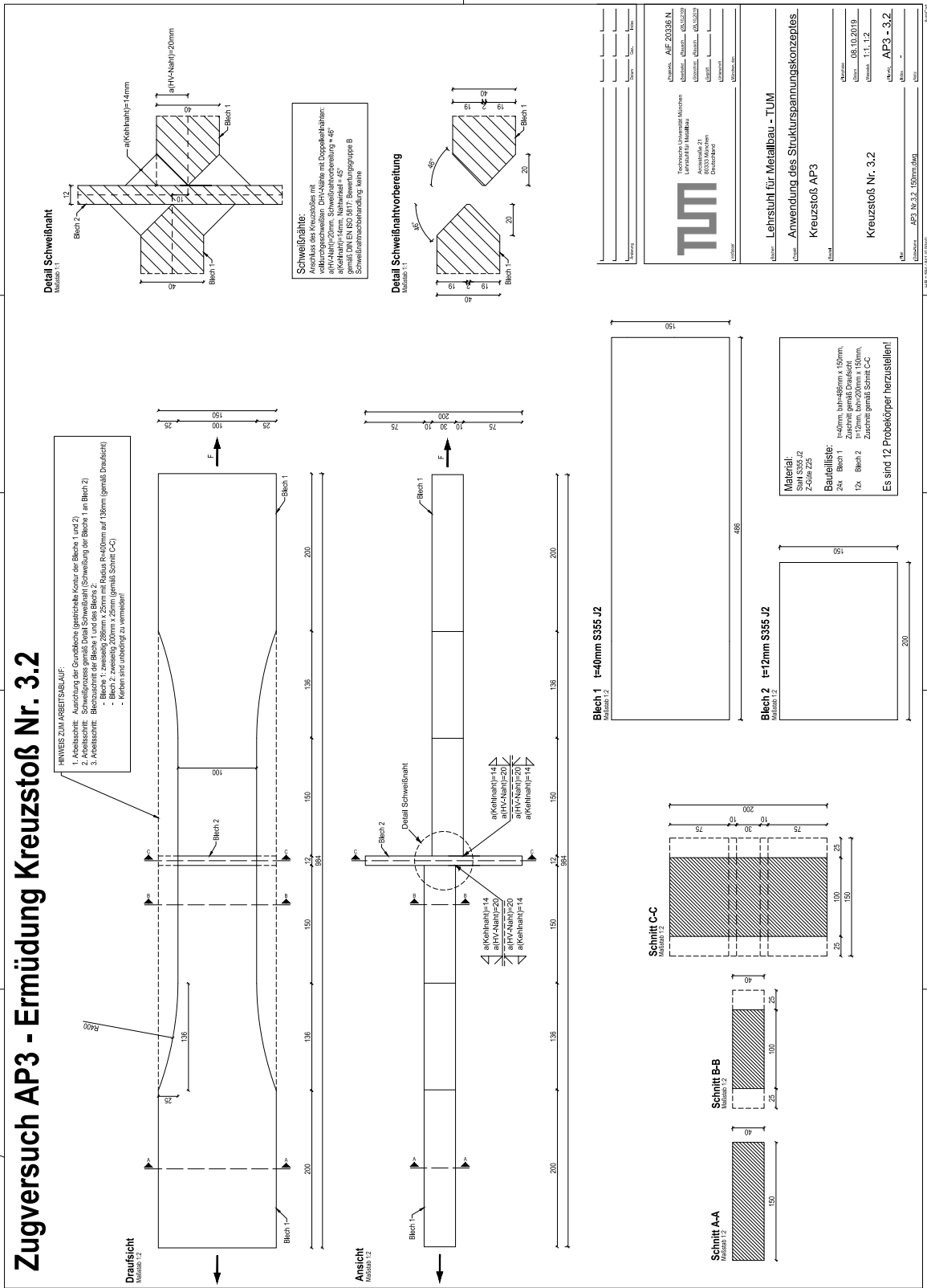


Technische Universität München Lehrstuhl für Metallbau - TUM Anwendung des Strukturspannungskonzeptes Kreuzstoß AP3 Kreuzstoß Nr. 2.1 AP3 - 2.1	
Datum: 08.10.2019 Version: 1.1, 1.2 Blatt: 1 von 1	Maßstab: 1:1 Zeichnung: AP3 - 2.1

Execution plan for cruciform joints of test group WP3_3.1



Execution plan for cruciform joints of test group WP3_3.2



Appendix B: Case studies on support parameters

Case (a)

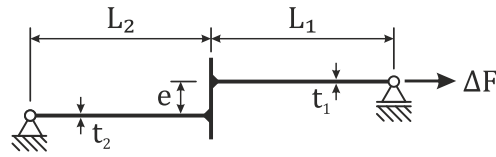


Figure 6-1: Case (a) according to Xing and Dong [5]

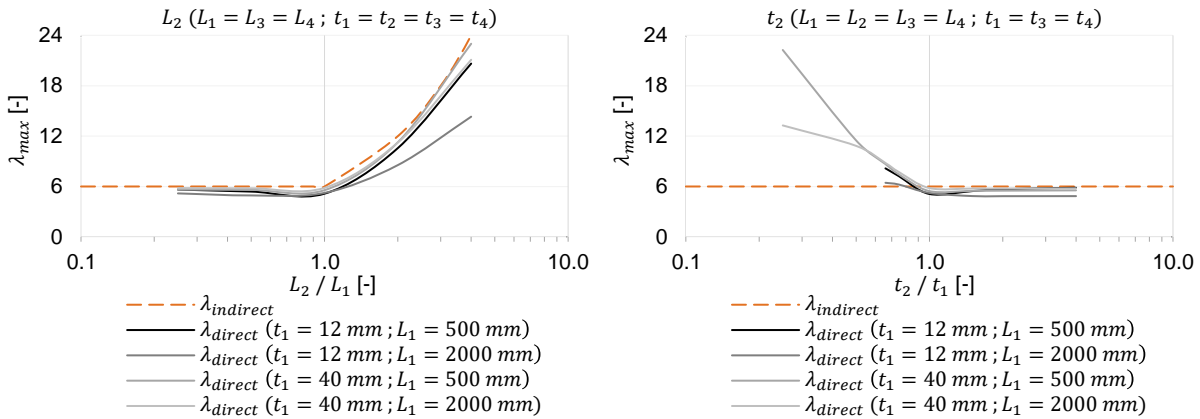


Figure 6-2: Relevant $\lambda_{indirect}$ results with comparison to relevant λ_{direct} results for L_2/L_1 ratio (left) and for t_2/t_1 ratio (right) for case (a) with axial misalignment $e/t_1 = 0.15$

Case (b)

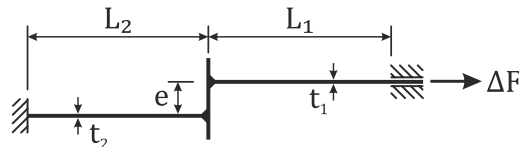


Figure 6-3: Case (b) according to Xing and Dong [5]

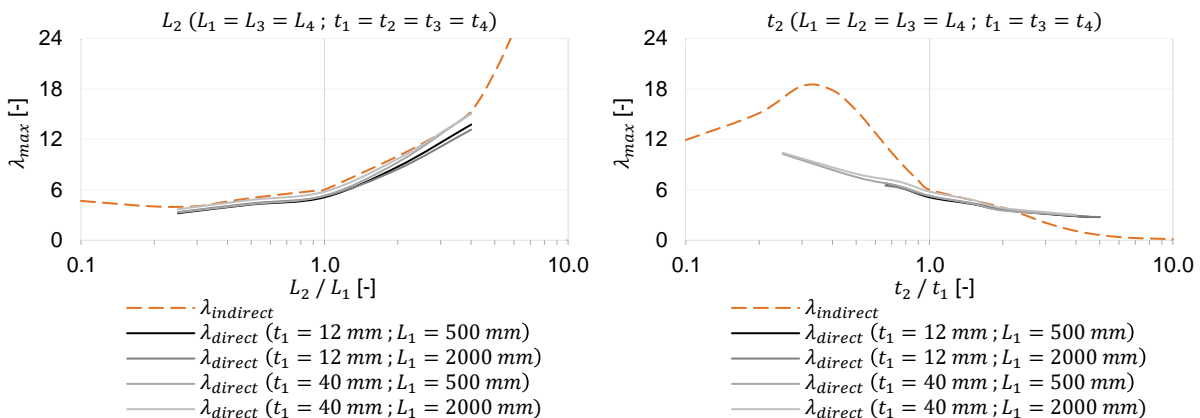


Figure 6-4: Relevant $\lambda_{indirect}$ results with comparison to relevant λ_{direct} results for L_2/L_1 ratio (left) and for t_2/t_1 ratio (right) for case (b) with axial misalignment $e/t_1 = 0.15$

Case (c)

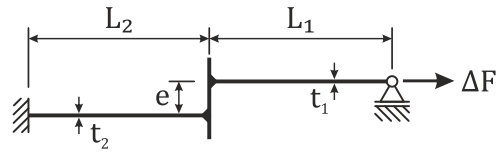


Figure 6-5: Case (c) according to Xing and Dong [5]

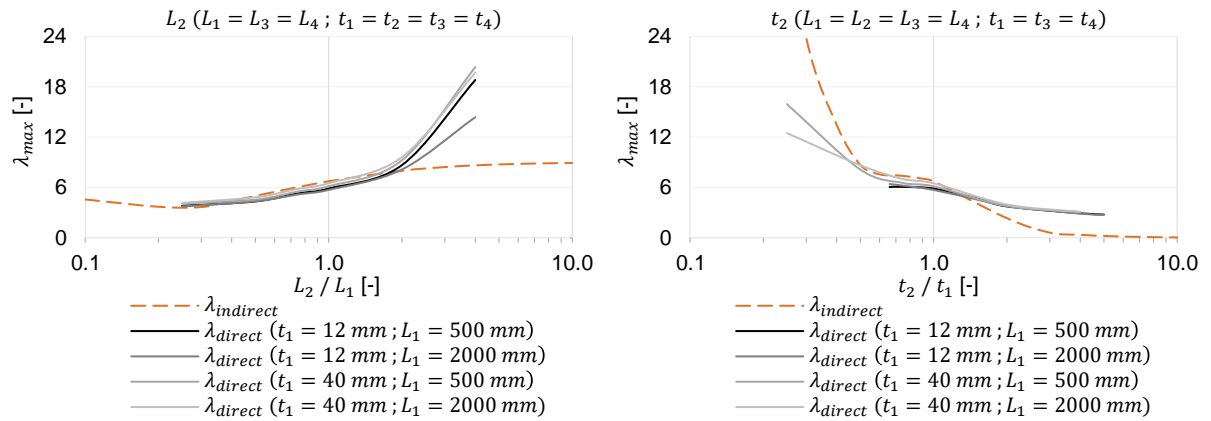


Figure 6-6: Relevant $\lambda_{indirect}$ results with comparison to relevant λ_{direct} results for L_2/L_1 ratio (left) and for t_2/t_1 ratio (right) for case (c) with axial misalignment $e/t_1 = 0.15$

Case (e)

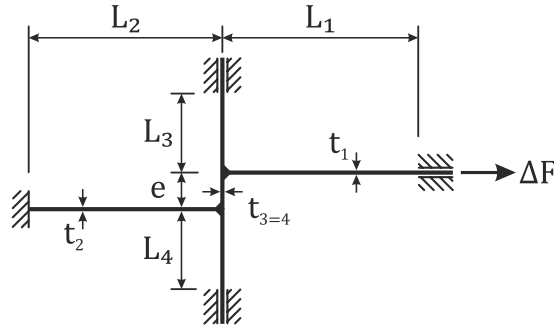
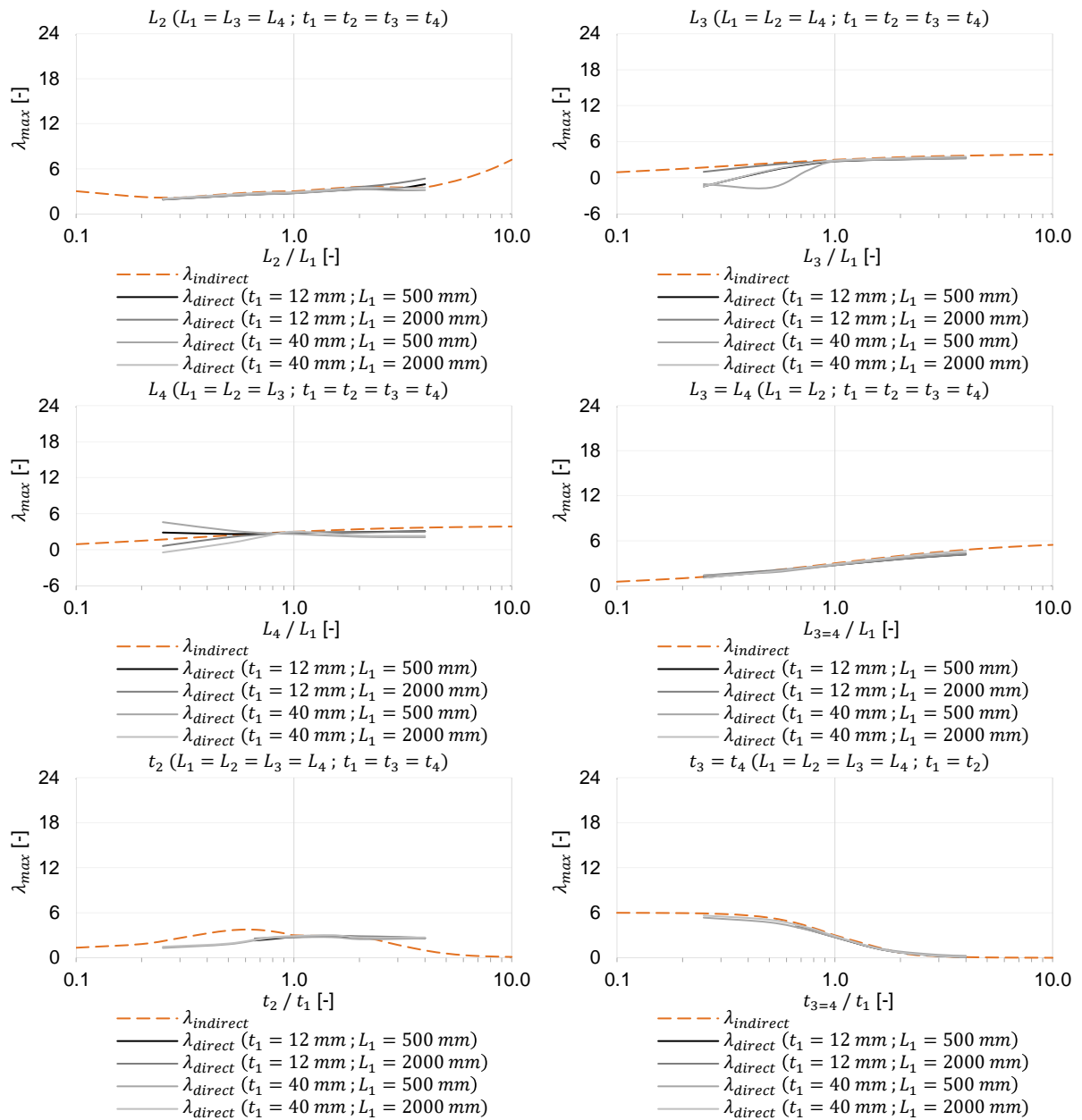


Figure 6-9: Case (e) according to Xing and Dong [5]



Case (f)

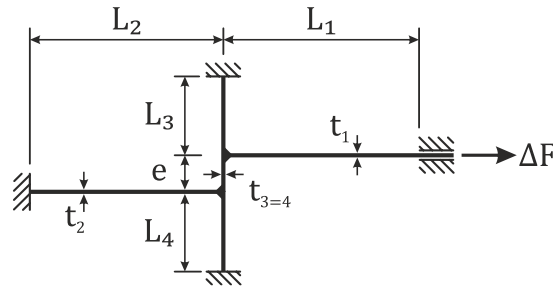
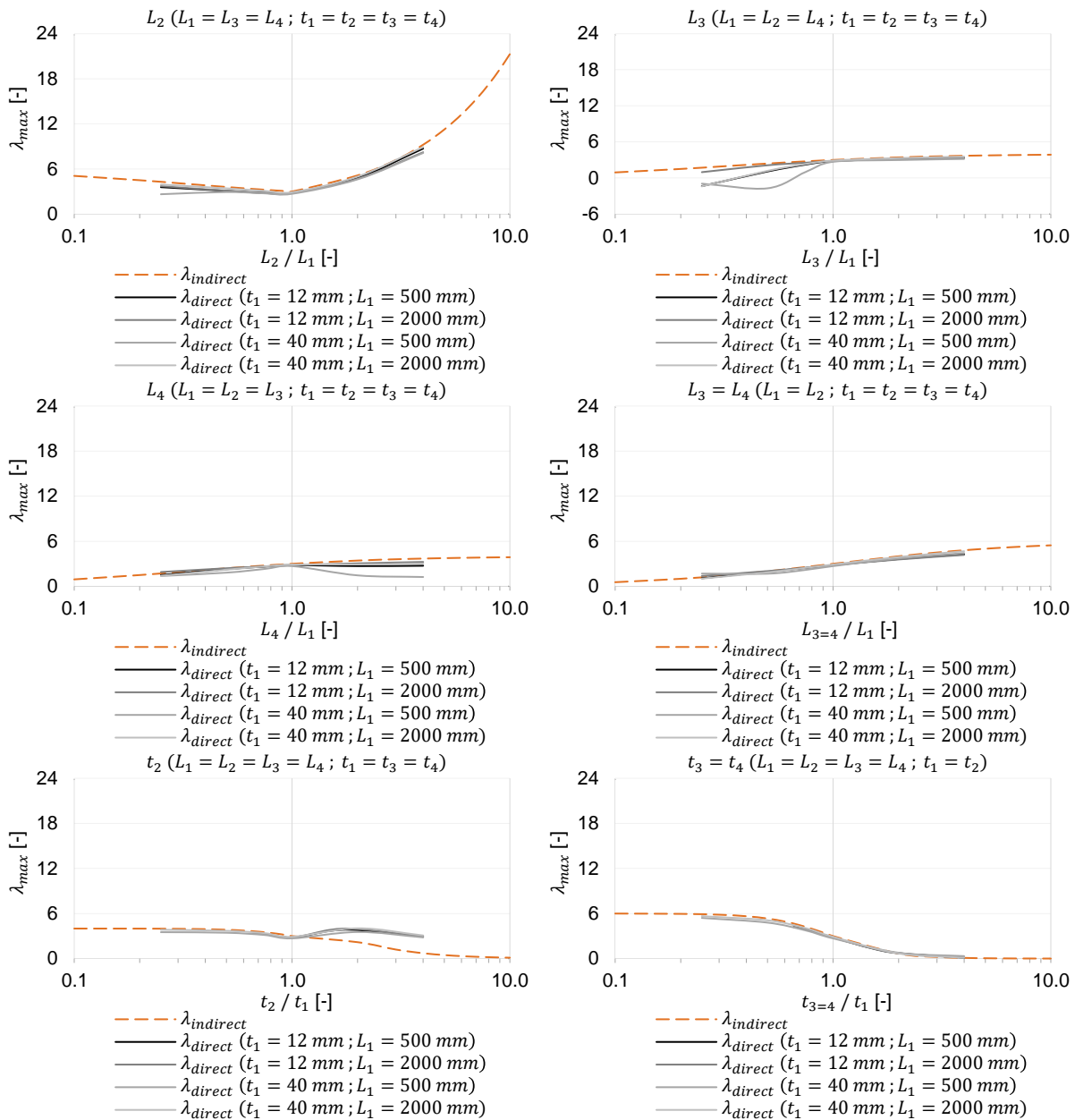


Figure 6-11: Case (f) according to Xing and Dong [5]

Figure 6-12: Relevant $\lambda_{indirect}$ results with comparison to relevant λ_{direct} results for L_2/L_1 ratio (top left), L_3/L_1 ratio (top right), L_4/L_1 ratio (centre left), $L_3=L_4/L_1$ ratio (centre right), t_2/t_1 ratio (bottom left) and $t_3=t_4/t_1$ ratio (bottom right) for case (f) with axial misalignment $e/t_1 = 0.15$

Case (g)

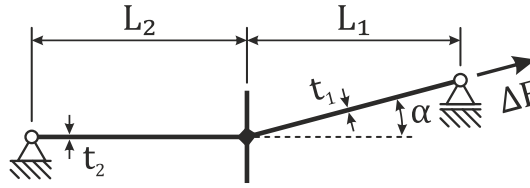


Figure 6-13: Case (g) according to Xing and Dong [5]

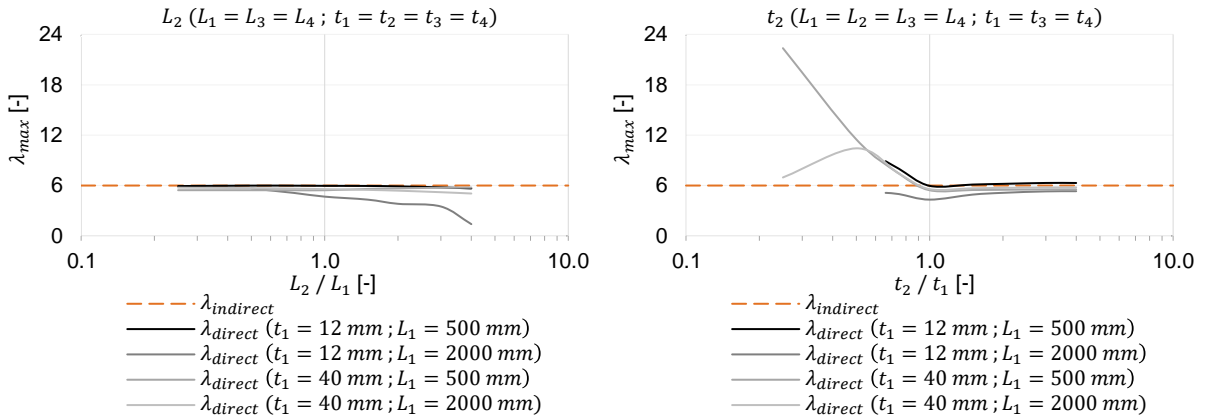


Figure 6-14: Relevant $\lambda_{indirect}$ results with comparison to relevant λ_{direct} results for L_2/L_1 ratio (left) and for t_2/t_1 ratio (right) for case (g) with angular misalignment $\alpha = 2^\circ$

Case (h)

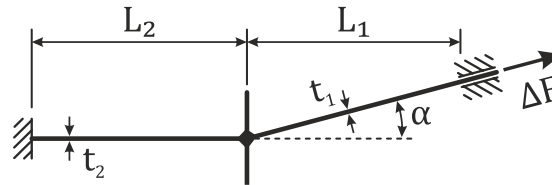


Figure 6-15: Case (h) according to Xing and Dong [5]

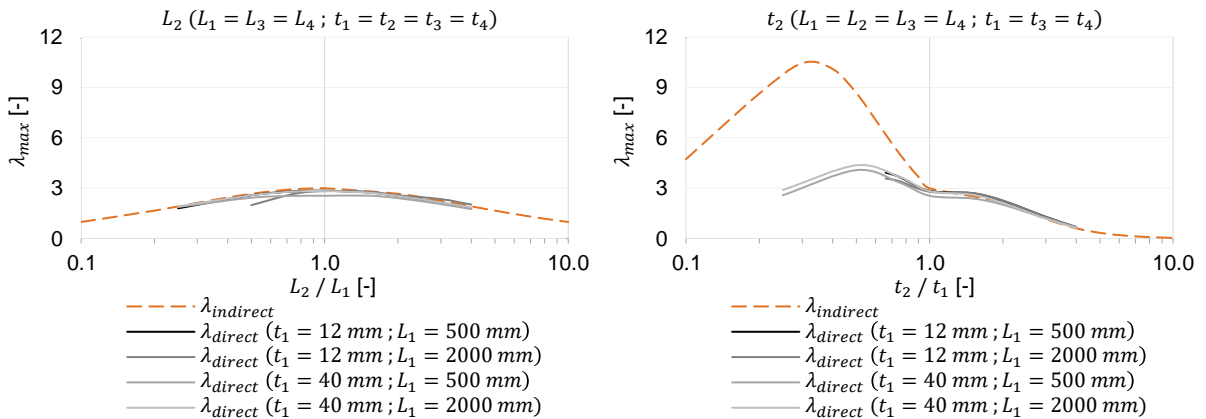


Figure 6-16: Relevant $\lambda_{indirect}$ results with comparison to relevant λ_{direct} results for L_2/L_1 ratio (left) and for t_2/t_1 ratio (right) for case (h) with angular misalignment $\alpha = 2^\circ$

Case (i)

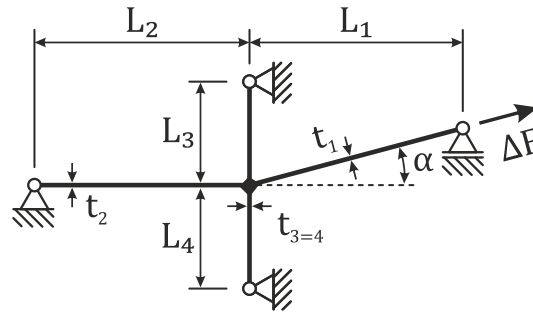


Figure 6-17: Case (i) according to Xing and Dong [5]

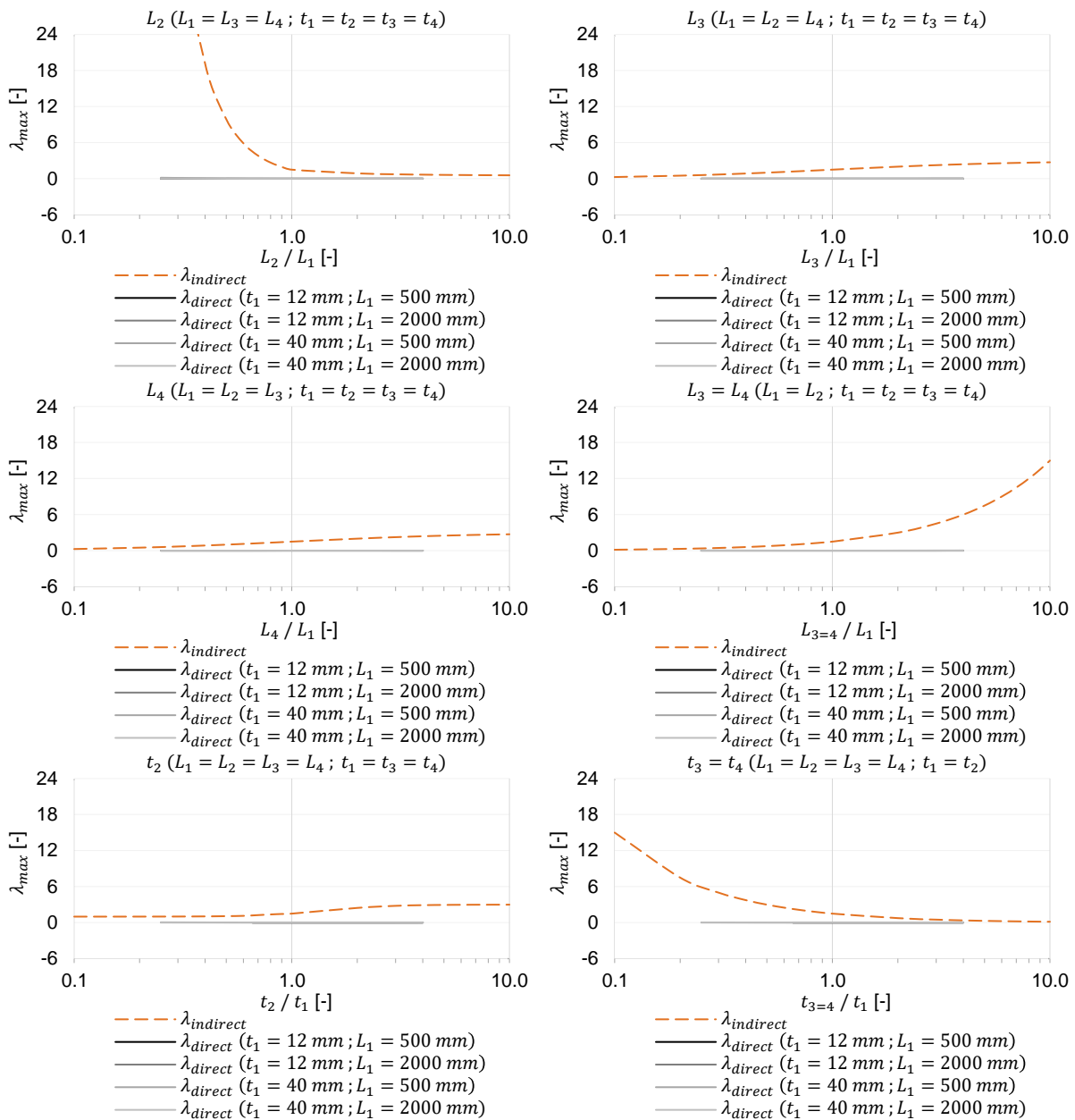


Figure 6-18: Relevant $\lambda_{indirect}$ results with comparison to relevant λ_{direct} results for L_2/L_1 ratio (top left), L_3/L_1 ratio (top right), L_4/L_1 ratio (centre left), $L_{3=4}/L_1$ ratio (centre right), t_2/t_1 ratio (bottom left) and $t_{3=4}/t_1$ ratio (bottom right) for case (i) with angular misalignment $\alpha = 2^\circ$

Case (j)

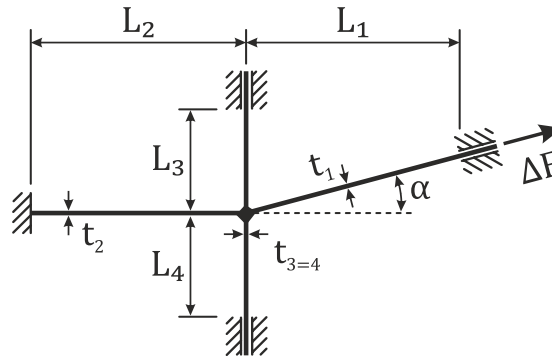


Figure 6-19: Case (j) according to Xing and Dong [5]

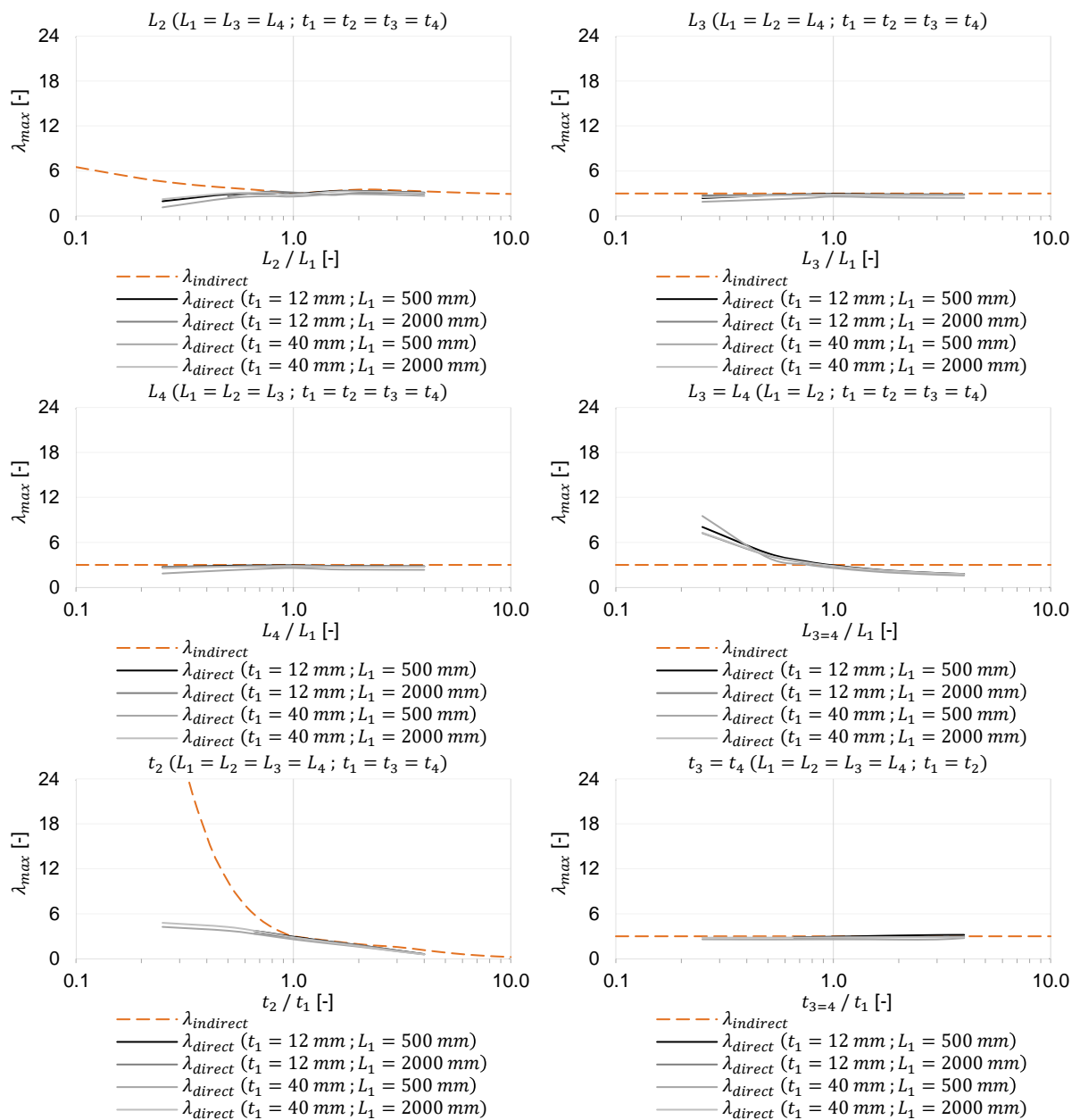


Figure 6-20: Relevant $\lambda_{indirect}$ results with comparison to relevant λ_{direct} results for L_2/L_1 ratio (top left), L_3/L_1 ratio (top right), L_4/L_1 ratio (centre left), $L_{3=4}/L_1$ ratio (centre right), t_2/t_1 ratio (bottom left) and $t_{3=4}/t_1$ ratio (bottom right) for case (j) with angular misalignment $\alpha = 2^\circ$

Case (k)

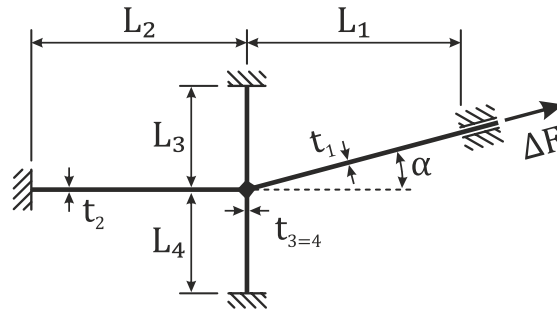


Figure 6-21: Case (k) according to Xing and Dong [5]

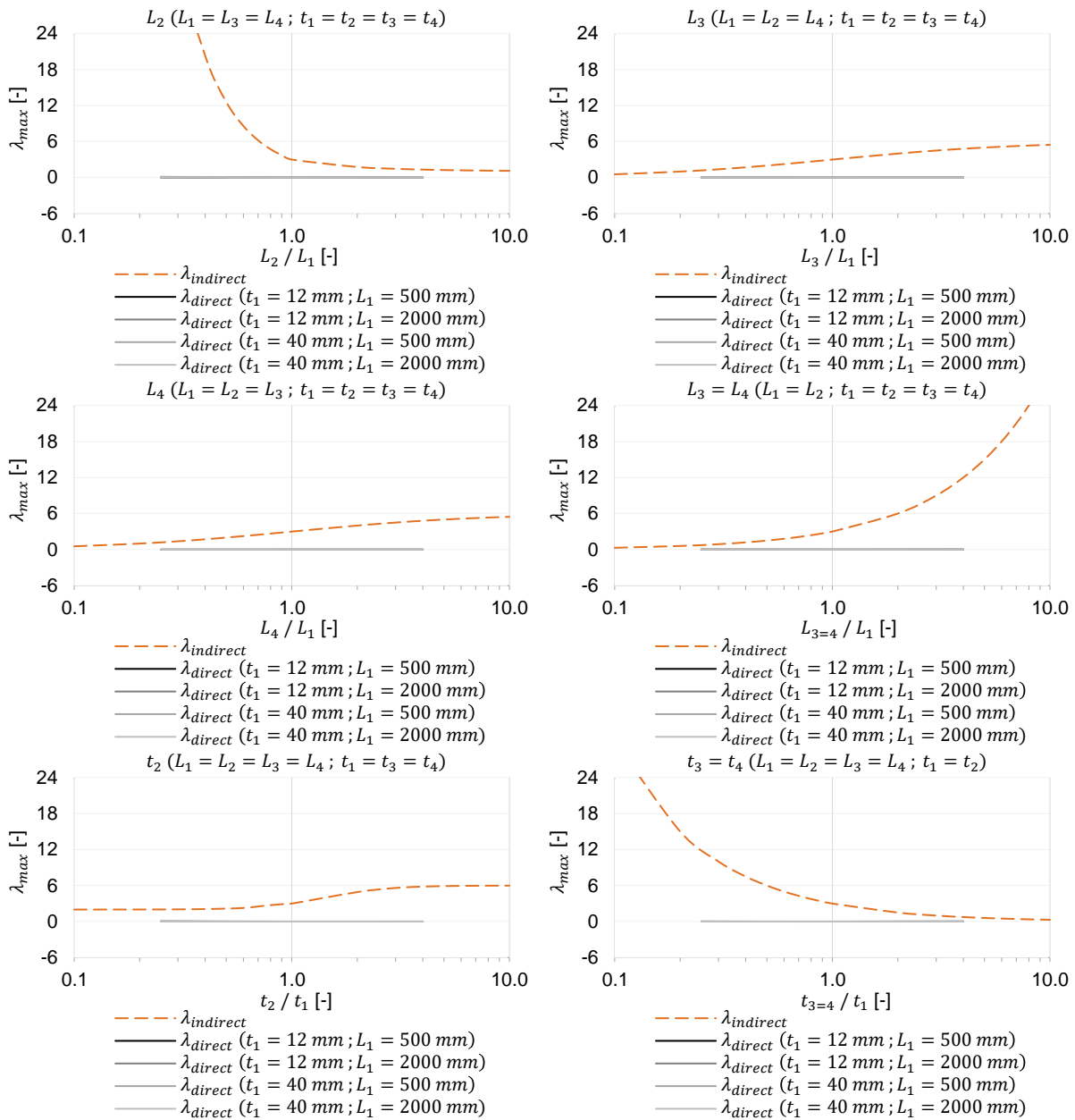


Figure 6-22: Relevant $\lambda_{indirect}$ results with comparison to relevant λ_{direct} results for L_2/L_1 ratio (top left), L_3/L_1 ratio (top right), L_4/L_1 ratio (centre left), $L_{3=4}/L_1$ ratio (centre right), t_2/t_1 ratio (bottom left) and $t_{3=4}/t_1$ ratio (bottom right) for case (k) with angular misalignment $\alpha = 2^\circ$

List of figures

Figure 2-1: Standardised fatigue resistance curve [16].....	6
Figure 2-2: Design S-N curves (left) and different fatigue resistances (right) for the nominal stress concept according to guidelines of the IIW [3] summarised by [6]	7
Figure 2-3: Permitted stress ranges derived from actual stress ranges according to a variety of design regulations [20, 21]	9
Figure 2-4: Scatter range in S-N curves according to IIW [3].....	9
Figure 2-5: Effective design value of the stress range [4]	10
Figure 2-6: Exemplary spectrum of stress ranges [16].....	11
Figure 2-7: Fatigue-relevant stresses at the notch [26].....	12
Figure 2-8: Surface methods (top row and bottom left), methods through plate thickness (bottom centre), δ -method (bottom right)	15
Figure 2-9: Linear stress extrapolation (left) and quadratic stress extrapolation (right) [31]	16
Figure 2-10: Hot-spot types <i>a</i> and <i>b</i> [12].....	16
Figure 2-11: One-point stress determination [35] (left) and method of Haibach [10, 31] (right).....	17
Figure 2-12: Distinction between structural and notch stresses [9, 37].....	18
Figure 2-13: Structural stress determination by stress linearisation over the thickness at the notch [35]	18
Figure 2-14: Definition of the structural stress according to Dong et al. [6] with continuous stress decrease (left), non-constant stress decrease (middle) and symmetrical stress curve (right)	19
Figure 2-15: One-millimetre method with reference detail (left), examined detail (middle) and trend of the associated double logarithmic S-N curves (right) [6].....	20
Figure 2-16: δ -method with stress distribution at the weld notch and at distance δ over the thickness t (left), linearised structural stress over the plate thickness t at the weld notch (A-A) determined by equilibrium conditions (B-B) (centre) and linearised structural stress by equilibrium conditions over the variable thickness t_1 (right) [42]	21
Figure 2-17: δ -method on shell models according to Dong [42].....	22
Figure 2-18: Procedure for the CAB method [31].....	22
Figure 2-19: First principal stress as relevant stress component (left) and resulting relevant perpendicular stress (right) for structural stress calculation [9].....	30
Figure 2-20: Relevant structural stress at multi-axial stress state for main plate with welded-on component according to prEN1993-1-9 [4] with first principal stress σ_1 longitudinal to the direction of tension and σ_2 transverse to the direction of tension as well as stress σ_{\perp} perpendicular to the weld... 34	34
Figure 2-21: Potential angular misalignment β of cruciform joints (left) and Potential bending of plates for laterally unsupported components according to DIN 1090-2 [27] systematically for the FEA (right) 40	40
Figure 2-22: Potential axial misalignment e of cruciform joints	41
Figure 2-23: Rotation of the welded-on plates around the global x -axis.....	42
Figure 2-24: Determination of the effective stress concentration factor $k_{m,eff}$ for permitted axial misalignment of $e_{max} = 0.1 \cdot t_{welded} - on plates$ (left) and $e_{max} \geq 0.15 \cdot t_{welded} - on plates$ (right)	46
Figure 2-25: λ -factor with axial misalignment and constant plate thicknesses $t_1 = t_2 = t_3 = t_4$ according to Xing and Dong [5] as a function of L_2/L_1 of plate 1 (left) and plate 2 (right)	55
Figure 2-26: λ -factor with axial misalignment and constant plate lengths $L_1 = L_2 = L_3 = L_4$ according to Xing and Dong [5] as a function of t_2/t_1 of plate 1 (left) and plate 2 (right).....	55

Figure 2-27: Maximum λ -factor of plate 1 and plate 2 with axial misalignment according to Xing and Dong [5] as a function of L_2/L_1 (left) and t_2/t_1 (right).....	56
Figure 2-28: λ -factor for axial misalignment according to Xing and Dong [5] as a function of $L_3/4/L_1$ (left) and $t_3/4/t_1$ (right).....	56
Figure 2-29: λ -factor with angular misalignment and constant plate thicknesses $t_1 = t_2 = t_3 = t_4$ according to Xing and Dong [5] as a function of L_2/L_1 of plate 1 (left) and plate 2 (right)	59
Figure 2-30: λ -factor with angular misalignment and constant plate lengths $L_1 = L_2 = L_3 = L_4$ according to Xing and Dong [5] as a function of t_2/t_1 of plate 1 (left) and plate 2 (right).....	59
Figure 2-31: Maximum λ -factor of plate 1 and plate 2 with angular misalignment according to Xing and Dong [5] as a function of L_2/L_1 (left) and t_2/t_1 (right).....	60
Figure 2-32: λ -factor for angular misalignment according to Xing and Dong [5] as a function of $L_3/4/L_1$ (left) and $t_3/4/t_1$ (right).....	60
Figure 2-33: λ -factor as a function of the L_c/L -ratio in relation to the clamping process of cruciform joints with axial misalignment (l) and angular misalignment (n) with the simplification $L_c = L_1$ according to Xing and Dong [5].....	62
Figure 2-34: Geometric size effect [29].....	66
Figure 2-35: Relevant parameters for the determination of the thickness effect [29].....	67
Figure 2-36: Reduction of the allowable stress cycles N due to the thickness effect ft with different thickness exponents k according to [50].....	72
Figure 2-37: Relevant parameters for the effective connection length L_t , the connection thickness t and the main plate thickness T according to DNVGL-RP-C203 [50].....	73
Figure 2-38: Reduction of the attainable stress cycles NR due to the thickness effect $f(t)$ using $teff$ with thickness exponent $k = 0.3$ according to [50].....	73
Figure 2-39: Relevant parameters for the effective connection length d , the connection thickness ta and the main plate thickness t according to DNVGL-CG-0129 [32].....	74
Figure 2-40: Factor ft for case A and B for relevant thickness exponents n according to the FKM [11].....	75
Figure 3-1: Illustration of eight node shell elements [69].....	78
Figure 3-2: Exemplary shell models for a K-joint (top left), a welded-on T-joint (top right) and a cover plate joint (bottom) with required modelling of the welds due to the decisive effect on the detail [6]	79
Figure 3-3: Modelling of welds in shell models by increasing the element thickness to ensure an enlarged stiffness in the area of the weld [71].....	80
Figure 3-4: Modelling of welds in shell models by inclined shell elements between the centre planes of the plates [3].....	81
Figure 3-5: Modelling of welds in shell models by inclined shell elements for full penetration welds (left) and fillet welds (right) [72]	81
Figure 3-6: Modelling of welds in shell models by inclined shell elements in combination with rigid links connecting the centre planes of the plates [3].....	82
Figure 3-7: Solid element with twenty nodes and a quadratic initial element function (left) and solid node with eight nodes and a linear initial element function (right) [69]	83
Figure 3-8: Shear locking effect with fully integrated first-order element (left) and hourglassing with reduced integrated first-order element (right) under bending loading.....	83
Figure 3-9: Position of reference points and associated meshing recommendations for the stress extrapolation according to the IIW [3].....	85

Figure 3-10: Characteristic meshing and stress extrapolation paths for shell element models without modelling of the weld (left) and solid element models with modelling of the weld (right) according to the guidelines of the IIW [3] 86

Figure 3-11: Linear stress extrapolation to determine the structural stress with a fine mesh model (left) and a coarse mesh model (right) according to prEN 1993-1-14 [12] 86

Figure 3-12: Quadratic stress extrapolation to determine the structural stress for hot-spot type *a* (left) and hot-spot type *b* (right) according to prEN 1993-1-14 [12] 87

Figure 3-13: Possible imperfections of cruciform joints with associated FE modelling for angular misalignment around the *y*global-axis (top left), axial misalignment in direction of *z*global-axis (top left) and rotation of the welded-on plates around the *x*global-axis (bottom) 91

Figure 3-14: Cruciform joint geometry with required parameters in the globally arranged coordinate system and highlighted clamping and load application section as well as auxiliary node for the modelling of the clamping process 92

Figure 3-15: Cruciform joint geometry with axial misalignment before clamping process (top) and deformed shape after clamping process (bottom) 93

Figure 3-16: Cruciform joint geometry with angular misalignment before clamping process (top) and deformed shape after clamping process (bottom) 93

Figure 3-17: Parameter study on stress concentration factors (SCF) of weld methods *WM1* to *WM4* with finely and coarsely meshed shell models and comparison to finely meshed solid model for different primary plate thicknesses $t_1 = t_2$ with an intermediate plate thickness of $t_3 = 12 \text{ mm}$ 106

Figure 3-18: Parameter study on stress concentration factors (SCF) of weld methods *WM1* to *WM4* with finely and coarsely meshed shell models and comparison to finely meshed solid model for different primary plate thicknesses $t_1 = t_2$ with an intermediate plate thickness of $t_3 = 40 \text{ mm}$ 106

Figure 3-19: Stress distributions of the stress concentration factor for $\Delta\sigma_R, 1.0 \cdot t$, $\Delta\sigma_R, 0.4 \cdot t$ and $\Delta\sigma_R, h_s$ over the component width for the linear stress extrapolation for finely and coarsely meshed *WM4* (left) and *WM1* (right) with $t_1 = t_2 = 12 \text{ mm}$ and $t_3 = 40 \text{ mm}$ 107

Figure 3-20: Stress distributions of the stress concentration factor for $\Delta\sigma_R, 1.0 \cdot t$, $\Delta\sigma_R, 0.4 \cdot t$ and $\Delta\sigma_R, h_s$ over the component width for the linear stress extrapolation for finely meshed *WM1* and solid model with $t_1 = t_2 = 12 \text{ mm}$ and $t_3 = 40 \text{ mm}$ 108

Figure 3-21: Stress distributions of the stress concentration factor for $\Delta\sigma_R, 1.0 \cdot t$, $\Delta\sigma_R, 0.4 \cdot t$ and $\Delta\sigma_R, h_s$ over the component width for the linear stress extrapolation for finely meshed *WM4* and solid model with $t_1 = t_2 = 12 \text{ mm}$ and $t_3 = 40 \text{ mm}$ 110

Figure 3-22: Stress distributions of the stress concentration factor for $\Delta\sigma_R, 1.0 \cdot t$, $\Delta\sigma_R, 0.4 \cdot t$ and $\Delta\sigma_R, h_s$ over the component width for the linear stress extrapolation for finely meshed *WM3* and solid model with $t_1 = t_2 = 12 \text{ mm}$ and $t_3 = 12 \text{ mm}$ 111

Figure 3-23: Stress distributions of the stress concentration factor for $\Delta\sigma_R, 1.0 \cdot t$, $\Delta\sigma_R, 0.4 \cdot t$ and $\Delta\sigma_R, h_s$ over the component width for the linear stress extrapolation for finely meshed *WM3* and solid model with $t_1 = t_2 = 40 \text{ mm}$ and $t_3 = 12 \text{ mm}$ 112

Figure 4-1: Stapled test specimens before the welding process (left) preheating process to reduce welding residual stresses (middle) and welding process (right) 125

Figure 4-2: Validation of the measurement data records by superposition of the point clouds of the measurements with imperfect FE models 127

Figure 4-3: Arrangement of support elements to compensate for the effects of axial misalignment of test group *WP3_3.2* 129

Figure 4-4: Strain gauge position for linear extrapolation to determine the structural stress [9] 130

Figure 4-5: Standardised position plan of the strain gauges for fatigue tests from [1] 130

Figure 4-6: Standardised test force sequence plan for static preliminary tests exemplarily for test specimen WP3_1.1_01	131
Figure 4-7: Strain measurements for SG1 to SG10 of static preliminary tests exemplarily for test specimen WP3_1.1_01	132
Figure 4-8: Determination of the equivalent misalignment <i>eequivalent</i> by calculated stress measurements on opposite plate sides.....	135
Figure 4-9: Exemplarily delayed measurement results for strain gauges SG 1 to SG 10 due to inaccurate synchronisation between the used measurement data acquisition systems (left) and corrected experimental data (right)	136
Figure 4-10: Exemplary evaluation of the maximum single cycle stresses (left) and minimum single cycle stresses (right) of all strain gauges over all cycles of the fatigue test.....	137
Figure 4-11: Definition for the evaluation of the initial crack	138
Figure 4-12: Validation of the clamping process for WP3_1.1_07 representatively for WP3_1.1	139
Figure 4-13: Validation of the clamping process for WP3_1.2_05 representatively for WP3_1.2	140
Figure 4-14: Validation of the clamping process for WP3_2.1_03 representatively for WP3_2.1	140
Figure 4-15: Validation of the clamping process for WP3_2.2NL_03 representatively for WP3_2.2	140
Figure 4-16: Validation of the clamping process for WP3_3.1_09 representatively for WP3_3.1	141
Figure 4-17: Validation of the clamping process for WP3_3.2_07 representatively for WP3_3.2	141
Figure 4-18: Validation of tensile load <i>Fmax</i> for WP3_1.1_07 representatively for WP3_1.1.....	142
Figure 4-19: Validation for tensile load <i>Fmax</i> for WP3_1.2_05 representatively for WP3_1.2	142
Figure 4-20: Validation for tensile load <i>Fmax</i> for WP3_2.1_03 representatively for WP3_2.1	142
Figure 4-21: Validation for tensile load <i>Fmax</i> for WP3_2.2NL_03 representatively for WP3_2.2.....	143
Figure 4-22: Validation for tensile load <i>Fmax</i> for WP3_3.1_09 representatively for WP3_3.1	143
Figure 4-23: Validation for tensile load <i>Fmax</i> for WP3_3.2_07 representatively for WP3_3.2	143
Figure 4-24: Results according to the nominal stress concept for the perfect and imperfect FE models and <i>NR, test</i> for test group WP3_1.1 with associated normative fatigue classes	148
Figure 4-25: Results according to the nominal stress concept for the perfect and imperfect FE models and <i>NR, test</i> for test group WP3_1.2 with associated normative fatigue classes	148
Figure 4-26: Results according to the nominal stress concept for the perfect and imperfect FE models and <i>NR, test</i> for test group WP3_1.2 without the abortive tests WP3_1.2_03 and WP3_1.2_10	149
Figure 4-27: Evaluation of the numerically determined perfect nominal stress $\Delta\sigma_{R, nom, 50\%, FEA, perfect}$ of the test specimens of test series WP3_1 in comparison to analytically determined uncorrected stress ranges of the nominal stress concept according to the normative regulations and guidelines.....	151
Figure 4-28: Evaluation of the numerically determined imperfect nominal stress $\Delta\sigma_{R, nom, 50\%, FEA, imperfect}$ of the test specimens of test series WP3_1 in comparison to analytically determined corrected stress ranges of the nominal stress concept according to the normative regulations and guidelines.....	151
Figure 4-29: Results according to the nominal stress concept for the perfect and imperfect FE models and <i>NR, test</i> for test group WP3_2.1 with associated normative fatigue classes	152
Figure 4-30: Results according to the nominal stress concept for the perfect and imperfect FE models and <i>NR, test</i> for test groups WP3_2.2 and WP3_2.2NL with associated normative fatigue classes.....	152
Figure 4-31: Results according to the nominal stress concept for the perfect and imperfect FE models and <i>NR, test</i> for the specimens WP3_2.2_06 and WP3_2.2NL_02 to WP3_2.2NL_05 with intentional imperfections $e \approx 3 \text{ mm}$ with associated normative fatigue classes	153

Figure 4-32: Evaluation of the numerically determined perfect nominal stress $\Delta\sigma_R, nom, 50\%, FEA, perfect$ of the test specimens of test series *WP3_2* in comparison to analytically determined uncorrected stress ranges of the nominal stress concept according to the normative regulations and guidelines 154

Figure 4-33: Evaluation of the numerically determined imperfect nominal stress $\Delta\sigma_R, nom, 50\%, FEA, imperfect$ of the test specimens of test series *WP3_2* in comparison to analytically determined uncorrected stress ranges of the nominal stress concept according to the normative regulations and guidelines 155

Figure 4-34: Results according to the nominal stress concept for the perfect and imperfect FE models and *NR, test* for test group *WP3_3.1* with associated normative fatigue classes 155

Figure 4-35: Results according to the nominal stress concept for the perfect and imperfect FE models and *NR, test* for test group *WP3_3.2* with associated normative fatigue classes 156

Figure 4-36: Evaluation of the numerically determined perfect nominal stress $\Delta\sigma_R, nom, 50\%, FEA, perfect$ of the test specimens of test series *WP3_3* in comparison to analytically determined uncorrected stress ranges of the nominal stress concept according to the normative regulations and guidelines 157

Figure 4-37: Evaluation of the numerically determined imperfect nominal stress $\Delta\sigma_R, nom, 50\%, FEA, imperfect$ of the test specimens of test series *WP3_3* in comparison to analytically determined uncorrected stress ranges of the nominal stress concept according to the normative regulations and guidelines 157

Figure 4-38: Fatigue strengths for *WP3* following the S-N curves according to the nominal stress concept for the perfect FE models and experimentally determined load cycle numbers *NR, test* with associated uncorrected normative fatigue classes 158

Figure 4-39: Fatigue strengths for *WP3* following the S-N curves according to the nominal stress concept for the imperfect FE models and experimentally determined load cycle numbers *NR, test* with associated corrected normative fatigue classes 159

Figure 4-40: Results according to the structural stress concept for the perfect and imperfect FE models and *NR, test* for test group *WP3_1.1* with associated normative fatigue classes 163

Figure 4-41: Results according to the structural stress concept for the perfect and imperfect FE models and *NR, test* for test group *WP3_1.2* with associated normative fatigue classes 164

Figure 4-42: Evaluation of the numerically determined perfect structural stress $\Delta\sigma_R, hs, 50\%, FEA, perfect$ of the test specimens of test series *WP3_1* in comparison to analytically determined uncorrected stress ranges of the structural stress concept according to the normative regulations and guidelines 166

Figure 4-43: Evaluation of the numerically determined imperfect structural stress $\Delta\sigma_R, hs, 50\%, FEA, imperfect$ of the test specimens of test series *WP3_1* in comparison to analytically determined corrected stress ranges of the structural stress concept according to the normative regulations and guidelines 166

Figure 4-44: Results according to the structural stress concept for the perfect and imperfect FE models and *NR, test* for test group *WP3_2.1* with associated normative fatigue classes 167

Figure 4-45: Results according to the structural stress concept for the perfect and imperfect FE models and *NR, test* for test group *WP3_2.2* and *WP3_2.2NL* with associated normative fatigue classes 167

Figure 4-46: Results according to the structural stress concept for the perfect and imperfect FE models and *NR, test* for the specimens *WP3_2.2_06* and *WP3_2.2NL_02* to *WP3_2.2NL_05* with intentional imperfections $e \approx 3 \text{ mm}$ with associated normative fatigue classes 168

Figure 4-47: Evaluation of the numerically determined perfect structural stress $\Delta\sigma_R, hs, 50\%, FEA, perfect$ of the test specimens of test series *WP3_2* in comparison to analytically determined uncorrected stress ranges of the structural stress concept according to the normative regulations and guidelines..... 169

Figure 4-48: Evaluation of the numerically determined imperfect structural stress $\Delta\sigma_R, hs, 50\%, FEA, imperfect$ of the test specimens of test series *WP3_2* in comparison to analytically determined corrected stress ranges of the structural stress concept according to the normative regulations and guidelines..... 169

Figure 4-49: Results according to the structural stress concept for the perfect and imperfect FE models and *NR, test* for test group *WP3_3.1* with associated normative fatigue classes 170

Figure 4-50: Results according to the structural stress concept for the perfect and imperfect FE models and *NR, test* for test group *WP3_3.2* with associated normative fatigue classes 171

Figure 4-51: Evaluation of the numerically determined perfect structural stress $\Delta\sigma_R, hs, 50\%, FEA, perfect$ of the test specimens of test series *WP3_3* in comparison to analytically determined uncorrected stress ranges of the structural stress concept according to the normative regulations and guidelines..... 172

Figure 4-52: Evaluation of the numerically determined imperfect structural stress $\Delta\sigma_R, hs, 50\%, FEA, imperfect$ of the test specimens of test series *WP3_3* in comparison to analytically determined corrected stress ranges of the structural stress concept according to the normative regulations and guidelines..... 172

Figure 4-53: Fatigue strengths for *WP3* following the S-N curves according to the structural stress concept for the perfect FE models and experimentally determined load cycle numbers *NR, test* with associated uncorrected normative fatigue classes 173

Figure 4-54: Fatigue strengths for *WP3* following the S-N curves according to the structural stress concept for the imperfect FE models and experimentally determined load cycle numbers *NR, test* with associated corrected normative fatigue classes 174

Figure 4-55: Utilisation rates for the ratio of numerically determined nominal or structural stress ranges to normative fatigue strengths according to the guidelines of the IIW [3] for an evaluation on perfect FE models without unintentional imperfections (left) and imperfect FE models (right) 176

Figure 4-56: Position of strain gauges *SG 2* and *SG 9* as well as *SG 8* and *SG 10* in the centre of the welded-on plates to determine secondary bending effects 177

Figure 4-57: Calculated equivalent imperfections *eequivalent* for strain gauges *SG 2* and *SG 9* as well as for *SG 8* and *SG 10* and associated test force *F* at load cycle *NR, test* = 25.000 exemplarily for test specimen *WP3_1.1_06* 178

Figure 4-58: Equivalent imperfections *eequivalent* under test load *Fmax* for strain gauges *SG 2* and *SG 9* as well as *SG 8* and *SG 10* over all cycles exemplarily for test specimen *WP3_1.1_06* 179

Figure 4-59: Comparison between numerical stress ranges $\Delta\sigma_R, eequivalent, FEA$ and experimental stress ranges $\Delta\sigma_R, eequivalent, test$ for test series *WP3_1* with reference to results of stress ranges determined on perfect FE models $\Delta\sigma_R, nom, FEA, perfect$ and imperfect FE models $\Delta\sigma_R, nom, FEA, imperfect$ 180

Figure 4-60: Comparison between numerical stress ranges $\Delta\sigma_R, eequivalent, FEA$ and experimental stress ranges $\Delta\sigma_R, eequivalent, test$ for test series *WP3_2* with reference to results of stress ranges determined on perfect FE models $\Delta\sigma_R, nom, FEA, perfect$ and imperfect FE models $\Delta\sigma_R, nom, FEA, imperfect$ 181

Figure 4-61: Comparison between numerical stress ranges $\Delta\sigma_R, eequivalent, FEA$ and experimental stress ranges $\Delta\sigma_R, eequivalent, test$ for test series *WP3_3* with reference to results of stress ranges

determined on perfect FE models $\Delta\sigma R, nom, FEA, perfect$ and imperfect FE models
 $\Delta\sigma R, nom, FEA, imperfect$ 181

Figure 4-62: Fatigue strengths for WP3 following the S-N curves according to the evaluation by equivalent misalignment *eequivalent* and experimentally determined load cycle numbers $NR, test$ according to the nominal stress concept 182

Figure 4-63: Fatigue strengths for WP3 following the S-N curves according to the evaluation by equivalent misalignment *eequivalent* and experimentally determined load cycle numbers $NR, test$ according to the structural stress concept 183

Figure 5-1: Parameter definition for indirect determination of the influence from axial misalignment according to Xing and Dong [5] 191

Figure 5-2: Evaluation of analytical stress concentration factors $km, angular, Xing\&Dong$ according to Xing and Dong [5] and numerical stress concentration factors $km, angular, FEA$ for nominal stress ranges of $1 N/mm^2$ and $100 N/mm^2$ in the FEA for cruciform joints with angular misalignment 192

Figure 5-3: Numerical parameter study of the axial stress concentration factor $km, axial, FEA$ and comparison with $km, axial, Xing\&Dong$ from [5] for $t1 = 2 = 10 mm$ (left), $t1 = 2 = 25 mm$ (middle) and $t1 = 2 = 40 mm$ (right) with total length $Ltotal = 600 mm$ (top) and $Ltotal = 1400 mm$ (bottom) 193

Figure 5-4: Parameter definition for indirect determination of the influence from angular misalignment according to Xing and Dong [5] 194

Figure 5-5: Numerical parameter study of the angular stress concentration factor $km, angular, FEA$ and comparison with $km, angular, Xing\&Dong$ from [5] for $t1 = 2 = 10 mm$ (left), $t1 = 2 = 25 mm$ (middle) and $t1 = 2 = 40 mm$ (right) with total length $Ltotal = 600 mm$ (top) and $Ltotal = 1400 mm$ (bottom) 194

Figure 5-6: Studies on the influence of the $t1 = 2/Ltotal$ -ratio on the correction factor between FEA and Xing and Dong [5] on axial misalignment (left) and angular misalignment (right) with analytically determined compensation curves 195

Figure 5-7: Numerical parameter study with $km, axial, mod$ for $t1 = 2 = 10 mm$ (left), $t1 = 2 = 25 mm$ (middle) and $t1 = 2 = 40 mm$ (right) with total length $Ltotal = 600 mm$ (top) and $Ltotal = 1400 mm$ (bottom) 197

Figure 5-8: Numerical parameter study with $km, angular, mod$ for $t1 = 2 = 10 mm$ (left), $t1 = 2 = 25 mm$ (middle) and $t1 = 2 = 40 mm$ (right) with total length $Ltotal = 600 mm$ (top) and $Ltotal = 1400 mm$ (bottom) 197

Figure 5-9: Numerical parameter study on cruciform joints with $t1 = 2 = 10 mm$ for the load-dependent correction factor $\Delta Ffactor$ for axial misalignment (left) and angular misalignment (right) with analytically derived results 198

Figure 5-10: Numerical parameter study with $t1 = 2 = 40 mm$ for the load-dependent correction factor $\Delta Ffactor$ for axial misalignment (left) and angular misalignment (right) with analytically derived results 199

Figure 5-11: Comparison between directly determined structural stress ranges by imperfect FE models and analytically calculated structural stress ranges by stress concentration factors for WP3_1 201

Figure 5-12: Comparison between directly determined structural stress ranges by imperfect FE models and analytically calculated structural stress ranges by stress concentration factors for WP3_2 201

Figure 5-13: Comparison between directly determined structural stress ranges by imperfect FE models and analytically calculated structural stress ranges by stress concentration factors for WP3_3 201

Figure 5-14: System (a) with hinged supports with freedom of rotation for axial misalignment 204

Figure 5-15: Comparison of numerical stress concentration factor km, FEA to analytical factors according to IIW [3] and Xing and Dong [5] for case (a) for axial misalignment with $t1 = 2 = 10 mm$ (left) and $t1 = 2 = 40 mm$ (right) 205

Figure 5-16: System (b) with restrained supports for axial misalignment..... 207

Figure 5-17: Comparison of numerical stress concentration factor km, FEA to analytical factors according to IIW [3] and Xing and Dong [5] for case (b) for axial misalignment with $t1 = 2 = 10 mm$ (left) and $t1 = 2 = 40 mm$ (right) 207

Figure 5-18: System (g) with hinged supports with freedom of rotation for angular misalignment 209

Figure 5-19: Comparison of numerical stress concentration factor km, FEA to analytical factors according to IIW [3] and Xing and Dong [5] for case (g) for angular misalignment with $t1 = 2 = 10 mm$ (left) and $t1 = 2 = 40 mm$ (right) 209

Figure 5-20: System (h) with restrained supports for angular misalignment..... 210

Figure 5-21: Comparison of numerical stress concentration factor km, FEA to analytical factors according to IIW [3] and Xing and Dong [5] for case (h) for angular misalignment with $t1 = 2 = 10 mm$ (left) and $t1 = 2 = 40 mm$ (right) 211

Figure 5-22: Case (a) (left), case (b) (middle) and case (c) (right) according to Xing and Dong [5].. 214

Figure 5-23: Support factor $\lambda_{plate 1}$ of plate 1 (left) and $\lambda_{plate 2}$ of plate 2 (right) for analytical support factor $\lambda_{indirect}$ with comparison to numerical support factors λ_{direct} for $L2/L1$ for case (a) with axial misalignment $e/t1 = 0.15$ 214

Figure 5-24: Relevant factor λ_{max} for analytical support factor $\lambda_{indirect}$ with comparison to numerical support factors λ_{direct} for $L2/L1$ ratio (left) and for for $t2/t1$ ratio (right) case (a) with $e/t1 = 0.15$. 215

Figure 5-25: Relevant factors λ_{max} for analytical support factor $\lambda_{indirect}$ with comparison to numerical support factors λ_{direct} for $L2/L1$ ratio (left) and for $t2/t1$ ratio (right) for case (b) with $e/t1 = 0.15$. 216

Figure 5-26: Relevant factors λ_{max} for analytical support factor $\lambda_{indirect}$ with comparison to numerical support factors λ_{direct} for $L2/L1$ ratio (left) and $t2/t1$ ratio (right) for case (c) with $e/t1 = 0.15$ 217

Figure 5-27: Case (d) (left) case (e) (middle) and case (f) (right) according to Xing and Dong [5]... 217

Figure 5-28: Relevant factors λ_{max} for analytical support factor $\lambda_{indirect}$ with comparison to numerical support factors λ_{direct} for $L2/L1$ ratio (left) and for $t2/t1$ ratio (right) for case (d) with $e/t1 = 0.15$. 217

Figure 5-29: Relevant factors λ_{max} for analytical support factor $\lambda_{indirect}$ with comparison to numerical support factors λ_{direct} for $L2/L1$ ratio (top left), $L4/L1$ ratio (top right), $t2/t1$ ratio (bottom left) and for $t3 = 4/t1$ ratio (bottom right) for case (e) with $e/t1 = 0.15$ 218

Figure 5-30: Relevant factors λ_{max} for analytical support factor $\lambda_{indirect}$ with comparison to numerical support factors λ_{direct} for $L2/L1$ ratio (left) and for $t2/t1$ ratio (right) for case (f) with $e/t1 = 0.15$. 218

Figure 5-31: Case (g) (left) and case (h) (right) according to Xing and Dong [5] 220

Figure 5-32: Relevant factors λ_{max} for analytical support factor $\lambda_{indirect}$ with comparison to numerical support factors λ_{direct} for $L2/L1$ ratio (left) and for $t2/t1$ ratio (right) for case (g) with $\alpha = 2^\circ$ 220

Figure 5-33: Relevant factors λ_{max} for analytical support factor $\lambda_{indirect}$ with comparison to numerical support factors λ_{direct} for $L2/L1$ ratio (left) and for $t2/t1$ ratio (right) for case (h) with $\alpha = 2^\circ$ 221

Figure 5-34: Case (i) (left), case (j) (middle) and case (k) (right) according to Xing and Dong [5]... 221

Figure 5-35: Relevant factors λ_{max} for support factors λ_{IIW} according to the IIW [3] with comparison to numerical support factors λ_{direct} for $L2/L1$ ratio (left) and for $t2/t1$ ratio (right) for case (i) with $\alpha = 2^\circ$ 222

Figure 5-36: Relevant factors λ_{max} for analytical support factor $\lambda_{indirect}$ with comparison to numerical support factors λ_{direct} for $L2/L1$ ratio (top left), $L3 = 4/L1$ ratio (top right), $t2/t1$ ratio (bottom left) and for $t3 = 4/t1$ ratio (bottom right) for case (j) with $\alpha = 2^\circ$ 223

Figure 5-37: Relevant factors λ_{max} for support factor λ_{IIW} according to guidelines of the IIW [3] with comparison to numerical support factors λ_{direct} for $L2/L1$ ratio (top left), $L3 = 4/L1$ ratio (top right), $t2/t1$ ratio (bottom left) and for $t3 = 4/t1$ ratio (bottom right) for case (k) with $\alpha = 2^\circ$ 224

Figure 6-1: Case (a) according to Xing and Dong [5]..... 242

Figure 6-2: Relevant $\lambda_{indirect}$ results with comparison to relevant λ_{direct} results for $L2/L1$ ratio (left) and for $t2/t1$ ratio (right) for case (a) with axial misalignment $e/t1 = 0.15$ 242

Figure 6-3: Case (b) according to Xing and Dong [5] 242

Figure 6-4: Relevant $\lambda_{indirect}$ results with comparison to relevant λ_{direct} results for $L2/L1$ ratio (left) and for $t2/t1$ ratio (right) for case (b) with axial misalignment $e/t1 = 0.15$ 242

Figure 6-5: Case (c) according to Xing and Dong [5] 243

Figure 6-6: Relevant $\lambda_{indirect}$ results with comparison to relevant λ_{direct} results for $L2/L1$ ratio (left) and for $t2/t1$ ratio (right) for case (c) with axial misalignment $e/t1 = 0.15$ 243

Figure 6-7: Case (d) according to Xing and Dong [5] 244

Figure 6-8: Relevant $\lambda_{indirect}$ results with comparison to relevant λ_{direct} results for $L2/L1$ ratio (top left), $L3/L1$ ratio (top right), $L4/L1$ ratio (centre left), $L3 = 4/L1$ ratio (centre right), $t2/t1$ ratio (bottom left) and $t3 = 4/t1$ ratio (bottom right) for case (d) with axial misalignment $e/t1 = 0.15$ 244

Figure 6-9: Case (e) according to Xing and Dong [5] 245

Figure 6-10: Relevant $\lambda_{indirect}$ results with comparison to relevant λ_{direct} results for $L2/L1$ ratio (top left), $L3/L1$ ratio (top right), $L4/L1$ ratio (centre left), $L3 = 4/L1$ ratio (centre right), $t2/t1$ ratio (bottom left) and $t3 = 4/t1$ ratio (bottom right) for case (e) with axial misalignment $e/t1 = 0.15$ 245

Figure 6-11: Case (f) according to Xing and Dong [5] 246

Figure 6-12: Relevant $\lambda_{indirect}$ results with comparison to relevant λ_{direct} results for $L2/L1$ ratio (top left), $L3/L1$ ratio (top right), $L4/L1$ ratio (centre left), $L3 = 4/L1$ ratio (centre right), $t2/t1$ ratio (bottom left) and $t3 = 4/t1$ ratio (bottom right) for case (f) with axial misalignment $e/t1 = 0.15$ 246

Figure 6-13: Case (g) according to Xing and Dong [5] 247

Figure 6-14: Relevant $\lambda_{indirect}$ results with comparison to relevant λ_{direct} results for $L2/L1$ ratio (left) and for $t2/t1$ ratio (right) for case (g) with angular misalignment $\alpha = 2^\circ$ 247

Figure 6-15: Case (h) according to Xing and Dong [5] 247

Figure 6-16: Relevant $\lambda_{indirect}$ results with comparison to relevant λ_{direct} results for $L2/L1$ ratio (left) and for $t2/t1$ ratio (right) for case (h) with angular misalignment $\alpha = 2^\circ$ 247

Figure 6-17: Case (i) according to Xing and Dong [5] 248

Figure 6-18: Relevant $\lambda_{indirect}$ results with comparison to relevant λ_{direct} results for $L2/L1$ ratio (top left), $L3/L1$ ratio (top right), $L4/L1$ ratio (centre left), $L3 = 4/L1$ ratio (centre right), $t2/t1$ ratio (bottom left) and $t3 = 4/t1$ ratio (bottom right) for case (i) with angular misalignment $\alpha = 2^\circ$ 248

Figure 6-19: Case (j) according to Xing and Dong [5] 249

Figure 6-20: Relevant $\lambda_{indirect}$ results with comparison to relevant λ_{direct} results for $L2/L1$ ratio (top left), $L3/L1$ ratio (top right), $L4/L1$ ratio (centre left), $L3 = 4/L1$ ratio (centre right), $t2/t1$ ratio (bottom left) and $t3 = 4/t1$ ratio (bottom right) for case (j) with angular misalignment $\alpha = 2^\circ$ 249

Figure 6-21: Case (k) according to Xing and Dong [5] 250

Figure 6-22: Relevant $\lambda_{indirect}$ results with comparison to relevant λ_{direct} results for $L2/L1$ ratio (top left), $L3/L1$ ratio (top right), $L4/L1$ ratio (centre left), $L3 = 4/L1$ ratio (centre right), $t2/t1$ ratio (bottom left) and $t3 = 4/t1$ ratio (bottom right) for case (k) with angular misalignment $\alpha = 2^\circ$ 250

List of tables

Table 2-1: Fatigue verifications in metal structures according to [3].....	12
Table 2-2: Fatigue strength and notch roundness on the basis of the effective notch stress concept according to table C.1 of prEN 1993-1-9 [4].....	24
Table 2-3: Meshing recommendations for element sizes at critical locations according to the effective notch stress concept according to Figure 7.7 of prEN 1993-1-14 [12].....	24
Table 2-4: Table 3.1 of DIN EN 1993-1-9 [2] for γM_f -factors with an influence on the fatigue strength	26
Table 2-5: Excerpt from Table 8.5 according to DIN EN 1993-1-9 [2] on the fatigue strength of cruciform joints applying the nominal stress concept.....	27
Table 2-6: Extract from fatigue classes for the structural stress concept on cruciform joints according to Annex B as specified in DIN EN 1993-1-9 [2]	28
Table 2-7: Excerpt from Table 3.1 of the IIW [3] on the fatigue strength of cruciform joints applying the nominal stress concept.....	29
Table 2-8: Excerpt from Table 3.1 of the IIW [3] on the fatigue strength of cruciform joints according to the structural stress concept	32
Table 2-9: γM_f -factors with regard to the fatigue strength according to prEN 1993-1-9 [4].....	32
Table 2-10: Extract from Table 10.6 of prEN 1993-1-9 [4] for the fatigue strength of cruciform joints applying the nominal stress concept	33
Table 2-11: Excerpt from Table B.1 of prEN 1993-1-9 [4] on the fatigue strength cruciform joints applying the structural stress concept.....	35
Table 2-12: Extract from Table 8 on cruciform joints according to DNVGL-CG-0129 applying the nominal stress concept [32].....	36
Table 2-13: Fatigue resistance and structural stress concentrations according to Table 2-1 DNVGL-RP-C203 [50]	37
Table 2-14: Extract from Table A-8 on cruciform joints according to DNVGL-RP-C203 applying the nominal stress concept [50].....	37
Table 2-15: Fatigue classes in normative regulations and guidelines of the nominal and structural stress concept with regard to cruciform joints with full penetration without weld toes ground.....	38
Table 2-16: Extract from Table 3.20 of the IIW [3] on specifications for stress concentration factors due to imperfections	43
Table 2-17: Stress concentration due to imperfections already considered in the fatigue resistances of cruciform joints	44
Table 2-18: Extract from Table 6.5 of the IIW [3] on axial and angular misalignment of cruciform joints	48
Table 2-19: Derivation of the λ -factor for a statically determined cruciform joint with axial misalignment	48
Table 2-20: Derivation of the λ -factor for a statically determined cruciform joint with angular misalignment	49
Table 2-21: Specifications on imperfections of cruciform joints according to DNVGL-RP-C203 [50]....	50
Table 2-22: Specifications for misalignment of cruciform joints according to BS 7910 [54]	52
Table 2-23: Investigations on axial misalignment of cruciform joints with varying support conditions ..	53
Table 2-24: Investigations on angular misalignment of cruciform joints with varying support conditions	57
Table 2-25: Interaction between λ -factor and clamping process	61

Table 2-26: Comparison of normative regulations and guidelines regarding the factor of the support condition λ of cruciform joints with axial misalignment	63
Table 2-27: Comparison of normative regulations and guidelines regarding the factor of the support condition λ of cruciform joints with angular misalignment	64
Table 2-28: Methods for the determination of the thickness correction factor $f(t)$ according to specifications from the literature	68
Table 2-29: Specifications for the thickness correction exponent n for determining the thickness correction factor $f(t)$ according to the guidelines of the IIW [3].....	71
Table 2-30: Thickness correction factor k according to DNVGL-RP-C203 [50].....	72
Table 2-31: Thickness exponent n for the thickness correction ft according to guideline of the FKM [11].....	75
Table 2-32: Summary for the normative determination of the thickness effect of cruciform joints according to different normative regulations and guidelines	76
Table 3-1: Recommended element sizes for relatively fine and relatively coarse models [9].....	85
Table 3-2: Specifications for linear and quadratic stress extrapolation according to prEN 1993-1-14 [12]	87
Table 3-3: Meshing specifications for models with three-dimensional solid elements according to generally existing local methods without the stress extrapolation.....	88
Table 3-4: Meshing specifications for models with two-dimensional shell elements according to generally existing local methods without the stress extrapolation.....	89
Table 3-5: Evaluation of the structural stresses resp. the stress concentration factor with the nominal and effective notch stress concept	99
Table 3-6: Evaluation of structural stresses resp. stress concentration factors according to different local methods for varying geometries (12 – 12), (12 – 40), (40 – 12) and (25 – 25) separately for finely and coarsely meshed solid and shell elements	100
Table 3-7: Deviation of the structural stresses resp. $SCFs$ of different local methods and the nominal stress and effective notch stress method from the results of the linear stress extrapolation for various geometries (12 – 12), (12 – 40), (40 – 12) and (25 – 25) separately for finely and coarsely meshed solid and shell elements	102
Table 3-8: Dimensions of cruciform joints for the parametric study of different weld modelling methods	105
Table 3-9: Comparison of the stress concentration factors SCF of the solid model to shell models with $WM1$ and normative positions of the required structural stress paths at $0.00 \cdot t3$ as well as adjusted positions at distance $0.25 \cdot t3$ for different cruciform joint geometries	109
Table 3-10: Maximal underestimation of the relevant structural stress $\Delta\sigma R, hs$ of finely meshed shell models with the modified method $WM1$ and unmodified method $WM3$ to finely meshed solid models	113
Table 4-1: Overview of experimental fatigue tests on cruciform joints	125
Table 4-2: Material properties of the steel batches of the fatigue tests according to [1].....	126
Table 4-3: Axial and angular misalignment as cumulative absolute values of the two welded-on plates	128
Table 4-4: Comparison of different approaches to convert normative fatigue classes $\Delta\sigma C$ to a survival probability of $P_s = 50\%$ based on the example of a fatigue class $\Delta\sigma C, 97.5\% = 71 N/mm^2$	133
Table 4-5: Memory plan for fatigue tests of [1].....	134
Table 4-6: Imperfections and maximum load F_{max} for exemplarily presented cruciform joints through the clamping process.....	139

Table 4-7: Fatigue classes according to nominal stress concept for the fatigue tests of *WP3* according to normative regulations and guidelines 145

Table 4-8: Stress concentration factors km due to already considered imperfections in the fatigue classes for cruciform joints of DIN EN 1993-1-9 [2] and prEN 1993-1-9 [4] as well as of the guidelines of the IIW [3] in the nominal stress concept 146

Table 4-9: Thickness concentration factor $f(t)$ of DIN EN 1993-1-9 [2], guidelines of the IIW [3] and prEN 1993-1-9 [4] according to the nominal stress concept 147

Table 4-10: Fatigue classes according to structural stress concept for the fatigue tests of *WP3* according to normative regulations and guidelines 161

Table 4-11: Stress concentration factors km due to already considered imperfections in the fatigue classes for cruciform joints of normative regulations and guidelines for the structural stress concept 162

Table 4-12: Thickness concentration factor $f(t)$ of DIN EN 1993-1-9 [2], guidelines of the IIW [3] and prEN 1993-1-9 [4] according to the structural stress concept 163

Table 5-1: Exceedances of the specifications for support parameters λ_{IIW} according to the IIW [3] by numerically determined support parameters λ_{direct} for systems (a) to (e) with $e/t_1 = 0.15$ 219

Table 5-2: Exceedances of the specifications for support parameters λ_{IIW} according to the guidelines of the IIW [3] by numerically determined support parameters λ_{direct} for systems (g) to (k) with $\alpha = 2^\circ$ 225

Bibliography

- [1] *Rausch, N.; Mensinger, M.*: Anwendung des Strukturspannungskonzeptes bei ermüdungsbeanspruchten Konstruktionen des Stahlbaus – Abschlussbericht zum IGF-Forschungsvorhaben Nr. 20336 N. Lehrstuhl für Metallbau, TUM, München, 2022.
- [2] DIN EN 1993-1-9:2010.
- [3] *Hobbacher, A.F.*: Recommendations for Fatigue Design of Welded Joints and Components, IIW Collection, Springer International Publishing, Cham, 2016.
- [4] prEN 1993-1-9:2021.
- [5] *Xing, S.; Dong, P.*: An analytical SCF solution method for joint misalignments and application in fatigue test data interpretation. *In: Marine Structures* 50 (2016), S. 143-161. <https://doi.org/10.1016/j.marstruc.2016.07.006>.
- [6] *Radaj, D.; Sonsino, C.M.; Fricke, W.*: Fatigue assessment of welded joints by local approaches, Woodhead publishing in materials, Woodhead Publ; CRC, Cambridge, 2006.
- [7] *XIAO, Z.*: A method of determining geometric stress for fatigue strength evaluation of steel welded joints. *In: International Journal of Fatigue* 26 (2004), Heft 12, S. 1277-1293. <https://doi.org/10.1016/j.ijfatigue.2004.05.001>.
- [8] *Radaj, D.*: Design and analysis of fatigue resistant welded structures, Woodhead Publishing Series in Welding and Other Joining Technologies, Abington, Cambridge, England, 1990.
- [9] *Niemi, E.; Fricke, W.; Maddox, S.J.*: Structural hot-spot stress approach to fatigue analysis of welded components – Designer's guide, IWW collection, Springer-Verlag, Singapore, 2018.
- [10] *Haibach, E. (Hrsg.)*: Die Schwingfestigkeit von Schweißverbindungen aus der Sicht einer örtlichen Beanspruchungsmessung. Hannover, Techn. Hochsch., Diss., 1968, Bericht / Laboratorium für Betriebsfestigkeit FB Heft 77,, Darmstadt, 1968.
- [11] *Rennert, R.; Kullig, E.; Vormwald, M.e.a.*: Rechnerischer Festigkeitsnachweis für Maschinenbauteile aus Stahl, Eisenguss- und Aluminiumwerkstoffen. Forschungskuratorium Maschinenbau, FKM-Richtlinie, VDMA-Verlag GmbH, Frankfurt am Main, 2012.
- [12] *Lotsberg, I.*: Assessment of the size effect in fatigue analysis of butt welds and cruciform joints. *In: International Conference on Offshore Mechanics and Arctic Engineering* (2014), Vol. 45455.
- [13] *Glenn, I. F., Paterson, R. B., Luznik, L., Dinovitzer, A., & Bayley, C.*: Fatigue resistant detail design guide for ship structures. No. SR-1386, 1999.
- [14] prEN 1993-1-14:2021. Ausgabe 2021.
- [15] *Geissler, K.*: Verbesserung der Praxistauglichkeit der Baunormen durch pränormative Arbeit – Teilantrag 3: Stahlbau, Forschungsinitiative Zukunft BauF 2964, Fraunhofer-IRB-Verl., Stuttgart, 2015.
- [16] *Ladinek, M.; Lang, R.; Lener, G.*: Ermüdungsfestigkeit nach EN 1993-1-9. *In: Stahlbau* 85 (2016), Heft 4, S. 274-280. <https://doi.org/10.1002/stab.201610373>.

- [17] *Nussbaumer, A.; Günther H.-P.*: Grundlagen und Erläuterung der neuen Ermüdungsnachweise nach Eurocode 3. In: Stahlbau-Kalender 2006. Hrsg.: Kuhlmann, U. Ernst & Sohn, Berlin, 2006.
- [18] *Deutsches Institut für Normung*: DIN EN ISO 19902, Petroleum and natural gas industries - fixed steel offshore structures (ISO 19902:2020) – = Erdöl- und Erdgasindustrie - gegründete Stahlplattformen (ISO 19902:2020). Deutsches Institut für Normung, Deutsche Norm, Beuth Verlag GmbH, Berlin, 2021.
- [19] *Ye, X.W.; Su, Y.H.; Han, J.P.*: A State-of-the-Art Review on Fatigue Life Assessment of Steel Bridges. In: Mathematical Problems in Engineering 2014 (2014), S. 1-13. <https://doi.org/10.1155/2014/956473>.
- [20] *Milana, G., Banisoleiman, K., González, A. (Hrsg.)*: Fatigue life assessment methods: the case of ship unloaders. 1st International Conference on Natural Hazards & Infrastructure (ICONHIC 2016): Protection, Design and Rehabilitation, Chania, Greece, 2016.
- [21] *A. Nussbaumer; H. P. Günther*: Stahlbau Kalender 2006 – Grundlagen und Erläuterung der neuen Ermüdungsnachweise nach Eurocode 3, Stahlbau Kalender Jahrgang 8, Ernest & Sohn, Berlin, op. 2006.
- [22] *Deutsches Institut für Normung*: DIN EN 1990 – Grundlagen der Tragwerksplanung - Deutsche Fassung, Deutsche Norm, Beuth Verlag GmbH, Berlin, 2021.
- [23] DIN EN 1993-1-9 - 2010-12, Eurocode 3: Bemessung und Konstruktion von Stahlbauten - Teil 1-9: Ermüdung. Norm,
- [24] *Fröhling, W.*: Bücher: Stahlbau Kalender 2006. By U. Kuhlmann. In: Bautechnik 83 (2006), Heft 10, S. 745. <https://doi.org/10.1002/bate.200690183>.
- [25] *Olivier, R.; Köttgen, V.B.*: Schwingfestigkeitsnachweise für Schweißverbindungen auf der Grundlage örtlicher Beanspruchungen – Abschlußbericht ; Vorhaben Nr. 105 ; Forschungszeitraum: 01.05.1986 - 31.12.1988. Fachgebiet Werkstoffmechanik, Technische Hochschule Darmstadt; Forschungskuratorium Maschinenbau, Forschungshefte. Forschungskuratorium Maschinenbau eV Heft 143,, Frankfurt am Main, 1989.
- [26] *Olivier, R.; Köttgen, V.B.; Seeger, T.*: Schweißverbindungen II – Bericht auf der FKM-Arbeitskreissitzung am 19. Juni 1991 in Frankfurt/Main, Fachgebiet Werkstoffmechanik, Technische Hochschule Darmstadt Heft 1991,4, Fachgebiet Werkstoffmechanik, Technische Hochsch, Darmstadt, 1991.
- [27] *Deutsches Institut für Normung*: DIN 50100. Deutsches Institut für Normung, Deutsche Norm, Beuth Verlag GmbH, Berlin, 2021.
- [28] *Det Norske Veritas*: DNVGL-RP-C203 2020-01: Fatigue design of offshore steel structures, 2020.
- [29] *Aygül, M.*: Fatigue evaluation of welded details - using the finite element method. Zugl.: Göteborg, Univ., Diss., 2013, Doktorsavhandlingar vid Chalmers Tekniska Högskolan. S., 3624, Chalmers Univ. of Technology, Göteborg, 2013.
- [30] *Gesellschaft für Schweißtechnik International mbH*: The Welding Engineer's Current Knowledge – Welding processes and equipment, Materials and their behaviour during welding, Construction and design, Fabrication. SLV Duisburg, 2015.

- [31] *Mashayekhizadeh, M.*: Fatigue assessment of complex structural components of steel bridges integrating finite element models and field-collected data – Doctoral dissertation. University of New Hampshire, 2019.
- [32] *Palmgren A.*: Die Lebensdauer von Kugellagern. *In: VDI-Z (1924), Heft 58, S. 339-341.*
- [33] *Miner M. A.*: Cumulative damage in fatigue. *In: J. Appl. Mech. (1945), Heft 12, S. 159-164.*
- [34] *Leander, J.*: Refining the fatigue assessment procedure of existing steel bridges – Doctoral dissertation. KTH Royal Institute of Technology, 2013.
- [35] *Hinkelmann, K.; Esderts, A.; Zenner, H.*: Ein verbessertes Verfahren zur Lebensdauerabschätzung mittels linearer Schadensakkumulation. *In: Materials Testing 52 (2010), Heft 5, S. 282-291. <https://doi.org/10.3139/120.110132>.*
- [36] *Martin Mensinger*: Zur Anwendung des Strukturspannungskonzeptes beim Ermüdungsnachweis nach EN 1993-1-9.
- [37] DIN EN 1090-2:2018.
- [38] *Schaumann & Keindorf Ingenieures.mbH*: Berechnungsmöglichkeiten für Strukturanalysen und Ermüdung, <https://ski-consult.de/taetigkeitsbereiche/strukturanalysen/> [Zugriff am: 14.01.2022].
- [39] *Bucak, Ö.; Lorenz, J.*: Ermüdungsverhalten unterschiedlicher Kerbdetails. *In: Stahlbau 80 (2011), Heft 8, S. 608-618. <https://doi.org/10.1002/stab.201101462>.*
- [40] *Möller, B.; Melz, T.; Baumgartner, J. et al.*: Bemessung zyklisch beanspruchter Schweißverbindungen aus höchst- und ultrahochfesten Stählen. *In: Stahlbau 84 (2015), Heft 9, S. 620-628. <https://doi.org/10.1002/stab.201510303>.*
- [41] *Al-Emrani, M.; Aygül, M.*: Fatigue Design of Steel and Composite Bridges – Report 2014:10. Chalmers University of Technology, Göteborg, Sweden, 2014.
- [42] *Heshmati, M.*: Fatigue Life Assessment of Bridge Details Using Finite Element Method – Master's thesis in the Master's Programme Structural Engineering and Building Performance Design. Department of Civil and Environmental Engineering, CHALMERS UNIVERSITY OF TECHNOLOGY, Gotheburg, Sweden, 2012.
- [43] *Stappers, T.*: Stress analysis for fatigue of aluminium welded joints – Thesis. Eindhoven University of Technology, Eindhoven, 2019.
- [44] *Beat Schmied, Schmied Engineering GmbH*: Statischer Festigkeitsnachweis von Schweißnähten mit örtlichen Spannungen, Schweizer Maschinenelemente Kolloquium (SMK2010),, 2010.
- [45] *Det Norske Veritas*: Fatigue assessment of ship structures: DNVGL-CG-0129 2018-01, 2018.
- [46] *Maddox, S.J.*: Hot-spot stress design curves for fatigue assessment of welded structures. *In: INTERNATIONAL JOURNAL OF OFFSHORE AND POLAR ENGINEERING 12 (2002), Heft 2, S. 134-141.*
- [47] *Lotsberg, I.; Sigurdsson, G.*: Hot Spot Stress S-N Curve for Fatigue Analysis of Plated Structures. ASME, NEW YORK, 2006.
- [48] *Borges A. L.; Davaine L.*: ECCS-SCI Eurocode design manuals – Fatigue Design of Steel and Composite Structures. European Convention for Constructional Steelwork; Steel Construction Institute. ECCS - European Convention for Constructional Steelwork, Brussels, Belgium, 2011.

- [49] *Kugler, P.; Dipl.-Ing., B.*: Analyse möglicher Ansätze zur Verlängerung der rechnerischen Restlebensdauer geschweißter Eisenbahnbrücken. Graz, Technische Universität Graz, Dissertation, 2019.
- [50] *Dong, P.*: A structural stress definition and numerical implementation for fatigue analysis of welded joints. *In: International Journal of Fatigue* (2001), Heft 23, S. 865-876.
- [51] *Dong, P.; Hong, J.K.; Jesus, A.M.P.*: Analysis of recent fatigue data using the structural stress procedure in ASME Div 2 Rewrite. *In: JOURNAL OF PRESSURE VESSEL TECHNOLOGY-TRANSACTIONS OF THE ASME* 129 (2007), Heft 3, S. 355-362.
- [52] *Remes, H.; Fricke, W.*: Influencing factors on fatigue strength of welded thin plates based on structural stress assessment. *In: Welding in the World* (2014), Heft 58, S. 915-923.
- [53] *Chen, C.*: A parametric study aimed at assessing fatigue performance of bolted connections – Doctoral dissertation. University of Kansas, 2016.
- [54] *Dong, P.; Hong, J.K.; Cao, Z.*: Structural stress based master S-N curve for welded joints, Paris 2002.
- [55] *Karssen, R.*: Searching for an improvement in fatigue assessment to increase lifetime expectancy, 2015.
- [56] *Poutiainen, I.; Tanskanen, P.; Marquis, G.*: Finite element methods for structural hot spot stress determination—a comparison of procedures. *In: International Journal of Fatigue* (2004), Heft 26, S. 1147-1157.
- [57] *Horn, A.M.; Andersen, M.R.; Biot, M. et al.*: Report of Committee III. 2: Fatigue and Fracture. *In: Proceeding of the 17th International Ship and Offshore Structures Congress* (2009), S. 475-585.
- [58] *Doerk, O.; Fricke, W.; & Weissenborn, C.*: Comparison of different calculation methods for structural stresses at welded joints. *In: International Journal of Fatigue* 2003, 25 (5), S. 359-369.
- [59] *Heshmati, M.; Al-Emrani, M.; Edlund, B.*: Fatigue assessment of weld terminations in welded cover-plate details; A comparison of local approaches. *In: Nordic Steel Construction Conference, Oslo* (2012), S. 781-790.
- [60] *Muscat, M.; Degiorgio, K.; Wood, J.*: Comparison Between Different Approaches for the Evaluation of the Hot Spot Structural Stress in Welded Pressure Vessel Components. *In: : Volume 3: Design and Analysis. ASMEDC, Prague, Czech Republic, 2009, S. 231-240.*
- [61] *NORSOK*: Standard: Design of steel structures – N-004, Rev, 2, 2004.
- [62] *Bayerisches Staatsministerium für Wohnen, Bau und Verkehr*: Bayerische Bauordnung – Bayerisches Staatsministerium für Wohnen, Bau und Verkehr – BayBO. Bayerisches Staatsministerium für Wohnen, Bau und Verkehr, 2021.
- [63] *Bayerisches Staatsministerium für Wohnen, Bau und Verkehr*: Bayerische Technische Baubestimmungen – Bayerisches Staatsministerium für Wohnen, Bau und Verkehr – BayTB. Bayerisches Staatsministerium für Wohnen, Bau und Verkehr, 2021.
- [64] *Deutsches Institut für Normung*: DIN EN 1993-1-12/NA:2011-08, Part 1-12, Beuth Verlag GmbH, Berlin, 2011.

- [65] *Niemi, E. (ed.):* Stress determination for fatigue analysis of welded components. International Institute of Welding. Abington in association with the International Institute of Welding, Cambridge, 1995.
- [66] *Det Norske Veritas:* Fatigue design of offshore steel structures: RP-C203 – Recommended practice DNVGL-RP-0005: 2014-06, 2014.
- [67] *Berge, S.; Myhre, H.:* Fatigue strength of misaligned cruciform and butt joints. *In:* Royal Norwegian Council for Scientific & Indus Res (1977), Volume: 5, p. 29-39.
- [68] DIN EN ISO 5817: DIN EN ISO 5817. Ausgabe 2014.
- [69] DIN EN ISO 6520-1:2007-11.
- [70] *TARAS, A.; Unterweger, H.:* NUMERICAL METHODS FOR THE FATIGUE ASSESSMENT OF WELDED JOINTS: INFLUENCE OF MISALIGNMENT AND GEOMETRIC WELD IMPERFECTIONS. *In:* Engineering Structures and Technologies 9 (2017), Heft 1, S. 9-24.
<https://doi.org/10.3846/2029882X.2017.1299968>.
- [71] *British Standards Institution:* Guide to methods for assessing the acceptability of flaws in metallic structures – British standard BS 7910:2005. British Standards Institution, BSI British standards no. 7910, BSI British Standards Institution, London, 2005.
- [72] *Berge, S.:* On the Effect of Plate Thickness in Fatigue of Welds. *In:* Engineering Fracture Mechanics 1985, Vol. 21, No. 2, S. 423-435.
- [73] *Berge, S.:* Effect of Plate Thickness in Fatigue Design of Welded Structures. *In:* OTC Paper (1984), Heft 4829.
- [74] *Berge, S.; Engesvik, K.:* Effect of Plate Thickness in Fatigue of Transverse Fillet Welds. *In:* Steel in Marine Structures Int. conf. Paris (1981).
- [75] *Gordon, J.R., Mohr, W.C., Dimitrakis, S.D. and Lawrence, F.V. (Hrsg.):* Fatigue Design of Offshore Structures, 1997.
- [76] *Gurney, T.R.:* Thickness Effect in “Relatively thin” Welded Joints. *In:* HSE 1995, Second impression (with amendments) (1997).
- [77] *Gurney, T.R.:* The influence of thickness in the fatigue strength of welded joints. Proceedings of the 2nd Int. Conference on the Behaviour of Offshore Structures. BHRA fluid Engineering, Cranfield, England, 1979.
- [78] *Gurney, T.R.:* The fatigue strength of transverse fillet welded joints – A study of the influence of joint geometry, An Abington Publishing Special Report, Abington Publishing, Cambridge, England, 1991.
- [79] *Maddox, S.J.:* The effect of plate thickness on the fatigue strength of fillet welded joints. Welding Institute. Welding Institute, Cambridge, 1987.
- [80] *Schumacher, A.; Costa Borges, L.; Nussbaumer, A.:* Critical Examination of the Size Effect for Welded Steel Tubular Joints. *In:* International Journal of Fatigue, Vol. 31, S. 1422-1433.
- [81] *Yagi, J.; Machida, S.; Tomita, Y. et al.:* Thickness Effect Criterion for Fatigue Evaluation of Welded Steel Structures. *In:* Proceedings of the 10th Int. Conf. on Offshore Mechanics and Arctic Engineering (1991), Volume III-Part B, ASME, S. 305-313.
- [82] *Yamamoto, N.; Mouri, M.; Okada, T. et al.:* Analytical and Experimental Study on the Thickness Effect to Fatigue Strength. *In:* IIW document XIII-2434-12 (2012).

- [83] *IACS: Common structural rules for bulk carriers and oil tankers*. DNV GL, Safer, smarter, greener, DNV GL, Maritime Headquarters, Hamburg, Germany, 2017.
- [84] *Burchitz, I.A.; Meinders, T.; Huetink, J.: Adaptive Through-Thickness Integration Strategy for Shell Elements*. In: AIP Conference Proceedings (2007), Vol. 908, No. 1, S. 699-704.
- [85] *ANSYS, Inc: ANSYS 19 Version R3: ANSYS Help*. ANSYS, 2021, <https://ansyshelp.ansys.com/account/secured?returnurl=/Views/Secured/corp/v191.html>.
- [86] *Echer, L.; Marczak, R.J.: A Formulation and Comparison of Different Shell FE Modeling Techniques for Fatigue Life Simulation of Welded Joints*. In: XXXIV Iberian Latin-American Congress on Computational Methods in Engineering (CILAMCE 2014) 2014.
- [87] *Goedel, F.; Mezzomo, G.P.; Pravia, Z.M.C.: Fatigue lifespan of a fillet welded joint - Hybrid approach to obtain the S-N curve with a reduced number of tests*. In: Latin American Journal of Solids and Structures 15 (2018), Heft 10. <https://doi.org/10.1590/1679-78255194>.
- [88] *Marin, T.; Nicoletto, G.: Fatigue design of welded joints using the finite element method and the 2007 ASME Div. 2 Master curve*. In: Frattura ed Integrità Strutturale 3 (2009), Heft 9, S. 76-84. <https://doi.org/10.3221/IGF-ESIS.09.08>.
- [89] *Fricke, W.: Recommended Hot Spot Analysis Procedure for Structural Details of FPSOs and Ships Based on Round-Robin FE Analyses*. The International Offshore and Polar Engineering Conference, Norway, 2001.
- [90] *Deutsches Institut für Normung: DIN 50125, Prüfung metallischer Werkstoffe - Zugproben – = Testing of metallic materials - tensile test pieces*. Deutsches Institut für Normung, Deutsche Norm, Beuth Verlag GmbH, Berlin, 2021.
- [91] *Deutsches Institut für Normung: DIN EN ISO 6892-1, Metallische Werkstoffe - Zugversuch. Teil 1, Prüfverfahren bei Raumtemperatur (ISO 6892-1:2019) – = Metallic materials - tensile testing. Part 1, Method of test at room temperature (ISO 6892-1:2019)*. Deutsches Institut für Normung, Deutsche Norm, Beuth Verlag GmbH, Berlin, 2020.
- [92] *Kuhlmann, U.: Stahlbau-Kalender 2012 – Eurocode 3 - Grundnorm, Brücken, Stahlbau-Kalender*, Wiley, Hoboken, 2014.
- [93] *Ummenhofer T., Herion S., Hrabowski J.: Ermüdungsverhalten kranzspezifischer Kerbdetails - Untersuchungen im Kurzzeitfestigkeitsbereich*. In: Stahlbau 82 (2013), Heft 4, S. 270-281. <https://doi.org/10.1002/stab.201310036>.